

**Biosynthesis of penilactones and peniphenones in
*Penicillium crustosum***

**Biosynthese von Penilactonen und Peniphenonen in
*Penicillium crustosum***

Dissertation
zur Erlangung des Doktorgrades
der Naturwissenschaften
(Dr. rer. nat.)

dem Fachbereich Pharmazie
der Philipps-Universität Marburg

vorgelegt von

Jie Fan
aus Linfen, China

Marburg an der Lahn, 2020

Erstgutachter: **Prof. Dr. Shu-Ming Li**

Zweitgutachter: **Prof. Dr. Michael Keusgen**

Eingereicht am 12. Februar 2020

Tag der mündlichen Prüfung: 27. März 2020

Hochschulkennziffer: 1180

Dedicated to my family

Table of contents

List of publications	III
Erklärung zum Eigenanteil	V
Abbreviations	VII
Summary	1
Zusammenfassung	3
1 Introduction	5
1.1 Ascomycota: rich source of diverse natural products	5
1.2 Biosynthesis of fungal natural products	7
1.2.1 Polyketide synthase.....	10
1.2.2 Polyketide synthase-nonribosomal peptide synthetase	13
1.3 Enzymatic oxidations and reductions in natural product biosynthesis	16
1.3.1 Nonheme Fe ^{II} /2-oxoglutarate-dependent oxygenases.....	18
1.3.2 Flavin-containing oxidoreductases	21
1.4 Non-enzymatic reactions in natural product formation	23
2 Aims of this thesis	25
3 Results and discussion	27
3.1 Peniphenone and penilactone formation in <i>Penicillium crustosum</i> via 1,4-Michael additions of <i>ortho</i> -quinone methide from hydroxyclavatul to γ -butyrolactones from tetronic acids.....	27
3.2 Terrestrial acid formation in <i>Penicillium crustosum</i> requires redox-assisted decarboxylation and stereoisomerization	31
3.3 Increasing structural diversity of natural products by Michael addition with <i>ortho</i> -quinone methide derived from hydroxyclavatul.....	35
4 Publications.....	41
4.1 Peniphenone and penilactone formation in <i>Penicillium crustosum</i> via 1,4-Michael additions of <i>ortho</i> -quinone methide from hydroxyclavatul to γ -butyrolactones from crustosic acid.	41
4.2 Formation of terrestrial acid in <i>Penicillium crustosum</i> requires redox-assisted decarboxylation and stereoisomerization.	123

TABLE OF CONTENTS

4.3 Increasing structural diversity of natural products by Michael addition with <i>ortho</i>-quinone methide as the acceptor.....	189
5 Conclusions and future prospects	257
6 References	259
Statutory Declaration.....	273
Acknowledgements	275
Curriculum Vitae	277

List of publications

1. **Jie Fan***, Ge Liao*, Florian Kindinger, Lena Ludwig-Radtke, Wen-Bing Yin, and Shu-Ming Li (2019), Peniphenone and penilactone formation in *Penicillium crustosum* via 1,4-Michael additions of *ortho*-quinone methide from hydroxyclovatol to γ -butyrolactones from crustosic acid. *Journal of the American Chemical Society*, 141 (10), 4225–4229, DOI: 10.1021/jacs.9b00110. (*equal contribution)
2. **Jie Fan***, Ge Liao*, Lena Ludwig-Radtke, Wen-Bing Yin, and Shu-Ming Li (2020), Formation of terrestrial acid in *Penicillium crustosum* requires redox-assisted decarboxylation and stereoisomerization. *Organic Letters*, 22 (1), 88–92, DOI: 10.1021/acs.orglett.9b04002. (*equal contribution)
3. Ge Liao*, **Jie Fan***, Lena Ludwig-Radtke, Katja Backhaus, and Shu-Ming Li (2020), Increasing structural diversity of natural products by Michael addition with *ortho*-quinone methide as the acceptor. *Journal of Organic Chemistry*, 85 (2), 1298–1307, DOI: 10.1021/acs.joc.9b02971 (*equal contribution)
4. Ge Liao*, Peter Mai*, **Jie Fan**, Georg Zocher, Thilo Stehle, and Shu-Ming Li (2018), Complete decoration of the indolyl residue in *cyclo*-L-Trp-L-Trp with geranyl moieties by using engineered dimethylallyl transferases. *Organic Letters*, 20 (22), 7201–7205, DOI: 10.1021/acs.orglett.8b03124. (*equal contribution)

Erklärung zum Eigenanteil

Titel der Publikation und Journal incl. Jahr, Heft, Seitzahl + doi	Autoren	geschätzter Eigenanteil in %	<u>Bitte angeben:</u> angenommen /eingereicht
<p>O: Originalarbeit Ü: Übersichtartikel/Review</p> <p>Peniphenone and penilactone formation in <i>Penicillium crustosum</i> via 1,4-Michael additions of <i>ortho</i>-quinone methide from hydroxyclovatol to γ-butyrolactones from crustosic acid. <i>Journal of the American Chemical Society</i>, 2019, 141 (10), 4225–4229 DOI: 10.1021/jacs.9b00110. Originalarbeit</p>	<p>Jie Fan*, Ge Liao*, Florian Kindinger, Lena Ludwig-Radtke, Wen-Bing Yin and Shu-Ming Li</p>	35	angenommen
<p>Formation of terrestric acid in <i>Penicillium crustosum</i> requires redox-assisted decarboxylation and stereoisomerization. <i>Organic Letters</i>, 2020, 22 (1), 88–92 DOI: 10.1021/acs.orglett.9b04002. Originalarbeit</p>	<p>Jie Fan*, Ge Liao*, Lena Ludwig-Radtke, Wen-Bing Yin and Shu-Ming Li</p>	40	angenommen
<p>Increasing structural diversity of natural products by Michael addition with <i>ortho</i>-quinone methide as the acceptor. <i>Journal of Organic Chemistry</i>, 2020, 85 (2), 1298–1307 DOI: 10.1021/acs.joc.9b02971 Originalarbeit</p>	<p>Ge Liao*, Jie Fan*, Lena Ludwig-Radtke, Katja Backhaus and Shu-Ming Li</p>	40	angenommen
<p>Complete decoration of the indolyl residue in <i>cyclo</i>-L-Trp-L-Trp with geranyl moieties by using engineered dimethylallyl transferases. <i>Organic Letters</i>, 2018, 20 (22), 7201–7205 DOI: 10.1021/acs.orglett.8b03124. Originalarbeit</p>	<p>Ge Liao*, Peter Mai*, Jie Fan, Georg Zocher, Thilo Stehle and Shu-Ming Li</p>	10	angenommen

*: These authors contributed equally to this work.

Kandidat(in)

Unterschrift Betreuer(in)

Abbreviations

The international system of units and units derived thereof have been used.

[M+H] ⁺	molecular ion plus proton
[M-H] ⁻	molecular ion minus proton
× <i>g</i>	gravitational acceleration
A domain	adenylation domain
<i>A. flavus</i>	<i>Aspergillus flavus</i>
<i>A. fumigatus</i>	<i>Aspergillus fumigatus</i>
<i>A. nidulans</i>	<i>Aspergillus nidulans</i>
<i>A. niger</i>	<i>Aspergillus niger</i>
<i>A. oryzae</i>	<i>Aspergillus oryzae</i>
<i>A. parasiticus</i>	<i>Aspergillus parasiticus</i>
<i>A. terreus</i>	<i>Aspergillus terreus</i>
aa	amino acid
ACP domain	acyl carrier protein domain
AT domain	acyltransferase domain
ATP	adenosine triphosphate
BGC	biosynthetic gene cluster
bp	base pair
br	broad (NMR signal)
C domain	condensation domain
<i>C. purpurea</i>	<i>Claviceps purpurea</i>
CD ₃ OD	deuterated methanol
CDCl ₃	deuterated chloroform
cDNA	copy deoxyribonucleic acid
cla	<u>clav</u> atol
CoA	coenzyme A
COSY	correlation spectroscopy
<i>cyclo</i> -L-Trp-L-Trp	<i>cyclo</i> -L-tryptophan-L-tryptophan
<i>cyclo</i> -L-Tyr-L-Tyr	<i>cyclo</i> -L-tyrosine-L-tyrosine
<i>cyclo</i> -L-Ser-L-Tyr	<i>cyclo</i> -L-serine-L-tyrosine

ABBREVIATIONS

d	doublet
D ₂ O	deuterium oxide
Da	dalton
dd	double doublet
ddd	double double doublet
DEBS	6-deoxyerythronolide B synthase
DH domain	dehydratase domain
DMA	dimethylallyl
DMAPP	dimethylallyl diphosphate
DMATS	dimethylallyltryptophan synthase
DMSO- <i>d</i> ₆	deuterated dimethyl sulfoxide
DNA	deoxyribonucleic acid
dq	double quartet
dt	double triplet
<i>E. coli</i>	<i>Escherichia coli</i>
<i>e.g.</i>	<i>exempli gratia</i>
EIC	extracted ion chromatogram
ER domain	enoyl reductase domain
ESI	electrospray ionization
EtOAc	ethyl acetate
FAD	flavin adenine dinucleotide
FMN	flavin mononucleotide
<i>F. begoniae</i>	<i>Fusarium begonia</i>
<i>F. fujikuroi</i>	<i>Fusarium fujikuroi</i>
<i>F. graminearum</i>	<i>Fusarium graminearum</i>
<i>F. tricinctum</i>	<i>Fusarium tricinctum</i>
gDNA	genomic DNA
GMM	glucose minimal medium
GPP	geranyl diphosphate
GTP	guanosine triphosphate
HC	hydroxyclavatul
HDA	hetero-Diels–Alder

ABBREVIATIONS

HE	heterologous expression
His ₆	Hexahistidine
HMBC	heteronuclear multiple bond correlation
HPLC	high performance liquid chromatography
<i>hph</i>	hygromycin B phosphotransferase gene
HRMS	high resolution mass spectrometry
HR-PKS	highly-reducing polyketide synthase
HSAF	dihydromaltophilin
HSQC	heteronuclear single quantum coherence
<i>Hz</i>	<i>hertz</i>
<i>i.e.</i>	id est
IEDDA	inverse electron-demand Diels-Alder
IMDA	intramolecular Diels-Alder reaction
IPP	isopentenyl diphosphate
<i>J</i>	coupling constant
JGI	Joint Genome Institute
kbp	kilo base pairs
<i>k_{cat}</i>	turnover number
kDa	kilodaltons
<i>K_M</i>	Michaelis-Menten constant
KR domain	β-ketoreductase domain
KS domain	β-ketoacyl synthase domain
LC-MS	liquid chromatography–mass spectrometry
m	multiplet
<i>m/z</i>	mass-to-charge ratio
mAU	milliabsorbance unit
Mb	mega base pairs
MEP	methylethritol phosphate
MHz	mega hertz
mRNA	messenger ribonucleic acid
MeT domain	methyltransferase domain
MeOH	methanol

ABBREVIATIONS

MS	mass spectroscopy
multi	multiplicity
MVA	mevalonic acid
NADH	nicotinamide adenine dinucleotide
NADPH	nicotinamide adenine dinucleotide phosphate
<i>N. fischeri</i>	<i>Neosartorya fischeri</i>
NMR	nuclear magnetic resonance
NP	natural product
NR-PKS	non-reducing polyketide synthase
nonheme Fe ^{II} /2-OG	nonheme Fe ^{II} /2-oxoglutarate
NRPS	nonribosomal peptide synthetase
<i>o</i> -QM	<i>ortho</i> -quinone methide
P450	cytochrome P450
<i>P. crustosum</i>	<i>Penicillium crustosum</i>
<i>P. citrinum</i>	<i>Penicillium citrinum</i>
<i>P. patulum</i>	<i>Penicillium patulum</i>
<i>P. griseofulvum</i>	<i>Penicillium griseofulvum</i>
<i>P. rubens</i>	<i>Penicillium rubens</i>
<i>P. verruculosum</i>	<i>Penicillium verruculosum</i>
PCP domain	peptidyl carrier protein domain
PCR	polymerase chain reaction
PD	potato dextrose
PDB	potato dextrose broth
PEG	polyethylene glycol
PFAM	protein family (database)
PKS	polyketide synthase
PKS-NRPS	polyketide synthase-nonribosomal peptide synthetase
PPi	inorganic pyrophosphate
ppm	parts per million
PR-PKS	partially-reducing polyketide synthase
PT	prenyltransferase
PT domain	product template domain

ABBREVIATIONS

q	quartet
R domain	reductase domain
RNA	ribonucleic acid
rpm	revolutions per minute
s	singlet
<i>S. cerevisiae</i>	<i>Saccharomyces cerevisiae</i>
<i>S. leeuwenhoekii</i>	<i>Streptomyces leeuwenhoekii</i>
SAT domain	starter unit acyltransferase domain
SDS-PAGE	sodium dodecyl sulfate polyacrylamide gel electrophoresis
SM	secondary metabolite
SMARTS	SMILES arbitrary target specification
SMILES	simplified molecular input line entry system
SMIRKS	a hybrid language of SMILES and SMARTS
t	triplet
tra	<u>ter</u> restric <u>a</u> cid
T domain	thiolation domain
TB	terrific broth
td	triple doublet
TE domain	thioesterase domain
Tris	tris(hydroxymethyl)aminomethane
UTR	untranslated region
UV	ultraviolet
v/v	volume per volume
w/v	weight per volume
WT	wild type
α -KG	α -ketoglutarate
δ_C	chemical shift of ^{13}C
δ_H	chemical shift of ^1H
6-DEB	6-deoxyerythronolide B
6-MSA	6-methylsalicylic acid

Summary

Secondary metabolites originated from plants, bacteria and fungi constitute a large group of compounds, which are not essential for the growth, development and reproduction of the organism, but necessary for protection, competition and species interactions. Microbes, e.g. fungi and bacteria, have been more important sources of natural products since the discovery of penicillin in 1928. With advanced isolation and characterization techniques for secondary metabolites from crude biological samples, diverse compounds from different groups including polyketides, nonribosomal peptides, alkaloids and terpenes have been identified. Producing organisms utilize a limited set of primary metabolic building blocks to produce different natural product skeletons, which are further modified by a number of tailoring enzymes to form a variety of end products. For example, a core structure of polyketide can be derived from acyl-CoAs by polyketide synthase(s) (PKS(s)) and catalyzed by a series of tailoring enzymes such as nonheme Fe^{II}/2-OG-dependent oxygenases, flavin-containing oxidoreductases, cytochrome P450s and prenyltransferases to create an amazing diversity of natural product architectures. To facilitate the biosynthetic mechanism, advanced bioinformatics, biological technologies and biochemical tools have been utilized to investigate the coding genes of these enzymes, which are usually located together as a biosynthetic gene cluster (BGC). However, post-biosynthetic non-enzymatic events can also be involved in natural product formation.

In this thesis, biosynthesis of secondary metabolites from a fungal strain, *Penicillium crustosum* PRB-2, was investigated in cooperation with Ge Liao. Penilactones A, B and D, as well as peniphenone D, structurally comprising clavatul and γ -butyrolactone moieties, were identified from the wild type. Two separate gene clusters were functionally characterized as building blocks of the complex penilactone and peniphenone structures by gene disruption in the native PRB-2 strain, heterologous expression in *Aspergillus nidulans* and precursor feeding experiment in the available deletion mutants. A non-reducing (NR) PKS ClaF from the clavatul cluster is responsible for the formation of clavatul. A hybrid PKS-NRPS TraA from the terrestric acid cluster is involved in the biosynthesis of crustosic acid and terrestric acid, which undergo C-C bond cleavage to give γ -butyrolactone moieties in penilactones and peniphenones. Oxidation of clavatul to hydroxyclavatul by a nonheme Fe^{II}/2-OG-dependent oxygenase ClaD and its spontaneous dehydration to an intermediate *ortho*-quinone methide initiate the non-enzymatic 1,4-Michael additions with γ -butyrolactones. Therefore, the cross-coupling of two moieties from two separate gene clusters leads to the formation of peniphenone D and penilactone D, which undergo a second Michael addition with *ortho*-quinone methide to give penilactones A and B. Our findings represent rare examples of complex structures derived from two separate clusters and formed through enzymatic and non-enzymatic approaches.

Afterwards, the investigation on terrestric acid formation was extended by using similar strategies. The hybrid PKS-NRPS TraA and the enoyl reductase TraG were demonstrated to be responsible for

SUMMARY

the accumulation of the tetronate core structure carboxylcrustic acid and viridicatic acid as precursors of crustosic acid in PRB-2. Biochemical characterizations proved that the conversion of crustosic acid to terrestric acid was achieved via oxidative decarboxylation catalyzed by a nonheme Fe^{II}/2-OG-dependent oxygenase TraH and subsequent stereospecific C-C double bond reduction by a flavin-containing oxidoreductase TraD. Among the two-step oxidative decarboxylation and stereospecific reduction, the mechanism with Fe^{IV}=O species as important intermediates was postulated for TraH-catalyzed olefination with or without CO₂ elimination. Results on the biosynthesis of terrestric acid also provide a valid experimental basis for understanding the formation of the fungal acyltetronates with different stereochemistry involving sequential redox-assisted decarboxylation and stereoisomerization.

In addition to penilactones and peniphenones, there are more clavatul-containing natural products from fungi. We wondered that these compounds are very likely synthesized from different precursors by nucleophilic attacking *ortho*-quinone methide derived from hydroxycavatul. This hypothesis triggered our interest to screen the reactivity of *ortho*-quinone methide with diverse natural products or natural product-like compounds. Coincubation of 102 selected reactants with hydroxycavatul under mild conditions (in nearly pH neutral aqueous solution) led to the detection of clavatul coupling products in 86 cases. As a result, 32 new clavatul-containing compounds were identified after isolation and structural elucidation. The conjugation between clavatul and the nucleophiles occurs mainly with the C-C bond formation at *para*- or *ortho*-positions of hydroxyl/amino group at the benzene ring and C-2 position of the indole skeleton. This study confirmed the activity of the *ortho*-quinone methide which is spontaneously derived from hydroxycavatul in an aqueous system and increased significantly the diversity of clavatul-containing products in nature.

Zusammenfassung

Die von Pflanzen, Bakterien und Pilzen stammenden Sekundärmetabolite bilden eine große Gruppe von Verbindungen, die nicht direkt mit dem Wachstum, der Entwicklung und der Vermehrung des Organismus zusammenhängen. Seit der Entdeckung des Penicillins im Jahr 1928 sind Mikroben, v.a. Pilze und Bakterien, wichtige Quellen für Naturstoffe. Durch verbesserte Isolierungs- und Charakterisierungsmethoden konnten diverse Sekundärmetabolite verschiedener Gruppen, wie z. B. Polyketide, nicht-ribosomale Polypeptide, Alkaloide und Terpene aus biologischen Proben identifiziert werden. Die Produzenten verwenden eine begrenzte Anzahl von Bausteinen aus dem Primärstoffwechsel, um verschiedene Naturstoffgerüste zu konstruieren. Diese können durch weitere Enzyme modifiziert werden, um eine Vielzahl von Endprodukten herzustellen. Eine Polyketid-Kernstruktur, die durch eine oder mehrere Polyketidsynthasen (PKSs) aus Acyl-CoAs zusammengebaut wird, kann durch eine Reihe von Enzymen, wie z.B. nonheme-Fe^{II}/2-OG-abhängige Oxygenasen, flavin-haltige Oxidoreduktasen, Cytochrom P450s und Prenyltransferasen modifiziert werden, so dass eine erstaunliche Vielfalt von Naturstoffen erzielt wird. Um die Biosynthese von Naturstoffen aufzuklären werden verschiedene Methoden, wie z.B. die Bioinformatik oder molekularbiologische und biochemische Verfahren angewandt. Somit können Funktionen der kodierenden Gene, die sich normalerweise zusammen in einem biosynthetischen Gencluster (BGC) befinden, genau untersucht werden. Dennoch können auch nicht-enzymatische Reaktionen nach der Biosynthese an der Naturstoffentstehung beteiligt sein.

In dieser Arbeit wurde die Sekundärmetabolit-Biosynthese in einem Pilzstamm, *Penicillium crustosum* PRB-2, in Zusammenarbeit mit Ge Liao untersucht. Penilactone A, B und D sowie Peniphenon D, die strukturell Clavatol- und γ -Butyrolacton-Einheiten enthalten, wurden in dem Wildtyp identifiziert. Zwei unterschiedliche DNA-Abschnitte wurden durch Geninaktivierung in dem PRB-2-Stamm, heterologe Expression in *Aspergillus nidulans* und Fütterungsexperimente in den Deletionsmutanten als verantwortliche Gencluster für die Produktion von Penilactone und Peniphenone identifiziert. Die nicht-reduzierende (NR) PKS ClaF aus dem Clavatol-Cluster ist für die Bildung von Clavatol verantwortlich. Die hybride PKS-NRPS TraA aus dem Terrestric acid-Cluster ist an der Biosynthese von Crustosic acid und Terrestric acid beteiligt, indem eine Spaltung der C-C-Bindung unter Bildung von γ -Butyrolactonen stattfindet. Die Oxidation von Clavatol zu Hydroxyclavatol durch die nonheme-Fe^{II}/2-OG-abhängige Oxygenase ClaD und dessen spontane Dehydratisierung zu einem Orthochinon-methid-Intermediat initiieren eine nicht enzymatische 1,4-Michael-Addition zu γ -Butyrolacton. Die Kreuzkupplung dieser zwei Einheiten aus zwei getrennten Genclustern führt zur Bildung von Peniphenon D und Penilacton D, die eine zweite Michael-Addition mit Orthochinonmethid zur Bildung von Penilacton A und B eingehen.

Die verwendeten Strategien wurden anschließend mit detaillierten Untersuchungen zur Biosynthese von Terrestric acid erweitert. Es wurde gezeigt, dass die hybride PKS-NRPS TraA und die

ZUSAMMENFASSUNG

Enoylreduktase TraG für die Entstehung der Carboxycrustic acid und Viridicatic acid mit der Tetronat-Grundstruktur als Vorläufer von Crustosic acid in *Penicillium Crustosum* PRB-2 verantwortlich sind. Biochemische Charakterisierungen haben gezeigt, dass die Umwandlung von Crustosic acid in Terrestric acid durch eine oxidative Decarboxylierung von der nonheme-Fe^{II}/2-O₂-abhängigen Oxygenase TraH und die anschließende stereospezifische C-C-Doppelbindungsreduktion von der Flavin-haltigen Oxidoreduktase TraD erfolgte. Ein Reaktionsmechanismus mit Fe^{IV}=O-Intermediaten wurde für die TraH-katalysierte Olefinierung mit oder ohne CO₂-Eliminierung postuliert. Unsere Ergebnisse zeigen, dass komplexe Strukturen von Genen aus zwei getrennten Clustern hergestellt und enzymatische und nicht-enzymatische Reaktionen involviert werden können. Die Ergebnisse zur Biosynthese von Terrestric acid liefern auch eine solide experimentelle Grundlage für die Entstehung pilzlicher Acyltetrone mit unterschiedlicher Stereochemie.

Neben Penilatonen und Peniphenonen sind weitere clavatul-haltige Naturstoffe bekannt. Wir vermuten, dass diese Verbindungen höchstwahrscheinlich auch durch den nucleophilen Angriff von aus Hydroxylavatul stammendem Orthochinonmethid synthetisiert werden. Diese Hypothese hat unser Interesse geweckt, die Reaktivität von Orthochinonmethid mit verschiedenen Naturstoffen zu untersuchen. Von 102 getesteten Substanzen führte die Coinkubation mit Hydroxylavatul unter milden Bedingungen in 86 Fällen zu nachweisbaren Clavatul-Kupplungsprodukten. Nach Isolierung und Strukturaufklärung wurden 32 neue clavatul-haltige Verbindungen identifiziert. Die Konjugationen zwischen Clavatul und den Nucleophilen erfolgt hauptsächlich mit Bildung einer C-C-Bindung an den *para*- oder *ortho*-Positionen der Hydroxyl-/Aminogruppe am Benzolring sowie der C2-Position des Indolrings. Diese Studie bestätigte die Reaktivität des aus Hydroxylavatul spontan entstandenen Orthochinonmethids in einem wässrigen System und erhöhte die Vielfalt der clavatul-haltigen Produkte in Natur.

1 Introduction

1.1 Ascomycota: rich source of diverse natural products

Ascomycota, comprising more than 33,000 named and a vast number of undescribed species, is the largest phylum of the fungal kingdom.^{1,2} Its members are commonly known as the sac fungi or ascomycetes. Many species are known as asexual fungi, called anamorphs, which produce asexual spores (conidia) on stalks.³ Correspondingly, their sexual phases, called teleomorphs, produce fruiting bodies for ascospore formation. The phylum of Ascomycota can be subdivided into three subphyla, the Pezizomycotina, the Saccharomycotina and the Taphrinomycotina.⁴ Ten or more classes are designated within the Pezizomycotina. This subphylum includes saprotrophs that grow on woody and non-woody plant tissues, as well as on herbivore dung, parasites of plants and animals (particularly invertebrates), and partners in lichen and mycorrhizal symbioses. In order to survive and reproduce, they compete with other organisms and have developed a number of strategies for protection and communication, one of which is the production of a variety of secondary metabolites (SMs), also known as natural products (NPs).⁵

So far, most of the described SMs are produced by ascomycetes in the asexual stage, especially *Aspergillus* and *Penicillium* as typical members of Pezizomycotina grown as filamentous fungi.⁶ Their conidial phases are crucial in biotechnological applications including fermentation, food, enzyme and antibiotic production. Structurally, SMs produced by Ascomycota mainly belong to polyketides,⁷ nonribosomal peptides,⁸ terpenes,⁹ alkaloids¹⁰ and even hybrid products like hybrid polyketide-nonribosomal peptides¹¹ (**Figure 1**). These chemical classes are defined by the type of starter substrates from the primary metabolism incorporated into their core structures by specialized backbone enzymes, *i.e.* polyketide synthases (PKSs), nonribosomal peptide synthetases (NRPSs), terpene cyclases (TCs) and hybrid polyketide synthase-nonribosomal peptide synthetases (hybrid PKS-NRPSs).

Correspondingly, primary metabolites are the molecules that influence the pathways essential for life, generation and storage of energy. Polyketides are generally derived from their central metabolic pathways and primary metabolite pools with acyl-CoAs as critical initial building blocks (**Figure 1**).¹² With an increasing number of acyl-CoAs as starter units or extender units identified and elucidated for their novel mechanisms, structural diversity of polyketide scaffolds have been represented.¹³ Examples are acetyl-CoA, propionyl-CoA, malonyl-CoA, benzoyl-CoA and 4-coumaroyl-CoA as starter units, and malonyl-CoA, methylmalonyl-CoA, ethylmalonyl-CoA and chloroethylmalonyl-CoA as extender units.¹⁴ 6-methylsalicylic acid (6-MSA) is a well-characterized fungal aromatic polyketide identified from *Penicillium patulum* Bainier (anamorph *P. griseofulvum* Dierckx).¹⁵ A natural polyketide citrinin, first isolated from *Penicillium citrinum*, was also further identified from other *Penicillium* species, *Monascus* species and *Aspergillus* species.^{16,17} Other prominent

INTRODUCTION

representatives of the pathology related polyketides are aflatoxin B₁¹⁸⁻²⁰ from *Aspergillus flavus* and *Aspergillus parasiticus* with highly hepatotoxic activity and lovastatin from *Aspergillus terreus* as a cholesterol-lowering drug (**Figure 1**).²¹ In addition, acetyl-CoA is also a building block for the biosynthesis of dimethylallyl and isopentenyl diphosphates (DMAPP and IPP) as fundamental metabolic precursors of terpenes and steroids, such as aristolochene and gibberellin A3 (**Figure 1**) via the mevalonic acid (MVA) pathway.²²⁻²⁶ This subgroup of compounds comprise about 60 % of known NPs.²⁷ An alternative pathway for terpene biosynthesis was derived from pyruvate and glycerol aldehyde-3 phosphate to construct the C₅ skeleton for isoprenoid biosynthesis.²⁸

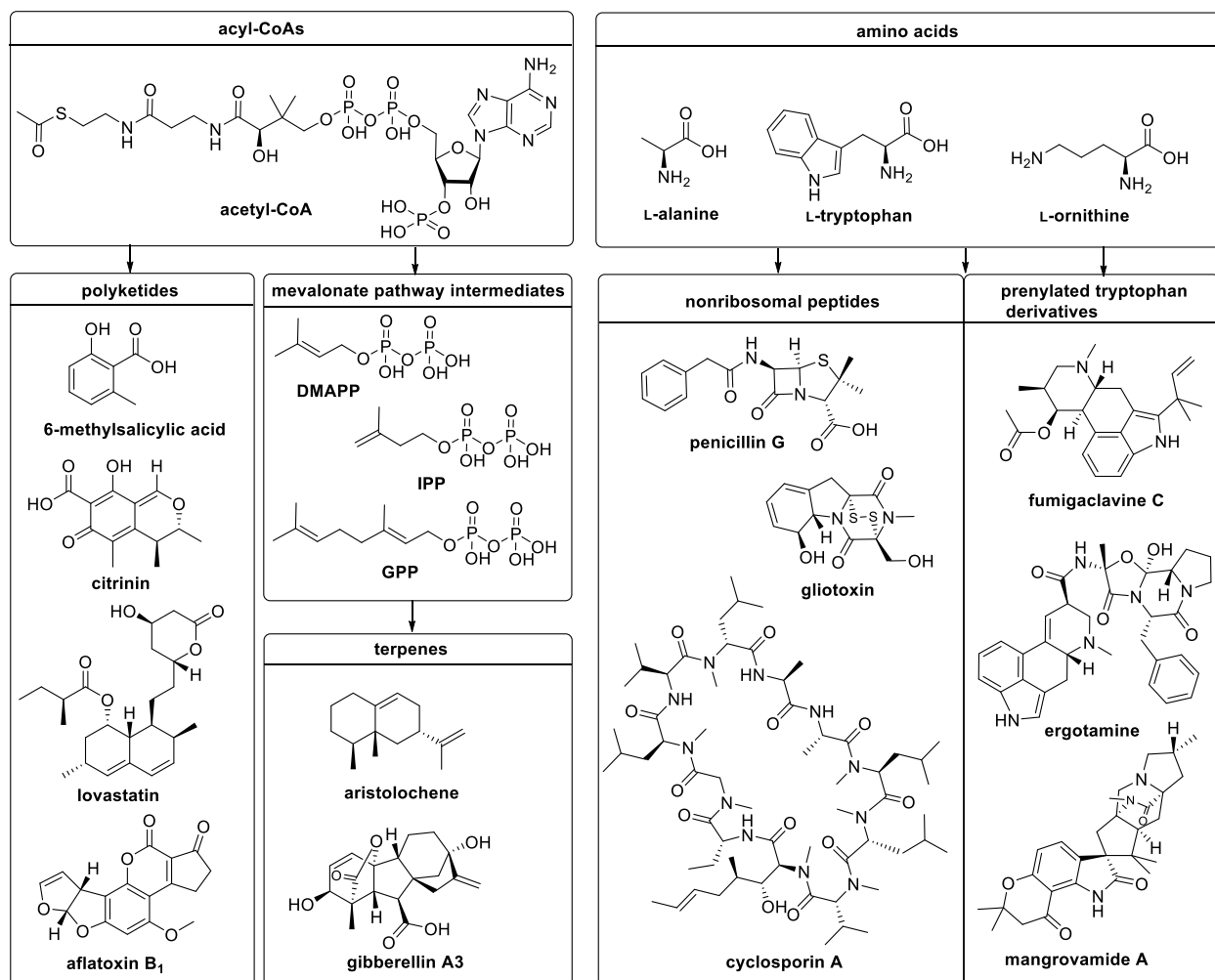


Figure 1. Diverse natural products identified in microorganisms

On the other hand, both proteinogenic and non-proteinogenic amino acids are used as building blocks for complex structures of peptides and amino acid-derived compounds (**Figure 1**). Nonribosomal peptides are mainly found in microorganisms with 2-48 amino acid residues in length.²⁹ The well-known representative is the antibiotic penicillin G produced by *Penicillium rubens* (formerly known as *Penicillium chrysogenum*).³⁰⁻³⁵ Gliotoxin, belonging to epipolythiodioxopiperazine

class of toxins, is synthesized by NRPS and has various biological activities.³⁶ Cyclosporin A is a cyclic undecapeptide with a variety of biological activities including immunosuppressive, anti-inflammatory, antifungal and antiparasitic activities.³⁷ Alkaloids also utilize primary proteinogenic amino acids as metabolic building blocks, e.g. fumigaclavine C derived from L-tryptophan (L-Trp) and ergotamine derived from L-Trp, L-alanine (L-Ala), L-phenylalanine (L-Phe), as well as L-proline (L-Pro).^{38,39} In addition, the non-proteinogenic amino acid L-ornithine was also proposed to be involved in the formation of mangrovamide A from *Penicillium* sp. (**Figure 1**).⁴⁰

Overall, a wide variety of NPs, which became therapeutic agents or inspired design of structural mimics, have attracted attention of researchers over the past 150-200 years on the basis of their diverse biologic activities, although 50 % of them have no synthetic counterparts yet. Tools with advanced version for metabolome analysis, such as mass spectroscopy (MS), single crystal X-ray diffraction, and nuclear magnetic resonance (NMR) spectrometry with increasingly sophisticated methods of chromatography, have made possible continuing discovery of more fungal metabolites and novel drugs.

1.2 Biosynthesis of fungal natural products

In the past decades, the development of genome, transcriptome, proteome, and metabolome analyses help researchers to better understand fungal biology, especially to exploit genes involved in the biosynthetic pathway of SMs. The genes required for modification of the chemical scaffold, transport of substrates and products, as well as specific regulatory genes are usually contiguously aligned in the genome leading to the concept of secondary metabolite biosynthetic gene clusters (BGCs).^{41,42} Diverse backbone enzymes, for instance, PKSs, NRPSs and TCs, are responsible for the core structures of SMs in fungi. The carbon skeletons are further modified by various tailoring enzymes, including oxidoreductases and transferases, which are encoded by genes located in BGCs. For example, the first fungal gene cluster identified was the penicillin cluster in *Penicillium rubens* and *Aspergillus nidulans* containing a NRPS (PcbAB) and two tailoring enzymes (PcbC and PenDE).³¹⁻³³

To identify BGCs and their products in fungi, the prerequisite is the cultivability of the targeted microorganisms to produce compounds of interest under laboratory conditions. The culture conditions, including nutrient source, redox status, pH, light, and temperature, can mimic the original natural environment to form SMs and even impact the metabolome significantly. Representatives are the pH-dependent expression of penicillin gene clusters and nitrogen-dependent expression of gibberellin gene cluster.^{22,34,35} Further genetic manipulation, such as replacement of the gene of interest with a hygromycin resistance cassette (*hph*) in the wild type strain enables the identification of more SMs, especially biosynthetic precursors (**Table 1, Figure 2**). Microbial cocultivation of two or more microorganisms in the same confined environment is another strategy for the expression of other cryptic genes, leading to the production of new microbial SMs (**Table 1**). It can be considered

INTRODUCTION

as an experimental imitation of the competition within natural microbe communities via signaling molecules and metabolic precursors produced by either one or both cultivated species. This approach has been utilized in the cocultivation of fungus with fungus or bacteria to produce luteoride D, pseurotin G, and subenniatins A and B (Table 1).^{43,44}

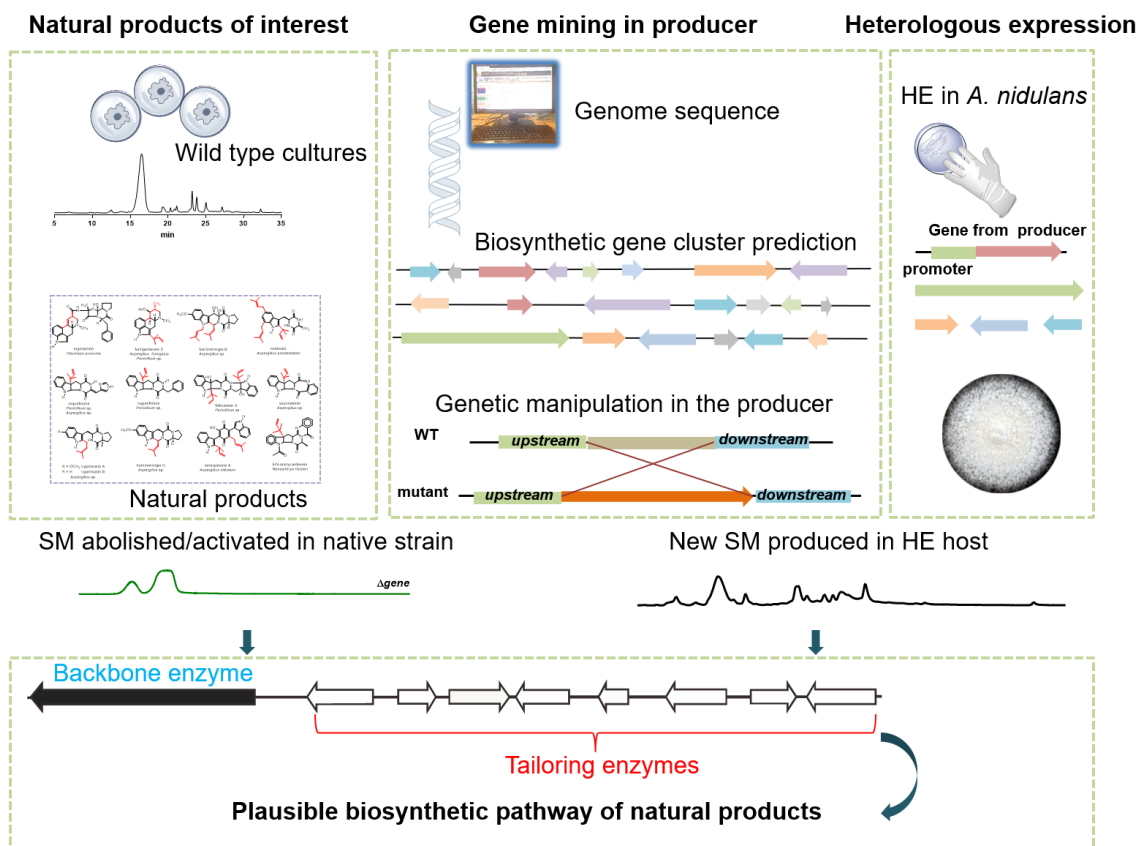


Figure 2. The strategy for the biosynthetic pathway identification of fungal secondary metabolites

Table 1. Methods used to identify secondary metabolite clusters and their products in fungi

metabolite	organism	references
conditional culture		
nidulanin A	<i>A. nidulans</i>	45
lovastatin	<i>A. terreus</i> , <i>P. citrinum</i>	46
penicillin/cephalosporin	<i>P. rubens</i> , <i>A. nidulans</i>	34,35
gibberellin	<i>F. fujikuroi</i>	22
bikaverin	<i>F. fujikuroi</i>	47
pleuromutilin	<i>Clitopilus passeckerianus</i>	48
co-cultivation		
luteoride D	<i>A. fumigatus</i> and <i>S. leeuwenhoekii</i>	43
pseurotin G	<i>A. fumigatus</i> and <i>S. leeuwenhoekii</i>	43
subenniatins A and B	<i>F. tricinctum</i> and <i>F. begoniae</i>	44
cluster-specific activation		
agglomerin F	<i>A. niger</i>	49

INTRODUCTION

monodictyphenone	<i>A. nidulans</i>		50
fumicyclines A and B	<i>A. fumigatus</i>		51
fusarielins F, G and H	<i>F. graminearum</i>		52
neosartoricin	<i>N. fischeri</i>		53
global regulator activation			
hexadehydroastechrome	<i>A. fumigatus</i>		54
endocrocin	<i>A. fumigatus</i>		55
tyrosine-derived alkaloids	<i>A. flavus</i>		56
terrequinone A	<i>A. nidulans</i>		57
ML-236B	<i>P. citrinum</i>		58
epigenetic modification			
meromusides A-H	<i>Metarhizium robertsii</i>		59
meromutides A and B	<i>Metarhizium robertsii</i>		59
asperthecin	<i>A. nidulans</i>		60
chladochromes F and G	<i>Cladosporium cladosporioides</i>		61
pestaloficins A-E	<i>Pestalotiopsis fici</i>		62
heterologous expression			
	donor organism	heterologous host	
asperfuranone	<i>A. terreus</i>	<i>A. nidulans</i>	63
leporin B	<i>A. flavus</i>	<i>A. nidulans</i>	64
citrinin	<i>Monascus purpureus</i> , <i>Monascus ruber</i>	<i>A. oryzae</i>	17,65
chrodrimanin B	<i>P. verruculosum</i>	<i>A. oryzae</i>	66
15 compounds	7 different strains from <i>Aspergillus</i> , <i>Trichoderma</i> , <i>Hypomyces</i> etc.	<i>S. cerevisiae</i>	67

Although both strategies mentioned above are easy and efficient to exploit metabolites, a vast number of BGCs have not been correctly assigned to their relative metabolites. One notable reason is that most BGCs are silent or only low expressed under laboratory cultivation. To activate these BGCs, genome mining strategies, including transcriptional regulator exploitation and heterologous expression (HE), have been developed for novel metabolite discovery and their biosynthetic analysis (**Figure 2**).^{12,68,69} About 50 % of fungal BGCs contain a putative cluster-specific regulator gene, which impacts the transcription of single BGC in quite a direct pattern. To date, several novel metabolites and their biosynthetic pathways have been identified by deletion or overexpression of cluster-specific regulators (**Table 1**). Zn(II)₂Cys₆ proteins and Cys₂His₂ zinc-finger proteins, for instance, AflR⁷⁰ identified in *Aspergillus nidulans* and TRI6 as well as TRI10⁷¹ identified in *Fusarium graminearum*, are common types of cluster-specific regulators. Agglomerin F, as a fungal acyltetronate, was identified in *Aspergillus niger* together with its precursor carlosic acid by a regulator overexpression.⁴⁹ On the other hand, global regulators represent another higher level of regulatory modulation of secondary metabolism. The discovery of the complex proteins LaeA with VeA as well as VelB first identified in *Aspergillus nidulans* explained the connection of fungal development to secondary metabolism.^{72,73} Subsequent identification of LaeB,⁷⁴ McrA,⁷⁵ and other regulators led to more novel secondary metabolism by up-regulating or down-regulating gene clusters (**Table 1**). Moreover, deletion of epigenetic factors such as histone acetyltransferase Hat1 from *Metarhizium robertsii* resulted in characterizations of 10 new polyketides, meromusides A-H, as well as meromutides A and B (**Table 1**).⁵⁹ Due to the limitation of laboratory cultivation and

genetically manipulation in native strain, heterologous expression in other microorganisms is another approach to survey cryptic fungal BGCs. In addition to *Escherichia coli*, fungi including *Saccharomyces cerevisiae*, *Aspergillus nidulans* and *Aspergillus oryzae* have been engineered to be synthetic biology tools to assemble and express synthetic DNAs (**Table 1, Figure 2**).^{17,63-67} More exploitation is in progress on other potential organisms, such as *Penicillium crustosum*.⁷⁶ Taken together, with the improvement of genome sequencing, particularly the third-generation sequencing, cooperation of different strategies has been developed to investigate the biosynthesis of fungal natural products (**Figure 2**). In the near future, more and more compounds with bioactivities, as well as their biosynthetic pathways, would be found and proved, which will provide new candidates for drug-development.

1.2.1 Polyketide synthase

Polyketide natural products are a remarkable class of compounds with complex structure diversity and medicinally important activities. Five structurally distinct subclasses of polyketides have been described, *i.e.* polycyclic aromatic polyketides, macrolactones, decalin-containing scaffolds, polyenes, and polyethers. All of them are built with equivalent logic, which borrows the chemical and protein precepts from fatty acid biosynthesis.⁷⁷ A polyketide synthase (PKS) consists of acyltransferase (AT), β -ketoacyl synthase (KS), as well as acyl carrier protein (ACP) as basic domains, and β -ketoacyl reductase (KR), dehydratase (DH), enoyl reductase (ER), methyltransferase (MeT), thioesterase (TE), as well as product template (PT) as accessory domains for the architecture of polyketide products. Generally, PKSs are classified into three distinct types depending upon their product structures and biochemistry (**Figure 3**). Type I PKSs are multifunctional enzymes that are organized structurally into modules. The catalytic domains of type II PKSs required for polyketide chain assembly are encoded within discrete proteins that are used in an iterative manner such as the biosynthesis of oxytetracycline.^{78,79} Type III PKS exemplified by naringenin uses a single KS-like active site to catalyze the repetitive condensation of acetate units to a CoA-derived starter molecule, typically yielding mono- and bi-cyclic aromatic products.⁸⁰

In bacteria, type I PKS with best known modular system is exemplified by the PKS responsible for the 6-deoxyerythronolide B (6-DEB) scaffold of erythromycin A.⁸¹ In modular type I PKS, the AT domain is the “gatekeeper” of the module for an appropriate acyl-CoA starter unit selection and recognizes the specific extender unit to be incorporated into the growing polyketide chain. After tethering the extender unit onto the sulfhydryl group of the ACP domain, the KS domain catalyzes the decarboxylative Claisen condensation to extend the polyketide chain (**Figure 4A**).⁸²⁻⁸⁴ Finally, the TE domain located at the C-terminal of the assembly line leads to the release of polyketide product.

INTRODUCTION

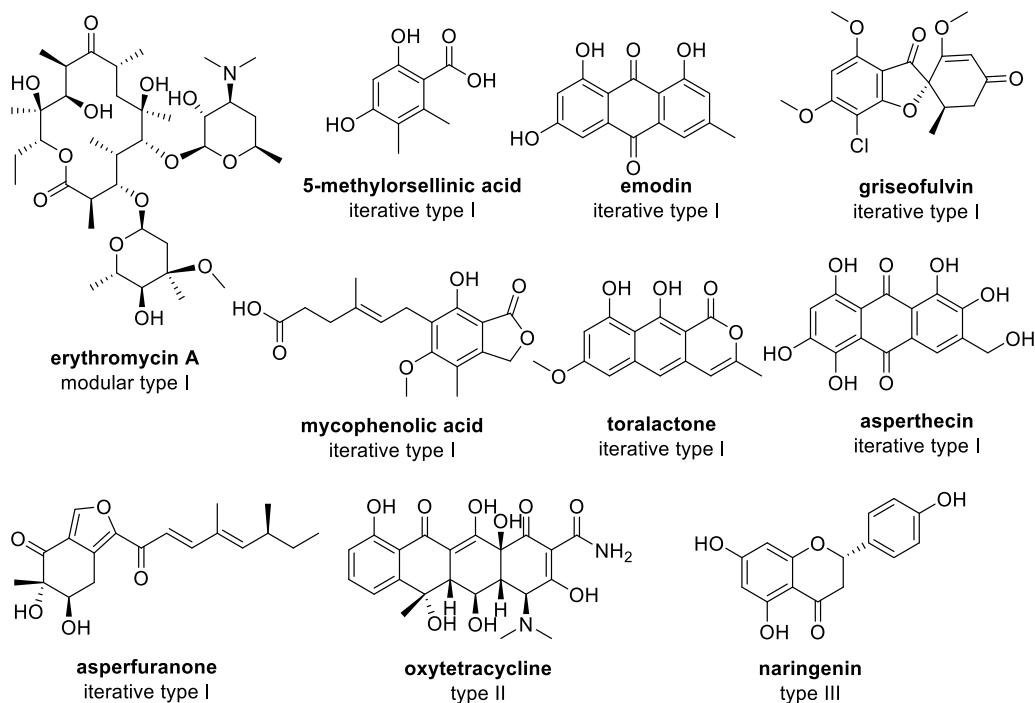


Figure 3. Polyketides derived from different types of PKS

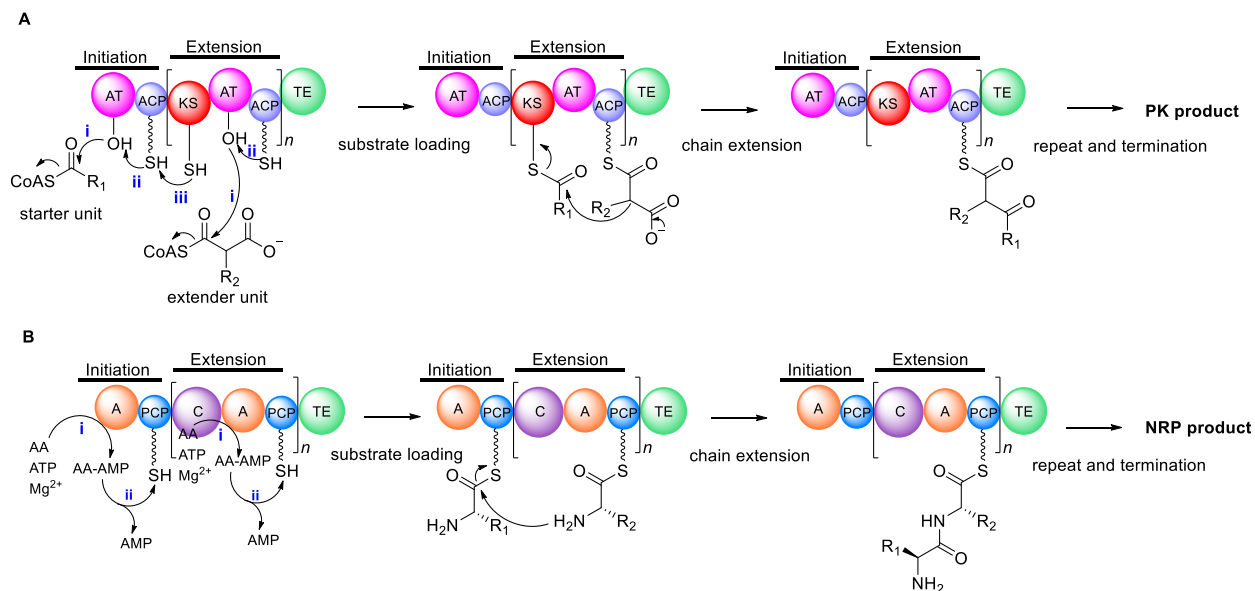


Figure 4. Biosynthetic cycles within modular type I PKS and NRPS

In comparison, iterative type I PKSs, commonly found in fungi, contain a single module that catalyzes polyketide chain elongation and modification iteratively to synthesize both aromatic and non-aromatic polyketides. They can be further divided into highly-reducing PKSs (HR-PKSs), partially-reducing PKSs (PR-PKSs), and non-reducing PKSs (NR-PKSs) depending on the presence or absence of reducing domains (**Figure 5**).

INTRODUCTION

HR-PKSs contain the full spectrum of possible reduction states in one molecule. In the case of lovastatin biosynthetic PKS LovB, the elongation intermediate was methylated by SAM-dependent MeT domain and subsequently reduced by the KR domain to form a hydroxyl group. Further reduction steps are achieved by DH domain and NADPH-dependent *trans*-ER domain consequently leading to a fully saturated product (**Figure 5A**).⁸⁵⁻⁸⁷ In contrast, releasing products of PR-PKSs differ from the fully reduction mechanism due to the absence of ER domain, such as 6-methylsalicylic acid (6-MSA) as the PR-PKS MSAS product (**Figure 5B**).^{15,88}

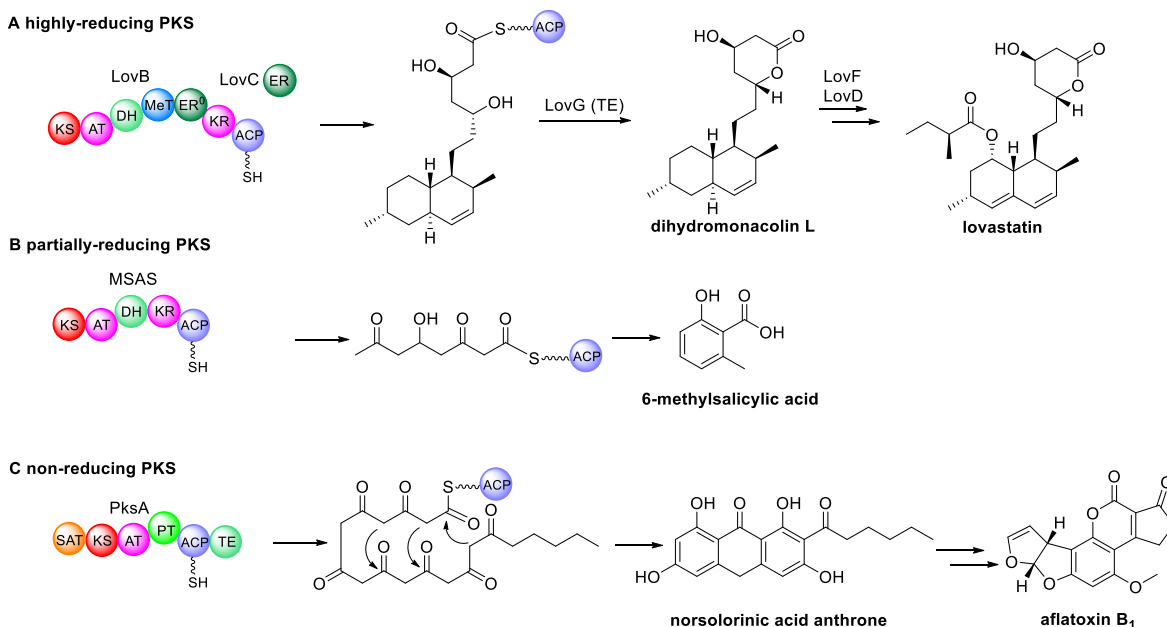


Figure 5. Representatives of HR-, PR-, and NR-PKS involved in the secondary metabolite biosynthesis

Unique to the NR-PKS family, the *N*-terminus is identified as a starter unit acyltransferase (SAT) domain, which accounts for the prime loading of polyketide extension and starter unit selection (**Figure 5C**).^{85,89} In most cases, the SAT domain is selective for acetyl-CoA, a fundamental metabolic building block.^{12,14} However, in the biosynthetic pathway of aflatoxin B₁, the SAT domain of PksA accepts a hexanoyl starter unit from a specialized fatty acid synthase subunits HexA/HexB and attached acetyl units onto either ACP domain or KS domain. Iterative rounds of decarboxylative Claisen condensation by KS domain are responsible for the linear poly- β -ketone intermediate formation. Afterward, the regiospecificity and timing of cyclization involve two successive aldol condensations by the PT domain, between C4-C9 and then C2-C11. The TE domain then mediates the C14-C1 thioclaisen-type of chain cyclization and release to yield norsolorinic acid anthrone (**Figures 5C and 6**).^{19,90} Instead, other cyclization patterns, including C2-C7 and C6-C11 aldol condensations, have been observed in the formation of aromatic polyketides.⁹¹⁻⁹³ The first ring of the naphthopyrone YWA1 is formed through the C2-C7 cyclization by the PT domain in the WA PKS

(**Figure 6**).^{94,95} C6-C11 first ring cyclization is involved in the biosynthesis of tricyclic fungal anthraquinones, such as endocrocin anthrone (**Figure 6**).^{96,97} In addition, several NR-PKSs, such as the well-studied 5-methylorsellinic acid synthase, also harbor a MeT domain catalyzing the methylation of the growing polyketide chain.⁹⁸

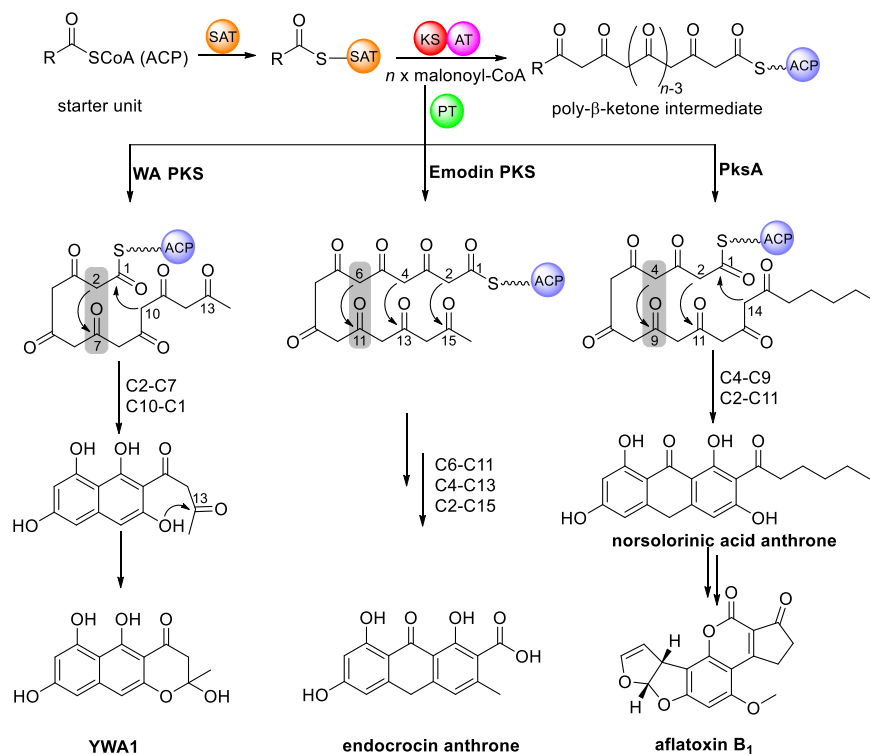


Figure 6. Three distinct regiospecificities for first ring formation by a protein template (PT) domain in fungal aromatic polyketides

With the help of advanced genetic, chemical and computational tools, structure insights into PKS architectures have been intensively studied to explain the complex diversity of polyketides in nature. Although recent progress has provided so many evidences for the formation of polyketides, there are still some questions remaining, for example, the complex interactions between the polyketide chain elongation and different domains as well as PKS docking-molecular dynamics.

1.2.2 Polyketide synthase-nonribosomal peptide synthetase

Given that polyketides built on assembly lines that tether elongating chains as phosphopantetheinyl-thioesters covalently attached to ACP domain, it is easy to understand that nonribosomal peptide synthetase (NRPS) assembly lines use a parallel chemical logic with amino acids as starters and peptidyl carrier protein (PCP) domain as covalent way station (**Figure 4B**).^{99,100} When a NRPS module is located upstream of a PKS module, the KS domain of PKS receives the aminoacyl group that is attached to the PCP domain followed by decarboxylative condensation with the malonyl-type

extender bound to ACP domain. As a result, a new C-C bond is formed as an aminoacyl-acyl hybrid chain (**Figure 7A**).¹⁰¹ Instead, when a PKS module is located upstream of a NRPS module, the condensation (C) domain of NRPS accommodates the acyl group, that is bound to the PKS ACP domain. Therefore, an acyl-aminoacyl hybrid chain is achieved by the N-C amide bond formation (**Figure 7B**).¹⁰¹ The molecules sometimes are on two distinct proteins within complex protein-protein interaction to guide the specific products. There are also single proteins with both PKS and NRPS domains, called hybrid polyketide synthase-nonribosomal peptide synthetase (hybrid PKS-NRPS) or hybrid NRPS-PKS.

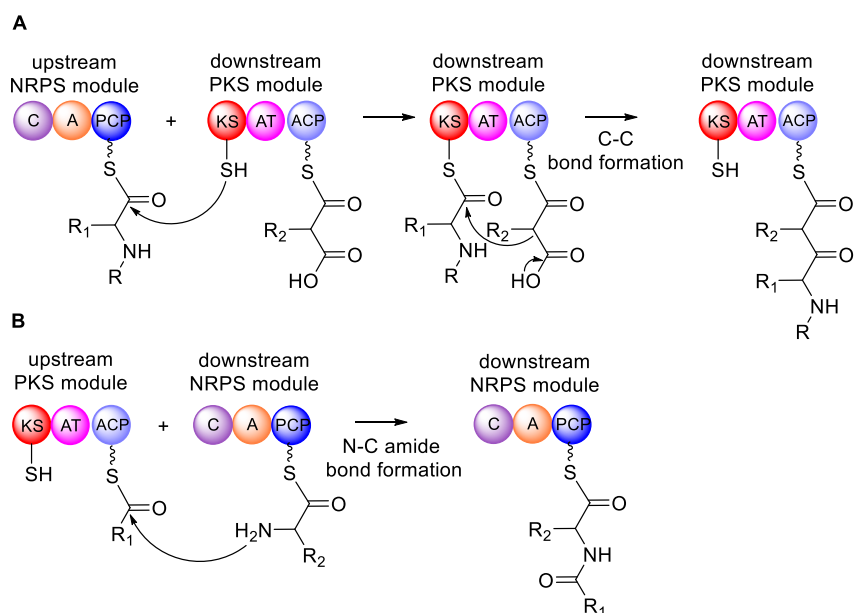


Figure 7. The mechanism of hybrid NRPS-PKS (A) and PKS-NRPS (B) module interfaces

Both hybrid PKS-NRPS and hybrid NRPS-PKS products are distributed in bacteria. In *Paenibacillus larvae*, a remarkably complex hybrid NRPS-PKS gene cluster (*pam*) was identified for the formation of the antibiotic paenilamicin B₁ (**Figure 8**).¹⁰² Multi-module systems of hybrid NRPS-PKS were also characterized in the althiomycin and didemnin B biosynthetic pathways.^{103,104} Polycyclic tetramate macrolactams, such as heat-stable antifungal factor dihydromaltophilin (HSAF) and frontalamdie A, are representative examples of bacterial hybrid PKS-NRPS products (**Figure 8**).^{11,105,106} In the case of HSAF, the PKS module is responsible for the biosynthesis of two different polyene hexaketide chains. Subsequently, the first polyene chain is transferred to the NRPS module and utilized for a condensation reaction with the δ -amino group of L-ornithine. Then the second polyene chain with β -keto group is condensed with the α -amino group of L-ornithine to result in the polyene-ornithine-polyene structure.

INTRODUCTION

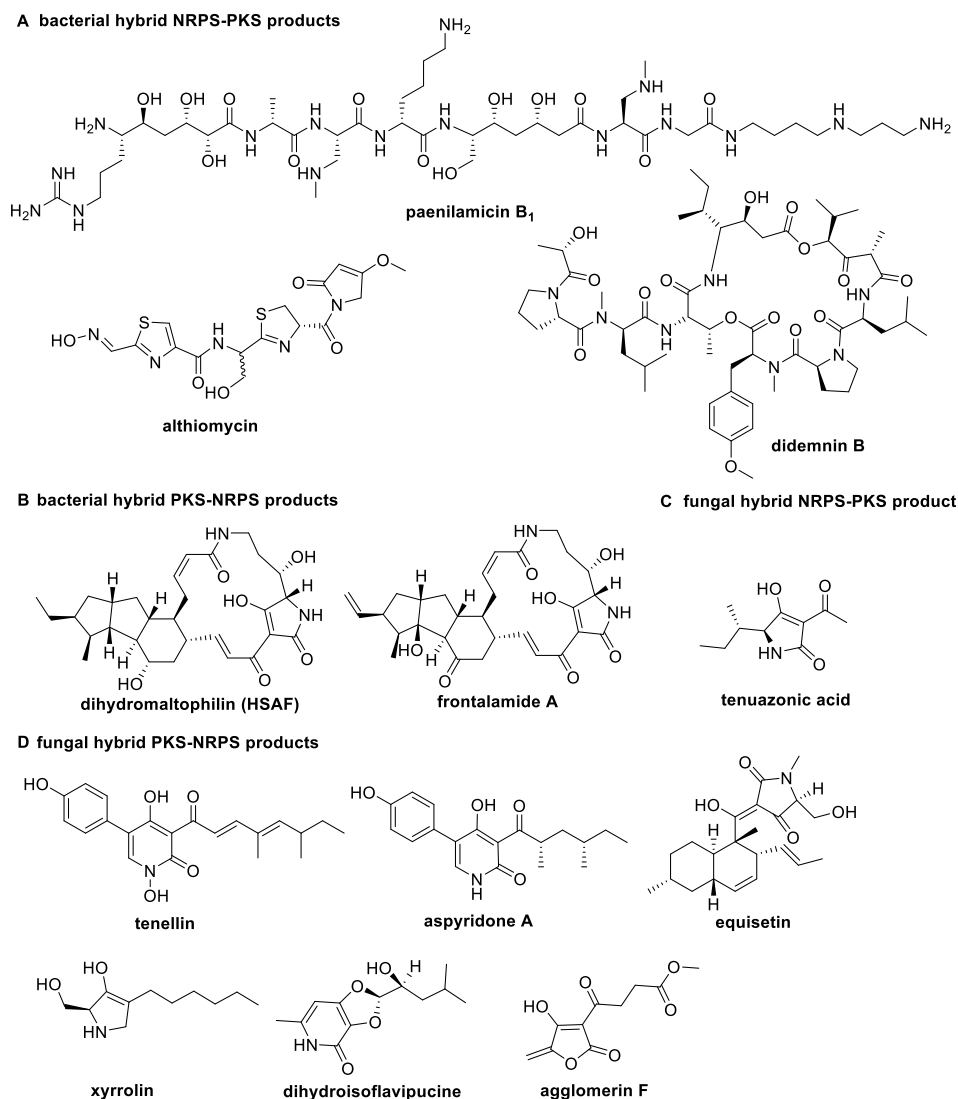


Figure 8. Natural products of hybrid PKS-NRPS or NRPS-PKS from microorganisms

In contrast, hybrid with *N*-terminal iterative PKS module tethered a *C*-terminal NRPS module is the popular architectural feature in fungi with an exception of tenuazonic acid. Tenellin,¹⁰⁷ aspyridone,^{108,109} equisetin,¹¹⁰ xyrrrolin,¹¹¹ and dihydroisoflavipucine¹¹² have been well studied involving iterative hybrid PKS-NRPS catalysis (**Figure 8**). All these enzymes contain an inactive enoyl reductase (ER) domain, *i.e.* ER⁰, and an extra *trans*-acting ER protein involved in the polyketide programming.^{11,113} For example, without coexpression of the ER gene *tenC*, heterologous expression of the hybrid PKS-NRPS *tenS* in *Aspergillus nidulans* led to the production of mis-programmed polyketides with low amount instead of pretenellin A (**Figure 9A**).¹¹⁴ Unlike the NRPS module of *TenS* accepting L-tyrosine, agglomerin F was proposed to involve L-malic acid activation by A domain of NRPS module. It is an exception for hybrid PKS-NRPS to accept an organic acid instead of proteinogenic or non-proteinogenic amino acids (**Figure 9B**).⁴⁹ More interestingly, TAS1,

INTRODUCTION

involved in tenuazonic acid biosynthesis, is a unique fungal hybrid NRPS-PKS enzyme that contains an NRPS module at its *N*-terminus (**Figure 9C**). The *C*-terminal PKS module contains only a KS domain, which is proposed to function in the cyclization and product release steps.¹¹⁵ With structural and biological approaches to understand the biosynthesis of hybrid polyketide-nonribosomal peptides, further studies on the connection and interaction within PKS and NRPS modules will provide a new approach to create novel and unusual compounds.

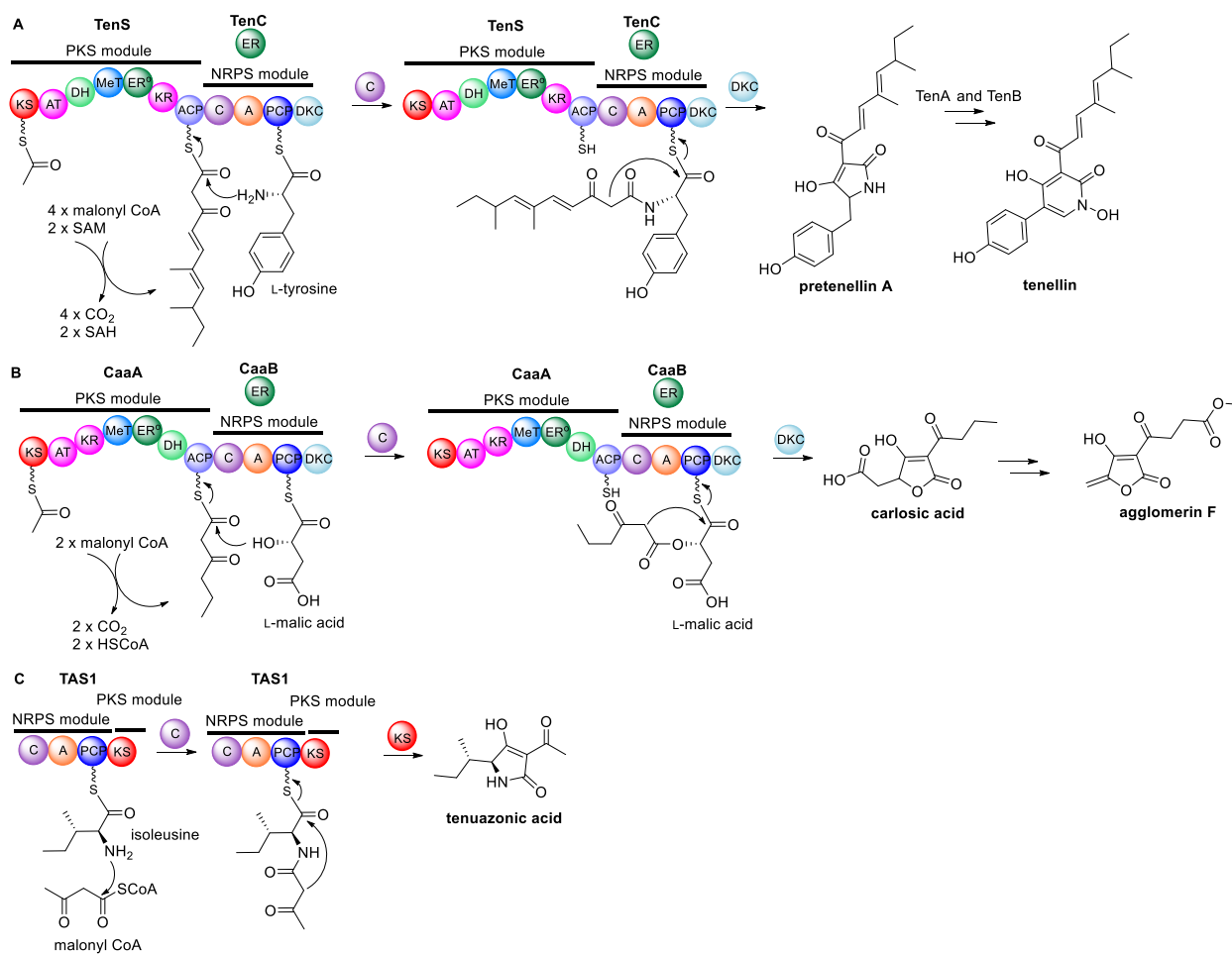


Figure 9. The mechanism of hybrid PKS-NRPS and NRPS-PKS reactions in fungi

1.3 Enzymatic oxidations and reductions in natural product biosynthesis

In the biosynthesis of natural products discussed before, the backbone enzymes are responsible for scaffold complexity of secondary metabolites. Further processing of the nascent scaffolds can occur in a set of post-assembly enzymatic tailoring steps, including acylations, glycosylations, methylations, prenylations, and redox reactions.¹¹⁶⁻¹¹⁸ Redox reactions involve electron transfers between two chemical species to trigger out reactions represented by hydroxylation, epoxidation, oxidation, desaturation and reduction. Enzymes being responsible for redox reactions show obligate

INTRODUCTION

requirements for either an organic coenzyme to act as an electron acceptor/donor or a redox-active transition metal to transmit electrons to another acceptor/donor (**Table 2**).¹¹⁹ For example, iron and copper between different redox states (Fe^{II} , Fe^{III} , and Fe^{IV} , Cu^{I} and Cu^{II}) can circulate by transferring one electron to O_2 to initiate radical reactions. Iron and heme-dependent cytochrome P450s form iron-porphyrin complexes to oxidize a vast multitude of different substrates using molecular oxygen.^{120,121} Nonheme Fe^{II} /2-oxoglutarate (Fe^{II} /2-OG)-dependent oxygenases require the extra Fe^{II} and α -ketoglutarate (α -KG) to fulfill multiple oxidative reactions.¹²²⁻¹²⁵

Table 2. Cofactors participating in enzymatic redox reactions

cofactors/prosthetic group (enzyme example)	reduced form \rightarrow oxidized form
nicotinamide adenine dinucleotides (NAD(P)H) (lactate dehydrogenase)	<p>NAD(P)H $\xrightarrow{2e^-}$ NAD(P)⁺</p> <p>R = </p>
biopterin (phenylalanine hydroxylase)	<p>5,6,7,8-tetrahydrobiopterin $\xrightarrow{2e^-}$ 7,8-dihydrobiopterin</p>
glutathione (glutathione peroxidase)	<p>2 x glutathione (GSH) $\xrightarrow{2e^-}$ glutathione disulfide (GSSG)</p>
lipoamide (dihydrolipoyl dehydrogenase)	<p>dihydrolipoate $\xrightarrow{2e^-}$ lipoate</p>
flavins (FAD and FMN) (succinate dehydrogenase)	<p>1,5-dihydroflavin FlH_2 $\xrightarrow{1e^-}$ flavin semiquinone FlH^\bullet $\xrightarrow{1e^-}$ oxidized flavin Fl_{ox}</p> <p>R = ribityl-P, FMN R = ribityl-ADP, FAD</p>
ascorbic acid (vitamin C) (nonheme Fe^{II} /2-OG-dependent oxygenase)	<p>ascorbic acid (reduced) $\xrightarrow{1e^-}$ ascorbate radical $\xrightarrow{1e^-}$ ascorbic acid (oxidized)</p>
iron / 2-oxoglutarate (nonheme Fe^{II} /2-OG-dependent oxygenase)	<p>Fe^{II} $\xrightarrow{2e^-}$ Fe^{IV}</p>
iron-sulfur clusters (Fe-S) _n (ferredoxins) n = 2 or 4	<p>enzyme-Fe^{II}-S-enzyme $\xrightarrow{1e^-}$ enzyme-Fe^{III}-S-enzyme</p> <p>(Fe-S)₂ cluster</p>

INTRODUCTION

heme (cytochrome oxidase)	
transition metal ions (laccase, catechol dioxygenase)	

Groups/atoms relevant to oxidation are marked in blue. NADP⁺ differs from NAD⁺ in having a phosphate group on OH marked in green (shown as (P)). Amino acid side chains, water, O₂, etc. provide the fifth and sixth ligands (X and Y) to heme iron.

1.3.1 Nonheme Fe^{II}/2-oxoglutarate-dependent oxygenases

Mononuclear nonheme Fe^{II}/2-oxoglutarate (Fe^{II}/2-OG)-dependent oxygenases comprise a large family of oxidative enzymes that are widely distributed in viruses,¹²⁶ bacteria,¹²⁷ fungi,¹²⁸ plants¹²⁹ as well as animals.¹³⁰ These enzymes activate molecular oxygen by Fe^{II} as the metallo-cofactor and mostly utilize α -KG as co-substrate to catalyze various types of oxidations (**Figure 10**). For example, AmbO5 is an example of nonheme Fe^{II}/2-OG-dependent halogenase catalyzing the chlorination of ambiguanes H, C, I, and L in analogy to WelO5.¹³¹ Hydroxylation is a common reaction catalyzed by nonheme Fe^{II}/2-OG-dependent oxygenases, such as the L-proline hydroxylase AIP4H catalyzing the formation of *trans*-4-hydroxy-L-proline¹³² and CitB installing a hydroxyl group in the biosynthesis of citrinin.¹⁷ O-demethylation of thebaine in morphinan alkaloid biosynthesis by the codeine O-demethylase CODM represents another subfamily of oxidative reactions catalyzed by the nonheme Fe^{II}/2-OG-dependent oxygenases.¹³³ Related to the development of plants, the dioxygenase for auxin oxidation (DAO) is responsible for the oxidation of a tryptophan derivative to form 2-oxindole-3-acetic acid (oxIAA).^{134,135} Notably, several nonheme Fe^{II}/2-OG-dependent oxygenases have been proven to catalyze multifunctional steps in secondary metabolite biosynthesis. CarC is a bifunctional nonheme Fe^{II}/2-OG-dependent enzyme catalyzing epimerization and desaturation.¹³⁶⁻¹³⁸ As a representative, AsqJ was well studied for the desaturation and epoxidation to produce cyclopeptin, which undergoes non-enzymatic rearrangement to viridicatin.^{139,140} FtmOx1 is an excellent example of an endoperoxidase to form verruculogen.¹⁴¹⁻¹⁴³ Three distinct steps including hydroxylation, ring formation and desaturation in the biosynthesis of clavulanic acid were observed for the nonheme Fe^{II}/2-OG-dependent clavaminic acid synthase (CAS) from *Streptomyces clavuligerus*.¹⁴⁴⁻¹⁴⁶ DAOCS/DACS is a bifunctional nonheme Fe^{II}/2-OG-dependent enzyme in *Cephalosporium acremonium* and catalyzes ring expansion and hydroxylation of penicillin N to form deacetylcephalosporin C.^{146,147} In addition, oxidative decarboxylation by nonheme Fe^{II}/2-OG-dependent enzymes have been also reported in recent years, e.g., IsnB and AmbI3 involved in the biosynthesis of isonitrile derivatives.¹⁴⁸⁻¹⁵¹ These oxidative transformations play crucial roles in biochemical processes and highlight their importance in nature. Therefore, extensive mechanism investigations on nonheme Fe^{II}/2-OG-dependent oxygenases have been reported.¹²³

INTRODUCTION

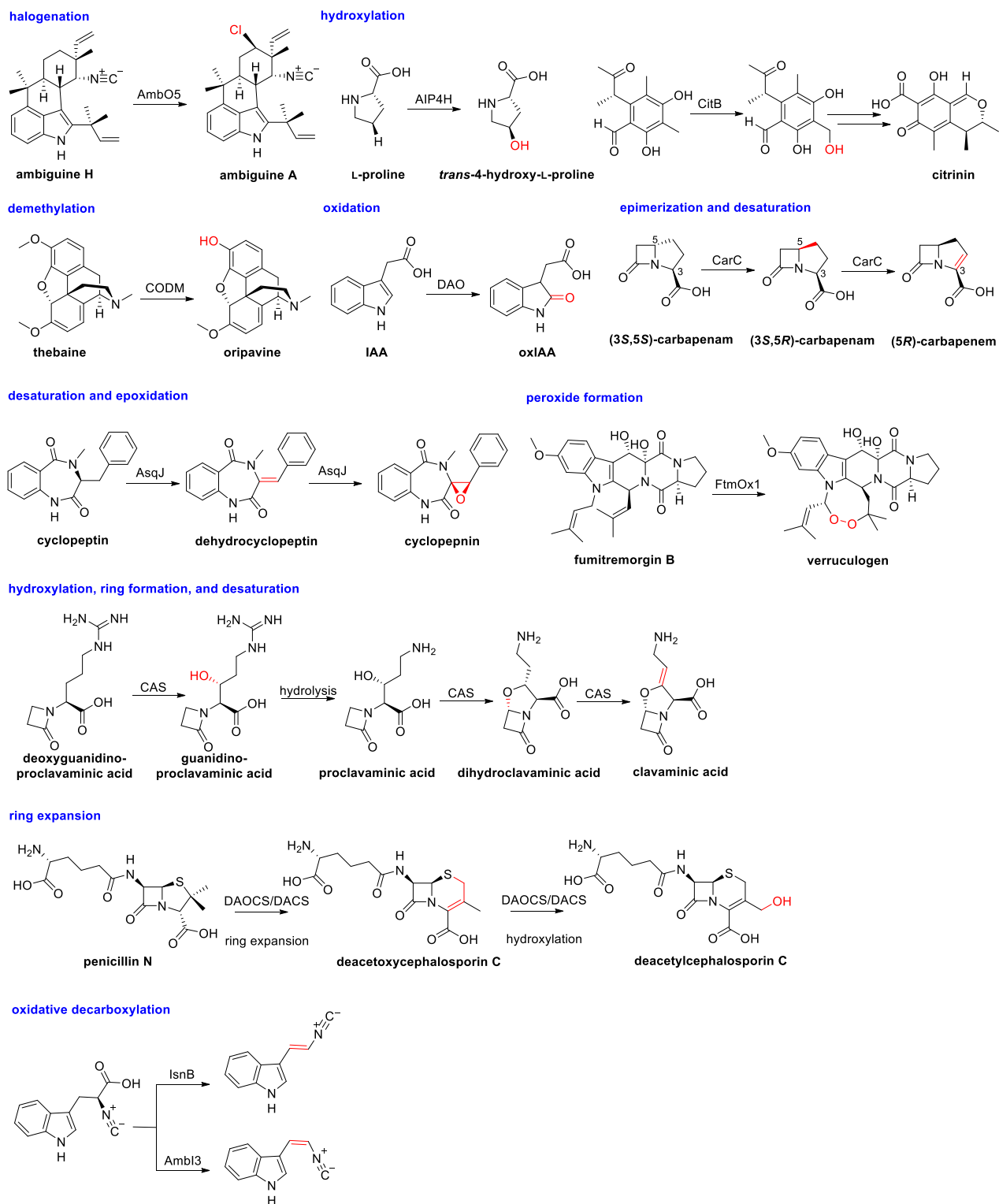


Figure 10. Reactions catalyzed by nonheme Fe^{II}/2-OG-dependent oxygenases

INTRODUCTION

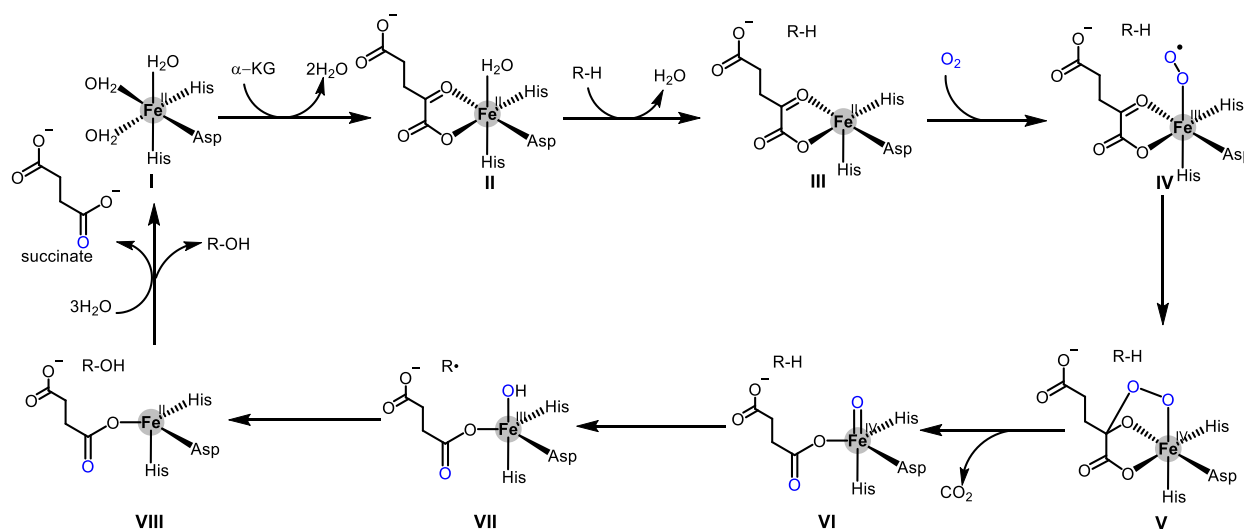


Figure 11. Reaction mechanism of the nonheme Fe^{II}/2-OG-dependent oxygenase-mediated hydroxylation

Crystallographic studies show that nonheme Fe^{II}/2-OG-dependent oxygenases comprise a double-stranded β -helix core fold composed of eight antiparallel β -strands forming a β -sandwich structure, which shares distinctive features of two His residues and a carboxylate Glu or Asp residue.¹⁵² As shown in **Figure 11** using a common hydroxylation reaction as an example, Fe^{II} is coordinated by conserved 2-His-1-carboxylate facial triad ligand and three water molecules (**Figure 11, I**).^{124,125} Binding of α -KG to the Fe^{II} center displaces two of the three metal-bound water molecules (**Figure 11, II**). Subsequently, the remaining water molecule is displaced to vacate a site for binding with the O₂ molecule and to generate the Fe^{III}-superoxo intermediate (**Figure 11, III**→**IV**). The distal oxygen atom of the Fe^{III}-superoxo species can attack carbon of α -KG to yield a peroxohemiketal bicyclic intermediate, which is abolished via an oxidative decarboxylation to construct a high valence Fe^{IV}=O (ferryl) intermediate (**Figure 11, IV**→**VI**). This ferryl species as a key intermediate can abstract a hydrogen atom from the substrate (R-H) to reduce the iron to the Fe^{III}-OH state accompanied by the substrate radical (R•) formation (**Figure 11, VII**). To complete the catalytic cycle, the hydroxylated product (R-OH) is formed due to the rebound of hydroxyl radical with the substrate radical, returning the iron back to the Fe^{II} species with concomitant formation of succinate release (**Figure 11, VIII**→**I**). Based on the generic mechanism mentioned above, more mechanisms of other reactions by nonheme Fe^{II}/2-OG-dependent oxygenases are studied with the help of *in vitro* investigations, site-specific mutagenesis, ¹⁸O labeling experiment and crystallographic analysis. In the cases of the oxidative decarboxylases IsnB and AmbI3, Huang et al. first proposed three different pathways, including the hydroxyl group formation, radical or cation intermediate pathway and O-H bond activation.¹⁴⁸ Finally, the mechanism involving radical or cation intermediate was proved to be more reasonable. A hydrogen atom from β -position of COOH is abstracted by Fe^{IV}=O species to generate the substrate radical. Subsequent radical-mediated electron transfer and C-C bond cleavage

eventually install the olefination accompanied by CO₂ elimination.¹⁴⁹ With advanced biochemical tools and the well-known mechanism study, more and more structural information and novel reactions are discovered for nonheme Fe^{II}/2-OG-dependent enzymes. Therefore, an increasing structure-function and structure-reactivity relationship will further enrich our knowledge on this enzyme family.

1.3.2 Flavin-containing oxidoreductases

In contrast to iron-based enzymes, flavin-containing enzymes utilize a flavin adenine dinucleotide (FAD) or flavin mononucleotide (FMN) as cofactor to undergo the catalytic cycle by two half reactions (**Table 2, Figure 12**).¹⁵³ In the reductive half reaction, four types of substrates with ester groups, alcohol, amine, thiol and dithiols are typically oxidized by the oxidized flavin (Fl_{ox}) coenzyme via two-electron pathway (**Figure 12A**). Representatively, the oxidase AknOx is a bifunctional enzyme, converting the alcohol group of aclacinomycin N (AcIN) to the ketone group and thereby acting as a typical flavin-dependent desaturase to yield aclacinomycin Y (AcIY) (**Figure 13A**).¹⁵⁴ The gliotoxin dithiol oxidase GliT is the last enzyme in the toxin assembly line and has recently been shown to play a self-protective role in the producer *Aspergillum fumigatus* (**Figure 13B**).^{155,156} For most flavin-containing enzymes, the second half reaction includes a directed reoxidation of a bound reduced dihydroflavin (FlH₂, *i.e.* FADH₂/FMNH₂) generated by the reductive half reactions. In this case, the oxygenating agent hydroperoxyflavin (Fl-4a-OOH) functions as an electrophile in most examples to deliver an OH⁺ equivalent to a nucleophilic substrate and the peroxyflavin (Fl-4a-OO⁻) serves as a nucleophile. The resultant Fl-4a-OH can decompose intramolecularly to give one molecule of water and regenerate the oxidized state Fl_{ox} in the enzyme active site (**Figure 12B**). For example, in the biosynthesis of gaudimycin C, the flavin-containing enzyme PgaE is responsible for the hydroxylation at C12-position.^{157,158} Analogously, NotB in the notoamide pathway is proposed to generate an indole epoxide intermediate from notoamide E (**Figure 13C and D**). Taken together, flavin-containing enzymes catalyze a large variety of oxidations including dehydrogenation, hydroxylation, epoxidation, Baeyer-Villiger oxidation and sulfoxidation.^{159,160}

Another major group of flavin-containing enzymes oxidizes NADPH to NADP by hydride transfer from the reduced nicotinamide coenzymes to N₅ of the bound FAD.^{121,161} Most of the NADPH-oxidizing flavin-containing enzymes found in the biosynthetic pathways are involved in co-substrate oxygenations by reoxidative half reactions from FlH₂. However, reduction/hydrogenation of this enzyme family was also reported. Representatively, the FAD-enzyme MurB utilizes NADPH as a hydride transfer agent to generate FADH₂ in the reductive half reaction. Subsequently, FADH₂ in the MurB active site is responsible for the hydride transfer to the olefinic terminus of the enol ether link in the substrate UDP-enoylpyruvyl-GlcNAc (**Figure 13E**).¹⁶²⁻¹⁶⁵ In summary, FAD and FMN use one- or two-electron transfer to yield different forms in redox reactions. They are electrophilic in the oxidized

INTRODUCTION

state and nucleophilic in the reduced state. Therefore, it is comprehensible that this enzyme family is responsible for a large number of crucial reactions in biosynthetic pathways.

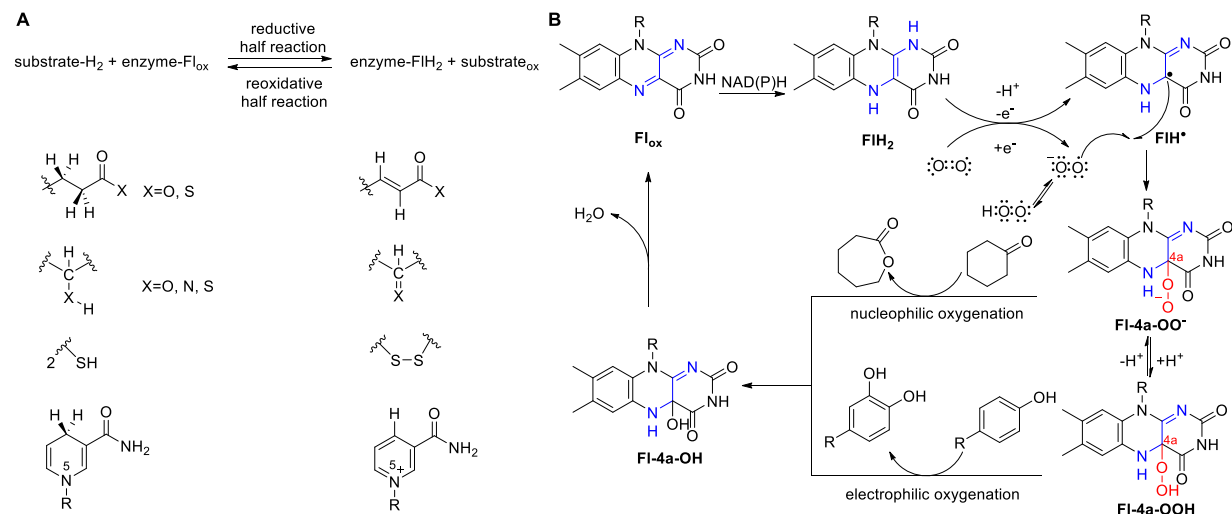


Figure 12. Mechanism of flavin-containing enzyme redox transformations. (A) Reductive half reaction and reoxidative half reaction between the oxidized flavin (Fl_{ox}) and reduced flavin (FlH_2). (B) Reoxidative half reaction of FlH_2 with O_2 via one-electron transfer.

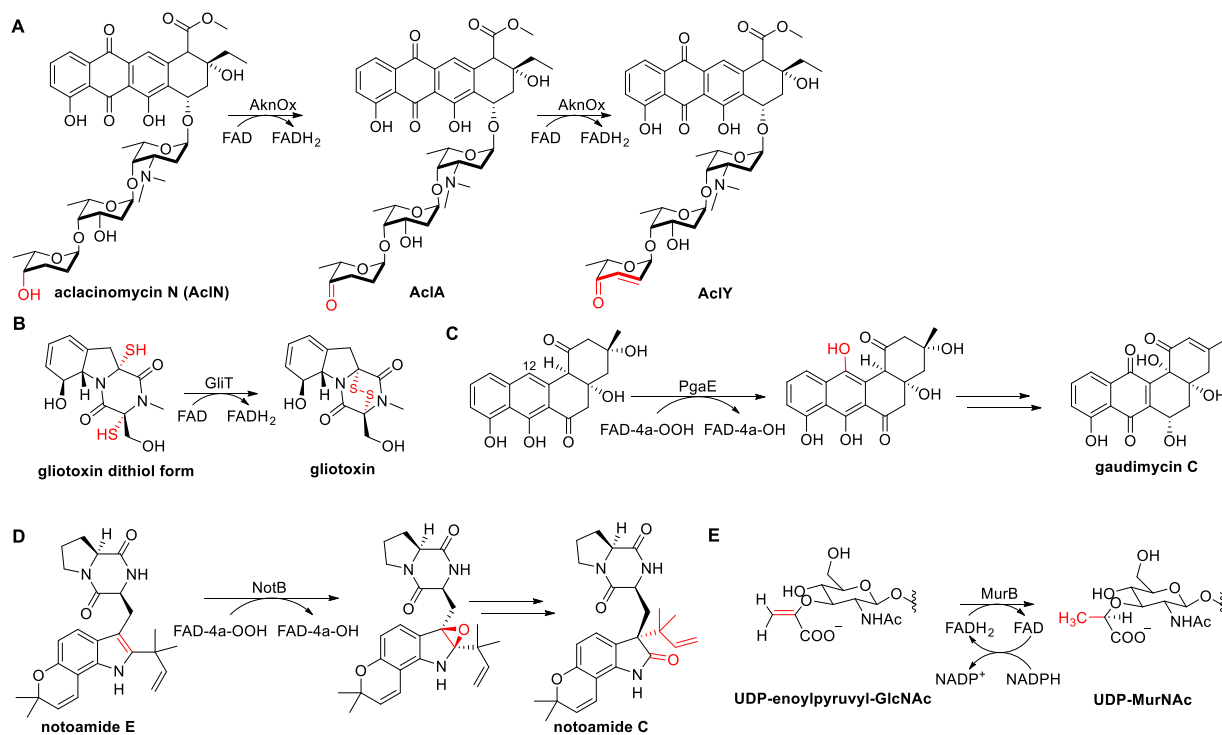


Figure 13. Reactions catalyzed by flavin-containing enzymes

1.4 Non-enzymatic reactions in natural product formation

Molecular biological and biochemical investigations showed that complex enzymatic reactions are performed in a sequential order in the biosynthesis of natural products.^{166,167} Although such multi-enzyme cascade reactions provide many advantages for compound design, there are a lot of non-enzymatic reactions observed during extraction, fractionation, analysis, handling and even storage.¹⁶⁸ These reactions can be induced by many stimuli including common organic solvents (*e.g.* alcohol, methanol, acetone and dichloromethane), slight changes on pH or temperature, exposure to light or air (*i.e.* oxygen) and even chromatography media. As a result, natural products can be converted to unexpected pseudo-natural products by ester formation, etherification, hydroxylation, cycloaddition, isomerization, or rearrangement. On the other hand, there are also diverse active intermediates spontaneously formed and undergoing miscellaneous chemical reactions in natural product formation.

Quinone methides (QMs) are highly reactive intermediates observed in complex natural product biosynthesis and have been extensively utilized in chemical synthesis.¹⁶⁹⁻¹⁷³ Diverse strategies, *e.g.* thermally driven,^{174,175} photolytically induced tautomerization^{176,177} and benzylic oxidation,^{178,179} have been developed to generate QMs. However, QMs can also be formed by spontaneous elimination of a stable molecule with concomitant dearomatization.^{180,181} They are susceptible to nucleophilic attack to form unexpected natural products by inverse electron-demand Diels-Alder (IEDDA) reactions or 1,4-Michael additions. For example, the *para*-quinone methide (*p*-QM) ppupehenone, isolated from a Caledonian sponge *Hyrtios* sp., yielded 15-methoxypuuephenone in methanol with asymmetric induction from adjacent chiral centers, and *vice versa* (**Figure 14A**).^{182,183} Pestapyrone B, isolated from the mangrove-derived fungus *Pestalotiopsis clavispora*, undergoes dehydration spontaneously to form an *ortho*-quinone methide (*o*-QM) intermediate, which is methylated spontaneously to deliver pestapyrone C (**Figure 14B**).¹⁸⁴ The *p*-QM elansolid A3 acts as a key intermediate in the biosynthesis of elansolids A1/A2 in *Chitinophaga sancti* (**Figure 14C**).^{185,186} Another *p*-QM intermediate derived from acyl-fluostatins (acyl-FSTs), such as FST D, is proposed to be responsible for the formation of FST C in water or methanol and involved in the dimerization of benzofluorene-containing difluostantin B via Michael addition (**Figure 14D**).¹⁸¹ The *o*-QM intermediates spontaneously lead to the formation of leprin C by hetero-Diels-Alder (HDA) reaction and its derivative by intramolecular Diels-Alder reaction (IMDA) (**Figure 14E**).⁶⁴ Chaetophenol E is produced through the acid-prompted generation of an *o*-QM from chaetophenol B, which is followed by an inverse-demand HDA reaction or a stepwise Michael addition (**Figure 14F**).¹⁸⁷ In summary, quinone methides as active intermediates are spontaneously involved in diverse natural product formation. This is likely to inspire the development of future methodology involving non-enzymatic reactions, which will be used not only in natural product synthesis but also in all fields of organic chemistry.

INTRODUCTION

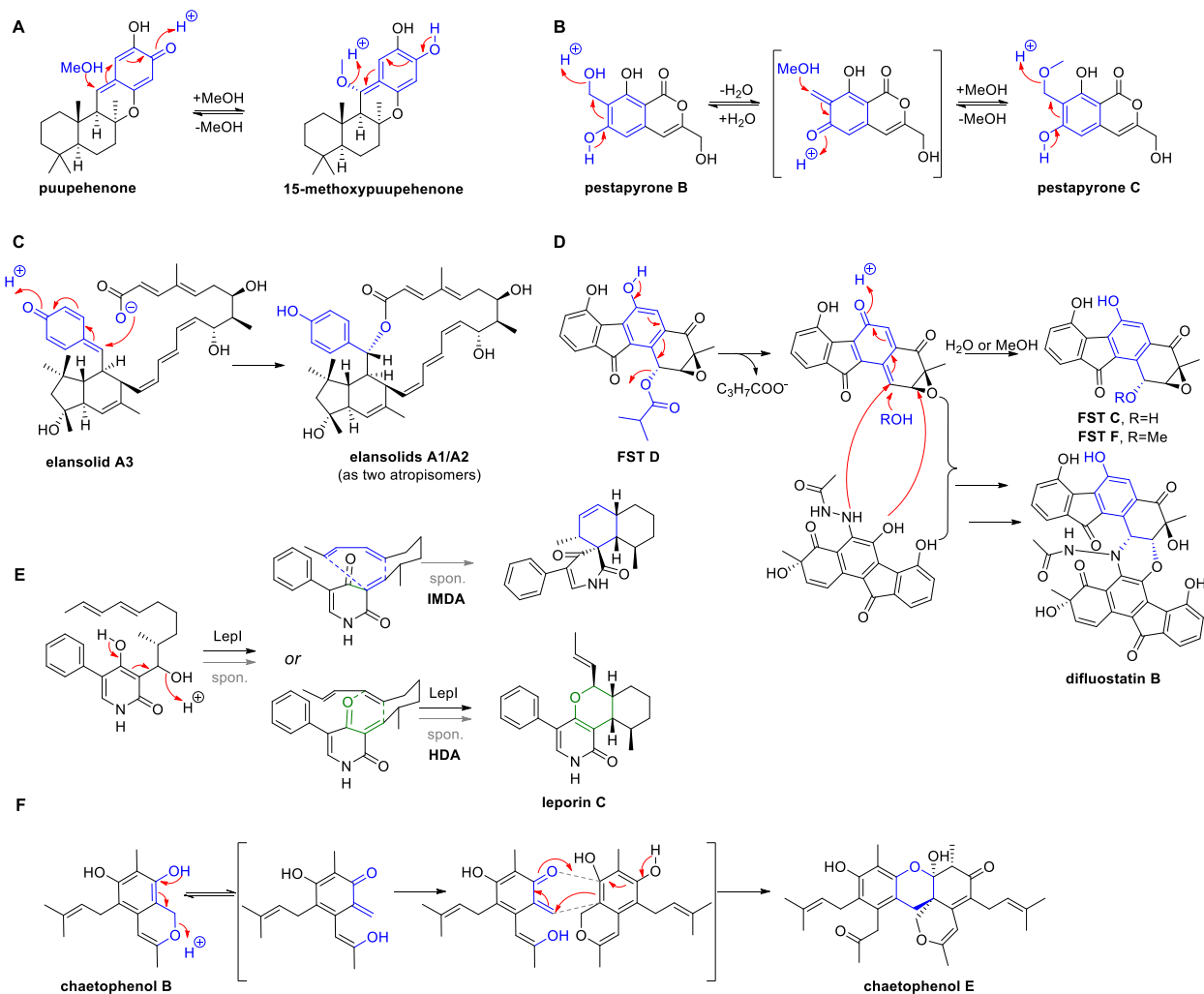


Figure 14. Biosynthesis of natural products via the active quinone methide intermediates

2 Aims of this thesis

The following issues have been addressed in this thesis:

Formation of peniphenones and penilactones in *Penicillium crustosum* requires coupling of products from two separate gene clusters via non-enzymatic 1,4-Michael additions

Penilactones A and B are rare fungal metabolites containing clavatol and γ -butyrolactone moieties. It was proposed that they are formed by 1,4-Michael additions of two clavatol molecules in its active form *ortho*-quinone methide with a γ -butyrolactone (tetronic acid), *i.e.* (5*R*)-methyl or (5*S*)-carboxymethyltetronic acid. Although this hypothesis was confirmed by a biomimetic synthesis, no genetic investigation on penilactones A and B biosynthesis was available prior to this study. The aim of this project is to find the biosynthetic origin of clavatol and γ -butyrolactone, as well as their coupling mechanism to yield the end products penilactones A and B in *Penicillium crustosum* PRB-2. The following experiments were carried out:

- Isolation and structural elucidation of secondary metabolites related to clavatol or γ -butyrolactone from *Penicillium crustosum* PRB-2
- Identification of the putative NR-PKS ClaF and hybrid PKS-NRPS TraA by sequence comparison
- Verification of the involvement of clavatol and terrestric acid gene clusters in the biosynthesis of penilactones A and B by gene deletion, feeding experiments, and heterologous expression
- Characterization of the nonheme Fe^{II}/2-OG-dependent oxygenase ClaD by biochemical investigation *in vitro*
- Detection of *o*-quinone methide derived from hydroxyclovatol
- Proof of the penilactone and peniphenone formation via non-enzymatic 1,4-Michael addition

Formation of crustosic acid and its stereospecific conversion to terrestric acid in *Penicillium crustosum*

Fungus-originated tetronates carry usually different acyl moieties at C3-position and differ from each other often in substituents at C5-position by an α -methyl, a β -carboxymethyl or an olefinic methylene group. Despite the occurrence of a number of such compounds in fungi, no detailed investigations on their biosynthesis were available prior to this study. The involvement of terrestric acid gene cluster in *Penicillium crustosum* PRB-2 was proposed in the formation of crustosic acid and terrestric acid in our previous efforts. In this study, we elucidated the biosynthetic pathway of crustosic acid with a β -carboxymethyl group and its stereospecific conversion to terrestric acid with an α -methyl group. The following experiments were carried out:

- Heterologous expression of the hybrid PKS-NRPS *traA* with or without the enoyl reductase *traG* in *Aspergillus nidulans* LO8030
- Identification of *traG* by gene deletion in *Penicillium crustosum* PRB-2
- Isolation and structural elucidation of crustosic acid precursors
- Overproduction of the recombinant flavin-containing oxidoreductase TraD and the nonheme Fe^{II}/2-OG-dependent oxygenase TraH in *E. coli*
- Performance of enzyme assays with TraD and TraH, as well as subsequent analysis by LC-MS
- Extraction, isolation and structural elucidation of enzyme products
- Determination of the kinetic parameters of the corresponding enzymes
- Postulation of a catalytic mechanism for TraH reaction

Application of *ortho*-quinone methide derived from hydroxyclovatol for increasing structural diversity of clavatul-containing pseudo-natural products under mild condition

A number of natural products containing a clavatul unit are found in fungi, especially in *Penicillium* species. In our previous study, we demonstrated that the formation of penilactones A and B requires two-step non-enzymatic 1,4-Michael additions between a γ -butyrolactone and two *ortho*-quinone methide molecules derived from hydroxyclovatol. *Ortho*-quinone methides, as transient intermediates with remarkable reactivity, have been utilized as useful reactants in chemical synthesis. Inspired by post-biosynthetic non-enzymatic event in the biosynthesis of penilactones A and B, *ortho*-quinone methide derived from hydroxyclovatol was used for increasing structural diversity of clavatul-containing products. The following experiments were carried out:

- Chemical synthesis of hydroxyclovatol (carried out by Lena Ludwig-Radtke)
- Incubation of hydroxyclovatol with 102 different reactants at 25 °C for 16 h or at 95 °C for 30 min without pH adjustment
- LC-MS analysis of incubation mixtures
- Isolation and structural elucidation of 32 selected clavatul-containing products
- Screen of isolated clavatul-containing products for their antibacterial, acetylcholinesterase, and α -glucosidase inhibition activities

The designed experiments of all the three projects have been successfully finished in cooperation with Ge Liao.

3 Results and discussion

3.1 Peniphenone and penilactone formation in *Penicillium crustosum* via 1,4-Michael additions of *ortho*-quinone methide from hydroxyclavatul to γ -butyrolactones from tetronic acids

Diverse penilactone and peniphenone natural products were identified in fungi, especially in *Penicillium* species.¹⁸⁸⁻¹⁹¹ Penilactones A (**1**) and B (**2**), together with their putative precursors peniphenone D (**3**) and penilactone D (**4**), were isolated from *Penicillium crustosum* PRB-2. They harbor structurally clavatul (**5**) and γ -butyrolactone (tetronic acid) moiety.¹⁸⁸ Biomimetic synthesis of **1**, **2**, and **4** were achieved by using an active intermediate *ortho*-quinone methide (**6**) and (5*R*)-methyl (**7**) or (5*S*)-carboxymethyltetronic acid (**8**) as reactants via Michael addition.^{174,175} However, their biosynthetic pathway still remained unknown prior to this study. Likewise, neither the biosynthesis nor the involvement of clavatul and γ -butyrolactones have been investigated before.

After optimization of culture conditions for secondary metabolite production in *Penicillium crustosum* PRB-2, two dominant peaks detected in 7 days-old PD shaking culture were identified as hydroxyclavatul (**9**) and hydroxyclavatul methyl ether (**10**)¹⁹² by isolation, NMR elucidation and X-ray diffraction. **5** and another clavatul-containing metabolite, hydroxyclavatul ethyl ether (**11**)¹⁹² as well as terrestrial acid (**12**)¹⁹³ were also obtained from PRB-2 from 7 days-old PD shaking culture by isolation and structural elucidation. **1** – **4** were clearly accumulated in a 14 days-old PD surface culture and a 30 days-old rice culture.^{188,191} Another new peak was proven to be a carboxylated derivative of **12**, termed crustosic acid (**13**). The CD spectra of **1** and **2** correspond very well to those reported previously.¹⁸⁸ The stereochemistry of **3** and **4** were determined by chemical synthesis from **7** and **8** with known configuration at C-5 respectively.^{174,175,194,195} The configurations of **12** and **13** were assigned by comparison with the optical rotation data of fungal acyltetrionic acids.¹⁹⁶

To investigate the biosynthetic pathway, the genome of *Penicillium crustosum* was sequenced and analyzed, leading to the prediction of 56 putative gene clusters by using AntiSMASH analysis.¹⁹⁷ Based on its aromatic character, **5** is expected to be assembled by a non-reducing PKS (NR-PKS).⁸⁴ Pcr3094, termed ClaF, was considered as the top candidate due to its sequence identity of 57.7 % with CitS from *Monascus ruber* (**Figure 15**).¹⁷ The disruption of *claF* from *clavatul* gene cluster by replacement with a hygromycin B cassette (*hph*) completely abolished the accumulation of **1** – **5** and **9** – **11**, which indicated that ClaF is responsible for the biosynthesis of **5** in PRB-2 (**Figure 17**). Feeding **5** to the Δ *claF* mutant restored the production of **1** – **4** and **9** – **11**. Further heterologous expression of *claF* in *Aspergillus nidulans* LO8030 confirmed the function of NR-PKS ClaF as clavatul synthase.

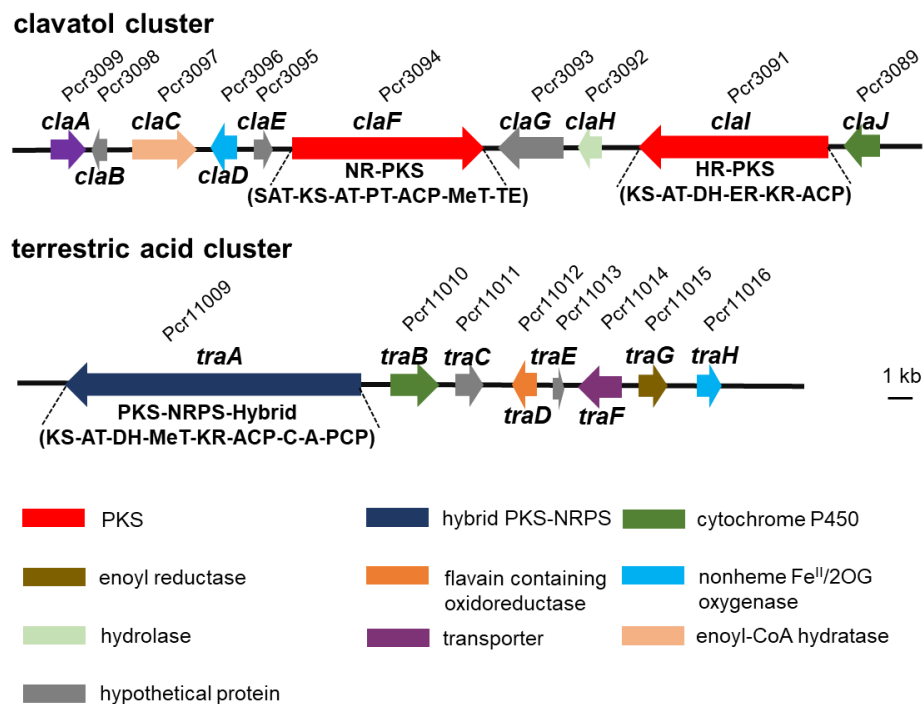


Figure 15. Schematic representation of clavatul and terrestric acid clusters in *P. crustosum* PRB-2

To identify the genetic potential for the formation of **7** and **8**, hybrid PKS-NRPS gene *pcr11009* from terrestric acid gene cluster, termed *traA*, was disrupted in the similar way as for *claF*, because its sequence homologue *caaA* was speculated for the formation of carlosic acid (**Figure 15**).⁴⁹ As expected, LC-MS analysis of the $\Delta traA$ mutant revealed the abolishment of **1** – **4** and the accumulation of **5** and **9** – **11**. Notably, the predominant peak of **12** observed in PRB-2, together with its carboxylated derivative **13**, were completely disappeared in the $\Delta traA$ mutant. Feeding **7** and **12** into the $\Delta traA$ mutant both restored the production of **1** and **3**, but not **2** and **4**. Instead, **2** and **4** were accumulated in the $\Delta traA$ mutant after feeding with **8**. Interestingly, feeding **13** into $\Delta traA$ mutant restored the production of **1** – **4**. This proved that TraA is involved in the biosynthesis of the γ -butyrolactone (tetronic acid) moiety. In addition, **12** and **13** are the precursors of **7** and **8**, respectively. **13** can be converted to **12**, which is further confirmed by inactivation of the encoding gene of the nonheme Fe^{II}/2-OG-dependent oxygenase (*traH*).

Having identified the backbone enzymes involved in building blocks, we intended to investigate the metabolism of **5** to **9**, **12** to **7**, as well as **13** to **12** and **8**. In the deletion mutants of the cytochrome P450 *traB* and the flavin-containing oxidoreductase *traD*, no accumulation of **12**, **13**, or **1** – **4** was detected, proving their roles in the **13** formation. In the deletion mutant of nonheme Fe^{II}/2-OG-dependent oxygenase *claD*, **1** – **4** and **9** were completely abolished, whereas **5** was clearly accumulated. Feeding **9** in the $\Delta claD$ mutant restored the production of **1** – **4**, proving its role in the conversion of **5** to **9**. Subsequently, the recombinant enzyme ClaD was incubated with **5** in the

presence of ascorbic acid, $\text{Fe}[(\text{NH}_4)_2(\text{SO}_4)_2]$ and 2-oxoglutarate. HPLC analysis confirmed the hydroxylation of **5** to **9**.

Regarding Michael addition, an active intermediate *ortho*-quinone methide (**6**) was speculated for the formation of **1** – **4**. To prove the conversion between **9** and **6**, **9** was incubated in H_2O and H_2^{18}O at 25°C for 16 h. MS data in positive and negative modes confirmed the incorporation of ^{18}O into **9** and therefore the equilibration (**Figures 16**). **6** was also detected in extracted ion chromatograms (EICs) in the incubation of **9** in different alcohols, which resulted in the formation of **10** and **11**.

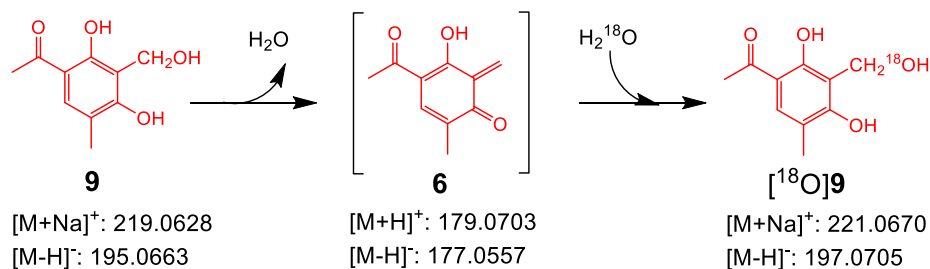


Figure 16. Determination of equilibration between hydroxyclovatol (**9**) and *ortho*-quinone methide (**6**)

Deletion of cytochrome P450 *claJ* resulted in the abolishment of **1** – **4**, but still retained the production of **5**, **9**, **12** and **13**. This suggested its role in the connection of the two building blocks via Michael addition. Therefore, we intended to feed the precursors in *claJ* heterologous expression mutant. Surprisingly, **1** as a minor product and **3** as a major product were detected in the control incubation of **7** with **9** in water at 25°C for overnight. In contrast, the incubation mixture of **8** with **9** in water led to the formation of **2** and **4**. When **3** and **4** were incubated with **9**, **1** and **2** were detected, respectively. It is obvious that the active intermediate **6** can be easily formed from **9** in aqueous system and initiates the non-enzymatic Michael additions by the intermolecular nucleophilic attacking under very mild condition (**Figure 17**). Consequently, these results indicate that *Claj* is responsible for other reactions instead of Michael addition.

Taken together, **1** – **4** are formed by enzymes from independent pathways of two separate gene clusters (**Figure 17**). Gene deletion, feeding experiments and biochemical investigations proved that a NR-PKS *Claf* is responsible for the formation of **5** and the hybrid PKS-NRPS *TraA* is involved in the formation of **13**, which undergoes decarboxylation and isomerization to **12**. Both acids deliver the two γ -butyrolactones **7** and **8**. Oxidation of **5** to **9** by *Clad* and its spontaneous dehydration form **6** initiate the two non-enzymatic Michael addition steps to yield **1** and **2**. This study provides an excellent example for natural products with complex structures by combination of enzymatic and non-enzymatic reactions. Thus, more clavatul-containing products reported before would also be formed in similar way via the active intermediate **6**.^{189,190,198-200}

RESULTS AND DISCUSSION

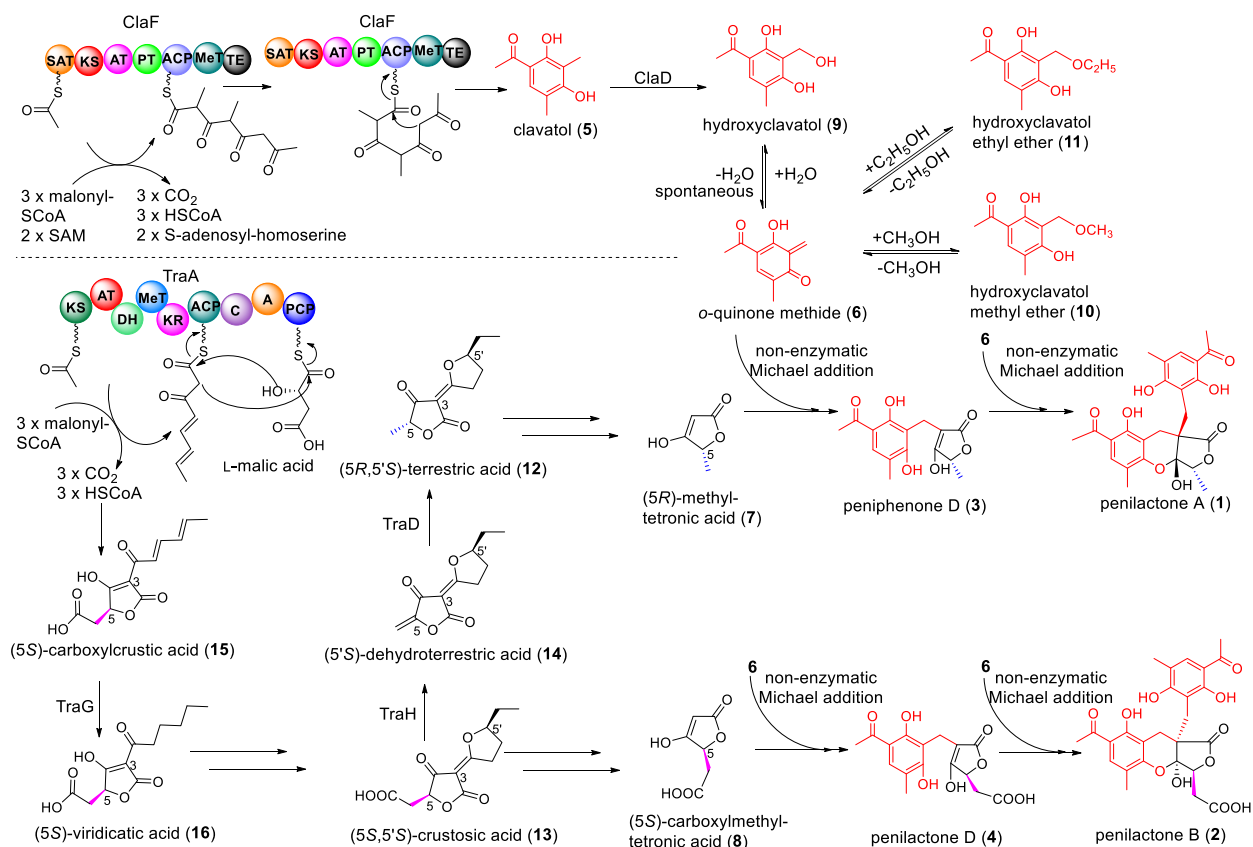


Figure 17. Proposed biosynthetic pathways of penilactones, peniphenone and terrestric acid in *P. crustosum* PRB-2

For details on this work, please see the publication (section 4.1)

Jie Fan*, Ge Liao*, Florian Kindinger, Lena Ludwig-Radtke, Wen-Bing Yin, and Shu-Ming Li (2019), Peniphenone and penilactone formation in *Penicillium crustosum* via 1,4-Michael additions of *ortho*-quinone methide from hydroxyclovatul to γ -butyrolactones from crustosic acid. *Journal of the American Chemical Society*, 141 (10), 4225–4229, DOI: 10.1021/jacs.9b00110. (*equal contribution)

3.2 Terrestrial acid formation in *Penicillium crustosum* requires redox-assisted decarboxylation and stereoisomerization

Natural products of the tetronate family with over 100 members display a wide variety of biological activities. Tetronate compounds mainly found in *Actinomycetes* consist of a linear fatty acid or polyketide backbone, decorated on one end with a characteristic γ -butyrolactone (tetronic acid) ring system (**Figure 18**).^{201,202} Fungus-originated tetronates carry different acyl moieties at C3-position and differ from each other often in substituents at C5-position by an α -methyl, a β -carboxymethyl or an olefinic methylene group.^{49,180,193,196,203-205} Representatives are terrestrial acid (**12**) and crustosic acid (**13**) from *Penicillium crustosum*, as well as dehydroterrestrial acid (**14**) from *Aspergillus hancockii* (**Figure 17**). Despite the interesting structural features of fungal acyltetronates, no detailed investigations on the biosynthesis of fungal tetronates were reported prior to this study. An hybrid PKS-NRPS CaaA responsible for the biosynthesis of carlosic acid with a β -carboxymethyl group was proposed after a regulator activation in *Aspergillus niger*, but without genetic and biochemical data.⁴⁹ As mentioned in section 3.1, the involvement of terrestrial acid cluster was proposed in the formation of **12** and **13**.¹⁸⁰ A nonheme Fe^{II}/2-OG-dependent oxygenase TraH was involved in the conversion of **13** to **12**. In this study, we continued the investigation on the formation of **13** in *Penicillium crustosum* PRB-2 and its conversion to **12**.

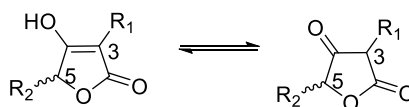


Figure 18. Tetronic acid tautomers

Based on the identification of TraA responsible for the core structure of **12** and **13** by gene deletion in *Penicillium crustosum*, its genome sequence *traA* was further introduced into *Aspergillus nidulans* LO8030. LC-MS analysis of the transformant JF15 harboring *traA* revealed the production of a new carboxylmethyltetronic acid derivative with an unsaturated acyl chain, termed carboxylcrustic acid (**15**) (**Figure 17**). This proved that the hybrid PKS-NRPS TraA alone acts as a carboxylcrustic acid synthase and differs from other PKS-NRPS enzymes requiring a *trans*-enoyl reductase (ER). Subsequently, heterologous expression of *traA* with the putative ER *traG* in *Aspergillus nidulans* led to accumulation of **16** as a predominant product and **15** as a minor product. Isolation and structural elucidation proved **16** to be viridicatic acid, which was also identified in *Penicillium crustosum* PRB-2. Structurally, **16** is a derivative of **15** with a saturated acyl chain, proving TraG for the reduction of C-C double bonds. Further disruption of *traG* in *Penicillium crustosum* showed completely abolishment of **12**, **13** as well as **16**, and accumulation of **15** as a main product in comparison with the wild type PRB-2. An additional product was identified as a decarboxylated stereoisomer of **15**, termed crustic acid (**17**), by comparing their optical rotation values and CD spectra (**Figure 19**). This result

RESULTS AND DISCUSSION

suggested that the enzymes involved in the conversion of **13** to **12** also catalyzed the conversion of **15** to **17** (Figures 17 and 19).

To prove the metabolism of **15** and **16** in the formation of **12** and **13**, they were fed in the available $\Delta traA$ and $\Delta traG$ mutants. LC-MS analysis of the EtOAc extracts revealed **15** can be converted to **12** and **17** in $\Delta traA$ mutant. **16** can be metabolized to **12** as the predominant product in both $\Delta traA$ and $\Delta traG$ mutants. In this way, **15** and **16** were confirmed to be precursors of **13** in the biosynthesis. Structural comparison revealed that **13** is an anhydrous form of a hydroxylated derivative of **16**. Incubation of **13** in D₂O proved the existence of its hydrous form, suggesting that an additional enzyme would be responsible for the hydroxylation of **16**. However, the responsible enzyme has not been identified yet.

Having identified the formation of **13**, we proceeded to investigate its conversion to **12**. Depending on the proposed involvement of the nonheme Fe^{II}/2-OG-dependent oxygenase TraH in this conversion in section 3.1, the recombinant TraH was first overproduced in *E. coli* and purified to near homogeneity as confirmed on SDS-PAGE (Figure 19). Surprisingly, incubation of TraH with **13** in the presence of ascorbic acid (AA), Fe[(NH₄)₂(SO₄)₂] (Fe^{II}), 2-oxoglutarate and dithiothreitol (DTT) revealed a product peak **14**, but not **12**. **14** was further identified as dehydroterrestric acid with an exocyclic double bond at C5-position after isolation and structure elucidation (Figure 19). This result proved that TraH catalyzes an oxidative decarboxylation of **13** to **14** instead of **12**.

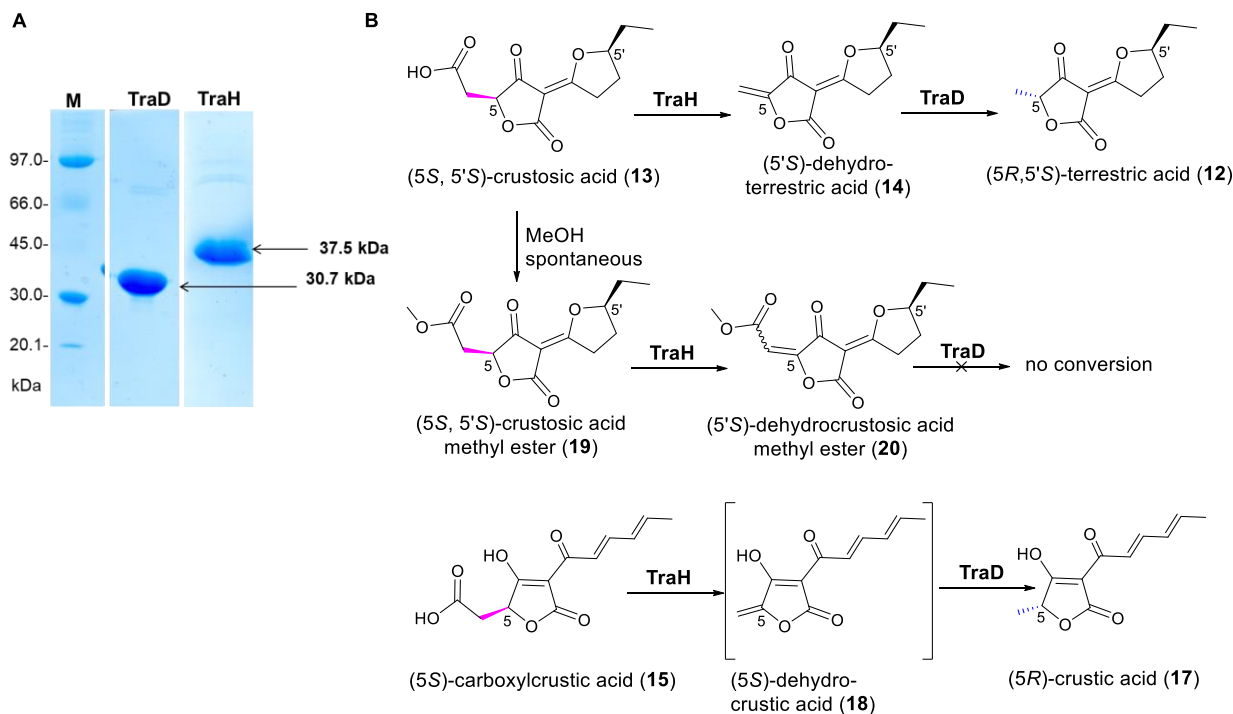


Figure 19. Analysis of the recombinant TraD and TraH on SDS-PAGE (A) and their enzymatic reactions (B)

Biochemical investigation of TraH implies the requirement of another enzyme responsible for the reduction of **14** to **12**. The flavin-containing oxidoreductase TraD from the terrestrial acid gene cluster was considered as a top candidate. Subsequently, the recombinant TraD was overproduced in *E. coli* in similar way to TraH and proved on SDS-PAGE (**Figure 19**). The enzyme assay of TraD with **14** was carried out in the presence of NADPH at 30 °C. LC-MS analysis revealed that 0.5 mM of **14** was completely converted to **12** by 0.6 μM TraD in 10 min. As speculated, the flavin-containing enzyme TraD catalyzed the reduction of the exocyclic double bond at C5-position of **14** to give **12**.

Subsequently, coincubation of **13** with TraH and TraD at different ratios in the presence of ascorbic acid (AA), Fe[(NH₄)₂(SO₄)₂] (Fe^{II}), 2-oxoglutarate, dithiothreitol (DTT) and NADPH revealed sequential production of **14** and **12**. The integrity of **12** isolated from the enzyme assay was confirmed by comparison with that isolated from *Penicillium crustosum* PRB-2. Therefore, the conversion of **13** to the stereospecific **12** requires an oxidative decarboxylation catalyzed by the nonheme Fe^{II}/2-OG-dependent oxygenase to give an exocyclic double bond and a sequent reduction by the flavin-containing oxidoreductase TraD. Incubation of **15** with TraH and TraD led to detection of **17** as a minor peak, proving the accumulation of **15** as a major and **17** as a minor product in Δ*traG* mutant. In analogy to the conversion of **13** to **12**, an intermediate dehydrocrustic acid (**18**) with an olefinic methylene group is likely involved in the conversion of **15** to **17**.

Regarding the TraH-catalyzed oxidative decarboxylation, we proposed that a hydrogen atom from β-position of COOH was abstracted by Fe^{IV}-oxo species to generate the substrate radical in analogy to the reported mechanisms.^{148-151,206-210} Subsequent radical-mediated electron transfer and C-C bond cleavage eventually install the exocyclic double bond in **14** accompanied by CO₂ elimination (**Figure 20**). To probe whether the decarboxylation is required for the olefination by TraH, crustosic acid methyl ester (**19**) was prepared by a spontaneous methylation of **13** in methanol. Incubation of TraH with **19** revealed a new product peak, termed dehydrocrustosic acid methyl ester (**20**), proving the sole olefination catalyzed by TraH when the carboxyl group was blocked. In comparison to the TraH-catalyzed oxidative decarboxylation of **13**, olefination of **19** by TraH seems to proceed via a second hydrogen abstraction from the α-position of COOCH₃ by Fe^{III}-OH species, resulting in two consecutive scissions of C-H bond to install the olefin group (**Figure 20**).

Taken together, the hybrid PKS-NRPS TraA and the ER TraG were assigned in the formation of **13**. Its conversion to **12** was proved by biochemical characterization of the nonheme Fe^{II}/2-OG-dependent oxygenase TraH and flavin-containing enzyme TraD. Differing from other nonheme Fe^{II}/2-OG-dependent oxygenases being responsible for decarboxylation-assisted olefination, TraH can catalyze the olefination with or without CO₂ elimination. In total, the redox-assisted decarboxylation and stereoisomerization provide new insights into the biosynthesis of fungal acyltetrates, especially their biosynthetic relationships with different stereochemistry in the three groups.

RESULTS AND DISCUSSION

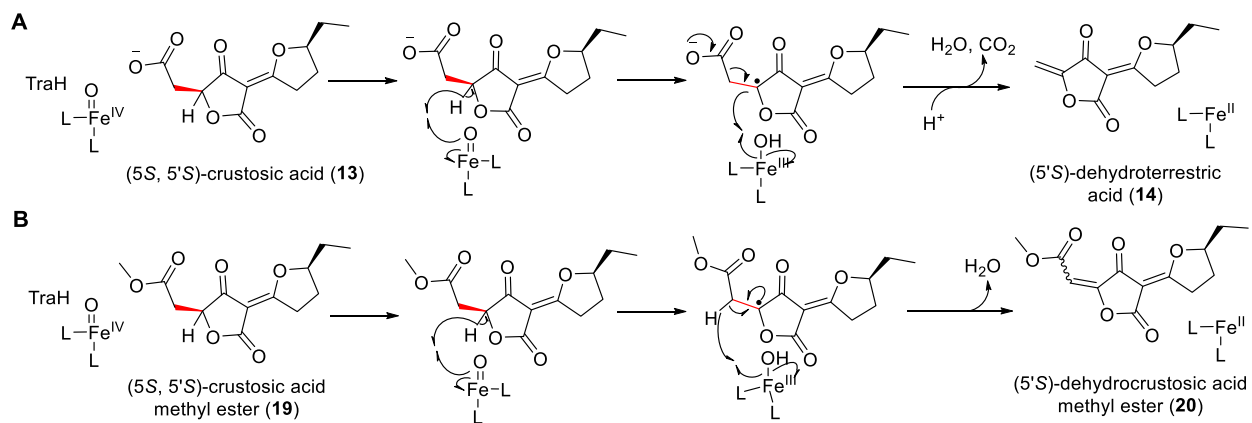


Figure 20. Mechanism of TraH-catalyzed olefination

For details on this work, please see the publication (section 4.2)

Jie Fan*, Ge Liao*, Lena Ludwig-Radtke, Wen-Bing Yin, and Shu-Ming Li (2020), Formation of terrestric acid in *Penicillium crustosum* requires redox-assisted decarboxylation and stereoisomerization. *Organic Letters*, 22 (1), 88-92, DOI: 10.1021/acs.orglett.9b04002. (*equal contribution)

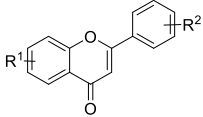
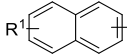
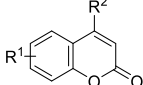
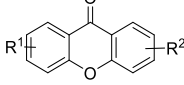
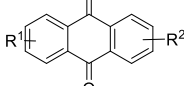
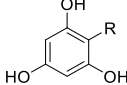
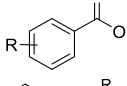
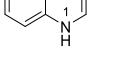
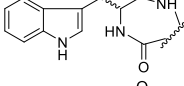
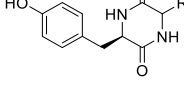
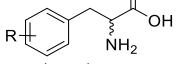
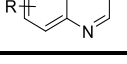
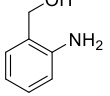
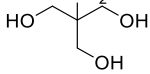
3.3 Increasing structural diversity of natural products by Michael addition with *ortho*-quinone methide derived from hydroxyclovatol

Ortho-quinone methides (*o*-QMs) are utilized in chemical synthesis due to its remarkable reactivity. Different synthetic strategies have been developed to generate *o*-QMs including spontaneous elimination of a stable molecule with concomitant dearomatization as an easier one.¹⁷⁴⁻¹⁸¹ *o*-QMs have been implicated in the formation of several natural products, as these versatile intermediates can readily participate in inverse electron-demand Diels-Alder (IEDDA) or 1,4-Michael additions.^{64,180,181,185,186,211} As described in section 3.1, penilactones A (**1**) and B (**2**) are formed via non-enzymatic 1,4-Michael addition of the *o*-QM (**6**) derived from hydroxyclovatol (**9**). Inspired by this non-enzymatic event, we wondered more coupling products of clavatol with lactones, phenols, indole derivatives and quinones found in fungi were assembled in a similar way.^{188-190,198-200,212}

To extend the activity of the *o*-QM intermediate (**6**) with diverse natural products, we incubated the chemical synthesized hydroxyclovatol (**9**) with 102 reactants from different substance classes (**Table 3**).^{174,213} Both hydroxyclovatol and reactants at a final concentration of 0.4 mM in 50 μ L H₂O were incubated at 25 °C for 16 h without pH adjustment. Encouraged by the clavatol-flavanone adduct isolated from *Penicillium griseoroseum*,¹⁹⁹ sixteen flavonoids including catechin were first screened with **9** under mild conditions. Fifteen of them revealed product peaks with [M+H]⁺ ions being 178 Da larger than the corresponding reactants. Masses of products harboring two clavatol units were also detected in eight cases. Subsequently, incubation of hydroxyclovatol with other phenolic substances including hydroxynaphthalenes, coumarins, xanthenes, anthraquinones, phloroglucinol derivatives and phenolic acids were carried out in similar way as mentioned above. Products were detected in incubation mixtures of nine of the eleven tested hydroxynaphthalenes, proving hydroxynaphthalenes to be suitable partners for coupling with the *o*-QM. Five of the tested coumarins with 4-hydroxycoumarin as an exception, six xanthenes and four anthraquinones were relatively poor Michael donors to couple with the *o*-QM and gave no product or only trace amount of products in their reaction mixtures. Clavatol-containing products with 10 % to 55 % conversion were detected in incubation mixtures of most selected phloroglucinol derivatives except for chalcone butein, suggesting that phloroglucinols are the most favorable nucleophiles to *o*-QM. Among selected phenolic acids, products were detectable in three of the nine selected nitrogen-free benzoic acids. No product from hydroxyphenyl acetic acids, propionic acids and acrylic acids as reactants was observed by LC-MS analysis.

RESULTS AND DISCUSSION

Table 3. Structures of tested reactants with hydroxyclovatol (**9**) from diverse subgroups

groups of reactants	total tested numbers	reactant numbers with detectable clavatul-containing products			no detectable product	
		conversions 10%-55%	conversions 1%-10%	detected only by EIC		
flavonoids including catechin		16	7	5	3	1
hydroxynaphthalenes		11	5	4	0	2
coumarins		5	1	0	2	2
xanthenes		6	0	5	0	1
anthraquinones		4	0	0	2	2
phloroglucinol derivatives		9	8	0	1	0
phenolic acids		10	3	1	0	6
indole derivatives		12	9	1	2	0
tryptophan-containing cyclic dipeptides		8	7	1	0	0
tyrosine-containing cyclic dipeptides		2	0	0	0	2
tyrosine analogues		8	3	0	5	0
quinolines		9	4	1	4	0
other tested reactants		conversion (%)				
2-aminobenzyl alcohol		28				
tris(hydroxymethyl)aminomethane (Tris)		35				

Afterwards, the identification of the clavatul-indole adduct communol B triggered our interest to probe the reactivity of *o*-QM (**6**) with indole derivatives. The incubation mixture of hydroxycavatul with indole derivatives showed the coupling products of up to 49 % conversion, while the replacement of nitrogen of the indole ring by sulfur or the methylation at N1-position reduced the activity (**Table 3**). Other nitrogen-containing reactants including cyclic dipeptides, tyrosine analogues and quinolines were also incubated with hydroxycavatul (**9**) under mild conditions. In the cases of eight tested tryptophan-containing cyclic dipeptides, all incubation mixtures showed coupling product formation with 9 to 29 % conversion. However, no product was detected in the incubation mixtures with *cyclo*-L-Tyr-L-Tyr and *cyclo*-L-Ser-L-Tyr as reactants. Furthermore, L-tyrosine and its analogues are relatively poor reaction partners coupling with clavatul. All quinolines serve as Michael donors to couple with the *o*-QM (**6**). In addition, a nitrogen-containing phenolic acid, 2-aminobenzoic acid, showed clavatul coupling product with the conversion of 42 %. Product peaks of hydroxycavatul with 2-aminobenzyl alcohol and tris(hydroxymethyl)aminomethane (Tris) were also observed by LC-MS analysis with conversion of up to 35 %.

Taken together, among the 102 tested reactants from diverse groups (**Table 3**), clavatul coupling products were detected in 86 cases under mild conditions. Product formation with 10 to 55 % conversion was observed for 49 reactants at 25 °C for 16 h. To facilitate the product isolation for structural elucidation, reactions mentioned above were carried out at 95 °C for 30 min, leading to generally 2 to 10-fold higher accumulation of the coupling products. Product formation with 30 to 99 % conversion was achieved for 58 reactants. Therefore, large scaled reactions of hydroxycavatul (**9**) with 23 reactants were further carried out at either 25 °C or 95 °C, resulting in the isolation of 32 products (**Figure 21**).

Structural elucidation proved that the majority of the coupling products are with a clavatul unit attached to the *ortho*- or *para*-position of a phenolic hydroxyl group at the benzene ring and or C2 or C3-position of the indole skeleton (**Figure 21**). Representatively, **24a** and **41** are examples for the attachment of a clavatul moiety onto the *para*-position of a hydroxyl group. Correlations of the methylene group to different aromatic carbons in the HMBC spectra supported the linkage between the clavatul part and meta-dihydroxylated benzene ring, such as flavonoids with a 5,7-dihydroxyl feature mainly leading to C8-adducts (**21**, **22a**, and **23a**). The C6-adduct **23b** as a byproduct from the reaction mixture of (+)-catechin with hydroxycavatul is an analogue of isopilosanol A–C.^{214,215} In analogy, **25** and **27** were identified as products of hydroxycavatul with 1,3-dihydroxynaphthalene/xanthone. These structures suggest that the clavatul-containing flavanone formation from *P. griseoroseum* might be the non-enzymatic event of incorporation of a clavatul unit into the exogenously fed flavanone.¹⁹⁹ Additionally, formation of **26** by the linkage between the clavatul unit and the α -pyrone moiety suggests that communol A from *P. commune* could be formed in a similar way.²⁰⁰ Anthraquinone and phloroglucinol derivatives harboring three hydroxyl groups at the benzene ring conjugated with a clavatul also via C-C bonds (**28**, **29**, **30**, **31**, and **32**). Indole

RESULTS AND DISCUSSION

derivatives including tryptophan-containing cyclic dipeptides linked with clavatul moiety mainly via C2-position of the indole skeleton to *o*-QM (**33**, (\pm)**34a**, **35**, **36**, **37**, **38a** and **39a**), indicating similar conjugation of communal B.²⁰⁰ C3-adducts were found in the case of *cyclo*-L-Trp-L-Trp and (*R*)-benzodiazepinedione, resulting in **38b** and **39b**. Only a few coupling products including (\pm)**34b**, **42b**, **42c**, and **43** were obtained via C-N bond formation. In addition, a *cyclo*-L-Trp-L-Trp derivative and a 2-aminobenzoic acid derivative carrying two clavatul units (**38c** and **42c**) were also identified. After structural elucidation, the obtained clavatul-containing products were screened for their biological activities. Detailed evaluation of the α -glucosidase inhibitory activity revealed the clavatul-coupling products **21**, **24a**, **25**, **27**, **35** and **40** showed clear inhibition, while their precursors showed no activity.

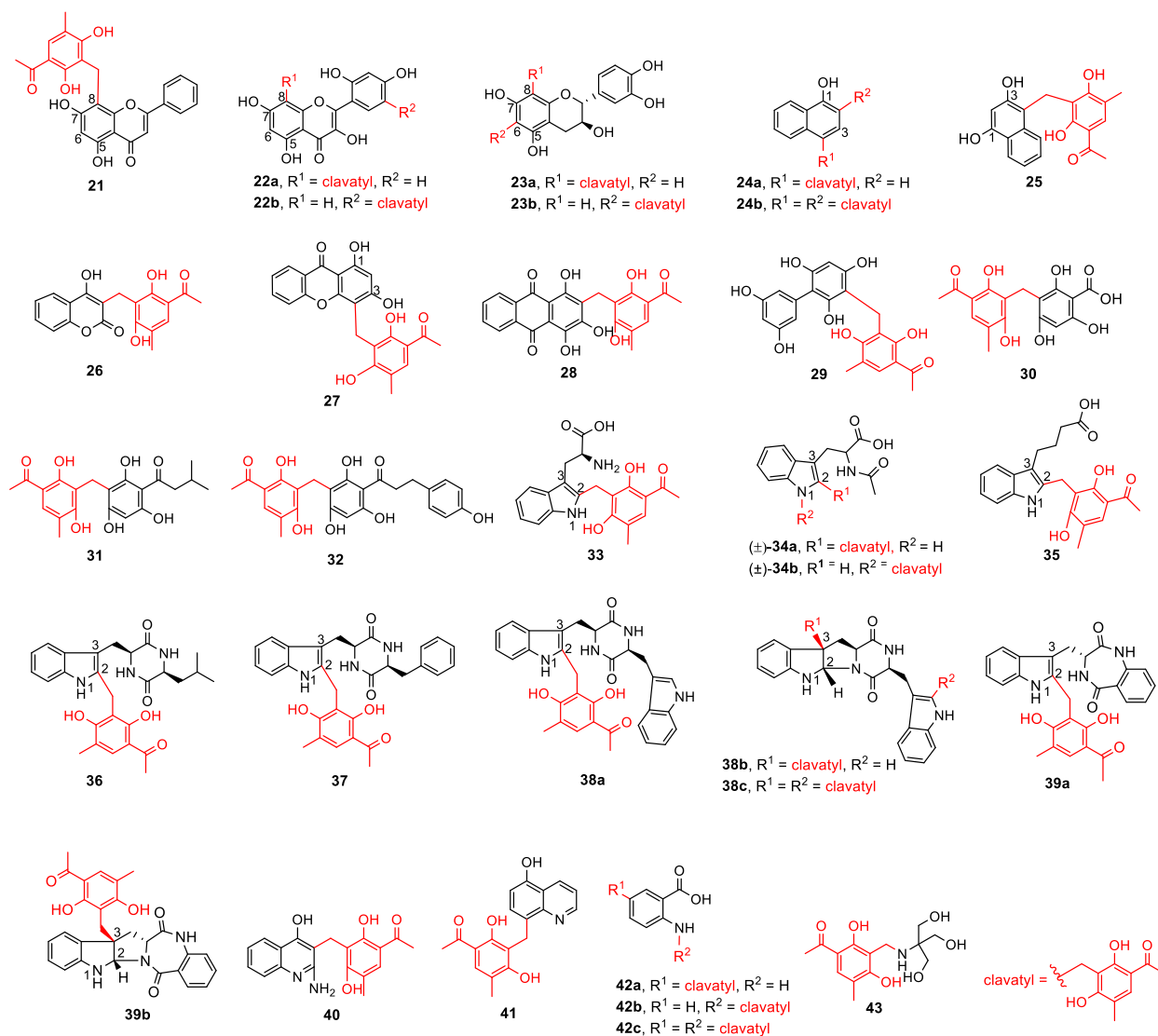


Figure 21. Isolated structures of diverse reactants coupling with *o*-QM intermediate

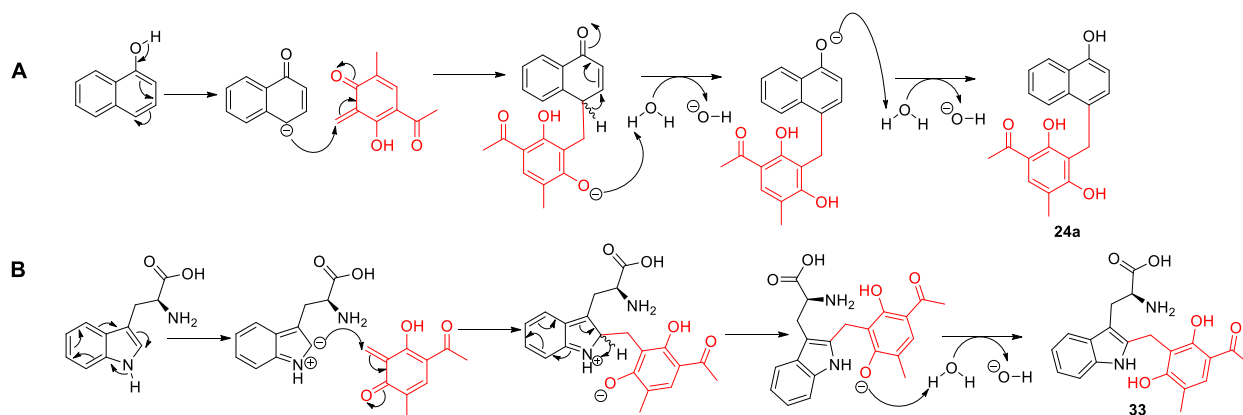


Figure 22. Reaction mechanisms of different nucleophile additions to the *o*-QM intermediate

In summary, the active form of clavatul, *o*-QM (**6**), generated from hydroxycavatul in an aqueous system was proposed to act as the Michael acceptor to initiate the non-enzymatic additions (**Figure 22**). It was demonstrated that the *o*-QM (**6**) can accept diverse natural or natural product-like compounds as nucleophiles under mild conditions to yield more clavatul-containing products. The clavatul moiety was mainly attached via C-C bonds to the *ortho*- or *para*-position of phenolic hydroxyl/amino groups. Represented by 1-naphthol, the incorporation of clavatul moiety was completed via 1,4-Michael addition to the *para*-position of hydroxyl group (**Figures 22A**). The conjugation between the clavatul unit and indole skeleton indicates that the electron transfer in the indole ring enabled the Michael addition mainly from C2 to the electrophilic methylene group of the *o*-QM (**6**) (**Figure 22B**). Additional C-N bond formation was also found in a few cases. It can be concluded that the cross-coupling between the nucleophiles and the *o*-QM (**6**) occurs preferentially via C-C bond formation. These results provide new insight into the non-enzymatic events in the natural product formation. It can be expected that more clavatul-containing compounds will be found in the near future from natural sources.

For details on this work, please see the publication (section 4.3)

Ge Liao*, **Jie Fan***, Lena Ludwig-Radtke, Katja Backhaus, and Shu-Ming Li (2020), Increasing structural diversity of natural products by Michael addition with *ortho*-quinone methide as the acceptor. *Journal of Organic Chemistry*, 85 (2), 1298-1307, DOI: 10.1021/acs.joc.9b02971 (*equal contribution)

4 Publications

4.1 Peniphenone and penilactone formation in *Penicillium crustosum* via 1,4-Michael additions of *ortho*-quinone methide from hydroxyclovatol to γ -butyrolactones from crustosic acid.

Peniphenone and Penilactone Formation in *Penicillium crustosum* via 1,4-Michael Additions of *ortho*-Quinone Methide from Hydroxylavatul to γ -Butyrolactones from Crustosic Acid

Jie Fan,^{†,§} Ge Liao,^{†,§} Florian Kindinger,[†] Lena Ludwig-Radtke,[†] Wen-Bing Yin,^{‡,§} and Shu-Ming Li^{*,†,§}

[†]Institut für Pharmazeutische Biologie und Biotechnologie, Philipps-Universität Marburg, Robert-Koch-Strasse 4, Marburg 35037, Germany

[‡]State Key Laboratory of Mycology, Institute of Microbiology, Chinese Academy of Sciences, Beijing 100101, China

Supporting Information

ABSTRACT: Penilactones A and B consist of a γ -butyrolactone and two clavatul moieties. We identified two separate gene clusters for the biosynthesis of these key building blocks in *Penicillium crustosum*. Gene deletion, feeding experiments, and biochemical investigations proved that a nonreducing PKS ClaF is responsible for the formation of clavatul and the PKS-NRPS hybrid TraA is involved in the formation of crustosic acid, which undergoes decarboxylation and isomerization to the predominant terrestric acid. Both acids are proposed to be converted to γ -butyrolactones with involvement of a cytochrome P₄₅₀ ClaJ. Oxidation of clavatul to hydroxylavatul by a nonheme Fe^{II}/2-oxoglutarate-dependent oxygenase ClaD and its spontaneous dehydration to an *ortho*-quinone methide initiate the two nonenzymatic 1,4-Michael addition steps. Spontaneous addition of the methide to the γ -butyrolactones led to peniphenone D and penilactone D, which undergo again stereospecific attacking by methide to give penilactones A/B.

Penilactones A (1) and B (2) (Figure 1A) are rare fungal metabolites and were first isolated from *Penicillium crustosum* PRB-2.¹ Together with their putative precursors peniphenone D (3) and penilactone D (4) (Figure 1A), they were also identified in other *Penicillium* species.^{2–4} Feeding experiments suggested that 1 and 2 are derived from acetyl-CoA and L-malic acid (Figure 1B).¹ It was proposed that 1 and 2 are formed by 1,4-Michael additions of two clavatul (5) molecules in its active form *ortho*-quinone methide (6) with a γ -butyrolactone (tetronic acid), i.e. (*R*)-5-methyl (7) or (*S*)-5-carboxymethyltetronic acid (8).^{1,2} This hypothesis was confirmed by a biomimetic synthesis.^{5–7} Acetate of hydroxylavatul (9) instead of 5 was used at 110 °C for the synthesis. Hydroxylavatul methyl ether (10) was also isolated from *P. crustosum*.³

5 can be considered as a polyketide synthase (PKS) product. However, the responsible enzyme is unknown before. Neither the direct precursor nor the biosynthesis of 7 and 8 has been reported. Michael addition as a thermodynamically controlled 1,4-addition of active methylenes to activated olefins such as α,β -unsaturated carbonyl derivatives⁸ are widely used in the

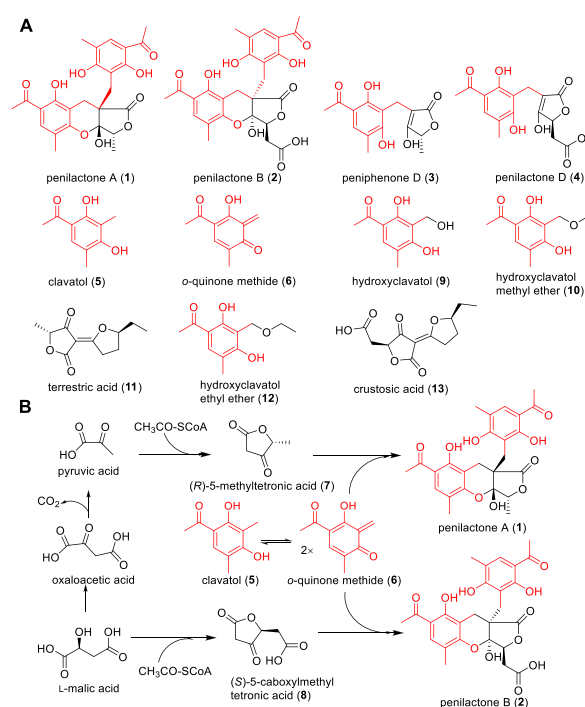


Figure 1. Metabolites from PRB-2 (A) and proposed biosynthetic routes to 1 and 2 (B).¹

chemical synthesis^{9–12} and also involved in the biosynthesis of natural products.¹³ However, the substrates, enzymes and conditions for Michael addition involved in the formation of 1–4 in nature have not been reported yet.

For secondary metabolite (SM) production in PRB-2, several culture conditions were tested and the extracts were analyzed on HPLC (Figure S1 in the Supplement Information (SI)). Three dominant peaks were detected in a 7 days-old PD culture (Figure S1), which were identified as 9, 10,¹⁴ and terrestric acid (11)¹⁵ after isolation and structure elucidation (see SI for details, NMR data and spectra are given in Tables S6–S10 and Figures S28–S45). The stereochemistry of 11 was confirmed by determination of its optical rotation and comparison with the published data.¹⁵ 9 has not been described before and therefore

Received: January 10, 2019

Published: February 27, 2019

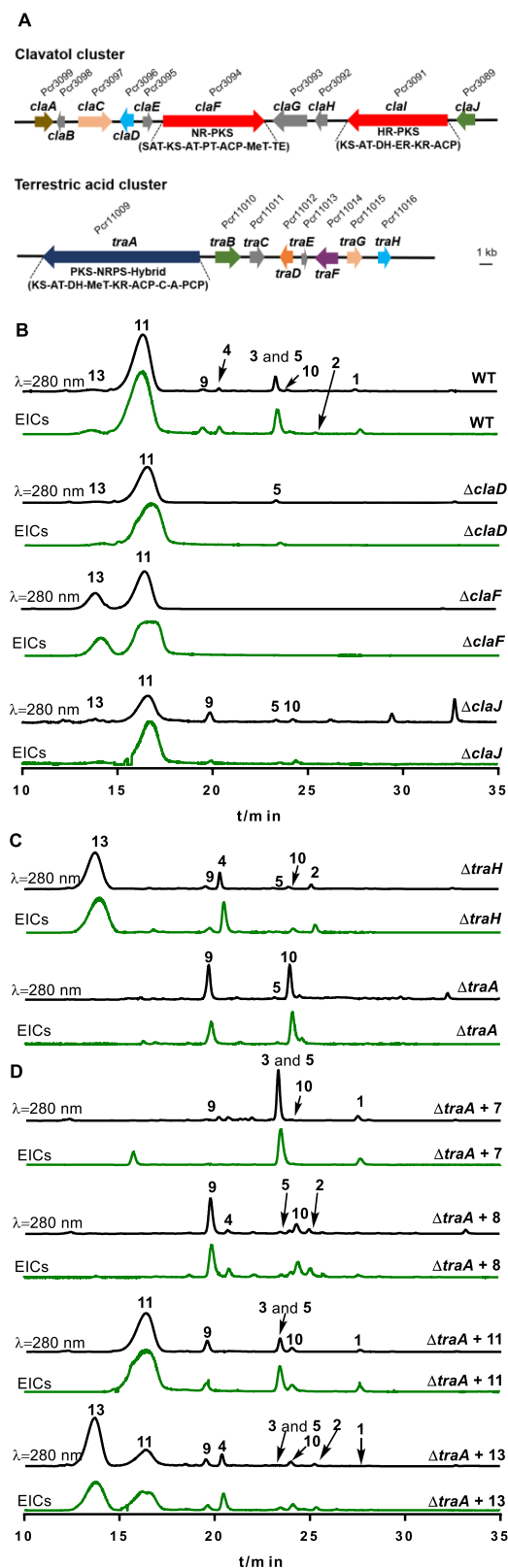


Figure 2. Schematic representation of clavatul and terrestric acid clusters in PRB-2 (A) and LC-MS results of deletion mutants (B and C) as well as $\Delta traA$ mutant fed with putative precursors (D). EICs refer $[M + H]^+$ ions of 1–6 and 11, 13 or $[M + Na]^+$ of 9 and 10 with tolerance ranges of ± 0.005 .

was confirmed by X-ray analysis (Table S11). Two additional minor peaks were proven to be 5 and hydroxylclavatul ethyl ether (12) (Figures 1A and S1).¹⁴

However, peniphenones and penilactones could only be detected in extracted ion chromatograms (EICs, data not shown). To increase their productivity, PRB-2 was cultivated in PD surface culture for 14 days. LC-MS analysis revealed clear accumulation of 1–4 (Figures 2, S1, and S2). A 30 days-old rice culture also accumulated 1–4 and was therefore used for isolation and structure elucidation by MS, NMR (Tables S6–S7 and Figures S28–S31), optical rotation, and CD spectra (Figures S46–S49).¹³ The CD spectra of 1 and 2 (Figures S46 and S47) correspond very well to those reported previously.¹ The stereochemistry of 3 and 4 was determined by chemical synthesis from 7 and 8 with known configuration at C-5 (Figure S21, see below for the formation of 3 from 7 and 4 from 8). Under these conditions, the production of 9 and 10 was strongly reduced. In comparison, 11 was detected as the predominant peak. Furthermore, a new peak was identified as carboxylated derivative of 11, termed crustosic acid (13) hereafter (Figures 1A, S44, and S45). 13 has an $[\alpha]_D^{20}$ value of -164.1 , while that of 11 at $+37.1$. The configuration of 13 was assigned by comparison with the optical rotation data of 5-methyl- and 5-carboxylmethyltetronic acids.¹⁶

For biosynthetic studies on 1 and 2, the genome of PRB-2 was sequenced and the draft genome sequence was used for prediction of putative gene clusters by using AntiSMASH.¹⁷ For gene inactivation, we established a gene replacement protocol using the split marker strategy and hygromycin B as selection marker, which significantly enhances the homologous recombination events at the target gene (Figure S3).¹⁸

Based on its aromatic character, 5 is expected to be assembled by a nonreducing PKS (NR-PKS).¹⁹ One of the six NR-PKS genes *pcr3094* within a 36.2 kbp large cluster (Figure 2A and Table S4) has a SAT-KS-AT-PT-ACP-MeT-TE domain structure (Abbreviations for PKS and NRPS domains as given before^{19,20}). It shares a sequence identity of 57.7% with CitS from *Monascus ruber*²¹ and 64.4% with EAW12049.1 from *Aspergillus clavatus* (Table S4). Deletion of *pcr3094*, termed *claF* (from the clavatul cluster) hereafter, completely abolished the production of 1–5, 9, and 10 (see SI for manipulation). The two tetronic acids 11 and 13 accumulated with much higher yields in the $\Delta claF$ mutant than in PRB-2 (Figures 2B, S4, and S6). Feeding 5 to the mutant restored the production of 1–4 and 9 (Figure S15).

To provide more evidence for the function of ClaF as a clavatul synthase, *pcr3094* was cloned into pYH-wA-pyrG and expressed in *A. nidulans*.^{22–24} The formation of 5 in the transformant JF11 was confirmed by LC-MS (Figure S20) and ¹H NMR analyses after isolation. These results proved that ClaF is responsible for 5 formation in the biosynthesis of 1–4 (Scheme 1).

To identify the genetic potential for 7 and 8, we focused on PKS-NRPS hybrid enzymes, because tetronic acids like carlosic acid are usually assembled by such enzymes.²⁵ Analysis of the draft sequence revealed the presence of a candidate gene *pcr11009*, termed *traA* (from the terrestric acid cluster), within a 33.6 kbp large cluster. TraA with a domain structure KS-AT-DH-MeT-KR-ACP-C-A-PCP (Figure 2A) shares a sequence identity of 69.6% with CaaA in the carlosic acid biosynthesis (Table S5).²⁵ Deletion of *traA* completely abolished the production of 1–4, indicating its involvement in the biosynthesis. As expected, 5, 9, and 10 were accumulated in the $\Delta traA$

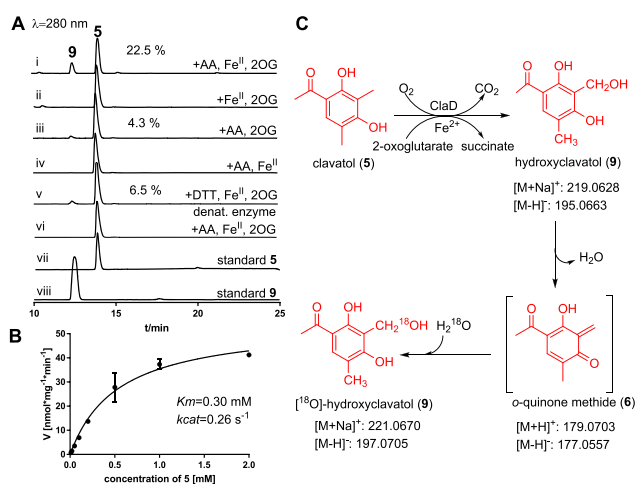
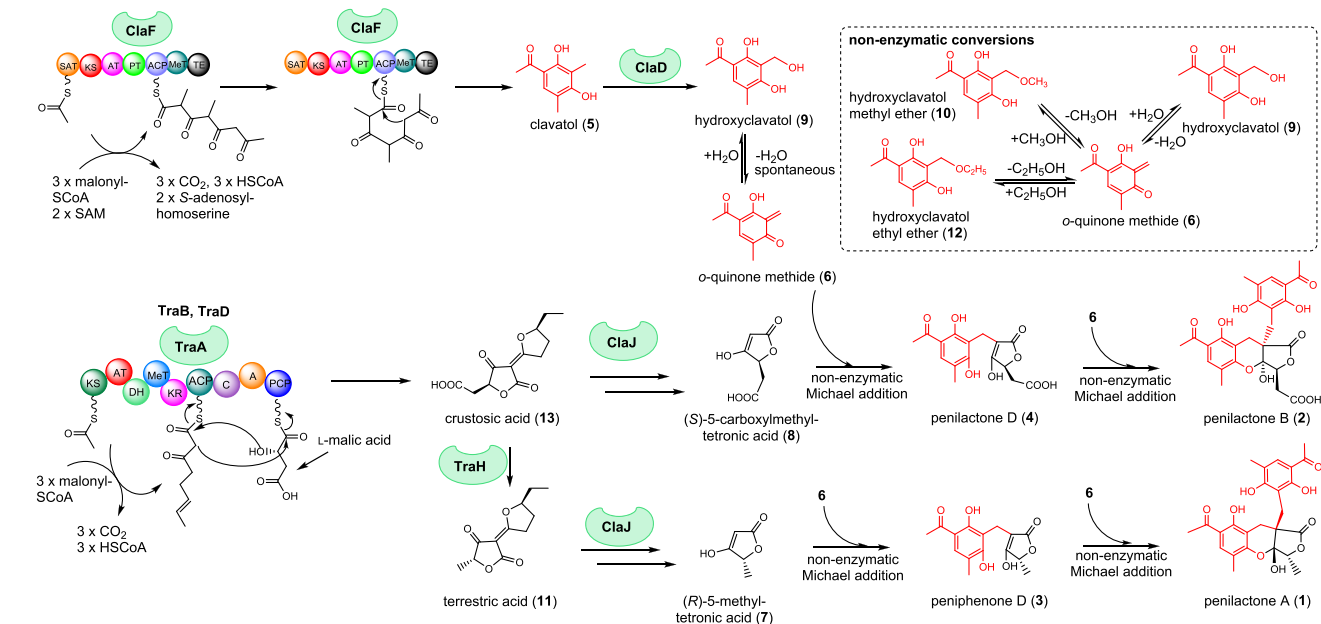
Scheme 1. Proposed Biosynthetic Pathways of Penilactones and Peniphenones in *P. crustosum*

Figure 3. Functional proof of ClaD as a nonheme Fe^{II}/2-oxoglutarate-dependent clavatul oxidase (A and B) and determination of the equilibration between 9 and 6 (C).

mutant (Figures 2C and S8). Surprisingly, the production of 11 and 13 were also totally blocked. To restore the production of 1–4, we chemically synthesized 7 and 8 (Figure S21)^{5,7,26,27} and fed them to the $\Delta traA$ mutant. LC-MS analysis revealed that feeding 7 restored the production of 1 and 3, but not 2 and 4. In contrast, 2 and 4, but not 1 and 3 were detected in the culture of $\Delta traA$ mutant fed with 8 (Figures 2C, S16, and S17). This proved that TraA is involved in the formation of 7 and 8, which cannot be converted to each other (Scheme 1).

For understanding the role of 11 and 13 for 1–4, they were isolated from $\Delta claF$ mutant and fed into $\Delta traA$ mutant. Feeding 11 only restored 1 and 3 production, while 1–4 were detected after feeding with 13 (Figures 2C, S18, and S19). More interestingly, 11 was also restored after feeding with 13, but not *vice versa* (Figure 2D). This proved that 13 is the precursor of both 8 and 11. 11 serves then as a precursor of 7 (Scheme 1).

It can be concluded that 13 is the product of TraA with or without other enzymes and mainly converted to the

predominant product 11 in PRB-2. Only small amounts of 11 and 13 undergo degradation to 7 and 8 for the formation of 1–4 (Figure 2D and Scheme 1).

Having the both backbone genes/enzymes identified, we intended to investigate the conversion of 13 to 8 and 11, 11 to 7, and the metabolism of 5. Inactivation of the oxygenase gene *traH* abolished the production of 1, 3, and 11, confirming its involvement in the decarboxylation and isomerization of 13 to 11 (Figures 2C and S13). In the deletion mutants of the cytochrome P₄₅₀ *traB* and the dehydrogenase *traD*, no accumulation of 11, 13, or 1–4 was detected (Figures S9 and S10), proving their roles in the 13 formation (Scheme 1). Deletion of *traE* and *traF* did not result in significant changes in SM production (Figures S11 and S12).

Regarding Michael addition, we presumed a more active intermediate than 5 for the formation of 6. Detailed inspection of the *cla* cluster (Figure 2A, Table S4) revealed the presence of genes coding for an oxygenase (*claD*) and a cytochrome P₄₅₀ (*claJ*). ClaD comprises 338 amino acids and shares a sequence identity of 53.8% with CitB in the citrinin biosynthesis.²¹ It also contains the typical conserved 2-His-1-Asp ion-binding triad (His₁₈₄, His₂₀₂ and Asp₁₈₇) of nonheme Fe^{II}/2-oxoglutarate-dependent oxygenases (Figure S22). Deletion of *claD* abolished the production of 1–4 and 9, whereas 5 was clearly accumulated (Figures 2B and S5). Feeding 9 in the $\Delta claD$ mutant restored the production of 1–4 (Figure S14), proving its role in the conversion of 5 to 9.

For biochemical characterization, *claD* was amplified and cloned into pET28a (+). The purified ClaD (Figure S23) was used for incubation with 5 in the presence of ascorbate (AA), Fe[(NH₄)₂(SO₄)₂], and 2-oxoglutarate (2OG).^{28,29} HPLC analysis confirmed the oxidation of 5 to 9 with a conversion yield of 22.5% after incubation with 2 μg protein at 37 °C for 30 min (Figure 3A). Nearly no consumption of 5 was detected in the assays without ascorbate or 2-oxoglutarate. Replacing ascorbate by dithiothreitol (DTT) or without additional Fe^{II} reduced the activity significantly. These results proved that ClaD acts as a nonheme Fe^{II}/2-oxoglutarate-dependent oxygenase and oxidizes 5 to yield 9. Determination of kinetic parameters

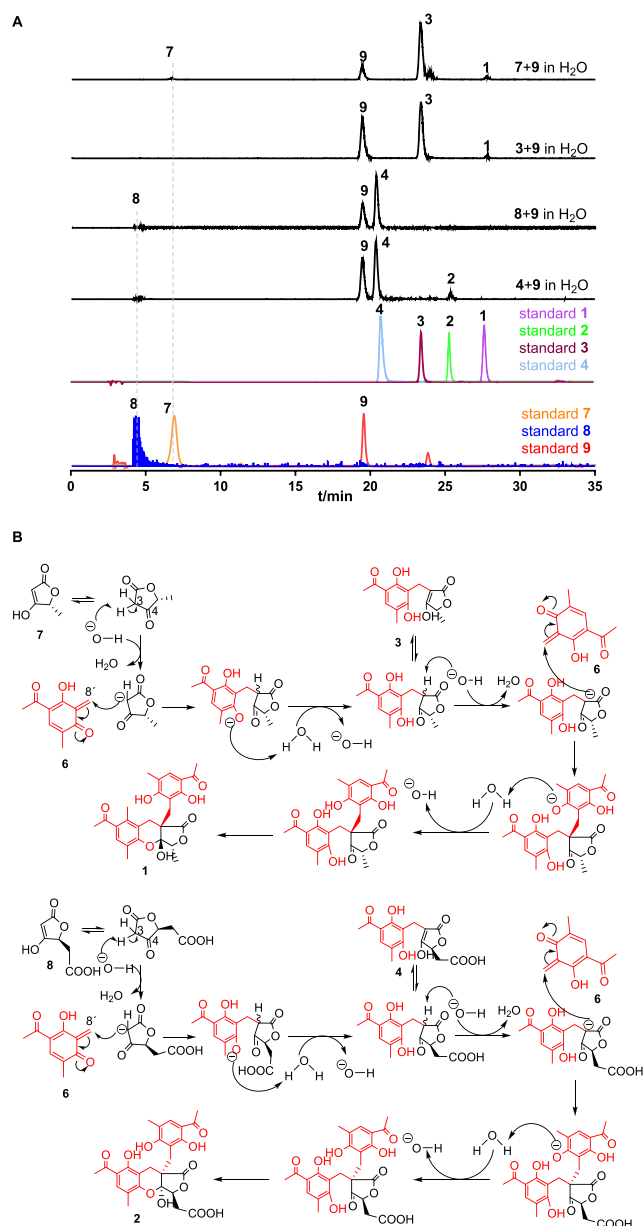


Figure 4. Nonenzymatic formation of penilactones and peniphenone. (A) LC-MS analysis of 48 h-incubation mixtures. Absorptions at 254 nm (1–4, 9) or EICs (7 and 8) are illustrated. (B) Proposed mechanism of nonenzymatic formation of 1–4 via Michael addition.

gave a K_M of 0.30 mM toward 5 and a turnover number (k_{cat}) of 0.26 s^{-1} (Figure 3B).

To prove the conversion between 9 and 6, 9 was incubated in H_2O and H_2^{18}O at 25°C for 16 h. MS data in positive and negative modes confirmed the incorporation of ^{18}O into 9 and therefore the equilibration (Figures 3C and S24).

Claj shares clear sequence homology with fungal cytochrome P_{450} enzymes, e.g. 42.0% identity with BAJ04372.1 from *Aspergillus oryzae*.³⁰ Deletion of *claj* resulted in the abolishment of 1–4 (Figures 2B and S7), but still retained the production of 5, 9, 11, and 13. This indicates its role in the C–C double bond cleavage of 11 and 13 (Scheme 1). However, Claj could also catalyze the connection of the two building blocks via Michael addition.

For preparing feeding experiments in $\Delta claj$, we carried out control incubations of 7 with 9 and 8 with 9 in water at 25°C ,

which delivered surprising results, i.e. the nonenzymatic Michael addition under these mild conditions (Figure 4A). In the first combination, 3 was detected as the major and 1 as a minor product, while 4 as the major and 2 as a minor product in the case of 8 with 9. When 3 and 4 were incubated with 9, 1 and 2 were detected (Figure 4A). Formation of 3 and 4 is time- and pH-dependent (Figures S25 and S26). 3 and 4 are formed under neutral or acidic conditions. When pH values were higher than 5.0, diclavato³ was also detected (Figure S26). It is obvious that the active intermediate 6 can be easily formed from 9 in aqueous system and initiates the Michael additions (Figure 4B), which was confirmed by incubation of 9, 10, and 12 in different solvents. They are stable in acetonitrile. Alcohols determined the end products of 6 (Figure S27, Scheme 1). All these results indicate that Claj is likely not involved in the Michael addition, probably in the conversion of 11 to 7 and 13 to 8 (Scheme 1).

Taken together, 1–4 are formed by enzymes from independent pathways of two separate gene clusters (Scheme 1). The *tra* cluster assembles 13, which is converted to 11. Both acids deliver the two γ -butyrolactones 7 and 8. The *cla* cluster provides the highly active 6 by a spontaneous dehydration of 9. This initiates the two step nonenzymatic Michael additions by the intermolecular nucleophile attacking of 6 to 7 or 8 and subsequent reaction with 3 and 4. Thus, this study provides an excellent example for SMs with complex structures that are formed by enzymes from different pathways and by combination of enzymatic and nonenzymatic reactions.

■ ASSOCIATED CONTENT

Supporting Information

The Supporting Information is available free of charge on the ACS Publications website at DOI: 10.1021/jacs.9b00110.

Materials, experimental procedures, physicochemical properties and spectroscopic data (PDF)

Data for $\text{C}_{10}\text{H}_{12}\text{O}_4$ (CIF)

■ AUTHOR INFORMATION

Corresponding Author

*S.-M. Li. E-mail: shuming.li@staff.uni-marburg.de.

ORCID

Wen-Bing Yin: 0000-0002-9184-3198

Shu-Ming Li: 0000-0003-4583-2655

Author Contributions

[§]These authors contributed equally to this work.

Notes

The authors declare no competing financial interest.

■ ACKNOWLEDGMENTS

We thank Tianjiao Zhu (Ocean University of China, Qingdao) for providing strain PRB-2, Rixa Kraut, Stefan Newel, and Andreas Heine (University of Marburg) for taking MS, NMR spectra and X-ray crystal analysis, respectively. This project was financially funded in part by the Deutsche Forschungsgemeinschaft (DFG, German Research Foundation) – Li844/11-1 and INST 160/620-1 as well as the National Natural Science Foundation of China – 31861133004. Jie Fan (201507565006) and Ge Liao (201607565014) are scholarship recipients from the China Scholarship Council.

REFERENCES

- (1) Wu, G.; Ma, H.; Zhu, T.; Li, J.; Gu, Q.; Li, D. Penilactones A and B, two novel polyketides from Antarctic deep-sea derived fungus *Penicillium crustosum* PRB-2. *Tetrahedron* **2012**, *68*, 9745.
- (2) Li, H.; Jiang, J.; Liu, Z.; Lin, S.; Xia, G.; Xia, X.; Ding, B.; He, L.; Lu, Y.; She, Z. Peniphenones A-D from the mangrove fungus *Penicillium dipodomycicola* HN4-3A as inhibitors of *Mycobacterium tuberculosis* phosphatase MtpB. *J. Nat. Prod.* **2014**, *77*, 800.
- (3) Wu, G. *Studies on secondary metabolites of three different marine environment-derived fungi: structures and bioactivities*. Dissertation, Ocean University of China, 2014.
- (4) Sun, W.; Chen, X.; Tong, Q.; Zhu, H.; He, Y.; Lei, L.; Xue, Y.; Yao, G.; Luo, Z.; Wang, J.; Li, H.; Zhang, Y. Novel small molecule 11beta-HSD1 inhibitor from the endophytic fungus *Penicillium commune*. *Sci. Rep.* **2016**, *6*, 26418.
- (5) Spence, J. T.; George, J. H. Biomimetic total synthesis of entpenilactone A and penilactone B. *Org. Lett.* **2013**, *15*, 3891.
- (6) Pantin, M.; Brimble, M. A.; Furkert, D. P. Total synthesis of (-)-peniphenone A. *J. Org. Chem.* **2018**, *83*, 7049.
- (7) Spence, J. T.; George, J. H. Total synthesis of peniphenones A-D via biomimetic reactions of a common o-quinone methide intermediate. *Org. Lett.* **2015**, *17*, 5970.
- (8) Tokoroyama, T. Discovery of the Michael reaction. *Eur. J. Org. Chem.* **2010**, *2010*, 2009.
- (9) Wadhwa, P.; Kharbanda, A.; Sharma, A. Thia-Michael addition: An emerging strategy in organic synthesis. *Asian J. Org. Chem.* **2018**, *7*, 634.
- (10) Mather, B. D.; Viswanathan, K.; Miller, K. M.; Long, T. E. Michael addition reactions in macromolecular design for emerging technologies. *Prog. Polym. Sci.* **2006**, *31*, 487.
- (11) Zhang, Y.; Wang, W. Recent advances in organocatalytic asymmetric Michael reactions. *Catal. Sci. Technol.* **2012**, *2*, 42.
- (12) Nising, C. F.; Bräse, S. The oxa-Michael reaction: from recent developments to applications in natural product synthesis. *Chem. Soc. Rev.* **2008**, *37*, 1218.
- (13) Miyanaga, A. Michael additions in polyketide biosynthesis. *Nat. Prod. Rep.* **2019**, DOI: 10.1039/C8NP00071A.
- (14) Astudillo, L.; Schmeda-Hirschmann, G.; Soto, R.; Sandoval, C.; Afonso, C.; Gonzalez, M. J.; Kijjoo, A. Acetophenone derivatives from Chilean isolate of *Trichoderma pseudokoningii* Rifai. *World J. Microbiol. Biotechnol.* **2000**, *16*, 585.
- (15) Nukina, M. Terrestrial acid as a phytotoxic metabolite from *Pyricularia oryzae* Cavara. *Agric. Biol. Chem.* **1988**, *52*, 2357.
- (16) Clutterbuck, P. W.; Haworth, W. N.; Raistrick, H.; Smith, G.; Stacey, M. Studies in the biochemistry of micro-organisms: The metabolic products of *Penicillium charlesii* G. Smith. *Biochem. J.* **1934**, *28*, 94.
- (17) Weber, T.; Blin, K.; Duddela, S.; Krug, D.; Kim, H. U.; Bruccoleri, R.; Lee, S. Y.; Fischbach, M. A.; Müller, R.; Wohlleben, W.; Breitling, R.; Takano, E.; Medema, M. H. antiSMASH 3.0 - a comprehensive resource for the genome mining of biosynthetic gene clusters. *Nucleic Acids Res.* **2015**, *43*, W237.
- (18) Goswami, R. S. Targeted gene replacement in fungi using a split-marker approach. *Methods Mol. Biol.* **2012**, *835*, 255.
- (19) Cox, R. J. Polyketides, proteins and genes in fungi: programmed nano-machines begin to reveal their secrets. *Org. Biomol. Chem.* **2007**, *5*, 2010.
- (20) Miyanaga, A.; Kudo, F.; Eguchi, T. Protein-protein interactions in polyketide synthase-nonribosomal peptide synthetase hybrid assembly lines. *Nat. Prod. Rep.* **2018**, *35*, 1185.
- (21) He, Y.; Cox, R. J. The molecular steps of citrinin biosynthesis in fungi. *Chem. Sci.* **2016**, *7*, 2119.
- (22) Yin, W. B.; Chooi, Y. H.; Smith, A. R.; Cacho, R. A.; Hu, Y.; White, T. C.; Tang, Y. Discovery of cryptic polyketide metabolites from dermatophytes using heterologous expression in *Aspergillus nidulans*. *ACS Synth. Biol.* **2013**, *2*, 629.
- (23) Li, W.; Fan, A.; Wang, L.; Zhang, P.; Liu, Z.; An, Z.; Yin, W.-B. Asperphenamate biosynthesis reveals a novel two-module NRPS system to synthesize amino acid esters in fungi. *Chem. Sci.* **2018**, *9*, 2589.
- (24) Chiang, Y. M.; Ahuja, M.; Oakley, C. E.; Entwistle, R.; Asokan, A.; Zutz, C.; Wang, C. C.; Oakley, B. R. Development of genetic dereplication strains in *Aspergillus nidulans* results in the discovery of aspercryptin. *Angew. Chem., Int. Ed.* **2016**, *55*, 1662.
- (25) Yang, X. L.; Awakawa, T.; Wakimoto, T.; Abe, I. Three acyltetric acid derivatives: noncanonical cryptic polyketides from *Aspergillus niger* identified by genome mining. *ChemBioChem* **2014**, *15*, 1578.
- (26) Adrian, J.; Stark, C. B. Total synthesis of muricadienin, the putative key precursor in the solamin biosynthesis. *Org. Lett.* **2014**, *16*, 5886.
- (27) Stebbins, N. D.; Yu, W.; Uhrich, K. E. Enzymatic polymerization of an ibuprofen-containing monomer and subsequent drug release. *Macromol. Biosci.* **2015**, *15*, 1115.
- (28) Ran, H.; Wohlgemuth, V.; Xie, X.; Li, S.-M. A non-heme FeII/2-oxoglutarate-dependent oxygenase catalyzes a double bond migration within a dimethylallyl moiety accompanied by hydroxylation. *ACS Chem. Biol.* **2018**, *13*, 2949.
- (29) Steffan, N.; Grundmann, A.; Afiyatullo, A.; Ruan, H.; Li, S.-M. FtmOx1, a non heme Fe(II) and alpha-ketoglutarate-dependent dioxygenase, catalyses the endoperoxide formation of verrucologen in *Aspergillus fumigatus*. *Org. Biomol. Chem.* **2009**, *7*, 4082.
- (30) Nazir, K. H. M. N. H.; Ichinose, H.; Wariishi, H. Molecular characterization and isolation of cytochrome P450 genes from the filamentous fungus *Aspergillus oryzae*. *Arch. Microbiol.* **2010**, *192*, 395.

SUPPORTING INFORMATION

Peniphenone and penilactone formation in *Penicillium crustosum* via 1,4-Michael additions of *ortho*-quinone methide from hydroxyclovatol to γ -butyrolactones from crustosic acid

Jie Fan,^{1,†} Ge Liao,^{1,†} Florian Kindinger,¹ Lena Ludwig-Radtke,¹ Wen-Bing Yin,² and Shu-Ming Li^{1,*}

¹ Institut für Pharmazeutische Biologie und Biotechnologie, Philipps-Universität Marburg, Robert-Koch-Strasse 4, Marburg 35037, Germany

² State Key Laboratory of Mycology, Institute of Microbiology, Chinese Academy of Sciences, Beijing 100101, China

[†]These authors contributed equally to this work.

Table content

Experiment Procedures	S5
1. Strains, media and growth conditions.....	S5
2. Genomic DNA isolation	S5
3. RNA isolation and cDNA synthesis.....	S5
4. Genome sequencing and sequence analysis	S5
5. PCR amplification, gene cloning and plasmid construction.....	S6
6. Genetic manipulation in <i>P. crustosum</i> and cultivation of deletion mutants	S6
7. Heterologous expression of <i>claF</i> in <i>A. nidulans</i>	S7
8. Precursor feeding in $\Delta claD$, $\Delta claF$, and $\Delta traA$-mutants.....	S7
9. Chemical synthesis of tetronic acids 7 and 8.....	S7
10. Overproduction and purification of ClaD	S7
11. <i>In vitro</i> assays of ClaD.....	S8
12. Proof of the existence of <i>ortho</i>-quinone methide	S8
13. Non-enzymatic formation of penilactones and peniphenones.....	S8
14. Large-scale fermentation, extraction and isolation of secondary metabolites ..	S8
15. HPLC and LC-MS analysis of secondary metabolites	S9
16. NMR analysis.....	S9
17. Measurement of optical rotations	S10
18. Circular dichroism (CD) spectroscopic analysis.....	S10
19. X-ray crystallographic analysis	S10
20. Physicochemical properties of the compounds described in this study	S10
Supplementary Tables	S12
Table S1. Strains used in this study.....	S12
Table S2. Plasmids used and constructed in this study.....	S13
Table S3. Primers used in this study	S14
Table S4. Putative functions of the genes from clavatul gene cluster.....	S17
Table S5. Putative functions of the genes from terrestric acid gene cluster	S18
Table S6. ¹H NMR data of compounds 1 and 2	S19
Table S7. ¹H NMR data of compounds 3 and 4	S20
Table S8. ¹H NMR data of compounds 5, 10 and 12	S21
Table S9. NMR data of compound 9.....	S22
Table S10. NMR data of 11 and 13	S23
Table S11. Crystal data and structure refinement of 9.....	S24
Figure S1. HPLC analysis of secondary metabolite profiles of <i>P. crustosum</i>.	S25
Figure S2. LC-MS analysis of secondary metabolites from a 14 days-old liquid PD surface culture of <i>P. crustosum</i>.	S26
Figure S3. Schematic representation of the gene deletion strategy in <i>P. crustosum</i>.	S27
Figure S4. PCR verification of deletion mutants of <i>P. crustosum</i>.	S28
Figure S5. LC-MS analysis of the metabolite profile of the $\Delta claD$-mutant.....	S29
Figure S6. LC-MS analysis of the metabolite profile of the $\Delta claF$-mutant.	S30
Figure S7. LC-MS analysis of the metabolite profile of the $\Delta claJ$-mutant.	S31
Figure S8. LC-MS analysis of the metabolite profile of the $\Delta traA$-mutant.	S32

Figure S9. LC-MS analysis of the metabolite profile of the $\Delta traB$ -mutant.	S33
Figure S10. LC-MS analysis of the metabolite profile of the $\Delta traD$ -mutant.	S34
Figure S11. LC-MS analysis of the metabolite profile of the $\Delta traE$ -mutant.....	S35
Figure S12. LC-MS analysis of the metabolite profile of the $\Delta traF$ -mutant.....	S36
Figure S13. LC-MS analysis of the metabolite profile of the $\Delta traH$ -mutant.	S37
Figure S14. LC-MS analysis of the metabolite profile of the $\Delta claD$ -mutant with and without feeding with 9.	S38
Figure S15. LC-MS analysis of the metabolite profile of the $\Delta claF$ -mutant with and without feeding with 5.	S39
Figure S16. LC-MS analysis of the metabolite profile of the $\Delta traA$ -mutant with and without feeding with 7.	S40
Figure S17. LC-MS analysis of the metabolite profile of the $\Delta traA$ -mutant with and without feeding with 8.	S41
Figure S18. LC-MS analysis of the metabolite profile of the $\Delta traA$ -mutant with and without feeding with 11.....	S42
Figure S19. LC-MS analysis of the metabolite profile of the $\Delta traA$ -mutant with and without feeding with 13.	S43
Figure S20. LC-MS analysis of the metabolite profile of different <i>A. nidulans</i> strains	S44
Figure S21. Chemical synthesis of the tetronic acids 7 and 8.....	S45
Figure S22. Sequence alignments of 2-OG-dependent oxygenases.....	S46
Figure S23. Analysis of ClaD on SDS PAGE.	S47
Figure S24. MS analysis of 9 after incubation in H ₂ O and in ¹⁸ O-enriched H ₂ ¹⁸ O...S48	S48
Figure S25. Time dependence of Michael addition reaction of 9 with 7 (A) or 8 (B).	S49
Figure S26. pH dependence on Michael addition reactions forming 3 and 4.	S50
Figure S27. HPLC analysis of 9, 10, and 12 after incubation in different solvents.S51	S51
Figure S28. ¹ H NMR spectrum of compound 1 in DMSO- <i>d</i> ₆ (500 MHz).	S52
Figure S29. ¹ H NMR spectrum of compound 2 in DMSO- <i>d</i> ₆ (500 MHz).	S53
Figure S30. ¹ H NMR spectrum of compound 3 in CDCl ₃ (500 MHz).....	S54
Figure S31. ¹ H NMR spectrum of compound 4 in DMSO- <i>d</i> ₆ (500 MHz).	S55
Figure S32. ¹ H NMR spectrum of compound 5 in CDCl ₃ (500MHz).....	S56
Figure S33. ¹ H NMR spectrum of compound 5 in DMSO- <i>d</i> ₆ (500MHz).	S57
Figure S34. ¹ H NMR spectrum of compound 7 in DMSO- <i>d</i> ₆ (400MHz).	S58
Figure S35. ¹ H NMR spectrum of compound 8 in CD ₃ OD (500MHz).....	S59
Figure S36. ¹ H NMR spectrum of compound 9 in CDCl ₃ (500MHz).....	S60
Figure S37. ¹ H NMR spectrum of compound 9 in DMSO- <i>d</i> ₆ (500MHz).	S61
Figure S38. ¹³ C NMR spectrum of compound 9 in CDCl ₃ (125MHz).	S62
Figure S39. HSQC spectrum of compound 9 in CDCl ₃	S63
Figure S40. HMBC spectrum of compound 9 in CDCl ₃	S64
Figure S41. ¹ H NMR spectrum of compound 10 in CDCl ₃ (500MHz).....	S65
Figure S42. ¹ H NMR spectrum of compound 11 in CDCl ₃ (500 MHz).....	S66
Figure S43. ¹ H NMR spectrum of compound 12 in CDCl ₃ (500 MHz).....	S67
Figure S44. ¹ H NMR spectrum of compound 13 in CDCl ₃ (500MHz).....	S68

Figure S45. ¹³ C NMR spectrum of compound 13 in CDCl ₃ (125MHz).....	S69
Figure S46. CD spectrum of penilactone A (1).....	S70
Figure S47. CD spectrum of penilactone B (2).	S70
Figure S48. CD spectrum of peniphenone D (3).....	S71
Figure S49. CD spectrum of penilactone D (4).	S71
Figure S50. CD spectrum of (<i>R</i>)-5-methyltetronic acid (7).	S72
Figure S51. CD spectrum of terrestric acid (11).	S72
Figure S52. CD spectrum of crustosic acid (13)	S73
Supplementary References	S74

Experiment Procedures

1. Strains, media and growth conditions

The fungal strains used in this study are summarized in Table S1. *Penicillium crustosum* strain PRB-2 was isolated from a deep-sea sediment collected in Prydz Bay at a depth of -526 m.¹ For detection of secondary metabolites (SMs), the strain PRB-2 was cultivated in PD medium (potato dextrose broth, Sigma) at 25°C. *Aspergillus nidulans* strains were grown at 37°C on GMM medium (1.0% glucose, 50 mL/L salt solution, 1 mL/L trace element solution, 1.6% agar) for sporulation and transformation with appropriate nutrition as required.²⁻⁴ The salt solution comprises (w/v) 12% NaNO₃, 1.04% KCl, 1.04% MgSO₄·7H₂O, and 3.04% KH₂PO₄. The trace element solution contains (w/v) 2.2% ZnSO₄·7H₂O, 1.1% H₃BO₃, 0.5% MnCl₂·4H₂O, 0.16% FeSO₄·7H₂O, 0.16% CoCl₂·5H₂O, 0.16% CuSO₄·5H₂O, 0.11% (NH₄)₆Mo₇O₂₄·4H₂O, and 5% Na₄EDTA. *Escherichia coli* DH5α and BL21(DE3) were grown in LB medium (1% NaCl, 1% tryptone, and 0.5% yeast extract) for standard DNA manipulation. 50 µg/mL carbenicillin or kanamycin were supplemented for cultivation of recombinant *E. coli* strains.

2. Genomic DNA isolation

The mycelia of *P. crustosum* and *A. nidulans* were collected in 2 mL Eppendorf tubes by centrifugation (13,000 rpm, 10 min). Four glass beads (2.85 mm in diameter) and 400 µL of LETS buffer (10 mM Tris-HCl pH 8.0, 20 mM EDTA pH 8.0, 0.5% SDS, and 0.1 M LiCl) were added to the tubes. After vigorous mixing for 4 min, 300 µL LETS buffer was added, and then the solution was treated with 700 µL phenol: chloroform: isoamyl alcohol (25: 24: 1). The genomic DNA was precipitated by addition of 900 µL absolute ethanol. After centrifugation at 13,000 rpm for 30 min and washing with 70% ethanol, the obtained DNA was dissolved in 50 µL distilled H₂O.

3. RNA isolation and cDNA synthesis

For isolation of RNA from *P. crustosum* PRB-2, the fungus was cultivated in liquid PD medium for 7 d and the cells were collected by centrifugation. RNA extraction was performed by using Fungal RNA Mini kit (VWR OMEGA bio-tek E.Z.N.A) according to the manufacturer's instruction. The ProtoScript II First Strand cDNA Synthesis kit (BioLabs) was used for cDNA synthesis with Oligo-dT primers.

4. Genome sequencing and sequence analysis

The genome of *P. crustosum* PRB-2 was sequenced by BerryGenomics (Beijing, China) using Nova-seq6000/X-ten (Illumina). Initial prediction and analysis of the clavato and terrestric acid biosynthetic gene clusters were carried out by using antiSMASH (<http://antismash.secondarymetabolites.org/>). Prediction of the open reading frames (ORFs) was performed with the online BLAST approaches (<http://blast.ncbi.nlm.nih.gov>). Detailed prediction for domain structures of PKS and PKS-NRPS hybrid enzymes was performed with the PKS/NRPS analysis tool (<http://nrps.igs.umaryland.edu/>). The genes in clavato and terrestric acid clusters were named as *claA-J* and *traA-H*, respectively (Figure 2A, Tables S4 and S5). The genomic DNA sequences of the clavato and terrestric acid clusters from *P. crustosum* PRB-2 reported in this study are available at GenBank under accession numbers MK360918 and MK360919, respectively.

5. PCR amplification, gene cloning and plasmid construction

Plasmids used in this study are listed in Table S2. The oligonucleotide sequences for PCR primers are given in Table S3. Primers were designed as described for gene deletion strategy (Figure S3) and synthesized by Seqlab GmbH (Göttingen, Germany). PCR amplification was carried out by using Phusion® High-Fidelity DNA polymerase from New England Biolabs (NEB) on a T100™ Thermal cycler from Bio-Rad. PCR reaction mixtures and thermal profiles were set as recommended by the manufacturer's instruction.

To identify the clavatul and terrestric acid biosynthetic gene clusters, we deleted genes of interest by using split-marker approach, which significantly enhances the homologous recombination events at the target genes.⁵ In this approach, two DNA fragments are constructed. One fragment comprises the upstream DNA region of the target gene and the two-third of the sequence of the selection marker at its 5'-end, e.g. the hygromycin B resistance gene in this study. The second fragment consists of two-third at the 3'-end of the selection marker and the downstream region of the target gene (Figure S3). 1.0–1.5 kbp upstream and downstream fragments of *claD*, *claF*, *claJ*, *traA*, *traB*, *traD*, *traE*, *traF* and *traH* were amplified from *P. crustosum* genomic DNA using the designed primers listed in Table S3.

To construct the plasmid for heterologous expression of *claF* in *A. nidulans*, an assembly approach based on the homologous recombination in *E. coli* was used.⁶ *claF* including its terminator of 480 bp was amplified from genomic DNA of *P. crustosum* by using primers A.n-claF-For/Rev (Table S3) and inserted into the corresponding sites of pYH-wA-pyrG with homologous flanking sequences of the *wA* gene.⁴ To construct the plasmid for expressing *claD* in *E. coli*, the coding region of *claD* was amplified by PCR from cDNA with the primers ClaD-28-For/Rev (Table S3). The DNA fragment was digested with BamHI and EcoRI and ligated into the same site of the expression vector pET-28a (+), yielding the expression plasmid pJF37, which was confirmed by sequencing (Seqlab GmbH).

6. Genetic manipulation in *P. crustosum* and cultivation of deletion mutants

Fresh spores of *P. crustosum* were inoculated into 30 mL LMM medium (1.0% glucose, 50 mL/L salt solution, 1 mL/L trace element solution, and 0.5% yeast extract) in 100 mL flask and incubated at 25°C and 230 rpm for germination. Mycelia were harvested after 11 h by centrifugation at 5,000 rpm for 10 min, and washed with distilled H₂O. The mycelia were then transferred into a 50 mL flask with 10 mL of osmotic buffer (1.2 M MgSO₄ in 10 mM sodium phosphate, pH 5.8) containing 50 mg lysing enzyme from *Trichoderma harzianum* (Sigma) and 20 mg yatalase from *Corynebacterium sp.* OZ-21 (OZEKI Co., Ltd.). After shaking at 30°C and 100 rpm for 2.5 h, the cells were transferred into a 50 mL falcon tube and overlaid gently with 10 mL of trapping buffer (0.6 M sorbitol in 0.1 M Tris-HCl, pH 7.0). After centrifugation at 4°C and 5,000 rpm for 10 min, the protoplasts were collected from the interface of the two buffer systems. The protoplasts were then transferred to a sterile 15 mL falcon tube and resuspended in 200 µL of STC buffer (1.2 M sorbitol, 10 mM CaCl₂, and 10 mM Tris-HCl, pH 7.5) for transformation.

The *via* PCR constructed gene deletion cassettes mentioned above were transformed into *P.*

crustosum by polyethylene glycol (PEG) mediated protoplast transformation. The DNA fragments were incubated with 100 μ L of the protoplasts for 50 min on ice. 1.25 mL of PEG solution (60% PEG 4000, 50 mM CaCl₂, 50 mM Tris-HCl, pH 7.5) was then added and gently mixed. After incubation at room temperature for 30 min, the mixture was transferred in 5 mL STC buffer and spread on plates with SMM bottom medium (1.0% glucose, 50 mL/L salt solution, 1 mL/L trace element solution, 1.2 M sorbitol, and 1.6% agar) containing 200 μ g/mL hygromycin B. SMM top medium (1.0% glucose, 50 mL/L salt solution, 1 mL/L trace element solution, 1.2 M sorbitol, and 0.8% agar) containing 100 μ g/mL hygromycin B was overlaid softly on the plates. Three days later, the transformants were transferred onto fresh PDA plates (PD medium with 1.6% agar) containing 200 μ g/mL hygromycin B for second selection. The obtained transformants were inoculated in PD medium for isolation of genomic DNA to verify the integrity, which was carried out by PCR amplification (Figure S4). After cultivation in PD liquid medium at 25°C for 14 days, the secondary metabolites of the deletion mutants were extracted with ethyl acetate, dissolved in MeOH and analyzed on LC-MS.

7. Heterologous expression of *claF* in *A. nidulans*

A. nidulans strain LO8030 was used as the recipient host.³ Fungal protoplast preparation and transformation were performed according to the method described previously.³ pJF18 containing the PKS gene *claF* was transformed into *A. nidulans* strain LO8030 to create the *claF* expression strain JF11. Potential transformants were verified by PCR using the primers *claF*-F/R (Table S3). Rice medium was used to cultivate the transformants (25°C, 7d) for LC-MS analysis of the secondary metabolite production.

8. Precursor feeding in Δ *claD*, Δ *claF*, and Δ *traA*-mutants

For feeding experiments, the precursors were dissolved in DMSO to give 1 M stock solutions. Adequate volumes of such solutions were then added to 10 mL of liquid PD cultures of respective deletion mutant, Δ *claF*, Δ *claD* or Δ *traA*, leading to final concentrations of 0.5 mM for clavatul (**5**) and hydroxyclavatul (**9**), 0.2 mM for terrestric acid (**11**), crustosic acid (**13**), (*R*)-5-methyltetronic acid (**7**), and (*S*)-5-carboxymethyltetronic acid (**8**). After further cultivation at 25°C for 14 d, the secondary metabolites were extracted with ethyl acetate, dissolved in MeOH and analyzed on LC-MS.

9. Chemical synthesis of tetronic acids **7** and **8**

For feeding experiments in deletion mutants, two tetronic acids (*R*)-5-methyltetronic acid (**7**) and (*S*)-5-carboxymethyltetronic acid (**8**) were synthesized chemically according to the published methods (Figure S21). **7** was synthesized in two steps from (*R*)-ethyl lactate⁷ and **8** in three steps from L-malic acid.^{8,9}

10. Overproduction and purification of ClaD

The expression plasmid pJF37 was constructed for *claD* expression in *E. coli* as mentioned above. The recombinant *E. coli* BL21(DE3) strain was cultivated in Terrific Broth medium (TB medium, with 2.4% yeast extract, 2.0% tryptone, 0.4% glycerol, 0.1 M phosphate buffer, pH 7.4) and *claD* expression was induced with 0.5 mM IPTG at 30°C for 6 h. The recombinant histidine-tagged ClaD was purified on Ni-NTA agaroses (Qiagen, Hilden) and proven on

SDS-PAGE (Figure S23).

11. *In vitro* assays of ClaD

To determine the enzyme activity toward clavatul (**5**), the enzyme assays (50 μ L) contained phosphate buffer (20 mM, pH 7.4), ascorbic acid (1 mM), clavatul (1 mM), $\text{Fe}[(\text{NH}_4)_2(\text{SO}_4)_2]$ (1 mM), 2-oxoglutarate (1 mM), glycerol (0.5–5%), DMSO (5%), and the purified recombinant ClaD (2 μ g). The enzyme assays were incubated at 37 °C for 30 min and terminated with one volume of acetonitrile. The reaction mixtures were centrifuged at 13,000 rpm for 30 min before further analysis on HPLC.

12. Proof of the existence of *ortho*-quinone methide

In order to provide evidence for the existence of *ortho*-quinone methide (**6**), hydroxycavatul (**9**) isolated from the fungal culture was dissolved in both H_2O and in ^{18}O -enriched H_2^{18}O . After incubation at room temperature for 16 h, the samples were analyzed by MS on positive and negative modes.

To prove their conversion *via* **6**, hydroxycavatul (**9**), hydroxycavatul methyl ether (**10**), and hydroxycavatul ethyl ether (**12**) were incubated in different solvents such as H_2O , acetonitrile, MeOH and EtOH at room temperature for 12 h. The mixtures were analyzed on HPLC by using method B.

13. Non-enzymatic formation of penilactones and peniphenones

To determine the non-enzymatic formation, hydroxycavatul (**9**) was incubated with (*R*)-5-methyltetronic acid (**7**) or (*S*)-5-carboxymethyltetronic acid (**8**) in H_2O at room temperature for 16 h. The dependence of the product formation on time (0, 5, 15, 30, 60, 120 min, and 24 h) was monitored on HPLC (method A) (Figure S25). pH dependence of the product formation was carried out by incubation in phosphate buffer saline (PBS, pH 3–10) for 12 h (Figure S26).

14. Large-scale fermentation, extraction and isolation of secondary metabolites

To isolate **5**, **9**, and **10–12**, *P. crustosum* PRB-2 spores were inoculated into 60x 250-mL flask containing 100 mL PD liquid medium each and incubated on a rotary shaker at 220 rpm and 25 °C for 7 d. The supernatant and mycelia were separated by filtration. The supernatant was extracted with equal volume of ethyl acetate for three times, and the mycelia were extracted with acetone. The acetone extract was concentrated under reduced pressure to afford an aqueous solution, and then extracted with ethyl acetate. The two ethyl acetate extracts were combined and evaporated under reduced pressure to give a crude extract (1.8 g). The crude extract was subjected to silica gel column chromatography by using stepwise gradient elution with the mixtures of $\text{CH}_2\text{Cl}_2/\text{MeOH}$ (100:1 to 20:1, v/v) to give eleven fractions (1–11). Fraction 3 eluted with $\text{CH}_2\text{Cl}_2/\text{MeOH}$ (80:1) was further purified on semi-preparative HPLC (ACN/ H_2O (70:30)) to yield clavatul (**5**) (15 mg), hydroxycavatul methyl ether (**10**) (7 mg) and hydroxycavatul ethyl ether (**12**) (4 mg). Hydroxycavatul (**9**) (17 mg) was obtained from fraction 7, which was eluted with $\text{CH}_2\text{Cl}_2/\text{MeOH}$ (40:1), by semi-preparative HPLC (ACN/ H_2O (60:40)). Fraction 8 eluted with $\text{CH}_2\text{Cl}_2/\text{MeOH}$ (20:1) was chromatographed over Sephadex LH-20

column and eluted with MeOH, resulting in terrestric acid (**11**) (40 mg).

To isolate **1–4**, *P. crustosum* PRB-2 was cultivated in 300x 250-mL flasks each containing 20 g rice, 30 mL H₂O, and 0.75 g soy flour at 25 °C for 30 days. The rice cultures were extracted with 15 L ethyl acetate and concentrated under reduced pressure to obtain a crude extract (35 g). The crude extract was applied to silica gel column chromatography and eluted with a stepwise gradient CH₂Cl₂/acetone (100:1, 50:1, 25:1, 19:1, and 1:1), yielding eight fractions (1–8). Subsequent elution with methanol gave 10 additional fractions (9–18). Fraction 4 was separated by repeated silica gel column chromatography with CH₂Cl₂/MeOH (50:1) and petroleum ether/EtOAc (1:1 and 1:6) as solvents to afford pure peniphenone D (**3**) (12 mg). Penilactone A (**1**) (7 mg) was obtained from fraction 7 by silica gel and Sephadex LH-20 column chromatography as well as by final purification on a semi-preparative HPLC (MeOH/H₂O (70:30) with 0.1% trifluoroacetic acid). In analogy, penilactone B (**2**) (5 mg) and penilactone D (**4**) (6 mg) were purified from fractions 12 and 18, respectively.

To isolate **13**, the Δ *claF*-mutant was cultivated in PD medium at 25°C for 14 d. The culture was extracted with ethyl acetate using the same procedure as mentioned above. 1.0 g crude extract was obtained from 4 L culture, and subjected to silica gel column chromatography by using petroleum ether/EtOAc (10:1, 3:1, 1:1, 1:3, 1:6) as elution solvents, giving 5 fractions (1–5). Pure **13** (20 mg) was obtained from fraction 5 after purification on Sephadex LH-20 column using MeOH as eluent.

15. HPLC and LC-MS analysis of secondary metabolites

Analysis of secondary metabolites was performed on an Agilent series 1200 HPLC (Agilent Technologies, Böblingen, Germany) with an Agilent Eclipse XDB-C18 column (150 × 4.6 mm, 5 μm). Water (A) and acetonitrile (B), both with 0.1% (v/v) formic acid, were used as solvents at flow rate of 0.5 mL/min. The substances were eluted with a linear gradient from 5–100% B in 15 min, then washed with 100% (v/v) solvent B for 5 min and equilibrated with 5% (v/v) solvent B for 5 min (method A) or with a linear gradient from 5–100% B in 40 min, then washed with 100% (v/v) solvent B for 5 min and equilibrated with 5% (v/v) solvent B for 10 min (method B). Absorptions at UV 280 nm were illustrated. Semi-preparative HPLC was performed on the same equipment with an Agilent Eclipse XDB-C18 column (9.4 × 250 mm, 5 μm) column and a flow rate of 2.5 mL/min.

LC-MS analysis was performed on an Agilent 1260 HPLC system equipped with a microTOF-Q III spectrometer (Bruker, Bremen, Germany) by using Multospher 120 RP18-5μ column (250 × 2 mm, 5 μm) (CS-Chromatographie Service GmbH) and method B for separation at flow rate of 0.25 mL/min. Electrospray positive or negative ionization mode was selected for determination of the exact masses. The capillary voltage was set to 4.5 kV and a collision energy of 8.0 eV. Sodium formate was used in each run for mass calibration. The masses were scanned in the range of m/z 100–1500. Data were evaluated with the Compass DataAnalysis 4.2 software (Bruker Daltonik, Bremen, Germany).

16. NMR analysis

NMR spectra were recorded on a JOEL ECA-500 MHz spectrometer (JEOL, Tokyo, Japan). All

spectra were processed with MestReNova 6.1.0 (Metrelab). Chemical shifts are referenced to those of the solvent signals. NMR data are given in Tables S6–S10 and spectra in Figures S28–S45.

17. Measurement of optical rotations

The optical rotation was measured with the polarimeter Jasco DIP-370 at 20°C using the D-line of the sodium lamp at $\lambda=589.3$ nm. Prior to the measurement, the polarimeter was calibrated with methanol as solvent.

18. Circular dichroism (CD) spectroscopic analysis

CD spectra were taken on a J-815 CD spectrometer (Jasco Deutschland GmbH, Pfungstadt, Germany). The samples were dissolved in methanol and measured in the range of 200–400 nm by using a 1 mm path length quartz cuvette (Hellma Analytics, Müllheim, Germany). The CD spectra are given in Figures S46–S52.

19. X-ray crystallographic analysis

Colorless crystals of hydroxyclovatol (**9**) were obtained in $\text{CH}_2\text{Cl}_2/\text{MeOH}$. Crystallographic data for **9** (Cu K α radiation) has been deposited in the Cambridge Crystallographic Data Centre with the deposition number CCDC 1883090 (Table S11). These data can be obtained free of charge via www.ccdc.cam.ac.uk/data_request/cif.

20. Physicochemical properties of the compounds described in this study

Penilactone A (**1**): Colorless solid; $[\alpha]_{\text{D}}^{20} = -14.8$ (*c* 0.25, MeOH); CD (MeOH) λ_{max} ($\Delta\epsilon$) 333 (-13.1), 295 (+28.2), 271 (-25.0), 240 (+17.2), 226 (-27.4) nm; HRMS (*m/z*): (ESI/[M + H]⁺) calcd. for $\text{C}_{25}\text{H}_{27}\text{O}_9$, 471.1650, found 471.1652.

Penilactone B (**2**): Colorless solid; $[\alpha]_{\text{D}}^{20} = +12.6$ (*c* 0.25, MeOH); CD (MeOH) λ_{max} ($\Delta\epsilon$) 335 (+9.6), 292 (-28.7), 270 (+18.9), 240 (-10.5), 227 (+11.4) nm; HRMS (*m/z*): (ESI/[M + H]⁺) calcd. for $\text{C}_{26}\text{H}_{27}\text{O}_{11}$, 515.1548, found 515.1570.

Peniphenone D (**3**): Colorless solid; $[\alpha]_{\text{D}}^{20} = +10.6$ (*c* 0.25, MeOH); CD (MeOH) λ_{max} ($\Delta\epsilon$) 254 (+2.4), 232 (-2.1), 200 (-3.0) nm; HRMS (*m/z*): (ESI/[M + H]⁺) calcd. for $\text{C}_{15}\text{H}_{17}\text{O}_6$, 293.1020, found 293.1040.

Penilactone D (**4**): Colorless solid; $[\alpha]_{\text{D}}^{20} = -15.9$ (*c* 0.20, MeOH); CD (MeOH) λ_{max} ($\Delta\epsilon$) 280 (-1.2), 242 (-3.0), 211 (+4.9) nm; HRMS (*m/z*): (ESI/[M + H]⁺) calcd. for $\text{C}_{16}\text{H}_{17}\text{O}_8$, 337.0918, found 337.0932.

Clavatol (**5**): Colorless solid; HRMS (*m/z*): (ESI/[M + H]⁺) calcd. for $\text{C}_{10}\text{H}_{13}\text{O}_3$, 181.0859, found 181.0860.

(*R*)-5-Methyltetronic acid (**7**): Yellow solid; ¹H NMR (400 MHz, DMSO-*d*6) δ 12.60 (s, 1H, 4-OH), 4.87 (s, 1H, H-3), 4.85 (q, *J* = 6.7 Hz, 1H, H-5), 1.33 (d, *J* = 6.7 Hz, 3H, H-6); $[\alpha]_{\text{D}}^{20} = -22.8$ (*c* 0.5, H₂O); CD (H₂O) λ_{max} ($\Delta\epsilon$) 309 (-9.3), 247 (+19.4) nm; HRMS (*m/z*): (ESI/[M + H]⁺) calcd. for $\text{C}_5\text{H}_7\text{O}_3$, 115.0390, found 115.0369.

(S)-5-carboxymethyltetronic acid (**8**): Yellow solid; ^1H NMR (500 MHz, CD_3OD) δ 5.18 (dd, $J = 8.8, 3.6$ Hz, 1H, H-5), 2.94 (dd, $J = 16.5, 3.6$ Hz, 1H, H-6a), 2.53 (dd, $J = 16.5, 8.8$ Hz, 1H, H-6b); $[\alpha]_{\text{D}}^{20} = -0.8$ (c 1.4, MeOH). HRMS (m/z): (ESI/[M + H] $^+$) calcd. for $\text{C}_6\text{H}_7\text{O}_5$, 159.0288, found 159.0272.

Hydroxyclovatol (**9**): Colorless crystal; HRMS (m/z): (ESI/[M + Na] $^+$) calcd. for $\text{C}_{10}\text{H}_{12}\text{NaO}_4$, 219.0628, found 219.0626. Crystallographic data for **9** (Cu K α radiation) has been deposited in the Cambridge Crystallographic Data Centre with the deposition number CCDC 1883090.

Hydroxyclovatol methyl ether (**10**): Colorless solid; HRMS (m/z): (ESI/[M + Na] $^+$) calcd. for $\text{C}_{11}\text{H}_{14}\text{NaO}_4$, 233.0784, found 233.0778.

Terrestric acid (**11**): Yellow oil; $[\alpha]_{\text{D}}^{20} = +37.1$ (c 0.80, MeOH); CD (MeOH) λ_{max} ($\Delta\epsilon$) 282 (+1.0), 234 (+2.8), 212 (+8.2) nm; HRMS (m/z): (ESI/[M + H] $^+$) calcd. for $\text{C}_{11}\text{H}_{15}\text{O}_4$, 211.0965, found 211.1003.

Hydroxyclovatol ethyl ether (**12**): Colorless solid; HRMS (m/z): (ESI/[M + Na] $^+$) calcd. for $\text{C}_{12}\text{H}_{16}\text{NaO}_4$, 247.0941, found 247.0959.

Crustosic acid (**13**): Yellow oil; $[\alpha]_{\text{D}}^{20} = -164.1$ (c 0.50, MeOH); CD (MeOH) λ_{max} ($\Delta\epsilon$) 272 (-11.2), 207 (-12.4) nm; HRMS (m/z): (ESI/[M + H] $^+$) calcd. for $\text{C}_{12}\text{H}_{15}\text{O}_6$, 255.0863, found 255.0876.

Supplementary Tables

Table S1. Strains used in this study

Strains	Genotype
Wild type	<i>Penicillium crustosum</i> PRB-2
Δ <i>claD</i>	Δ <i>claD</i> :: <i>hph</i> in <i>P. crustosum</i> PRB-2
Δ <i>claF</i>	Δ <i>claF</i> :: <i>hph</i> in <i>P. crustosum</i> PRB-2
Δ <i>claJ</i>	Δ <i>claJ</i> :: <i>hph</i> in <i>P. crustosum</i> PRB-2
Δ <i>traA</i>	Δ <i>traA</i> :: <i>hph</i> in <i>P. crustosum</i> PRB-2
Δ <i>traB</i>	Δ <i>traB</i> :: <i>hph</i> in <i>P. crustosum</i> PRB-2
Δ <i>traD</i>	Δ <i>traD</i> :: <i>hph</i> in <i>P. crustosum</i> PRB-2
Δ <i>traE</i>	Δ <i>traE</i> :: <i>hph</i> in <i>P. crustosum</i> PRB-2
Δ <i>traF</i>	Δ <i>traF</i> :: <i>hph</i> in <i>P. crustosum</i> PRB-2
Δ <i>traH</i>	Δ <i>traH</i> :: <i>hph</i> in <i>P. crustosum</i> PRB-2
<i>Aspergillus nidulans</i> LO8030 ^{2,3}	<i>pyroA4</i> , <i>riboB2</i> , <i>pyrG89</i> , <i>nkuA</i> :: <i>argB</i> , sterigmatocystin cluster (<i>AN7804-AN7825</i>) Δ , emericellamide cluster (<i>AN2545-AN2549</i>) Δ , asperfuranone cluster (<i>AN1039-AN1029</i>) Δ , monodictyphenone cluster (<i>AN10023-AN10021</i>) Δ , terrequinone cluster (<i>AN8512-AN8520</i>) Δ , austinol cluster part 1 (<i>AN8379-AN8384</i>) Δ , austinol cluster part 2 (<i>AN9246-AN9259</i>) Δ , F9775 cluster (<i>AN7906-AN7915</i>) Δ , asperthecin cluster (<i>AN6000-AN6002</i>) Δ
JF10	<i>pYH- wA -pyrG</i> in <i>A. nidulans</i> LO8030
JF11	<i>gpdA</i> :: <i>claF</i> :: <i>AfpYrG</i> in <i>A. nidulans</i> LO8030

Table S2. Plasmids used and constructed in this study

Plasmids	Description
pESC-URA	<i>Saccharomyces cerevisiae</i> shuttle vector.
pUChph	vector with hygromycin B (<i>hph</i>) resistance originate.
pET28a(+)	vector with T7 promoter, 6xHis tag, T7 terminator, kanamycin resistance.
p5HY	Two-third of the <i>hph</i> resistance gene at the 5'-end, originated from the pUChph and inserted into pESC-URA. For gene replacement using <i>hph</i> as selection marker.
p3YG	Two-third of the <i>hph</i> resistance gene at the 3'-end, originated from the pUChph and inserted into pESC-URA. For gene replacement using <i>hph</i> as selection marker.
pJF19 (p5HY- <i>claD</i>)	a 1012 bp US PCR fragment of <i>claD</i> from genomic DNA of <i>P. crustosum</i> PRB-2 inserted in p5HY.
pJF20 (p3YG- <i>claD</i>)	a 1008 bp DS PCR fragment of <i>claD</i> from genomic DNA of <i>P. crustosum</i> PRB-2 inserted in p3YG.
pJF40 (p5HY- <i>claF</i>)	a 1560 bp US PCR fragment of <i>claF</i> from genomic DNA of <i>P. crustosum</i> PRB-2 inserted in p5HY.
pJF41 (p3YG- <i>claF</i>)	a 1426 bp DS PCR fragment of <i>claF</i> from genomic DNA of <i>P. crustosum</i> PRB-2 inserted in p3YG.
pJF21 (p5HY- <i>claJ</i>)	a 1367 bp US PCR fragment of <i>claJ</i> from genomic DNA of <i>P. crustosum</i> PRB-2 inserted in p5HY.
pJF22 (p3YG- <i>claJ</i>)	a 1259 bp DS PCR fragment of <i>claJ</i> from genomic DNA of <i>P. crustosum</i> PRB-2 inserted in p3YG.
pJF38 (p5HY- <i>traA</i>)	a 1500 bp US PCR fragment of <i>traA</i> from genomic DNA of <i>P. crustosum</i> PRB-2 inserted in p5HY.
pJF39 (p3YG- <i>traA</i>)	a 1496 bp DS PCR fragment of <i>traA</i> from genomic DNA of <i>P. crustosum</i> PRB-2 inserted in p3YG.
pJF56 (p5HY- <i>traB</i>)	a 1388 bp US PCR fragment of <i>traB</i> from genomic DNA of <i>P. crustosum</i> PRB-2 inserted in p5HY.
pJF57 (p3YG- <i>traB</i>)	a 1067 bp DS PCR fragment of <i>traB</i> from genomic DNA of <i>P. crustosum</i> PRB-2 inserted in p3YG.
pJF54 (p5HY- <i>traD</i>)	a 1170 bp US PCR fragment of <i>traD</i> from genomic DNA of <i>P. crustosum</i> PRB-2 inserted in p5HY.
pJF55 (p3YG- <i>traD</i>)	a 1139 bp DS PCR fragment of <i>traD</i> from genomic DNA of <i>P. crustosum</i> PRB-2 inserted in p3YG.
pJF52 (p5HY- <i>traE</i>)	a 1130 bp US PCR fragment of <i>traE</i> from genomic DNA of <i>P. crustosum</i> PRB-2 inserted in p5HY.
pJF53 (p3YG- <i>traE</i>)	a 1027 bp DS PCR fragment of <i>traE</i> from genomic DNA of <i>P. crustosum</i> PRB-2 inserted in p3YG.
pJF50 (p5HY- <i>traF</i>)	a 977 bp US PCR fragment of <i>traF</i> from genomic DNA of <i>P. crustosum</i> PRB-2 inserted in p5HY.
pJF51 (p3YG- <i>traF</i>)	a 1031 bp DS PCR fragment of <i>traF</i> from genomic DNA of <i>P. crustosum</i> PRB-2 inserted in p3YG.
pJF48 (p5HY- <i>traH</i>)	a 1101 bp US PCR fragment of <i>traH</i> from genomic DNA of <i>P. crustosum</i> PRB-2 inserted in p5HY.
pJF49 (p3YG- <i>traH</i>)	a 1114 bp DS PCR fragment of <i>traH</i> from genomic DNA of <i>P. crustosum</i> PRB-2 inserted in p3YG.
pYH-wA-pyrG	<i>URA3</i> , <i>wA</i> flanking, <i>AfpyrG</i> , <i>Amp</i>
pJF18	<i>pYH-wA-claF</i> ; a 8119 bp fragment of <i>claF</i> with its terminator from genomic DNA of <i>P. crustosum</i> PRB-2 inserted in <i>pYH-wA</i>
pJF37	<i>pET-28a(+)-claD</i> ; a 1017 bp fragment of <i>claD</i> from cDNA of <i>P. crustosum</i> PRB-2 inserted in <i>pET28a(+)</i>

US: upstream; DS: downstream

Table S3. Primers used in this study

Primers	Sequence 5'-3'	Targeted amplification
P5HY-1	TGCGGCCGCCCTTTAGTGAGGGTTGAATTAGCTCTCCAAAGGGCG	Two-third of the <i>hph</i> resistance gene at the 5'-end from pUChph to construct p5HY
P5HY-2	CCTATAGTGAGTCGTATTACGGATCCAAGACCAATGCGGAGCATATAC	
P3YG-1	TGCGGCCGCCCTTTAGTGAGGGTTGAATTGATTCCGGAAGTGCTTGAC	Two-third of the <i>hph</i> resistance gene at the 3'-end from pUChph to construct p3YG
P3YG-2	CCTATAGTGAGTCGTATTACGGATCTCGGTGGAGCCAAG	
5F-R	GCTGAAGTCGATTTGAGTCCAC	US of <i>hph</i> to verify 5F of <i>P. crustosum</i> mutant
3F-F	GCATTAATGCATTGGACCTCGC	DS of <i>hph</i> to verify 3F of <i>P. crustosum</i> mutant
claD-up-F	AAGAATTGTTAATTAAGAGCTCAGATCTGTAGAGCAGGCTGGCGGATAC	1012 bp US fragment of <i>claD</i> to construct pJF19
claD-up-R	AACCCTCACTAAAGGGCGGCCGCACTAGTGTCTTTCGCGGATGATAAAC	
claD-down-F	ATACGACTCACTATAGGGCCCCGGCGTTCGACCTGGAAGGGGGAGCCTTG	1008 bp DS fragment of <i>claD</i> to construct pJF20
claD-down-R	GCTAGCCGCGGTACCAAGCTTACTCGAGCGGTGCTGGTGGTACCTATC	
claD-F	ATGCCTGTTCTAAGCAATCC	1017 bp partial fragment of <i>claD</i>
claD-R	TTAAATGGCATAACTCGCCGTC	
claD-5F-F	CTCGCAATCCATGGACGTG	US of <i>hph</i> to verify Δ <i>claD</i> mutant
claD-3F-R	GCGCTTTGGTTATTGCGAG	DS of <i>hph</i> to verify Δ <i>claD</i> mutant
claF-up-F	AAGAATTGTTAATTAAGAGCTCAGATCAGAGAACTGAGCTTTAGATTGG	1560 bp US fragment of <i>claF</i> to construct pJF40
claF-up-R	CCTCACTAAAGGGCGGCCGCACTAGCGATTGCAGCTATACCCG	
claF-down-F	ACTCACTATAGGGCCCCGGCGTTCGAGCCTGATGGCCTATTGTAC	1426 bp DS of <i>claF</i> to construct pJF41
claF-down-R	TAGCCGCGGTACCAAGCTTACTCGAGATGCAGGATATACGTTTCCAC	
claF-F	GCGAATGACTGATGCAGTG	1845 bp partial fragment of <i>claF</i>
claF-R	GAAGTTCACTCGGCAGAGC	
claF-5F-F	CATCGCTATAGATGTCTGGTCC	US of <i>hph</i> to verify Δ <i>claF</i> mutant
claF-3F-R	CAACCCACAACCTGGATCG	DS of <i>hph</i> to verify Δ <i>claF</i> mutant
claJ-up-F	GAATTGTTAATTAAGAGCTCAGATCTCTTGTGTAATGCCCAAATGCC	1367 bp US fragment of <i>claJ</i> to construct pJF21
claJ-up-R	CCCTCACTAAAGGGCGGCCGCACTAGTCCGTCATAGTTGAAGCGCAG	
claJ-down-F	CTCACTATAGGGCCCCGGCGTTCGACATATTAATTTAGGTAGCACGAG	1259 bp DS fragment of <i>claJ</i> to construct pJF22
claJ-down-R	CTAGCCGCGGTACCAAGCTTACTCGAGGCTATTGCTAGGATGTCACGC	
claJ--F	ATGAAAGGTCCAATTGTCCGC	867 bp partial fragment of <i>claJ</i>
claJ-R	AAGGTATGGAAGCTTCTGGGC	
claJ-5F-F	CTAGTTAGCAGCACTCGTC	US of <i>hph</i> to verify Δ <i>claJ</i> mutant
claJ-3F-R	CTATAGCAGTGGTCTCAACGGC	DS of <i>hph</i> to verify Δ <i>claJ</i> mutant
traA-up-F	AAGAATTGTTAATTAAGAGCTCAGATCTTCGTGGTTTGTAACTGC	1500 bp US fragment of <i>traA</i> to construct pJF38
traA-up-R	CCTCACTAAAGGGCGGCCGCACTAGATCTTTGAGGGTTATCTTACAGC	
traA-down-F	ACTCACTATAGGGCCCCGGCGTTCGAGTTAGTTGTAGTAGCACTACTGC	1496 bp DS fragment of <i>traA</i> to construct pJF39
traA-down-R	TAGCCGCGGTACCAAGCTTACTCGACCAGTACCGTAAATATCTGG	

Table S3. Primers used in this study (continued)

traA-F	TGCATCTGTAGAGCTCGC	1819 bp partial fragment of <i>traA</i>
traA-R	GAGGGCGTTTTAGAATCAATTG	
traA-5F-F	GGACACACAGTTAAATGCAG	US of <i>hph</i> to verify $\Delta traA$ mutant
traA-3F-R	CCTAGGCCATGTTAGATTGC	DS of <i>hph</i> to verify $\Delta traA$ mutant
traB-up-F	GAATTGTTAATTAAGAGCTCAGATCTCTGACGAATGAGGCATTCAATG	1388 bp US fragment of <i>traB</i> to construct pJF56
traB-up-R	ACCCTCACTAAAGGGCGGCCGCACTAGCATGGCTTGACAGCGCTCTC	
traB-down-F	GACTCACTATAGGGCCCGGGCGTCGACGGCCCTCCCCTTGCTATTTC	1067 bp DS fragment of <i>traB</i> to construct pJF57
traB-down-R	CTAGCCGCGGTACCAAGCTTACTCGAGCGTCCGACGATCATGATCCC	
traB-F	GAATGCGTATTGCACTAGTATG	1037 bp partial fragment of <i>traB</i>
traB-R	CCAGTTATACCACGACACC	
traB-5F-F	CCTGCTGTACCTTCTGTATGC	US of <i>hph</i> to verify $\Delta traB$ mutant
traB-3F-R	GTGGCTACGGTTACCACTG	DS of <i>hph</i> to verify $\Delta traB$ mutant
traD-up-F	GAATTGTTAATTAAGAGCTCAGATCTGGCTCAGATCTTCCAGTGAAC	1170 bp US fragment of <i>traD</i> to construct pJF54
traD-up-R	CAACCCTCACTAAAGGGCGGCCGCACTAGGTTGCAGCTAGGTGGGTG	
traD-down-F	CTCACTATAGGGCCCGGGCGTCGACCTACCATACTGCCTTTTCTGAC	1139 bp DS fragment of <i>traD</i> to construct pJF55
traD-down-R	GCTAGCCGCGGTACCAAGCTTACTCGAGGGACCGCTCTGCTCTCATACT	
traD--F	ATGAAAGTTTTGATTATTTTTGCCACC	942 bp partial fragment of <i>traD</i>
traD-R	TCACGCTTCTTTGACGTCCG	
traD-5F-F	GGTAGAGCAGCGCGGTCTA	US of <i>hph</i> to verify $\Delta traD$ mutant
traD-3F-R	CAAAGGCTGAGCCAGAGACTC	DS of <i>hph</i> to verify $\Delta traD$ mutant
traE-up-F	GAATTGTTAATTAAGAGCTCAGATCTCCGCATATGCTTCAGCTGAC	1030 bp US fragment of <i>traE</i> to construct pJF52
traE-up-R	CCCTCACTAAAGGGCGGCCGCACTAGCAAATTATGCAGTGGTGCACG	
traE-down-F	CTCACTATAGGGCCCGGGCGTCGACGATAGTATGAGAGCAGAGCGGTC	1027 bp DS fragment of <i>traE</i> to construct pJF53
traE-down-R	GCTAGCCGCGGTACCAAGCTTACTCGAGGGCAGTATTCTGATGCCTGC	
traE-F	ATGGCCGACCAGCACTTC	471 bp partial fragment of <i>traE</i>
traE-R	CTATTTGCCGAAAAGTCCAG	
traE-5F-F	CAATGTTCTTCTCCGTATCGGTC	US of <i>hph</i> to verify $\Delta traE$ mutant
traE-3F-R	CTGTTGACGCTGTACATGGG	DS of <i>hph</i> to verify $\Delta traE$ mutant
traF-up-F	GAAGAATTGTTAATTAAGAGCTCAGATCTCAACCGCATATCGCCAAG	977 bp US fragment of <i>traF</i> to construct pJF50
traF-up-R	CCCTCACTAAAGGGCGGCCGCACTAGCACGACAGCCTTTGTCCG	
traF-down-F	GACTCACTATAGGGCCCGGGCGTCGACAGCAATCGTCAATTTGCAAAC	1031 bp DS of <i>traF</i> to construct pJF51
traF-down-R	CTAGCCGCGGTACCAAGCTTACTCGAGCGTATTCGGCCCCATTGAAAC	
traF-F	ATGACCTCCGGCACTGAG	1795 bp partial fragment of <i>traF</i>
traF-R	CTAATGCGCTGTAAACTTGCTC	
traF-5F-F	CAGCCAATCGAAGATCCTTGC	US of <i>hph</i> to verify $\Delta traF$ mutant
traF-3F-R	CATGTTTGCCTTGGAGCAGG	DS of <i>hph</i> to verify $\Delta traF$ mutant

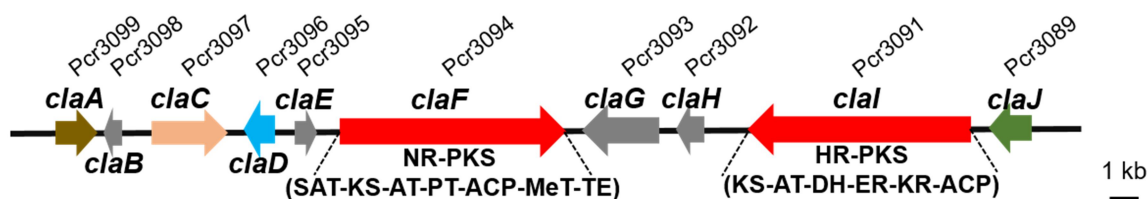
Table S3. Primers used in this study (continued)

traH-up-F	GAATTGTTAATTAAGAGCTCAGATCTCCCATCCATGGTCCGATTGAG	1101 bp US fragment of <i>traH</i> to construct pJF48
traH-up-R	CCTCACTAAAGGGCGGCCGCACTAGGATTGCTTATGTGACGTGCTTTTG	
traH-down-F	CTCACTATAGGGCCCGGGCGTGCACCGTTACAGCCAAGACATTGATG	1114 bp DS fragment of <i>traH</i> to construct pJF49
traH-down-R	CTAGCCGCGGTACCAAGCTTACTCGAGCGCAGGACTCGACATGGATC	
traH-F	GCGAAGGTCATTGAGCAAGTG	1097 bp partial fragment of <i>traH</i>
traH-R	CACTACATACTGTGAATGCTATCACC	
traH-5F-F	GCGGTGGAGTTGACGGTAAG	US of <i>hph</i> to verify $\Delta traH$ mutant
traH-3F-R	GTCTCTCTGCCCCACCAC	DS of <i>hph</i> to verify $\Delta traH$ mutant
A.n-claF-For	TATTCATCTTCCCATCCAAGAACCCTTAATCATGCCGTCTGAGTCTTAC	DNA of <i>claF</i> with its 480 bp terminator from <i>P. crustosum</i> to construct pJF18
A.n-claF-Rev	CATATTTTCGTGACACACAGAATAACTCTCCATGTTATTAGGGACCATGG	
ClaD-28-For	GTGGACAGCAAATGGGTCGCGGATCCATGCCTGTTCTAAGCAATCCATC	1017 bp fragment of <i>claD</i> to construct pJF37
ClaD-28-Rev	CAAGCTTGTCGACGGAGCTCGAATTCTTAAATGGCATAACTCGCCGTCA	

US: upstream; DS: downstream

Table S4. Putative functions of the genes from clavatul gene cluster

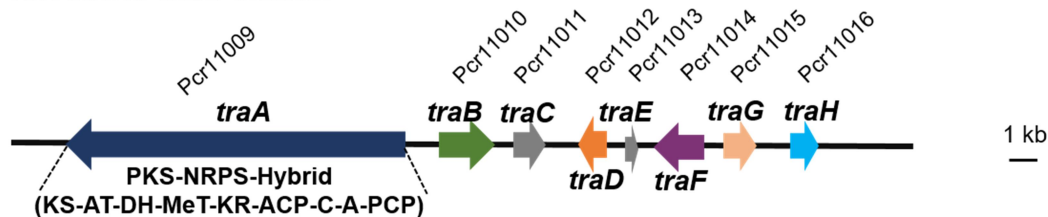
Clavatul cluster



Protein	No. in genome	Size (AA)	Homologous known protein	Identity (%)	Putative function
ClaA	Pcr3099	476	C6 transcription factor (ANF07281) from <i>Byssoschlamys fulva</i> ¹⁰	53.1	transcription activator
ClaB	Pcr3098	214	hypothetical protein AUD_9432 (GAO90472) from <i>Aspergillus udagawae</i> ¹¹	38.8	hypothetical protein
ClaC	Pcr3097	878	enoyl-CoA hydratase/isomerase family protein (OCK96737) from <i>Cenococcum geophilum</i> ¹²	53.6	enoyl-CoA hydratase/isomerase
ClaD	Pcr3096	338	Fe ^{II} /2-oxoglutarate-dependent oxygenase CitB (ALI92653) from <i>Monascus ruber</i> M7 ¹³	53.8	clavatul oxidase
ClaE	Pcr3095	265	citrinin biosynthesis protein CitA (ALI92654) from <i>Monascus ruber</i> M7 ¹³	64.8	hypothetical protein
ClaF	Pcr3094	2587	clavatul polyketide synthase CitS (ALI92655) from <i>Monascus ruber</i> M7 ¹³	57.7	clavatul synthase
ClaG	Pcr3093	743	hypothetical protein (XP_020058556.1) from <i>Aspergillus aculeatus</i> ATCC 16872	47.0	hypothetical protein
ClaH	Pcr3092	308	thiohydrolase in the brefeldin A biosynthesis (A0A068ACU9.1) from <i>Penicillium brefeldianum</i> ¹⁴	44.0	hydrolase
ClaI	Pcr3091	2346	polyketide synthase (AFP89392) from <i>Cladosporium phlei</i> ¹⁵	42.8	polyketide synthase
ClaJ	Pcr3089	438	cytochrome P450 monooxygenase (BAJ04372.1) from <i>Aspergillus oryzae</i>	42.0	cytochrome P450

Table S5. Putative functions of the genes from terrestrial acid gene cluster

Terrestrial acid cluster



Protein	No. in genome	Size (AA)	homologous known protein	Identity (%)	Putative Function
TraA	Pcr11009	3856	NRPS/PKS hybrid enzyme (XP_001392496) from <i>Aspergillus niger</i> CBS 513.88 ¹⁶	69.6	PKS-NRPS hybrid enzyme
TraB	Pcr11010	509	cytochrome P450 monooxygenase (XP_001392495) in toxin biosynthesis in <i>Aspergillus niger</i> CBS 513.88 ¹⁶	65.5	cytochrome P450
TraC	Pcr11011	417	hypothetical protein (OQD61093) from <i>Penicillium polonicum</i>	81.0	hypothetical protein
TraD	Pcr11012	267	NAD(P)H dehydrogenase (AEO48230) from <i>Rhodospirillum rubrum</i> F11 ¹⁷	63.4	flavodoxin family protein
TraE	Pcr11013	156	hypothetical protein (XP_001392493) from <i>Aspergillus niger</i> CBS 513.88 ¹⁶	49.0	hypothetical protein
TraF	Pcr11014	482	MFS multidrug transporter (XP_001392492) from <i>Aspergillus niger</i> CBS 513.88 ¹⁶	68.9	transporter
TraG	Pcr11015	364	enoyl reductase (XP_001392491) from <i>Aspergillus niger</i> CBS 513.88 ¹⁶	68.9	enoyl reductase
TraH	Pcr11016	327	2-oxoglutarate-dependent oxygenase (XP_001392490) from <i>Aspergillus niger</i> CBS 513.88 ¹⁶	66.0	2-oxoglutarate-dependent oxygenase

Table S6. ^1H NMR data of compounds **1** and **2**

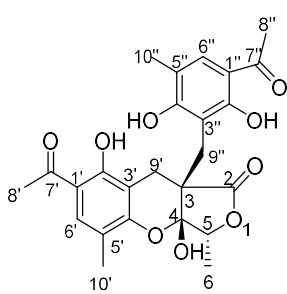
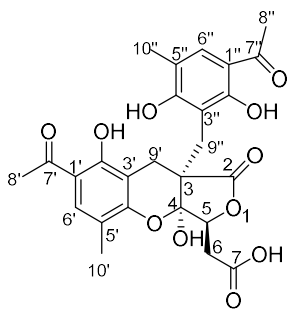
Compound		
	Penilactone A (1 , DMSO- d_6)	Penilactone B (2 , DMSO- d_6)
Position	δ_{H} , multi., J in Hz	δ_{H} , multi., J in Hz
5	5.00, q, 6.4, 1H	5.22, dd, 9.6, 2.1, 1H
6	1.51, d, 6.4, 3H	3.18, t, 9.6, 1H
	-	2.66, dd, 16.9, 9.6, 1H
6'	7.57, s, 1H	7.59, s, 1H
8'	2.55, s, 3H	2.56, s, 3H
9'	2.97, d, 17.0, 1H	2.96, d, 17.4, 1H
	2.79, d, 17.0, 1H	2.82, d, 17.4, 1H
10'	2.13, s, 3H	2.13, s, 3H
6''	7.61, s, 1H	7.62, s, 1H
8''	2.52, s, 3H	2.53, s, 3H
9''	3.25, d, 12.3, 1H	3.25, d, 13.8, 1H
	3.13, d, 12.3, 1H	3.17, d, 13.8, 1H
10''	2.16, s, 3H	2.16, s, 3H
4-OH	8.15, s, 1H	8.32, s, 1H
2'-OH	12.82, s, 1H	12.81, s, 1H
2''-OH	13.01, s, 1H	13.03, s, 1H
4''-OH	9.78, s, 1H	9.84, s, 1H

Table S7. ^1H NMR data of compounds **3** and **4**

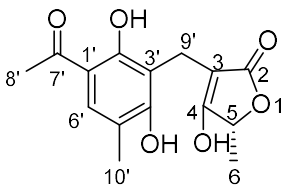
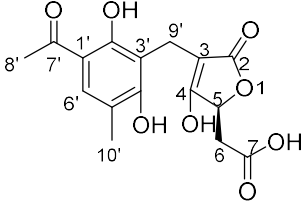
Compound		
	Peniphenone D (3 , CDCl_3)	Penilactone D (4 , $\text{DMSO-}d_6$)
Position	δ_{H} , multi., J in Hz	δ_{H} , multi., J in Hz
5	4.83, q, 6.8, 1H	4.96, dd, 9.6, 3.0, 1H
6	1.46, d, 6.8, 3H	2.89, dd, 16.2, 3.0, 1H
	-	2.25, dd, 16.2, 9.6, 1H
6'	7.40, s, 1H	7.53, s, 1H
8'	2.56, s, 3H	2.52, s, 3H
9'	3.47, d, 15.1, 1H	3.41, d, 14.5, 1H
	3.42, d, 15.1, 1H	3.37, d, 14.5, 1H
10'	2.20, s, 3H	2.13, s, 3H
2'-OH	13.98, s, 1H	12.94, s, 1H

Table S8. ¹H NMR data of compounds **5**, **10** and **12**

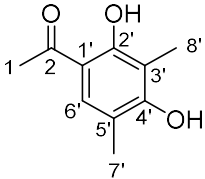
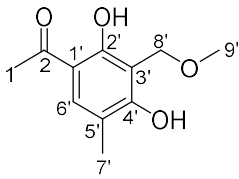
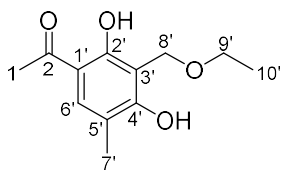
Compound				
	Clavatul (5)	Hydroxyclovatul methyl ether (10 , CDCl ₃)	Hydroxyclovatul ethyl ether (12 , CDCl ₃)	
Position	δ_{H} , multi., <i>J</i> in Hz (CDCl ₃)	δ_{H} , multi., <i>J</i> in Hz (DMSO- <i>d</i> ₆)	δ_{H} , multi., <i>J</i> in Hz	δ_{H} , multi., <i>J</i> in Hz
1	2.56, s, 3H	2.56, s, 3H	2.54, s, 3H	2.54, s, 3H
6'	7.37, s, 1H	7.56, s, 1H	7.41, s, 1H	7.41, s, 1H
7'	2.14, s, 3H	2.05, s, 3H	2.16, s, 3H	2.16, s, 3H
8'	2.21, s, 3H	2.18, s, 3H	4.84, s, 2H	4.88, s, 2H
9'	-	-	3.50, s, 3H	3.67, q, 7.1, 2H
10'	-	-	-	1.31, t, 7.1, 3H
2'-OH	12.89, s, 1H	12.94, s, 1H	12.95, s, 1H	12.95, s, 1H
4'-OH	-	9.48, s, 1H	9.15, s, 1H	9.44, s, 1H

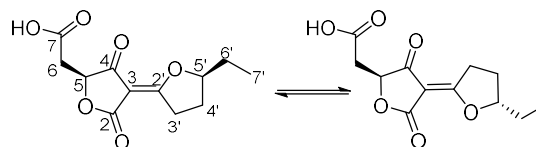
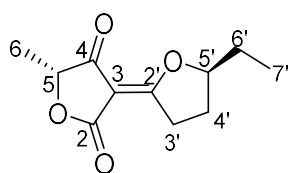
Table S9. NMR data of compound **9**

Compound

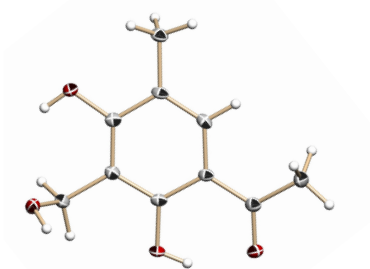
Hydroxyclovatol (**9**)

Position	δ_{H} , multi., J in Hz (CDCl ₃)	δ_{H} , multi., J in Hz (DMSO- <i>d</i> ₆)	δ_{C} (CDCl ₃)	Key HMBC correlations
1	2.53, s, 3H	2.53, s, 3H	26.4	C-2
2	-	-	203.0	
1'	-	-	112.6	
2'	-	-	159.8	
3'	-	-	110.3	
4'	-	-	162.4	
5'	-	-	117.2	
6'	7.40, s, 1H	7.61, s, 1H	131.9	C-2, C-2', C-4'
7'	2.17, s, 3H	2.11, s, 3H	15.5	C-4', C-5', C-6'
8'	5.07, s, 2H	4.70, s, 2H	58.9	C-3'
2'-OH	12.93, s, 1H	12.98, s, 1H	-	C-1', C-2'
4'-OH	9.13, s, 1H	10.23, s, 1H	-	C-4'
8'-OH	-	5.75, s, 1H	-	

Table S10. NMR data of **11** and **13**



Compound	Terrestrial acid (11 , CDCl ₃)		Crustosic acid (13 , CDCl ₃)	
Position	δ_{H} , multi., J in Hz	δ_{H} , multi., J in Hz	δ_{H} , multi., J in Hz	δ_{C}
2	-	-	-	167.5/170.7
3	-	-	-	95.2/95.6
4	-	-	-	197.4/193.8
5	4.61, q, 7.0, 1H	4.81, dd, 6.4, 4.0, 1H	4.81, dd, 6.4, 4.0, 1H	78.6/78.3
6	1.46, d, 7.0, 3H	3.00, ddd, 17.2, 9.3, 4.0, 1H	3.00, ddd, 17.2, 9.3, 4.0, 1H	35.8/35.7
	-	2.82, td, 17.2, 6.4, 1H	2.82, td, 17.2, 6.4, 1H	-
7	-	-	-	173.8/173.6
2'	-	-	-	187.6/187.0
3'	3.60, ddd, 20.1, 9.3, 1.5, 1H	3.58, ddd, 19.9, 9.3, 4.1, 1H	3.58, ddd, 19.9, 9.3, 4.1, 1H	33.9/34.2
	3.27, ddd, 20.1, 9.7, 8.5, 1H	3.26, ddd, 19.9, 9.6, 9.0, 1H	3.26, ddd, 19.9, 9.6, 9.0, 1H	-
4'	2.36, m, 1H	2.37, m, 1H	2.37, m, 1H	27.7/27.7
	1.87, m, 1H	1.86, m, 1H	1.86, m, 1H	-
5'	4.93, m, 1H	4.94, m, 1H	4.94, m, 1H	93.0/93.6
6'	1.96, m, 1H	1.94, m, 1H	1.94, m, 1H	26.5/26.4
	1.79, m, 1H	1.77, m, 1H	1.77, m, 1H	-
7'	1.06, t, 7.5, 3H	1.04, t, 7.4, 3H	1.04, t, 7.4, 3H	9.6/9.5
7-OH	-	8.59, s, 1H	8.59, s, 1H	-

Table S11. Crystal data and structure refinement of **9**Perspective drawing of the X-ray structure of **9**

Name	Hydroxyclovatol	
Identification code	CCDC 1883090	
Empirical formula	C ₁₀ H ₁₂ O ₄	
Formula weight	196.20	
Temperature	113(2) K	
Wavelength	1.54178 Å	
Crystal system	Triclinic	
Space group	P -1	
Unit cell dimensions	a = 7.7553(9) Å	α = 77.750(5)°.
	b = 8.2119(10) Å	β = 69.610(4)°.
	c = 8.3575(10) Å	γ = 66.847(5)°.
Volume	456.97(10) Å ³	
Z	2	
Density (calculated)	1.426 mg/m ³	
Absorption coefficient	0.929 mm ⁻¹	
F(000)	208	
Crystal size	0.900 x 0.500 x 0.200 mm ³	
Theta range for data collection	5.669 to 64.115°.	
Index ranges	-8 ≤ h ≤ 9, -9 ≤ k ≤ 9, -9 ≤ l ≤ 9	
Reflections collected	3969	
Independent reflections	1409 [R(int) = 0.0585]	
Completeness to theta = 64.115°	92.6%	
Refinement method	Full-matrix least-squares on F ²	
Data / restraints / parameters	1409 / 8 / 134	
Goodness-of-fit on F ²	1.589	
Final R indices [I > 2σ(I)]	R1 = 0.0535, wR2 = 0.1801	
R indices (all data)	R1 = 0.0542, wR2 = 0.1834	
Extinction coefficient	0.044(8)	
Largest diff. peak and hole	0.391 and -0.328 e.Å ⁻³	

Supplementary Figures

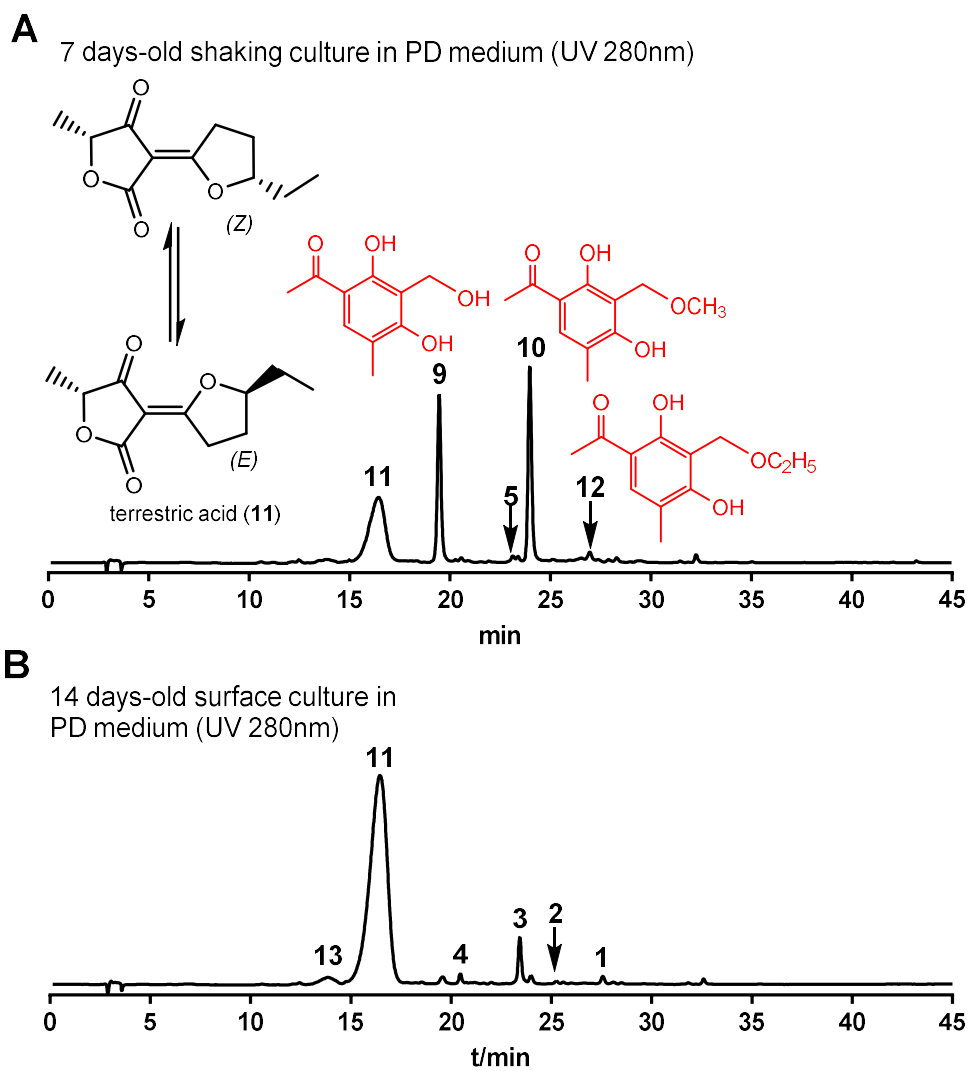


Figure S1. HPLC analysis of secondary metabolite profiles of *P. crustosum*

(A) in 7 days-old PD liquid shaking culture at 230 rpm. (B) in 14 days-old PD liquid surface culture. Absorptions at 280 nm are illustrated.

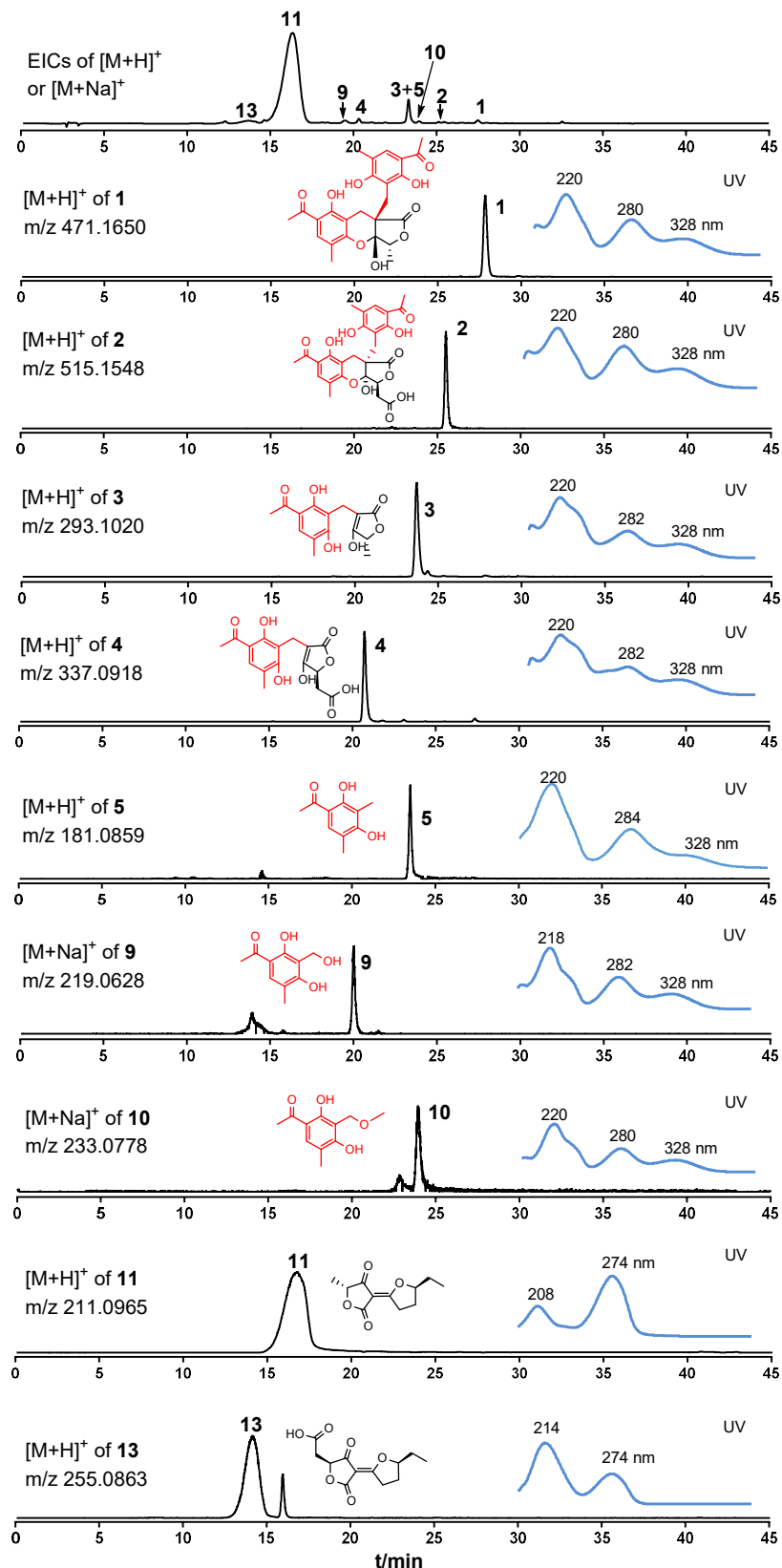


Figure S2. LC-MS analysis of secondary metabolites from a 14 days-old liquid PD surface culture of *P. crustosum*

EICs of 1–5, 9, 10, 11, and 13 are selected with a tolerance range of ± 0.005 . UV spectra are shown in blue.

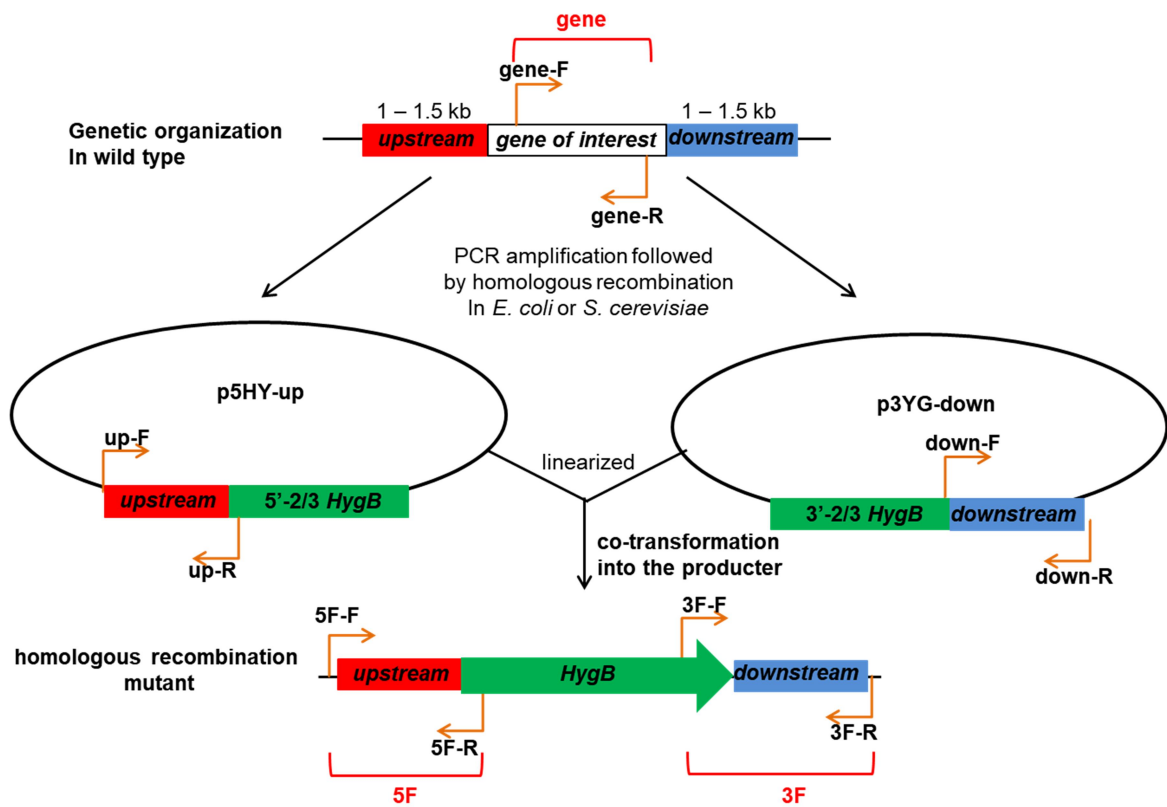


Figure S3. Schematic representation of the gene deletion strategy in *P. crustosum*

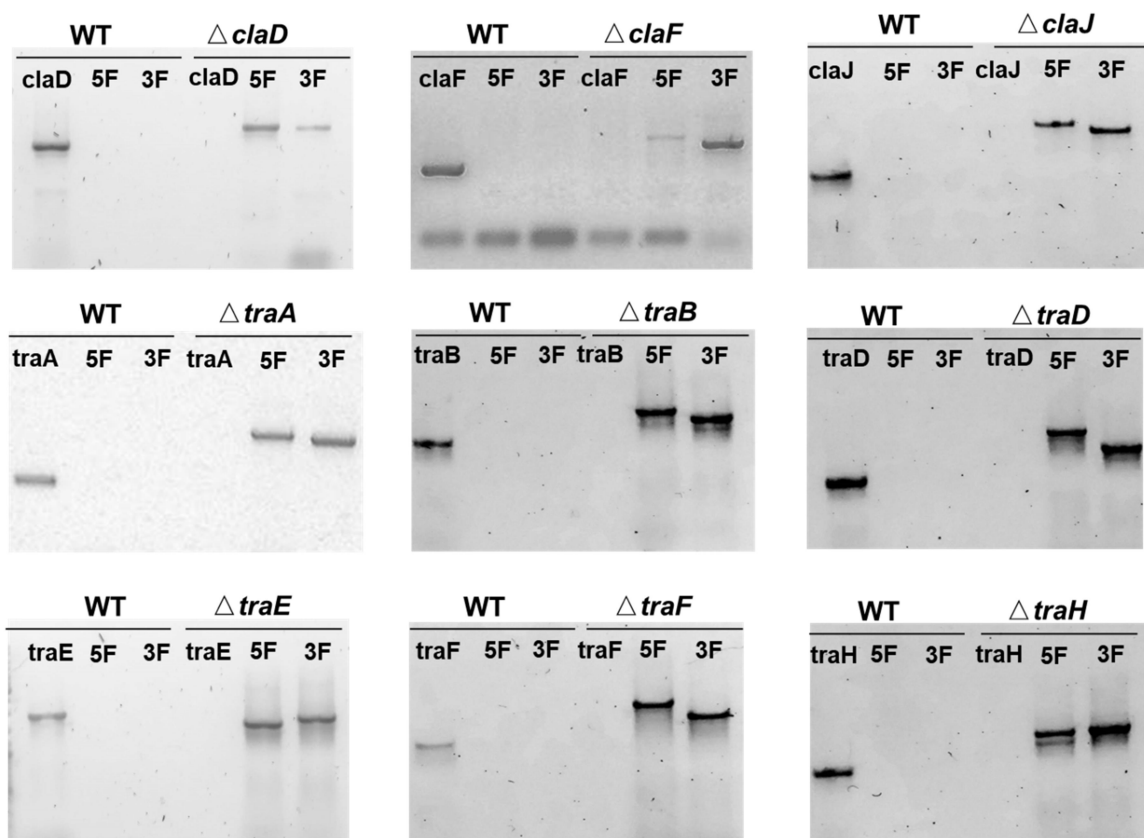


Figure S4. PCR verification of deletion mutants of *P. crustosum*

PCR amplification for three different fragments from genomic DNA of WT and deletion mutants was used to prove the presence/absence of the gene of interest and its site specific integration with the help of up- and downstream regions. The PCR primers are given in Table S3.

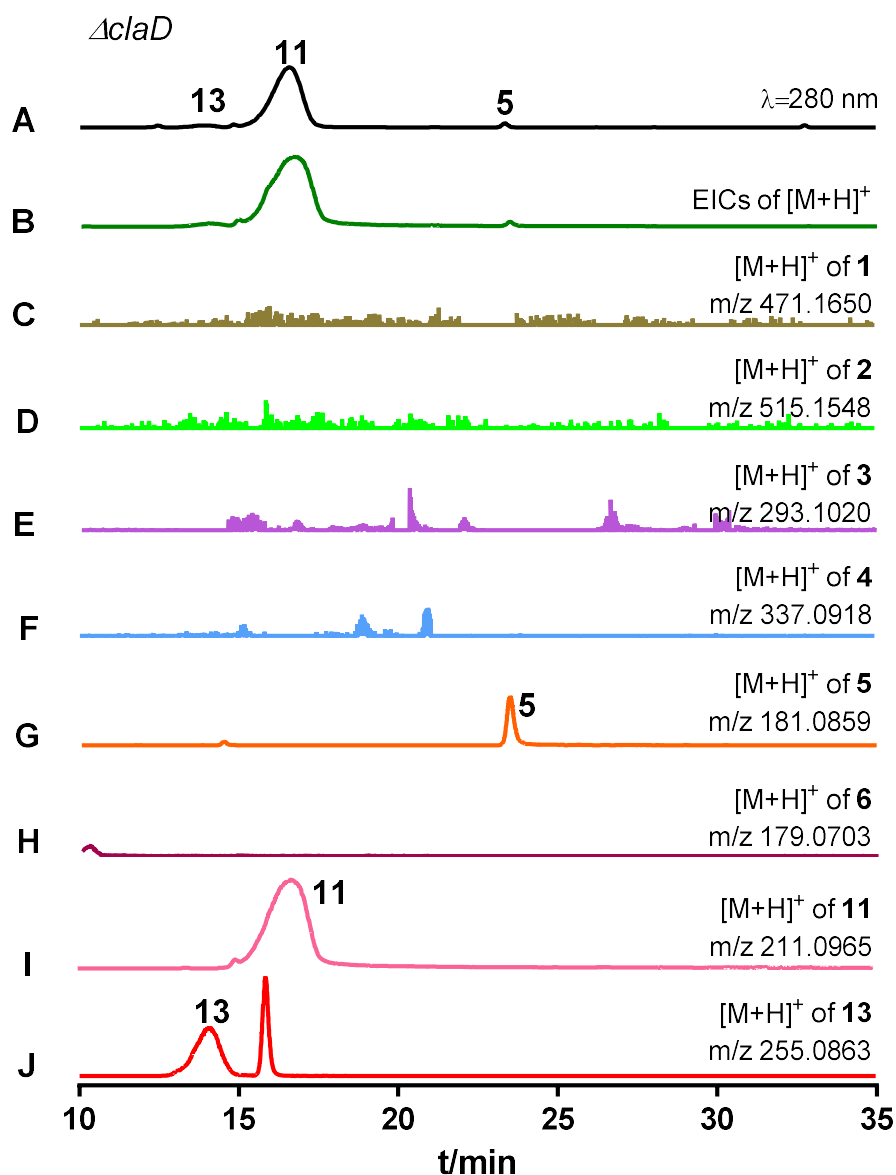


Figure S5. LC-MS analysis of the metabolite profile of the $\Delta claD$ -mutant

Absorptions at 280 nm are illustrated in black (A). EICs in dark green (B) refer total $[M+H]^+$ ions of 1–6, 11, and 13 with a tolerance range of ± 0.005 , and in other colors refer $[M+H]^+$ ions of 1–6, 11, and 13 (C–J), respectively.

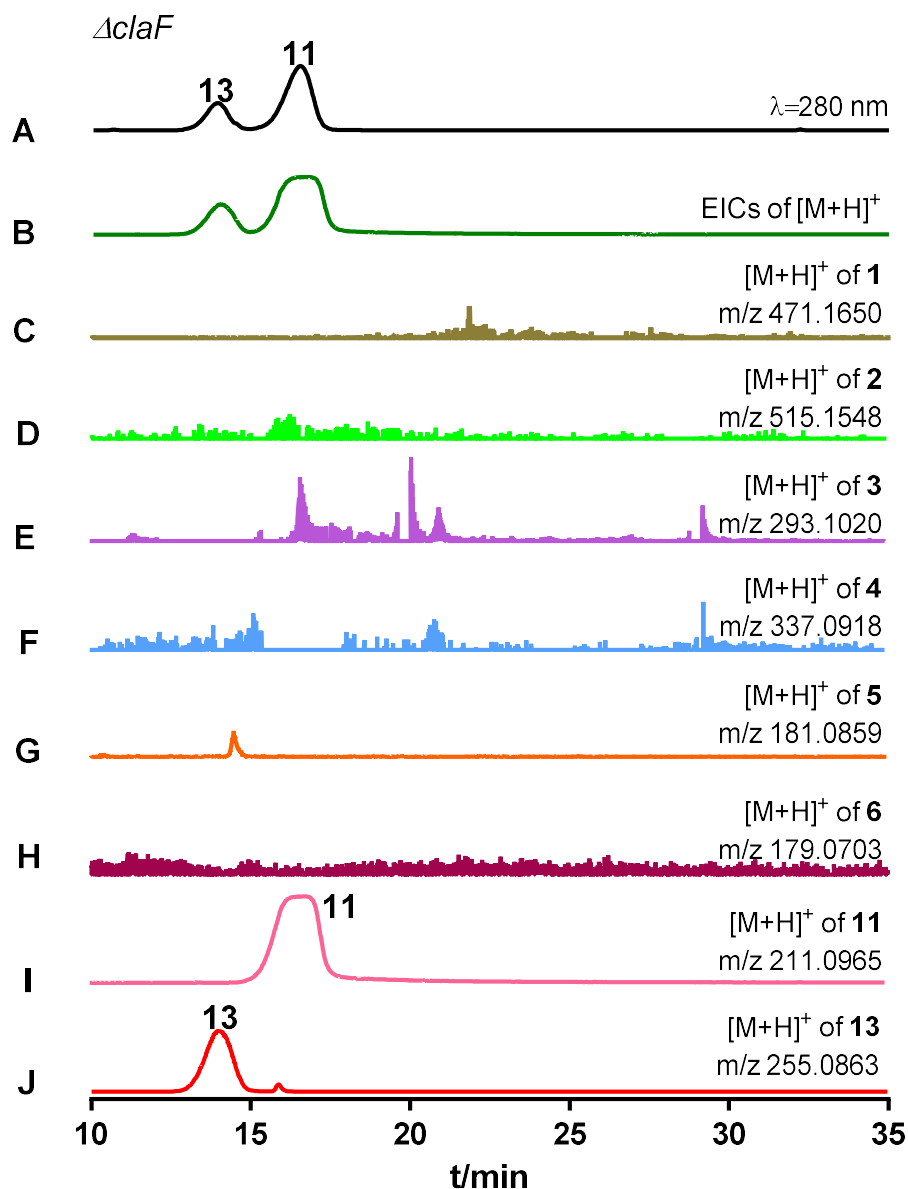


Figure S6. LC-MS analysis of the metabolite profile of the $\Delta claF$ -mutant

Absorptions at 280 nm are illustrated in black (A). EICs in dark green (B) refer total $[M+H]^+$ ions of 1–6, 11, and 13 with a tolerance range of ± 0.005 , and in other colors refer $[M+H]^+$ ions of 1–6, 11, and 13 (C–J), respectively.

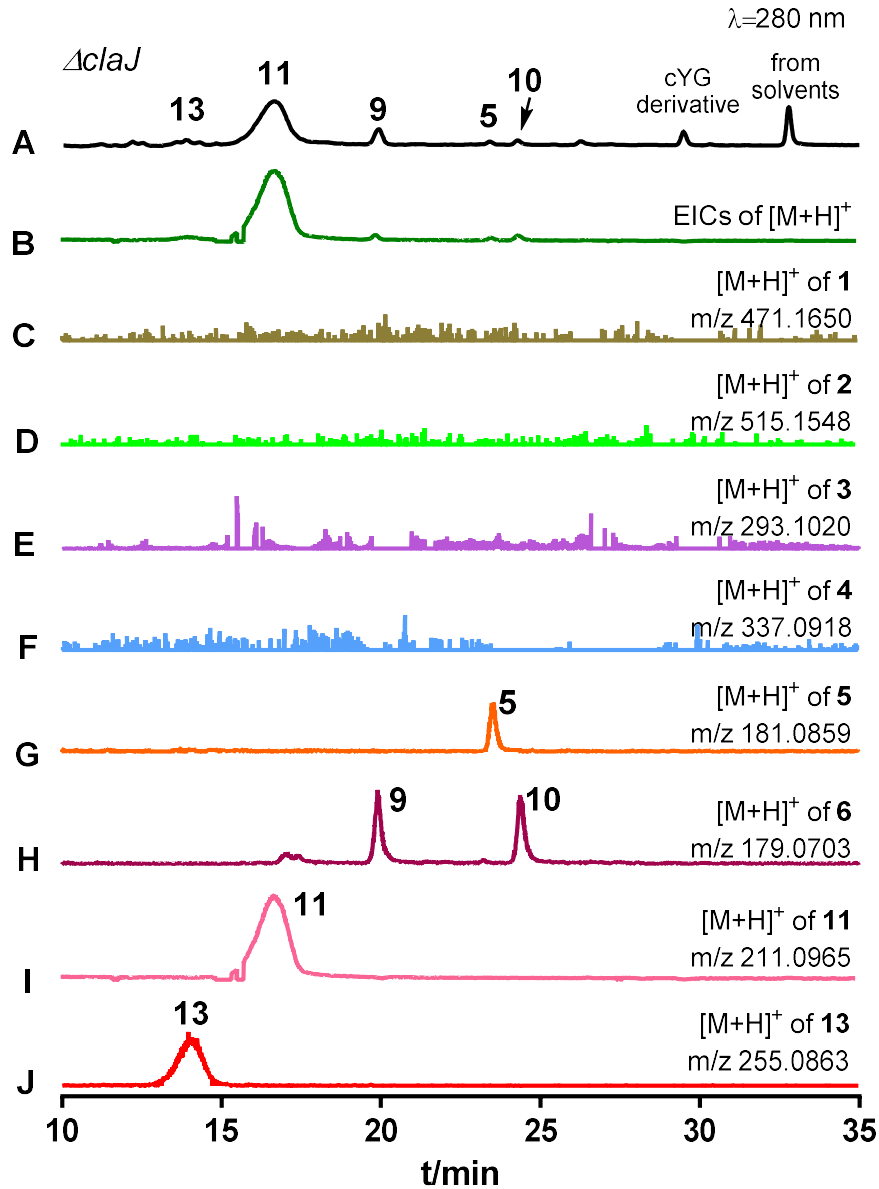


Figure S7. LC-MS analysis of the metabolite profile of the $\Delta cIaJ$ -mutant

Absorptions at 280 nm are illustrated in black (A). EICs in dark green (B) refer total $[M+H]^+$ ions of 1–6, 11, and 13 with a tolerance range of ± 0.005 , and in other colors refer $[M+H]^+$ ions of 1–6, 11, and 13 (C–J), respectively. The peak at 29.3 min, which is very likely derived from the cyclodipeptide of tyrosine and glycine (cYG), was isolated and identified as the enantiomer of *cis*-Bis(methylthio)silvatin¹⁸ (data not shown). The peak at 33.5 min was also detected in the control chromatogram with methanol as a sample.

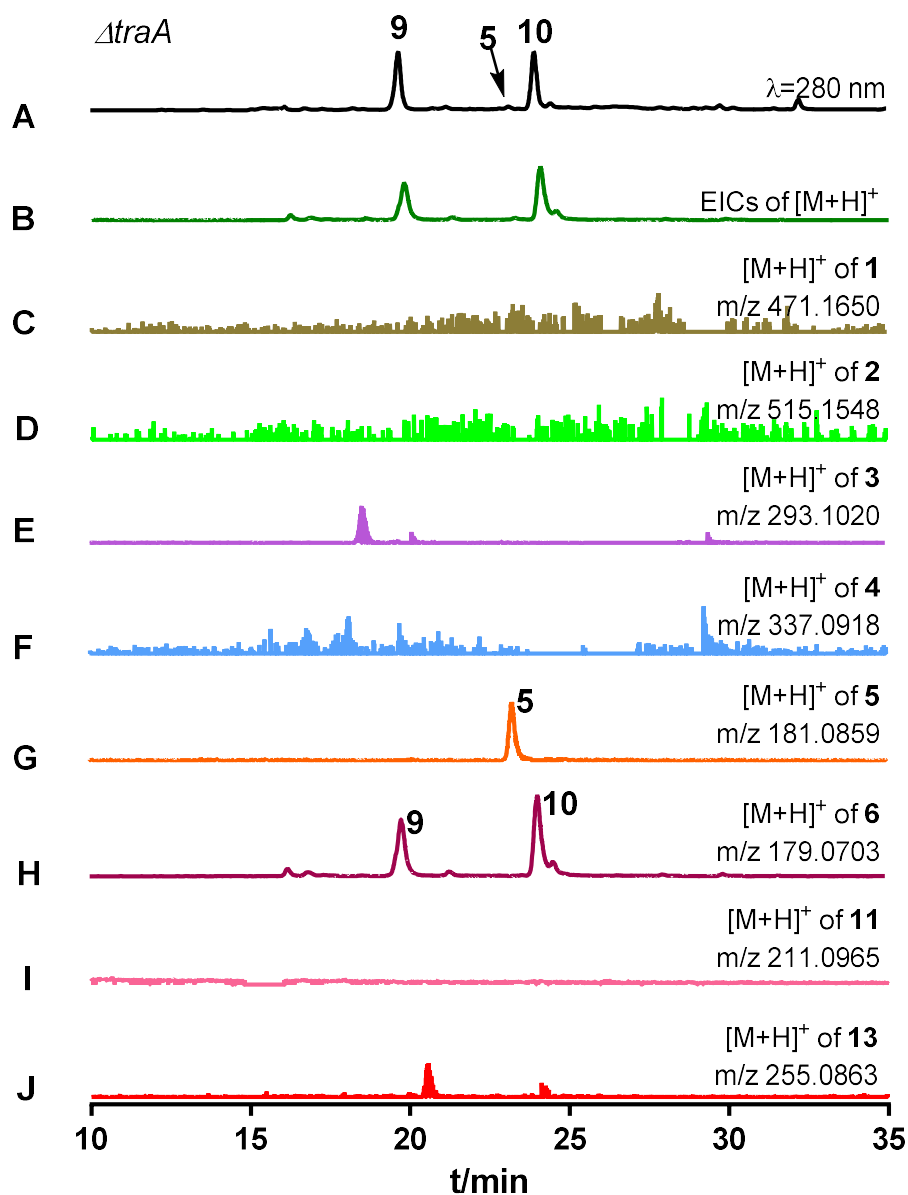


Figure S8. LC-MS analysis of the metabolite profile of the $\Delta traA$ -mutant

Absorptions at 280 nm are illustrated in black (A). EICs in dark green (B) refer total $[M+H]^+$ ions of 1–6, 11, and 13 with a tolerance range of ± 0.005 , and in other colors refer $[M+H]^+$ ions of 1–6, 11, and 13 (C–J), respectively.

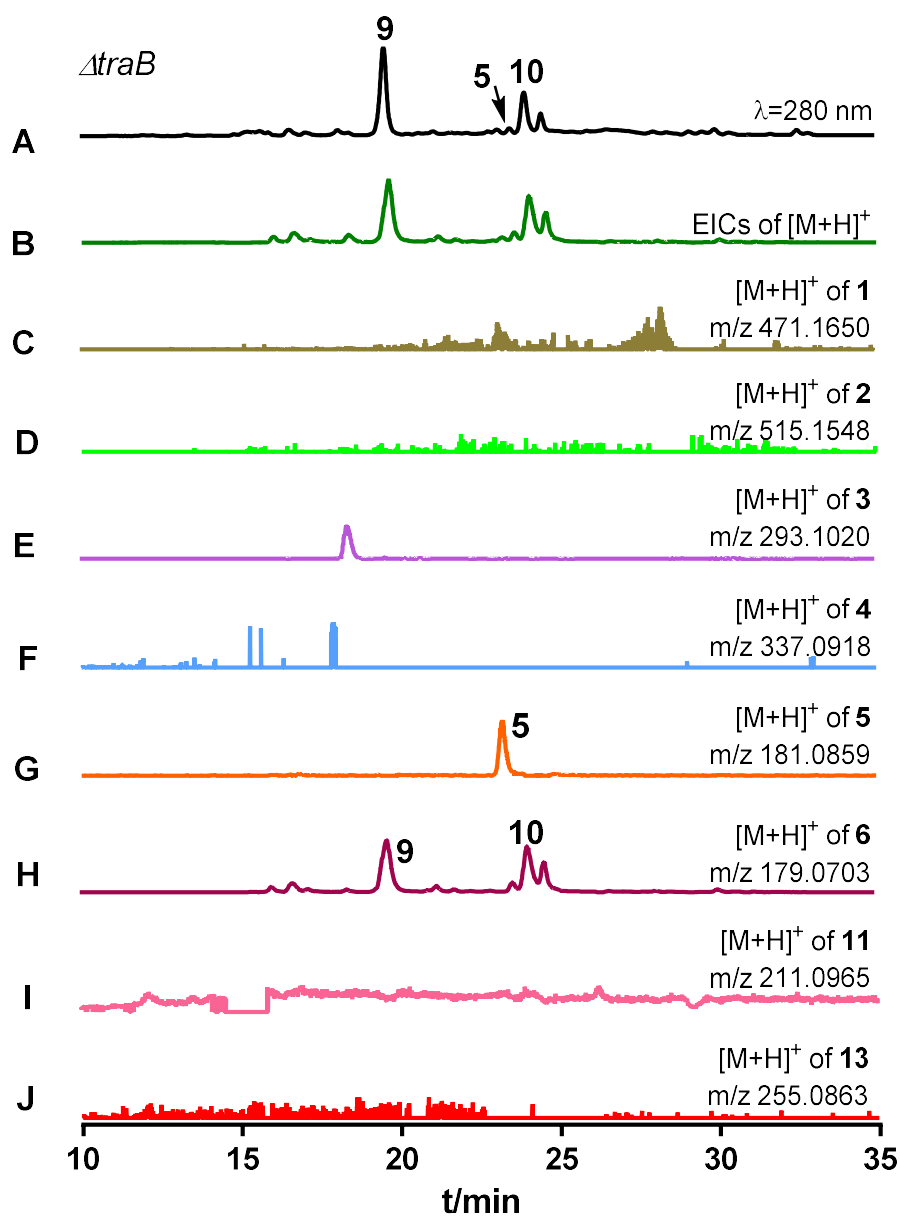


Figure S9. LC-MS analysis of the metabolite profile of the $\Delta traB$ -mutant

Absorptions at 280 nm are illustrated in black (A). EICs in dark green (B) refer total $[M+H]^+$ ions of 1–6, 11, and 13 with a tolerance range of ± 0.005 , and in other colors refer $[M+H]^+$ ions of 1–6, 11, and 13 (C–J), respectively.

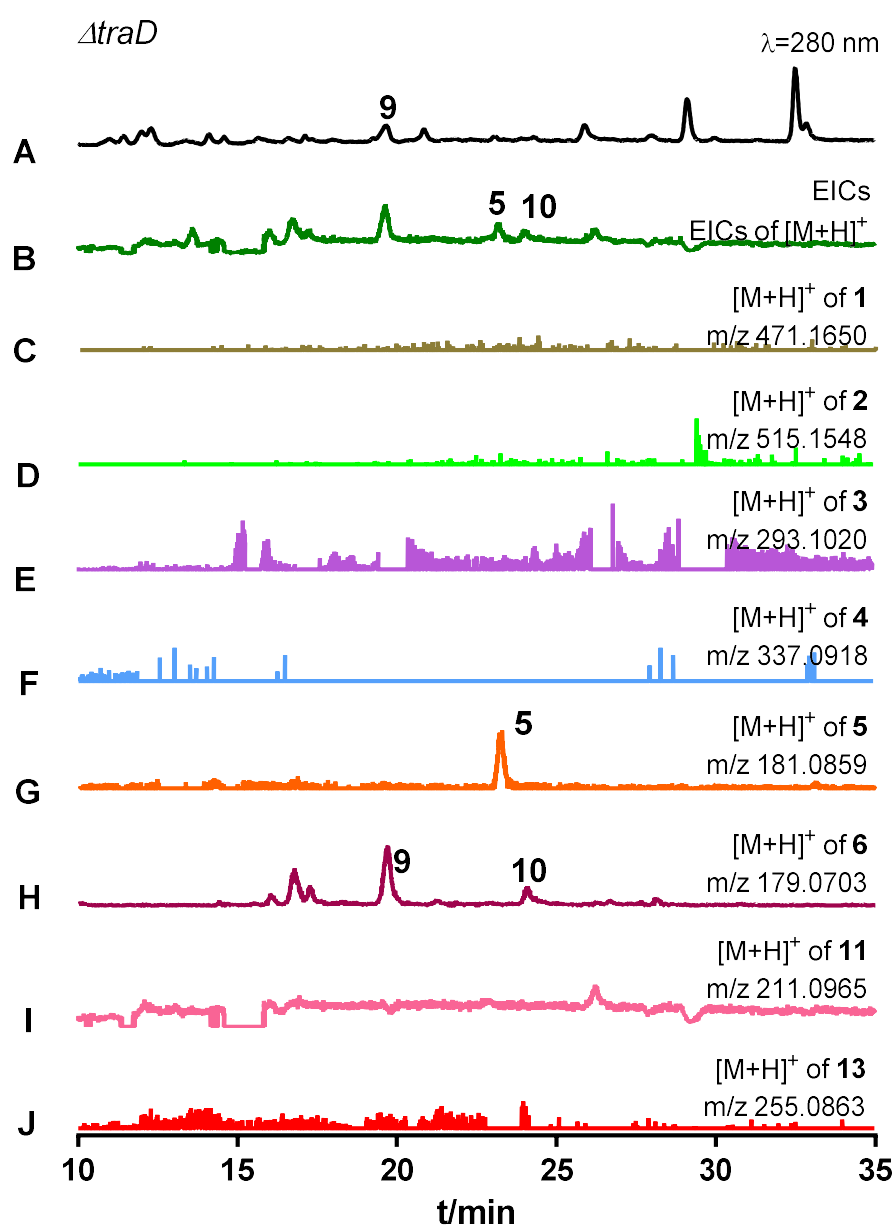


Figure S10. LC-MS analysis of the metabolite profile of the $\Delta traD$ -mutant

Absorptions at 280 nm are illustrated in black (A). EICs in dark green (B) refer total $[M+H]^+$ ions of 1–6, 11, and 13 with a tolerance range of ± 0.005 , and in other colors refer $[M+H]^+$ ions of 1–6, 11, and 13 (C–J), respectively.

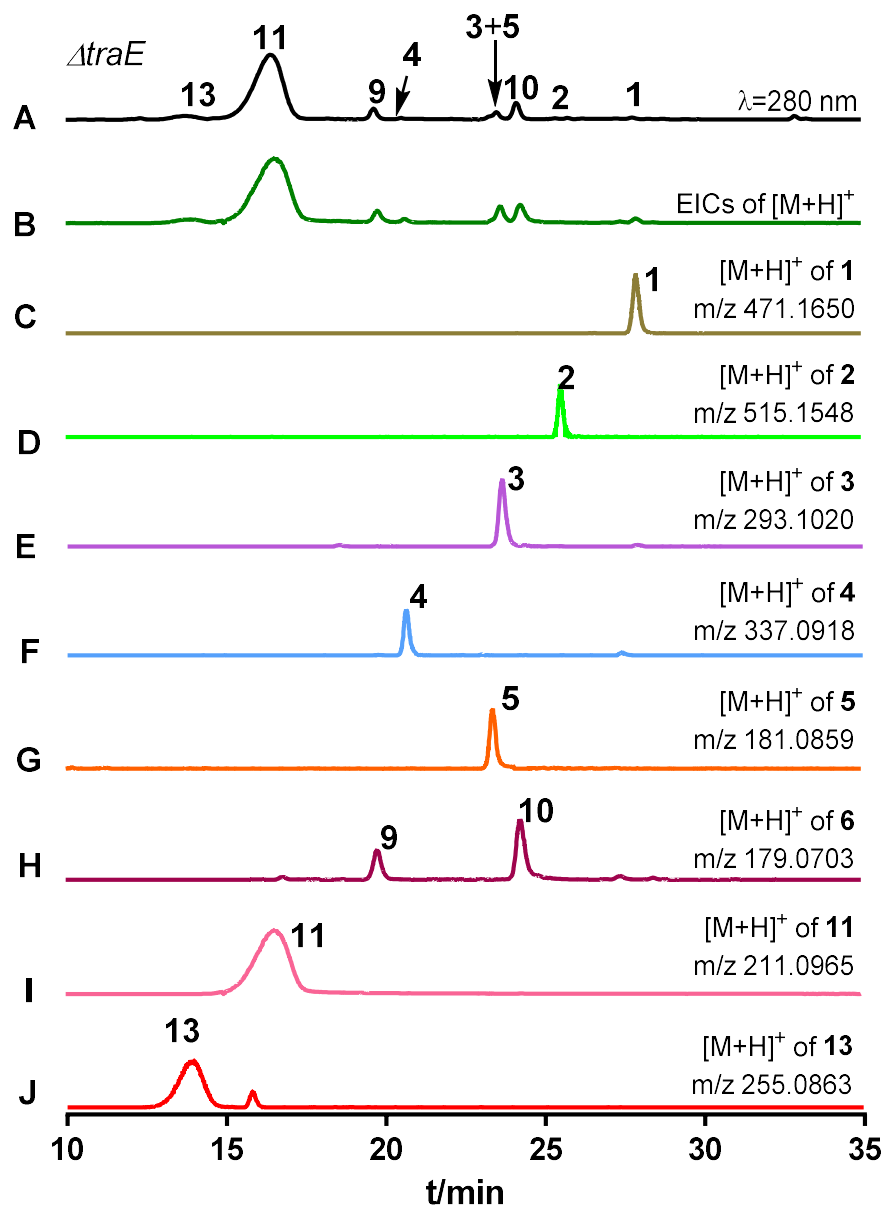


Figure S11. LC-MS analysis of the metabolite profile of the $\Delta traE$ -mutant

Absorptions at 280 nm are illustrated in black (A). EICs in dark green (B) refer total $[M+H]^+$ ions of 1–6, 11, and 13 with a tolerance range of ± 0.005 , and in other colors refer $[M+H]^+$ ions of 1–6, 11, and 13 (C–J), respectively.

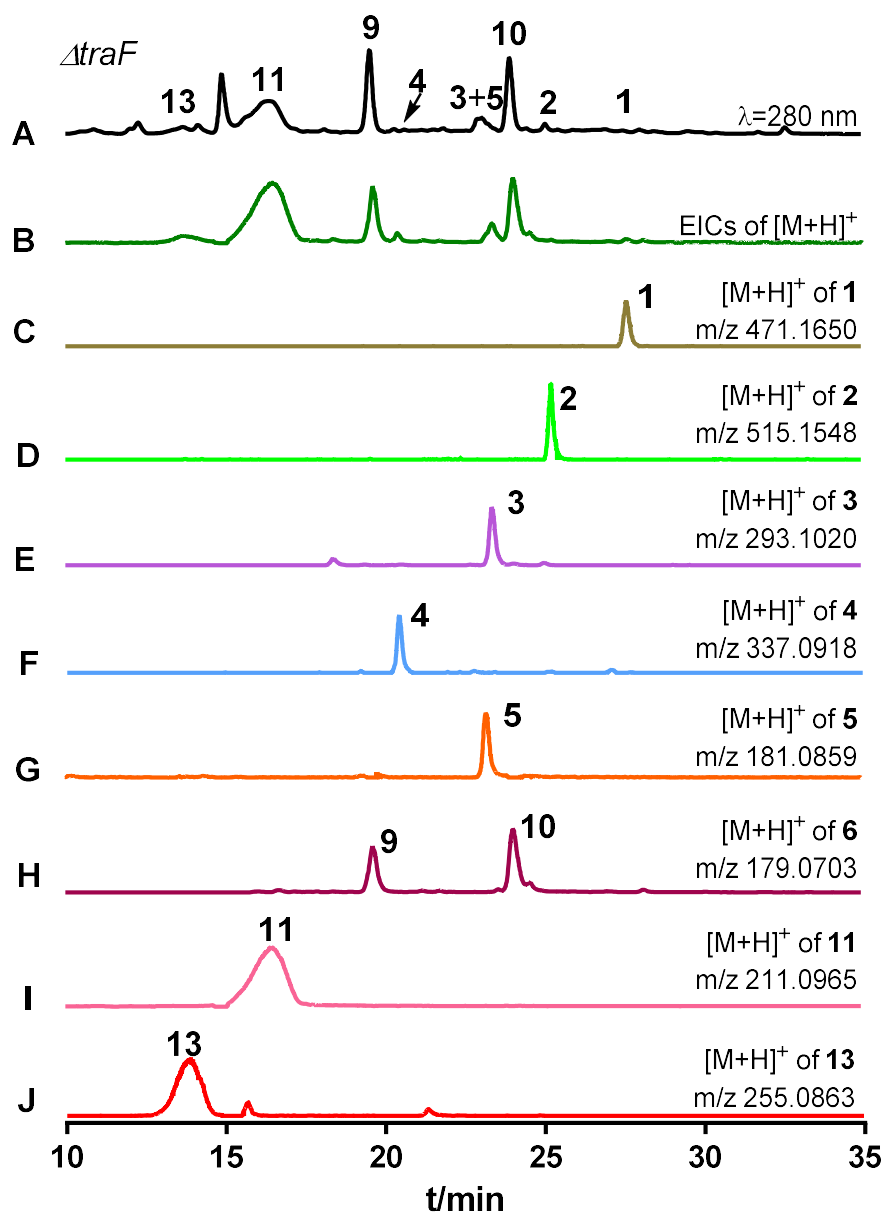


Figure S12. LC-MS analysis of the metabolite profile of the $\Delta traF$ -mutant

Absorptions at 280 nm are illustrated in black (A). EICs in dark green (B) refer total $[M+H]^+$ ions of 1–6, 11, and 13 with a tolerance range of ± 0.005 , and in other colors refer $[M+H]^+$ ions of 1–6, 11, and 13 (C–J), respectively.

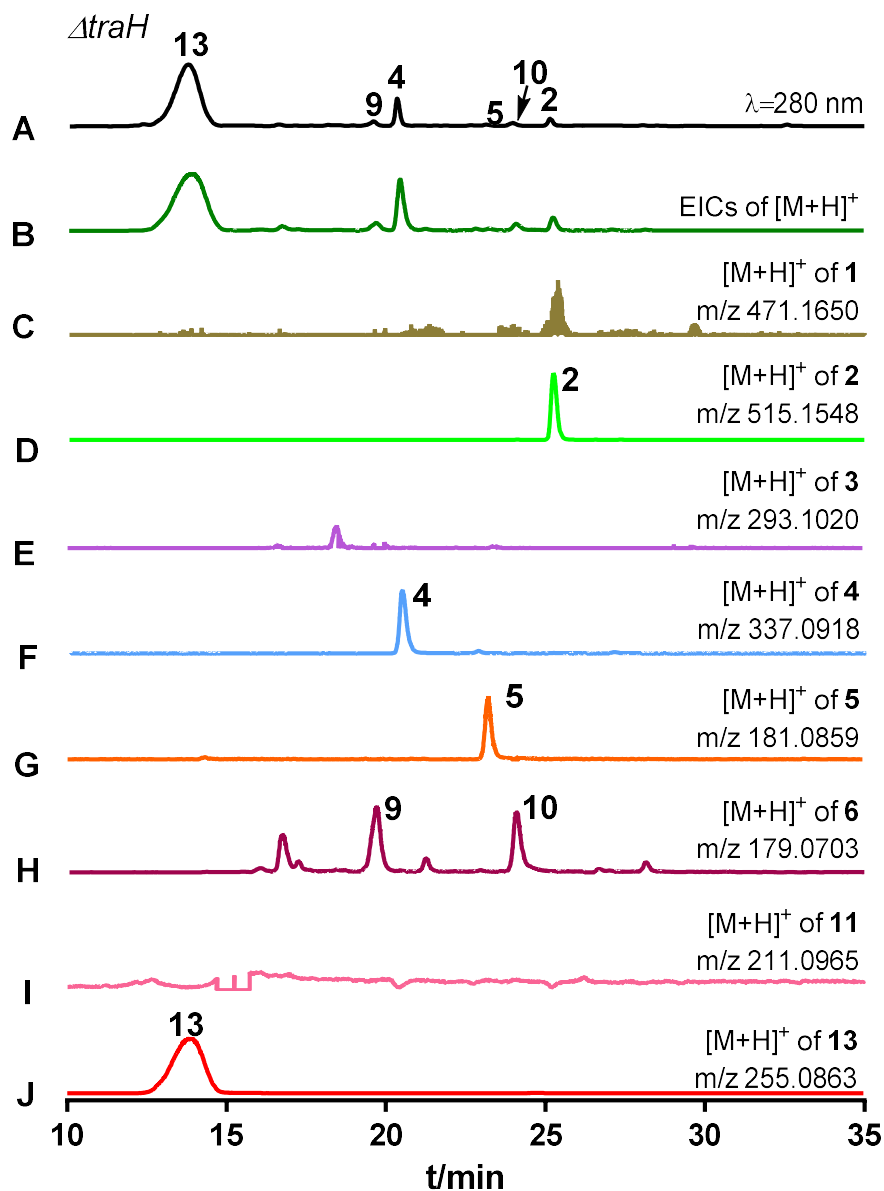


Figure S13. LC-MS analysis of the metabolite profile of the $\Delta traH$ -mutant

Absorptions at 280 nm are illustrated in black (A). EICs in dark green (B) refer total $[M+H]^+$ ions of 1–6, 11, and 13 with a tolerance range of ± 0.005 , and in other colors refer $[M+H]^+$ ions of 1–6, 11, and 13 (C–J), respectively.

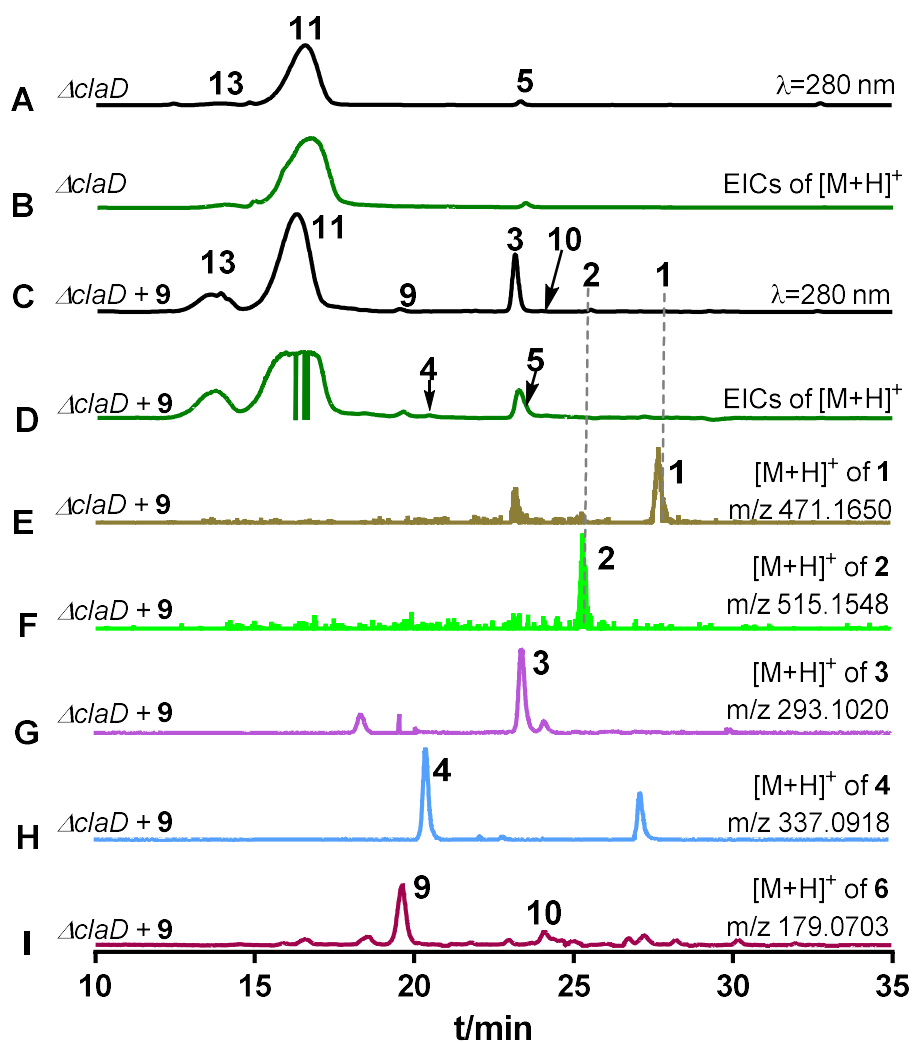


Figure S14. LC-MS analysis of the metabolite profile of the $\Delta claD$ -mutant with and without feeding with **9**

Absorptions at 280 nm are illustrated in black (A and C). EICs in dark green (B and D) refer total $[M+H]^+$ ions of **1–6**, **11**, and **13** with a tolerance range of ± 0.005 , and in other colors refer $[M+H]^+$ ions of **1–4** and **6** (E–I), respectively.

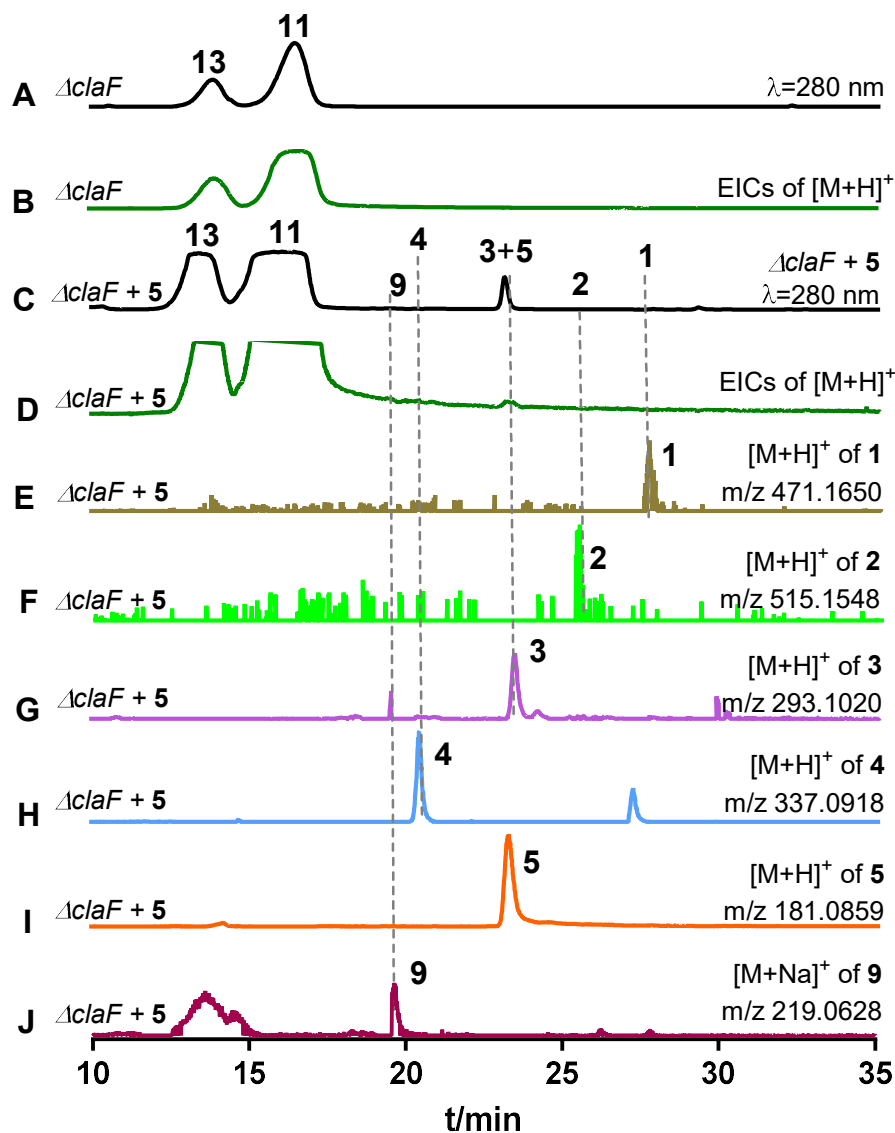


Figure S15. LC-MS analysis of the metabolite profile of the $\Delta claF$ -mutant with and without feeding with 5

Absorptions at 280 nm are illustrated in black (A and C). EICs in dark green (B and D) refer total $[M+H]^+$ ions of 1–6, 11, and 13 with a tolerance range of ± 0.005 , and in other colors refer $[M+H]^+$ ions of 1–5 (E–I) or $[M+Na]^+$ ion of 9 (J).

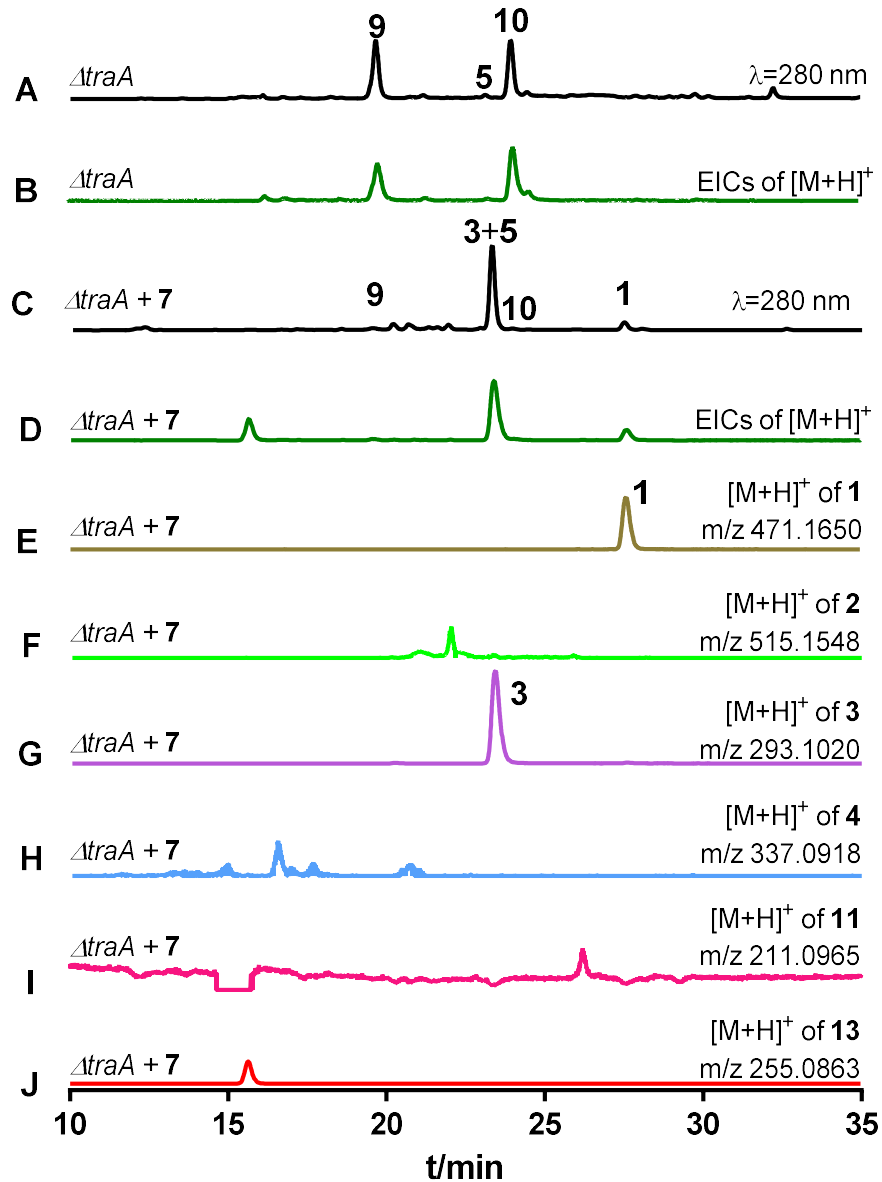


Figure S16. LC-MS analysis of the metabolite profile of the $\Delta traA$ -mutant with and without feeding with 7

Absorptions at 280 nm are illustrated in black (A and C). EICs in dark green (B and D) refer total $[M+H]^+$ ions of 1–6, 11, and 13 with a tolerance range of ± 0.005 , in other colors refer $[M+H]^+$ ions of 1–4, 11, and 13 (E–J), respectively.

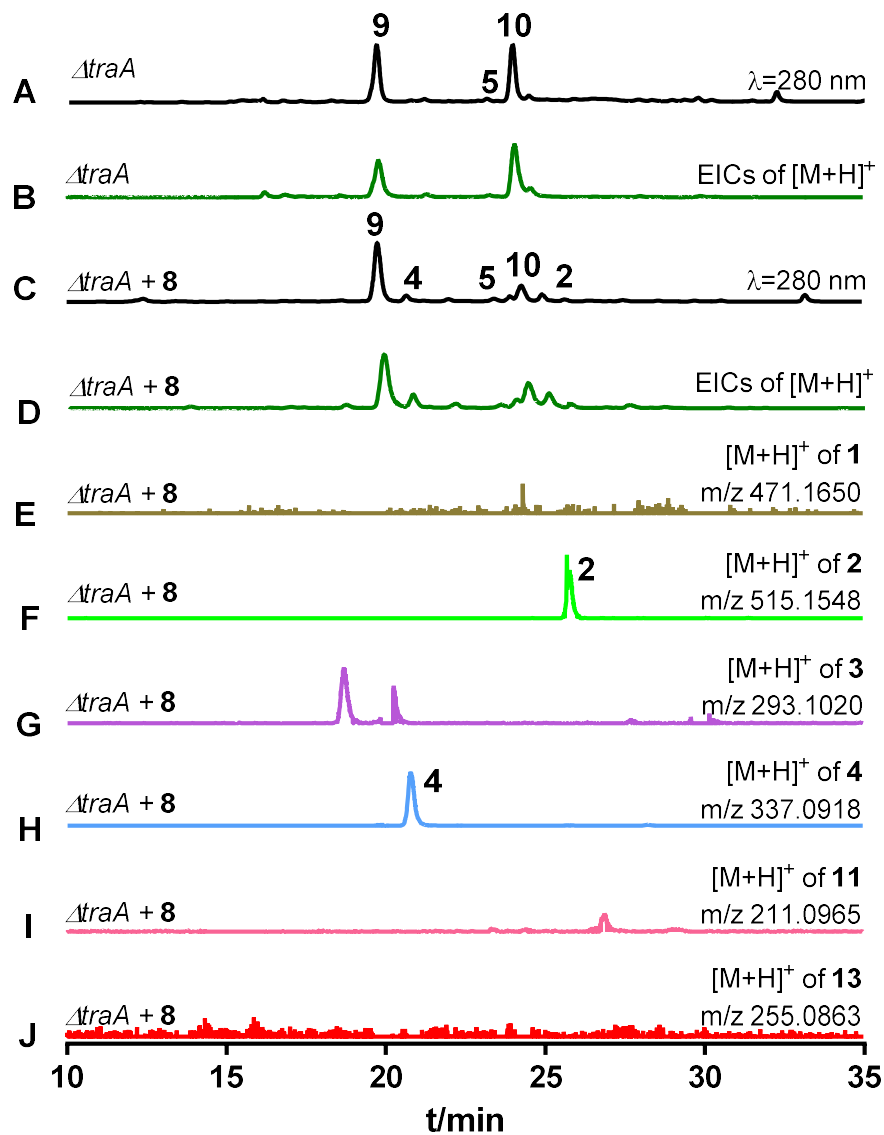


Figure S17. LC-MS analysis of the metabolite profile of the $\Delta traA$ -mutant with and without feeding with **8**

Absorptions at 280 nm are illustrated in black (A and C). EICs in dark green refer $[M+H]^+$ ions of **1–6**, **11**, and **13** (B and D) with a tolerance range of ± 0.005 , and in other colors refer $[M+H]^+$ ions of **1–4**, **11**, and **13** (E–J), respectively.

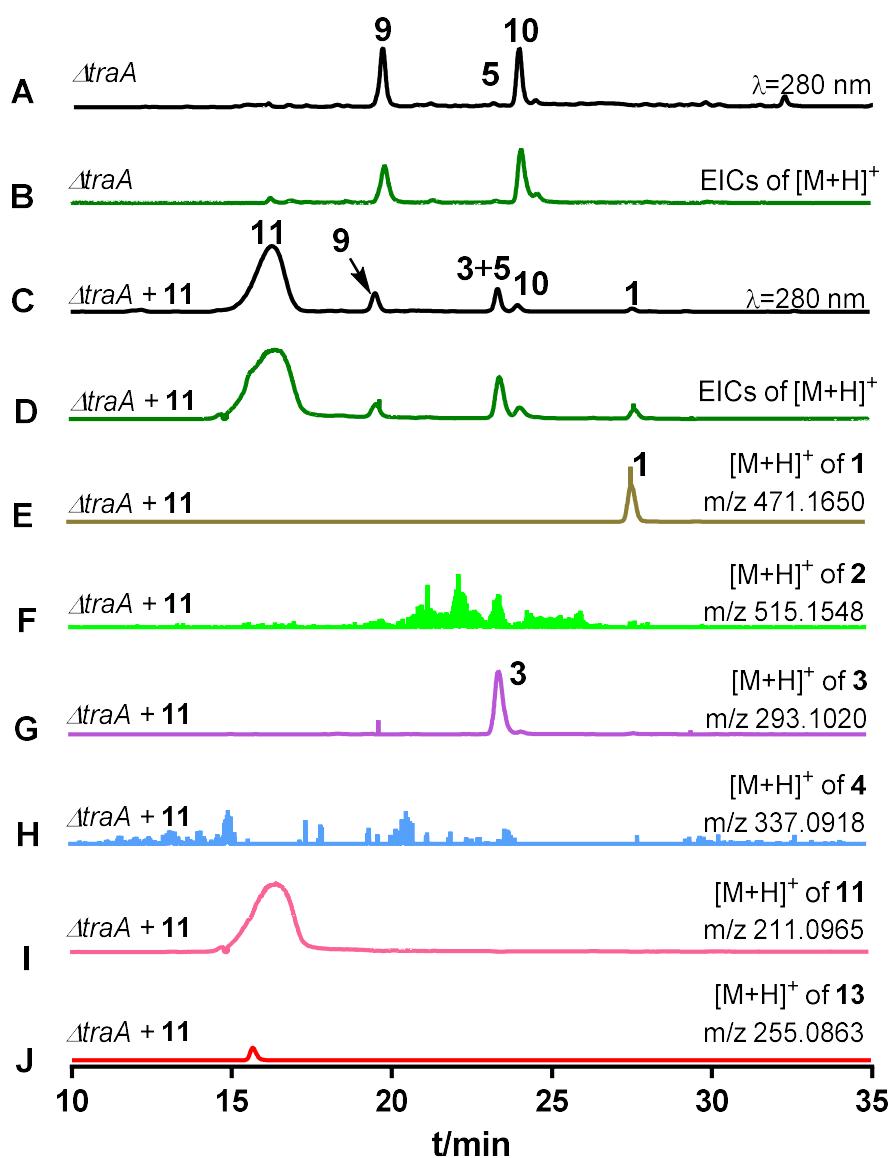


Figure S18. LC-MS analysis of the metabolite profile of the $\Delta traA$ -mutant with and without feeding with **11**

Absorptions at 280 nm are illustrated in black (A and C). EICs in dark green refer $[M+H]^+$ ions of **1–6**, **11**, and **13** (B and D with a tolerance range of ± 0.005 , and in other different colors refer $[M+H]^+$ ions of **1–4**, **11**, and **13** (E–J), respectively.

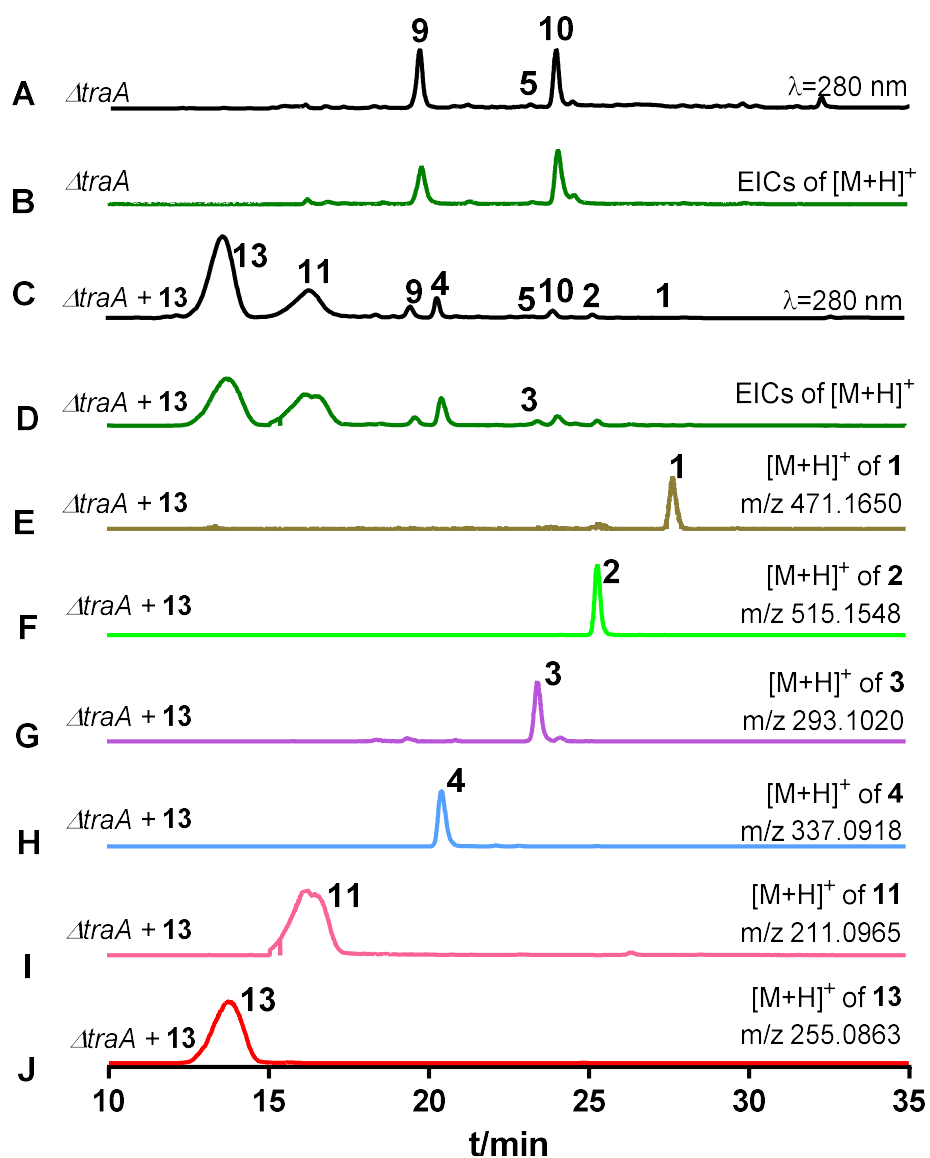


Figure S19. LC-MS analysis of the metabolite profile of the $\Delta traA$ -mutant with and without feeding with 13

Absorptions at 280 nm are illustrated in black (A and C). EICs in dark green refer $[M+H]^+$ ions of 1–6, 11, and 13 (B and D) with a tolerance range of ± 0.005 , and in other different colors refer $[M+H]^+$ ions of 1–4, 11, and 13 (E–J), respectively.

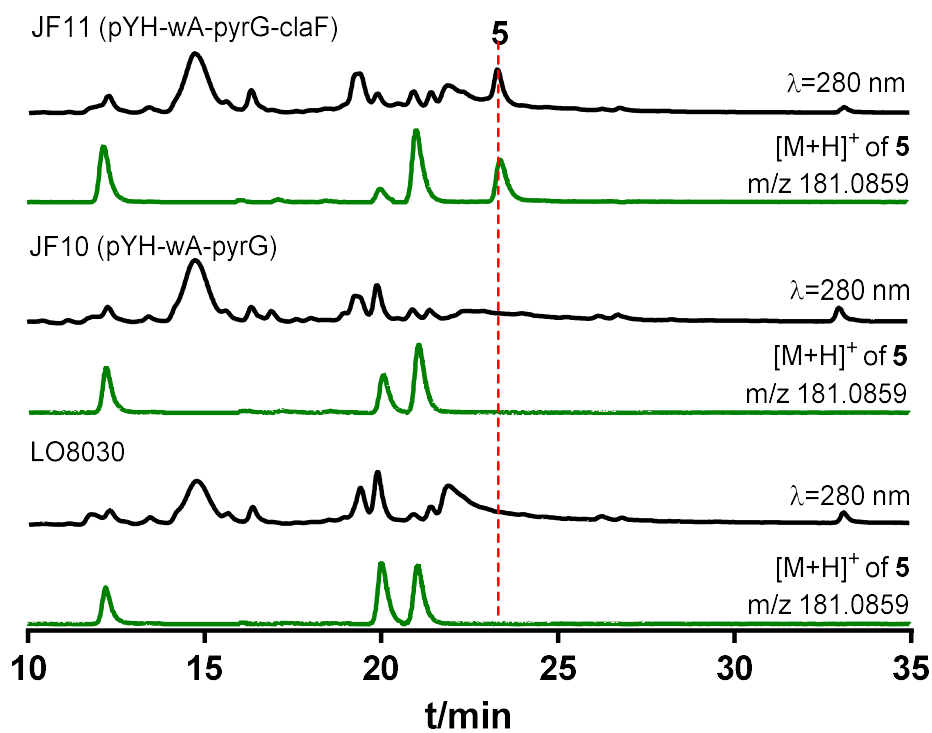


Figure S20. LC-MS analysis of the metabolite profile of different *A. nidulans* strains. Absorptions at 280 nm and $[M+H]^+$ of (5) m/z 181.0859 are illustrated. JF11 carries the expression construct for *claF* in *A. nidulans* LO8030 and JF10 the empty vector pYH-wA-pyrG.

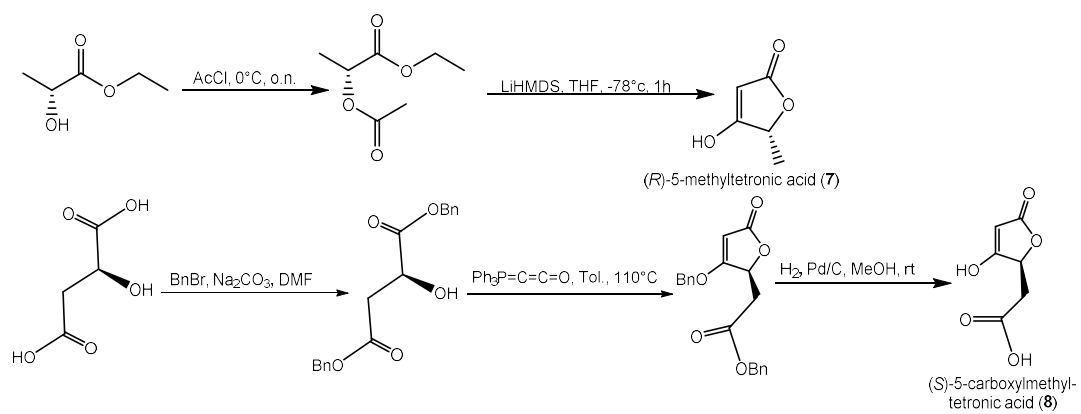


Figure S21. Chemical synthesis of the tetronic acids **7** and **8**

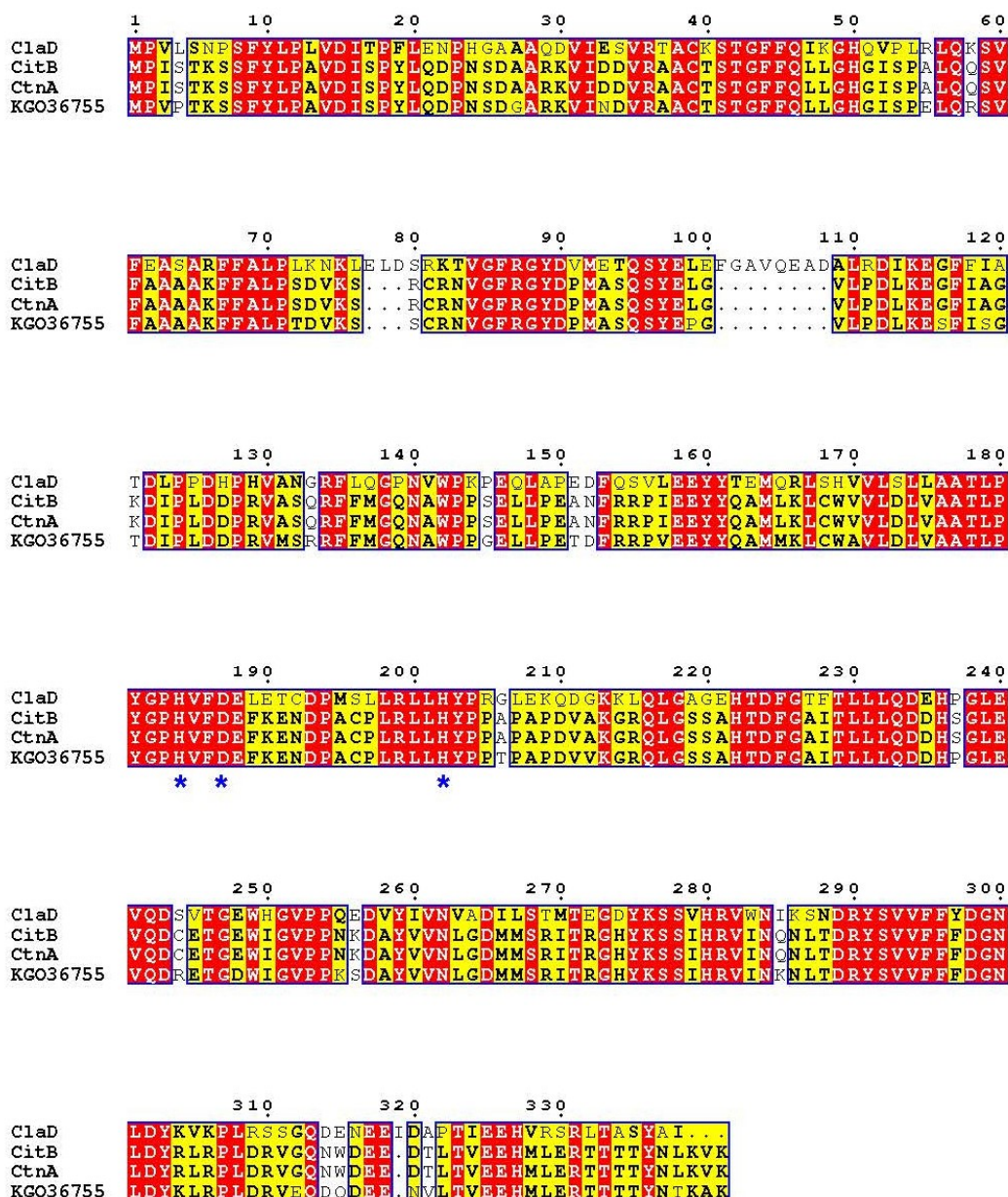


Figure S22. Sequence alignments of 2-OG-dependent oxygenases

CitB (ALI92653), CtnA (BAE95338), and KGO36755 are from *Monascus ruber* M7, *Monascus purpureus*, and *Penicillium expansum* and share sequence identities of 53.8, 53.8, and 53.6% with ClaD, respectively. ClaD also contains the typical conserved 2-His-1-Asp ion-binding triad of non-heme Fe^{II}/2-oxoglutarate-dependent oxygenases (His₁₈₄, His₂₀₂ and Asp₁₈₇) (marked with *).¹³ Protein sequence alignments were carried out by using the sequence alignment function of MEGA 5.2 and visualized with ESPrnt 3.0 (<http://esprnt.ibcp.fr/ESPrnt/ESPrnt/>).

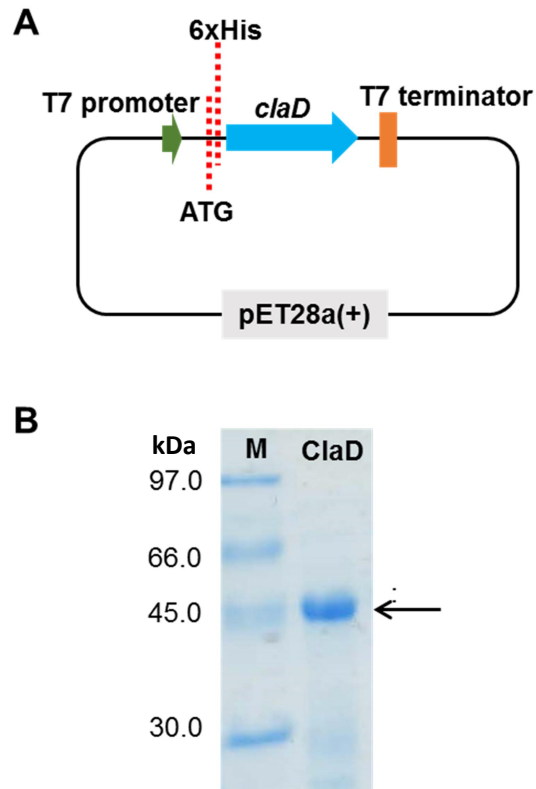


Figure S23. Analysis of ClaD on SDS PAGE

(A) *claD* was inserted into pET28a(+) with 6xHis at its N-terminal. (B) The recombinant histidine-tagged ClaD was purified and separated on a 12% gel after induction with 0.5 mM IPTG at 30°C for 6 h in TB medium.

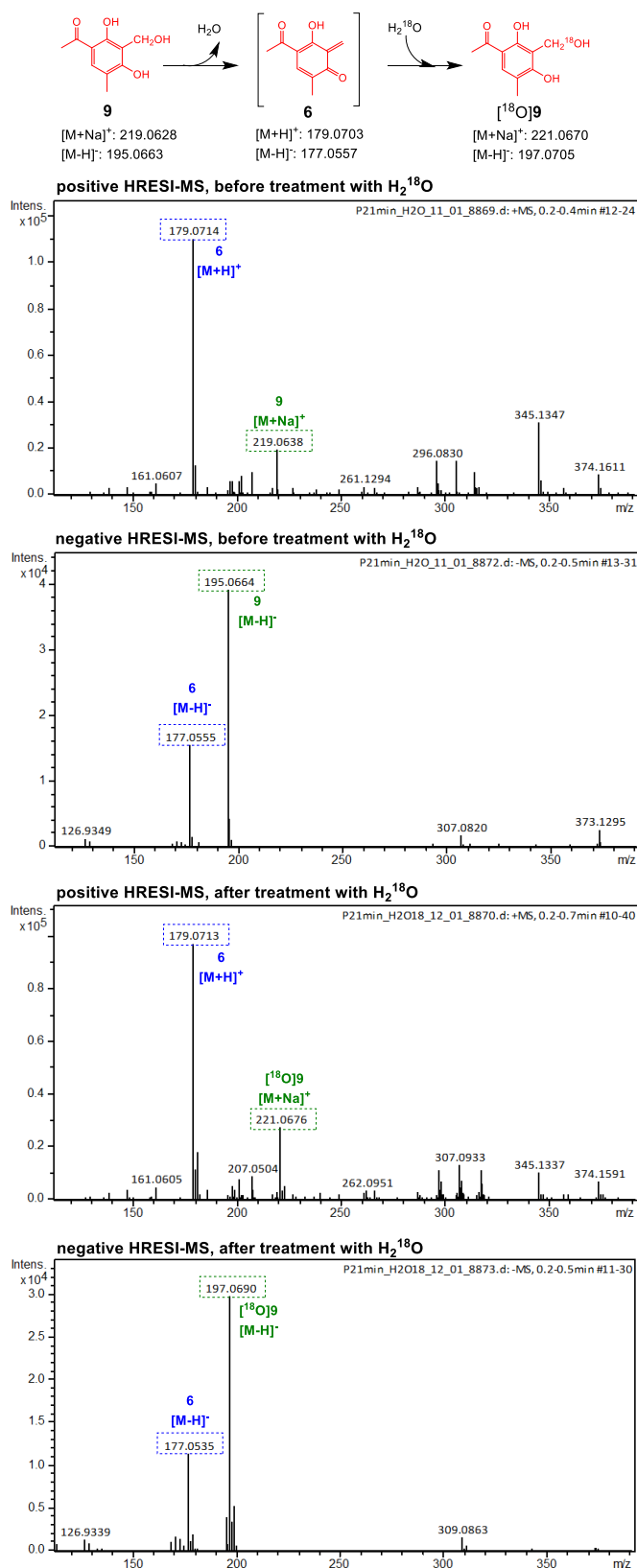


Figure S24. MS analysis of **9** after incubation in H₂O and in ¹⁸O-enriched H₂¹⁸O Hydroxyclovatol (**9**) was dissolved in H₂O and ¹⁸O-enriched H₂¹⁸O and incubated at room temperature for 16 h. MS data of two samples were collected in both positive and negative modes.

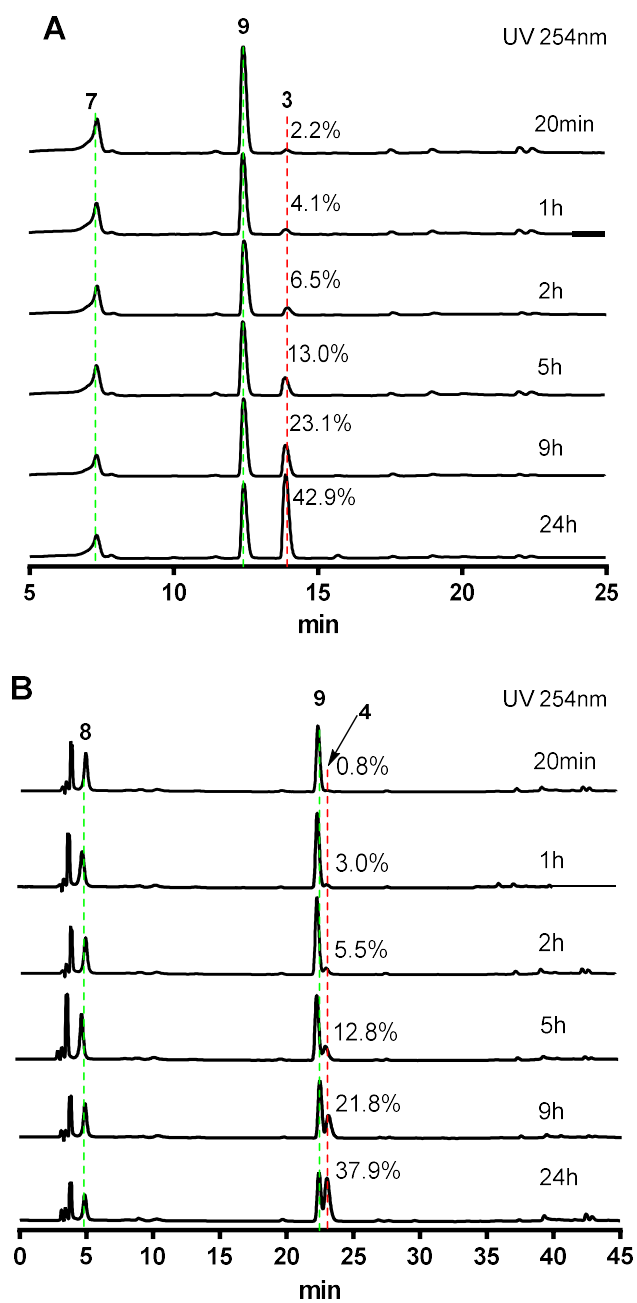


Figure S25. Time dependence of Michael addition reaction of **9** with **7** (A) or **8** (B) The incubations were carried out at room temperature in distilled H₂O. Absorptions at 254 nm are illustrated.

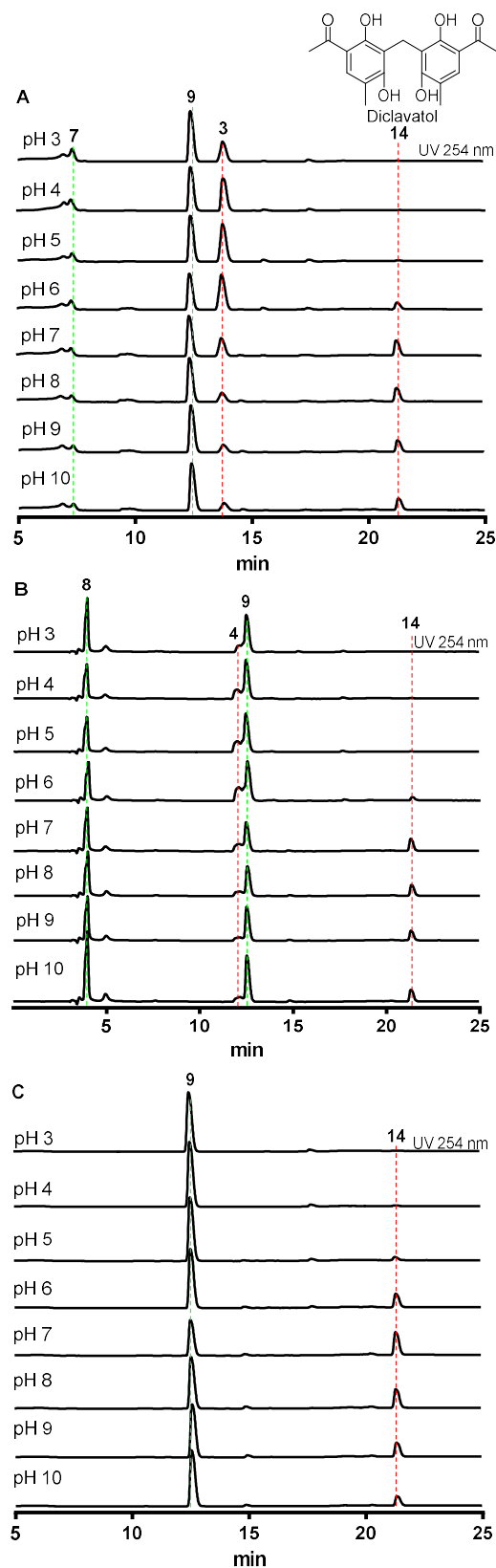


Figure S26. pH dependence on Michael addition reactions forming **3** and **4**
HPLC analysis of mixtures of **9** with **7** (A), **8** (B) or alone (C) in phosphate saline buffer with different pH values at room temperature for 12 h. Absorptions at 254 nm are illustrated.

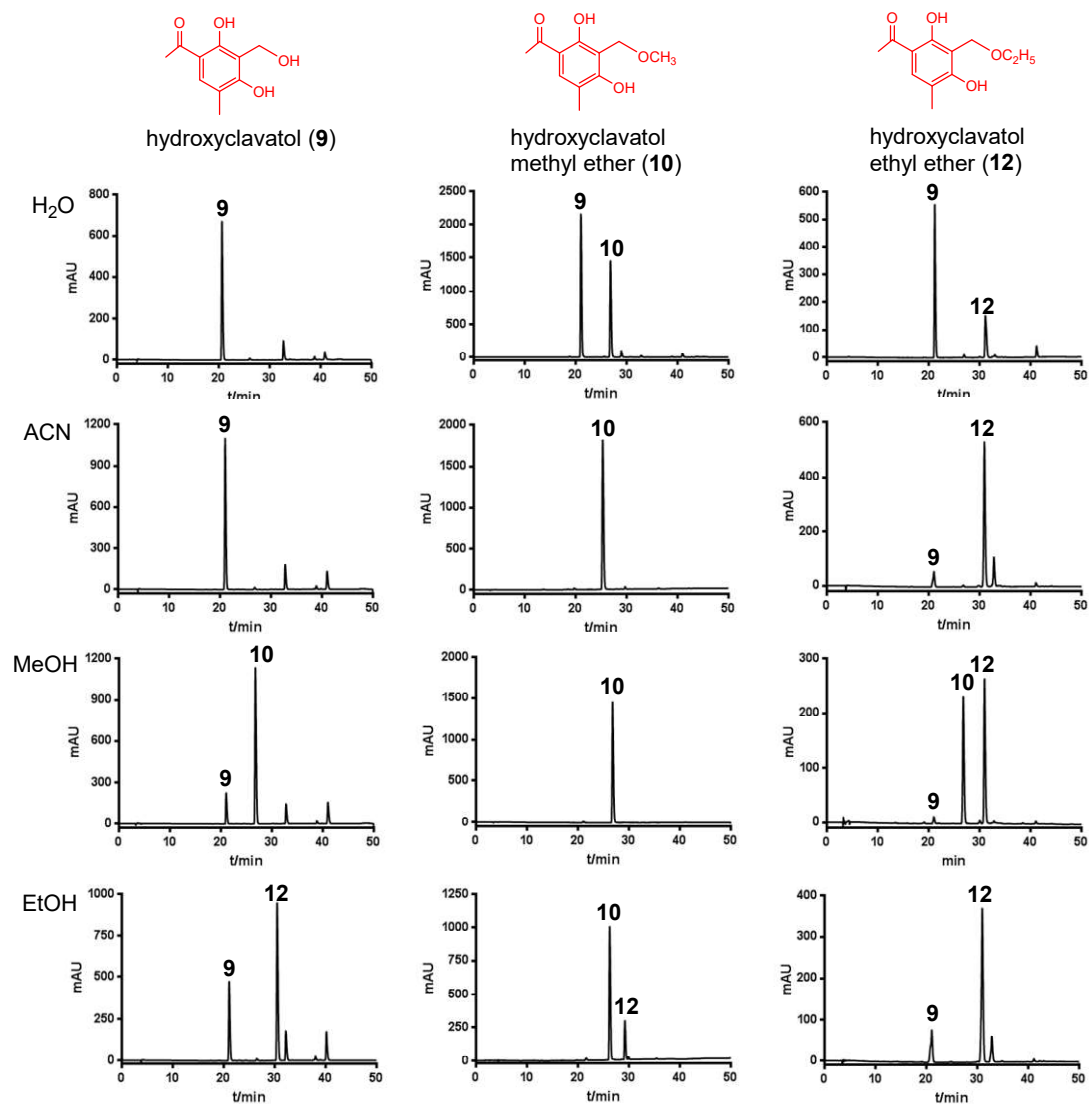
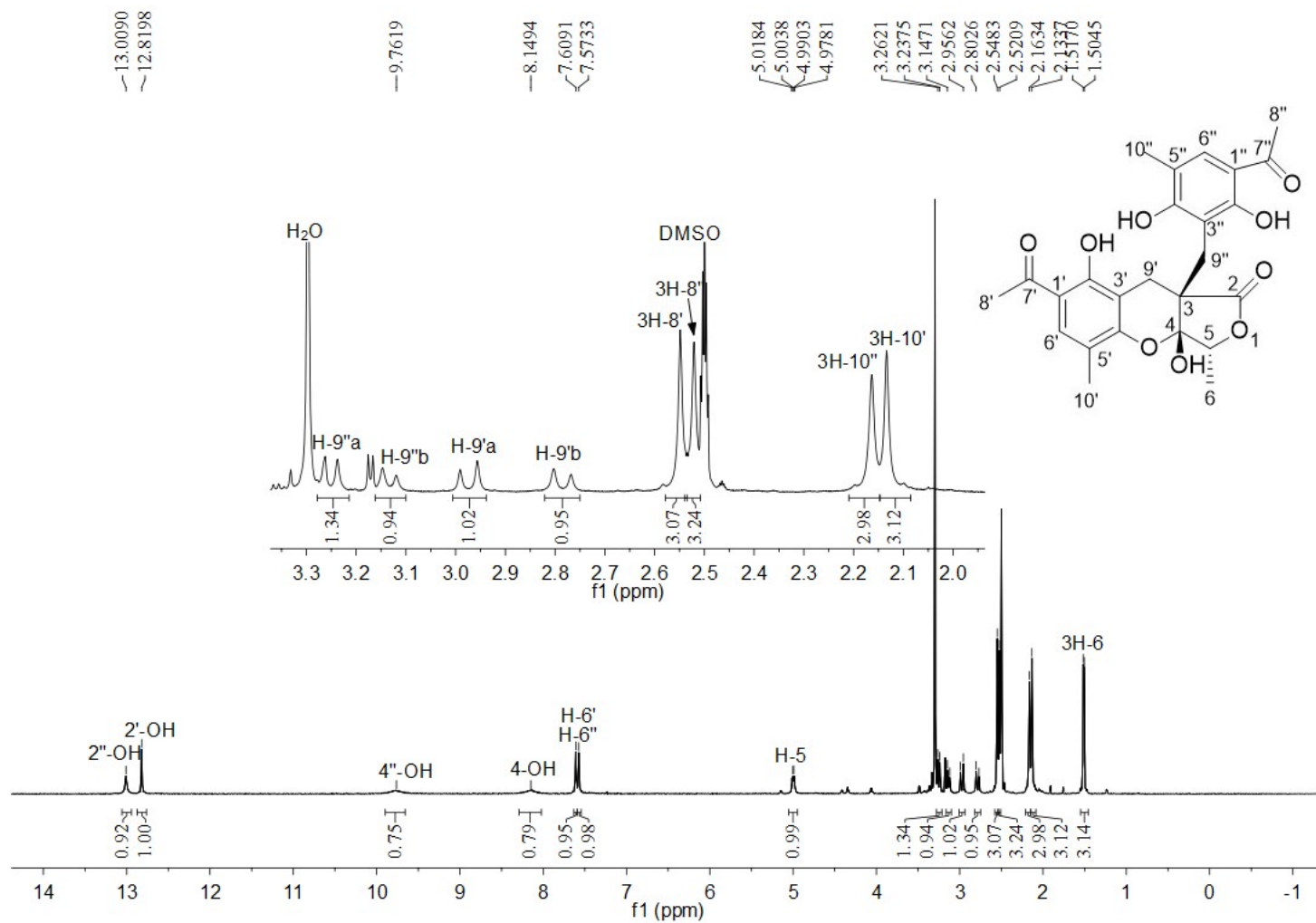


Figure S27. HPLC analysis of **9**, **10**, and **12** after incubation in different solvents. Incubation of hydroxyclovatol (**9**), hydroxyclovatol methyl ether (**10**), and hydroxyclovatol ethyl ether (**12**) in H₂O, acetonitrile, MeOH and EtOH at room temperature for 12 h. Absorptions at 280 nm are illustrated.



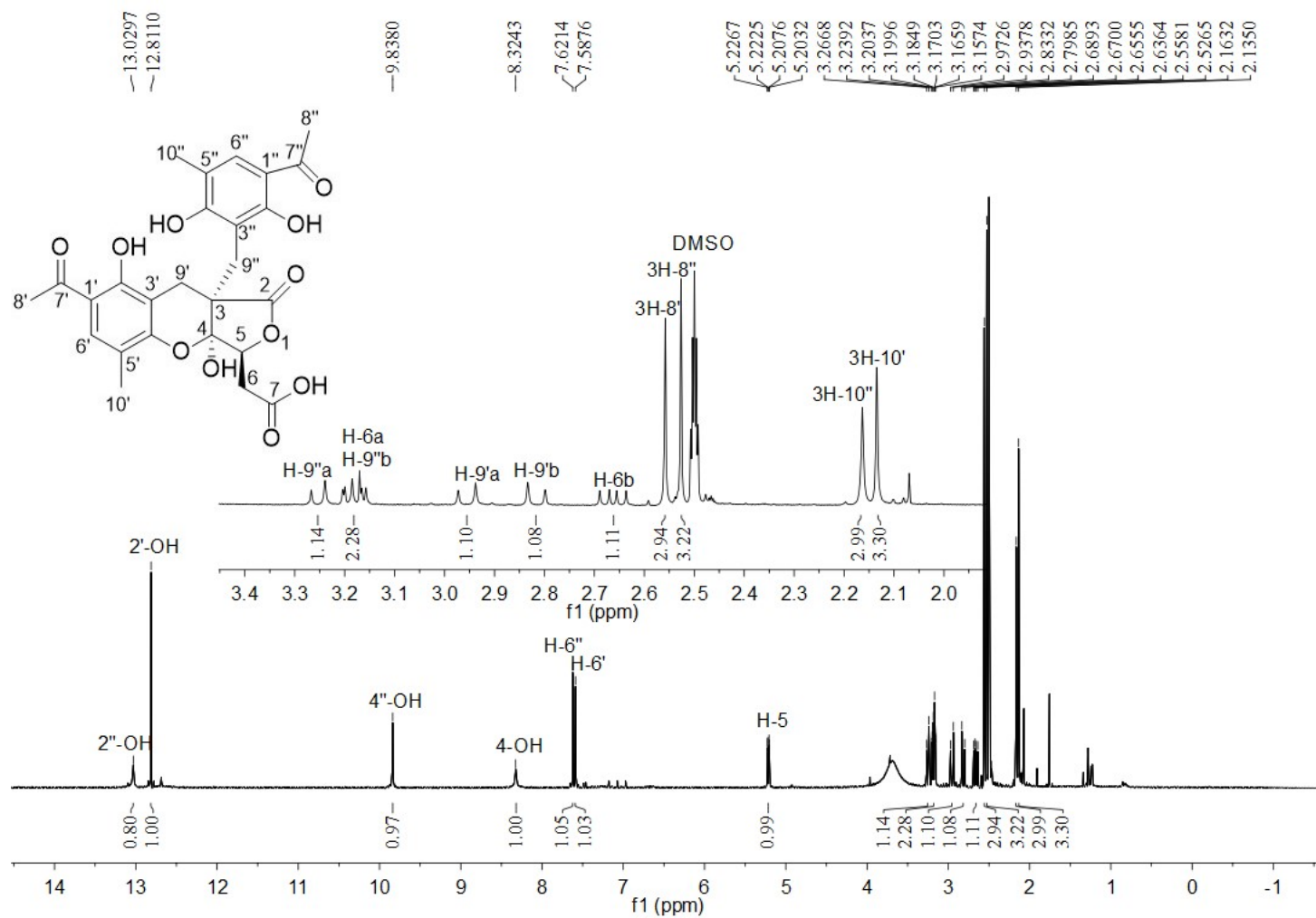


Figure S29. ^1H NMR spectrum of compound **2** in $\text{DMSO-}d_6$ (500 MHz)

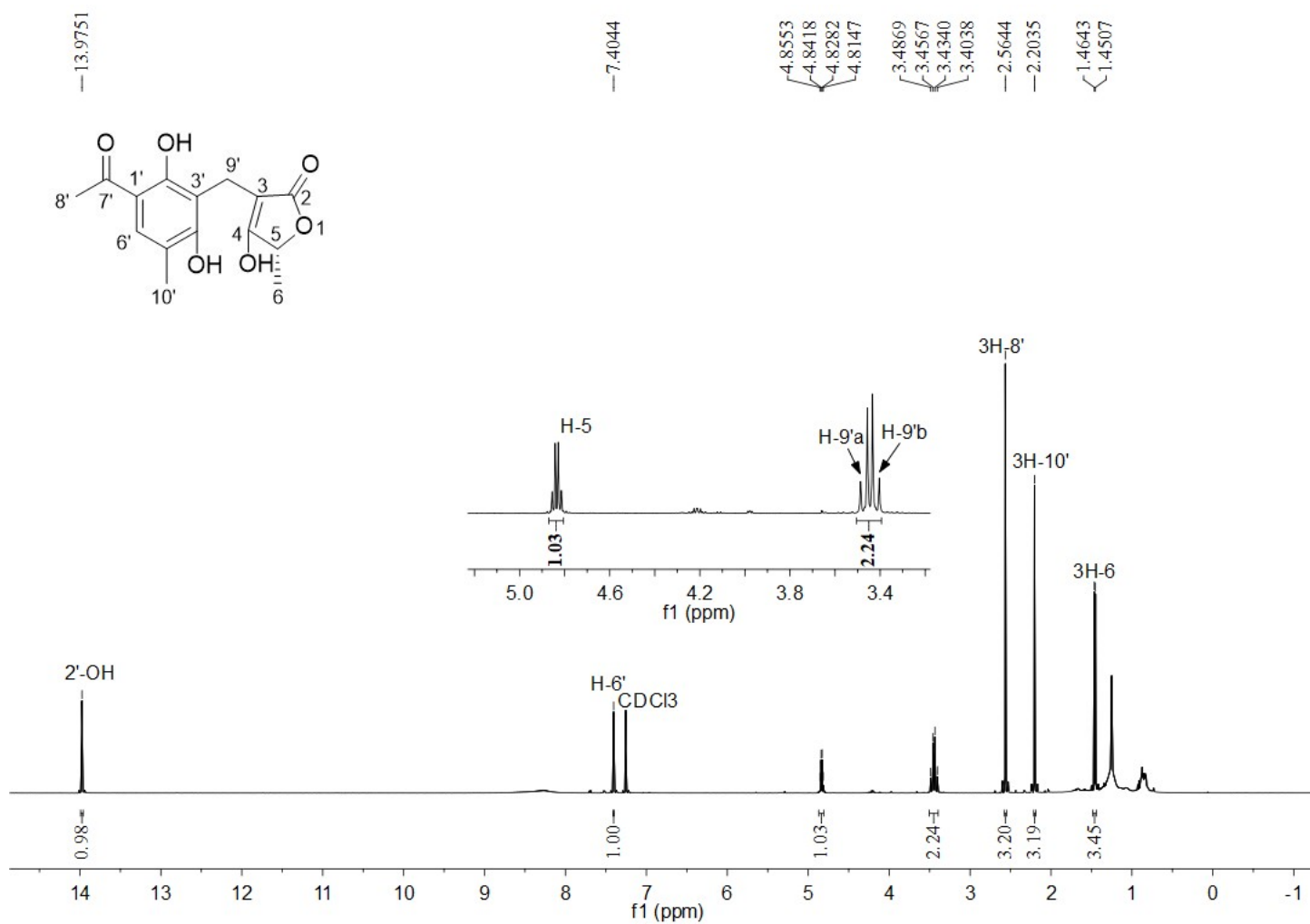


Figure S30. ¹H NMR spectrum of compound **3** in CDCl₃ (500 MHz)

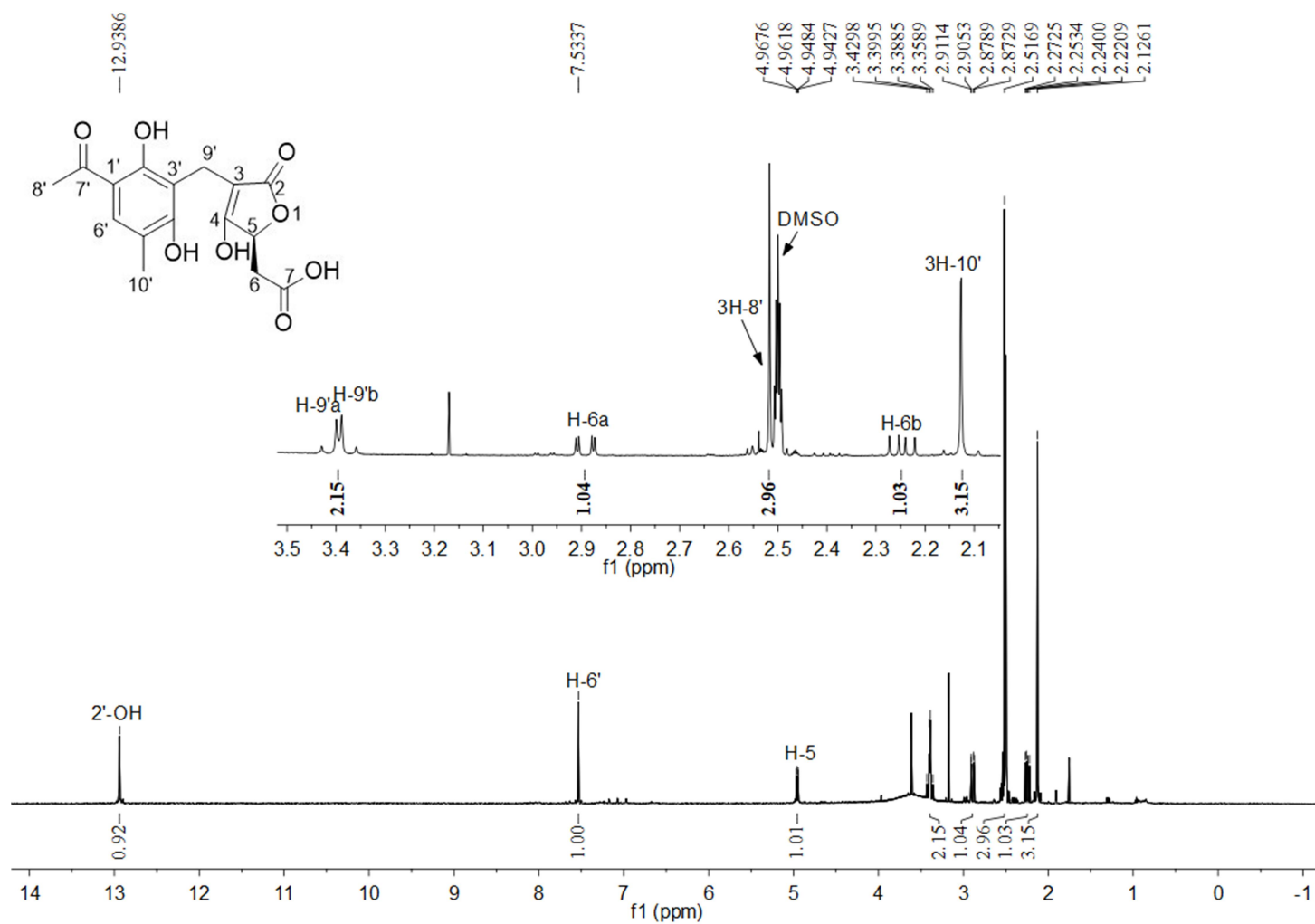


Figure S31. ^1H NMR spectrum of compound **4** in $\text{DMSO-}d_6$ (500 MHz)

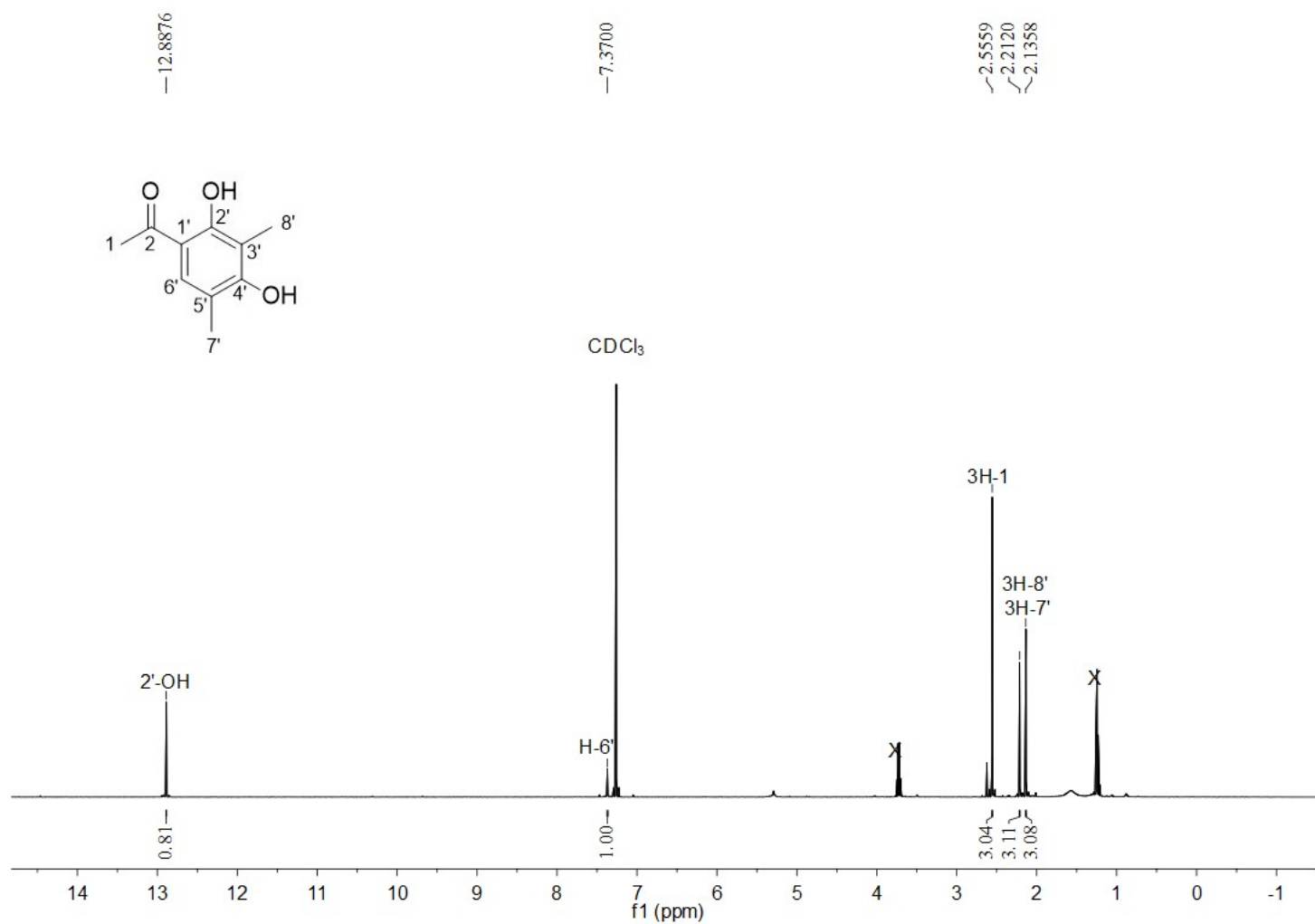


Figure S32. ¹H NMR spectrum of compound **5** in CDCl₃ (500MHz)

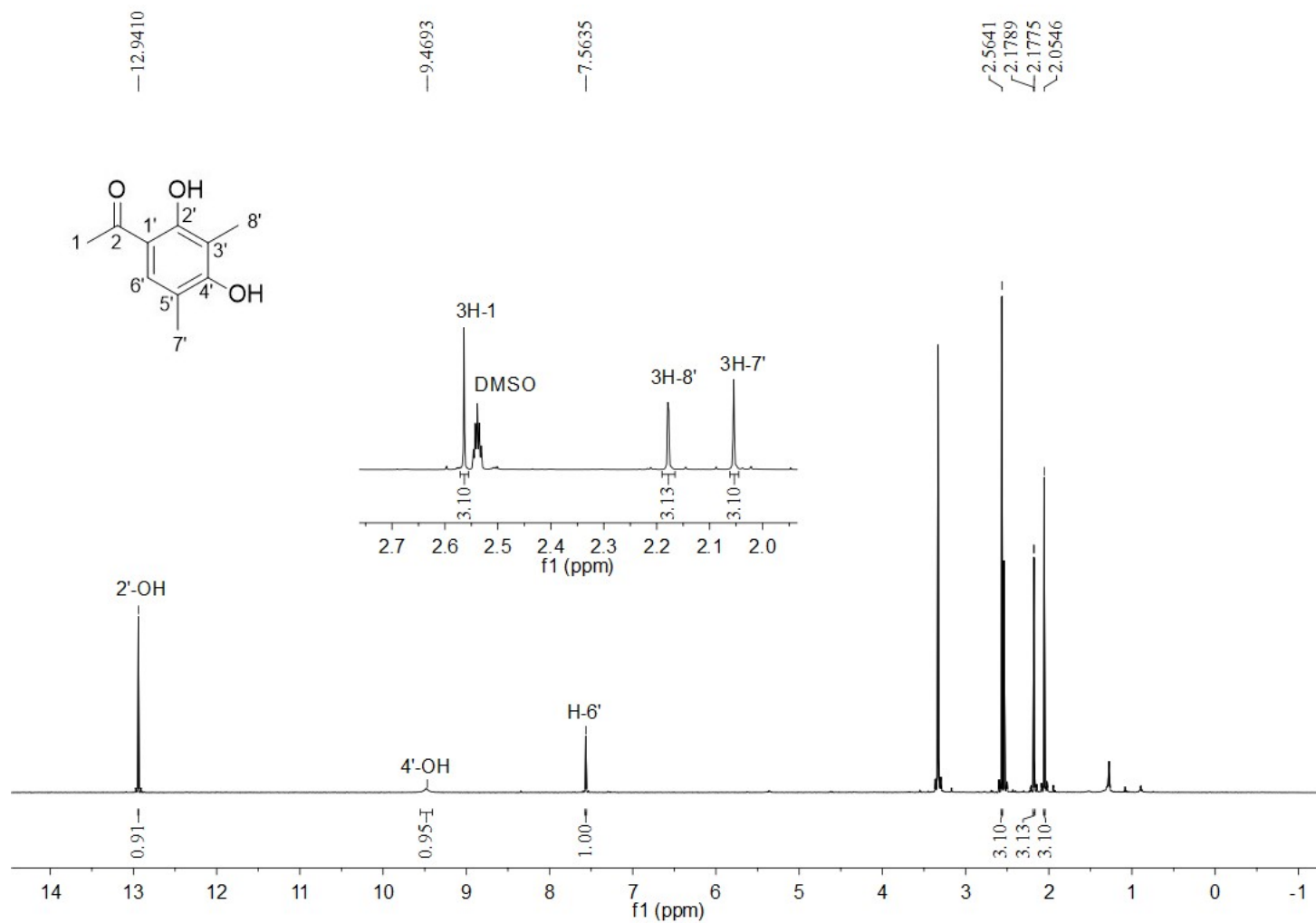


Figure S33. ^1H NMR spectrum of compound **5** in $\text{DMSO}-d_6$ (500MHz)

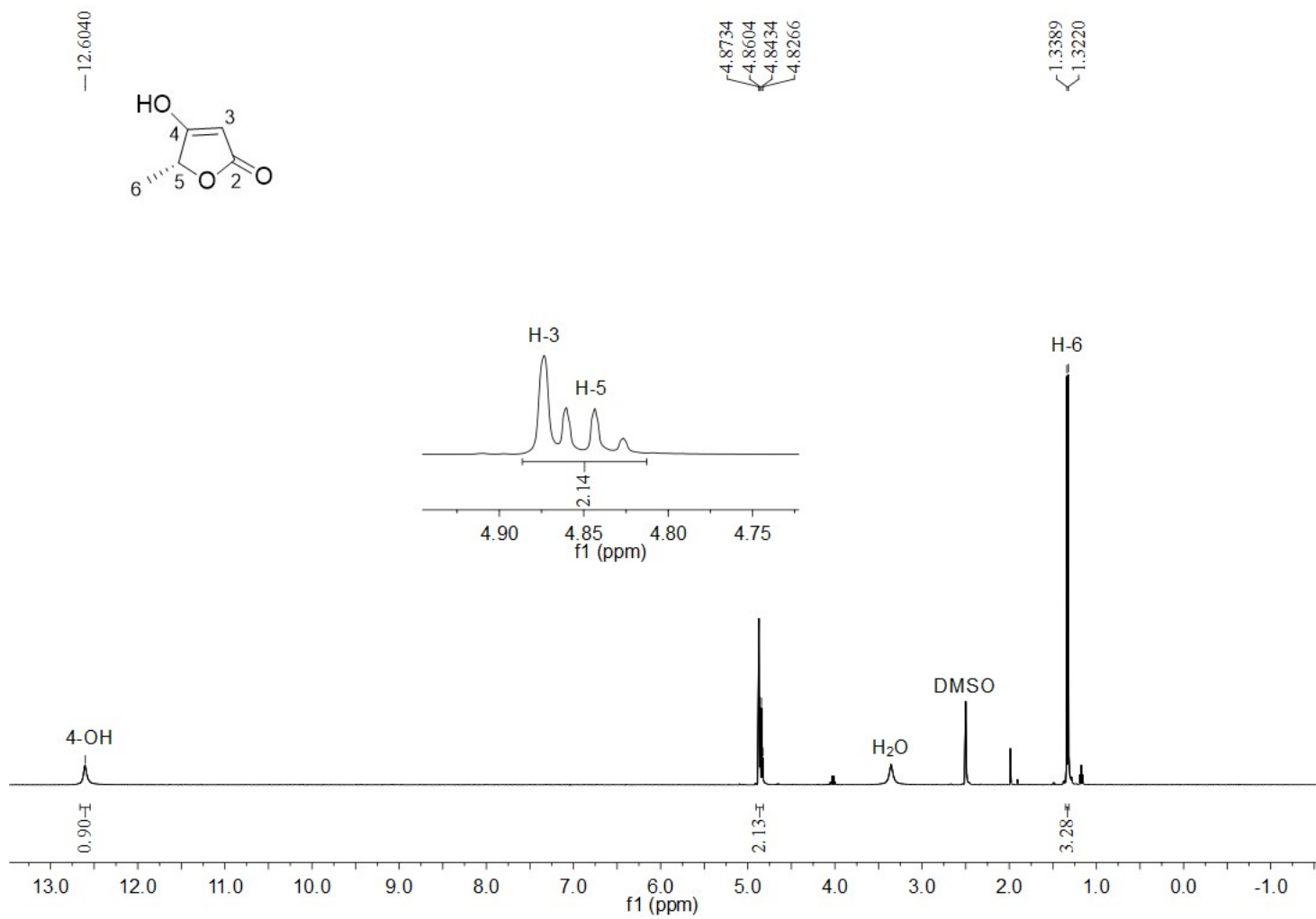


Figure S34. ¹H NMR spectrum of compound **7** in DMSO-*d*₆ (400MHz)

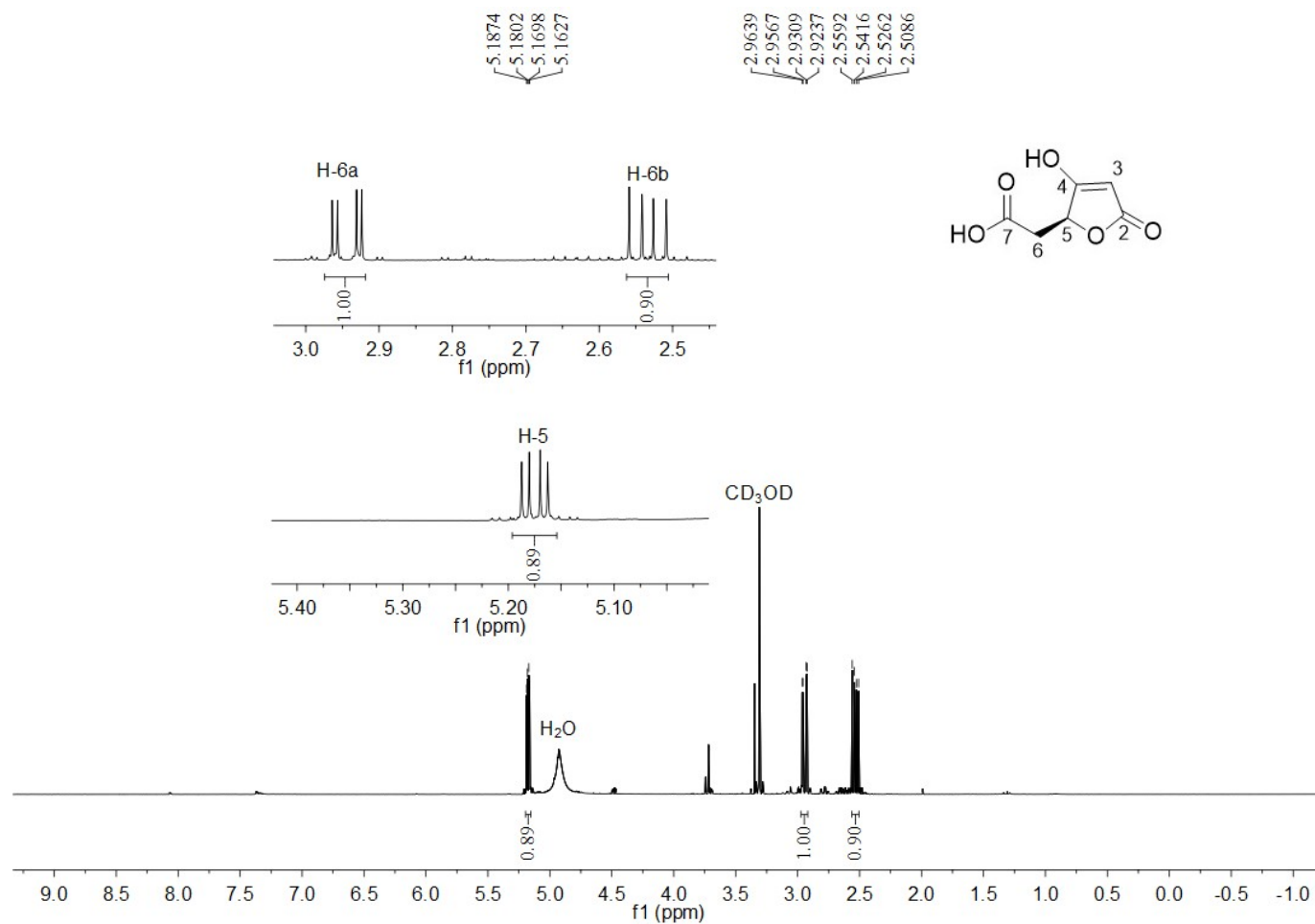


Figure S35. ^1H NMR spectrum of compound **8** in CD_3OD (500MHz)

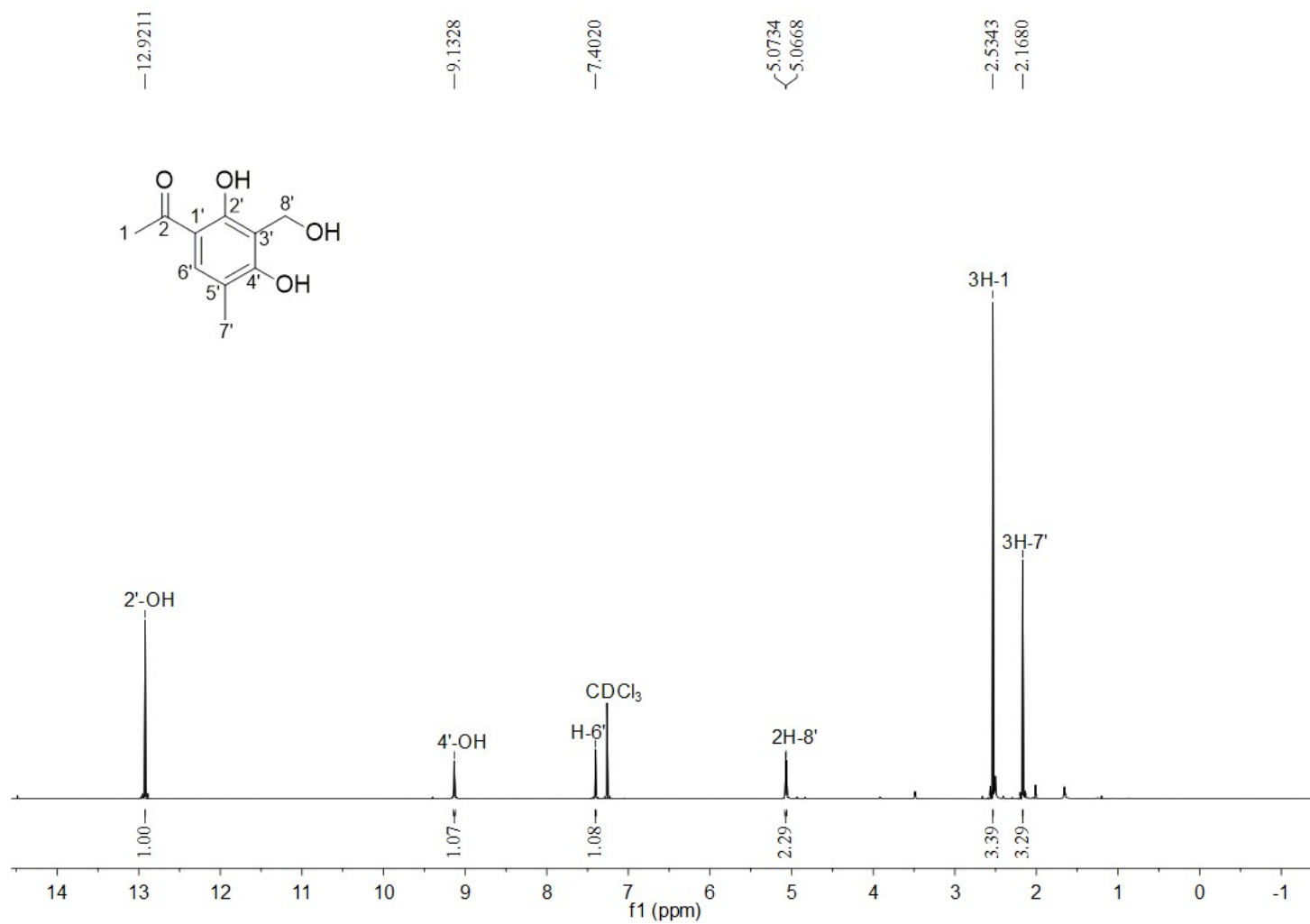


Figure S36. ^1H NMR spectrum of compound **9** in CDCl_3 (500MHz)

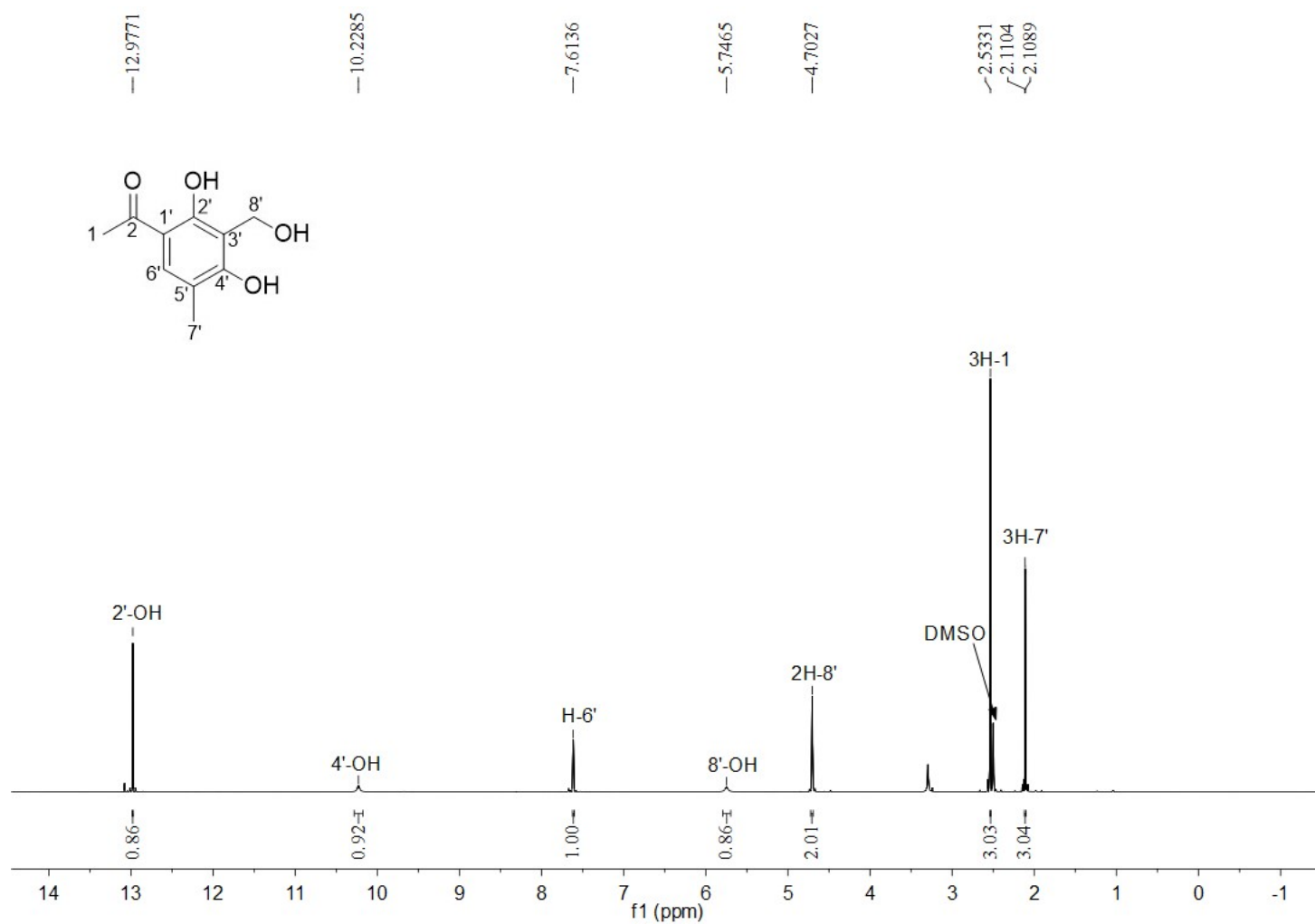


Figure S37. ¹H NMR spectrum of compound **9** in DMSO-*d*₆ (500MHz)

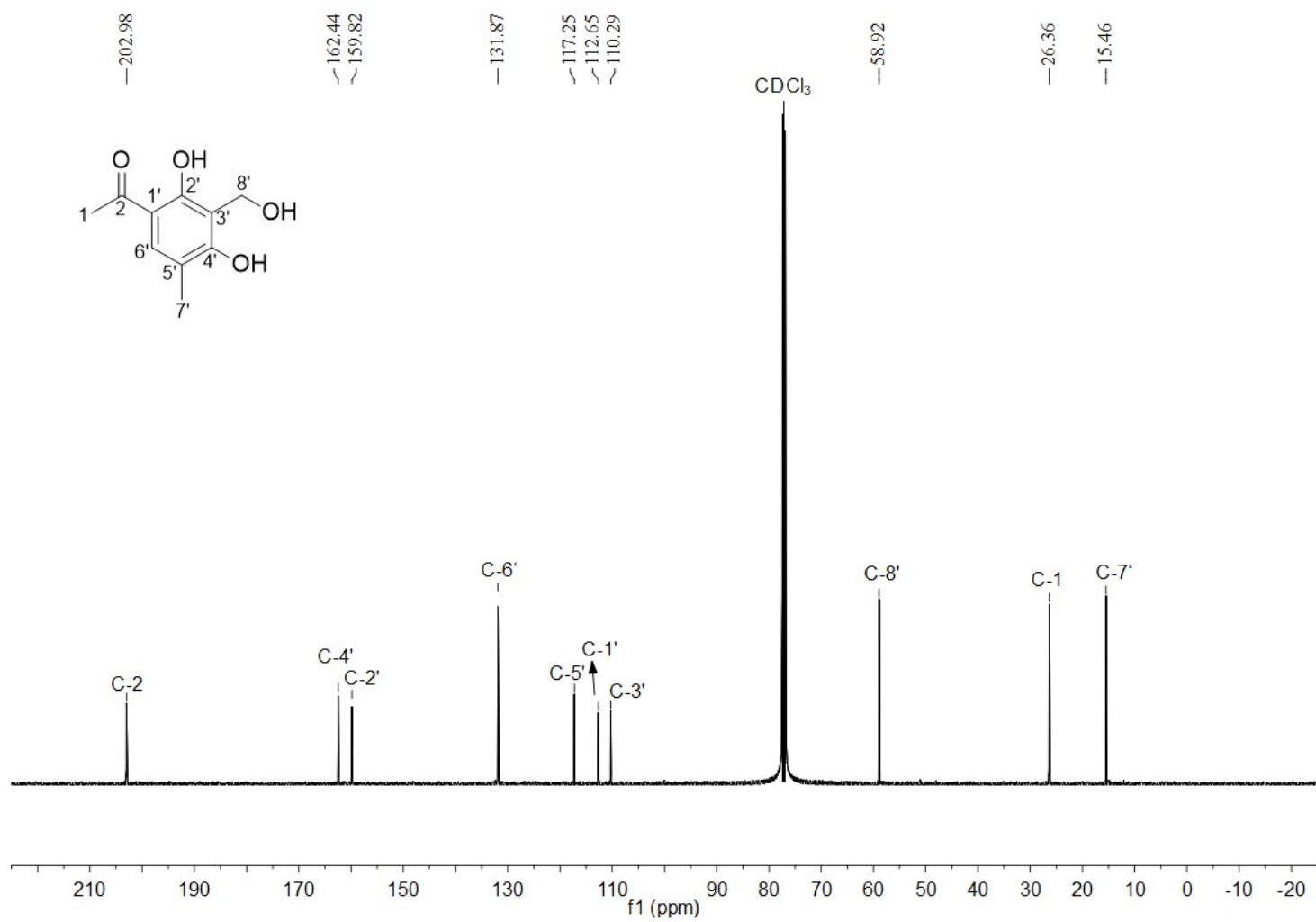


Figure S38. ^{13}C NMR spectrum of compound **9** in CDCl_3 (125MHz)

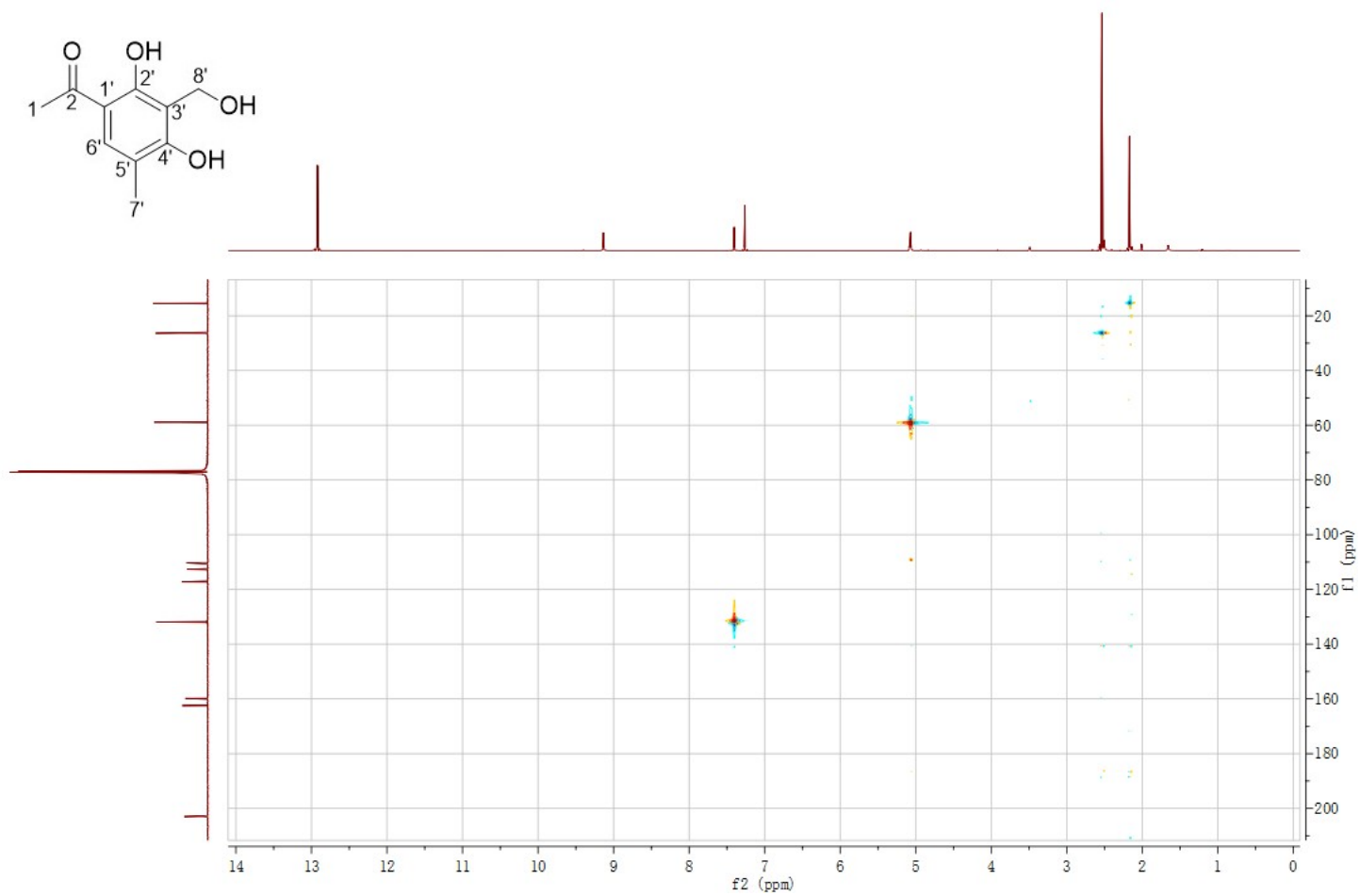


Figure S39. HMQC spectrum of compound **9** in CDCl₃

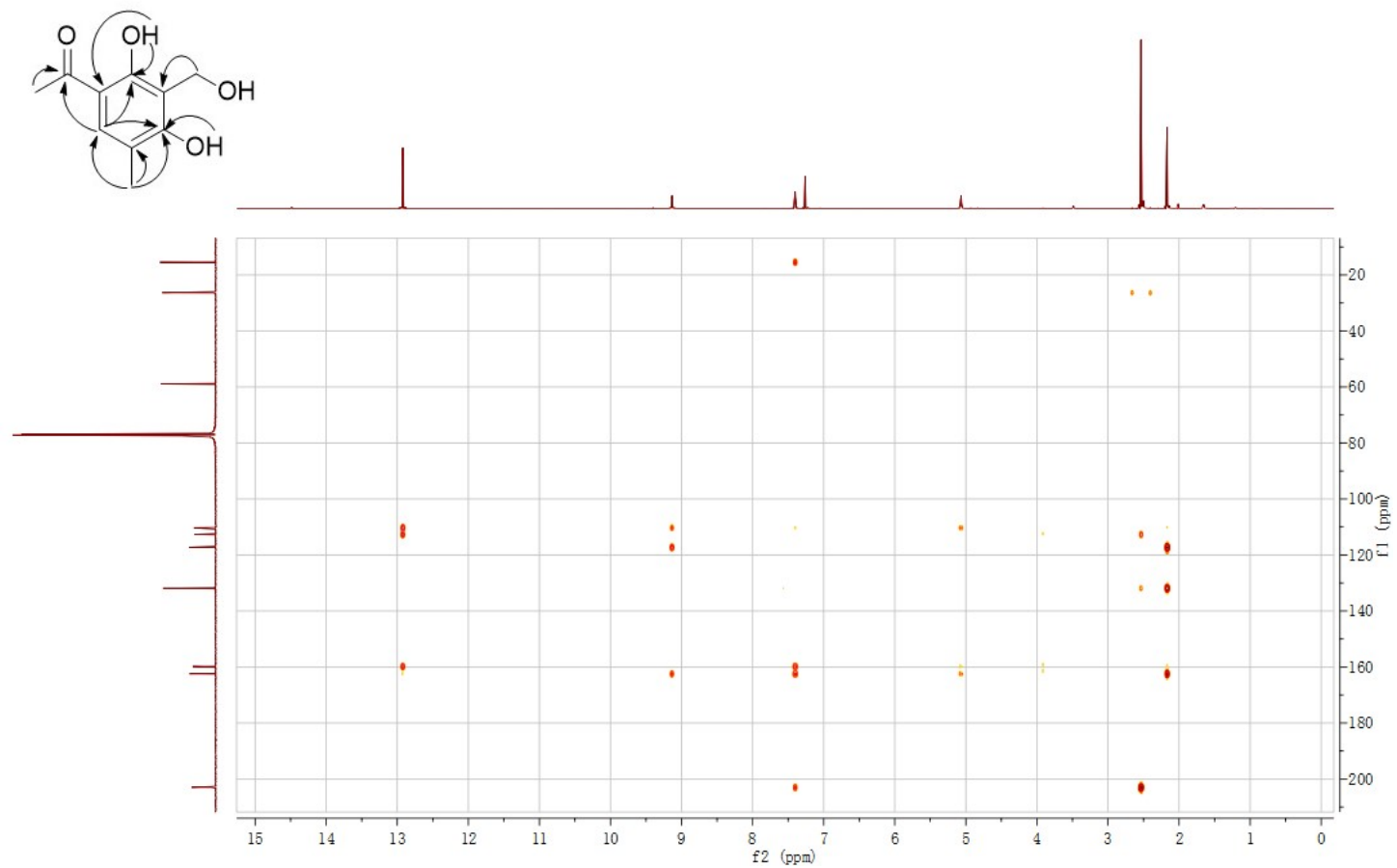


Figure S40. HMBC spectrum of compound **9** in CDCl₃

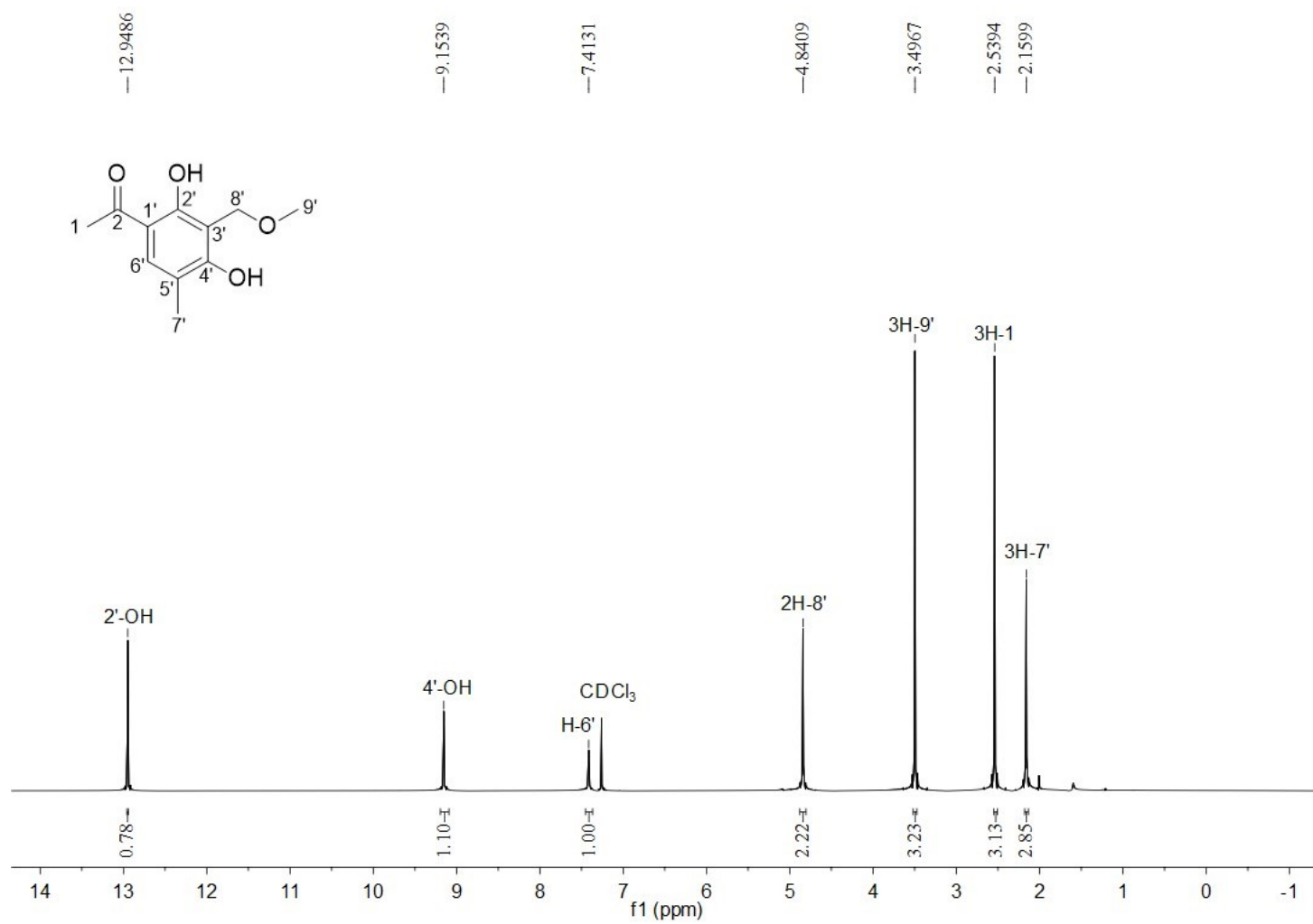


Figure S41. ¹H NMR spectrum of compound **10** in CDCl₃ (500MHz)

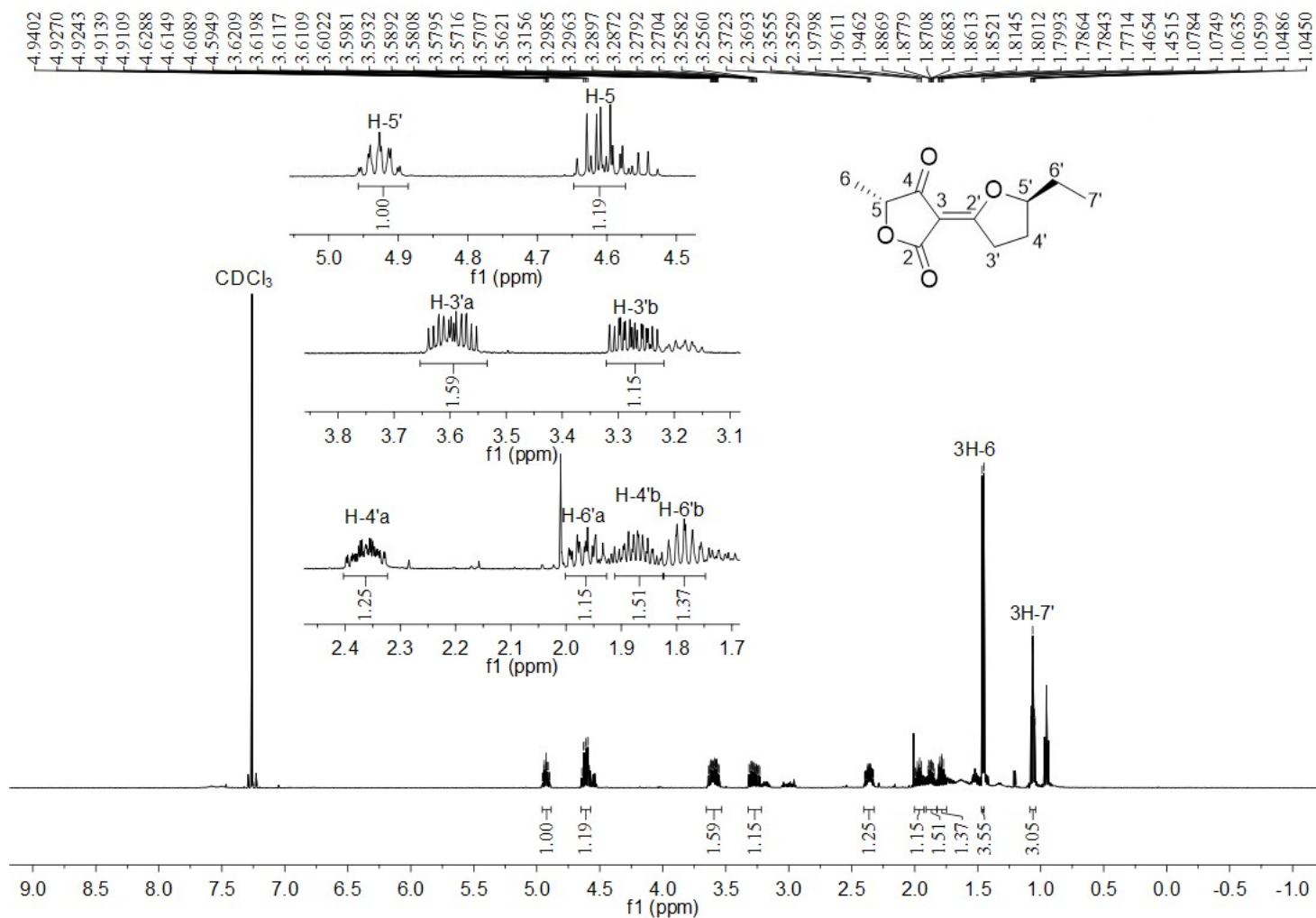


Figure S42. ¹H NMR spectrum of compound **11** in CDCl₃ (500 MHz)

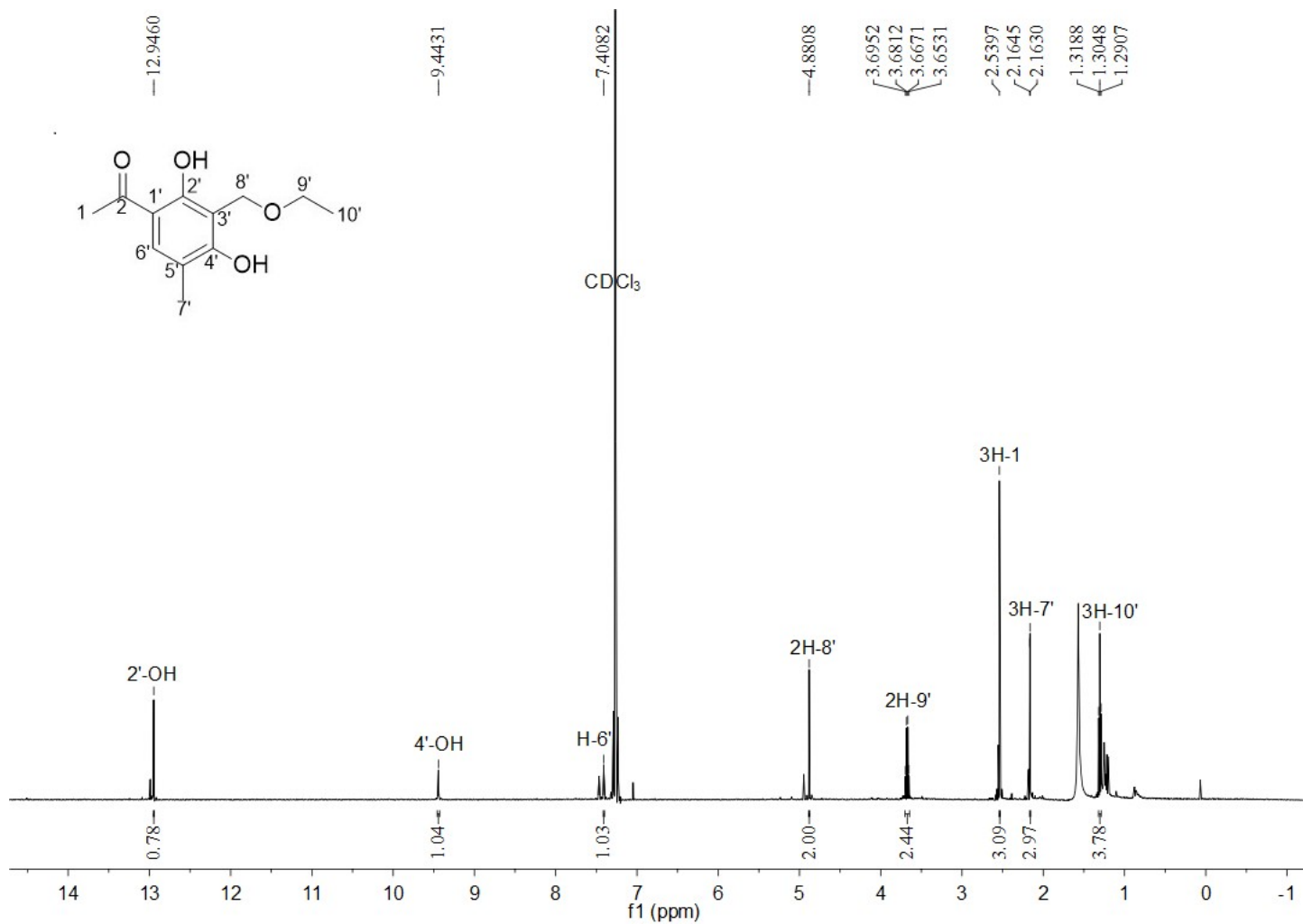


Figure S43. ¹H NMR spectrum of compound **12** in CDCl₃ (500 MHz)

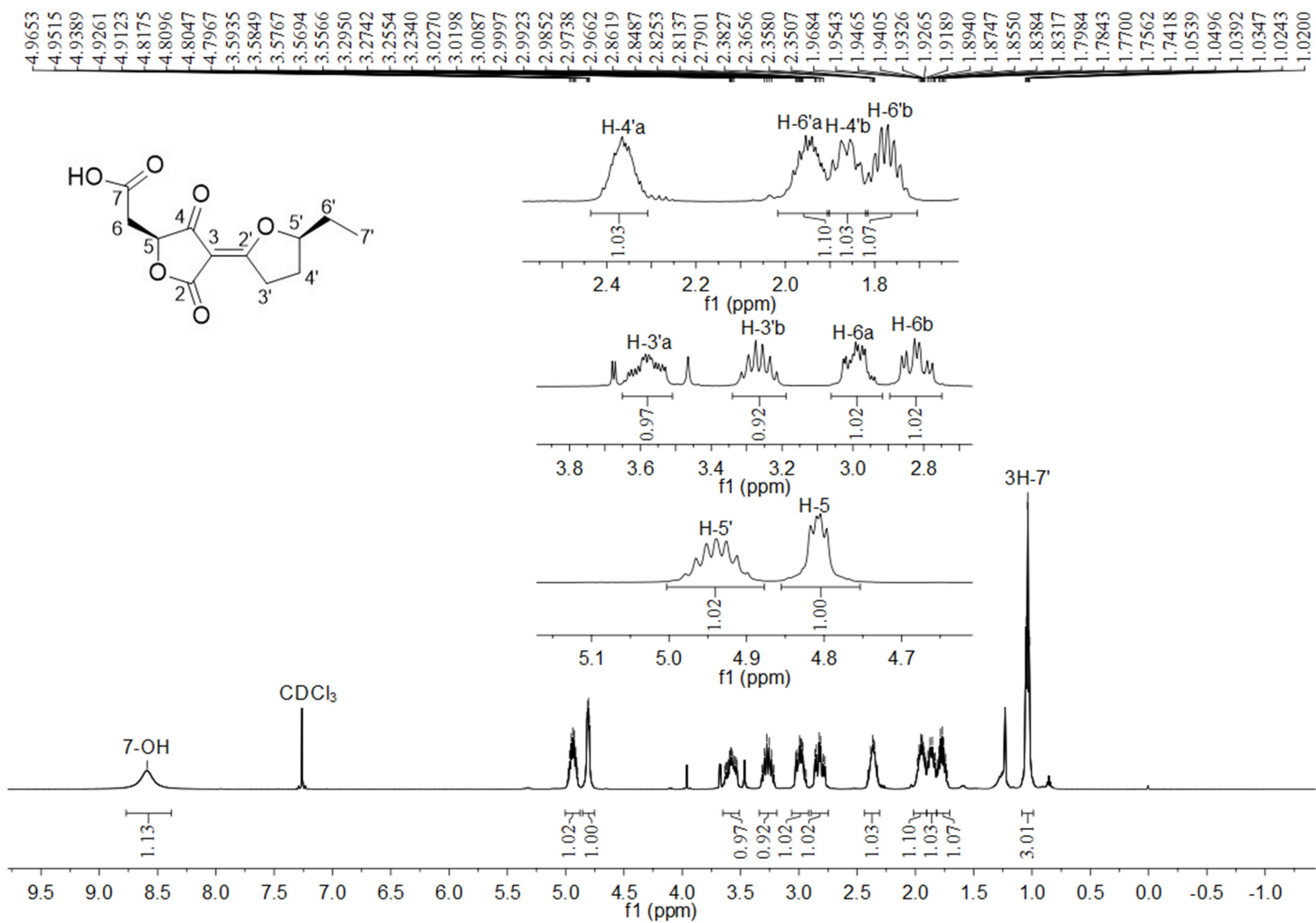


Figure S44. ^1H NMR spectrum of compound **13** in CDCl_3 (500MHz)

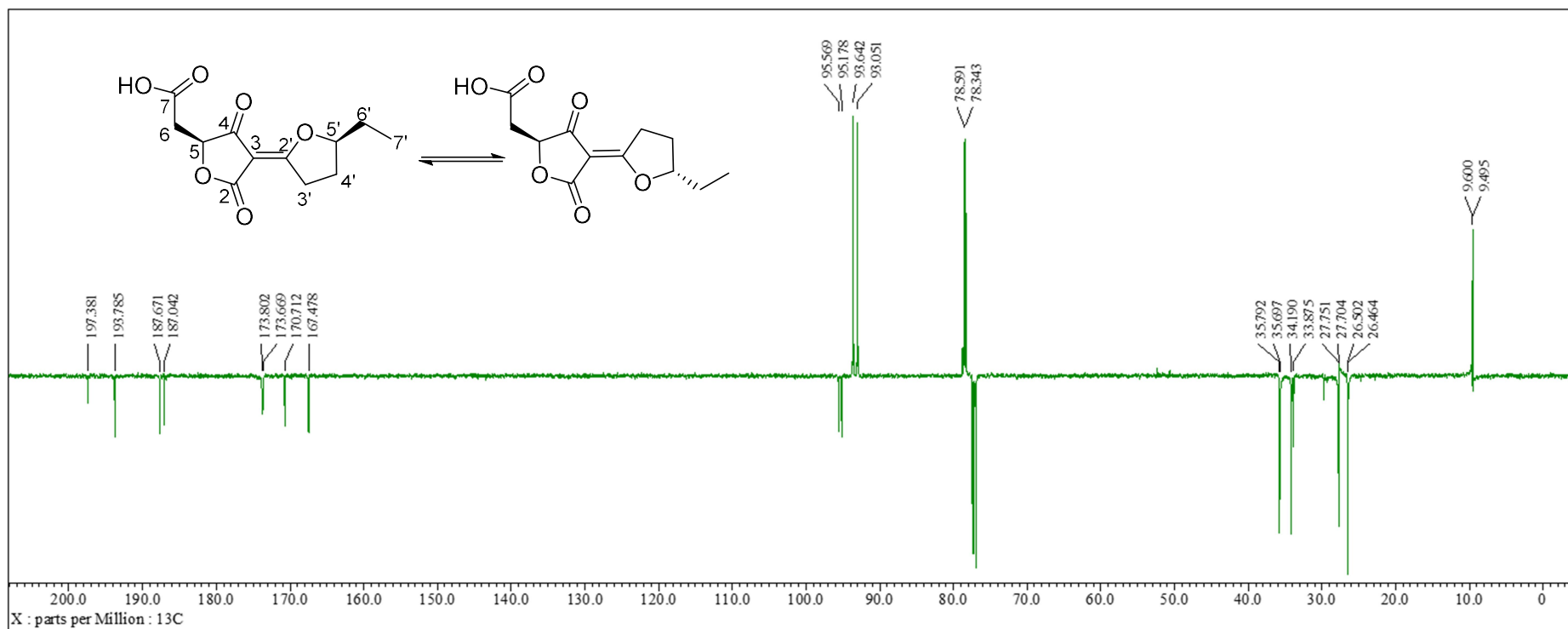


Figure S45. ^{13}C NMR spectrum of compound 13 in CDCl_3 (125MHz)

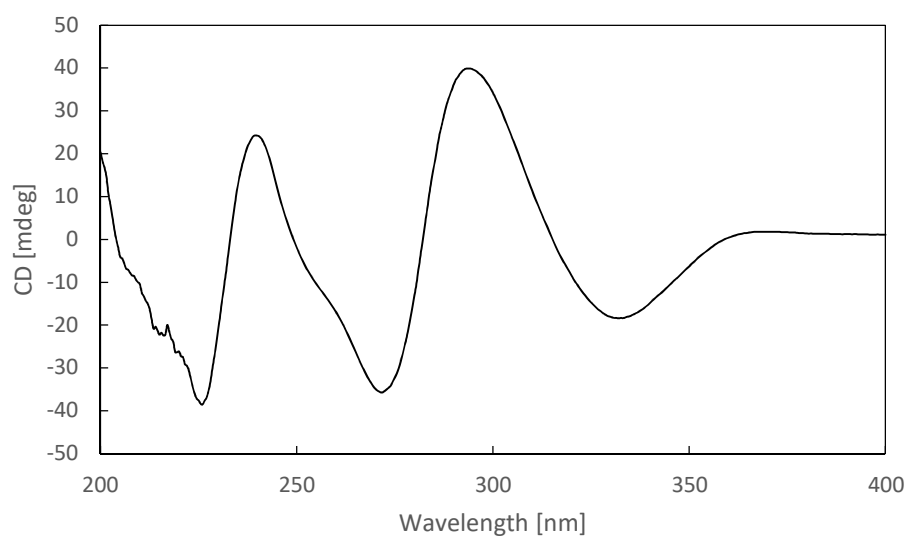


Figure S46. CD spectrum of penilactone A (1)

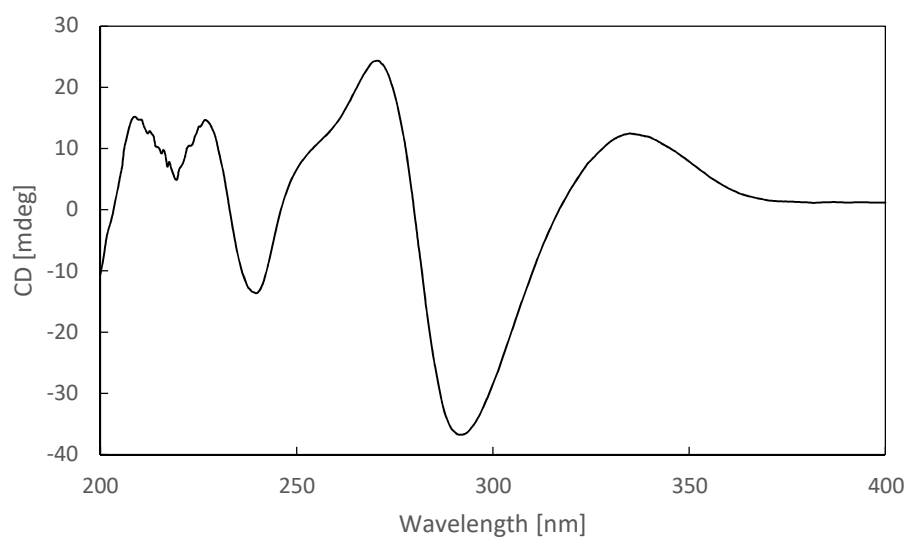


Figure S47. CD spectrum of penilactone B (2)

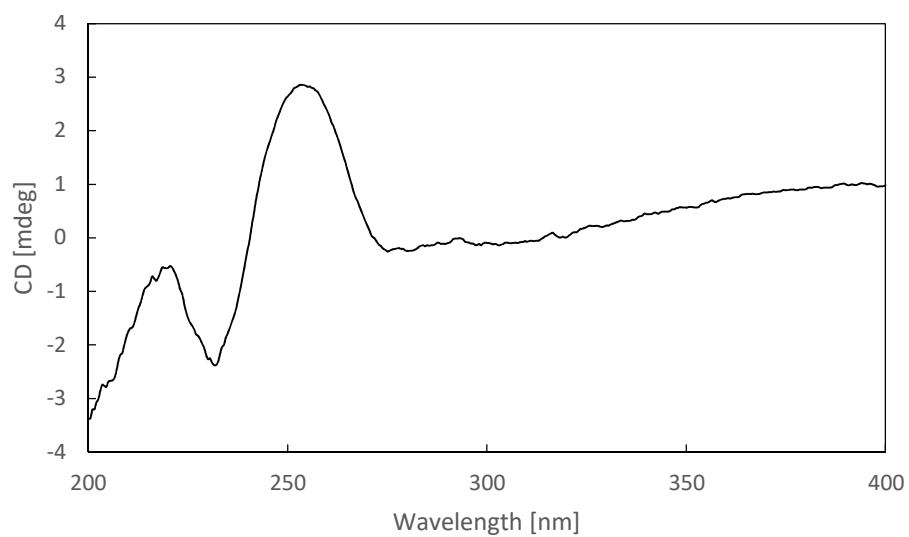


Figure S48. CD spectrum of peniphenone D (3)

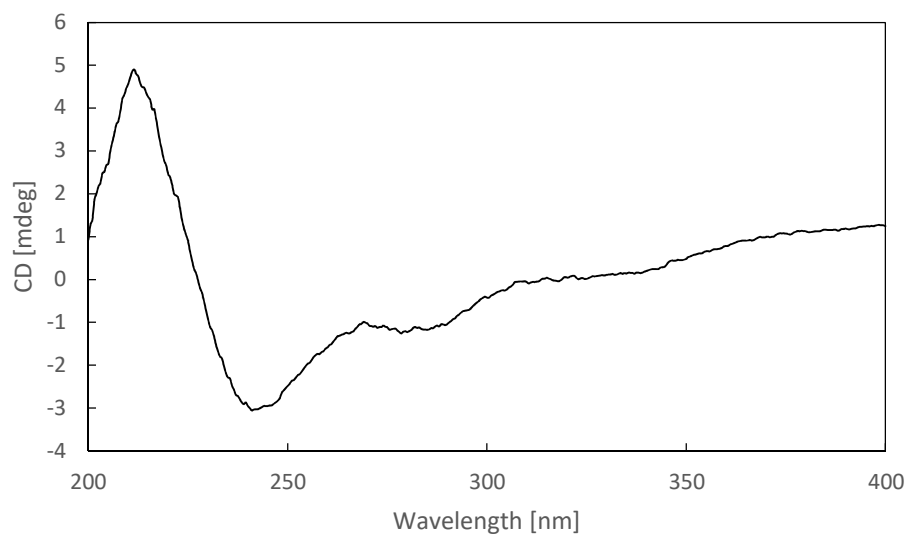


Figure S49. CD spectrum of penilactone D (4)

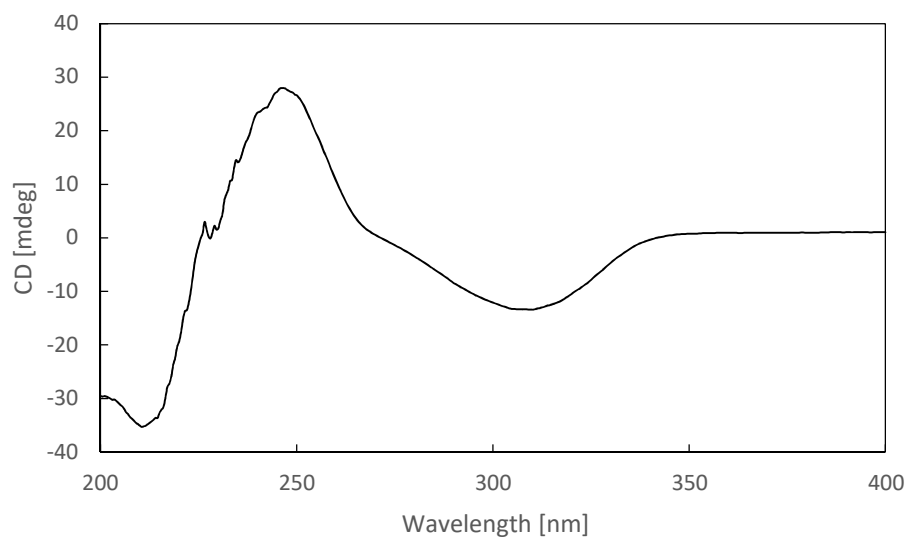


Figure S50. CD spectrum of (*R*)-5-methyltetronic acid (**7**)

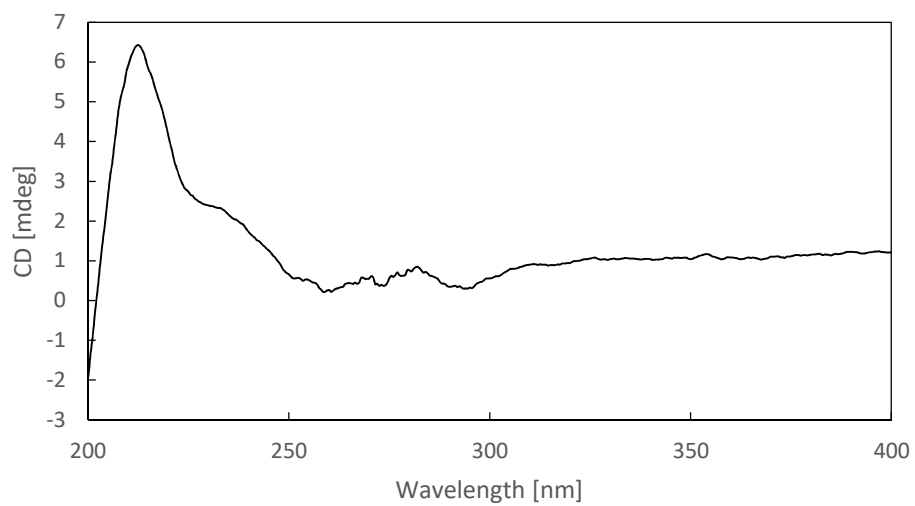


Figure S51. CD spectrum of terrestric acid (**11**)

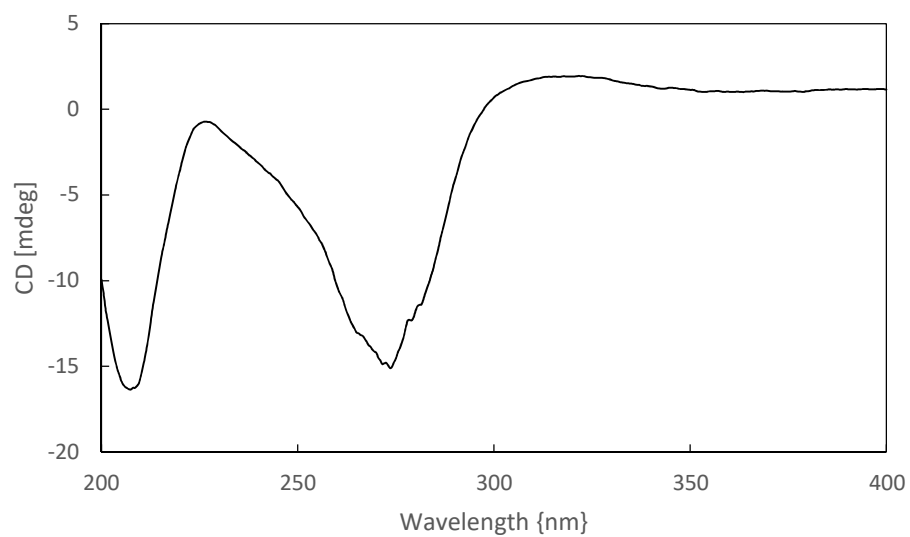


Figure S52. CD spectrum of crustosic acid (**13**)

Supplementary References

- (1) Wu, G.; Ma, H.; Zhu, T.; Li, J.; Gu, Q.; Li, D. Penilactones A and B, two novel polyketides from Antarctic deep-sea derived fungus *Penicillium crustosum* PRB-2. *Tetrahedron* **2012**, *68*, 9745.
- (2) Li, W.; Fan, A.; Wang, L.; Zhang, P.; Liu, Z.; An, Z.; Yin, W.-B. Asperphenamate biosynthesis reveals a novel two-module NRPS system to synthesize amino acid esters in fungi. *Chem. Sci.* **2018**, *9*, 2589.
- (3) Chiang, Y. M.; Ahuja, M.; Oakley, C. E.; Entwistle, R.; Asokan, A.; Zutz, C.; Wang, C. C.; Oakley, B. R. Development of genetic dereplication strains in *Aspergillus nidulans* results in the discovery of aspercryptin. *Angew. Chem. Int. Ed. Engl.* **2016**, *55*, 1662.
- (4) Yin, W. B.; Chooi, Y. H.; Smith, A. R.; Cacho, R. A.; Hu, Y.; White, T. C.; Tang, Y. Discovery of cryptic polyketide metabolites from dermatophytes using heterologous expression in *Aspergillus nidulans*. *ACS Synth. Biol.* **2013**, *2*, 629.
- (5) Goswami, R. S. Targeted gene replacement in fungi using a split-marker approach. *Methods Mol. Biol.* **2012**, *835*, 255.
- (6) Jacobus, A. P. and Gross, J. Optimal cloning of PCR fragments by homologous recombination in *Escherichia coli*. *PLoS. One.* **2015**, *10*, e0119221.
- (7) Adrian, J. and Stark, C. B. Total synthesis of muricadienin, the putative key precursor in the solamin biosynthesis. *Org. Lett.* **2014**, *16*, 5886.
- (8) Spence, J. T. and George, J. H. Biomimetic total synthesis of ent-penilactone A and penilactone B. *Org. Lett.* **2013**, *15*, 3891.
- (9) Stebbins, N. D.; Yu, W.; Uhrich, K. E. Enzymatic polymerization of an ibuprofen-containing monomer and subsequent drug release. *Macromol. Biosci.* **2015**, *15*, 1115.
- (10) Williams, K.; Szwalbe, A. J.; Mulholland, N. P.; Vincent, J. L.; Bailey, A. M.; Willis, C. L.; Simpson, T. J.; Cox, R. J. Heterologous production of fungal maleidrides reveals the cryptic cyclization involved in their biosynthesis. *Angew. Chem. Int. Ed. Engl.* **2016**, *55*, 6784.
- (11) Kusuya, Y.; Takahashi-Nakaguchi, A.; Takahashi, H.; Yaguchi, T. Draft genome sequence of the pathogenic filamentous fungus *Aspergillus udagawae* strain IFM 46973T. *Genome Announc.* **2015**, *3*, e00834-15.
- (12) Peter, M.; Kohler, A.; Ohm, R. A.; Kuo, A.; Krutzmann, J.; Morin, E.; Arend, M.; Barry, K. W.; Binder, M.; Choi, C.; Clum, A.; Copeland, A.; Grisel, N.; Haridas, S.; Kipfer, T.; LaButti, K.; Lindquist, E.; Lipzen, A.; Maire, R.; Meier, B.; Mihaltcheva, S.; Molinier, V.; Murat, C.; Pöggeler, S.; Quandt, C. A.; Sperisen, C.; Tritt, A.; Tisserant, E.; Crous, P. W.; Henrissat, B.; Nehls, U.; Egli, S.; Spatafora, J. W.; Grigoriev, I. V.; Martin, F. M. Ectomycorrhizal ecology is imprinted in the genome of the dominant symbiotic fungus *Cenococcum geophilum*. *Nat. Commun.* **2016**, *7*, 12662.
- (13) He, Y. and Cox, R. J. The molecular steps of citrinin biosynthesis in fungi. *Chem. Sci.* **2016**, *7*, 2119.
- (14) Zabala, A. O.; Chooi, Y. H.; Choi, M. S.; Lin, H. C.; Tang, Y. Fungal polyketide synthase product chain-length control by partnering thiohydrolase. *ACS Chem. Biol.* **2014**, *9*, 1576.
- (15) So, K. K.; Kim, J. M.; Nguyen, N. L.; Park, J. A.; Kim, B. T.; Park, S. M.; Hwang, K. J.; Kim, D. H. Rapid screening of an ordered fosmid library to clone multiple polyketide synthase genes of the phytopathogenic fungus *Cladosporium phlei*. *J. Microbiol. Methods* **2012**, *91*, 412.
- (16) Yang, X. L.; Awakawa, T.; Wakimoto, T.; Abe, I. Three acyltetronic acid derivatives: noncanonical cryptic polyketides from *Aspergillus niger* identified by genome mining. *Chembiochem.* **2014**, *15*, 1578.
- (17) Lonjers, Z. T.; Dickson, E. L.; Chu, T. P.; Kreutz, J. E.; Neacsu, F. A.; Anders, K. R.; Shepherd, J. N.

Identification of a new gene required for the biosynthesis of rhodoquinone in *Rhodospirillum rubrum*. *J. Bacteriol.* **2012**, *194*, 965.

(18) Usami, Y.; Aoki, S.; Hara, T.; Numata, A. New dioxopiperazine metabolites from a *Fusarium* species separated from a marine alga. *J. Antibiot. (Tokyo)* **2002**, *55*, 655.

4.2 Formation of terrestric acid in *Penicillium crustosum* requires redox-assisted decarboxylation and stereoisomerization.

Formation of Terrestrial Acid in *Penicillium crustosum* Requires Redox-Assisted Decarboxylation and Stereoisomerization

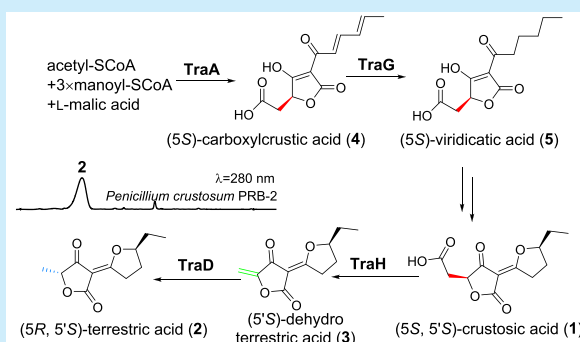
Jie Fan,^{†,§} Ge Liao,^{†,§} Lena Ludwig-Radtke,[†] Wen-Bing Yin,^{‡,§} and Shu-Ming Li^{*,†,§}

[†]Institut für Pharmazeutische Biologie und Biotechnologie, Philipps-Universität Marburg, Robert-Koch-Straße 4, Marburg 35037, Germany

[‡]State Key Laboratory of Mycology, Institute of Microbiology, Chinese Academy of Sciences, Beijing 100101, China

S Supporting Information

ABSTRACT: Crustosic acid (**1**) differs from terrestrial acid (**2**) by a 5 β -carboxymethyl at the tetronate ring instead of a 5 α -methyl group in *Penicillium crustosum*. The formation of **1** via carboxylcrustic and viridicatic acid was confirmed by gene deletion and heterologous expression. The conversion of **1** to **2** requires a decarboxylation-mediated olefination by TraH and subsequent reduction by TraD. The redox-assisted decarboxylation and stereoisomerization proved the biosynthetic relationships of fungal acyltetronates with different stereochemistry.



Natural products of the tetronate family with over 100 members contain a characteristic γ -butyrolactone ring and are mainly found in *Actinomycetes*.^{1,2} Fungus-originated tetronates carry different acyl moieties at C3 and differ from each other often in substituents at C5. Representatives are crustosic acid (**1**), carlic acid, and carlosic acid with a 5 β -carboxymethyl moiety, terrestrial acid (**2**), carolic acid, and carolinic acid with a 5 α -methyl group, as well as dehydroterrestrial acid (**3**), dehydrocarolic acid, and agglomerin F with an olefinic methylene group at the corresponding position (Figure 1A).^{3–9} Despite the interesting structural features of these fungal tetronates, no detailed investigation on their biosynthesis was reported prior to this study. The biosynthesis of agglomerin F in *Aspergillus niger* was proposed after a regulator activation and product isolation (Figure 1B).⁷ In this pathway, the hybrid polyketide synthase–nonribosomal peptide synthetase (PKS–NRPS) CaaA should be responsible for the formation of carlosic acid and the P450 oxygenase CaaC for the oxidative decarboxylation to install the exocyclic double bond. The nonheme Fe^{II}/2-oxoglutarate (Fe^{II}-2OG)-dependent oxygenase CaaD was speculated for the oxidation of the terminal methyl group at the acyl chain. However, no genetic and biochemical data support the hypothesis.

We recently identified the terrestrial acid biosynthetic gene cluster (*traA-H*, *pcr11009-pcr11016*) in *Penicillium crustosum* PRB-2 and proved the involvement of the hybrid PKS–NRPS TraA in the formation of **1**. The nonheme Fe^{II}-2OG-dependent oxygenase TraH was proposed for the conversion of **1** to **2** (Figure S1, see Supporting Information (SI)).⁹ In this study, we report the functions of TraA and the enoyl reductase TraG to give precursors of **1**. Biochemical investigations proved that the conversion of **1** to **2** was achieved via an

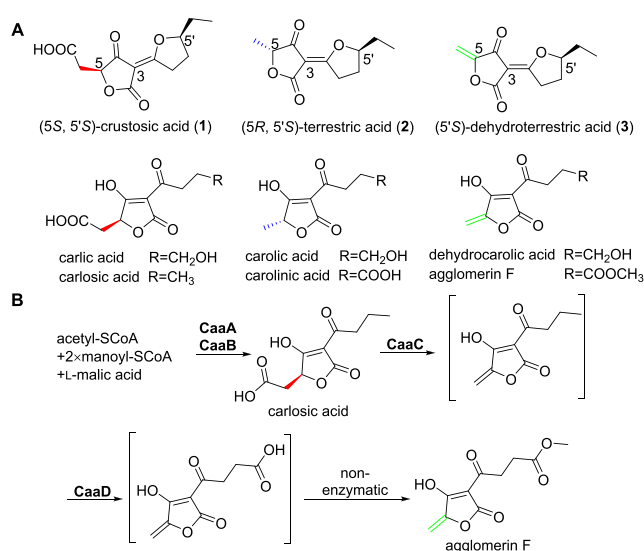


Figure 1. Representatives of acyltetronic acids in fungi (A) and proposed biosynthetic pathway of agglomerin F in *A. niger* (B).

oxidative decarboxylation catalyzed by TraH and a subsequent stereospecific reduction with the flavin-containing oxidoreductase TraD.

To identify its function, the genomic sequence of *traA* was introduced into *Aspergillus nidulans* LO8030 by PEG-mediated protoplast transformation (Tables S1–S3 and Figure S2).^{10–12}

Received: November 8, 2019

Published: December 13, 2019

A transformant JF15 harboring *traA* was cultivated as a PD surface culture for 7 days. LC-MS analysis of the EtOAc extract revealed the presence of two new product peaks 4 and 4* with $[M + H]^+$ ions at m/z 253.071 \pm 0.005 and almost the same UV spectra (Figures 2A and S3). Both peaks were

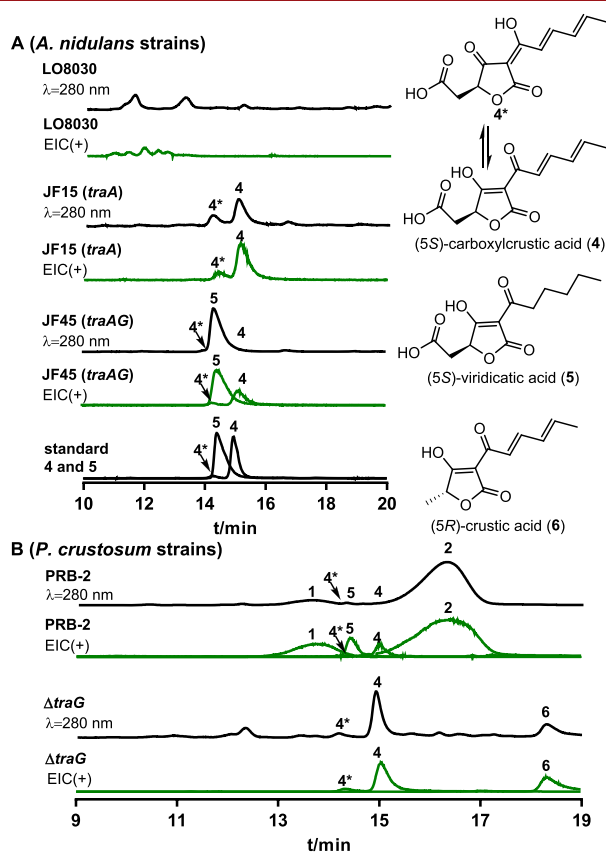


Figure 2. LC-MS analysis of extracts from *A. nidulans* (A) and *P. crustosum* (B). UV absorptions at 280 nm are illustrated. Extracted ion chromatograms (EICs) for $[M + H]^+$ ions of 1–6 are given with a tolerance range of \pm 0.005.

interchangeable, which was observed during the isolation procedure. Isolation and structure elucidation (Table S5 and Figures S23–S26) proved 4 as the stable form in CD₃OD and identified to be a carboxylmethyltetronic acid derivative with an unsaturated acyl chain, termed carboxylcrustic acid. We proposed 4* as a tautomer of 4 (Figures 2A and S3). Therefore, TraA, sharing 59.5% sequence identity with CaaA on the amino acid level, functions alone as a tetronate synthase and differs from other known PKS–NRPS enzymes, requiring a *trans*-acting enoyl reductase (ER) for product releasing.^{13,14}

Subsequently, coexpression of *traA* and the putative ER *traG* in LO8030 led to accumulation of a predominant peak 5 with an $[M + H]^+$ ion at m/z 257.1038 in the obtained transformant JF45, together with the PKS–NRPS product 4 as a minor product (Figures 2A and S3). Isolation and NMR analysis proved 5 to be viridicatic acid, which was also identified in the wild-type PRB-2 (Table S6 and Figures S5 and S27–S31).¹⁵ Obviously, TraG, with sequence identity of 68.9% with CaaB, acts as an enoyl reductase for the reduction of the two double bonds at the acyl chain. This was further confirmed by replacing *traG* with a hygromycin B cassette in PRB-2 (Figures 2B, S4, and S7).^{9,16} In comparison to PRB-2, the production of 1, 2, and 5 was completely abolished in the $\Delta traG$ mutant,

whereas 4 as the putative substrate of TraG was accumulated and confirmed by ¹H NMR analysis. One additional minor peak with an $[M + H]^+$ ion at m/z 209.0827 was identified as a decarboxylated stereoisomer of 4, termed crustic acid (6), by comparing their optical rotation values and CD spectra (Table S7 and Figures S32–S34 and S38). Detection of 6 as a minor metabolite indicates that the enzyme(s) for the conversion of 1 to 2 can also use 4 as substrate, but with low activity.

To identify their metabolism in the biosynthesis, 4 and 5 were fed in the available $\Delta traA$ and $\Delta traG$ mutants, respectively (Figures S6–S9). LC-MS analysis revealed that 4 was metabolized to 2 and 6 in the $\Delta traA$ mutant. Feeding 5 also restored the accumulation of 2 as the predominant product in both $\Delta traA$ and $\Delta traG$ mutants, suggesting their involvement in the biosynthesis of 2.

Structural comparison revealed that 1 is an anhydrous form of a hydroxylated derivative of 5. Existence of the open form of 1 was confirmed by LC-MS analysis after incubation in D₂O (Figure S10). The equilibrium between the open and closed forms explains well the presence of broad peaks in the LC-MS chromatograms of 1 and 2 (Figures 2B and S5). The responsible enzyme for the hydroxylation of 5 has not been identified yet. It cannot be excluded that the responsible structure gene is located outside the *tra* cluster.

Having identified the formation of 1 with 4 and 5 as precursors, we proceeded to investigate its conversion to 2. In our previous study, the involvement of the putative Fe^{II}-2OG-dependent oxygenase TraH in the conversion of 1 to 2 was proved by the accumulation of 1 in a $\Delta traH$ mutant.⁹ TraH comprises 327 amino acids and shares a sequence identity of 66% with the aforementioned CaaD (Figure 1B). Sequence alignments showed the typical conserved 2-His-1-Asp ion-binding triad (His₁₉₈, His₂₁₁, and Asp₁₁₂) in TraH (Figure S11).^{17,18} For biochemical characterization, the coding sequence of *traH* was amplified from cDNA and cloned into pET28a (+) for overexpression in *Escherichia coli*.^{19,20} The recombinant N-terminally His₆-tagged protein was purified to near homogeneity as confirmed on SDS-PAGE, yielding 4.5 mg of purified TraH per liter of bacterial culture (Figure S12). TraH (5.4 μ M) was then incubated with 0.5 mM of 1 in the presence of ascorbic acid (AA), Fe[(NH₄)₂(SO₄)₂] (Fe^{II}), 2-oxoglutarate (2OG), and dithiothreitol (DTT) at 37 °C for 30 min.²¹ Surprisingly, LC-MS analysis of the full assay showed a product peak with an $[M + H]^+$ ion at m/z 209.0806, corresponding to the molecular formula of C₁₁H₁₃O₄, but not the expected C₁₁H₁₅O₄ for 2 (Figures 3A and S13). Subsequent incubation of TraH with 1 in a large scale enabled us to identify this product as dehydroterrestrial acid (3) with an exocyclic double bond at the C5-position, which had been identified in *Aspergillus hancockii* (Table S4 and Figure S22).⁸ Detailed investigations demonstrated that the activity of TraH is strictly dependent on the presence of 2OG and can be enhanced by externally added Fe^{II} (Figure S14). A K_M value at 0.49 mM and a turnover number (k_{cat}) at 0.02 s⁻¹ were determined for TraH reaction with 1 (Figure S13). These results proved that TraH catalyzes an oxidative decarboxylation of 1 to yield 3 instead of 2 (Scheme 1A).

Differing slightly from the previous hypothesis, conversion of 1 to 3 by TraH implies one additional enzyme required for the reduction of 3 to 2. We took the flavin-containing oxidoreductase TraD as a top candidate for the reduction of the double bond of 3 to the α -methyl group of 2. TraD comprises 267 amino acids with a well-known conserved FAD-

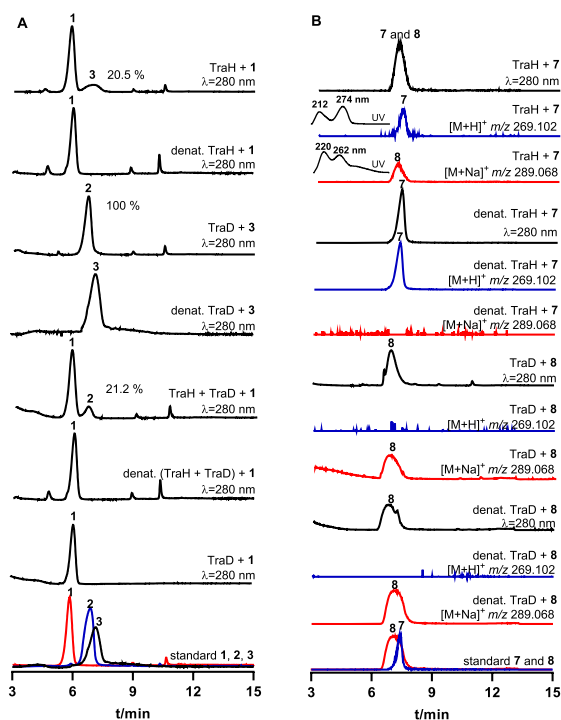


Figure 3. LC-MS analysis of enzyme assays of TraH without or together with TraD with 1, TraD with 1 or 3 (A), TraH with 7, and TraD with 8 (B). UV absorptions at 280 nm are illustrated. EICs refer to $[M + H]^+$ of 7 at m/z 269.102 and $[M + Na]^+$ of 8 at m/z 289.068 with a tolerance range of ± 0.005 .

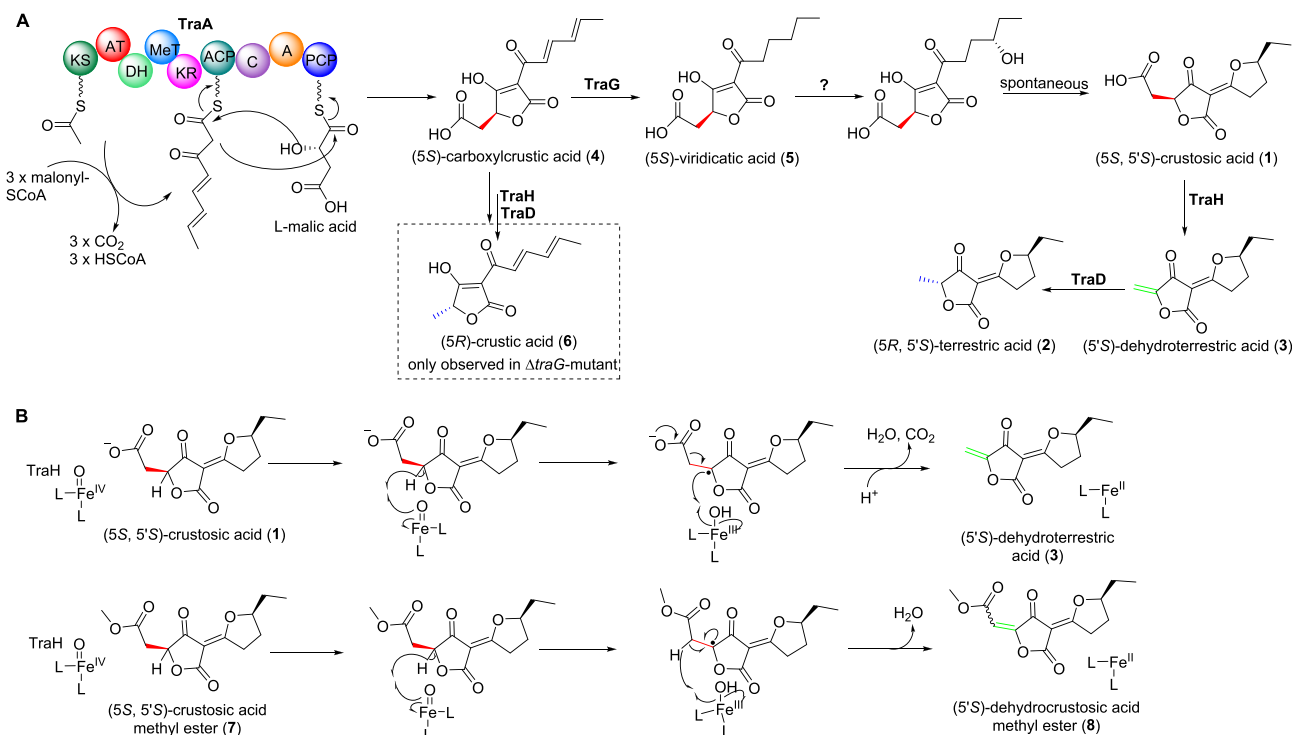
binding motif (GXXXGXG).^{22–24} To verify its function *in vitro*, TraD was successfully overproduced in *E. coli* BL21-(DE3) in a similar way to TraH. With the aid of Ni-NTA resin,

TraD was obtained in a yellow color with a yield of 10.6 mg per liter of bacterial culture (Figure S12). The enzyme assay with 0.6 μ M of TraD and 0.5 mM of 3 was carried out in the presence of NADPH at 30 °C. LC-MS analysis revealed that 3 was completely converted to 2 in 10 min (Figure 3A). The high efficiency of the TraD reaction was confirmed by incubation of 3 with different protein amounts. An amount of 23% of a 0.5 mM solution of 3 was consumed by 6 nM of TraD in 10 min (Figure S15). This proved that the reduction of the exocyclic double bond at the C5-position by TraD was much more efficient than the oxidative decarboxylation of 1 by TraH, which was also confirmed by coincubation of 1 with TraH and TraD.

Incubations of 0.5 mM of 1 with TraH and TraD at different ratios in the presence of AA, Fe^{II}, 2OG, and NADPH at 30 °C for 30 min showed sequential formation of the intermediate 3 and final product 2 (Figures 3A and S16). The integrity of 2 from the enzyme assay was confirmed by isolation and comparison of its ¹H NMR and CD spectra with those of 2 from PRB-2 (Table S4 and Figures S17 and S21).⁹ Therefore, it can be concluded that the flavin-containing oxidoreductase TraD is responsible for the stereospecific reduction of 3 to yield 2 with a 5 α -methyl group. The product yields of 2 and 3 in different assays confirmed the high efficiency of TraD toward 3, which was only detected at very low TraD concentration. This proved that the conversion of 1 to 2 was controlled by the TraH-catalyzed oxidative decarboxylation of 1 and provides evidence for the absence of 3 in the wild-type PRB-2.

Incubation of 4 with TraH and TraD led to the detection of a very weak peak with the same retention time and fragmentation pattern as those of 6. The proposed intermediate dehydrocrustic acid with an $[M + H]^+$ at m/z

Scheme 1. Proposed Terrestrial Acid Biosynthetic Pathway in *P. crustosum* PRB-2 (A) and Mechanisms of TraH-Catalyzed Olefination (B)



207.0662 was also detected in the TraH assay with **4** (Figure S18). These results proved that TraH and TraD can also convert **4** to **6**, but only with very low efficiency, as observed in the $\Delta traG$ mutant (Scheme 1A).

Taken together, our results proved that the conversion of **1** to **2** required sequential two-step reactions, i.e., oxidative decarboxylation by the nonheme Fe^{II}-2OG-dependent oxygenase TraH and double-bond reduction by the flavin-containing oxidoreductase TraD (Scheme 1A). Oxidative decarboxylations have been reported for enzymes from different families, e.g., the cytochrome P450 OleT,²⁵ the FAD-dependent decarboxylase CndG,²⁶ and the radical S-adenosyl-L-methionine (SAM) enzyme HemN,²⁷ as well as the nonheme iron oxidase UndA^{28,29} and the nonheme Fe^{II}-2OG-dependent oxygenases IsnB, AmbI3, and ScoE.^{30–33} Differing from IsnB, AmbI3, and ScoE with indole vinyl isonitriles as final products, TraH provides a transient intermediate for further reduction, which accomplishes decarboxylation and stereoisomerization in the biosynthesis of fungal acyltetronates with different stereochemistry. In analogy to IsnB, the oxidative decarboxylation by TraH would very likely undergo the abstraction of a hydrogen atom from the β -position of COOH by Fe^{IV}-oxo species to generate the substrate radical. Subsequent radical-mediated electron transfer and C–C bond scission eventually install the exocyclic double bond in **3** accompanied by CO₂ elimination (Scheme 1B).

To probe whether the decarboxylation is required for the olefination by TraH, crustosic acid methyl ester (**7**) was prepared by spontaneous methylation of **1** in methanol (Table S8 and Figures S19, S35, and S36). The enzyme assay of **7** with TraH was carried out in a similar way as **1** with TraH. LC-MS analysis revealed the presence of an enzyme product with almost the same retention time as **7** (Figures 3B and S20). Subsequent isolation and structure elucidation by comparison of its ¹H NMR data with that of **7** (Tables S8 and S9 and Figures S35 and S37) led to the unequivocal identification of dehydrocrustosic acid methyl ester (**8**) as the enzyme product, although no ¹³C NMR data of **8** could be obtained due to low conversion. In comparison to the reported oxidative decarboxylations catalyzed by nonheme Fe^{II}-2OG-dependent oxygenases,^{30–32} methylation of **1** redirected the TraH reaction from oxidative decarboxylation of **1** to the sole olefination of **7**. Conversion of **7** to the dehydrogenated product **8** by TraH seems to proceed via a second hydrogen abstraction from the α -position of COOCH₃ by Fe^{III}–OH species. In total, two consecutive cleavages of the C–H bond with H₂O elimination completed the olefin installation (Scheme 1B). **7** with a K_M at 0.11 mM and k_{cat} at 0.03 s⁻¹ seem to be even a better substrate for TraH than **1** (Figure S20). However, neither **7** nor **8** was detected in *P. crustosum* PRB-2. Further incubation of TraD with **8** showed no product formation, indicating the necessity of the terminal double bond for the reduction by TraD.

In summary, our study provides new insights into the biosynthesis of fungal acyltetronic acids, especially the formation of the skeleton and the relationships between different stereoisomers. Heterologous expression and feeding experiments suggested that **4** and **5**, as the products of TraA and TraG, respectively, serve as precursors of **1**, carrying a β -carboxymethyl group. Chemically, the conversion of **1** to **2** is a decarboxylation with epimerization. We demonstrated that **1** was first converted by the nonheme Fe^{II}-2OG-dependent oxygenase TraH, via an oxidative decarboxylation, to a transient intermediate **3** carrying an exocyclic double bond.

Subsequent stereospecific reduction by the flavin-containing oxidoreductase TraD led to the formation of the final product **2** bearing a 5 α -methyl group. Among the two-step conversion, the oxidative decarboxylation seems to be the rate-controlling reaction, and its product **3** was immediately consumed by TraD with high efficiency. Differing from other nonheme Fe^{II}-2OG-dependent oxygenases being responsible for decarboxylation-assisted olefination,^{30–32} TraH is capable of catalyzing dehydrogenation with or without simultaneous decarboxylation, as demonstrated with **1** and **7** as substrates. It can be speculated that other fungal stereospecific acyltetronic acids mentioned in Figure 1A are very likely biosynthesized in a similar way.

■ ASSOCIATED CONTENT

Supporting Information

The Supporting Information is available free of charge at <https://pubs.acs.org/doi/10.1021/acs.orglett.9b04002>.

Experimental procedures, physicochemical properties, and NMR spectra (PDF)

■ AUTHOR INFORMATION

Corresponding Author

*E-mail: shuming.li@staff.uni-marburg.de.

ORCID

Wen-Bing Yin: 0000-0002-9184-3198

Shu-Ming Li: 0000-0003-4583-2655

Author Contributions

[§]J.F. and G.L. contributed equally to this work.

Notes

The authors declare no competing financial interest.

■ ACKNOWLEDGMENTS

We thank Rixa Kraut and Stefan Newel (Philipps-Universität Marburg) for taking MS and NMR spectra, respectively. This project was financially funded in part by the Deutsche Forschungsgemeinschaft (DFG, German Research Foundation)—Li844/11-1 and INST 160/620-1—as well as the National Natural Science Foundation of China—31861133004. Jie Fan (201507565006) and Ge Liao (201607565014) are scholarship recipients from the China Scholarship Council.

■ REFERENCES

- (1) Vieweg, L.; Reichau, S.; Schobert, R.; Leadlay, P. F.; Sussmuth, R. D. *Nat. Prod. Rep.* **2014**, *31*, 1554.
- (2) Schobert, R.; Schlenk, A. *Bioorg. Med. Chem.* **2008**, *16*, 4203.
- (3) Clutterbuck, P. W.; Haworth, W. N.; Raistrick, H.; Smith, G.; Stacey, M. *Biochem. J.* **1934**, *28*, 94.
- (4) Bentley, R.; Bhate, D. S.; Keil, J. G. *J. Biol. Chem.* **1962**, *237*, 859.
- (5) Bracken, A.; Raistrick, H. *Biochem. J.* **1947**, *41*, 569.
- (6) Nukina, M. *Agric. Biol. Chem.* **1988**, *52*, 2357.
- (7) Yang, X. L.; Awakawa, T.; Wakimoto, T.; Abe, I. *ChemBioChem* **2014**, *15*, 1578.
- (8) Pitt, J. I.; Lange, L.; Lacey, A. E.; Vuong, D.; Midgley, D. J.; Greenfield, P.; Bradbury, M. I.; Lacey, E.; Busk, P. K.; Pilgaard, B.; Chooi, Y. H.; Piggott, A. M. *PLoS One* **2017**, *12*, No. e0170254.
- (9) Fan, J.; Liao, G.; Kindinger, F.; Ludwig-Radtke, L.; Yin, W.-B.; Li, S.-M. *J. Am. Chem. Soc.* **2019**, *141*, 4225.
- (10) Yin, W. B.; Chooi, Y. H.; Smith, A. R.; Cacho, R. A.; Hu, Y.; White, T. C.; Tang, Y. *ACS Synth. Biol.* **2013**, *2*, 629.

- (11) Li, W.; Fan, A.; Wang, L.; Zhang, P.; Liu, Z.; An, Z.; Yin, W.-B. *Chem.Sci.* **2018**, *9*, 2589.
- (12) Chiang, Y. M.; Ahuja, M.; Oakley, C. E.; Entwistle, R.; Asokan, A.; Zutz, C.; Wang, C. C.; Oakley, B. R. *Angew. Chem., Int. Ed.* **2016**, *55*, 1662.
- (13) Halo, L. M.; Marshall, J. W.; Yakasai, A. A.; Song, Z.; Butts, C. P.; Crump, M. P.; Heneghan, M.; Bailey, A. M.; Simpson, T. J.; Lazarus, C. M.; Cox, R. J. *ChemBioChem* **2008**, *9*, 585.
- (14) Xu, W.; Cai, X.; Jung, M. E.; Tang, Y. J. *Am. Chem. Soc.* **2010**, *132*, 13604.
- (15) Birkinshaw, J. H.; Samant, M. S. *Biochem. J.* **1960**, *74*, 369.
- (16) Goswami, R. S. *Methods Mol. Biol.* **2012**, *835*, 255.
- (17) Gao, S.-S.; Naowarajna, N.; Cheng, R.; Liu, X.; Liu, P. *Nat. Prod. Rep.* **2018**, *35*, 792.
- (18) Nakamura, H.; Matsuda, Y.; Abe, I. *Nat. Prod. Rep.* **2018**, *35*, 633.
- (19) Yu, H.; Li, S.-M. *Org. Lett.* **2019**, *21*, 7094.
- (20) Yu, X.; Li, S.-M. *Methods Enzymol.* **2012**, *516*, 259.
- (21) Steffan, N.; Grundmann, A.; Afiyatullo, A.; Ruan, H.; Li, S.-M. *Org. Biomol. Chem.* **2009**, *7*, 4082.
- (22) Bottoms, C. A.; Smith, P. E.; Tanner, J. J. *Protein Sci.* **2002**, *11*, 2125.
- (23) Hanukoglu, I. J. *Mol. Evol.* **2017**, *85*, 205.
- (24) Romeo, C.; Moriwaki, N.; Yasunobu, K. T.; Gunsalus, I. C.; Koga, H. J. *Protein Chem.* **1987**, *6*, 253.
- (25) Grant, J. L.; Hsieh, C. H.; Makris, T. M. *J. Am. Chem. Soc.* **2015**, *137*, 4940.
- (26) Rachid, S.; Revermann, O.; Dauth, C.; Kazmaier, U.; Müller, R. *J. Biol. Chem.* **2010**, *285*, 12482.
- (27) Ji, X.; Mo, T.; Liu, W. Q.; Ding, W.; Deng, Z.; Zhang, Q. *Angew. Chem., Int. Ed.* **2019**, *58*, 6235.
- (28) Rui, Z.; Li, X.; Zhu, X.; Liu, J.; Domigan, B.; Barr, I.; Cate, J. H. D.; Zhang, W. *Proc. Natl. Acad. Sci. U. S. A.* **2014**, *111*, 18237.
- (29) Manley, O. M.; Fan, R.; Guo, Y.; Makris, T. M. *J. Am. Chem. Soc.* **2019**, *141*, 8684.
- (30) Chang, W. C.; Sanyal, D.; Huang, J. L.; Ittiarnkul, K.; Zhu, Q.; Liu, X. *Org. Lett.* **2017**, *19*, 1208.
- (31) Huang, J. L.; Tang, Y.; Yu, C. P.; Sanyal, D.; Jia, X.; Liu, X.; Guo, Y.; Chang, W. C. *Biochemistry* **2018**, *57*, 1838.
- (32) Yu, C. P.; Tang, Y.; Cha, L.; Milikisyan, S.; Smirnova, T. I.; Smirnov, A. I.; Guo, Y.; Chang, W. C. *J. Am. Chem. Soc.* **2018**, *140*, 15190.
- (33) Harris, N. C.; Born, D. A.; Cai, W.; Huang, Y.; Martin, J.; Khalaf, R.; Drennan, C. L.; Zhang, W. *Angew. Chem., Int. Ed.* **2018**, *57*, 9707.

Supporting Information

Formation of terrestrial acid in *Penicillium crustosum* requires redox-assisted decarboxylation and stereoisomerization

Jie Fan,^{1,†} Ge Liao,^{1,†} Lena Ludwig-Radtke,¹ Wen-Bing Yin,² and Shu-Ming Li^{1,*}

¹Institut für Pharmazeutische Biologie und Biotechnologie, Philipps-Universität Marburg, Robert-Koch-Straße 4, Marburg 35037, Germany

²State Key Laboratory of Mycology, Institute of Microbiology, Chinese Academy of Sciences, Beijing 100101, China

[†]These authors contributed equally to this work.

Table of content

Experiment Procedures	4
1. Computer-assisted sequence analysis	4
2. Strains, media and growth conditions	4
3. Genomic DNA isolation.....	4
4. RNA isolation and cDNA synthesis	4
5. PCR amplification, gene cloning and plasmid construction	5
6. Deletion of <i>traG</i> in <i>P. crustosum</i> and cultivation of deletion mutants.....	5
7. Heterologous expression of <i>traA</i> and <i>traG</i> in <i>A. nidulans</i>	6
8. Precursor feeding in <i>P. crustosum</i> deletion mutants	6
9. Overproduction and purification of TraD and TraH	6
10. <i>In vitro</i> assays of TraD and TraH.....	7
11. Large-scale fermentation, extraction and isolation of secondary metabolites	8
12. Determination of kinetic parameters	8
13. HPLC and LC-MS analysis of secondary metabolites	9
14. NMR analysis	9
15. Circular dichroism (CD) spectroscopic analysis	9
16. Measurement of optical rotations.....	9
17. Physicochemical properties of the compounds described in this study.....	9
Supplementary Tables	11
Table S1. Strains used in this study	11
Table S2. Plasmids used and constructed in this study	12
Table S3. Primers used in this study.....	13
Table S4. ¹ H NMR data of compounds 2 and 3.....	14
Table S5. NMR data of compound 4	15
Table S6. NMR data of compound 5	16
Table S7. NMR data of compound 6	17
Table S8. NMR data of compound 7	18
Table S9. ¹ H NMR data of compound 8	19
Supplementary Figures	20
Figure S1. Deduced functions of ORFs in terrestrial acid gene cluster of <i>P. crustosum</i> PRB-2	20
Figure S2. Constructs used for heterologous expression of <i>traA</i> and <i>traAG</i> in <i>A. nidulans</i> ...	21
Figure S3. LC-MS analysis of the metabolite profile of different <i>A. nidulans</i> strains	22
Figure S4. Verification of $\Delta traG$ -mutant from <i>P. crustosum</i> PRB-2.....	23
Figure S5. LC-MS detection of secondary metabolites from a 7 days-old liquid PD surface culture of <i>P. crustosum</i> PRB-2.....	24
Figure S6. LC-MS detection of the metabolites in the terrestrial acid biosynthesis in $\Delta traA$ -mutant obtained from a previous study	25
Figure S7. LC-MS detection of the metabolites in the terrestrial acid biosynthesis in $\Delta traG$ -mutant.....	26
Figure S8. LC-MS detection of the metabolite profile of $\Delta traA$ mutant after feeding with 4.....	27
Figure S9. LC-MS detection of the metabolite profile of $\Delta traA$ and $\Delta traG$ mutants after feeding with 5	28

SUPPORTING INFORMATION

Figure S10. Incorporation of deuterium in 1 via E/Z-isomerization in D ₂ O-enriched milieu.....	29
Figure S11. Sequence alignments of non-heme Fe ^{II} -2OG-dependent decarboxylases	30
Figure S12. Analysis of recombinant TraD and TraH on SDS-PAGE.....	31
Figure S13. Oxidative decarboxylation of 1 catalyzed by TraH	32
Figure S14. HPLC analysis of the incubation mixtures of 1 with TraH	33
Figure S15. HPLC analysis of incubation mixtures of 3 with TraD at different concentrations	34
Figure S16. HPLC analysis of sequential reaction products in enzyme assays of TraH and TraD with 1	35
Figure S17. Comparison of CD spectra of two terrestrial acid samples	36
Figure S18. LC-MS analysis of enzyme assays of 4 with TraH without or together with TraD	37
Figure S19. LC-MS analysis of spontaneous ester formation of 1 with different alcohols	38
Figure S20. Conversion of 7 to 8 catalyzed by TraH.....	39
Figure S21. ¹ H NMR spectrum of compound 2 isolated from an incubation mixture of 1 with TraH and TraD in CDCl ₃ (500MHz).....	40
Figure S22. ¹ H NMR spectrum of compound 3 in DMSO- <i>d</i> ₆ (500MHz)	41
Figure S23. ¹ H NMR spectrum of compound 4 isolated from <i>A. nidulans</i> JF15 harboring <i>traA</i> in CD ₃ OD (500MHz).....	42
Figure S24. ¹ H NMR spectrum of compound 4 isolated from Δ <i>traG</i> -mutant in CD ₃ OD (500MHz)	43
Figure S25. ¹³ C NMR spectrum of compound 4 isolated from <i>A. nidulans</i> JF15 harboring <i>traA</i> in CD ₃ OD (125MHz).....	44
Figure S26. HMBC spectrum of compound 4 isolated from <i>A. nidulans</i> JF15 harboring <i>traA</i> in CD ₃ OD.....	45
Figure S27. ¹ H NMR spectrum of compound 5 isolated from <i>P. crustosum</i> PRB-2 in DMSO- <i>d</i> ₆ (500MHz).....	46
Figure S28. ¹ H NMR spectrum of compound 5 isolated from <i>A. nidulans</i> JF45 harboring <i>traAG</i> in DMSO- <i>d</i> ₆ (500MHz)	47
Figure S29. ¹³ C NMR spectrum of compound 5 isolated from <i>A. nidulans</i> JF45 harboring <i>traAG</i> in DMSO- <i>d</i> ₆ (125MHz)	48
Figure S30. HMBC spectrum of compound 5 isolated from <i>A. nidulans</i> JF45 harboring <i>traAG</i> in DMSO- <i>d</i> ₆	49
Figure S31. ¹ H- ¹ H COSY spectrum of compound 5 isolated from <i>A. nidulans</i> JF45 harboring <i>traAG</i> in DMSO- <i>d</i> ₆	50
Figure S32. ¹ H NMR spectrum of compound 6 in CD ₃ OD (500MHz).....	51
Figure S33. ¹³ C NMR spectrum of compound 6 in CD ₃ OD (125MHz).....	52
Figure S34. HMBC spectrum of compound 6 in CD ₃ OD	53
Figure S35. ¹ H NMR spectrum of compound 7 in CDCl ₃ (500MHz)	54
Figure S36. ¹³ C NMR spectrum of compound 7 in CDCl ₃ (125MHz)	55
Figure S37. ¹ H NMR spectrum of compound 8 in CDCl ₃ (500MHz)	56
Figure S38. CD spectra of compounds 4 – 6	57
Supplementary References	58

Experiment Procedures

1. Computer-assisted sequence analysis

Sequence analysis of terrestrial acid gene cluster was carried out by antiSMASH (<http://antismash.secondarymetabolites.org/>) and by comparison with known entries in database. The genomic DNA sequence of the terrestrial acid cluster from *P. crustosum* PRB-2 reported in this study is available at GenBank under the accession number MK360919. Multiple sequence alignments for TraH and analogues were carried out with the program ClustalW and visualized with ESPript 3.2 (<http://esprict.ibcp.fr/ESPript/cgi-bin/ESPript.cgi>) to identify strictly conserved amino acid residues.

2. Strains, media and growth conditions

The fungal strains used in this study are summarized in Table S1. *Penicillium crustosum* strain PRB-2 was isolated from a deep-sea sediment collected in Prydz Bay at a depth of -526 m.¹ The wild type strain PRB-2 and deletion mutants $\Delta traA$ and $\Delta traG$ were cultivated on PDA plates (potato dextrose broth, Sigma) with 1.6% agar at 25°C for sporulation and in PD surface culture at 25°C for 7 days for detection of secondary metabolites (SMs).

Aspergillus nidulans strains were grown at 37°C on GMM medium (1.0% glucose, 50 mL/L salt solution, 1 mL/L trace element solution, 1.6% agar) for sporulation and transformation with appropriate nutrition as required, and incubated at 25°C in PD medium for 7 days for SM detection.²⁻⁴ The salt solution contains (w/v) 12% NaNO₃, 1.04% KCl, 1.04% MgSO₄·7H₂O, and 3.04% KH₂PO₄. The trace element solution comprises (w/v) 2.2% ZnSO₄·7H₂O, 1.1% H₃BO₃, 0.5% MnCl₂·4H₂O, 0.16% FeSO₄·7H₂O, 0.16% CoCl₂·5H₂O, 0.16% CuSO₄·5H₂O, 0.11% (NH₄)₆Mo₇O₂₄·4H₂O, and 5% Na₄EDTA.

Escherichia coli DH5 α and BL21(DE3) were grown in liquid or on solid Luria-Bertani (LB) medium (1% NaCl, 1% tryptone, and 0.5% yeast extract) for standard DNA manipulation. 50 μ g/mL carbenicillin or 25 μ g/mL kanamycin were supplemented for cultivation of recombinant *E. coli* strains.

3. Genomic DNA isolation

The mycelia of *P. crustosum* and *A. nidulans* were collected on sterilized filter paper and then suspended in 400 μ L of LETS buffer (10 mM Tris-HCl pH 8.0, 20 mM EDTA pH 8.0, 0.5% SDS, and 0.1 M LiCl) in 2 mL Eppendorf tubes and vigorous vortexed with four glass beads (2.85 mm in diameter). 300 μ L LETS buffer were added in the solution, which was subsequently treated with 700 μ L phenol: chloroform: isoamylol (25:24:1). The genomic DNA (gDNA) was precipitated by addition of 900 μ L absolute ethanol and centrifugation at 17,000 x g for 30 min. After washing with 70% ethanol and drying, the obtained DNA was dissolved in 50 μ L distilled H₂O.

4. RNA isolation and cDNA synthesis

For isolation of RNA from *P. crustosum* PRB-2, the fungus was cultivated in liquid PD medium shaking at 230 rpm for 7 days and the cells were collected by centrifugation. RNA extraction was performed by using Fungal RNA Mini kit (VWR OMEGA bio-tek E.Z.N.A) according to the standard manufacturer's instruction. The ProtoScript II First Strand cDNA Synthesis kit (BioLabs) was used for cDNA synthesis with Oligo-dT primers.

5. PCR amplification, gene cloning and plasmid construction

Plasmids used in this study are listed in Table S2. The oligonucleotide sequences for PCR amplification are given in Table S3. Genetic manipulation in *E. coli* was carried out according to the protocol by Sambrook and Russell.⁵ All primers were synthesized by SeqLab GmbH (Göttingen, Germany). PCR amplification was carried out by using Phusion® High-Fidelity DNA polymerase from New England Biolabs (NEB) on a T100TM Thermal cycler from Bio-Rad. PCR reaction mixtures and thermal profiles were set as recommended by the manufacturer's instruction.

To construct pJF80 and pJF81 for *traG* deletion, primers were designed with split-marker strategy by using p5HY and p3YG vectors (Figure S4).^{6,7} To construct the plasmids for heterologous expression of *traA* and *traAG* in *A. nidulans*, an assembly approach based on the homologous recombination in *E. coli* was used (Figure S2).⁸ Full length of *traA* including its terminator of 497 bp was amplified from gDNA of *P. crustosum* PRB-2 as the template by PCR with primer pairs A.n-*traA*-1F-For/1F-Rev and A.n-*traA*-2F-For/2F-Rev (Table S3) and inserted into the corresponding sites of pYH-*wA*-*pyrG* with homologous flanking sequences of the *wA* gene to create pJF27.⁴ For co-expression of *traA* and *traG*, *traA* including *gpdA* promoter and its terminator of 497 bp from pJF27, and *traG* with its 778 bp promoter and 568 bp terminator from *P. crustosum* PRB-2 were cloned into pYWB2 by homologous recombination with flanking sequences of the *wA* gene to create pJF91.⁹ Herein, primers A.n-*traAG*-1F-For/*traA*-1F-Rev, A.n-*traA*-2F-For/*traAG*-1F-Rev and A.n-*traAG*-2F-For/2F-Rev (Table S3) were used for PCR amplification.

To construct the plasmid for expressing *traD* and *traH* in *E. coli*, the coding region of *traD* and *traH* were amplified by PCR from cDNA with the primer pairs TraD-28-For/Rev and TraH-28-For/Rev (Table S3). The expression vector pET-28a (+) was digested with BamHI and EcoRI, and ligated with DNA fragments by homologous recombination yielding the expression plasmid pJF72 for TraD and pJF74 for TraH, which were confirmed by sequencing (SeqLab GmbH).

6. Deletion of *traG* in *P. crustosum* and cultivation of deletion mutants.

Fresh conidia from 7-day PDA culture of *P. crustosum* PRB-2 were inoculated into 30 mL LMM medium (1.0% glucose, 50 mL/L salt solution, 1 mL/L trace element solution, and 0.5% yeast extract) in 100 mL flask and incubated at 25°C and 230 rpm for germination. Mycelia were harvested after 11 h by centrifugation at 2,800 x *g* for 10 min, and washed with distilled H₂O. The mycelia were then transferred into a 50 mL flask with 10 mL of osmotic buffer (1.2 M MgSO₄ in 10 mM sodium phosphate, pH 5.8) containing 50 mg lysing enzyme from *Trichoderma harzianum* (Sigma) and 20 mg yatalase from *Corynebacterium sp.* OZ-21 (OZEKI Co., Ltd.). After shaking at 30°C and 100 rpm for 2.5 h, the cells were transferred into a 50 mL falcon tube and overlaid gently with 10 mL of trapping buffer (0.6 M sorbitol in 0.1 M Tris-HCl, pH 7.0). After centrifugation at 4°C and 2,800 x *g* for 10 min, the protoplasts were collected from the interface of the two buffer systems. The protoplasts were then transferred to a sterile 15 mL falcon tube and resuspended in 200 µL of STC buffer (1.2 M sorbitol, 10 mM CaCl₂, and 10 mM Tris-HCl, pH 7.5) for transformation.

The *via* PCR constructed gene deletion cassettes mentioned above were transformed into *P. crustosum* by polyethylene glycol (PEG) mediated protoplast transformation. The DNA fragments (2 µg) were incubated with 100 µL of the protoplasts for 50 min on ice. 1.25 mL of PEG solution (60% PEG 4000, 50 mM CaCl₂, 50 mM Tris-HCl, pH 7.5) was then added and gently mixed. After incubation at room temperature for 30 min, the mixture was transferred in 5 mL STC buffer and spread on plates with SMM bottom medium (1.0% glucose, 50 mL/L salt solution, 1 mL/L trace element solution, 1.2 M sorbitol, and 1.6% agar) containing 200 µg/mL hygromycin B. SMM top medium (1.0% glucose, 50 mL/L salt solution, 1 mL/L trace element solution, 1.2 M sorbitol, and 0.8% agar) containing 100 µg/mL hygromycin B was overlaid softly on the plates. Three days later, the transformants were transferred onto fresh PDA plates containing 200 µg/mL hygromycin B for second round selection. The obtained transformants were inoculated in PD medium for isolation of genomic DNA to verify the integrity, which was carried out by PCR amplification (Figure S4). The obtained $\Delta traG$ mutant was cultivated in PD liquid medium at 25 °C for 7 days, together with $\Delta traA$ mutant in a previous study.⁶ For SM detection of the deletion mutants, cultures were extracted with ethyl acetate, dissolved in a mixture of MeOH and H₂O (8 : 2) and analyzed on LC-MS by method B (see below for methods of HPLC and LC-MS analysis).

7. Heterologous expression of *traA* and *traG* in *A. nidulans*

A. nidulans strain LO8030 was used as the recipient host.³ Fungal protoplast preparation and transformation were performed according to the method described previously.³ pJF27 containing the PKS-NRPS gene *traA* was transformed into LO8030 to create the *traA* expression strain JF15. pJF91 containing both *traA* and *traG* was transformed into LO8030 to create the *traAG* expression strain JF45. Potential transformants were verified by PCR using the primers traA-F/R or traG-F/R (Table S3). Differing from *P. crustosum*, germination condition was at 37°C with appropriate nutrition as supplements (0.75 µM riboflavin and 0.5 µM pyridoxine for JF15, 5% uracil, 6% uridine and 0.5 µM pyridoxine for JF45) for 6 h. Protoplastation condition was at 37°C for 2.5 h. *A. nidulans* strains were cultivated in PD liquid medium at 25°C for 7 days for LC-MS analysis (method B) of the SM production.

8. Precursor feeding in *P. crustosum* deletion mutants

For feeding experiments, the precursors (5*S*)-carboxylcrustic acid (**4**) and (5*S*)-viridicatic acid (**5**) were dissolved in DMSO to give 1 M stock solution, and added to 10 mL of PD cultures of respective deletion mutants, **4** to $\Delta traA$ mutant, and **5** to $\Delta traA$ and $\Delta traG$, leading to final concentrations of 0.4 mM. After further cultivation at 25°C for 7 d in PD medium, the secondary metabolites were extracted with ethyl acetate, dissolved in a mixture of MeOH and H₂O (8 : 2) and analyzed on LC-MS by method B (see below for methods of HPLC and LC-MS analysis).

9. Overproduction and purification of TraD and TraH

The expression plasmids pJF72 and pJF74 were constructed for TraD and TraH expression in *E. coli* as mentioned above. The recombinant *E. coli* BL21(DE3) strains were cultivated in Terrific Broth (TB) medium (2.4% yeast extract, 2.0% tryptone, 0.4% glycerol, 0.1 M phosphate buffer, pH 7.4). TraH expression was induced with 0.5 mM IPTG at 20°C for 16 h and TraD at 16°C for 16 h. The recombinant His₆-tagged protein were purified on Ni-NTA affinity chromatography

(Qiagen, Hilden) using the published procedures.^{10,11} The purity for TraH and TraD were confirmed on sodium dodecyl sulfate-polyacrylamide gel electrophoresis (SDS-PAGE) (Figure S12). The protein concentration was determined on Nanodrop 2000c spectrophotometer (Thermo Scientific, Braunschweig, Germany). 4.5 mg/L of protein can be obtained for TraH, 10.6 mg/L of protein can be obtained for TraD from the bacterial culture.

10. *In vitro* assays of TraD and TraH

To determine the enzyme activity of TraH toward (5*S*, 5'*S*)-crustolic acid (**1**) or (5*S*, 5'*S*)-crustolic acid methyl ester (**7**), the enzyme assays (50 μ L) contained phosphate buffer (20 mM, pH 7.4), ascorbic acid (1 mM), (5*S*, 5'*S*)-crustolic acid (**1**, 0.5 mM) or (5*S*, 5'*S*)-crustolic acid methyl ester (**7**, 0.5 mM), DTT (1 mM), Fe[(NH₄)₂(SO₄)₂] (1 mM), 2-oxoglutarate (1 mM), glycerol (0.5 – 5%), DMSO (5%), and the purified recombinant TraH (5.4 μ M). The enzyme assays were carried out at 37 °C for 30 min and terminated with one volume of acetonitrile. The reaction mixtures were centrifuged at 17,000 x *g* for 30 min before further analysis on HPLC and LC-MS by method A (see below for methods of HPLC and LC-MS analysis).

To determine the enzyme activity of TraD toward dehydroterrestric acid (**3**), the enzyme assays (50 μ L) contained phosphate buffer (20 mM, pH 7.4), NAD(P)H (2 mM), glycerol (0.5 – 5%), DMSO (5%), dehydroterrestric acid (**3**, 0.5 mM), and the purified recombinant TraD (0.6 μ M). The enzyme assays were incubated at 30 °C for 10 min and terminated with one volume of acetonitrile. The reaction mixtures were centrifuged at 17,000 x *g* for 30 min before further analysis on HPLC and LC-MS by method A. The same reaction condition was used for the enzyme assay of TraD with (5'*S*)-dehydrocrustolic acid methyl ester (**8**).

To prove the conversion of (5*S*, 5'*S*)-crustolic acid (**1**) by TraH and TraD, the enzyme assays (50 μ L) contained phosphate buffer (20 mM, pH 7.4), ascorbic acid (1 mM), (5*S*, 5'*S*)-crustolic acid (**1**, 0.5 mM), Fe[(NH₄)₂(SO₄)₂] (1 mM), 2-oxoglutarate (1 mM), NADPH (2 mM), glycerol (0.5 – 5%), DMSO (5%), and the purified recombinant TraH (5.4 μ M) and TraD (0.6 μ M). The enzyme assays were incubated at 30 °C for 30 min and terminated with one volume of acetonitrile. The reaction mixtures were centrifuged at 17,000 x *g* for 30 min before further analysis on HPLC and LC-MS by method A.

To prove the conversion of (5*S*)-carboxylcrustic acid (**4**) to (5*R*)-crustic acid (**6**) by TraH and TraD, the enzyme assays (50 μ L) containing phosphate buffer (20 mM, pH 7.4), ascorbic acid (1 mM), (5*S*)-carboxylcrustic acid (**4**, 0.5 mM), DTT (1 mM), Fe[(NH₄)₂(SO₄)₂] (1 mM), 2-oxoglutarate (1 mM), NAD(P)H (2 mM), glycerol (0.5 – 5%), DMSO (5%), and the purified recombinant TraH (12 μ M) and TraD (6 μ M) were incubated at 30°C for 16 h and terminated with one volume of acetonitrile. The reaction mixtures were centrifuged at 17,000 x *g* for 30 min before further analysis on HPLC and LC-MS by method A. In addition, (5*S*)-carboxylcrustic acid (**4**, 0.5 mM) was incubated with TraH (12 μ M) in the presence of ascorbic acid (1 mM), DTT (1 mM), Fe[(NH₄)₂(SO₄)₂] (1 mM), 2-oxoglutarate (1 mM) at 37°C for 16 h. After terminated with acetonitrile and centrifugation, the enzyme assay was further analyzed on HPLC and LC-MS by method A.

11. Large-scale fermentation, extraction and isolation of secondary metabolites

To isolate **4** from *A. nidulans* carrying *traA*, the transformant JF15 was cultivated in 60 x 250 mL flasks each containing 50 mL PD liquid medium with appropriate nutrition as supplement at 25°C for 7 days. The supernatant and mycelia were separated, and extracted with ethyl acetate and acetone, separately. The acetone extract was concentrated under reduced pressure to afford an aqueous solution, and then extracted with ethyl acetate. The two ethyl acetate extracts were combined and evaporated under reduced pressure to give a crude extract (0.8 g). The crude extract was applied to Sephadex LH-20 column eluted with methanol, yielding twenty fractions (1 – 20). Fraction 8 was purified on a semi-preparative HPLC (acetonitrile / H₂O (40 : 60) with 0.1% trifluoroacetic acid) yielding compound **4** (8 mg).

To isolate **5** from *A. nidulans* carrying *traA* and *traG*, the transformant JF45 was cultivated in 10 x 1 L flasks each containing 100 g rice and 150 mL H₂O (with appropriate nutrition as supplement) at 25°C for 7 days. After extracting with 15 L ethyl acetate and concentrated under reduced pressure, the crude extract (2.5 g) obtained from JF45 cultivation was applied to silica gel column chromatography by using petroleum ether / EtOAc (1 : 1, 1 : 3, and 1 : 5, v/v) as elution solvents, giving fractions 1 – 10. **5** (15 mg) was obtained from fraction 3 after purification on Sephadex LH-20 column using MeOH as eluent.

To isolate **5** from *P. crustosum* PRB-2, spores were inoculated in 4 L PD liquid medium and cultivated at 25°C for 14 days. 1.0 g crude extract was obtained after extraction, and subjected to silica gel column chromatography by using petroleum ether / EtOAc (10 : 1, 3 : 1, 1 : 1, 1 : 3, 1 : 6, v/v) as elution solvents, giving fractions 1 – 5. **5** (3 mg) was obtained from fraction 3 by applying to Sephadex LH-20 column using MeOH as eluent.

To isolate the accumulated products **4** and **6** from $\Delta traG$ mutant, the strain was cultivated in 6 L PD liquid medium at 25°C for 14 days and extracted as mentioned above. The resulted crude extract (2.5 g) was subjected to silica gel column chromatography by using stepwise gradient elution with the mixtures of petroleum ether / EtOAc (10 : 1, 5 : 1, 3 : 1, and 1 : 1, v/v) to give 25 fractions. Subsequent purification on semi-preparative HPLC with isocratic elution using acetonitrile / H₂O (40 : 60) supplied with 0.1% trifluoroacetic acid yielded 3 mg of **4**, using acetonitrile / H₂O (70 : 30) with 0.1% trifluoroacetic acid yielded 5 mg of **6**.

To prepare the enzyme products for structural elucidation, assays were carried out in large scales (10 – 20 mL) using the reaction conditions mentioned above. The reaction mixtures were extracted with double volume of ethyl acetate for three times. The organic phases were combined and concentrated under vacuum. The resulted residues were dissolved in acetonitrile and centrifuged at 17,000 x *g* for 20 min. After isolation on semi-preparative HPLC eluted with 40% acetonitrile containing 0.1% trifluoroacetic acid, compound **2** from the incubation mixture of TraH, TraD and **1**, compound **3** from TraH and **1**, and **5** from TraH and **4**, were obtained.

12. Determination of kinetic parameters

For determination of kinetic parameters of TraH toward **1** or **7**, the enzyme assays were carried out in a similar way as mentioned above, excepting that substrates at final concentrations of

SUPPORTING INFORMATION

0.01, 0.02, 0.05, 0.1, 0.2, 0.5, 1, 2, 5 mM, respectively. The enzyme assays were incubated at 37°C for 30 min and terminated with one volume of acetonitrile. The supernatants were subjected to HPLC analysis by method A after centrifuging at 17,000 $\times g$ for 30 min. The K_M and k_{cat} values were obtained by analysis with GraphPad Prism 8.

13. HPLC and LC-MS analysis of secondary metabolites

Analysis of SMs was performed on an Agilent series 1200 HPLC (Agilent Technologies, Böblingen, Germany) with an Agilent Eclipse XDB-C18 column (150 \times 4.6 mm, 5 μ m). Water (A) and acetonitrile (B), both with 0.1% (v/v) formic acid, were used as solvents at flow rate of 0.5 mL/min. The substances were eluted with a linear gradient from 5 – 100% B in 15 min, then washed with 100% (v/v) solvent B for 5 min and equilibrated with 5% (v/v) solvent B for 5 min (method A) or with a linear gradient from 5 – 100% B in 40 min, then washed with 100% (v/v) solvent B for 5 min and equilibrated with 5% (v/v) solvent B for 10 min (method B). UV absorptions at 280 nm were illustrated in this study. Semi-preparative HPLC was performed on the same equipment with an Agilent Eclipse XDB-C18 column (9.4 \times 250 mm, 5 μ m) column and a flow rate of 2 mL/min.

LC-MS analysis was performed on an Agilent 1260 HPLC system equipped with a microTOF-Q III spectrometer (Bruker, Bremen, Germany) by using Multospher 120 RP18-5 μ column (250 \times 2 mm, 5 μ m) (CS-Chromatographie Service GmbH) and method A or method B for separation at flow rate of 0.25 mL/min. Electrospray positive or negative ionization mode was selected for determination of the exact masses. The capillary voltage was set to 4.5 kV and a collision energy of 8.0 eV. Sodium formate was used in each run for mass calibration. The masses were scanned in the range of m/z 100 – 1500. Data were evaluated with the Compass DataAnalysis 4.2 software (Bruker Daltonik, Bremen, Germany).

14. NMR analysis

NMR spectra were recorded on a JEOL ECA-500 MHz spectrometer (JEOL, Tokyo, Japan). The spectra were processed with MestReNova 6.1.0 (Metrelab) or Delta 5.0.4 (JEOL). Chemical shifts are referenced to those of the solvent signals. NMR data are given in Tables S4 – S8 and spectra in Figures S21 – S35.

15. Circular dichroism (CD) spectroscopic analysis

CD spectra were taken on a J-815 CD spectrometer (Jasco Deutschland GmbH, Pfungstadt, Germany). The samples were dissolved in methanol and measured in the range of 200–400 nm by using a 1 mm path length quartz cuvette (Hellma Analytics, Müllheim, Germany). The CD spectra are given in Figures S36.

16. Measurement of optical rotations

The optical rotation was measured with the polarimeter Jasco DIP-370 at 20°C using the D-line of the sodium lamp at $\lambda=589.3$ nm. Prior to the measurement, the polarimeter was calibrated with methanol or ethanol as solvent.

17. Physicochemical properties of the compounds described in this study

(5*R*, 5'*S*)-terrestric acid (**2**): Yellow oil; CD (MeOH): λ_{max} ($\Delta\epsilon$) 282 (+0.9) nm, 228 (+2.8), 212

SUPPORTING INFORMATION

(+7.5); HRMS (m/z): (ESI/[M+H]⁺) calcd. for C₁₁H₁₅O₄, 211.0965, found 211.0963.

(5'S)-dehydroterrestric acid (**3**): White powder; HRMS (m/z): (ESI/[M+H]⁺) calcd. for C₁₁H₁₃O₄, 209.0808, found 209.0806.

(5S)-carboxylcrustic acid (**4**): Yellow oil; $[\alpha]_D^{20} = -46.5$ (c 0.40, MeOH); HRMS (m/z): (ESI/[M+H]⁺) calcd. for C₁₂H₁₃O₆, 253.0707, found 253.0719

CD spectrum (MeOH) of sample isolated from a *A. nidulans* strain JF15 harboring *traA*: $\lambda_{\max} (\Delta\epsilon)$ 332 (-1.9), 268 (-1.7), 228 (-4.1) nm .

CD spectrum (MeOH) of sample isolated from $\Delta traG$ mutant of *P. crustosum*: $\lambda_{\max} (\Delta\epsilon)$ 346 (-2.8), 279 (-3.9), 223 (-6.0) nm.

(5S)-viridicatic acid (**5**): Yellow oil; $[\alpha]_D^{20} = -73.6$ (c 1.0, EtOH); HRMS (m/z): (ESI/[M+H]⁺) calcd. for C₁₂H₁₇O₆, 257.1020, found 257.1038.

CD spectrum (MeOH) of sample isolated from a *A. nidulans* strain JF45 harboring *traA* and *traG*: $\lambda_{\max} (\Delta\epsilon)$ 258 (-11.4), 230 (-11.3) nm.

CD spectrum (MeOH) of sample isolated from *P. crustosum* PRB-2: $\lambda_{\max} (\Delta\epsilon)$ 259 (-7.0), 230 (-7.6) nm.

(5R)-crustic acid (**6**): Yellow oil; $[\alpha]_D^{20} = +19.1$ (c 0.25, MeOH); CD (MeOH) $\lambda_{\max} (\Delta\epsilon)$ 317 (+0.2), 258 (+2.1), 228 (+5.2) nm; HRMS (m/z): (ESI/[M+H]⁺) calcd. for C₁₁H₁₃O₄, 209.0808, found 209.0827.

(5S, 5'S)-custosic acid methyl ester (**7**): Yellow oil; HRMS (m/z): (ESI/[M+H]⁺) calcd. for C₁₃H₁₇O₆, 269.1020, found 269.1037.

(5'S)-dehydrocrustosic acid methyl ester (**8**): White powder; HRMS (m/z): (ESI/[M+Na]⁺) calcd. for C₁₃H₁₄NaO₆, 289.0683, found 289.0700.

SUPPORTING INFORMATION

Supplementary Tables

Table S1. Strains used in this study

Strains	Genotype	Source/Ref.
<i>Penicillium crustosum</i>		
PRB-2	Wild type	1
$\Delta traA$	$\Delta traA::hph$ in <i>P. crustosum</i> PRB-2	6
$\Delta traG$	$\Delta traG::hph$ in <i>P. crustosum</i> PRB-2	This study
<i>Aspergillus nidulans</i>		
LO8030	<i>pyroA4, riboB2, pyrG89, nkuA::argB,</i> sterigmatocystin cluster (<i>AN7804-AN7825</i>) Δ , emericellamide cluster (<i>AN2545-AN2549</i>) Δ , asperfuranone cluster (<i>AN1039-AN1029</i>) Δ , monodictyphenone cluster (<i>AN10023-AN10021</i>) Δ , terrequinone cluster (<i>AN8512-AN8520</i>) Δ , austinol cluster part 1 (<i>AN8379-AN8384</i>) Δ , austinol cluster part 2 (<i>AN9246-AN9259</i>) Δ , F9775 cluster (<i>AN7906-AN7915</i>) Δ , asperthecin cluster (<i>AN6000-AN6002</i>) Δ	2,3
JF15	<i>gpdA::traA::AfpyrG</i> in <i>A. nidulans</i> LO8030	This study
JF45	<i>gpdA::traA::traG::Ribo</i> in <i>A. nidulans</i> LO8030	This study

SUPPORTING INFORMATION

Table S2. Plasmids used and constructed in this study

Plasmids	Description	Source/Ref.
p5HY	Two-third of the <i>hph</i> resistance gene at the 5'-end, originated from the pUChph and inserted into pESC-URA. For gene replacement using <i>hph</i> as selection marker.	6
p3YG	Two-third of the <i>hph</i> resistance gene at the 3'-end, originated from the pUChph and inserted into pESC-URA. For gene replacement using <i>hph</i> as selection marker.	6
pJF80	A 1054 bp US PCR fragment of <i>traG</i> from genomic DNA of <i>P. crustosum</i> PRB-2 inserted in p5HY.	This study
pJF81	A 939 bp DS PCR fragment of <i>traG</i> from genomic DNA of <i>P. crustosum</i> PRB-2 inserted in p3YG.	This study
pYH-wA-pyrG	<i>URA3, wA flanking, AfpyrG, Amp</i>	4
pYWB2	<i>URA3, wA flanking, Afribo, Amp</i>	9
pJF27	<i>pYH-wA-traA</i> ; a 12068 bp fragment of <i>traA</i> with its terminator from genomic DNA of <i>P. crustosum</i> PRB-2 inserted in <i>pYH-wA-gpdA</i>	This study
pJF91	<i>pYH-wA-traAG</i> ; a 12788 bp fragment of <i>traA</i> with <i>gpdA</i> promoter and its terminator from pJF27, and a 2528 bp fragment of <i>traG</i> with its promoter and terminator from genomic DNA of <i>P. crustosum</i> PRB-2 inserted in <i>pYWB2</i>	This study
pJF72	<i>pET-28a(+)-traD</i> ; a 804 bp fragment of <i>traD</i> from cDNA of <i>P. crustosum</i> PRB-2 with BamHI and EcoRI inserted in pET28a(+)	This study
pJF74	<i>pET-28a(+)-traH</i> ; a 984 bp fragment of <i>traH</i> from cDNA of <i>P. crustosum</i> PRB-2 with BamHI and EcoRI inserted in pET28a(+)	This study

US: upstream; DS: downstream

SUPPORTING INFORMATION

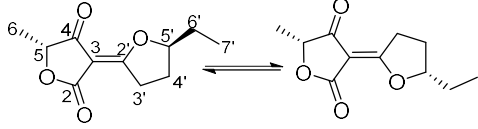
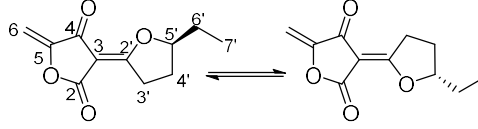
Table S3. Primers used in this study

Primers	Sequence 5'-3'	Targeted amplification
5F-R	GCTGAAGTCGATTTGAGTCCAC	US of <i>hph</i> to verify 5F of <i>P. crustosum</i> mutant
3F-F	GCATTAATGCATTGGACCTCGC	DS of <i>hph</i> to verify 3F of <i>P. crustosum</i> mutant
traA-F	TGCATCTTGAGAGCTCGC	1819 bp partial fragment of <i>traA</i>
traA-R	GAGGGCGGTTTTAGAATCAATTG	
traG-up-F	GAATTGTTAATTAAGAGCTCAGATCTCTAGCAGGACTCATCACAGACG	1054 bp upstream fragment of <i>traG</i> to construct pJF80
traG-up-R	CAACCCTCACTAAAGGGCGGCCGCACTAGCCGGGCTTCAGGGAAATTC	
traG-down-F	CGACTCACTATAGGGCCCGGGCGTGCACCCATGGTCCGATTGAGCTGG	939 bp downstream fragment of <i>traG</i> to construct pJF81
traG-down-R	CTAGCCGCGGTACCAAGCTTACTCGAGGCATGATTTGCCTCTAGACCCC	
traG-F	CAACACAATGTCACGGTACC	1071 bp partial fragment of <i>traG</i>
traG-R	CAGACATGGCCTGGGTACG	
traG-5F-F	CCGACAGACGAATATGGTGCC	US of <i>hph</i> to verify $\Delta traG$ mutant
traG-3F-R	CAGACATGCTTTCCGCAC	DS of <i>hph</i> to verify $\Delta traG$ mutant
A.n-traA-1F-For	CATCTTCCCATCCAAGAACCTTTAATCATGGTTCTACCCAGCCC	DNA of 1st <i>traA</i> fragment 5442 bp from <i>P. crustosum</i> to construct pJF27
A.n-traA-1F-Rev	CTCATCAAGCCCGTGACGAGCAAATGACTGTGAGCAACCACCATAG	
A.n-traA-2F-For	CTATGGTGGTTGCTCACAGTCATTTGCTCGTCCACGGGCTTGATGAG	DNA of 2nd <i>traA</i> fragment 6176 bp with its 497 bp terminator from <i>P. crustosum</i> to construct pJF27
A.n-traA-2F-Rev	GACACAGAATAACTCTCGCTAGCGTAGCTGGCAAATATAGTTACCT	
A.n-traAG-1F-For	CTTGACTCTCCTTCTCCTGATCGGATCCCATGCGGAGAGACGGACG	DNA of 6190 bp from pJF27 with A.n-traA-1F-Rev to construct pJF91
A.n-traAG-1R-Rev	TTAGTTTGCAAATCGACGATTGCTGTAGCTGGCAAATATAGTTACCTA	DNA of 6673 bp from pJF27 with A.n-traA-2F-For to construct pJF91
A.n-traAG-2F-For	GATAGGTAAGTATATTTGCCAGCTACAGCAATCGTCGATTTTGCAAAC	DNA of <i>traG</i> with its 788 bp promoter and 568 bp terminator from <i>P. crustosum</i> to construct pJF91
A.n-traAG-2R-Rev	CAACACCATATTTAATCCCATGTGCATGGATACTCAGGTGGTATAATT	
TraD-28-For	GTGGACAGCAAATGGGTCGCGGATCCATGAAAGTTTTGATTATTTTTGC	804 bp fragment of <i>traD</i> to construct pJF72
TraD-28-Rev	GCAAGCTTGTGACGGAGCTCGAATTCTCACGCTTCTTTGACGTCG	
TraH-28-For	CTGGTGGACAGCAAATGGGTCGCGGATCCATGTCTGTGTCGATGCGGCC	984 bp fragment of <i>traH</i> to construct pJF74
TraH-28-Rev	CAAGCTTGTGACGGAGCTCGAATTCCTACAATGAAGTATCATCCGTCA	

US: upstream; DS: downstream

SUPPORTING INFORMATION

Table S4. ^1H NMR data of compounds **2** and **3**

Compound		
	(5 <i>R</i> , 5' <i>S</i>)-terrestric acid (2 , CDCl_3) ¹²	(5' <i>S</i>)-dehydroterrestric acid (3 , $\text{DMSO-}d_6$) ¹³
Position	δ_{H} , multi., <i>J</i> in Hz	δ_{H} , multi., <i>J</i> in Hz
5	4.62, q, 7.0, 1H	-
6	1.48, d, 7.0, 3H	5.18, d, 2.5, 1H
	-	5.01, d, 2.5, 1H
3'	3.60, ddd, 20.0, 9.6, 4.5, 1H	3.56, ddd, 19.9, 9.4, 4.2, 1H ^a
	3.27, ddd, 20.0, 9.6, 5.1, 1H	3.48, ddd, 19.9, 9.4, 4.2, 1H ^a
4'	2.36, m, 1H	2.33, m, 1H
	1.87, m, 1H	1.84, m, 1H
5'	4.93, m, 1H	5.02, m, 1H
6'	1.97, m, 1H	1.81, m, 1H
	1.79, m, 1H	1.74, m, 1H
7'	1.07, t, 7.5, 3H	0.97, t, 7.4, 3H

Note: Due to the *Z/E* isomerization, there were two sets of signals in a ratio of 1:1 showed in the ^1H NMR spectra. The corresponding signals are overlapping in most cases with each other. Therefore, only one set of the NMR data was listed in the table. The *Z/E* isomerization was proved by deuterium incorporation after incubation of (5*S*, 5'*S*)-crustosic acid (**1**) in D_2O -enriched milieu (Figure S10).

^a signals overlapped with those of water.

Compounds **3** and **2** were isolated from incubation mixtures of **1** with TraH alone and with TraH and TraD, respectively. Their NMR data correspond very well to those reported previously.^{12,13}

SUPPORTING INFORMATION

Table S5. NMR data of compound **4**

Compound

(5*S*)-carboxylcrustic acid (**4**, CD₃OD)

Position	δ_{H} , multi., J in Hz	δ_{C}	Key HMBC correlations
2	-	167.8 ^a	
3	-	n.d. ^b	
4	-	n.d. ^b	
5	4.95, dd, 5.9, 4.1, 1H	80.2	C-2, C-13
6	-	178.5	
7	7.10, d, 15.3, 1H	119.0	C-6, C-9
8	7.68, dd, 15.3, 9.9, 1H	149.5	C-6, C-10
9	6.50, m, 1H	132.2	C-8, C-11
10	6.50, m, 1H	146.5	C-8, C-11
11	1.96, d, 5.5, 3H	19.3	C-9, C-10
12	2.99, dd, 17.4, 4.1, 1H	35.8	C-5, C-13
	2.88, dd, 17.4, 5.9, 1H	-	
13	-	172.2	

Note: ^a Signals acquired from HMBC correlations.

^b Signals not detected in neither ¹³C NMR nor HMBC spectrum.

Compound **4** was isolated from *A. nidulans* JF15 harboring pJF27 with *traA*.

SUPPORTING INFORMATION

Table S6. NMR data of compound **5**

Position	δ_{H} , multi., J in Hz	δ_{C}	Key HMBC correlations
2	-	174.2	
3	-	94.2	
4	-	171.8	
5	4.37, dd, 9.3, 3.5, 1H	75.7	C-2, C-4, C-13
6	-	194.2	
7	2.61, dd, 8.5, 6.9, 2H	40.1 ^a	C-6, C-8, C-9
8	1.45, m, 2H	24.2	C-6, C-9, C-10
9	1.25, m, 2H	31.3	C-10
10	1.25, m, 2H	22.0	C-9
11	0.85, t, 7.0, 3H	13.9	C-9, C-10
12	2.69, dd, 16.0, 3.5, 1H 2.20, dd, 16.0, 9.3, 1H	37.6 -	C-5, C-13
13	-	193.7	
13-OH	12.44, s, 1H	-	

Note: ^a signals overlapped with those of solvents.

Compound **5** was isolated from *A. nidulans* JF45 harboring pJF91 with *traA* and *traG*.

SUPPORTING INFORMATION

Table S7. NMR data of compound **6**

(5*R*)-crustic acid (**6**, CD₃OD)

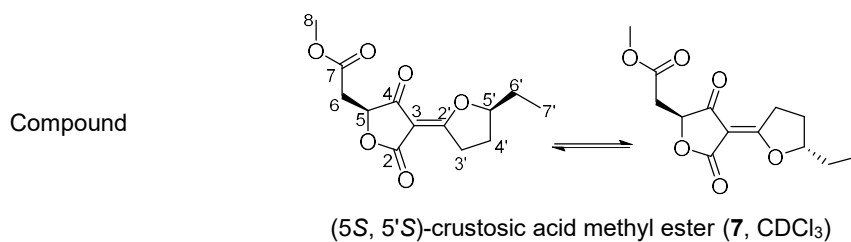
Position	δ_{H} , multi., J in Hz	δ_{C}	Key HMBC correlations
2	-	173.7	
3	-	96.8	
4	-	201.4 ^a	
5	4.79, q, 7.0, 1H	80.8	C-2, C-4
6	-	179.4	
7	7.11, d, 15.2, 1H	119.0	C-6, C-9
8	7.69, dd, 15.2, 9.9, 1H	149.9	C-6, C-10
9	6.50, m, 1H	132.2	C-7, C-11
10	6.50, m, 1H	146.9	C-8, C-11
11	1.96, d, 5.6, 3H	19.4	C-9, C-10
12	1.45, d, 7.0, 3H	17.0	C-4, C-5

Note: ^a Signal acquired from HMBC correlations.

Compound **6** was isolated from a $\Delta traG$ -mutant.

SUPPORTING INFORMATION

Table S8. NMR data of compound **7**



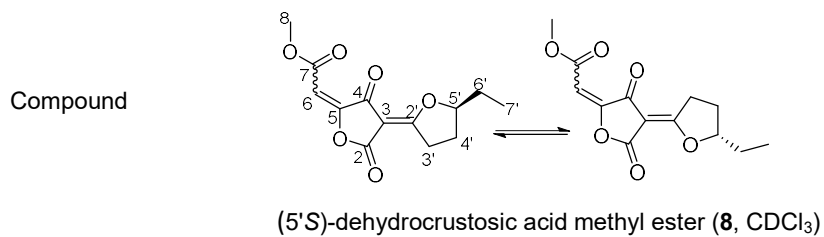
Position	δ_{H} , multi., <i>J</i> in Hz	δ_{C}
2	-	170.6/167.2
3	-	95.8/95.3
4	-	197.5/193.7
5	4.83, dd, 6.9, 4.1, 1H	78.8/78.6
6	3.00, dd, 9.0, 4.1, 1H	35.9/35.9
	2.85, dd, 9.0, 6.9, 1H	-
7	-	169.8/169.8
8	3.70, s, 3H	52.3/52.3
9	-	-
10	-	-
11	-	-
12	-	-
2'	-	187.0/186.3
3'	3.61, ddd, 14.0, 8.7, 4.2, 1H	34.1/33.8
	3.28, ddd, 14.0, 9.5, 8.6, 1H	-
4'	2.37, m, 1H	27.9/27.8
	1.87, m, 1H	-
5'	4.93, m, 1H	93.3/92.8
6'	1.98, m, 1H	26.6/26.6
	1.79, m, 1H	-
7'	1.06, t, 7.5, 3H	9.7/9.5

Note: due to the *Z/E* isomerization, there were two sets of signals in a ratio of 1:1 showed in the ¹H NMR spectra. The corresponding signals are overlapping in most cases with each other. Therefore, only one set of the NMR data was listed in the table.

Compound **7** was isolated from a methanol solution of **1**.

SUPPORTING INFORMATION

Table S9. ^1H NMR data of compound **8**



Position	δ_{H} , multi., J in Hz
6	5.91, s, 1H
8	3.81, s, 3H
3'	3.68, ddd, 20.3, 9.4, 4.0, 1H
	3.35, m, 1H
4'	2.43, m, 1H
	2.01, m, 1H ^a
5'	5.02, m, 1H
6'	1.93, m, 1H ^a
	1.83, m, 1H
7'	1.08, t, 7.4, 3H

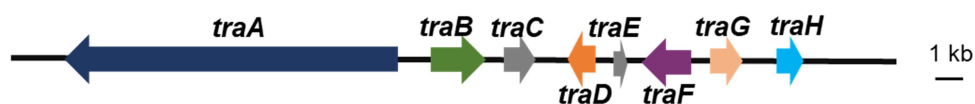
Note: due to the *Z/E* isomerization, there were two sets of signals in a ratio of 1:1 showed in the ^1H NMR spectra. The corresponding signals are overlapping in most cases with each other. Therefore, only one set of the NMR data was listed in the table.

^a signals overlapped with those of water.

Compound **8** was isolated from incubation mixture of **7** with TraH.

Supplementary Figures

Terrestrial acid cluster



Protein	Putative function
TraA	carboxylcrustic acid synthase KS-AT-DH-MeT-KR-ACP-C-A-PCP
TraB	cytochrome P450
TraC	hypothetical protein
TraD	flavin containing dehydroterrestrial acid hydrogenase
TraE	hypothetical protein
TraF	transporter
TraG	crustic acid reductase
TraH	2-oxoglutarate-dependent crustosic acid decarboxylase

The domain organization of TraA was deduced as ketosynthase (KS), acyltransferase (AT), dehydratase (DH), methyltransferase (MeT), ketoreductase (KR), and acyl carrier protein (ACP) domains of PKS, and the condensation (C), adenylation (A), peptidyl carrier protein (PCP) domains of NRPS.^{14,15}

Figure S1. Deduced functions of ORFs in terrestrial acid gene cluster of *P. crustosum* PRB-2⁶

SUPPORTING INFORMATION

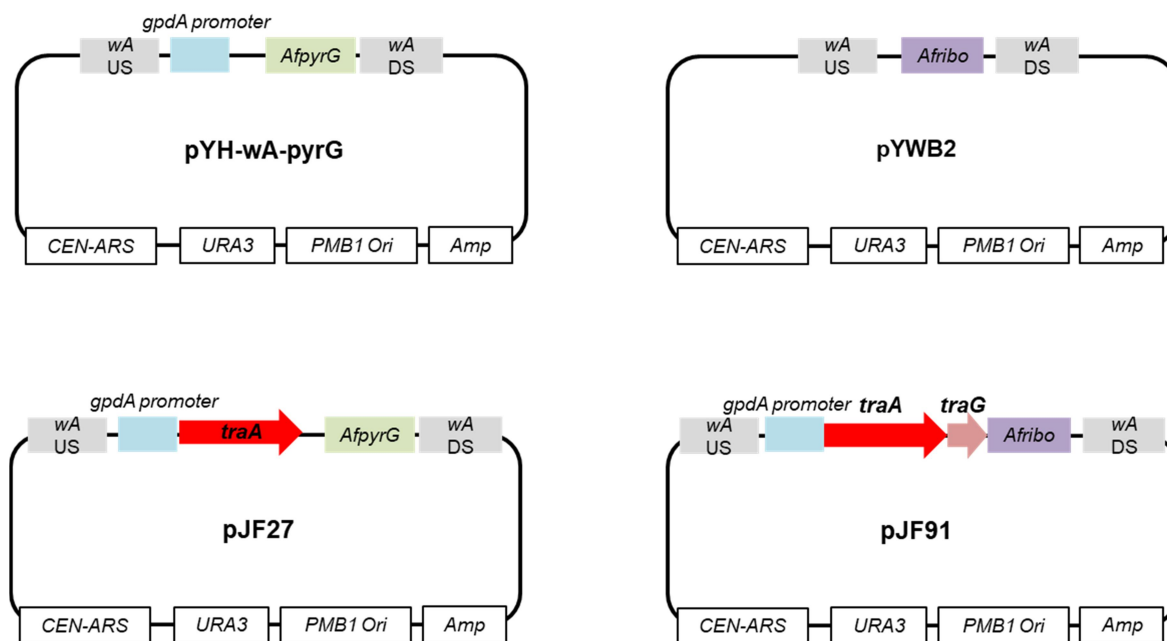


Figure S2. Constructs used for heterologous expression of *traA* and *traAG* in *A. nidulans*

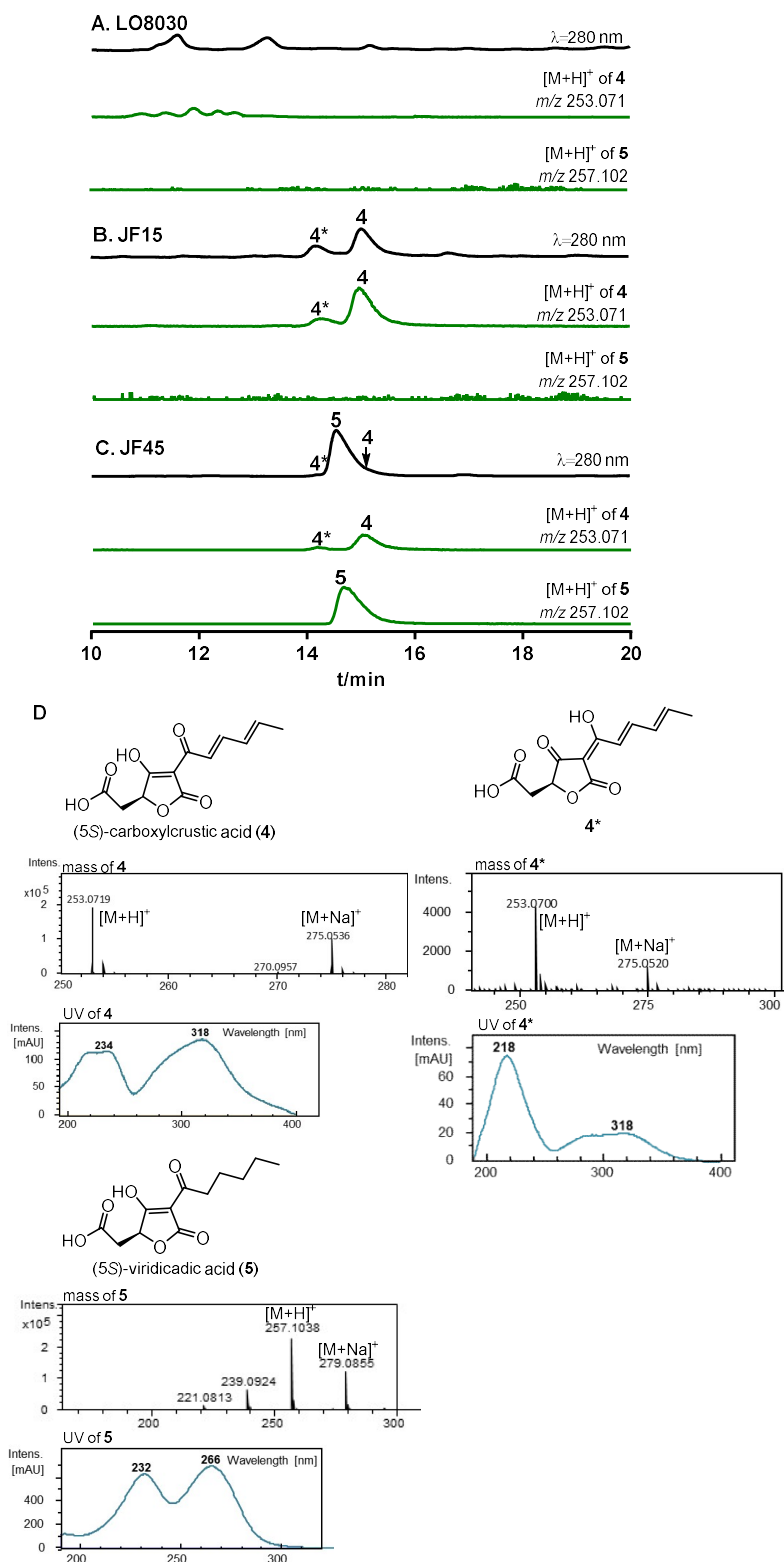


Figure S3. LC-MS analysis of the metabolite profile of different *A. nidulans* strains LO8030 as an expression host in (A), JF15 carrying the expression construct for *traA* (B), JF45 for co-expression of *traA* and *traG* (C) were cultivated in PD medium at 25 °C for 7 days. UV absorptions at 280 nm, [M+H]⁺ of **4** at m/z 253.071 ± 0.005 and [M+H]⁺ of **5** at m/z 257.102 ± 0.005 are illustrated. Structures, mass, and UV spectra of **4**, **4*** and **5** are shown in (D).

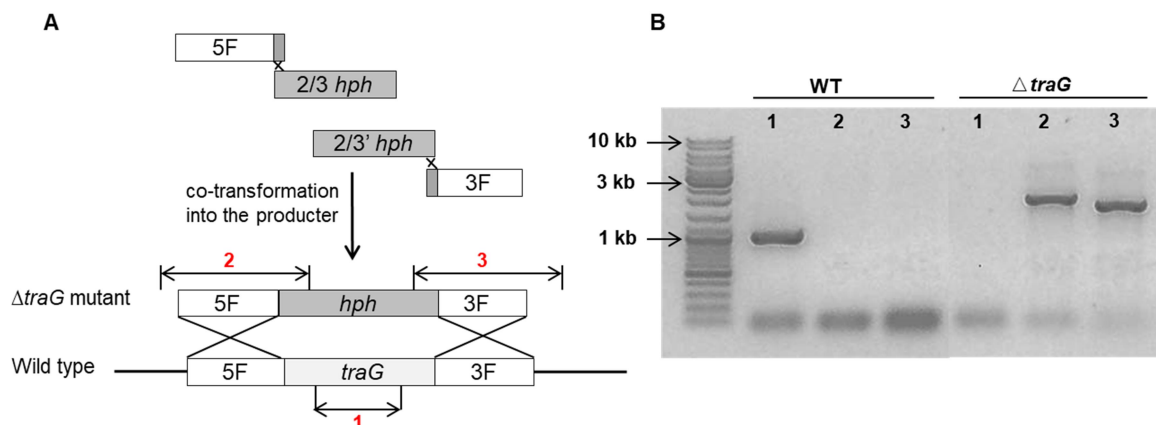


Figure S4. Verification of $\Delta traG$ -mutant from *P. crustosum* PRB-2

Gene deletion strategy in *P. crustosum* was schematically represented in (A). PCR amplification for three different fragments from genomic DNA of WT and $\Delta traG$ -mutant was used to prove the presence/absence of *traG* and its site specific integration with the help of up- and downstream regions (B). The PCR primers are given in Table S3.

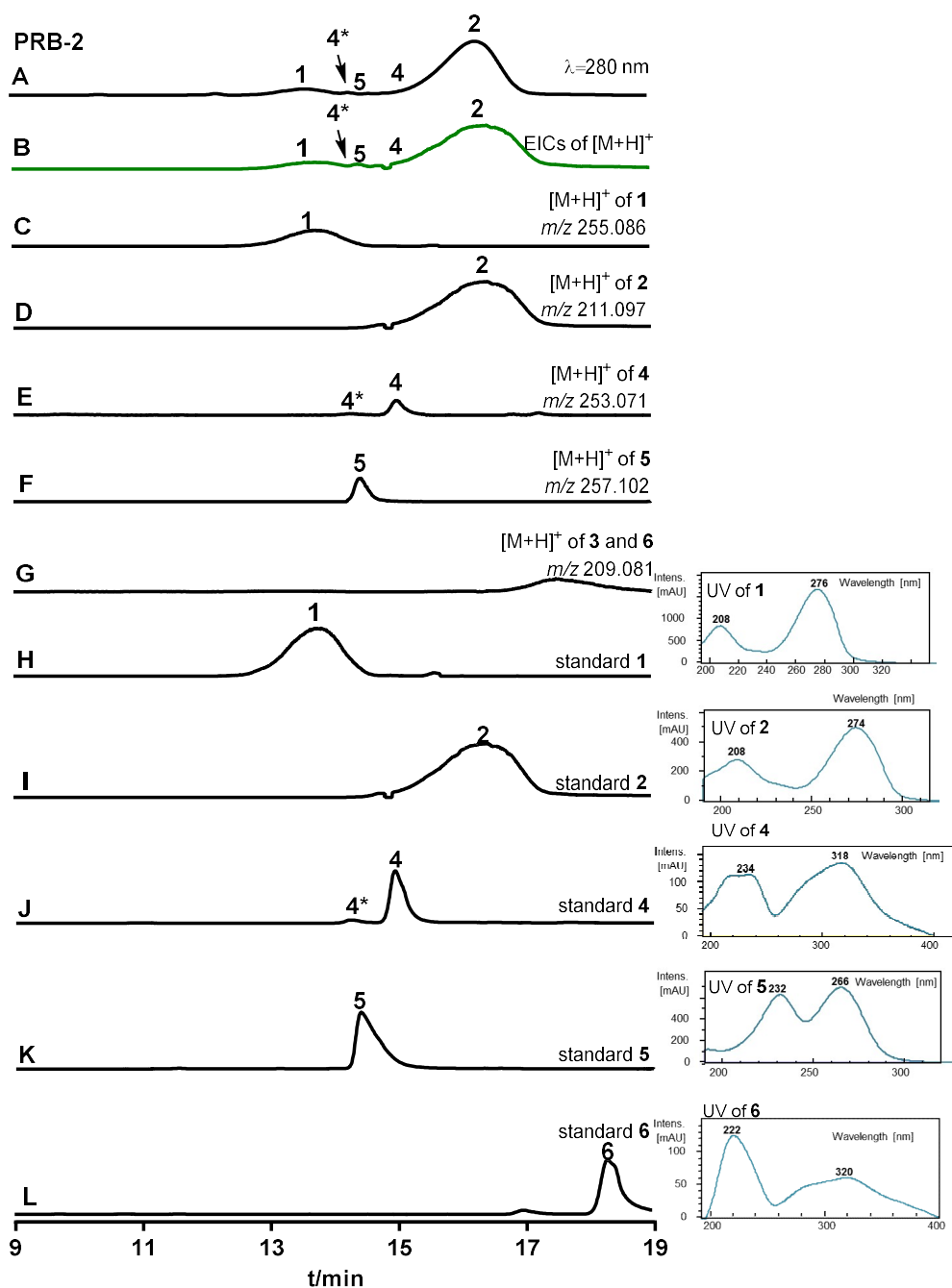


Figure S5. LC-MS detection of secondary metabolites from a 7 days-old liquid PD surface culture of *P. crustosum* PRB-2

UV absorptions at 280 nm are illustrated in (A). EICs in dark green refer total $[M+H]^+$ ions of **1** – **6** with a tolerance range of ± 0.005 (B), and in black refer $[M+H]^+$ ions of **1** – **6** (C – G), respectively. Standards of **1**, **2**, **4** – **6** are shown in H – L.

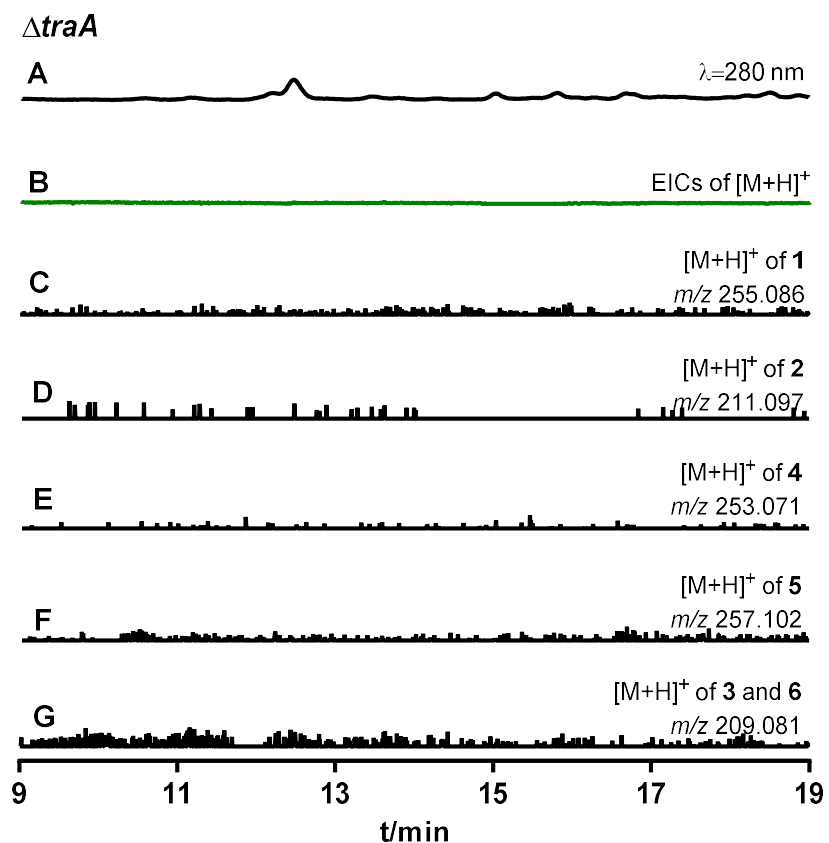


Figure S6. LC-MS detection of the metabolites in the terrestrial acid biosynthesis in $\Delta traA$ -mutant obtained from a previous study⁶. UV absorptions at 280 nm are illustrated in (A). EICs in dark green refer total $[M+H]^+$ ions of **1** – **6** with a tolerance range of ± 0.005 (B), and in black refer $[M+H]^+$ ions of **1** – **6** (C – G), respectively.

SUPPORTING INFORMATION

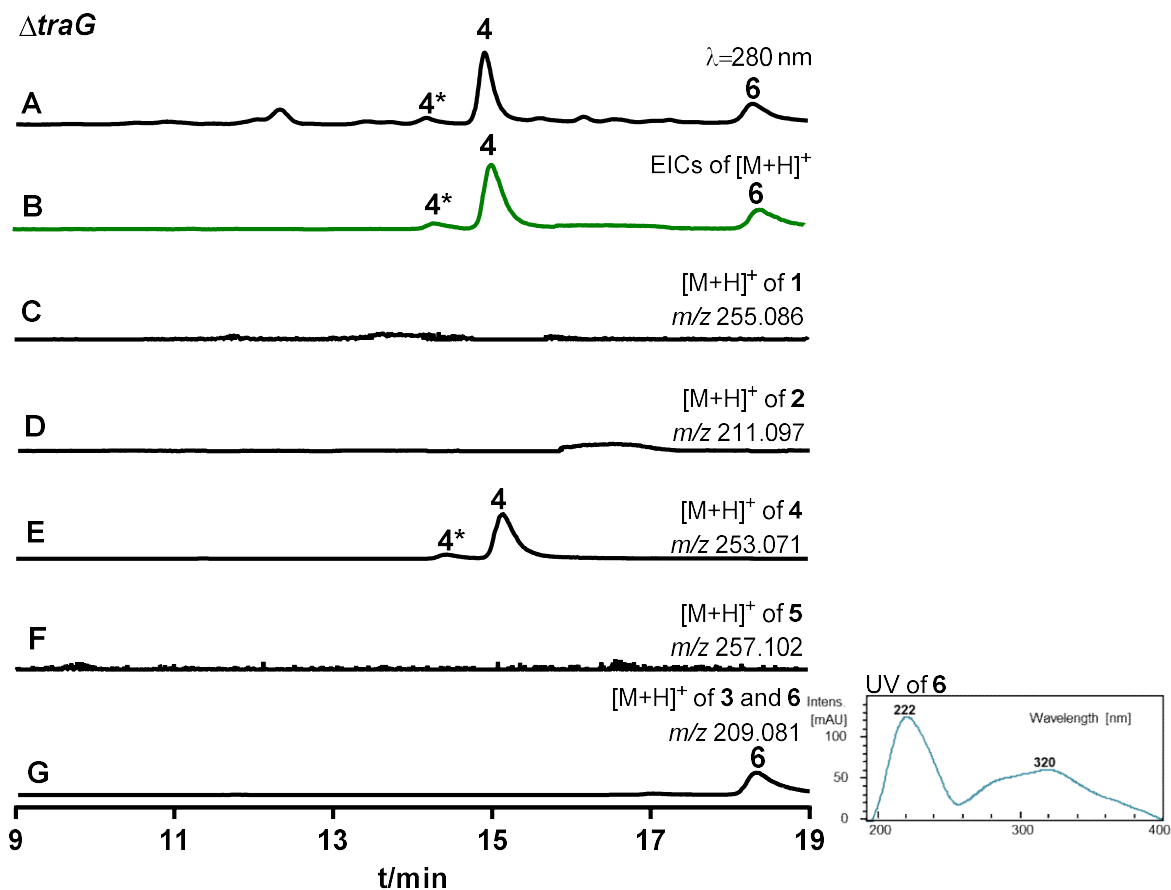


Figure S7. LC-MS detection of the metabolites in the terrestrial acid biosynthesis in $\Delta traG$ -mutant UV absorptions at 280 nm are illustrated in (A). EICs in dark green refer total $[M+H]^+$ ions of **1** – **6** with a tolerance range of ± 0.005 (B), and in black refer $[M+H]^+$ ions of **1** – **6** (C–G), respectively.

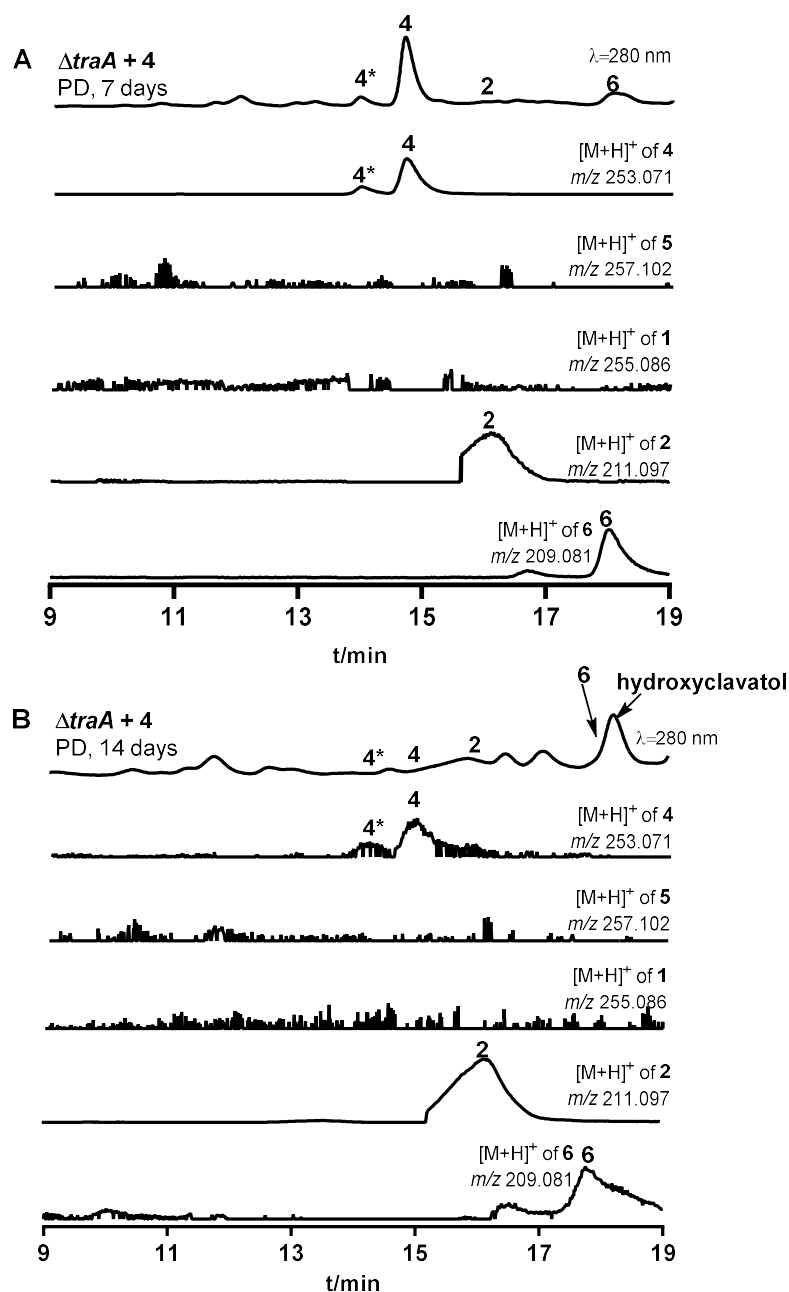


Figure S8. LC-MS detection of the metabolite profile of $\Delta traA$ mutant after feeding with **4**. $\Delta traA$ culture were fed with **4** and maintained for 7 days (A) and 14 days (B). UV absorptions at 280 nm are illustrated. EICs refer $[M+H]^+$ ions of **1**, **2**, **4**, **5** and **6** with a tolerance range of ± 0.005 .

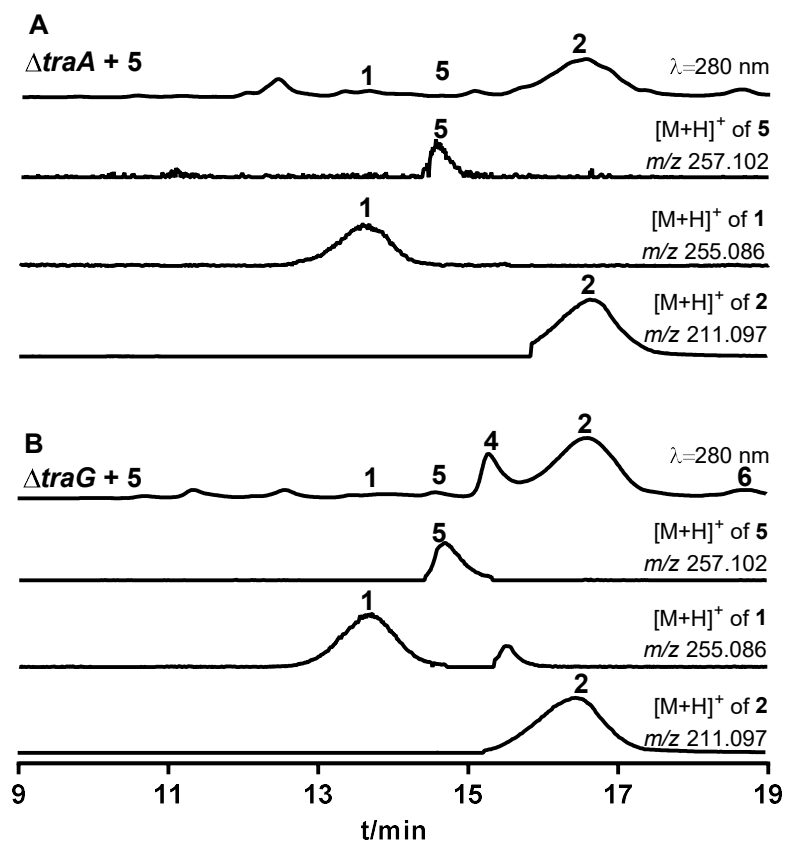


Figure S9. LC-MS detection of the metabolite profile of $\Delta traA$ and $\Delta traG$ mutants after feeding with **5**

$\Delta traA$ (A) and $\Delta traG$ (B) cultures were fed with **5** and maintained for 7 days. UV absorptions at 280 nm are illustrated. EICs refer $[M+H]^+$ ions of **1**, **2** and **5** with a tolerance range of ± 0.005 .

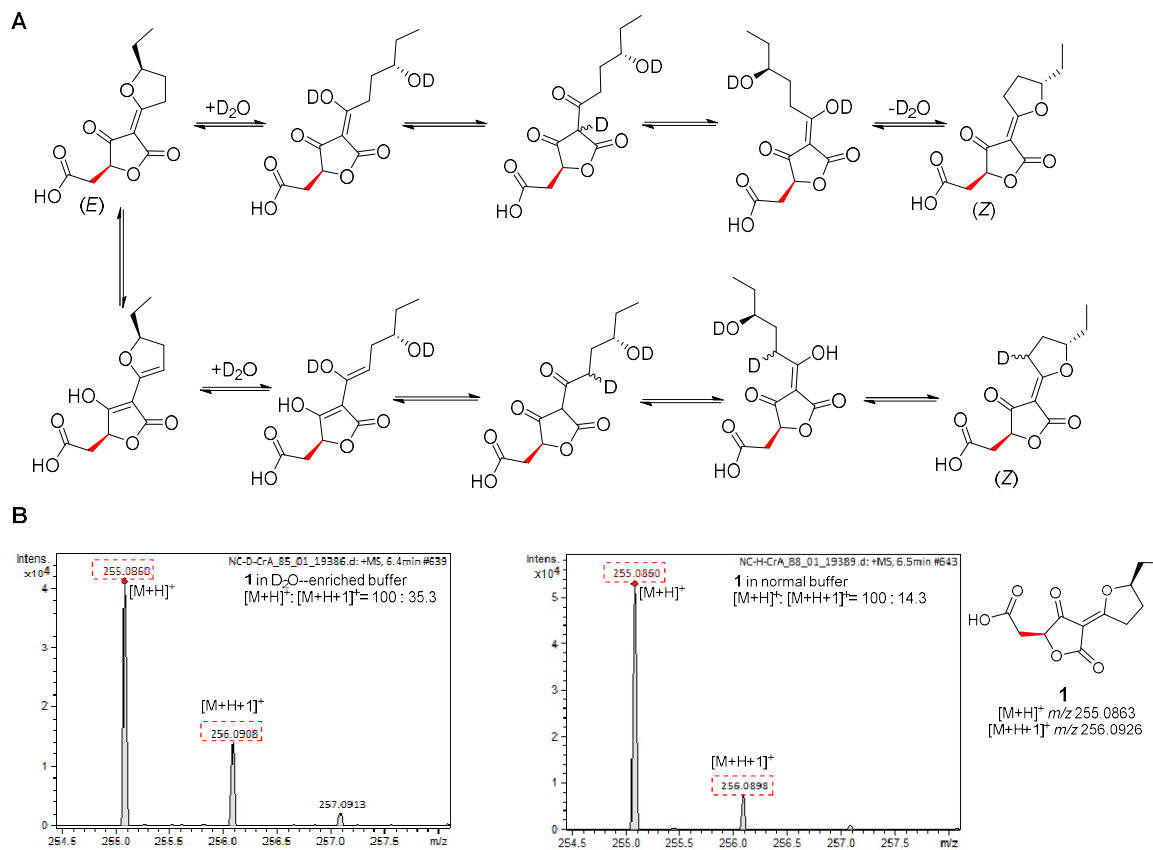


Figure S10. Incorporation of deuterium in **1** via *E/Z*-isomerization in D₂O-enriched milieu

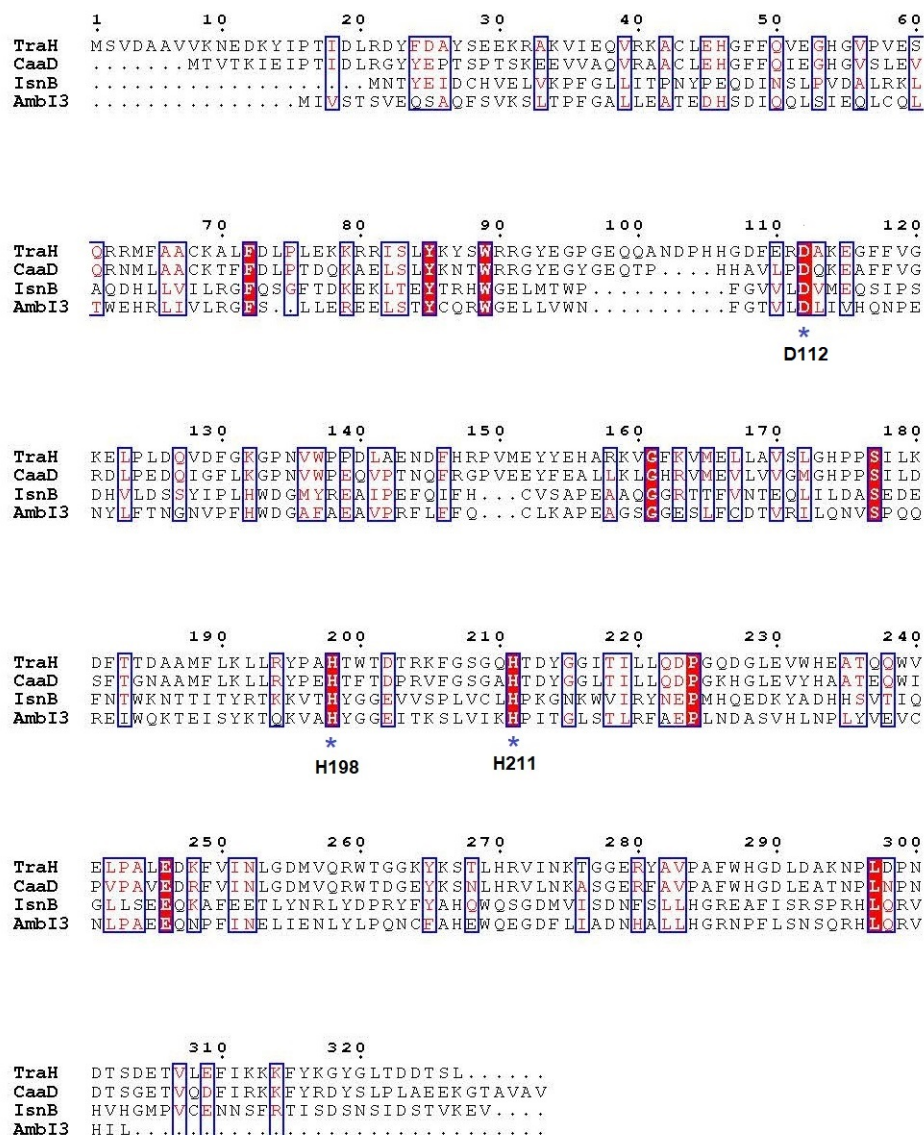


Figure S11. Sequence alignments of non-heme Fe^{II}-2OG-dependent decarboxylases CaaD (XP_001392490), IsnB (CEK22194.1), and AmbI3 (AIJ28554.1) are from *Aspergillus niger*, *Xenorhabdus nematophila*, and *Fischerella ambigua*, respectively.¹⁶⁻¹⁸ TraH also contains the typical conserved 2-His-1-Asp ion-binding triad of non-heme Fe^{II}/2-oxoglutarate-dependent enzyme (His₁₉₈, His₂₁₁ and Asp₁₁₂) (marked with *). Protein sequence alignments were carried out by using the sequence alignment function of ClustalW and visualized with ESPript 3.0 (<http://esprict.ibcp.fr/ESPript/ESPript/>).

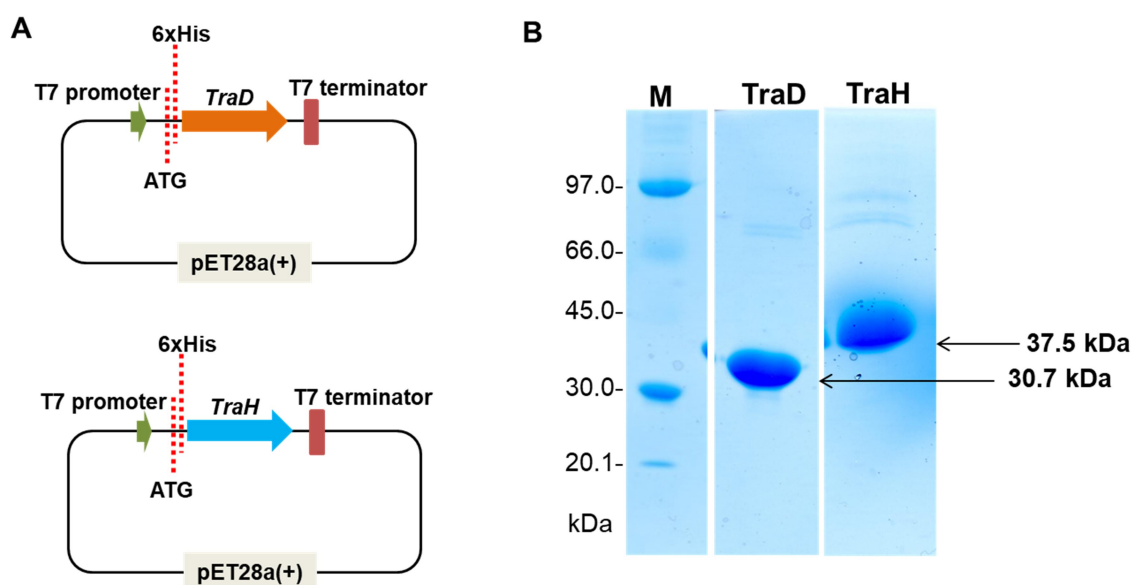


Figure S12. Analysis of recombinant TraD and TraH on SDS-PAGE

TraD and *traH* were separately inserted into pET28a(+) with 6xHis-tag at its N-terminal (A). The purified recombinant histidine-tagged TraD and TraH were separated on a 12% SDS-PAGE (B).

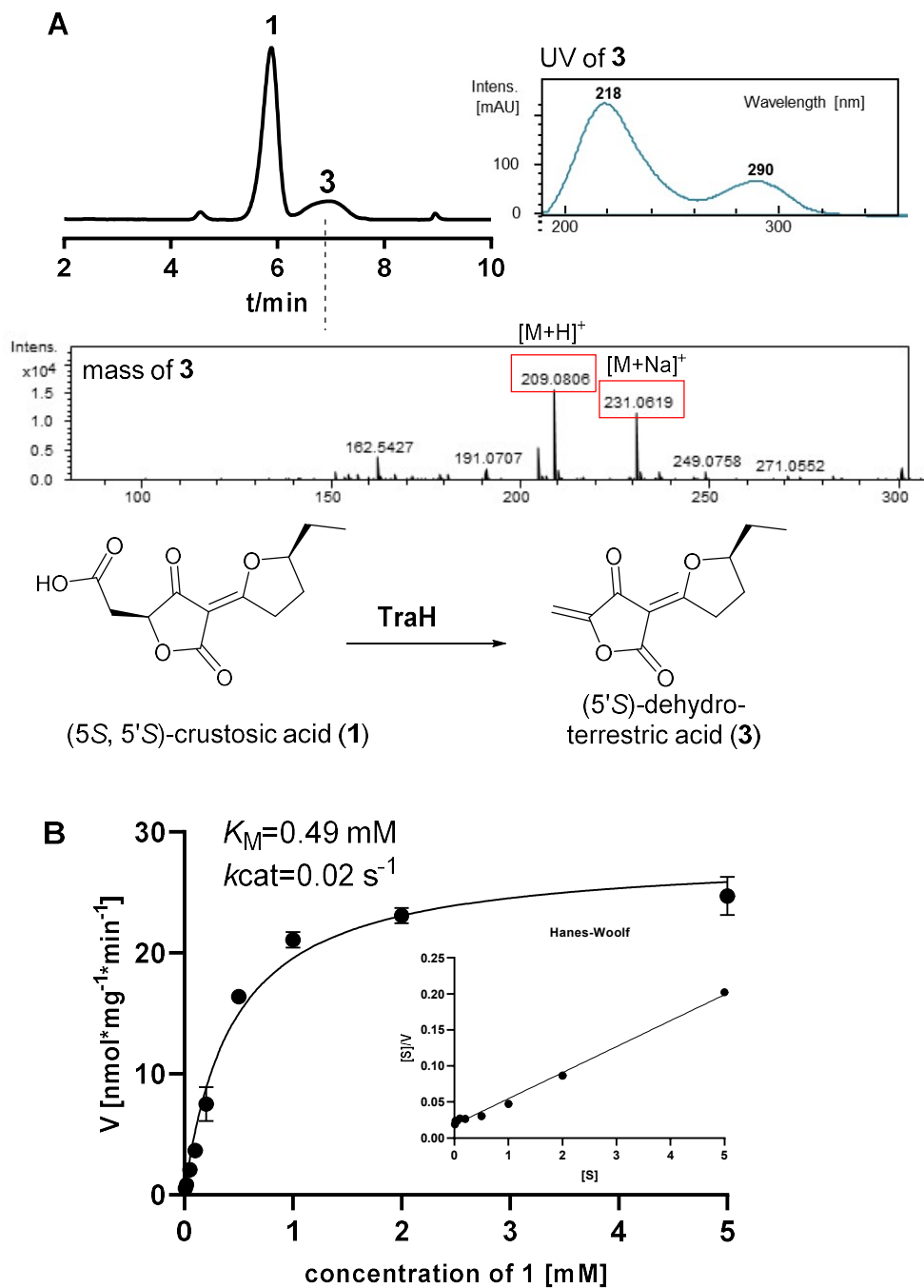


Figure S13. Oxidative decarboxylation of **1** catalyzed by TraH
LC-MS analysis of incubation mixture of **1** with TraH (A), determination of kinetic parameter of the TraH toward **1** (B).

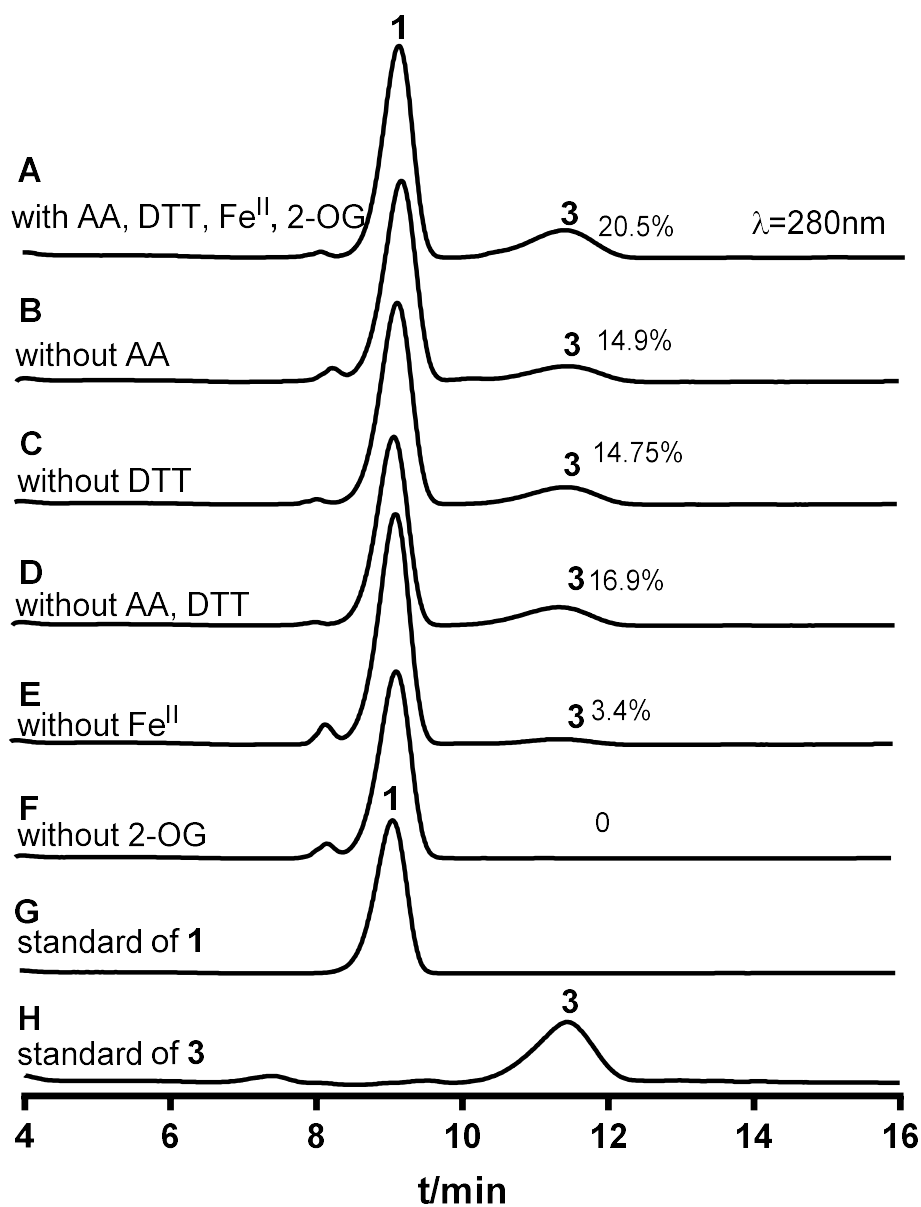


Figure S14. HPLC analysis of the incubation mixtures of **1** with TraH 5.4 μM TraH in the full assay with ascorbic acid (AA), dithiothreitol (DTT), $\text{Fe}[(\text{NH}_4)_2(\text{SO}_4)_2]$ (Fe^{II}) and 2-oxoglutarate (2OG) (A); full assay without AA (B); full assay without DTT (C); full assay without AA and DTT (D); full assay without exogenous Fe^{II} (E); full assay without 2OG (F), standards of **1** (G) and **3** (H). UV absorptions at 280 nm are illustrated.

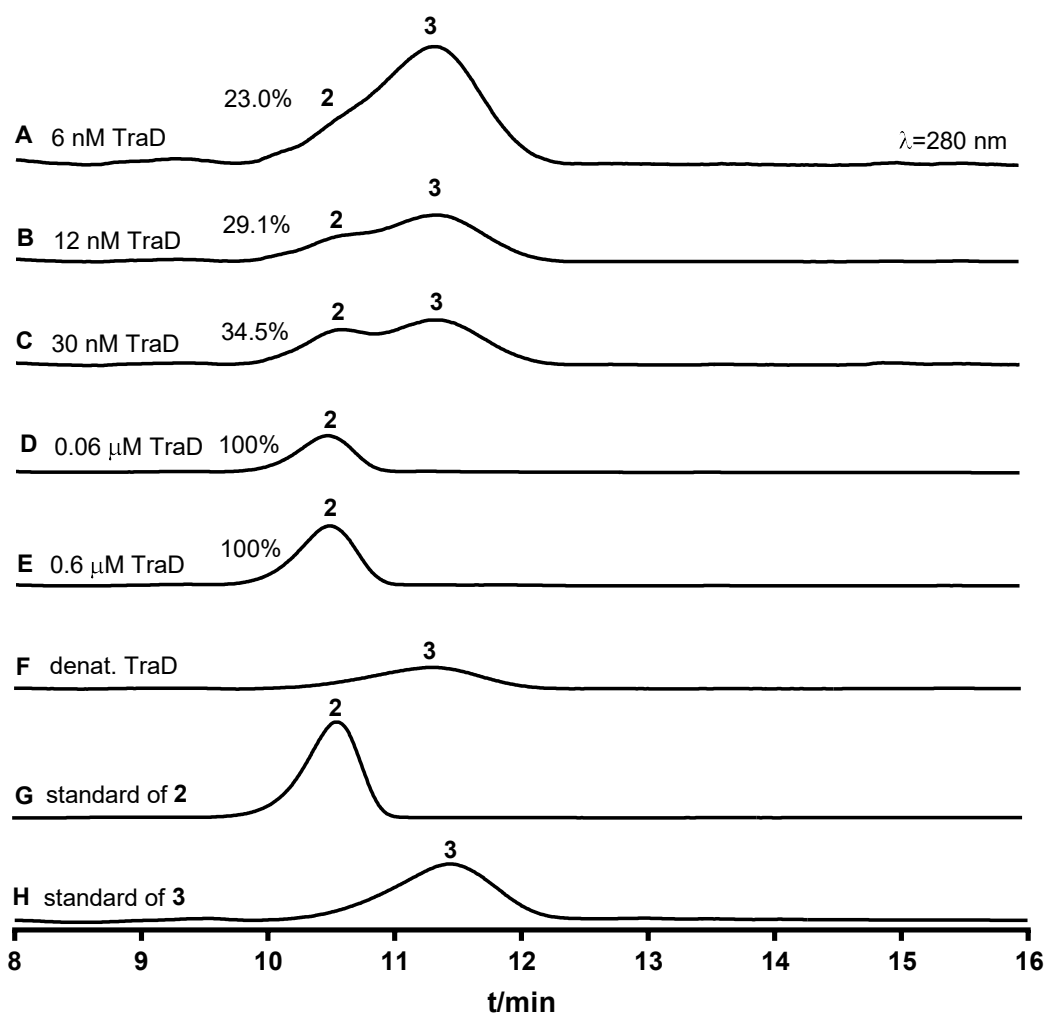


Figure S15. HPLC analysis of incubation mixtures of **3** with TraD at different concentrations

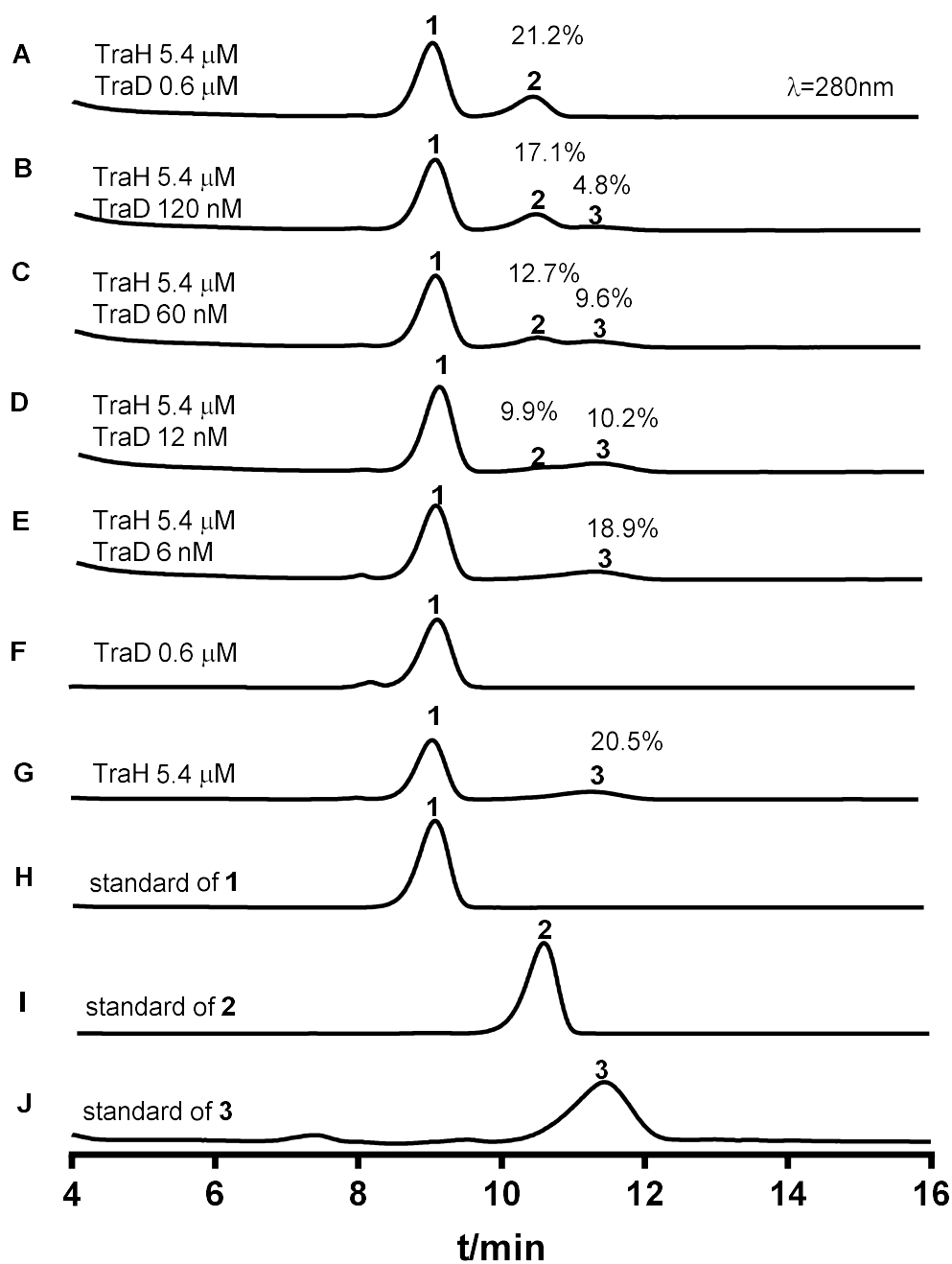


Figure S16. HPLC analysis of sequential reaction products in enzyme assays of TraH and TraD with 1

SUPPORTING INFORMATION

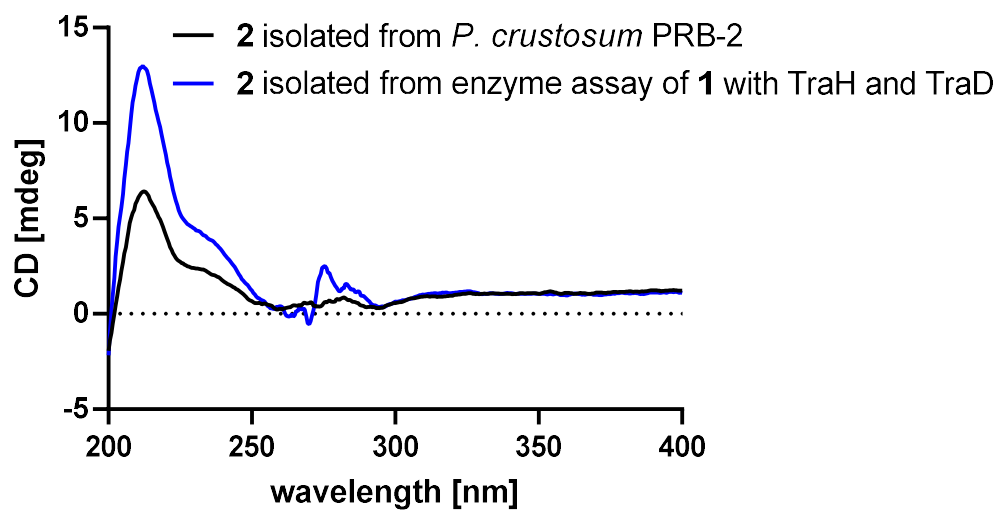
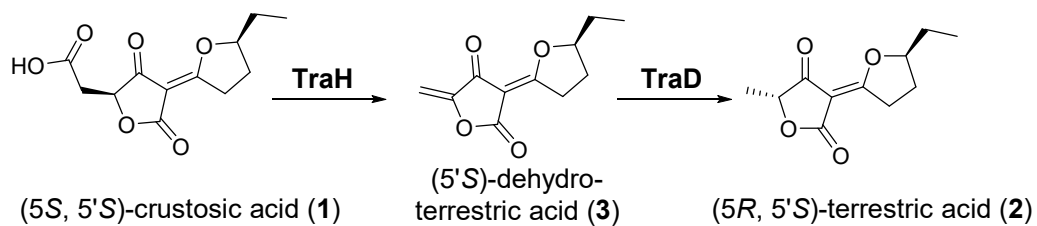


Figure S17. Comparison of CD spectra of two terrestric acid samples

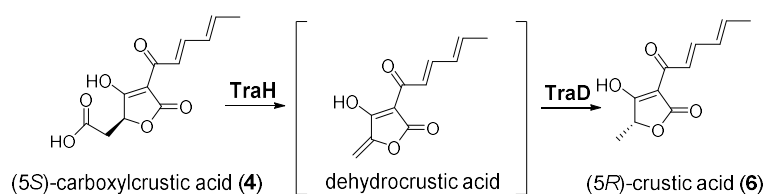
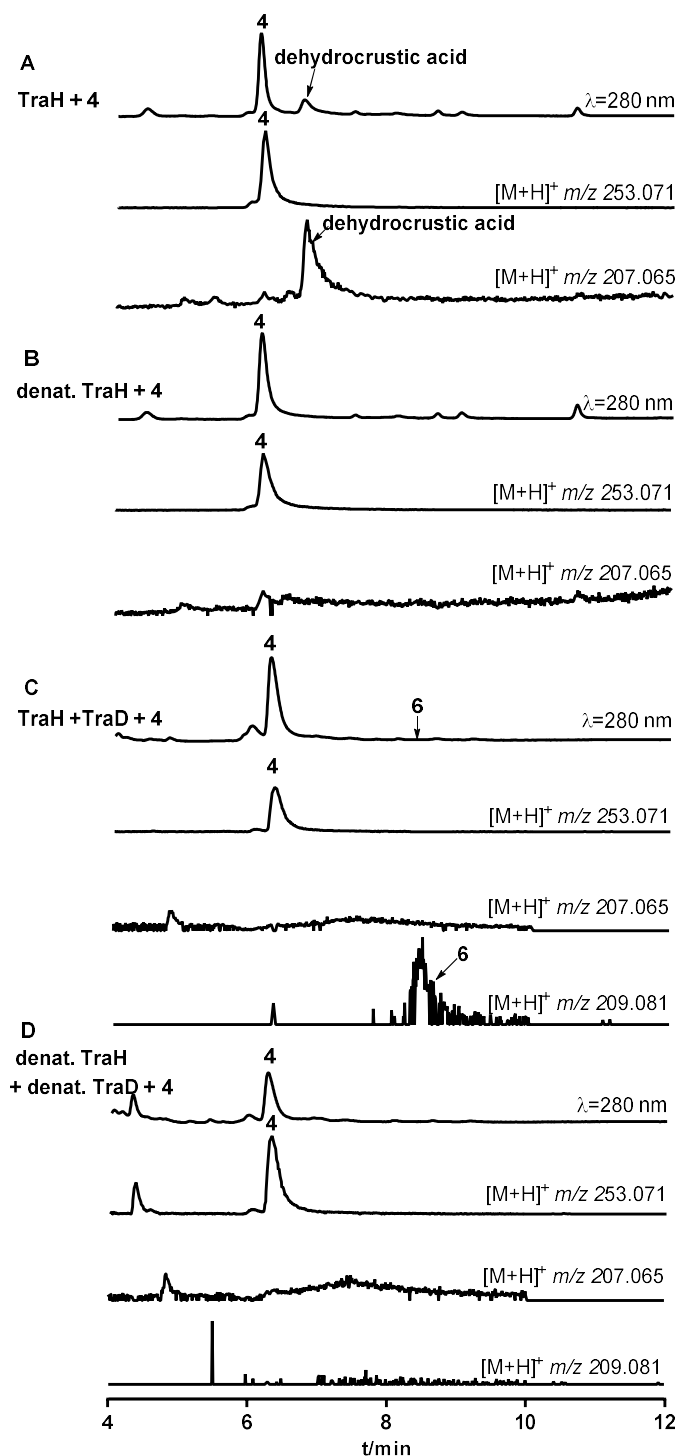


Figure S18. LC-MS analysis of enzyme assays of **4** with TraH without or together with TraD. Incubation mixtures of **4** with TraH (A), **4** with denat TraH (B) at 37°C for 16 h, **4** with TraH and TraD (C), and **4** with denat TraH and TraD (D) at 30°C for 16 h. EICs refer $[M+H]^+$ ions of **4**, **6** and dehydrocrustic acid with a tolerance range of ± 0.005 .

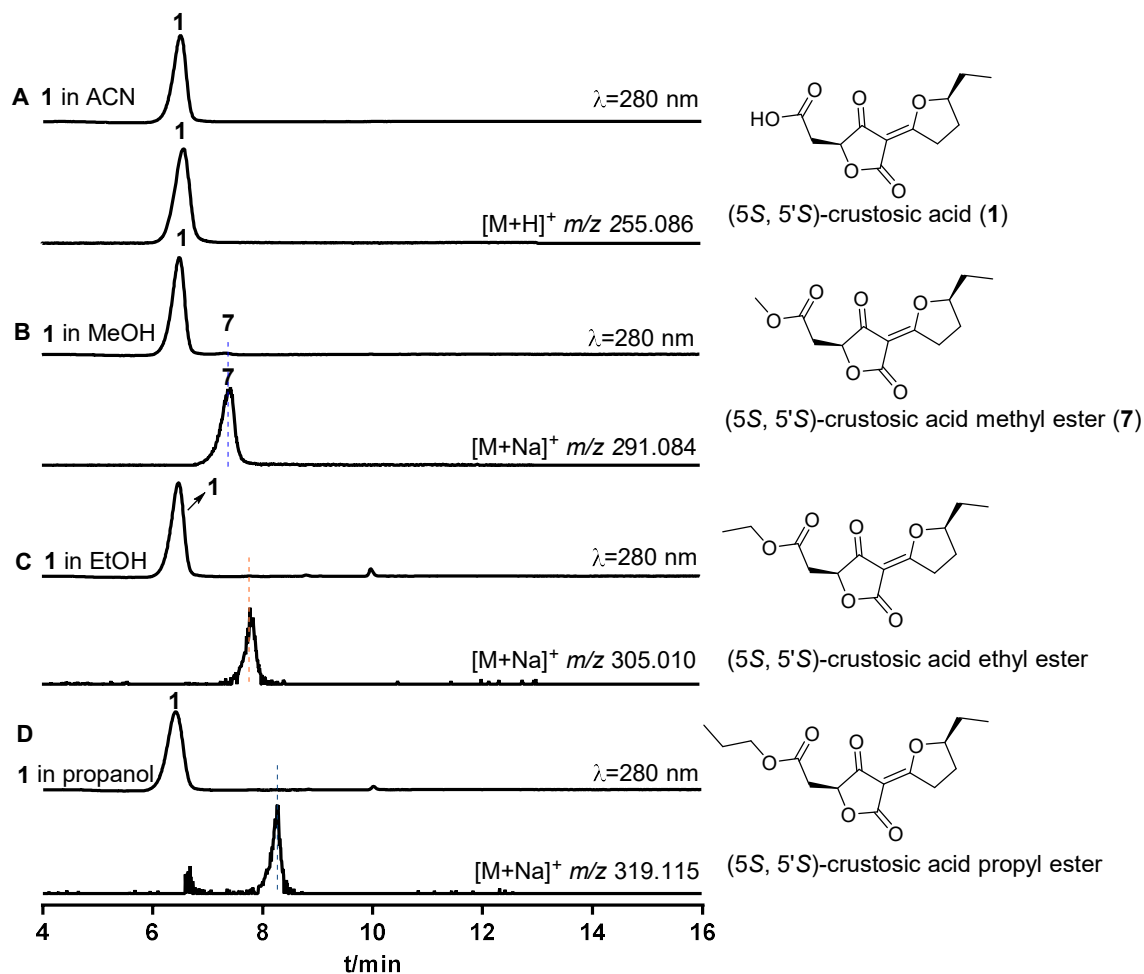


Figure S19. LC-MS analysis of spontaneous ester formation of **1** with different alcohols. 0.4 mM solutions of crustosic acid (**1**) in ACN, MeOH, EtOH or *n*-propanol were kept at 25°C for 24 h and subjected directly to LC-MS analysis. UV absorptions at 280 nm are illustrated. EIC at m/z 255.086 \pm 0.005 refer [M+H]⁺ ion of (5*S*, 5'*S*)-crustosic acid (**1**), EICs at m/z 291.084 \pm 0.005, 305.010 \pm 0.005, 319.115 \pm 0.005 refer [M+Na]⁺ ion of its methyl ester (**7**), ethyl ester, propyl ester, respectively.

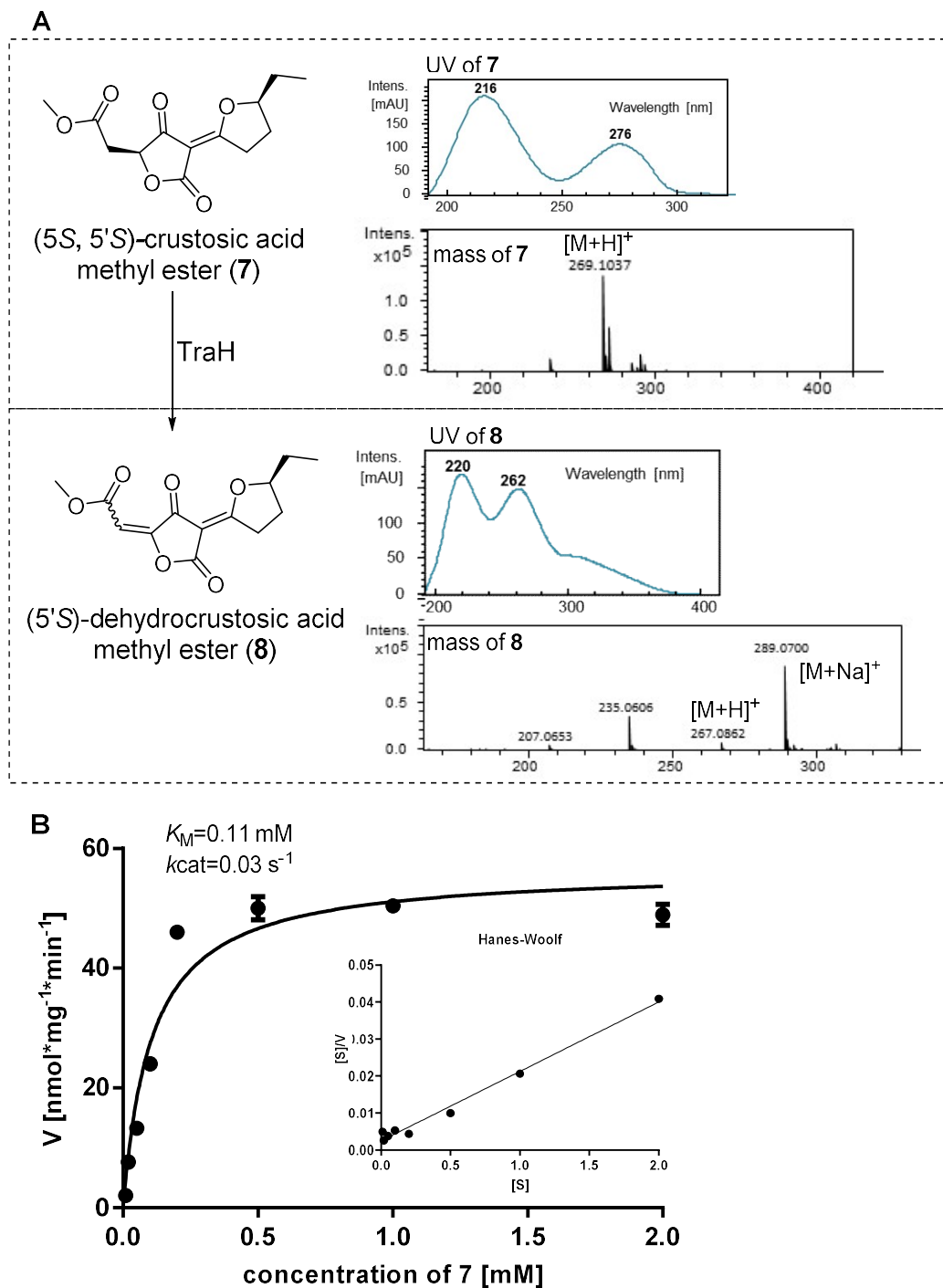


Figure S20. Conversion of **7** to **8** catalyzed by TraH
LC-MS analysis of incubation mixture of **7** with TraH (A), determination of kinetic parameter of the TraH toward **7** (B).

SUPPORTING INFORMATION

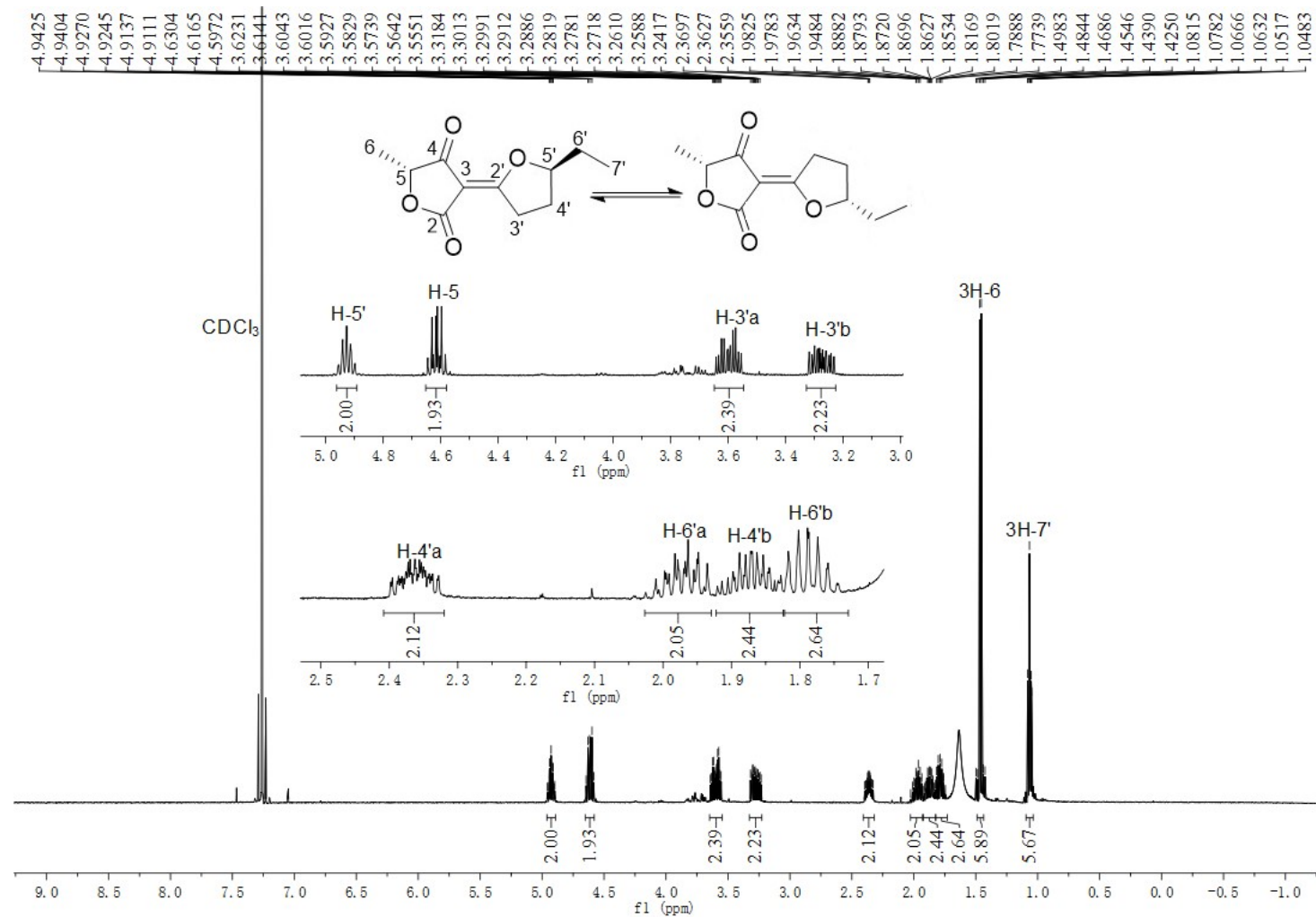


Figure S21. ¹H NMR spectrum of compound **2** isolated from an incubation mixture of **1** with TraH and TraD in CDCl₃ (500MHz)

SUPPORTING INFORMATION

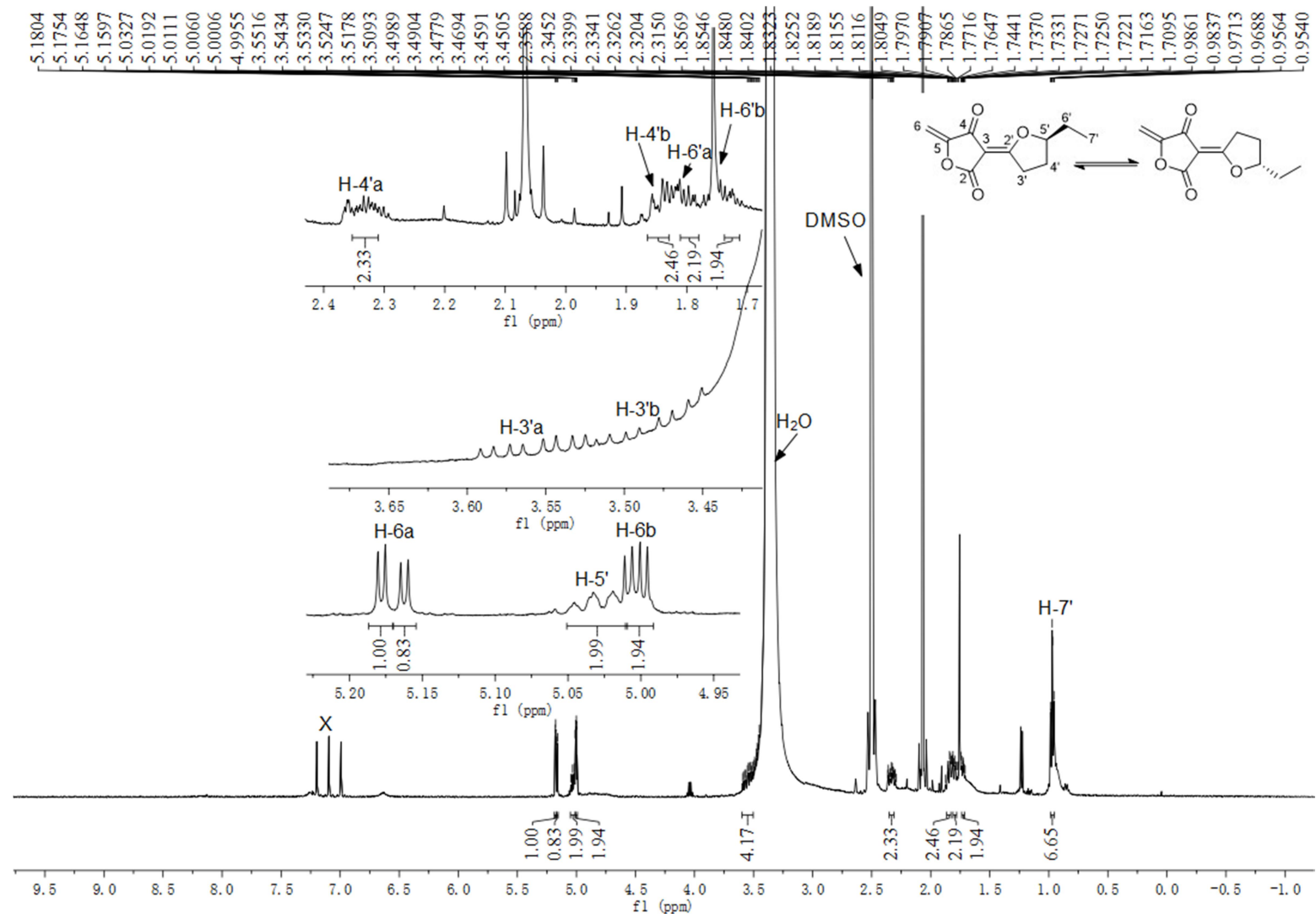


Figure S22. ^1H NMR spectrum of compound 3 in $\text{DMSO-}d_6$ (500MHz)

SUPPORTING INFORMATION

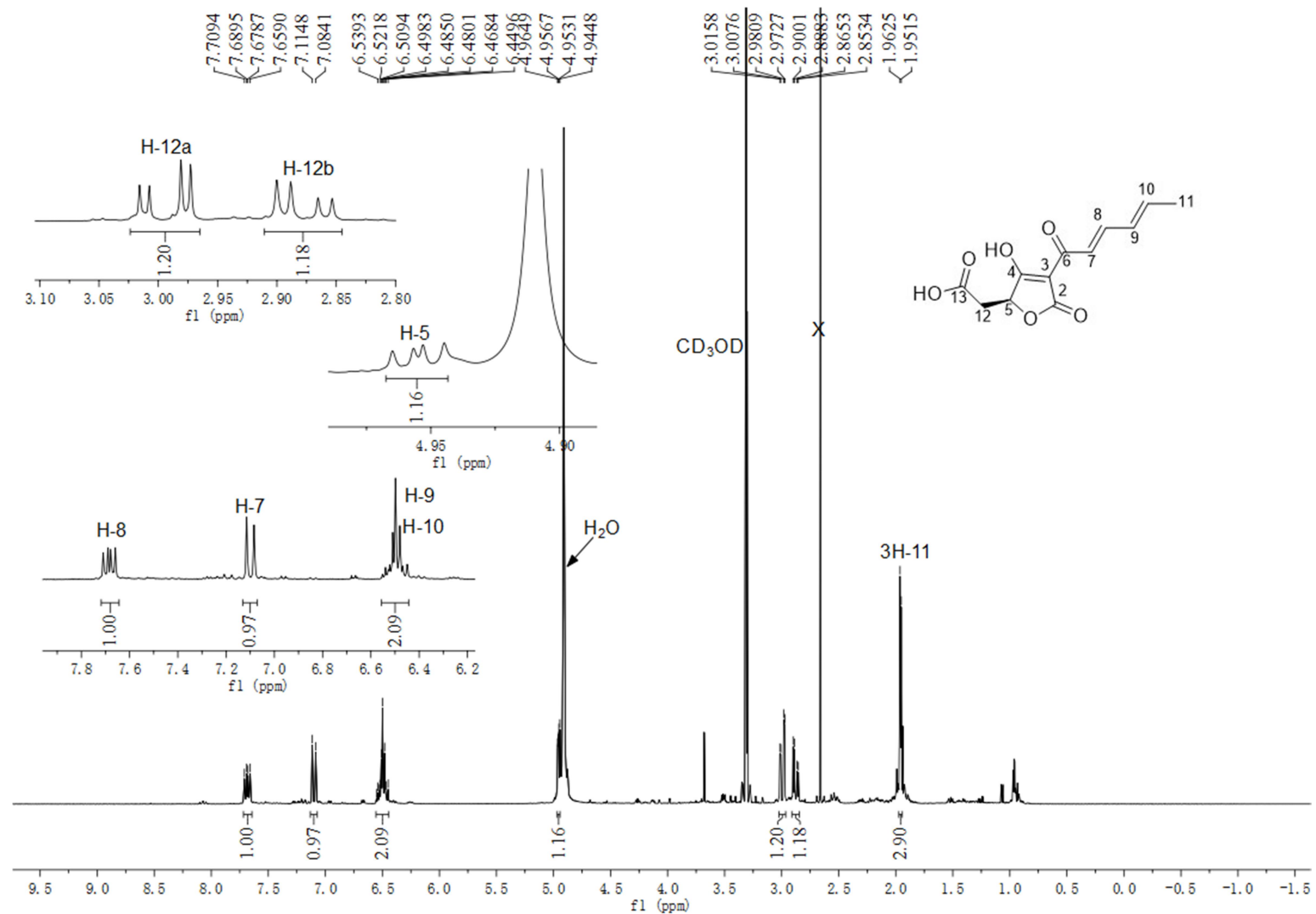


Figure S23. ^1H NMR spectrum of compound **4** isolated from *A. nidulans* JF15 harboring *traA* in CD_3OD (500MHz)

SUPPORTING INFORMATION

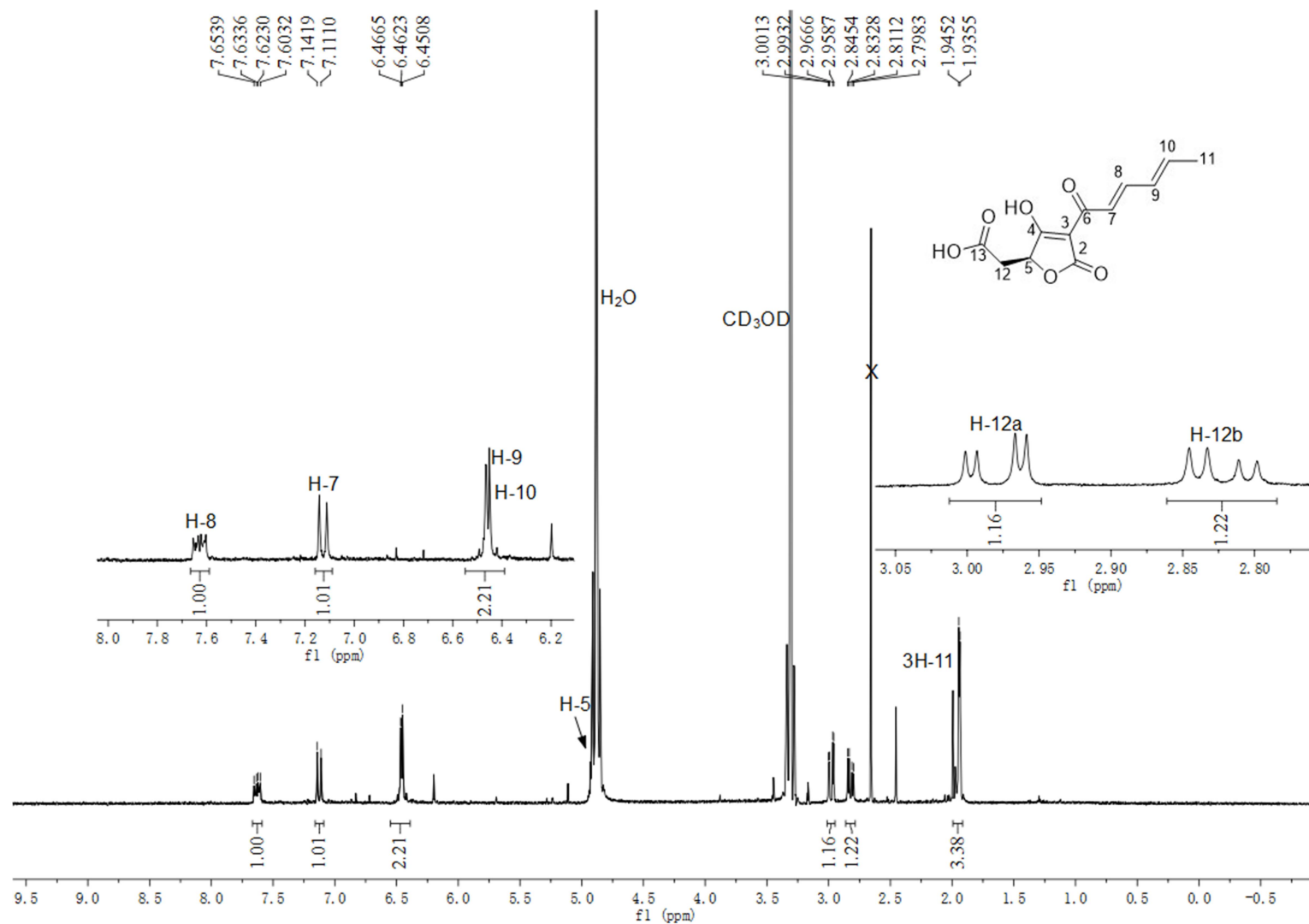


Figure S24. ¹H NMR spectrum of compound 4 isolated from *ΔtraG*-mutant in CD₃OD (500MHz)

SUPPORTING INFORMATION

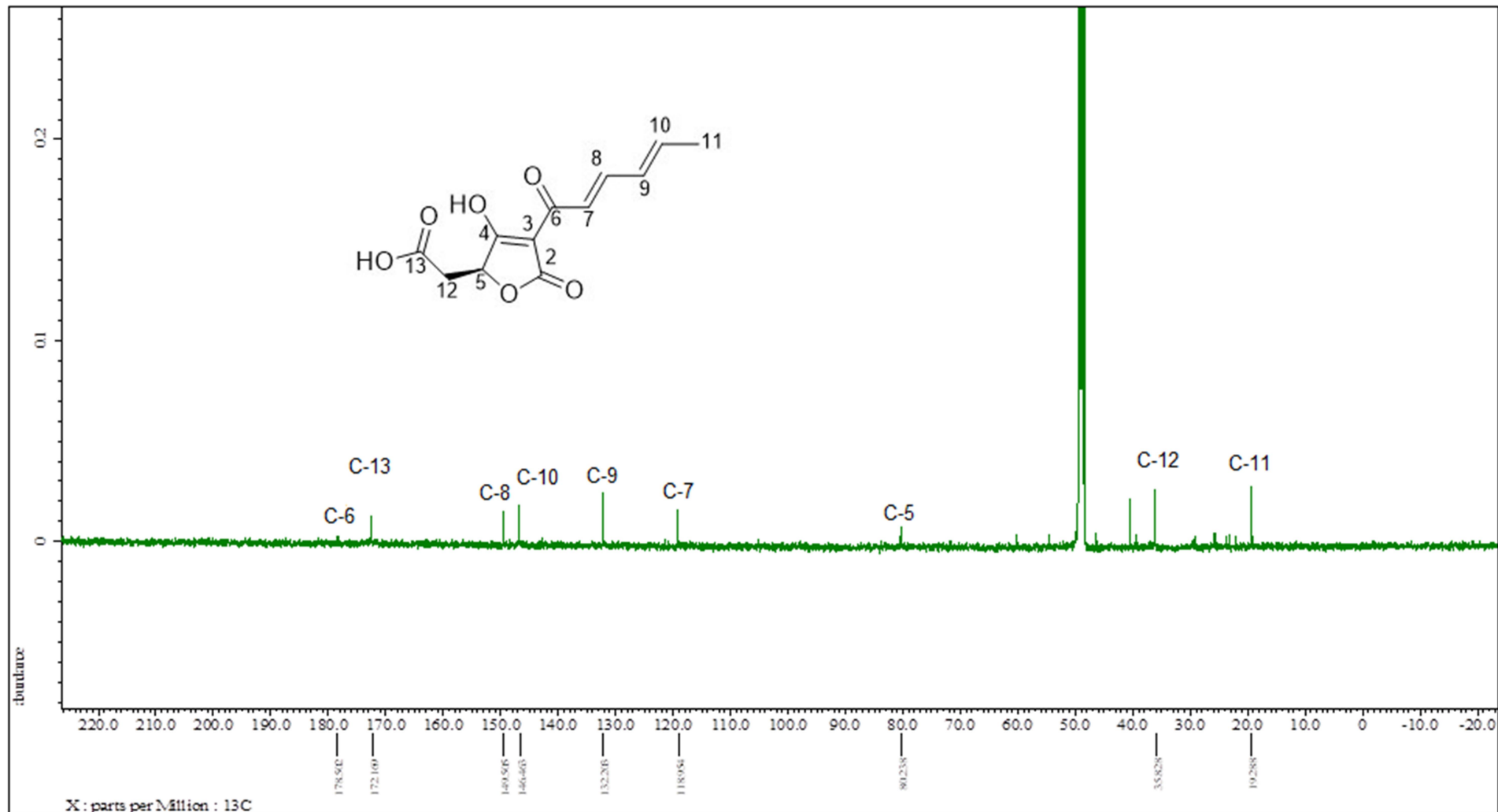


Figure S25. ^{13}C NMR spectrum of compound **4** isolated from *A. nidulans* JF15 harboring *traA* in CD_3OD (125MHz)

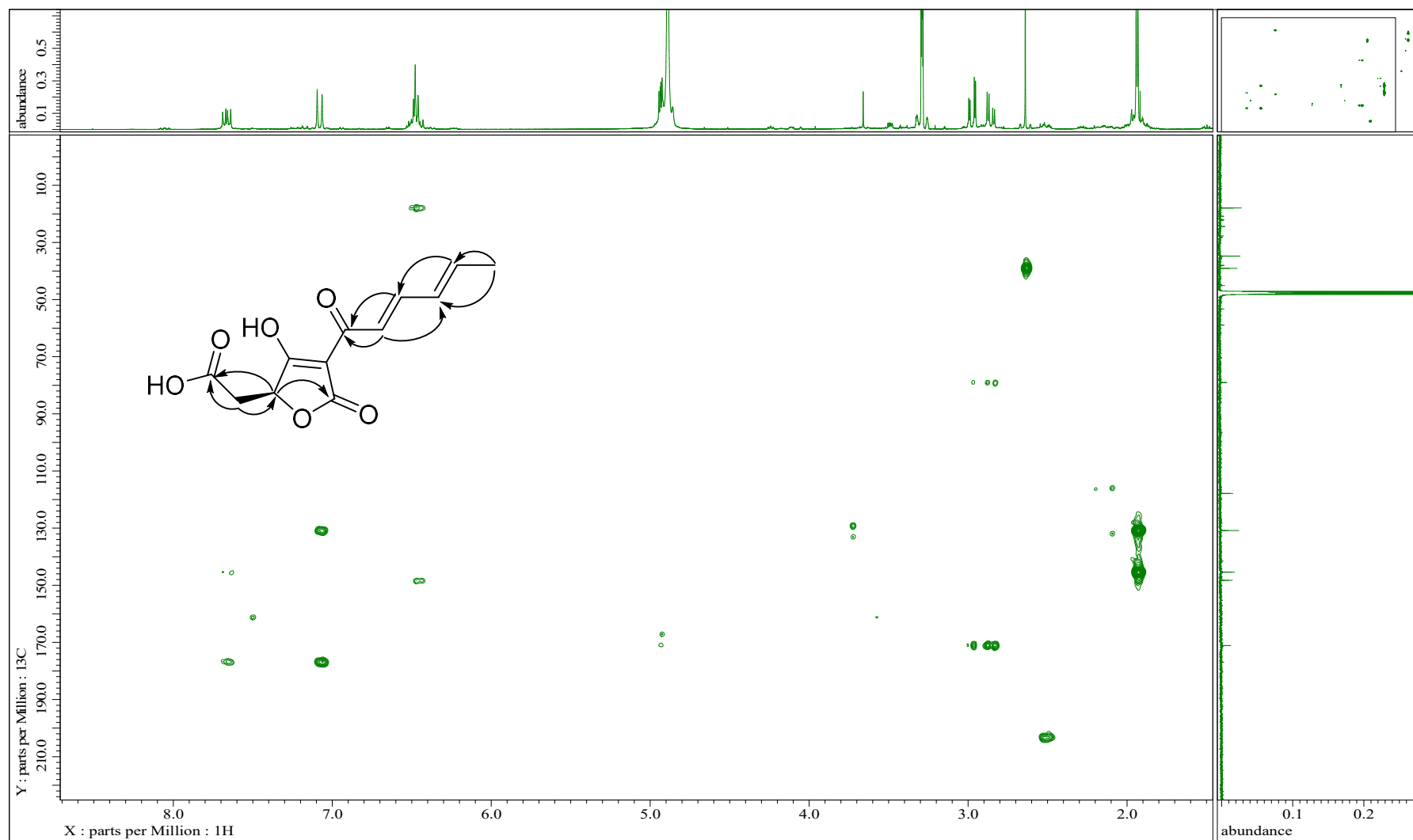


Figure S26. HMBC spectrum of compound **4** isolated from *A. nidulans* JF15 harboring *traA* in CD₃OD

SUPPORTING INFORMATION

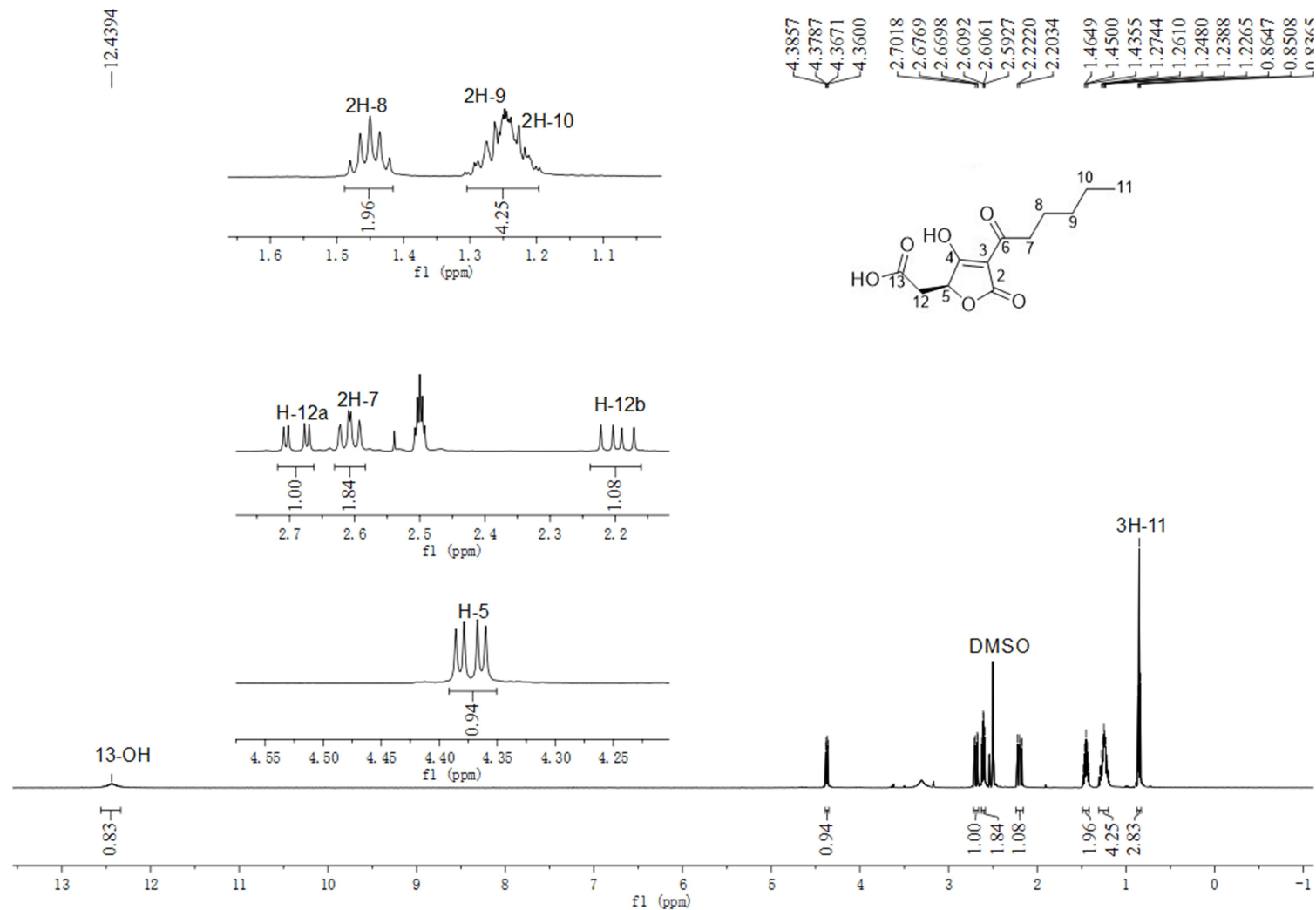


Figure S27. ¹H NMR spectrum of compound **5** isolated from *P. crustosum* PRB-2 in DMSO-*d*₆ (500MHz)

SUPPORTING INFORMATION

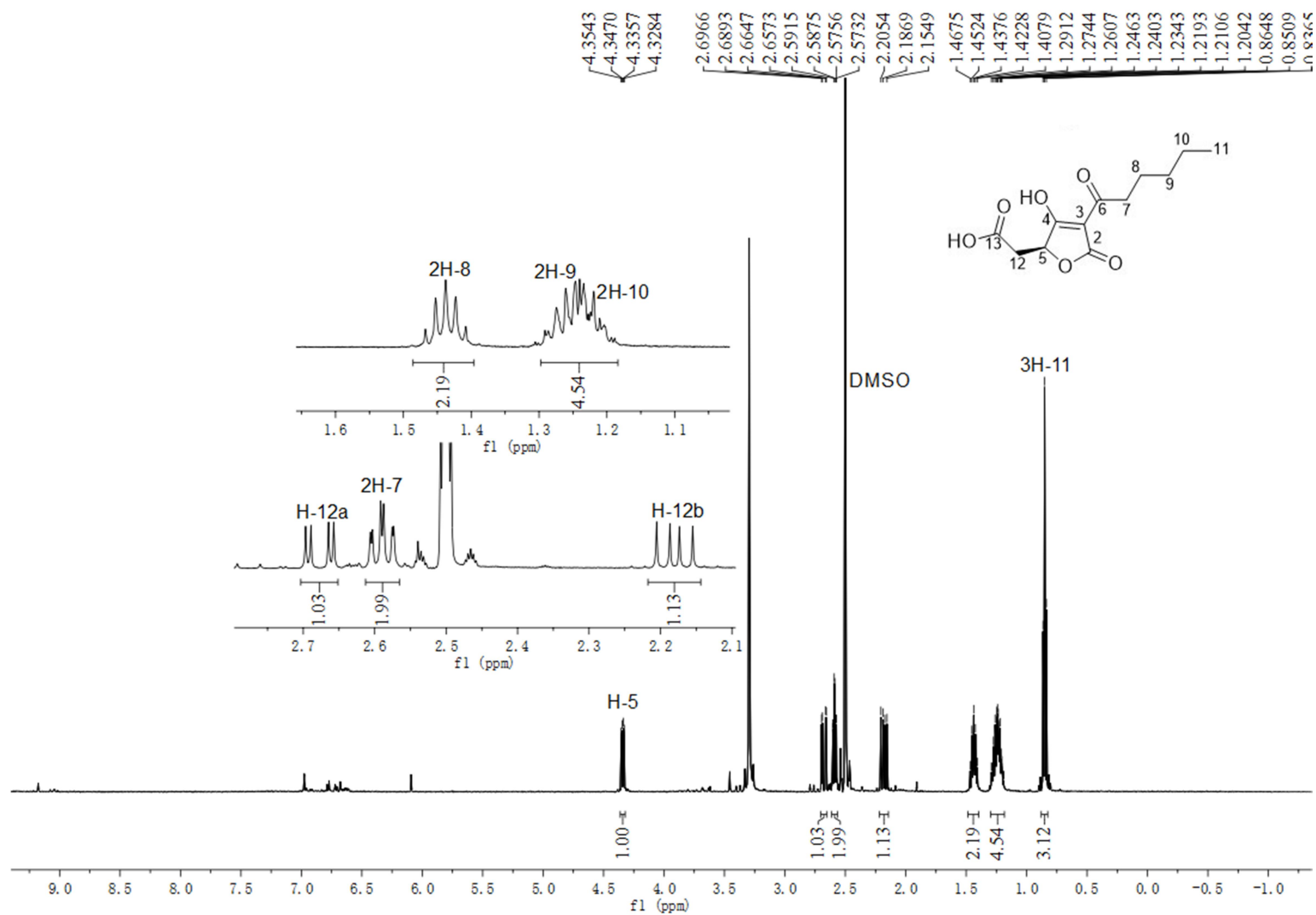


Figure S28. ^1H NMR spectrum of compound **5** isolated from *A. nidulans* JF45 harboring *traAG* in $\text{DMSO-}d_6$ (500MHz)

SUPPORTING INFORMATION

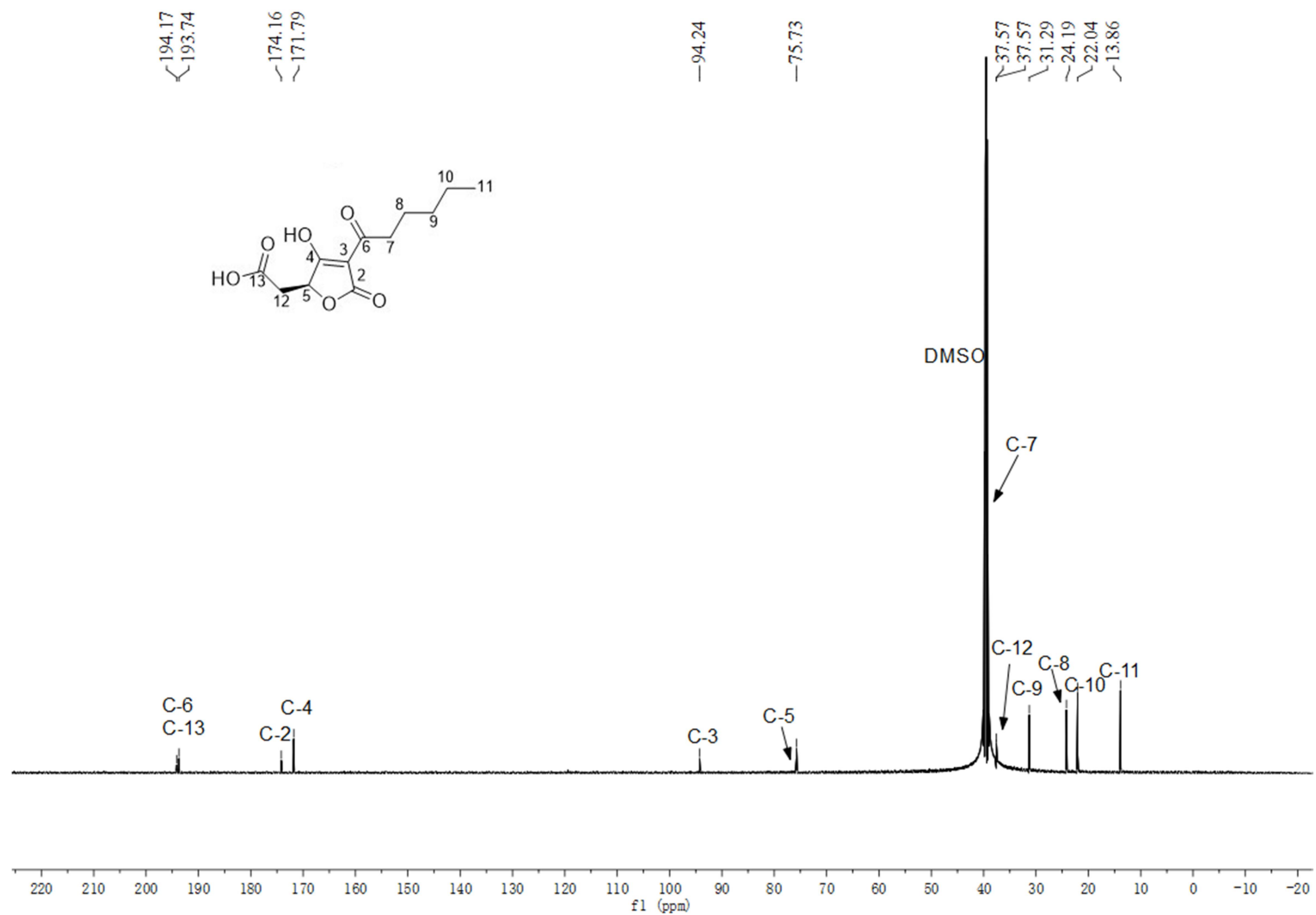


Figure S29. ¹³C NMR spectrum of compound **5** isolated from *A. nidulans* JF45 harboring *traAG* in DMSO-*d*₆ (125MHz)

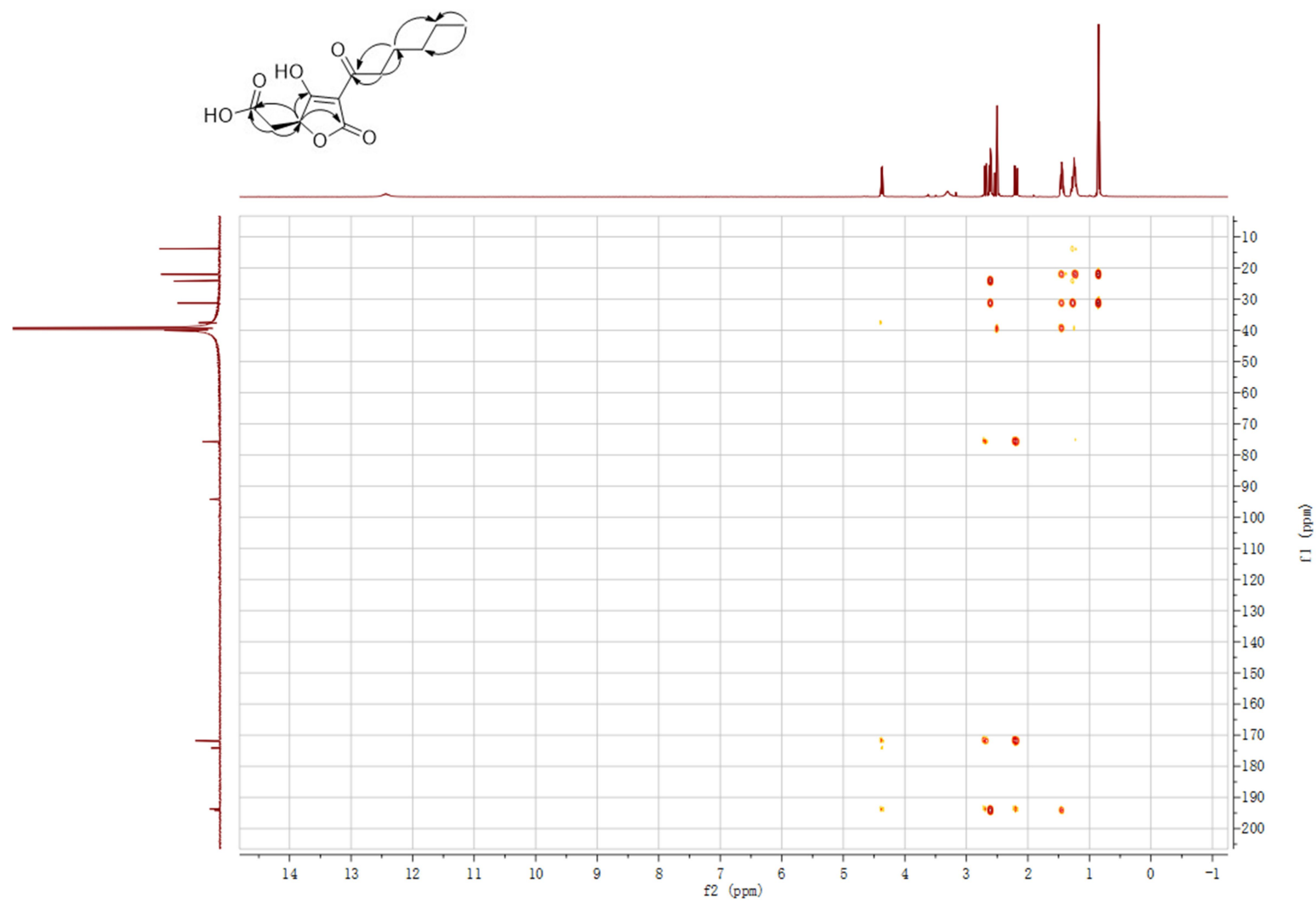


Figure S30. HMBC spectrum of compound **5** isolated from *A. nidulans* JF45 harboring *traAG* in DMSO-*d*₆

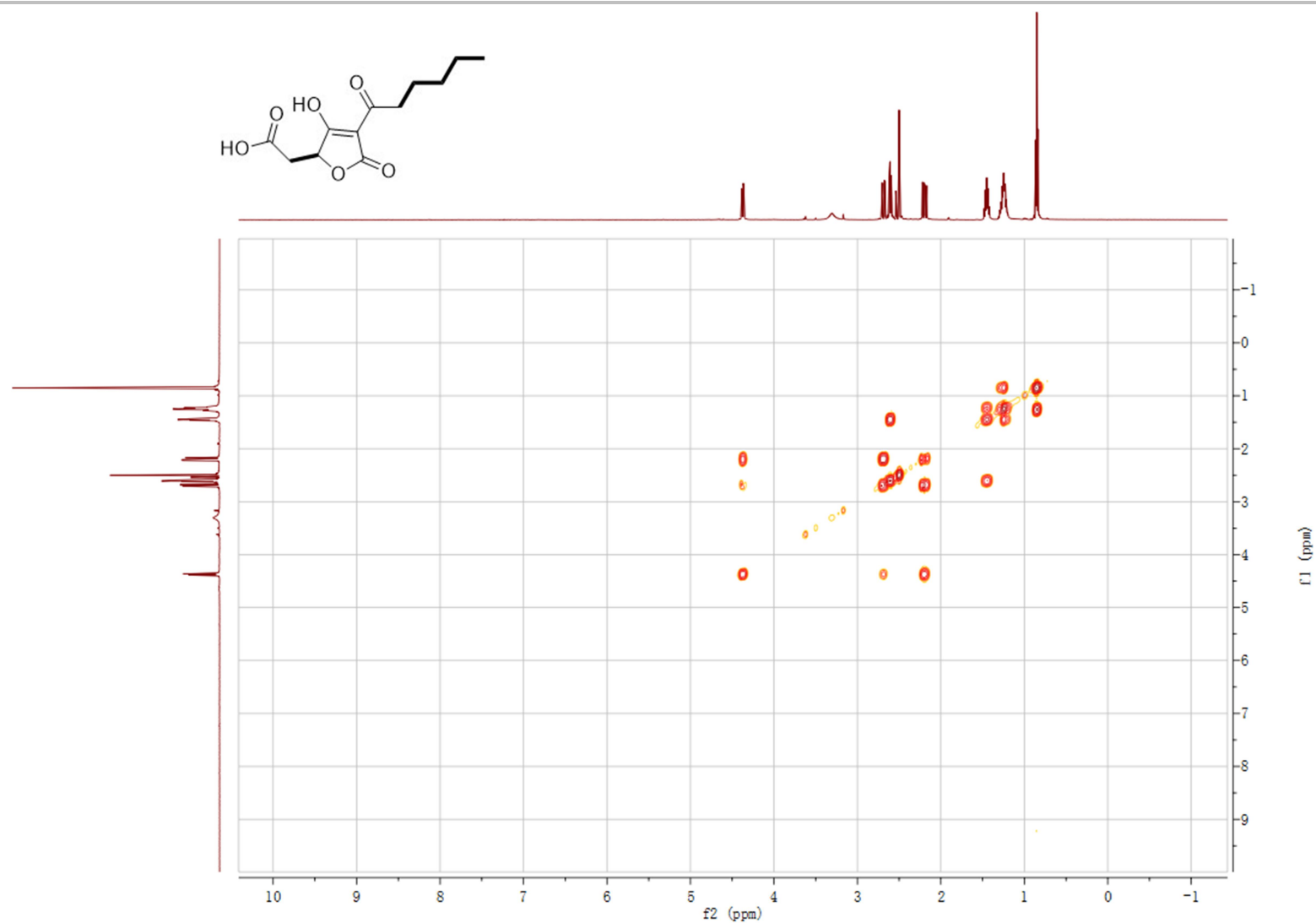


Figure S31. ^1H - ^1H COSY spectrum of compound **5** isolated from *A. nidulans* JF45 harboring *traAG* in $\text{DMSO-}d_6$

SUPPORTING INFORMATION

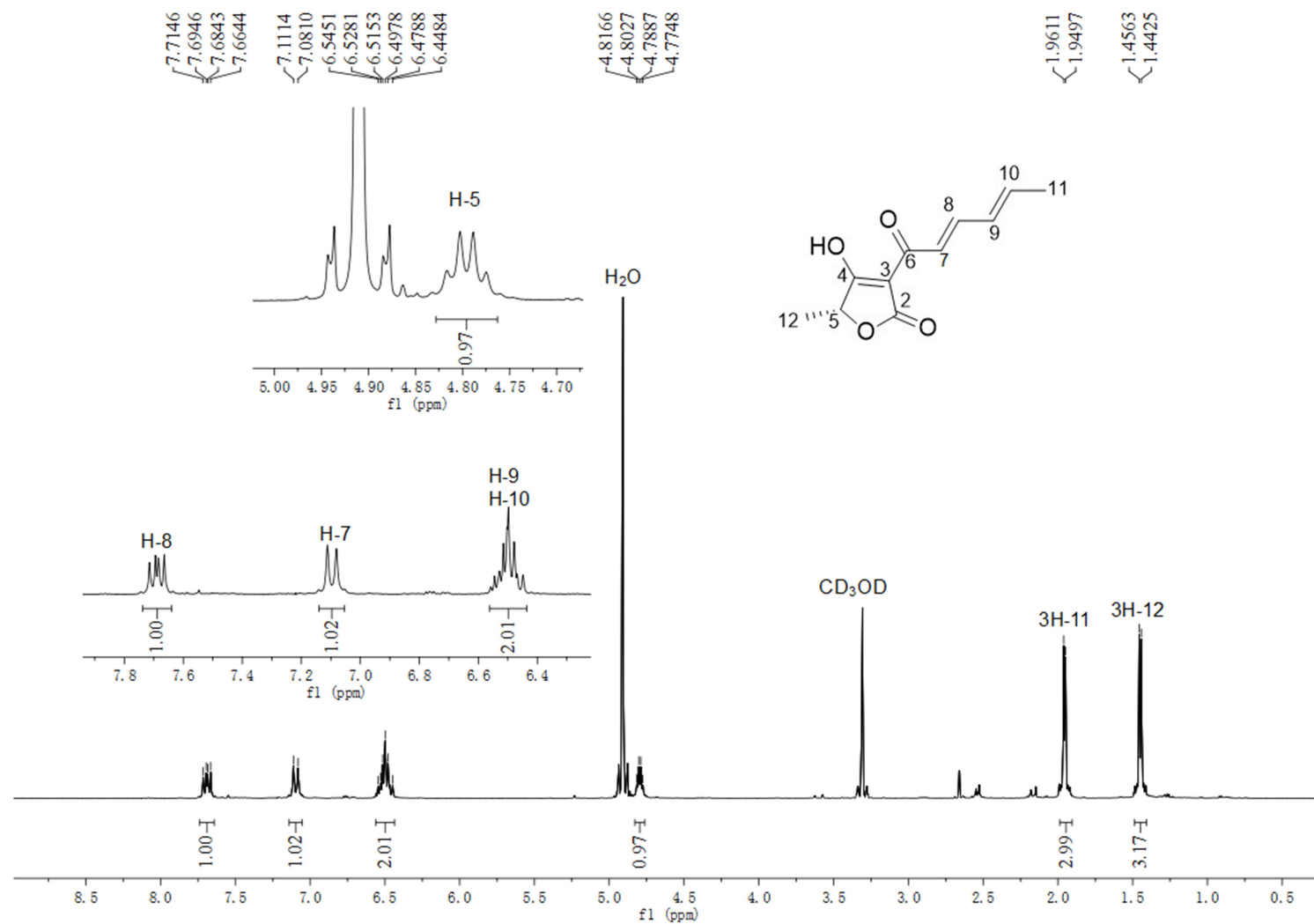


Figure S32. ¹H NMR spectrum of compound 6 in CD₃OD (500MHz)

SUPPORTING INFORMATION

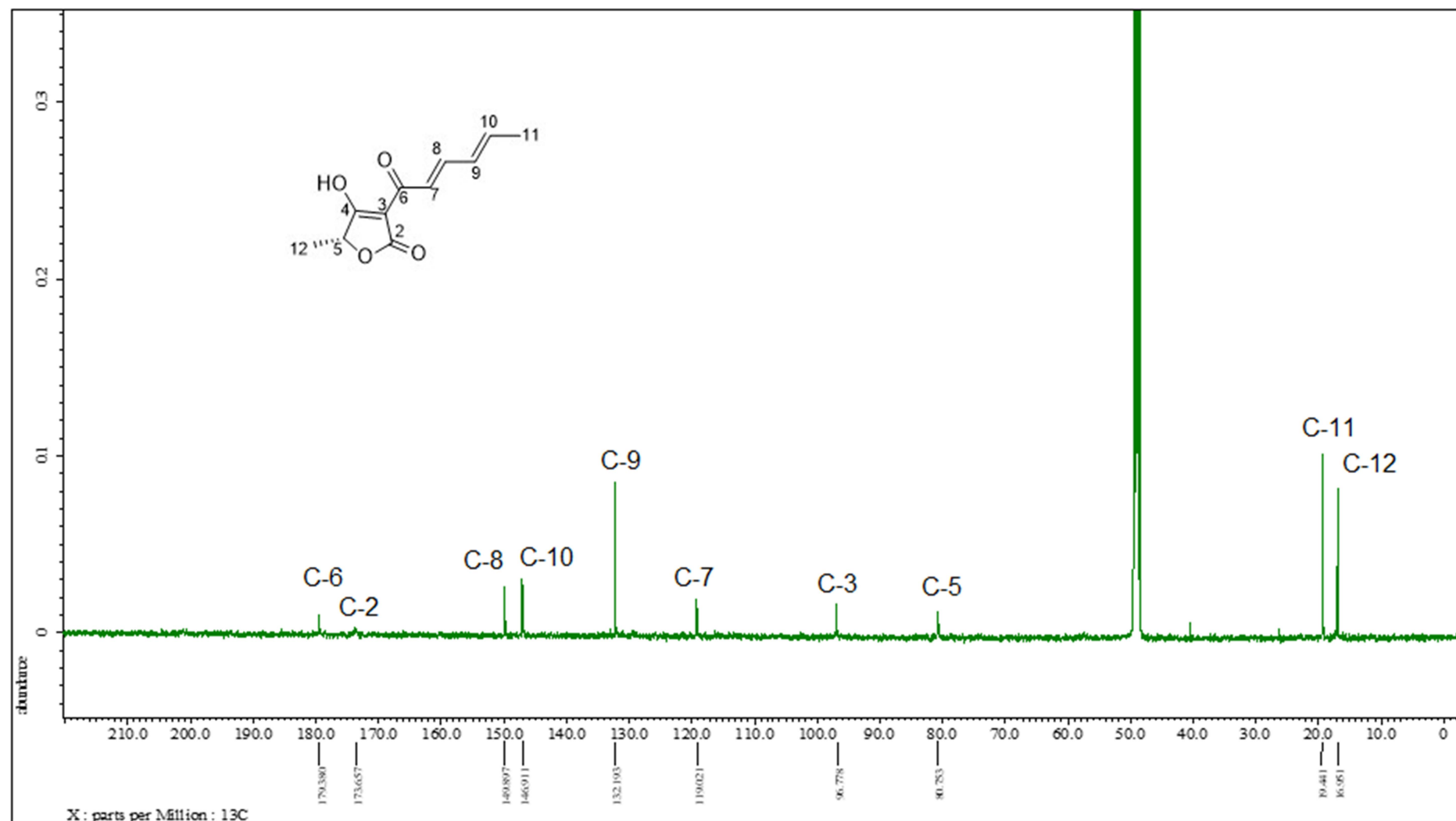


Figure S33. ^{13}C NMR spectrum of compound 6 in CD_3OD (125MHz)

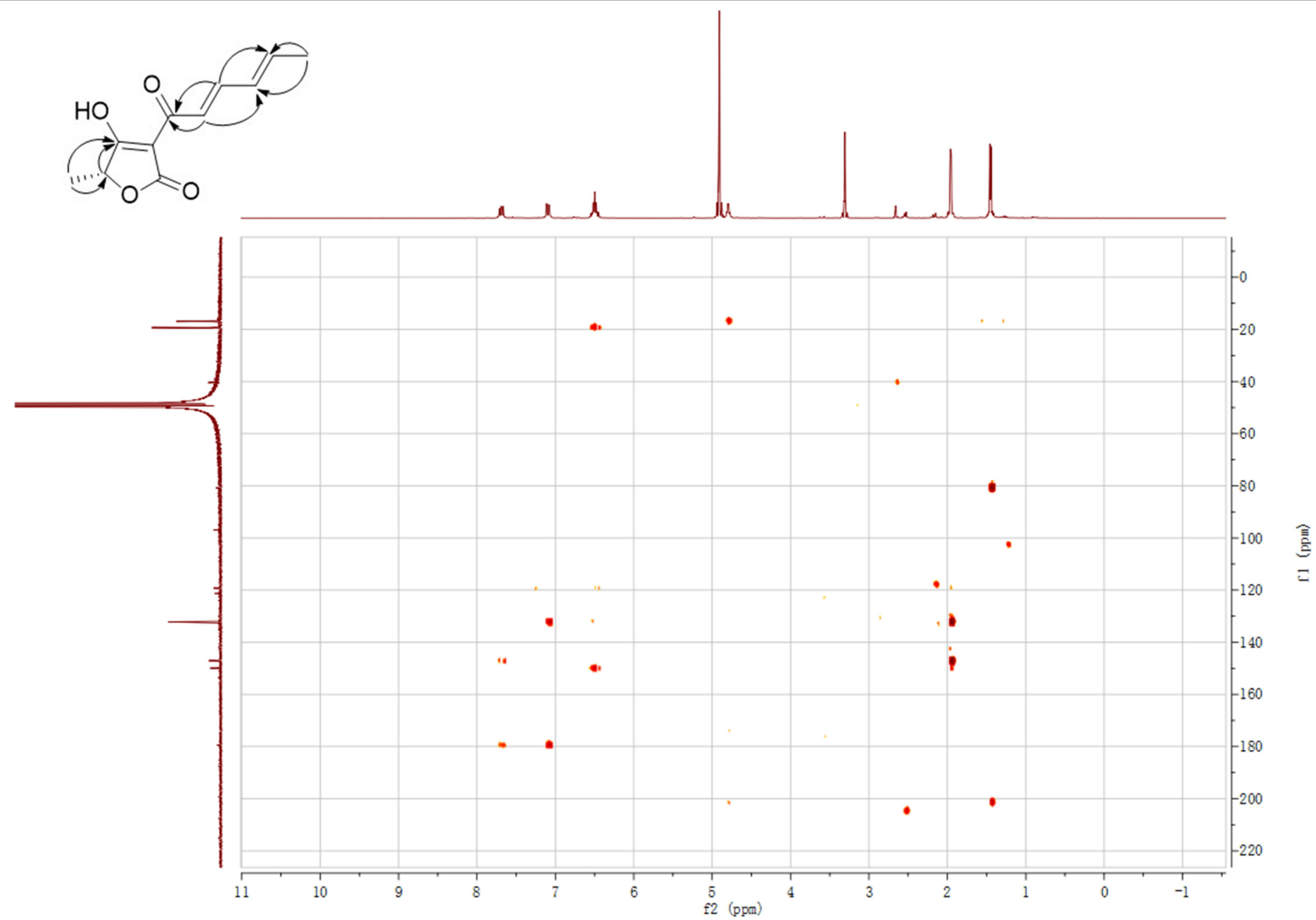


Figure S34. HMBC spectrum of compound 6 in CD₃OD

SUPPORTING INFORMATION

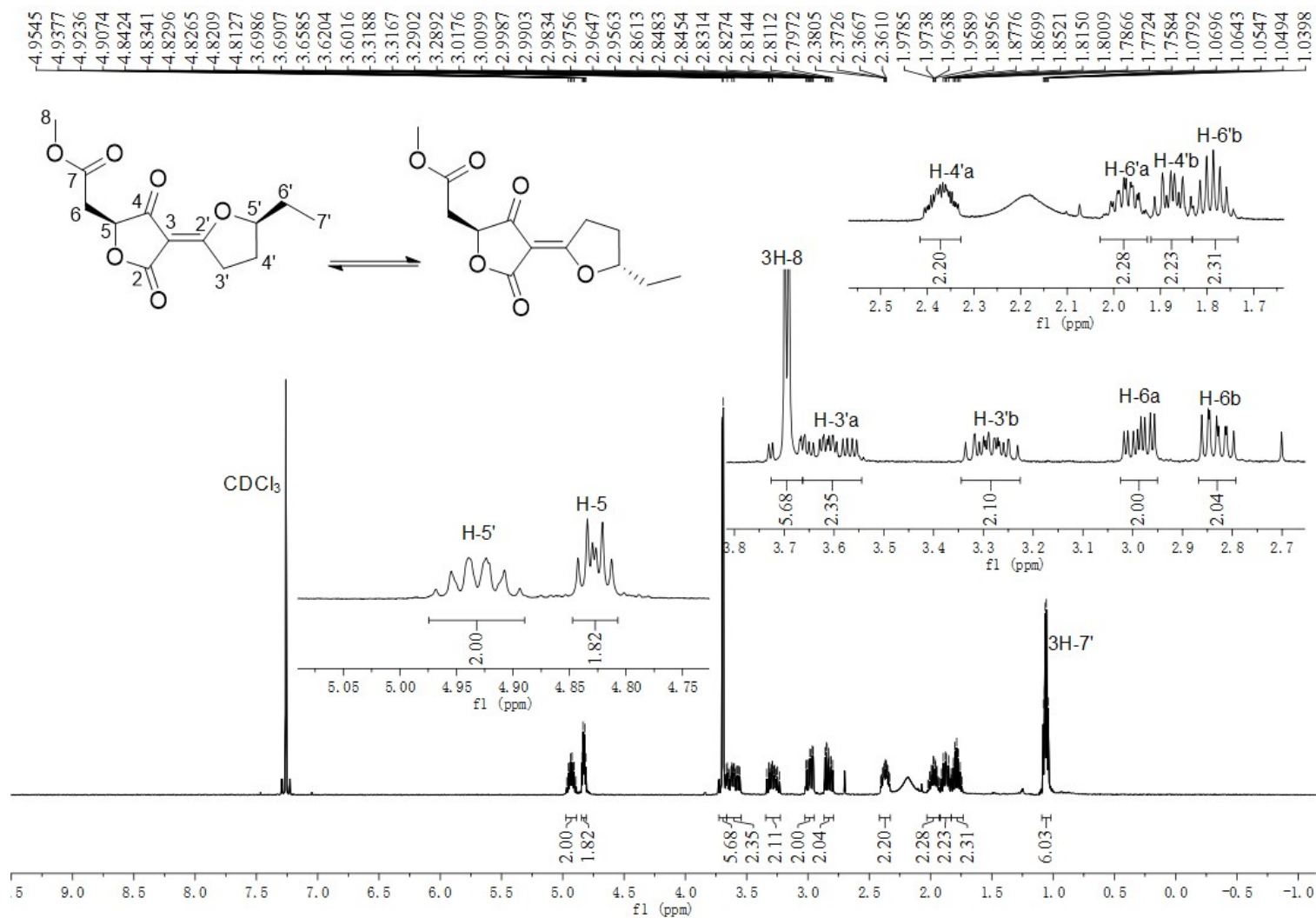


Figure S35. ¹H NMR spectrum of compound 7 in CDCl₃ (500MHz)

SUPPORTING INFORMATION

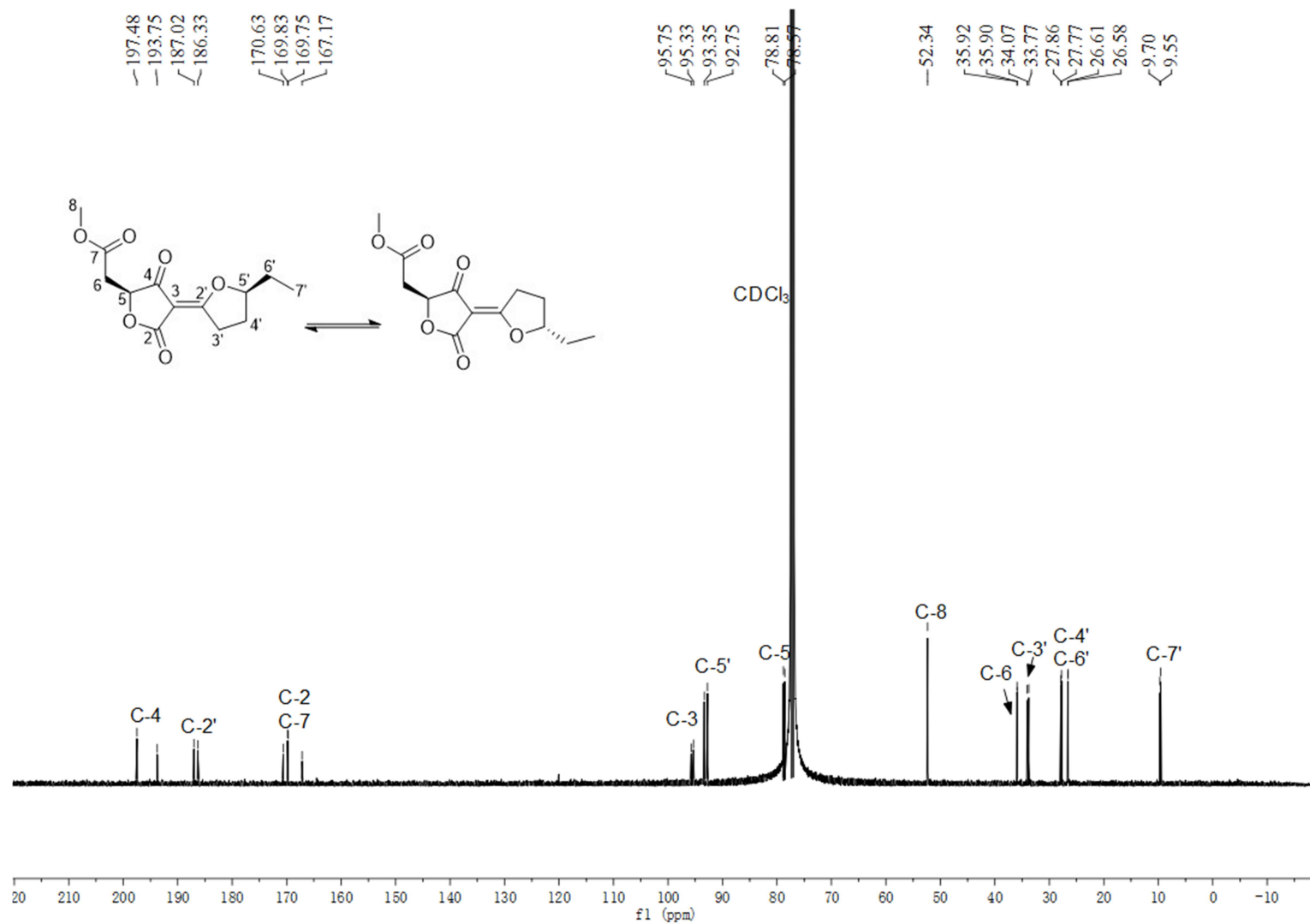


Figure S36. ¹³C NMR spectrum of compound 7 in CDCl₃ (125MHz)

SUPPORTING INFORMATION

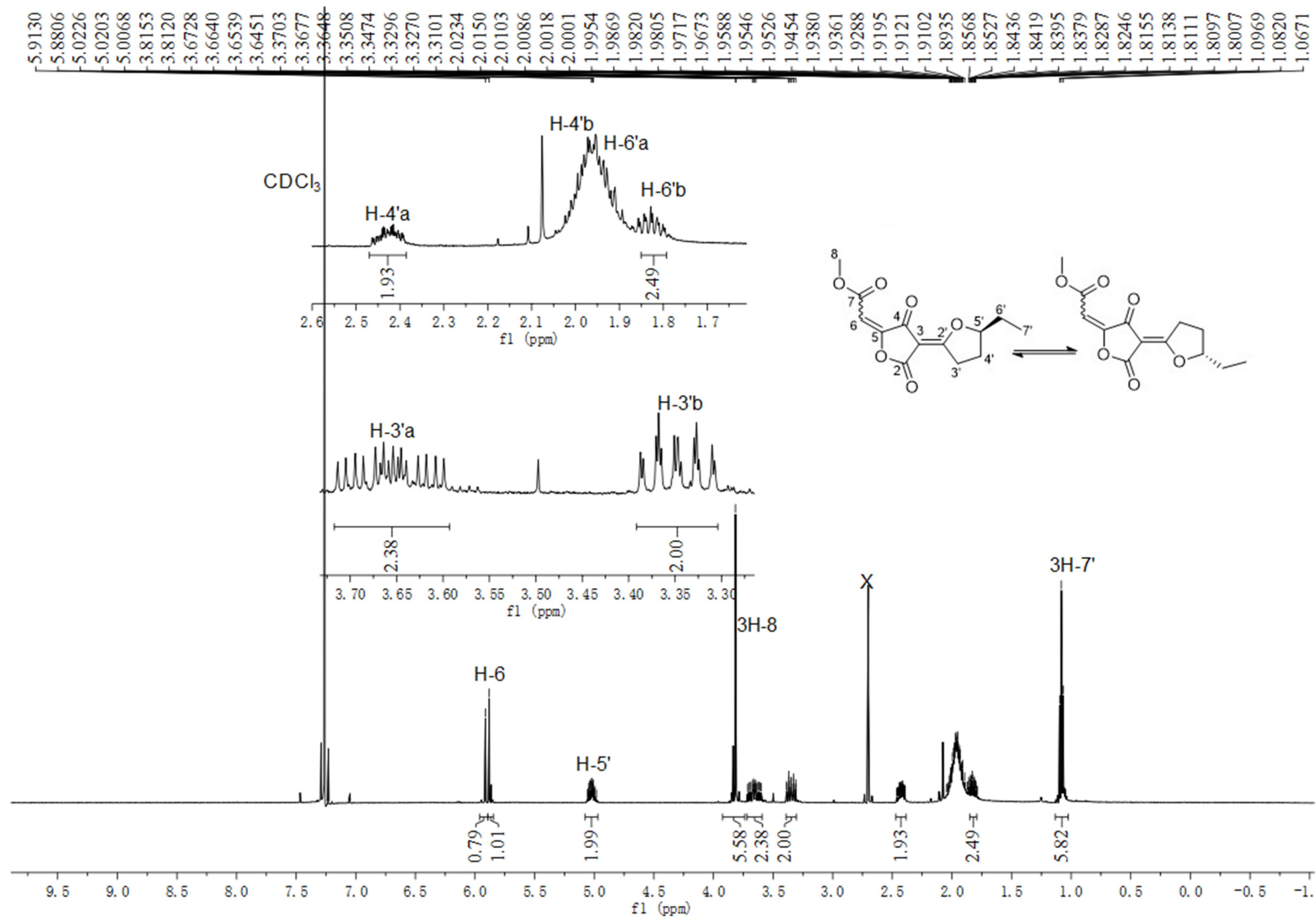


Figure S37. ^1H NMR spectrum of compound **8** in CDCl_3 (500MHz)

SUPPORTING INFORMATION

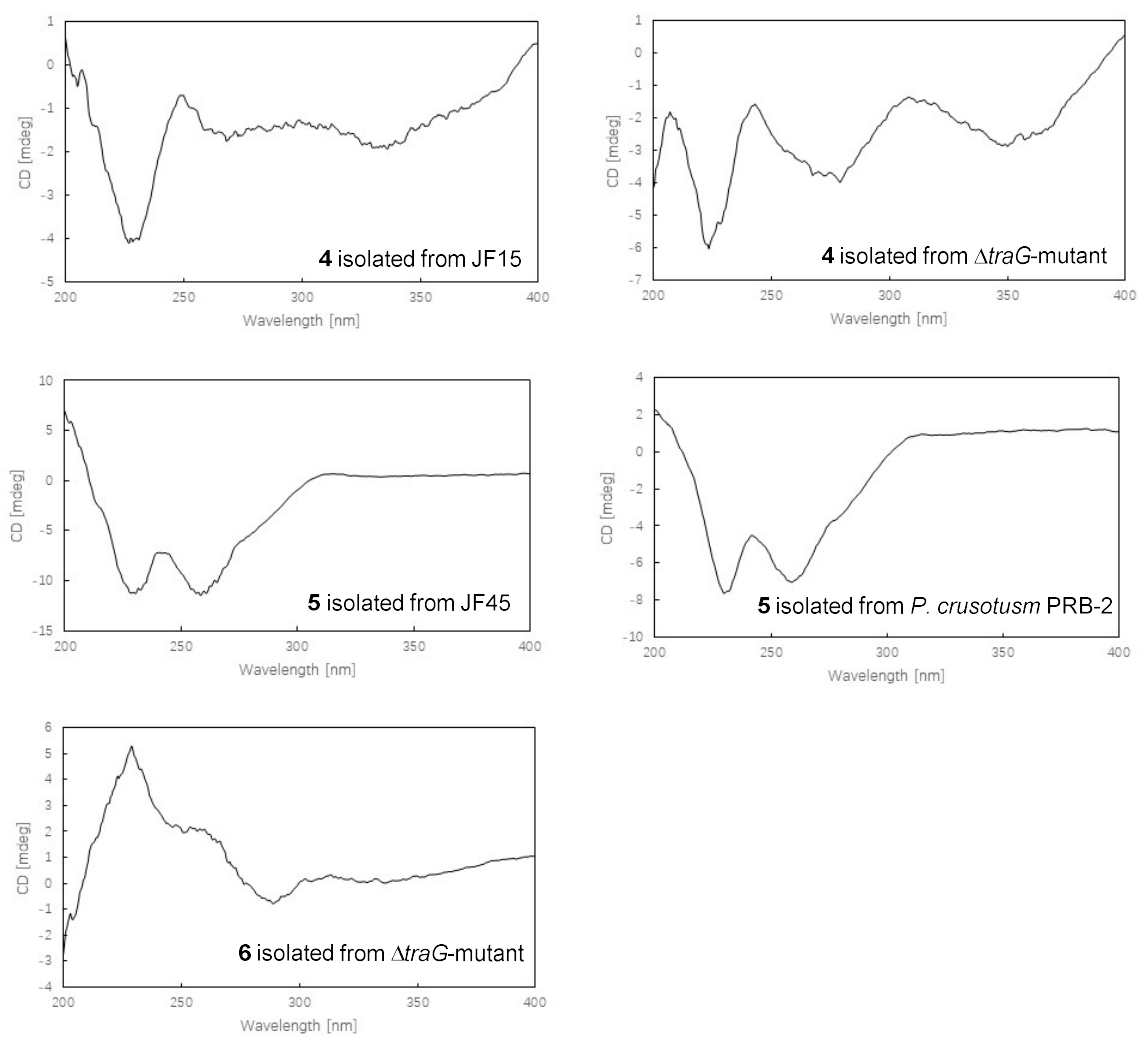


Figure S38. CD spectra of compounds **4 – 6**

Supplementary References

- (1) Wu, G.; Ma, H.; Zhu, T.; Li, J.; Gu, Q.; Li, D. Penilactones A and B, two novel polyketides from Antarctic deep-sea derived fungus *Penicillium crustosum* PRB-2. *Tetrahedron* **2012**, *68*, 9745.
- (2) Li, W.; Fan, A.; Wang, L.; Zhang, P.; Liu, Z.; An, Z.; Yin, W.-B. Asperphenamate biosynthesis reveals a novel two-module NRPS system to synthesize amino acid esters in fungi. *Chem. Sci.* **2018**, *9*, 2589.
- (3) Chiang, Y. M.; Ahuja, M.; Oakley, C. E.; Entwistle, R.; Asokan, A.; Zutz, C.; Wang, C. C.; Oakley, B. R. Development of genetic dereplication strains in *Aspergillus nidulans* results in the discovery of aspercryptin. *Angew. Chem. Int. Ed. Engl.* **2016**, *55*, 1662.
- (4) Yin, W. B.; Chooi, Y. H.; Smith, A. R.; Cacho, R. A.; Hu, Y.; White, T. C.; Tang, Y. Discovery of cryptic polyketide metabolites from dermatophytes using heterologous expression in *Aspergillus nidulans*. *ACS Synth. Biol.* **2013**, *2*, 629.
- (5) Sambrook, J.; Russell, D. W. *Molecular cloning: a laboratory manual*; 3rd ed.; Cold Spring Harbor Laboratory Press, Cold Spring Harbor: New York, 2001.
- (6) Fan, J.; Liao, G.; Kindinger, F.; Ludwig-Radtke, L.; Yin, W.-B.; Li, S.-M. Peniphenone and penilactone formation in *Penicillium crustosum* via 1,4-Michael additions of *ortho*-quinone methide from hydroxyclovatol to γ -butyrolactones from crustosic acid. *J. Am. Chem. Soc.* **2019**, *141*, 4225.
- (7) Goswami, R. S. Targeted gene replacement in fungi using a split-marker approach. *Methods Mol. Biol.* **2012**, *835*, 255.
- (8) Jacobus, A. P. and Gross, J. Optimal cloning of PCR fragments by homologous recombination in *Escherichia coli*. *PLoS. One.* **2015**, *10*, e0119221.
- (9) Zhang, P.; Wang, X.; Fan, A.; Zheng, Y.; Liu, X.; Wang, S.; Zou, H.; Oakley, B. R.; Keller, N. P.; Yin, W. B. A cryptic pigment biosynthetic pathway uncovered by heterologous expression is essential for conidial development in *Pestalotiopsis fici*. *Mol. Microbiol.* **2017**, *105*, 469.
- (10) Yu, X. and Li, S.-M. Prenyltransferases of the dimethylallyltryptophan synthase superfamily. *Methods Enzymol.* **2012**, *516*, 259.
- (11) Yu, H. and Li, S.-M. Two cytochrome P450 enzymes from *Streptomyces* sp. NRRL S-1868 catalyze distinct dimerization of tryptophan-containing cyclodipeptides. *Org. Lett.* **2019**, *21*, 7094.
- (12) Jacobsen, J. P.; Refstrup, T.; Cox, R. E.; Holker, J. S. E.; Boll, P. M. Revision of the structures of the naturally occurring acyl tetronic acids: dehydrocarolic acid, terrestrial acid and carlic acid. *Tetrahedron Lett.* **1978**, *19*, 1081.
- (13) Pitt, J. I.; Lange, L.; Lacey, A. E.; Vuong, D.; Midgley, D. J.; Greenfield, P.; Bradbury, M. I.; Lacey, E.; Busk, P. K.; Pilgaard, B.; Chooi, Y. H.; Piggott, A. M. *Aspergillus hancockii* sp. nov., a biosynthetically talented fungus endemic to southeastern Australian soils. *PLoS. One.* **2017**, *12*, e0170254.
- (14) Cox, R. J. Polyketides, proteins and genes in fungi: programmed nano-machines begin to reveal their secrets. *Org. Biomol. Chem.* **2007**, *5*, 2010.
- (15) Miyanaga, A.; Kudo, F.; Eguchi, T. Protein-protein interactions in polyketide synthase-nonribosomal peptide synthetase hybrid assembly lines. *Nat. Prod. Rep.* **2018**, *35*, 1185.
- (16) Huang, J. L.; Tang, Y.; Yu, C. P.; Sanyal, D.; Jia, X.; Liu, X.; Guo, Y.; Chang, W. C. Mechanistic investigation of oxidative decarboxylation catalyzed by two iron(II)- and 2-oxoglutarate-dependent enzymes. *Biochemistry* **2018**, *57*, 1838.
- (17) Yu, C. P.; Tang, Y.; Cha, L.; Milikisiyants, S.; Smirnova, T. I.; Smirnov, A. I.; Guo, Y.; Chang, W. C. Elucidating the reaction pathway of decarboxylation-assisted olefination catalyzed by a mononuclear non-heme iron enzyme. *J Am. Chem. Soc.* **2018**, *140*, 15190.
- (18) Yang, X. L.; Awakawa, T.; Wakimoto, T.; Abe, I. Three acyltetronic acid derivatives: noncanonical cryptic polyketides from *Aspergillus niger* identified by genome mining. *Chembiochem* **2014**, *15*, 1578.

**4.3 Increasing structural diversity of natural products by
Michael addition with *ortho*-quinone methide as the acceptor.**

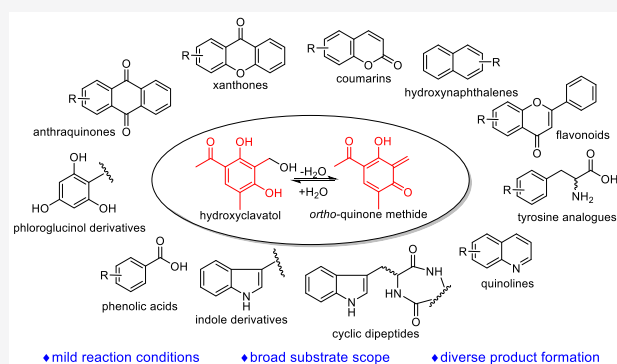
Increasing Structural Diversity of Natural Products by Michael Addition with *ortho*-Quinone Methide as the Acceptor

Ge Liao,[†] Jie Fan,[†] Lena Ludwig-Radtke, Katja Backhaus, and Shu-Ming Li*[‡]

Institut für Pharmazeutische Biologie und Biotechnologie, Philipps-Universität Marburg, Robert-Koch Straße 4, Marburg 35037, Germany

Supporting Information

ABSTRACT: The active form of clavatul, *ortho*-quinone methide, can be generated from hydroxycavatul in an aqueous system and used as a highly reactive intermediate for coupling with diverse natural products under very mild conditions. These include flavonoids, hydroxynaphthalenes, coumarins, xanthenes, anthraquinones, phloroglucinols, phenolic acids, indole derivatives, tyrosine analogues, and quinolines. The clavatul moiety was mainly attached via C–C bonds to the *ortho*- or *para*-positions of phenolic hydroxyl/amino groups and the C2-position of the indole ring.



Ortho-quinone methides (*o*-QMs), as transient intermediates with remarkable reactivity, have been utilized as useful reactants in chemical synthesis.^{1–5} A wide range of strategies, e.g., thermally driven,^{6,7} photolytically induced tautomerization,^{8,9} and benzylic oxidation,^{10,11} were developed to generate *o*-QMs. However, *o*-QMs can also be formed by spontaneous elimination of a stable molecule with concomitant dearomatization.^{12,13}

Recently, we reported the formation of penilactones A and B by two-step nonenzymatic Michael additions between a γ -butyrolactone and two *o*-QM molecules. The key precursor hydroxycavatul was the oxidation product of clavatul by the nonheme Fe^{II}/2-oxoglutarate dependent oxygenase ClaD and undergoes spontaneous water elimination, resulting in the active *o*-QM intermediate (Figure 1i).¹²

In addition to penilactones A and B from *Penicillium crustosum*,¹⁴ a number of natural products containing a clavatul unit are found in fungi, especially in *Penicillium* species.^{14–20} These include a clavatul–flavanone adduct from *Penicillium griseoroseum*¹⁶ as well as coupling products of clavatul with α -pyrone (communal A) and indole (communal B) from *Penicillium commune*¹⁷ (Figure 1ii). More coupling products of clavatul with diverse lactones, phenols, and quinones are listed in Figure S1 (see Supporting Information (SI)).

The occurrence of these natural products implies the involvement of clavatul, very likely via the *o*-QM intermediate, in their formation. Inspired by the postbiosynthetic non-enzymatic event in the formation of penilactones A and B, we wondered whether these clavatul-containing compounds are also pseudonatural products.

This hypothesis triggered our interest to prove the reactivity of the *o*-QM intermediate derived from hydroxycavatul with

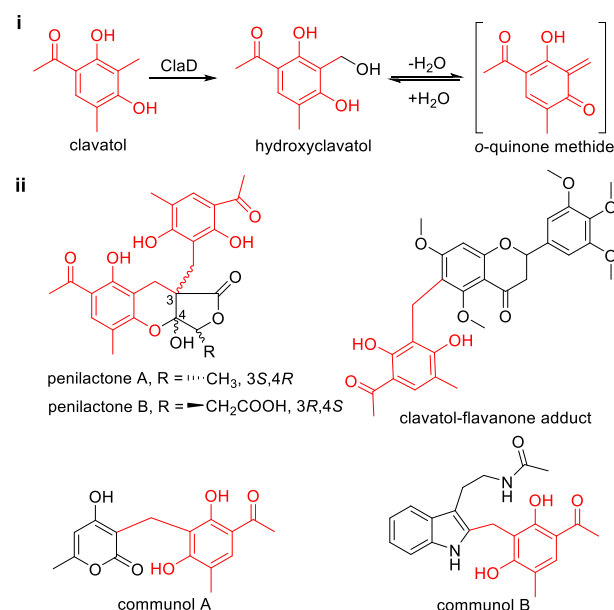


Figure 1. Formation of hydroxycavatul and its equilibration with the *o*-QM intermediate (i). Representative examples of clavatul-containing natural products (ii). See Figure S1 for more examples.

diverse natural products. Encouraged by accumulation of the clavatul–flavanone adduct in *P. griseoroseum*,¹⁶ we synthesized hydroxycavatul chemically (Scheme S1)^{6,21} and screened its reactivity with 16 flavonoids including catechin (1a–16a)

Received: November 1, 2019

Published: December 20, 2019

under mild conditions (Figures S2–S4). Both hydroxycavato and reactants at a final concentration of 0.4 mM in 50 μ L of H₂O were incubated at 25 °C for 16 h without pH adjustment. LC–MS analysis of the incubation mixtures showed that, with the exception for 10a, [M + H]⁺ ions being 178 Da larger than the corresponding reactants were detected. These proved the formation of the coupling products of flavonoids with clavato. Masses of products harboring two clavato units were also detected when using 4a, 5a, 8a, 9a, and 12a–15a as reactants.

Subsequent assays of hydroxycavato with other phenolic substances, including hydroxynaphthalenes (17a–27a), coumarins (28a–32a), xanthenes (33a–38a), anthraquinones (39a–42a), phloroglucinol derivatives (43a–51a), and phenolic acids (52a–60a) were carried out in a similar way as mentioned above. Products were detected in incubation mixtures of hydroxycavato with 9 of 11 tested hydroxynaphthalenes. This proved hydroxynaphthalenes as suitable reactants for coupling with the *o*-QM (Figures S2–S4). Coumarins with 29a as an exception, xanthenes, and anthraquinones were relatively poor reaction partners for the *o*-QM and gave no product or only trace amount of products in their reaction mixtures (Figures S2–S5). Among all the tested phenolic substances, phloroglucinol derivatives were found to be the most favorable Michael donors for the *o*-QM intermediate, with 10 to 55% conversion (Figures S2 and S6). In addition, coupling products of benzoic acids (52a–54a) were also observed by LC–MS analysis, while products from hydroxyphenyl acetic acid (55a), propionic acids (56a and 57a), and acrylic acids (58a – 60a) were not detectable (Figures S2–S4).

We speculated that the formation of the clavato–indole adduct communol B from *P. commune*¹⁷ was also a non-enzymatic event and therefore investigated the reaction activity of hydroxycavato with indole derivatives (61a–72a). The incubation mixture of L-tryptophan (61a) with hydroxycavato showed a coupling product with a conversion of 20%, while replacement of the nitrogen of the indole ring by sulfur (62a) and methylation at the N1 position (63a) significantly reduced the activity. Other indole derivatives carrying different side chains at C3 coupled with clavato with up to 49% conversion (Figures S2, S3, and S7).

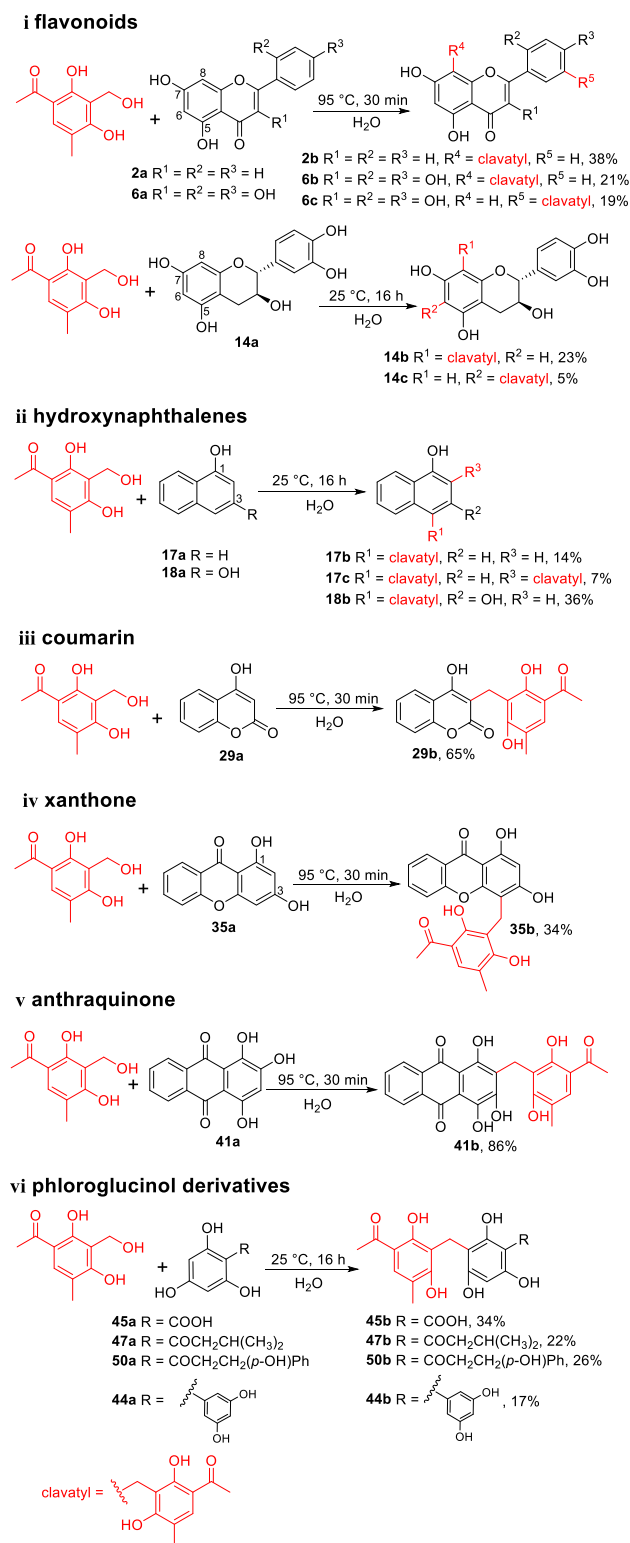
Subsequently, cyclic dipeptides (73a–82a) were tested by coinubation with hydroxycavato. All tryptophan-containing cyclic dipeptides (73a–80a) showed UV detectable product formation with 9 to 29% conversion. No product formation was detected for the incubation mixtures of *cyclo*-L-Tyr–L-Tyr (81a) and *cyclo*-L-Ser–L-Tyr (82a) (Figures S2–4, S7, and S8). In contrast to the easy coupling of L-tryptophan with the *o*-QM, L-tyrosine and its analogues (83a – 87a) were generally poorly converted to their clavato adducts. 88a–90a with an amino group at the benzene ring showed UV detectable product formation (Figures S2 and S3). All selected quinolines (91a–99a) served as Michael donors to couple with the *o*-QM, especially 92a, 94a, 95a, and 98a with obvious product peaks in UV chromatograms (Figures S2, S3, and S8).

In addition, clear product formation was also detected for the *o*-QM with other nitrogen-containing reactants, including 2-aminobenzyl alcohol (100a), 2-aminobenzoic acid (101a), and even tris(hydroxymethyl)aminomethane (Tris, 102a) prepared as Tris–HCl buffer (pH 7.5) (Figures S2 and S8).

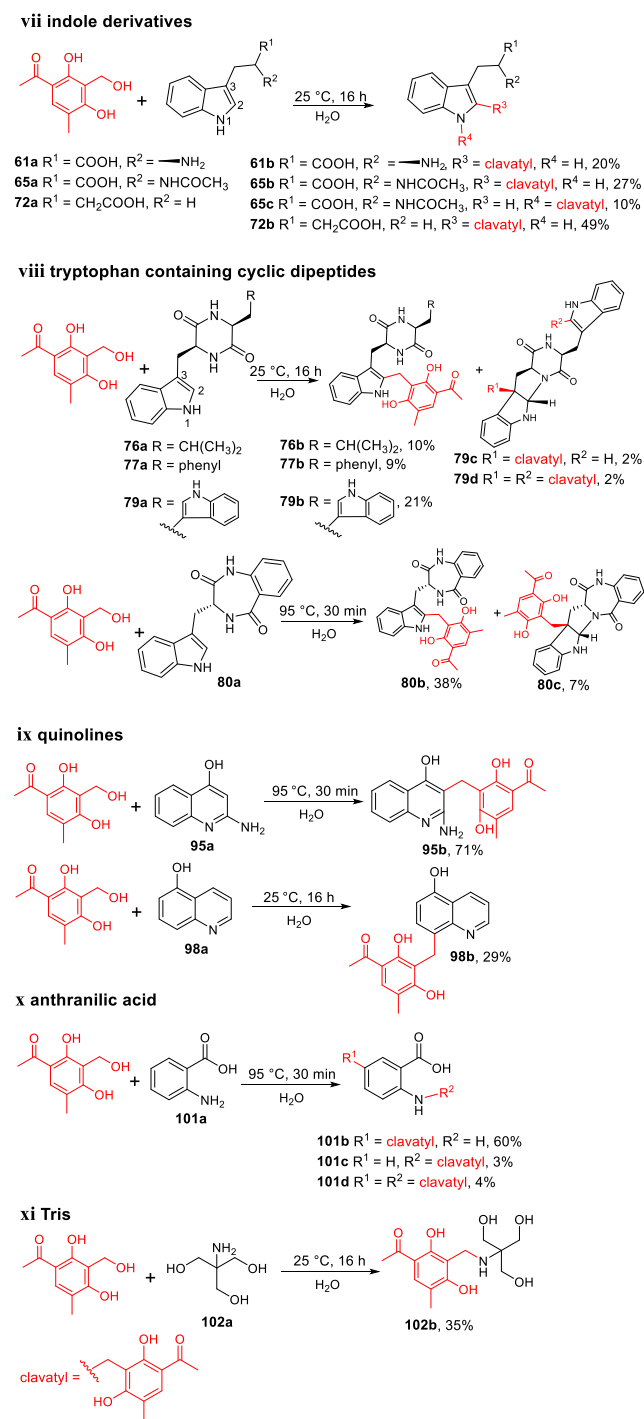
In summary, we demonstrated in a previous study that Michael additions between the *o*-QM and γ -butyrolactones took place easily under neutral or acidic conditions.¹²

Therefore, hydroxycavato was incubated in this study with 101 natural products or natural-product-like compounds at 25 °C and a nearly neutral pH value, which led to the detection of coupling products in 85 cases. Product formation with 10 to 55% conversion was detected for 49 reactants (Schemes 1 and 2 and Figures S5–S10). To facilitate the isolation of the

Scheme 1. Reactions of Hydroxycavato with Nitrogen-Free Reactants



Scheme 2. Reactions of Hydroxyclovatol with Nitrogen-Containing Reactants



products for structural elucidation, we changed the reaction temperature for all the incubations to 95 °C for 30 min to improve the product yields. As shown in Figures S5–S10, the majority of the reactions was promoted by increased temperature, leading to generally 2 to 10-fold higher accumulation of the coupling products. Taking purpurin (41a) as an example, its coupling with clavatul was improved dramatically from a trace amount to 86%. In total, product formation with 30 to 99% conversion was achieved for 58 reactants at 95 °C for 30 min. However, in a few cases, no significant change was observed for reactions performed at 25

and 95 °C (Figures S5–S10). Therefore, large scaled reactions of hydroxyclovatol with 23 reactants of different structural skeletons were carried out at either 25 or 95 °C, resulting in the isolation of 32 products, which were further subjected to HR-ESI-MS and NMR analyses (Figures S12–S86).

Structural elucidation of the coupling products of phenolic reactants confirmed the attachment of the clavatul unit to the *ortho*- or *para*-positions of the hydroxyl group at the benzene ring. Herein, the *o*-QM formed from hydroxyclovatol in an aqueous system was proposed to act as the Michael acceptor for the phenolic substances (Figure S11i,ii). The formation of 17b and 98b represents examples for the attachment of a clavatul moiety onto the *para*-position of the hydroxyl group (Schemes 1 and 2 and Figures S5 and S8). For flavan derivatives with a 5,7-dihydroxyl feature (2a, 6a, and 14a), C8-adducts (2b, 6b, and 14b) were identified as main products, and the C6-adduct (14c) was identified as a byproduct (Scheme 1 and Figure S5). The clavatul-containing flavanone from *P. griseoroseum* (Figure 1) was identified by feeding 5,7,3',4',5'-pentamethoxyflavanone into the culture.¹⁶ The incorporation of the clavatul unit into the exogenous flavanone might be also a nonenzymatic product. In analogy, 18b and 35b were identified as products of hydroxyclovatol with 1,3-dihydroxynaphthalene (18a) and 1,3-dihydroxyxanthone (35a) (Scheme 1 and Figures S5 and S6). Additionally, formation of 29b by the linkage between the clavatul unit and the α -pyrone moiety of 29a suggests that communal A from *P. commune* could be formed in a similar way (Scheme 1 and Figure S5). Phloroglucinol derivatives harboring three hydroxyl groups at the benzene ring conjugated with a clavatul also via C–C bonds (44b, 45b, 47b, and 50b) (Scheme 1 and Figure S6).

The indole ring in the tryptophanyl moiety contributes greatly to structural complexity by enzymatic modifications and spontaneous rearrangement.^{22,23} Communal B mentioned above represents a coupling example of a clavatul moiety with an indole skeleton.¹⁷ Accordingly, incubation of L-tryptophan (61a) with hydroxyclovatol enabled us to obtain the product (61b) with a similar structure to communal B (Scheme 2 and Figure S7). Subsequent isolation of clavatul adducts with different indole derivatives ((\pm)-65b and 72b) confirmed the spontaneous addition of the indole moiety via C2 to the *o*-QM (Scheme 2 and Figure S7). Furthermore, a number of coupling products of clavatul with tryptophan-containing cyclic dipeptides were also identified. Among them, C2-adducts were obtained as main products (76b, 77b, 79b, and 80b), and C3-adducts (79c and 80c) were obtained as byproducts (Scheme 2 and Figures S7 and S8). In addition, a *cyclo*-L-Trp-L-Trp derivative carrying two clavatul units (79d) was also identified (Scheme 2 and Figure S7). The conjugation between the clavatul unit and indole skeleton indicates that the electron transfer in the indole ring enabled the Michael addition from C2 to the electrophilic methylene group of the *o*-QM (Figure S11iii).

Steinmetz et al.²⁴ reported C–N coupling compounds as Michael addition products of different nucleophiles via their amino groups to the *p*-quinone methide, i.e., elansolid A3. However, only a few coupling products were obtained via C–N bond formation in this study. Examples are (\pm)-65c as a byproduct from the incubation of hydroxyclovatol with *N*-acetyl-DL-tryptophan ((\pm)-65a), 101c, and 101d from 2-aminobenzoic acid (101a) and 102b from Tris (102a) (Scheme 2 and Figures S7, S8, and S11iv). It can be concluded

that the cross-coupling between the nucleophiles tested above and the *o*-QM from hydroxyclavatul occurs preferentially via C–C bond formation. In addition, the C–N bond in **101d** seems unstable and can be easily hydrolyzed, which was observed by inspection of the ¹H NMR spectrum of **101d** (Figure S83) and comparison of the impurity signals with those of **101b** (Figure S79).

After structure elucidation, the obtained clavatul-containing products were screened for their antibacterial, acetylcholinesterase, and α -glucosidase inhibition activities. Detailed evaluation of the α -glucosidase inhibitory activity revealed the clavatul-coupling products **2b**, **17b**, **18b**, **35b**, **72b**, and **95b** showed clear inhibition with IC₅₀ values ranging from 43.8 ± 1.0 to 231.0 ± 7.5 μ M, while their precursors showed no activity. These concentrations are significantly lower than that of the control substance acarbose with an IC₅₀ at 766.2 ± 37.8 μ M (Table 1), indicating that conjugation of low-molecular-weight compounds with clavatul has the potential to increase the biological activity.

Table 1. Inhibitory Effects of the Selected Compounds against α -Glucosidase

reactants	IC ₅₀ (μ M)	products	IC ₅₀ (μ M)
2a	n.i.	2b	60.1 ± 0.6
17a	n.i.	17b	167.8 ± 2.3
18a	n.i.	18b	231.0 ± 7.5
35a	n.i.	35b	43.8 ± 1.0
72a	n.i.	72b	140.1 ± 1.3
95a	n.i.	95b	52.0 ± 2.4
acarbose ^a	766.2 ± 37.8		

^aPositive control. n.i.: no inhibition. The IC₅₀ data with standard deviation are mean values of three independent experiments.

In summary, our extended study on the utility of hydroxyclavatul proved that the *o*-QM generated from hydroxyclavatul can be considered as an excellent Michael acceptor for a variety of substances. The coupling reactions occurred under very mild conditions, i.e., overnight incubation at 25 °C in water. Increasing the reaction temperature can accelerate the reaction rate and promote the product accumulation. Diverse clavatul-containing products were identified in this study by incorporation of a clavatul unit onto the *ortho*- or *para*-positions of the hydroxyl group of different phenolic compounds as well as connection between the methylene group of the clavatul unit and the C2 of indole skeletons. Additional C–N bond formation of clavatul-coupling products was also observed in a few cases.

Despite of the wide application of QMs in chemical synthesis,^{1–5} QMs have also been reported to be involved in the assembly of natural products in recent years. For example, elansolid A3 acts as a key intermediate in the biosynthesis of elansolids.^{25,26} Spontaneous Diels–Alder addition via an *o*-QM intermediate was suggested for the formation of leprins.²⁷ Another QM-like intermediate is likely responsible for the dimerization of benzofluorene-containing angucyclines.¹³ In analogy, it is plausible that the clavatul-containing natural products listed in Figures 1 and S1 are formed by nonenzymatic Michael addition with involvement of the *o*-QM derived from hydroxyclavatul. Furthermore, it can be expected that more clavatul-coupling natural products will be discovered in the near future.

EXPERIMENTAL SECTION

Chemicals. **35a–38a**, **46a–48a**, **73a**, **75a**, **79a**, and **80a** were chemically synthesized as previously reported.^{28–34} Other chemicals used in this study were purchased from Bachem (Bubendorf, Switzerland), ABCR (Karlsruhe, Germany), TCI Europe (Zwijndrecht, Belgium), Alfa Aesar (Kandel, Germany), Carl Roth (Karlsruhe, Germany), Sigma-Aldrich (St. Louis, USA), or Acros (Merelbeke, Belgium).

Reaction Conditions of Hydroxyclavatul with the Tested Aromatic Compounds. Stock solutions of the tested compounds were prepared at 20 mM in DMSO or DMSO/H₂O (*v/v*, 1:1). Reactions were initiated by adding hydroxyclavatul (0.4 mM) and reactants (0.4 mM) into 50 μ L of distilled H₂O without pH adjustment. As a result, the reactions generally took place in the pH environment of 5.0–7.5. After incubation at 25 °C for 16 h, 50 μ L of ACN was added into the reaction mixture. A 5 μ L aliquot of supernatant was injected into LC–MS for analysis after centrifugation at 13 000 rpm for 30 min. Conversions were calculated from peak areas of products and reactants with UV detection. Two independent experiments were performed. In addition, reactions of all reactants were also carried out at 95 °C for 30 min.

LC–MS Analysis of Reaction Mixtures. LC–MS analysis was performed on a microTOF-Q III spectrometer (Bruker, Bremen, Germany) with an Agilent 1260 HPLC system (Agilent Technologies, Böblingen, Germany), using the Multosphere 120 RP18-5 μ column (250 × 2 mm, 5 μ m) (CS-Chromatographie Service GmbH). H₂O (A) and ACN (B), both with 0.1% (*v/v*) HCOOH, were used as solvents at flow rate of 0.25 mL/min. The substances were eluted with a linear gradient from 5–100% (*v/v*) B in 15 min. The column was then washed with 100% (*v/v*) solvent B for 5 min and equilibrated with 5% (*v/v*) solvent B for 5 min. Detection was carried out on a photodiode array detector, and UV absorptions at 280 nm are illustrated in this study. Electrospray ionization in positive or negative mode was set for the determination of the accuracy masses. HCOONa was used in each run for mass calibration. The capillary voltage was set to 4.5 kV, and collision energy was set to 8.0 eV. Data were evaluated with the Compass DataAnalysis 4.2 software (Bruker Daltonik, Bremen, Germany). The masses were scanned in the range of *m/z* 100–1500.

Isolation and Identification of the Reaction Products. To isolate the reaction products for structural elucidation, reactions were carried out in large scaled incubations (40 or 200 mL) containing hydroxyclavatul (0.4 mM), different reactants (0.4–0.8 mM), and up to 2% (*v/v*) DMSO. After incubation at 25 °C for 16 h or heating at 95 °C for 30 min, the reaction mixtures were extracted with a double volume of EtOAc three times. The organic phases were combined and concentrated under vacuum. The resulted residues were dissolved in MeOH and centrifuged at 13 000 rpm for 20 min. The products were then purified by silica gel column chromatography with a stepwise gradient of petroleum ether/EtOAc or on a Sephadex LH20 column with MeOH as elution solvent. A semipreparative HPLC equipped with an Agilent ZORBAX Eclipse XDB-C18 HPLC column (250 × 9.4 mm, 5 μ m) was also applied for purification by using isocratic elution with H₂O and ACN containing 0.1% trifluoroacetic acid (TFA). NMR spectra were recorded on a JEOL ECA-500 MHz spectrometer (JEOL, Tokyo, Japan). The spectra were processed with MestReNova 6.1.0 (Metrelab). Chemical shifts are referenced to those of the solvent signals.

Structural Elucidation. Characteristic signals of the clavatul moiety were observed in ¹H NMR spectra of all the isolated products as a set of signals for an aromatic proton at approximately 7.5 ppm, a singlet between 12–14 ppm, a methylene group mostly between 3–4 ppm, and two methyl groups at around 2.5 and 2.1 ppm. The clavatul-coupling products generally belong to two major groups. The majority is with the clavatul unit attached to the *ortho*- or *para*-position of a phenolic hydroxyl group at the benzene ring and other products carrying clavatul moieties attached to C2 or C3 of the indole skeleton.

In the cases of **17b** and **98b**, the linkage between the methylene group of the clavatul unit and the *para*-position of the hydroxy group

was proven by HMBC correlations (Figures S27–S30 and S76–S78). In analogy, correlations of the methylene group to different aromatic carbons in the HMBC spectra supported the linkage between the clavatul part and meta-dihydroxylated benzene ring, such as **2b** (Figures S12–S14), **6b** (Figures S15–S17), **6c** (Figures S18–S20), **14b** (Figures S21–S25), **18b** (Figures S32–S34), **35b** (Figures S38–S40), and **41b** (Figures S41–S43). **14c** obtained as the byproduct from the reaction mixture of (+)-catechin (**14a**) with hydroxycavatul is an analogue of isopilosanol A–C. Its structure was confirmed by comparison of ^1H NMR spectra with those of reported data (Figure S26).^{35,36} Since **44b**, **45b**, **47b**, and **50b** are formed via coupling of clavatul unit with phloroglucinol derivatives, the attachment of clavatul to the phloroglucinol moiety in **44b** and **47b** was proven by HMBC correlations as examples (Figures S44–S46 and S48–S50). The structures of **45b** and **50b** are deduced according to their molecular weight and ^1H NMR data (Figures S47 and S51). **29b** and **95b** showed two sets of signals in their ^1H NMR, one set for the clavatul subunit and one set of four coupling aromatic protons for the ortho-disubstituted benzene ring, suggesting the attachment of the clavatul unit to the α -pyrone ring in **29b** (Figures S35–S37) and to the pyridine ring in **95b** (Figures S73–S75).

61b, (\pm)-**65b**, and **72b** are indole derivatives with the clavatul unit linked at C2-position and differ only at the side chain of the C3-position. Therefore, their structures were determined by comparison of the NMR data (Figures S52–S54 and S60) with the known compound communol B.¹⁷ (\pm)-**65c** is an example of C–N bond formation between the clavatul moiety and the indole skeleton, which was confirmed by HMBC correlations (Figures S55–S59). **76b**, **77b**, **79b**, **79c**, **79d**, **80b**, and **80c** are coupling products of clavatul with tryptophan-containing cyclic dipeptides (Figures S61–S72). The structures of **79b** and **80b** were unequivocally confirmed by ^1H and ^{13}C NMR data as well as HMBC correlations (Figures S63–S66 and S69–S71). Other products are analogues of **79b**, and their structures were determined according to the C2- and C3-substitution patterns of the indole ring as reported before.³⁷

In the cases of **101b**–**101d** obtained from 2-aminobenzoic acid (**101a**), detailed inspection of the ^1H NMR revealed that **101b** and **101c** are products with one clavatul moiety, and **101d** is a product harboring two clavatul units. The presence of one set of characteristic signals for an ABX system in the ^1H NMR spectrum of **101b** revealed a para-substitution of the amino group at the benzene ring. The structure of **101b** was further confirmed by ^{13}C NMR and HMBC analyses (Figures S79–S81). In the ^1H NMR spectrum of **101c**, the coupling pattern consisting of four protons at the benzene ring, and a downfield shift of the methylene group from 3.95 to 4.51 ppm (Figure S82) indicated clavatul attachment to the amino group of **101a**. Similarly, one clavatul at the para-position of the amino group and one at the amino group can be concluded for the structure of **101d** (Figure S83). **102b** is another clavatul-coupling derivative via a C–N linkage, which was supported by the slightly downfield shifts of the methylene group at 4.49 ppm in the ^1H NMR spectrum and confirmed by HMBC correlations (Figure S84–S86).

Characterization Data. 8-(3-Acetyl-2,6-dihydroxy-5-methylbenzyl)-5,7-dihydroxy-2-phenyl-4H-chromen-4-one (**2b**). The title compound was prepared using **2a** (0.106 mmol, 32.0 mg) and hydroxycavatul (0.102 mmol, 20.0 mg) as reactants. The product was isolated in 39% yield (17.3 mg) as yellow amorphous solid. Eluent: petroleum ether/EtOAc (5:1, v/v). ^1H NMR (500 MHz, DMSO- d_6) δ 13.00 (s, 1H), 8.00 (dd, J = 8.4, 1.5 Hz, 2H), 7.59 (tt, J = 7.5, 1.5 Hz, 1H), 7.54–7.49 (m, 2H), 7.52 (s, 1H), 6.91 (s, 1H), 6.25 (s, 1H), 4.10 (s, 2H), 2.49 (s, 3H), 2.11 (s, 3H). $^{13}\text{C}\{^1\text{H}\}$ NMR (125 MHz, DMSO- d_6) δ 203.2, 182.2, 163.4, 162.2, 160.9, 160.9, 159.1, 155.0, 131.8, 131.1, 130.8, 128.9, 128.9, 126.5, 126.5, 115.8, 113.1, 112.1, 105.5, 104.8, 103.8, 98.4, 26.1, 16.6, 16.2. HRMS (ESI-TOF) m/z : [$M + H$] $^+$ Calcd for $\text{C}_{25}\text{H}_{21}\text{O}_7$, 433.1282; Found 433.1272.

8-(3-Acetyl-2,6-dihydroxy-5-methylbenzyl)-2-(2,4-dihydroxyphenyl)-3,5,7-trihydroxy-4H-chromen-4-one (**6b**). The title compound was prepared using **6a** (0.108 mmol, 32.9 mg) and hydroxycavatul (0.066 mmol, 12.9 mg) as reactants. The product was isolated in 17% yield (5.5 mg) as yellow amorphous solid. Eluent:

ACN/ H_2O (55:45, v/v) supplied with 0.1% TFA. ^1H NMR (500 MHz, DMSO- d_6) δ 12.82 (s, 1H), 12.64 (s, 1H), 9.74 (s, 1H), 7.48 (s, 1H), 7.09 (d, J = 8.5 Hz, 1H), 6.37 (d, J = 2.3 Hz, 1H), 6.30 (dd, J = 8.5, 2.3 Hz, 1H), 6.20 (s, 1H), 3.95 (s, 2H), 2.49 (s, 3H), 2.07 (s, 3H). $^{13}\text{C}\{^1\text{H}\}$ NMR (125 MHz, DMSO- d_6) δ 202.8, 176.3, 160.9, 160.9, 160.4, 160.4, 158.4, 156.5, 154.5, 148.7, 135.4, 131.1, 130.5, 115.6, 113.1, 112.0, 109.5, 107.0, 104.7, 103.4, 102.9, 97.5, 26.1, 16.2. HRMS (ESI-TOF) m/z : [$M + H$] $^+$ Calcd for $\text{C}_{25}\text{H}_{21}\text{O}_{10}$, 481.1129; Found 481.1151.

2-(5-(3-Acetyl-2,6-dihydroxy-5-methylbenzyl)-2,4-dihydroxyphenyl)-3,5,7-trihydroxy-4H-chromen-4-one (**6c**). The title compound was prepared using **6a** (0.108 mmol, 32.9 mg) and hydroxycavatul (0.066 mmol, 12.9 mg) as reactants. The product was isolated in 21% yield (6.7 mg) as yellow amorphous solid. Eluent: ACN/ H_2O (55:45, v/v) supplied with 0.1% TFA. ^1H NMR (500 MHz, DMSO- d_6) δ 12.95 (s, 1H), 10.66 (s, 1H), 7.58 (s, 1H), 6.79 (s, 1H), 6.50 (s, 1H), 6.18 (d, J = 2.2 Hz, 1H), 6.14 (d, J = 2.2 Hz, 1H), 3.78 (s, 2H), 2.52 (s, 3H), 2.15 (s, 3H). $^{13}\text{C}\{^1\text{H}\}$ NMR (125 MHz, DMSO- d_6) δ 203.2, 176.0, 163.6, 160.9, 160.7, 160.6, 157.4, 156.7, 154.4, 148.9, 136.0, 131.1, 129.9, 117.6, 116.0, 113.2, 112.3, 109.0, 103.4, 102.6, 98.0, 93.1, 26.1, 21.1, 16.1. HRMS (ESI-TOF) m/z : [$M + H$] $^+$ Calcd for $\text{C}_{25}\text{H}_{21}\text{O}_{10}$, 481.1129; Found 481.1147.

1-(3-(((2R,3S)-2-(3,4-Dihydroxyphenyl)-3,5,7-trihydroxychroman-8-yl)methyl)-2,4-dihydroxy-5-methylphenyl)ethan-1-one (**14b**). The title compound was prepared using **14a** (0.106 mmol, 30.8 mg) and hydroxycavatul (0.066 mmol, 12.9 mg) as reactants. The product was isolated in 28% yield (8.6 mg) as brown oil. Eluent: ACN/ H_2O (55:45, v/v) supplied with 0.1% TFA. ^1H NMR (500 MHz, acetone- d_6) δ 14.26 (s, 1H), 7.59 (s, 1H), 6.99 (d, J = 1.2 Hz, 1H), 6.86 (s, 1H), 6.86 (s, 1H), 6.11 (s, 1H), 4.81 (d, J = 7.8 Hz, 1H), 4.15 (ddd, J = 8.5, 7.8, 5.5 Hz, 1H), 3.81 (d, J = 15.6 Hz, 1H), 3.77 (d, J = 15.6 Hz, 1H), 2.97 (dd, J = 16.3, 5.5 Hz, 1H), 2.61 (dd, J = 16.3, 8.5 Hz, 1H), 2.53 (s, 3H), 2.09 (s, 3H). ^1H NMR (500 MHz, pyridine- d_6) δ 7.62 (d, J = 2.1 Hz, 1H), 7.47 (s, 1H), 7.30 (d, J = 8.1 Hz, 1H), 7.25 (dd, J = 8.1, 2.1 Hz, 1H), 6.67 (s, 1H), 5.31 (d, J = 7.7 Hz, 1H), 4.57 (ddd, J = 8.4, 7.7, 5.4 Hz, 1H), 4.47 (d, J = 15.1 Hz, 1H), 4.35 (d, J = 15.1 Hz, 1H), 3.63 (dd, J = 16.1, 5.4 Hz, 1H), 3.31 (dd, J = 16.1, 8.4 Hz, 1H), 2.46 (s, 3H), 2.20 (s, 3H). ^1H NMR (500 MHz, DMSO- d_6) δ 12.90 (s, 1H), 9.67 (s, 1H), 9.11 (s, 1H), 8.95 (s, 1H), 7.48 (s, 1H), 6.66 (d, J = 2.0 Hz, 1H), 6.60 (d, J = 8.1 Hz, 1H), 6.46 (dd, J = 8.1, 2.0 Hz, 1H), 6.03 (s, 1H), 4.54 (d, J = 7.1 Hz, 1H), 3.82–3.78 (m, 1H), 3.76 (d, J = 14.8 Hz, 1H), 3.68 (d, J = 14.8 Hz, 1H), 2.62 (dd, J = 16.2, 5.3 Hz, 1H), 2.49 (s, 3H), 2.37 (dd, J = 16.2, 7.7 Hz, 1H), 2.04 (s, 3H). $^{13}\text{C}\{^1\text{H}\}$ NMR (125 MHz, DMSO- d_6) δ 202.6, 160.6, 160.4, 154.0, 153.0, 152.8, 144.6, 144.5, 130.3, 130.2, 117.9, 115.6, 114.9, 114.4, 113.5, 112.2, 103.2, 99.8, 94.8, 81.2, 66.0, 30.6, 27.7, 26.2, 15.8. $[\alpha]_{\text{D}}^{20}$ = +25 (c 0.1, MeOH); HRMS (ESI-TOF) m/z : [$M + H$] $^+$ Calcd for $\text{C}_{25}\text{H}_{25}\text{O}_9$, 469.1493; Found 469.1493.

1-(3-(((2R,3S)-2-(3,4-Dihydroxyphenyl)-3,5,7-trihydroxychroman-6-yl)methyl)-2,4-dihydroxy-5-methylphenyl)ethan-1-one (**14c**). The title compound was prepared using **14a** (0.106 mmol, 30.8 mg) and hydroxycavatul (0.066 mmol, 12.9 mg) as reactants. The product was isolated in 6% yield (1.8 mg) as brown oil. Eluent: ACN/ H_2O (55:45, v/v) supplied with 0.1% TFA. ^1H NMR (500 MHz, acetone- d_6) δ 14.5 (s, 1H), 7.67 (s, 1H), 6.85 (d, J = 2.0 Hz, 1H), 6.77 (d, J = 8.1 Hz, 1H), 6.71 (dd, J = 8.1, 2.0 Hz, 1H), 6.10 (s, 1H), 4.57 (d, J = 7.5 Hz, 1H), 3.98 (ddd, J = 8.5, 7.5, 5.3 Hz, 1H), 3.86 (s, 2H), 2.87 (dd, J = 16.2, 5.3 Hz, 1H), 2.60 (s, 3H), 2.54 (dd, J = 16.2, 8.5 Hz, 1H), 2.15 (s, 3H). $[\alpha]_{\text{D}}^{20}$ = +23 (c 0.1, MeOH); HRMS (ESI-TOF) m/z : [$M + H$] $^+$ Calcd for $\text{C}_{25}\text{H}_{25}\text{O}_9$, 469.1493; Found 469.1496.

1-(2,4-Dihydroxy-3-((4-hydroxynaphthalen-1-yl)methyl)-5-methylphenyl)ethan-1-one (**17b**). The title compound was prepared using **17a** (0.179 mmol, 25.9 mg) and hydroxycavatul (0.076 mmol, 14.9 mg) as reactants. The product was isolated in 21% yield (5.0 mg) as yellow amorphous solid. Eluent: ACN/ H_2O (70:30, v/v). ^1H NMR (500 MHz, acetone- d_6) δ 13.09 (s, 1H), 8.28 (dd, J = 8.6, 1.5 Hz, 1H), 8.23 (dd, J = 8.6, 1.5 Hz, 1H), 7.71 (s, 1H), 7.56 (ddd, J = 8.6, 7.0, 1.5 Hz, 1H), 7.48 (ddd, J = 8.6, 7.0, 1.5 Hz, 1H), 6.71 (s, 2H),

4.38 (s, 2H), 2.60 (s, 3H), 2.25 (s, 3H). ¹H NMR (500 MHz, DMSO-*d*₆) δ 12.95 (s, 1H), 9.78 (s, 1H), 9.54 (s, 1H), 8.22 (d, *J* = 8.5 Hz, 1H), 8.16 (d, *J* = 8.5 Hz, 1H), 7.66 (s, 1H), 7.55 (dd, *J* = 8.5, 6.8 Hz, 1H), 7.46 (dd, *J* = 8.5, 6.8 Hz, 1H), 6.67 (d, *J* = 8.0 Hz, 1H), 6.63 (d, *J* = 8.0 Hz, 1H), 4.26 (s, 2H), 2.57 (s, 3H), 2.19 (s, 3H). ¹³C{¹H} NMR (125 MHz, DMSO-*d*₆) δ 203.2, 161.1, 160.9, 151.4, 132.8, 131.3, 125.8, 125.6, 124.8, 124.1, 124.0, 123.6, 122.4, 116.0, 113.1, 112.3, 107.3, 26.2, 24.3, 16.2. HRMS (ESI-TOF) *m/z*: [M - H]⁻ Calcd for C₂₀H₁₇O₄ 321.1132; Found 321.1159.

1,1'-((4-Hydroxynaphthalene-1,3-diyl)bis(methylene))bis(2,4-dihydroxy-5-methyl-3,1-phenylene)bis(ethan-1-one) (17c). The title compound was prepared using 17a (0.179 mmol, 25.9 mg) and hydroxycavatul (0.076 mmol, 14.9 mg) as reactants. The product was isolated in 6% yield (1.5 mg) as yellow amorphous solid. Eluent: ACN/H₂O (70:30, *v/v*). ¹H NMR (500 MHz, acetone-*d*₆) δ 13.11 (s, 1H), 13.00 (s, 1H), 8.27 (d, *J* = 8.4 Hz, 1H), 8.16 (d, *J* = 8.4 Hz, 1H), 7.69 (s, 1H), 7.54 (s, 1H), 7.50 (dd, *J* = 8.4, 6.8 Hz, 1H), 7.47 (dd, *J* = 8.4, 6.8 Hz, 1H), 7.00 (s, 1H), 4.30 (s, 2H), 3.98 (s, 2H), 2.63 (s, 3H), 2.55 (s, 3H), 2.24 (s, 3H), 2.15 (s, 3H). HRMS (ESI-TOF) *m/z*: [M - H]⁻ Calcd for C₃₀H₂₇O₇ 499.1762; Found 499.1773.

1-(3-((2,4-Dihydroxynaphthalen-1-yl)methyl)-2,4-dihydroxy-5-methylphenyl)ethan-1-one (18b). The title compound was prepared using 18a (0.161 mmol, 25.9 mg) and hydroxycavatul (0.089 mmol, 17.4 mg) as reactants. The product was isolated in 24% yield (7.3 mg) as white amorphous solid. Eluent: ACN/H₂O (65:35, *v/v*) supplied with 0.1% TFA. ¹H NMR (500 MHz, DMSO-*d*₆) δ 13.66 (s, 1H), 10.11 (s, 1H), 8.32 (d, *J* = 8.9 Hz, 1H), 8.00 (d, *J* = 8.9 Hz, 1H), 7.55 (s, 1H), 7.37 (dd, *J* = 8.9, 6.7 Hz, 1H), 7.19 (dd, *J* = 8.9, 6.7 Hz, 1H), 6.71 (s, 1H), 4.18 (s, 2H), 2.54 (s, 3H), 2.04 (s, 3H). ¹³C{¹H} NMR (125 MHz, DMSO-*d*₆) δ 203.4, 160.9, 159.9, 153.1, 150.9, 134.1, 131.0, 126.6, 123.5, 122.2, 121.5, 120.8, 116.1, 113.3, 112.1, 107.9, 99.6, 26.2, 17.1, 15.7. HRMS (ESI-TOF) *m/z*: [M - H]⁻ Calcd for C₂₀H₁₇O₅ 337.1081; Found 337.1097.

3-(3-Acetyl-2,6-dihydroxy-5-methylbenzyl)-4-hydroxy-2H-chromen-2-one (29b). The title compound was prepared using 29a (0.173 mmol, 28.1 mg) and hydroxycavatul (0.076 mmol, 14.9 mg) as reactants. The product was isolated in 43% yield (11.2 mg) as white amorphous solid. Eluent: ACN/H₂O (90:10, *v/v*) supplied with 0.1% TFA. ¹H NMR (500 MHz, CDCl₃) δ 14.70 (s, 1H), 10.28 (s, 1H), 10.23 (s, 1H), 7.93 (dd, *J* = 8.5, 1.6 Hz, 1H), 7.56 (ddd, *J* = 8.5, 7.0, 1.6 Hz, 1H), 7.43 (s, 1H), 7.35 (dd, *J* = 8.5, 1.6 Hz, 1H), 7.33 (ddd, *J* = 8.5, 7.0, 1.6 Hz, 1H), 3.87 (s, 2H), 2.58 (s, 3H), 2.21 (s, 3H). ¹³C{¹H} NMR (125 MHz, CDCl₃) δ 203.6, 168.4, 163.4, 162.0, 158.9, 152.3, 132.6, 131.1, 124.8, 123.9, 119.8, 116.7, 116.3, 112.6, 112.3, 103.5, 26.0, 18.2, 16.2. HRMS (ESI-TOF) *m/z*: [M + H]⁺ Calcd for C₁₉H₁₇O₆ 341.1020; Found 341.1013.

4-(3-Acetyl-2,6-dihydroxy-5-methylbenzyl)-1,3-dihydroxy-9H-xanthen-9-one (35b). The title compound was prepared using 35a (0.122 mmol, 27.9 mg) and hydroxycavatul (0.071 mmol, 13.9 mg) as reactants. The product was isolated in 31% yield (9.1 mg) as white amorphous solid. Eluent: ACN/H₂O (80:20, *v/v*) supplied with 0.1% TFA. ¹H NMR (500 MHz, DMSO-*d*₆) δ 13.04 (s, 1H), 12.76 (s, 1H), 8.08 (dd, *J* = 8.0, 1.6 Hz, 1H), 7.83 (ddd, *J* = 8.0, 7.2, 1.6 Hz, 1H), 7.52 (s, 1H), 7.42 (ddd, *J* = 8.0, 7.2, 1.6 Hz, 1H), 7.39 (dd, *J* = 8.0, 1.6 Hz, 1H), 6.28 (s, 1H), 4.06 (s, 2H), 2.50 (s, 3H), 2.16 (s, 3H). ¹³C{¹H} NMR (125 MHz, DMSO-*d*₆) δ 203.1, 179.9, 161.0, 161.0, 160.3, 160.3, 155.3, 154.8, 135.5, 130.7, 125.1, 124.1, 119.4, 117.3, 115.7, 113.4, 112.0, 105.5, 102.1, 97.5, 26.1, 16.3, 16.2. HRMS (ESI-TOF) *m/z*: [M + H]⁺ Calcd for C₂₃H₁₉O₇ 407.1125; Found 407.1116.

2-(3-Acetyl-2,6-dihydroxy-5-methylbenzyl)-1,3,4-trihydroxyanthracene-9,10-dione (41b). The title compound was prepared using 41a (0.094 mmol, 24.1 mg) and hydroxycavatul (0.058 mmol, 11.4 mg) as reactants. The product was isolated in 33% yield (8.3 mg) as red amorphous solid. Eluent: ACN/H₂O (75:25, *v/v*) supplied with 0.1% TFA. ¹H NMR (500 MHz, DMSO-*d*₆) δ 14.24 (s, 1H), 13.46 (s, 1H), 12.95 (s, 1H), 8.27 (dd, *J* = 7.6, 1.3 Hz, 1H), 8.26 (dd, *J* = 7.6, 1.3 Hz, 1H), 7.93 (td, *J* = 7.6, 1.3 Hz, 1H), 7.89 (td, *J* = 7.6, 1.3 Hz, 1H), 7.51 (s, 1H), 3.99 (s, 2H), 2.50 (s, 3H), 2.11 (s, 3H). ¹³C{¹H} NMR (125 MHz, DMSO-*d*₆) δ 202.9, 184.8, 181.8, 161.2, 160.9,

160.9, 155.8, 134.7, 133.7, 133.6, 132.4, 130.7, 126.3, 126.2, 123.2, 115.8, 112.5, 112.2, 112.0, 109.8, 26.2, 17.5, 16.2. HRMS (ESI-TOF) *m/z*: [M + H]⁺ Calcd for C₂₄H₁₉O₈ 435.1074; Found 435.1069.

1-(2,4-Dihydroxy-5-methyl-3-((2,3',4,5',6-pentahydroxy-[1,1'-biphenyl]-3-yl)methyl)phenyl)ethan-1-one (44b). The title compound was prepared using 44a (0.128 mmol, 30.0 mg) and hydroxycavatul (0.076 mmol, 14.9 mg) as reactants. The product was isolated in 28% yield (8.9 mg) as brown oil. Eluent: ACN/H₂O (60:40, *v/v*) supplied with 0.1% TFA. ¹H NMR (500 MHz, DMSO-*d*₆) δ 13.96 (s, 1H), 8.90 (s, 1H), 8.87 (s, 1H), 7.64 (s, 1H), 6.10 (s, 1H), 6.06–6.04 (m, 3H), 3.73 (s, 2H), 2.56 (s, 3H), 2.12 (s, 3H). ¹³C{¹H} NMR (125 MHz, DMSO-*d*₆) δ 203.8, 160.6, 158.7, 157.4, 157.4, 154.2, 152.9, 152.8, 136.3, 131.1, 117.2, 113.2, 112.2, 110.1, 109.4, 109.4, 103.4, 100.5, 94.9, 48.6, 26.1, 15.7. HRMS (ESI-TOF) *m/z*: [M + H]⁺ Calcd for C₂₂H₂₁O₈ 413.1231; Found 413.1242.

3-(3-Acetyl-2,6-dihydroxy-5-methylbenzyl)-2,4,6-trihydroxybenzoic acid (45b). The title compound was prepared using 45a (0.024 mmol, 4.2 mg) and hydroxycavatul (0.016 mmol, 3.1 mg) as reactants. The product was isolated in 44% yield (2.5 mg) as white amorphous solid. Eluent: ACN/H₂O (60:40, *v/v*) supplied with 0.1% TFA. ¹H NMR (500 MHz, acetone-*d*₆) δ 14.42 (s, 1H), 7.64 (s, 1H), 6.04 (s, 1H), 3.82 (s, 2H), 2.59 (s, 3H), 2.13 (s, 3H). HRMS (ESI-TOF) *m/z*: [M + H]⁺ Calcd for C₁₇H₁₇O₈ 349.0918; Found 349.0925.

1-(3-(3-Acetyl-2,6-dihydroxy-5-methylbenzyl)-2,4,6-trihydroxyphenyl)-3-methylbutan-1-one (47b). The title compound was prepared using 29a (0.142 mmol, 30.0 mg) and hydroxycavatul (0.076 mmol, 14.9 mg) as reactants. The product was isolated in 31% yield (9.1 mg) as yellow amorphous solid. Eluent: ACN/H₂O (90:10, *v/v*) supplied with 0.1% TFA. ¹H NMR (500 MHz, DMSO-*d*₆) δ 13.09 (s, 1H), 10.69 (s, 1H), 7.51 (s, 1H), 5.96 (s, 1H), 3.74 (s, 2H), 2.87 (d, *J* = 6.7 Hz, 1H), 2.51 (s, 3H), 2.14 (m, 1H), 2.08 (s, 3H), 0.90 (d, *J* = 6.7 Hz, 3H), 0.90 (d, *J* = 6.7 Hz, 3H). ¹³C{¹H} NMR (125 MHz, DMSO-*d*₆) δ 205.1, 203.0, 163.4, 162.3, 160.8, 160.7, 160.3, 130.4, 115.7, 113.3, 112.0, 104.4, 103.7, 94.4, 51.8, 48.6, 26.1, 24.8, 22.6, 22.6, 15.9. HRMS (ESI-TOF) *m/z*: [M + H]⁺ Calcd for C₂₁H₂₅O₇ 389.1595; Found 389.1597.

1-(3-(3-Acetyl-2,6-dihydroxy-5-methylbenzyl)-2,4,6-trihydroxyphenyl)-3-(4-hydroxyphenyl)propan-1-one (50b). The title compound was prepared using 50a (0.028 mmol, 7.9 mg) and hydroxycavatul (0.024 mmol, 4.7 mg) as reactants. The product was isolated in 19% yield (2.0 mg) as white amorphous solid. Eluent: ACN/H₂O (80:20, *v/v*) supplied with 0.1% TFA. ¹H NMR (500 MHz, acetone-*d*₆) δ 14.53 (s, 1H), 7.66 (s, 1H), 7.10 (d, *J* = 8.6 Hz, 2H), 6.75 (d, *J* = 8.6 Hz, 2H), 6.08 (s, 1H), 3.85 (s, 2H), 3.39 (t, *J* = 7.5 Hz, 2H), 2.90 (t, *J* = 7.5 Hz, 2H), 2.59 (s, 3H), 2.14 (s, 3H). HRMS (ESI-TOF) *m/z*: [M + H]⁺ Calcd for C₂₅H₂₅O₈ 453.1544; Found 453.1561.

(S)-3-(2-(3-Acetyl-2,6-dihydroxy-5-methylbenzyl)-1H-indol-3-yl)-2-aminopropanoic acid (61b). The title compound was prepared using 61a (0.160 mmol, 44.0 mg) and hydroxycavatul (0.102 mmol, 20.0 mg) as reactants. The product was isolated in 27% yield (10.4 mg) as yellow amorphous solid. Eluent: CH₂Cl₂. ¹H NMR (500 MHz, DMSO-*d*₆) δ 10.19 (s, 1H), 7.56 (s, 1H), 7.51 (d, *J* = 8.0 Hz, 1H), 7.26 (d, *J* = 8.0 Hz, 1H), 6.94 (dd, *J* = 8.0, 6.8 Hz, 1H), 6.90 (dd, *J* = 8.0, 6.8 Hz, 1H), 4.14 (d, *J* = 15.2 Hz, 1H), 4.07 (d, *J* = 15.2 Hz, 1H), 3.41 (dd, *J* = 6.8, 5.8 Hz, 1H), 3.18 (dd, *J* = 14.7, 5.8 Hz, 1H), 3.03 (dd, *J* = 14.7, 6.8 Hz, 1H), 2.52 (s, 3H), 2.11 (s, 3H). ¹³C{¹H} NMR (125 MHz, DMSO-*d*₆) δ 202.1, 171.2, 161.5, 136.1, 134.9, 130.8, 128.4, 119.8, 118.2, 118.0, 117.2, 111.9, 111.4, 110.9, 105.1, 55.0, 26.1, 25.9, 20.0, 16.5. [α]_D²⁰ = -6 (c 0.2, acetone); HRMS (ESI-TOF) *m/z*: [M + H]⁺ Calcd for C₂₁H₂₃N₂O₅ 383.1601; Found 383.1609.

2-Acetamido-3-(2-(3-acetyl-2,6-dihydroxy-5-methylbenzyl)-1H-indol-3-yl)propanoic acid ((±)-65b). The title compound was prepared using (±)-65a (0.178 mmol, 44.0 mg) and hydroxycavatul (0.069 mmol, 13.5 mg) as reactants. The product was isolated in 29% yield (8.6 mg) as brown oil. Eluent: ACN/H₂O (55:45, *v/v*) supplied with 0.1% TFA. ¹H NMR (500 MHz, acetone-*d*₆) δ 13.26 (s, 1H), 7.66 (s, 1H), 7.53 (d, *J* = 7.4 Hz, 1H), 7.23 (d, *J* = 7.4 Hz, 1H), 6.96 (t, *J* = 7.4 Hz, 1H), 6.92 (t, *J* = 7.4 Hz, 1H), 4.81 (ddd, *J* = 8.2, 7.7,

6.0 Hz, 1H), 4.21 (d, J = 15.0 Hz, 1H), 4.18 (d, J = 15.0 Hz, 1H), 3.45 (dd, J = 14.7, 6.0 Hz, 1H), 3.33 (dd, J = 14.7, 7.7 Hz, 1H), 2.57 (s, 3H), 2.26 (s, 3H), 1.85 (s, 3H). HRMS (ESI-TOF) m/z : [M + H]⁺ Calcd for C₂₃H₂₅N₂O₆ 425.1707; Found 425.1713.

N^o-Acetyl-1-(3-acetyl-2,6-dihydroxy-5-methylbenzyl)tryptophan ((±)-**65c**). The title compound was prepared using (±)-**65a** (0.178 mmol, 44.0 mg) and hydroxyclovatol (0.069 mmol, 13.5 mg) as reactants. The product was isolated in 14% yield (4.3 mg) as brown oil. Eluent: ACN/H₂O (55:45, v/v) supplied with 0.1% TFA. ¹H NMR (500 MHz, acetone-*d*₆) δ 13.31 (s, 1H), 7.71 (s, 1H), 7.70 (d, J = 8.2 Hz, 1H), 7.51 (d, J = 8.2 Hz, 1H), 7.29 (s, 1H), 7.09 (dd, J = 8.2, 7.0 Hz, 1H), 6.97 (dd, J = 8.2, 7.0 Hz, 1H), 5.33 (s, 2H), 4.68 (ddd, J = 8.2, 7.5, 5.6 Hz, 1H), 3.27 (dd, J = 14.7, 5.6 Hz, 1H), 3.10 (dd, J = 14.7, 7.5 Hz, 3H), 2.56 (s, 3H), 2.27 (s, 3H), 1.83 (s, 3H). ¹H NMR (500 MHz, DMSO-*d*₆) δ 13.19 (s, 1H), 8.06 (d, J = 8.4 Hz, 1H), 7.69 (s, 1H), 7.65 (d, J = 8.2 Hz, 1H), 7.48 (d, J = 8.2 Hz, 1H), 7.15 (s, 1H), 7.10 (dd, J = 8.2, 7.0 Hz, 1H), 6.98 (dd, J = 8.2, 7.0 Hz, 1H), 5.25 (s, 2H), 4.38 (td, J = 9.2, 5.1 Hz, 1H), 3.11 (dd, J = 15.0, 5.1 Hz, 1H), 2.90 (dd, J = 15.0, 9.2 Hz, 1H), 2.54 (s, 3H), 2.17 (s, 3H), 1.75 (s, 3H). ¹³C{¹H} NMR (125 MHz, DMSO-*d*₆) δ 203.4, 173.4, 169.0, 161.0, 161.0, 136.0, 133.1, 127.3, 127.2, 120.8, 118.3, 118.1, 116.1, 112.4, 111.1, 110.2, 109.1, 52.8, 37.5, 26.9, 26.2, 22.2, 16.2. HRMS (ESI-TOF) m/z : [M + H]⁺ Calcd for C₂₃H₂₅N₂O₆ 425.1707; Found 425.1708.

4-(2-(3-Acetyl-2,6-dihydroxy-5-methylbenzyl)-1H-indol-3-yl)-butanoic acid (**72b**). The title compound was prepared using **72a** (0.008 mmol, 1.6 mg) and hydroxyclovatol (0.008 mmol, 1.6 mg) as reactants. The product was isolated in 46% yield (1.4 mg) as brown oil. Eluent: ACN/H₂O (65:35, v/v) supplied with 0.1% TFA. ¹H NMR (500 MHz, CDCl₃) δ 13.30 (s, 1H), 8.57 (s, 1H), 7.49 (d, J = 8.0 Hz, 1H), 7.40 (s, 1H), 7.24 (d, J = 8.0 Hz, 1H), 7.08 (dd, J = 8.0, 7.0 Hz, 1H), 7.03 (dd, J = 8.0, 7.0 Hz, 1H), 4.14 (s, 2H), 2.95 (t, J = 7.0 Hz, 2H), 2.57 (s, 3H), 2.50 (t, J = 7.0 Hz, 2H), 2.18 (s, 3H), 2.07–2.01 (m, 2H). HRMS (ESI-TOF) m/z : [M + H]⁺ Calcd for C₂₂H₂₄NO₅ 382.1649; Found 382.1662.

(3*S*,6*S*)-3-((2-(3-Acetyl-2,6-dihydroxy-5-methylbenzyl)-1H-indol-3-yl)methyl)-6-isobutylpiperazine-2,5-dione (**76b**). The title compound was prepared using **76a** (0.016 mmol, 4.8 mg) and hydroxyclovatol (0.016 mmol, 3.2 mg) as reactants. The product was isolated in 13% yield (1.0 mg) as white amorphous solid. Eluent: ACN/H₂O (60:40, v/v). ¹H NMR (500 MHz, CDCl₃) δ 13.40 (s, 1H), 8.77 (s, 1H), 7.51 (d, J = 8.0 Hz, 1H), 7.46 (s, 1H), 7.25 (d, J = 8.0 Hz, 1H), 7.12 (dd, J = 8.0, 7.1 Hz, 1H), 7.07 (dd, J = 8.0, 7.1 Hz, 1H), 6.39 (s, 1H), 5.99 (s, 1H), 4.40 (d, J = 8.9 Hz, 1H), 4.16 (d, J = 15.0 Hz, 1H), 4.13 (d, J = 15.0 Hz, 1H), 3.94 (d, J = 10.0 Hz, 1H), 3.65 (dd, J = 14.8, 3.2 Hz, 1H), 3.28 (dd, J = 14.8, 8.9 Hz, 1H), 2.60 (s, 3H), 2.23 (s, 3H), 1.68–1.60 (m, 1H), 1.61–1.56 (m, 1H), 1.17 (ddd, 13.7, 10.0, 4.5 Hz, 1H), 0.86 (d, J = 6.2 Hz, 1H), 0.85 (d, J = 6.2 Hz, 1H). [α]_D²⁰ = −41 (c 0.1, CHCl₃); HRMS (ESI-TOF) m/z : [M + H]⁺ Calcd for C₂₇H₃₂N₃O₅ 478.2336; Found 478.2339.

(3*S*,6*S*)-3-((2-(3-Acetyl-2,6-dihydroxy-5-methylbenzyl)-1H-indol-3-yl)methyl)-6-benzylpiperazine-2,5-dione (**77b**). The title compound was prepared using **77a** (0.032 mmol, 10.7 mg) and hydroxyclovatol (0.032 mmol, 3.1 mg) as reactants. The product was isolated in 24% yield (2.0 mg) as white amorphous solid. Eluent: ACN/H₂O (55:45, v/v). ¹H NMR (500 MHz, DMSO-*d*₆) δ 13.04 (s, 1H), 9.96 (s, 1H), 9.63 (s, 1H), 7.94 (d, J = 3.0 Hz, 1H), 7.64 (d, J = 3.3 Hz, 1H), 7.62 (s, 1H), 7.43 (d, J = 7.6 Hz, 1H), 7.22 (d, J = 7.6 Hz, 1H), 7.16–7.10 (m, 3H), 6.95 (dd, J = 7.6, 6.5 Hz, 1H), 6.92 (dd, J = 7.6, 6.5 Hz, 1H), 6.62 (dd, J = 7.5, 2.3 Hz, 2H), 4.05 (d, J = 15.7 Hz, 1H), 4.07–4.04 (m, 1H), 4.01 (d, J = 15.7 Hz, 1H), 3.80–3.76 (m, 1H), 3.05 (dd, J = 14.7, 4.7 Hz, 1H), 2.98 (dd, J = 14.7, 5.4 Hz, 1H), 2.55 (s, 3H), 2.47 (m, 1H), 2.18 (s, 3H), 1.61 (dd, J = 13.7, 7.9 Hz, 1H). [α]_D²⁰ = −49 (c 0.2, MeOH); HRMS (ESI-TOF) m/z : [M + H]⁺ Calcd for C₃₀H₃₀N₃O₅ 512.2180; Found 512.2200.

3-((1*H*-Indol-3-yl)methyl)-6-((2-(3-acetyl-2,6-dihydroxy-5-methylbenzyl)-1*H*-indol-3-yl)methyl)piperazine-2,5-dione (**79b**). The title compound was prepared using **79a** (0.040 mmol, 14.9 mg) and hydroxyclovatol (0.033 mmol, 6.5 mg) as reactants. The product was isolated in 30% yield (5.4 mg) as white amorphous solid. Eluent:

ACN/H₂O (65:35, v/v). ¹H NMR (500 MHz, CDCl₃) δ 13.40 (s, 1H), 8.74 (s, 1H), 8.01 (s, 1H), 7.48 (s, 1H), 7.47 (d, J = 8.0, 1H), 7.46 (d, J = 8.2, 1H), 7.34 (d, J = 8.2 Hz, 1H), 7.24 (d, J = 8.0 Hz, 1H), 7.17 (dd, J = 8.2, 7.2 Hz, 1H), 7.11 (dd, J = 8.2, 7.2 Hz, 1H), 7.08 (dd, J = 8.0, 7.1 Hz, 1H), 7.05 (dd, J = 8.0, 7.1 Hz, 1H), 6.58 (s, 1H), 6.48 (s, 1H), 5.84 (s, 1H), 4.36 (d, J = 7.7 Hz, 1H), 4.20 (d, J = 10.1 Hz, 1H), 4.08 (d, J = 15.1 Hz, 1H), 4.04 (d, J = 15.1 Hz, 1H), 3.45 (dd, J = 14.7, 3.2 Hz, 1H), 3.30 (dd, J = 14.5, 3.2 Hz, 1H), 3.08 (dd, J = 14.5, 7.7 Hz, 1H), 2.61 (s, 3H), 2.27–2.24 (m, 1H), 2.23 (s, 3H). ¹H NMR (500 MHz, DMSO-*d*₆) δ 13.04 (s, 1H), 10.75 (d, J = 1.9 Hz, 1H), 9.92 (s, 1H), 9.61 (s, 1H), 7.85 (d, J = 2.5 Hz, 1H), 7.62 (s, 1H), 7.60 (d, J = 2.7 Hz, 1H), 7.30 (d, J = 8.0 Hz, 1H), 7.27 (d, J = 8.2 Hz, 1H), 7.25 (d, J = 8.2 Hz, 1H), 7.21 (d, J = 8.0 Hz, 1H), 6.98 (dd, J = 8.0, 7.0 Hz, 1H), 6.93 (dd, J = 8.0, 7.0 Hz, 1H), 6.90 (dd, J = 8.0, 7.0 Hz, 1H), 6.88 (dd, J = 8.0, 7.0 Hz, 1H), 6.37 (d, J = 2.1 Hz, 1H), 4.02 (dd, J = 8.1, 3.8 Hz, 1H), 3.97 (d, J = 15.4 Hz, 1H), 3.91 (d, J = 15.4 Hz, 1H), 3.81–3.76 (m, 1H), 2.99 (dd, J = 14.4, 4.6 Hz, 1H), 2.88 (dd, J = 14.4, 5.4 Hz, 1H), 2.71 (dd, J = 14.4, 3.8 Hz, 1H), 2.55 (s, 3H), 2.17 (s, 3H), 1.85 (dd, J = 14.4, 8.1 Hz, 1H). ¹³C{¹H} NMR (125 MHz, DMSO-*d*₆) δ 203.1, 167.0, 166.5, 160.7, 160.6, 136.1, 136.1, 135.2, 131.4, 128.4, 127.0, 124.2, 120.7, 119.8, 119.4, 118.2, 118.1, 118.0, 115.9, 112.5, 112.5, 111.1, 110.8, 108.8, 104.9, 55.9, 55.3, 30.6, 30.6, 26.2, 19.3, 16.2. [α]_D²⁰ = −38 (c 0.1, CHCl₃); HRMS (ESI-TOF) m/z : [M + H]⁺ Calcd for C₃₂H₃₁N₄O₅ 551.2289; Found 551.2313.

(3*S*,5*S*,10*bS*,11*aS*)-3-((1*H*-Indol-3-yl)methyl)-10*b*-(3-acetyl-2,6-dihydroxy-5-methylbenzyl)-2,3,6,10*b*,11,11*a*-hexahydro-4*H*-pyrazino[1',2':1,5]pyrrolo[2,3-*b*]indole-1,4(5*aH*)-dione (**79c**). The title compound was prepared using **79a** (0.040 mmol, 14.9 mg) and hydroxyclovatol (0.033 mmol, 6.5 mg) as reactants. The product was isolated in 3% yield (0.6 mg) as white amorphous solid. Eluent: ACN/H₂O (65:35, v/v). ¹H NMR (500 MHz, CDCl₃) δ 13.01 (s, 1H), 8.11 (s, 1H), 7.51 (d, J = 8.0 Hz, 1H), 7.44 (s, 1H), 7.38 (d, J = 8.0 Hz, 1H), 7.21 (dd, J = 8.0, 7.0 Hz, 1H), 7.15 (dd, J = 8.0, 7.0 Hz, 1H), 7.11 (d, J = 8.0 Hz, 1H), 7.10 (dd, J = 8.0, 7.0 Hz, 1H), 7.06 (s, 1H), 6.82 (dd, J = 8.0, 7.0 Hz, 1H), 6.72 (d, J = 8.0 Hz, 1H), 5.60 (s, 1H), 5.47 (s, 1H), 4.29 (d, J = 11.0 Hz, 1H), 3.92 (dd, J = 11.3, 5.8 Hz, 1H), 3.69 (dd, J = 15.0, 3.5 Hz, 1H), 3.21 (d, J = 14.0 Hz, 1H), 2.97 (d, J = 14.0 Hz, 1H), 2.90 (dd, J = 15.0, 11.0 Hz, 1H), 2.74 (dd, J = 13.2, 5.8 Hz, 1H), 2.57 (s, 3H), 2.37 (dd, J = 13.2, 11.3 Hz, 1H), 2.18 (s, 3H). [α]_D²⁰ = −58 (c 0.06, CHCl₃); HRMS (ESI-TOF) m/z : [M + H]⁺ Calcd for C₃₂H₃₁N₄O₅ 551.2289; Found 551.2314.

(3*S*,5*S*,10*bS*,11*aS*)-10*b*-(3-Acetyl-2,6-dihydroxy-5-methylbenzyl)-3-((2-(3-acetyl-2,6-dihydroxy-5-methylbenzyl)-1*H*-indol-3-yl)methyl)-2,3,6,10*b*,11,11*a*-hexahydro-4*H*-pyrazino[1',2':1,5]pyrrolo[2,3-*b*]indole-1,4(5*aH*)-dione (**79d**). The title compound was prepared using **79a** (0.040 mmol, 14.9 mg) and hydroxyclovatol (0.033 mmol, 6.5 mg) as reactants. The product was isolated in 4% yield (1.0 mg) as white amorphous solid. Eluent: ACN/H₂O (65:35, v/v). ¹H NMR (500 MHz, CDCl₃) δ 12.98 (s, 1H), 12.92 (s, 1H), 8.18 (s, 1H), 7.59 (d, J = 8.0 Hz, 1H), 7.42 (s, 1H), 7.40 (d, J = 8.0 Hz, 1H), 7.24–7.21 (m, 1H), 7.19 (t, J = 7.5, 1H), 7.12 (dd, J = 8.0, 7.0 Hz, 1H), 7.12 (s, 1H), 6.89 (d, J = 7.5 Hz, 1H), 6.79 (d, J = 7.5 Hz, 1H), 6.71 (t, J = 7.5 Hz, 1H), 5.69 (s, 1H), 5.52 (s, 1H), 4.76 (d, J = 15.2 Hz, 1H), 4.54 (d, J = 15.2 Hz, 1H), 4.46 (dd, J = 10.0, 3.4 Hz, 1H), 3.99 (dd, J = 11.9, 5.5 Hz, 1H), 3.70 (dd, J = 15.0, 3.4 Hz, 1H), 3.12 (dd, J = 15.0, 10.0 Hz, 1H), 2.78 (s, 2H), 2.69 (dd, J = 13.0, 5.5 Hz, 1H), 2.55 (s, 3H), 2.51 (s, 3H), 2.28 (s, 3H), 2.04 (dd, J = 13.0, 11.9 Hz, 1H), 1.99 (s, 3H). [α]_D²⁰ = −63 (c 0.1, CHCl₃); HRMS (ESI-TOF) m/z : [M + H]⁺ Calcd for C₄₂H₄₁N₄O₈ 729.2919; Found 729.2932.

(*R*)-3-((2-(3-Acetyl-2,6-dihydroxy-5-methylbenzyl)-1*H*-indol-3-yl)methyl)-3,4-dihydro-1*H*-benzo[e][1,4]diazepine-2,5-dione (**80b**). The title compound was prepared using **80a** (0.080 mmol, 24.5 mg) and hydroxyclovatol (0.051 mmol, 10.0 mg) as reactants. The product was isolated in 21% yield (5.3 mg) as white amorphous solid. Eluent: ACN/H₂O (55:45, v/v). ¹H NMR (500 MHz, acetone-*d*₆) δ 13.30 (s, 1H), 9.71 (s, 1H), 9.52 (s, 1H), 7.71 (d, J = 8.0 Hz, 1H), 7.62 (s, 1H), 7.52 (dd, J = 8.0, 7.2 Hz, 1H), 7.45 (d, J = 8.0 Hz, 1H), 7.23 (d, J = 8.0 Hz, 1H), 7.21 (d, J = 8.0 Hz, 1H), 7.20 (dd, J = 8.0, 7.2 Hz,

1H), 6.93 (dd, $J = 8.0, 7.0$ Hz, 1H), 6.84 (dd, $J = 8.0, 7.0$ Hz, 1H), 4.28 (d, $J = 15.0$ Hz, 1H), 4.25 (dd, $J = 9.0, 5.9$ Hz, 1H), 4.22 (d, $J = 15.0$ Hz, 1H), 3.51 (dd, $J = 15.0, 5.9$ Hz, 1H), 3.34 (dd, $J = 15.0, 9.0$ Hz, 1H), 2.56 (s, 3H), 2.24 (s, 3H). $^{13}\text{C}\{^1\text{H}\}$ NMR (125 MHz, acetone- d_6) δ 203.9, 172.7, 168.5, 161.4, 161.4, 137.5, 136.6, 136.5, 133.3, 132.4, 131.8, 128.9, 127.1, 125.1, 121.9, 121.6, 119.5, 118.5, 117.0, 114.2, 113.8, 111.7, 106.3, 53.2, 26.4, 24.4, 20.2, 16.3. $[\alpha]_{\text{D}}^{20} = -52$ (c 0.1, acetone); HRMS (ESI-TOF) m/z : $[\text{M} + \text{H}]^+$ Calcd for $\text{C}_{28}\text{H}_{26}\text{N}_3\text{O}_5$, 484.1867; Found 484.1870.

(5*aS*, 13*aR*, 14*aS*)-14*a*-(3-Acetyl-2,6-dihydroxy-5-methylbenzyl)-5*a*, 13*a*, 14, 14*a*-tetrahydrobenzo[5',6']-[1,4]diazepino[1',2':1,5]-pyrrolo[2,3-*b*]indole-7,13(5*H*,12*H*)-dione (80*c*). The title compound was prepared using 80*a* (0.080 mmol, 24.5 mg) and hydroxycyclavotol (0.051 mmol, 10.0 mg) as reactants. The product was isolated in 4% yield (1.0 mg) as white amorphous solid. Eluent: ACN/H₂O (55:45, v/v). ^1H NMR (500 MHz, acetone- d_6) δ 13.14 (s, 1H), 9.54 (s, 1H), 8.63 (s, 1H), 7.76 (d, $J = 8.0$ Hz, 1H), 7.64 (s, 1H), 7.48 (dd, $J = 8.0, 7.3$ Hz, 1H), 7.20 (dd, $J = 8.0, 7.3$ Hz, 1H), 7.16 (dd, $J = 8.2$ Hz, 1H), 7.12 (d, $J = 8.0$ Hz, 1H), 6.97 (dd, $J = 8.2, 7.7$ Hz, 1H), 6.67 (d, $J = 8.2$ Hz, 1H), 6.61 (dd, $J = 8.2, 7.7$ Hz, 1H), 6.31 (s, 1H), 5.65 (s, 1H), 4.01 (dd, $J = 8.2, 7.0$ Hz, 1H), 3.22 (d, $J = 14.0$ Hz, 1H), 3.17 (d, $J = 14.0$ Hz, 1H), 3.17 (dd, $J = 14.0, 7.0$ Hz, 1H), 2.56 (s, 3H), 2.47 (dd, $J = 14.0, 8.2$ Hz, 1H), 2.25 (s, 1H). $[\alpha]_{\text{D}}^{20} = -47$ (c 0.1, acetone); HRMS (ESI-TOF) m/z : $[\text{M} + \text{H}]^+$ Calcd for $\text{C}_{28}\text{H}_{26}\text{N}_3\text{O}_5$, 484.1867; Found 484.1874.

1-(3-((2-Amino-4-hydroxyquinolin-3-yl)methyl)-2,4-dihydroxy-5-methylphenyl)ethan-1-one (95*b*). The title compound was prepared using 95*a* (0.128 mmol, 20.6 mg) and hydroxycyclavotol (0.058 mmol, 11.3 mg) as reactants. The product was isolated in 46% yield (9.0 mg) as brown amorphous solid. Eluent: ACN/H₂O (75:25, v/v) supplied with 0.1% TFA. ^1H NMR (500 MHz, DMSO- d_6) δ 13.93 (s, 1H), 11.52 (s, 1H), 8.05 (d, $J = 8.2$ Hz, 1H), 7.56 (s, 1H), 7.55 (dd, $J = 8.2, 7.1$ Hz, 1H), 7.36 (d, $J = 8.2$ Hz, 1H), 7.25 (dd, $J = 8.2, 7.1$ Hz, 1H), 6.67 (s, 2H), 3.70 (s, 2H), 2.53 (s, 3H), 2.08 (s, 3H). $^{13}\text{C}\{^1\text{H}\}$ NMR (125 MHz, DMSO- d_6) δ 202.9, 174.0, 164.1, 159.4, 153.0, 136.9, 130.9, 130.8, 124.4, 122.3, 120.6, 117.7, 116.3, 113.1, 111.0, 101.0, 25.8, 17.6, 15.9. HRMS (ESI-TOF) m/z : $[\text{M} + \text{H}]^+$ Calcd for $\text{C}_{19}\text{H}_{19}\text{N}_2\text{O}_4$, 339.1339; Found 339.1357.

1-(2,4-Dihydroxy-3-((5-hydroxyquinolin-8-yl)methyl)-5-methylphenyl)ethan-1-one (98*b*). The title compound was prepared using 98*a* (0.157 mmol, 22.9 mg) and hydroxycyclavotol (0.059 mmol, 11.5 mg) as reactants. The product was isolated in 38% yield (7.1 mg) as yellow amorphous solid. Eluent: ACN/H₂O (80:20, v/v) supplied with 0.1% TFA. ^1H NMR (500 MHz, DMSO- d_6) δ 13.19 (s, 1H), 10.59 (s, 1H), 9.01 (dd, $J = 4.5, 1.7$ Hz, 1H), 8.69 (dd, $J = 8.4, 1.7$ Hz, 1H), 7.75 (d, $J = 8.0$ Hz, 1H), 7.63 (dd, $J = 8.4, 4.5$ Hz, 1H), 7.55 (s, 1H), 6.96 (d, $J = 8.0$ Hz, 1H), 4.23 (s, 2H), 2.51 (s, 3H), 2.12 (s, 3H). $^{13}\text{C}\{^1\text{H}\}$ NMR (125 MHz, DMSO- d_6) δ 203.1, 161.2, 160.9, 152.0, 148.6, 144.4, 133.7, 132.1, 130.7, 126.9, 120.2, 120.1, 117.3, 114.1, 112.0, 109.0, 26.1, 24.5, 15.9. HRMS (ESI-TOF) m/z : $[\text{M} + \text{H}]^+$ Calcd for $\text{C}_{19}\text{H}_{18}\text{NO}_4$, 324.1230; Found 324.1235.

5-(3-Acetyl-2,6-dihydroxy-5-methylbenzyl)-2-aminobenzoic acid (101*b*). The title compound was prepared using 101*a* (0.167 mmol, 23.0 mg) and hydroxycyclavotol (0.066 mmol, 12.9 mg) as reactants. The product was isolated in 23% yield (4.7 mg) as brown amorphous solid. Eluent: ACN/H₂O (65:35, v/v) supplied with 0.1% TFA. ^1H NMR (500 MHz, acetone- d_6) δ 13.08 (s, 1H), 7.72 (d, $J = 2.1$ Hz, 1H), 7.62 (s, 1H), 7.37 (dd, $J = 8.4, 2.1$ Hz, 1H), 6.68 (d, $J = 8.4$ Hz, 1H), 3.95 (s, 2H), 2.56 (s, 3H), 2.24 (s, 3H). $^{13}\text{C}\{^1\text{H}\}$ NMR (125 MHz, acetone- d_6) δ 204.0, 163.7, 162.0, 161.6, 146.0, 136.8, 132.2, 132.1, 129.8, 116.4, 115.5, 114.0, 114.0, 112.6, 27.9, 26.4, 16.3. HRMS (ESI-TOF) m/z : $[\text{M} + \text{H}]^+$ Calcd for $\text{C}_{17}\text{H}_{18}\text{NO}_5$, 316.1179; Found 316.1169.

2-((3-Acetyl-2,6-dihydroxy-5-methylbenzyl)amino)benzoic acid (101*c*). The title compound was prepared using 101*a* (0.167 mmol, 23.0 mg) and hydroxycyclavotol (0.066 mmol, 12.9 mg) as reactants. The product was isolated in 6% yield (1.2 mg) as brown amorphous solid. Eluent: ACN/H₂O (65:35, v/v) supplied with 0.1% TFA. ^1H NMR (500 MHz, acetone- d_6) δ 13.23 (s, 1H), 7.89 (d, $J = 8.0$ Hz, 1H), 7.68 (s, 1H), 7.37 (dd, $J = 8.0, 7.1$ Hz, 1H), 7.05 (d, $J = 8.0$ Hz,

1H), 6.59 (dd, $J = 8.0, 7.1$ Hz, 1H), 4.51 (s, 2H), 2.56 (s, 3H), 2.21 (s, 3H). HRMS (ESI-TOF) m/z : $[\text{M} + \text{H}]^+$ Calcd for $\text{C}_{17}\text{H}_{18}\text{NO}_5$, 316.1179; Found 316.1181.

5-(3-Acetyl-2,6-dihydroxy-5-methylbenzyl)-2-((3-acetyl-2,6-dihydroxy-5-methylbenzyl)amino)benzoic acid (101*d*). The title compound was prepared using 101*a* (0.167 mmol, 23.0 mg) and hydroxycyclavotol (0.066 mmol, 12.9 mg) as reactants. The product was isolated in 3% yield (0.9 mg) as yellow amorphous solid. Eluent: ACN/H₂O (65:35, v/v) supplied with 0.1% TFA. ^1H NMR (500 MHz, acetone- d_6) δ 13.21 (s, 1H), 13.06 (s, 1H), 7.89 (d, $J = 2.1$ Hz, 1H), 7.64 (s, 1H), 7.59 (s, 1H), 7.32 (dd, $J = 8.6, 2.1$ Hz, 1H), 6.92 (d, $J = 8.6$ Hz, 1H), 4.49 (s, 2H), 3.91 (s, 2H), 2.55 (s, 3H), 2.54 (s, 3H), 2.22 (s, 3H), 2.17 (s, 3H). HRMS (ESI-TOF) m/z : $[\text{M} + \text{H}]^+$ Calcd for $\text{C}_{27}\text{H}_{28}\text{NO}_8$, 494.1809; Found 494.1823.

1-(3-(((1,3-Dihydroxy-2-(hydroxymethyl)propan-2-yl)amino)-methyl)-2,4-dihydroxy-5-methylphenyl)ethan-1-one (102*b*). The title compound was prepared by using 102*a* (1.0 mmol, 122.0 mg, prepared as Tris-HCl buffer, pH 7.5) and hydroxycyclavotol (0.066 mmol, 12.9 mg) as reactants. The product was isolated in 16% yield (3.2 mg) as brown oil. Eluent: ACN/H₂O (70:30, v/v) supplied with 0.1% TFA. ^1H NMR (500 MHz, CD₃OD) δ 7.72 (s, 1H), 4.49 (s, 2H), 3.82 (s, 6H), 2.56 (s, 3H), 2.22 (s, 3H). $^{13}\text{C}\{^1\text{H}\}$ NMR (125 MHz, CD₃OD) δ 204.9, 162.5, 162.4, 135.5, 117.3, 114.4, 107.3, 67.5, 59.7, 59.7, 59.7, 36.5, 26.3, 16.1. HRMS (ESI-TOF) m/z : $[\text{M} + \text{H}]^+$ Calcd for $\text{C}_{14}\text{H}_{22}\text{NO}_6$, 300.1442; Found 300.1445.

α -Glucosidase Inhibition Assay. The α -glucosidase inhibition activity was evaluated by modified procedures reported previously.^{38,39} The assays contained 100 mM phosphate buffer (pH 6.8), α -glucosidase (1.3 U/mL) (Sigma-Aldrich, St. Louis, USA), and 10 μL of a 2 mM DMSO solution of compounds to be tested. After preincubation at 37 °C for 15 min, the assays were initiated by addition of 40 μL of 2.5 mM *p*-nitrophenyl- α -D-glucopyranoside solution (Sigma-Aldrich, St. Louis, USA) to a final volume of 150 μL . After incubation at 37 °C for a further 15 min, the absorbance at 405 nm was recorded on a microplate reader (BMG Labtech, Offenburg, Germany). DMSO was used as a negative control, and acarbose (TCI Europe, Zwiindrecht, Belgium) was used as positive control. All assays were performed in triplicate. The IC₅₀ value was determined by regression analysis.^{40,41}

■ ASSOCIATED CONTENT

Supporting Information

The Supporting Information is available free of charge at <https://pubs.acs.org/doi/10.1021/acs.joc.9b02971>.

Chemical synthesis of hydroxycyclavotol, structural overview of all reactants, LC-MS chromatograms of selected reactions, NMR spectra of coupling products (PDF)

■ AUTHOR INFORMATION

Corresponding Author

*E-mail: shuming.li@staff.uni-marburg.de.

ORCID

Shu-Ming Li: 0000-0003-4583-2655

Author Contributions

[†]G.L. and J.F. contributed equally to this work.

Notes

The authors declare no competing financial interest.

■ ACKNOWLEDGMENTS

We thank Rixa Kraut and Stefan Newel (University of Marburg) for taking MS and NMR spectra, respectively. S.-M.L. acknowledges the DFG for funding the Bruker microTOF QIII mass spectrometer (INST 160/620-1). G.L. (201607565014) and J.F. (201507565006) are scholarship recipients from the China Scholarship Council.

REFERENCES

- (1) Van De Water, R. W.; Pettus, T. R. R. *o*-Quinone methides: intermediates underdeveloped and underutilized in organic synthesis. *Tetrahedron* **2002**, *58* (27), 5367–5406.
- (2) Bai, W. J.; David, J. G.; Feng, Z. G.; Weaver, M. G.; Wu, K. L.; Pettus, T. R. R. The domestication of *ortho*-quinone methides. *Acc. Chem. Res.* **2014**, *47* (12), 3655–3664.
- (3) Nielsen, C. D. T.; Abas, H.; Spivey, A. C. Stereoselective reactions of *ortho*-quinone methide and *ortho*-quinone methide imines and their utility in natural product synthesis. *Synthesis* **2018**, *50* (20), 4008–4018.
- (4) Pathak, T. P.; Sigman, M. S. Applications of *ortho*-quinone methide intermediates in catalysis and asymmetric synthesis. *J. Org. Chem.* **2011**, *76* (22), 9210–9215.
- (5) Willis, N. J.; Bray, C. D. *ortho*-Quinone methides in natural product synthesis. *Chem. - Eur. J.* **2012**, *18* (30), 9160–9173.
- (6) Spence, J. T.; George, J. H. Biomimetic total synthesis of entpenilactone A and penilactone B. *Org. Lett.* **2013**, *15* (15), 3891–3893.
- (7) Spence, J. T.; George, J. H. Total synthesis of peniphenones A-D via biomimetic reactions of a common *o*-quinone methide intermediate. *Org. Lett.* **2015**, *17* (24), 5970–5973.
- (8) Forest, K.; Wan, P.; Preston, C. M. Catechin and hydroxybenzhydrols as models for the environmental photochemistry of tannins and lignins. *Photochem. Photobiol. Sci.* **2004**, *3* (5), 463–472.
- (9) Chen, Y.; Steinmetz, M. G. Photoactivation of amino-substituted 1,4-benzoquinones for release of carboxylate and phenolate leaving groups using visible light. *J. Org. Chem.* **2006**, *71* (16), 6053–6060.
- (10) Bishop, L. M.; Winkler, M.; Houk, K. N.; Bergman, R. G.; Trauner, D. Mechanistic investigations of the acid-catalyzed cyclization of a vinyl *ortho*-quinone methide. *Chem. - Eur. J.* **2008**, *14* (18), 5405–5408.
- (11) Patel, A.; Netscher, T.; Rosenau, T. Stabilization of *ortho*-quinone methides by a bis (sulfonium ylide) derived from 2, 5-dihydroxy-[1, 4] benzoquinone. *Tetrahedron Lett.* **2008**, *49* (15), 2442–2445.
- (12) Fan, J.; Liao, G.; Kindinger, F.; Ludwig-Radtke, L.; Yin, W.-B.; Li, S.-M. Peniphenone and penilactone formation in *Penicillium crustosum* via 1,4-Michael additions of *ortho*-quinone methide from hydroxycyclavotol to γ -butyrolactones from crustosic acid. *J. Am. Chem. Soc.* **2019**, *141*, 4225–4229.
- (13) Huang, C.; Yang, C.; Zhang, W.; Zhang, L.; De, B. C.; Zhu, Y.; Jiang, X.; Fang, C.; Zhang, Q.; Yuan, C. S.; Liu, H. W.; Zhang, C. Molecular basis of dimer formation during the biosynthesis of benzofluorene-containing atypical angucyclines. *Nat. Commun.* **2018**, *9* (1), 2088.
- (14) Wu, G.; Ma, H.; Zhu, T.; Li, J.; Gu, Q.; Li, D. Penilactones A and B, two novel polyketides from Antarctic deep-sea derived fungus *Penicillium crustosum* PRB-2. *Tetrahedron* **2012**, *68*, 9745–9749.
- (15) Tomoda, H.; Tabata, N.; Masuma, R.; Si, S. Y.; Omura, S. Erabulenols, inhibitors of cholesterol ester transfer protein produced by *Penicillium* sp. FO-5637. I. Production, isolation and biological properties. *J. Antibiot.* **1998**, *51* (7), 618–623.
- (16) da Silva, B. F.; Rodrigues-Fo, E. Production of a benzylated flavonoid from 5,7,3',4',5'-pentamethoxyflavanone by *Penicillium griseoreseum*. *J. Mol. Catal. B: Enzym.* **2010**, *67* (3–4), 184–188.
- (17) Wang, J.; Liu, P.; Wang, Y.; Wang, H.; Li, J.; Zhuang, Y.; Zhu, W. Antimicrobial aromatic polyketides from Gorgonian-associated fungus, *Penicillium commune* 518. *Chin. J. Chem.* **2012**, *30*, 1236–1242.
- (18) Li, H.; Jiang, J.; Liu, Z.; Lin, S.; Xia, G.; Xia, X.; Ding, B.; He, L.; Lu, Y.; She, Z. Peniphenones A-D from the mangrove fungus *Penicillium dipodomycicola* HN4–3A as inhibitors of *Mycobacterium tuberculosis* phosphatase MptpB. *J. Nat. Prod.* **2014**, *77* (4), 800–806.
- (19) Sun, W.; Chen, X.; Tong, Q.; Zhu, H.; He, Y.; Lei, L.; Xue, Y.; Yao, G.; Luo, Z.; Wang, J.; Li, H.; Zhang, Y. Novel small molecule 11 β -HSD1 inhibitor from the endophytic fungus *Penicillium commune*. *Sci. Rep.* **2016**, *6*, 26418.
- (20) Yu, G.; Sun, Z.; Peng, J.; Zhu, M.; Che, Q.; Zhang, G.; Zhu, T.; Gu, Q.; Li, D. Secondary metabolites produced by combined culture of *Penicillium crustosum* and a *Xylaria* sp. *J. Nat. Prod.* **2019**, *82* (7), 2013–2017.
- (21) Davies, M. W.; Maskell, L.; Shipman, M.; Slawin, A. M.; Vidot, S. M.; Whatmore, J. L. Studies toward the synthesis of luminacin D: assembly of simplified analogues devoid of the epoxide displaying antiangiogenic activity. *Org. Lett.* **2004**, *6* (22), 3909–3912.
- (22) Walsh, C. T. Biological matching of chemical reactivity: pairing indole nucleophilicity with electrophilic isoprenoids. *ACS Chem. Biol.* **2014**, *9* (12), 2718–2728.
- (23) Alkhalaf, L. M.; Ryan, K. S. Biosynthetic manipulation of tryptophan in bacteria: Pathways and mechanisms. *Chem. Biol.* **2015**, *22* (3), 317–328.
- (24) Steinmetz, H.; Zander, W.; Shushni, M. A. M.; Jansen, R.; Gerth, K.; Dehn, R.; Dräger, G.; Kirschning, A.; Müller, R. Precursor-directed syntheses and biological evaluation of new elansolid derivatives. *ChemBioChem* **2012**, *13* (12), 1813–1817.
- (25) Jansen, R.; Gerth, K.; Steinmetz, H.; Reinecke, S.; Kessler, W.; Kirschning, A.; Müller, R. Elansolid A3, a unique *p*-quinone methide antibiotic from *Chitinophaga sancti*. *Chem. - Eur. J.* **2011**, *17* (28), 7739–7744.
- (26) Dehn, R.; Katsuyama, Y.; Weber, A.; Gerth, K.; Jansen, R.; Steinmetz, H.; Höfle, G.; Müller, R.; Kirschning, A. Molecular basis of elansolid biosynthesis: evidence for an unprecedented quinone methide initiated intramolecular Diels-Alder cycloaddition/macrolactonization. *Angew. Chem., Int. Ed.* **2011**, *50* (17), 3882–3887.
- (27) Ohashi, M.; Liu, F.; Hai, Y.; Chen, M.; Tang, M. C.; Yang, Z.; Sato, M.; Watanabe, K.; Houk, K. N.; Tang, Y. SAM-dependent enzyme-catalyzed pericyclic reactions in natural product biosynthesis. *Nature* **2017**, *549* (7673), 502–506.
- (28) Liu, Y.; Zou, L.; Ma, L.; Chen, W.-H.; Wang, B.; Xu, Z.-L. Synthesis and pharmacological activities of xanthone derivatives as α -glucosidase inhibitors. *Bioorg. Med. Chem.* **2006**, *14* (16), 5683–5690.
- (29) Grover, P. K.; Shah, G. D.; Shah, R. C. Xanthenes. Part IV. A new synthesis of hydroxyxanthenes and hydroxybenzophenones. *J. Chem. Soc.* **1955**, 3982–3985.
- (30) Morkunas, M.; Dube, L.; Gotz, F.; Maier, M.-E. Synthesis of the acylphloroglucinols rhodomyrtonone and rhodomyrtonone B. *Tetrahedron* **2013**, *69* (40), 8559–8563.
- (31) Pepper, H. P.; Lam, H. C.; Bloch, W. M.; George, J. H. Biomimetic total synthesis of (\pm)-garcibracteatone. *Org. Lett.* **2012**, *14* (19), 5162–5164.
- (32) Caballero, E.; Avedaño, C.; Menéndez, J. C. Stereochemical issues related to the synthesis and reactivity of pyrazino[2',1'-5,1]pyrrolo[2,3-b]indole-1,4-diones. *Tetrahedron: Asymmetry* **1998**, *9* (6), 967–981.
- (33) Cacciatore, I.; Cocco, A.; Costa, M.; Fontana, M.; Lucente, G.; Pecci, L.; Pinnen, F. Biochemical properties of new synthetic carnosine analogues containing the residue of 2,3-diaminopropionic acid: the effect of N-acetylation. *Amino Acids* **2005**, *28* (1), 77–83.
- (34) George, J.-H.; Hesse, M.-D.; Baldwin, E.; Adlington, R.-M. Biomimetic synthesis of polycyclic polyprenylated acylphloroglucinol natural products isolated from *Hypericum papuanum*. *Org. Lett.* **2010**, *12* (15), 3532–3535.
- (35) Kasai, S.; Watanabe, S.; Kawabata, J.; Tahara, S.; Mizutani, J. Antimicrobial catechin derivatives of *Agrimonia pilosa*. *Phytochemistry* **1992**, *31* (3), 787–789.
- (36) Kim, H. W.; Park, J.; Kang, K. B.; Kim, T. B.; Oh, W. K.; Kim, J.; Sung, S. H. Acylphloroglucinolated catechin and phenylethyl isocoumarin derivatives from *Agrimonia pilosa*. *J. Nat. Prod.* **2016**, *79* (9), 2376–2383.
- (37) Liao, G.; Mai, P.; Fan, J.; Zocher, G.; Stehle, T.; Li, S.-M. Complete decoration of the indolyl residue in *cyclo*-L-Trp-L-Trp with geranyl moieties by using engineered dimethylallyl transferases. *Org. Lett.* **2018**, *20*, 7201–7205.
- (38) Matsui, T.; Yoshimoto, C.; Osajima, K.; Oki, T.; Osajima, Y. *In vitro* survey of α -glucosidase inhibitory food components. *Biosci., Biotechnol., Biochem.* **1996**, *60* (12), 2019–2022.

(39) Matsui, T.; Oki, T.; Osajima, Y. Isolation and identification of peptidic α -glucosidase inhibitors derived from sardine muscle hydrolyzate. *Z. Naturforsch., C: J. Biosci.* **1999**, *54* (3–4), 259–263.

(40) Rivera-Chávez, G.; González-Andrade, M.; González, M. d. C.; Glenn, A. E.; Mata, R. Thielavins A, J and K: α -glucosidase inhibitors from MEXU 27095, an endophytic fungus from *Hintonia latiflora*. *Phytochemistry* **2013**, *94*, 198–205.

(41) Rivera-Chávez, G.; Figueroa, M.; González, M. d. C.; Glenn, A. E.; Mata, R. α -Glucosidase inhibitors from a *Xylaria feejeensis* associated with *Hintonia latiflora*. *J. Nat. Prod.* **2015**, *78* (4), 730–735.

Supporting Information

Increasing structural diversity of natural products by Michael addition with *ortho*-quinone methide as the acceptor

Ge Liao,[†] Jie Fan,[†] Lena Ludwig-Radtke, Katja Backhaus, and Shu-Ming Li*

Institut für Pharmazeutische Biologie und Biotechnologie, Philipps-Universität Marburg, Robert-Koch Straße 4, Marburg 35037, Germany

Corresponding Author

*E-mail: shuming.li@staff.uni-marburg.de

[†]These authors contributed equally to this work.

Table of contents

Chemical synthesis of hydroxyclovatol.	S5
Scheme S1 Chemical synthesis of hydroxyclovatol.....	S5
Figure S1. Examples of fungal clavatul-containing natural products.	S6
Figure S2. Structures of tested reactants with conversions between 10% – 55%.	S7
Figure S3. Structures of tested reactants with conversions between 1% – 10% (A), and only detected by EIC of $[M+H]^+/[M-H]^-$ ions (B).	S8
Figure S4. Structures of tested reactants with no detectable product by EIC of $[M+H]^+/[M-H]^-$ ions. .	S9
Figure S5. LC-MS analysis of reaction mixtures of hydroxyclovatol with different reactants.	S10
Figure S6. LC-MS analysis of reaction mixtures of hydroxyclovatol with different reactants.	S11
Figure S7. LC-MS analysis of reaction mixtures of hydroxyclovatol with different reactants.	S12
Figure S8. LC-MS analysis of reaction mixtures of hydroxyclovatol with different reactants.	S13
Figure S9. Conversions of hydroxyclovatol reactions with nitrogen-free reactants at 25 °C (left) or 95 °C (right).	S14
Figure S10. Conversions of hydroxyclovatol reactions with nitrogen-containing reactants at 25 °C (left) or 95 °C (right).	S15
Figure S11. Reaction mechanisms of different nucleophile additions to the <i>ortho</i> -quinone methide intermediate.	S16
Figure S12. ^1H NMR spectrum of 2b in DMSO- d_6 (500 MHz).	S17
Figure S13. $^{13}\text{C}\{^1\text{H}\}$ NMR spectrum of 2b in DMSO- d_6 (125 MHz).	S17
Figure S14. HMBC spectrum of 2b in DMSO- d_6	S18
Figure S15. ^1H NMR spectrum of 6b in DMSO- d_6 (500 MHz).	S18
Figure S16. $^{13}\text{C}\{^1\text{H}\}$ NMR spectrum of 6b in DMSO- d_6 (125 MHz).	S19
Figure S17. HMBC spectrum of 6b in DMSO- d_6	S19
Figure S18. ^1H NMR spectrum of 6c in DMSO- d_6 (500 MHz).	S20
Figure S19. $^{13}\text{C}\{^1\text{H}\}$ NMR spectrum of 6c in DMSO- d_6 (125 MHz).	S20
Figure S20. HMBC spectrum of 6c in DMSO- d_6	S21
Figure S21. ^1H NMR spectrum of 14b in acetone- d_6 (500 MHz).	S21
Figure S22. ^1H NMR spectrum of 14b in pyridine- d_5 (500 MHz).	S22
Figure S23. ^1H NMR spectrum of 14b in DMSO- d_6 (500 MHz).	S22
Figure S24. $^{13}\text{C}\{^1\text{H}\}$ NMR spectrum of 14b in DMSO- d_6 (125 MHz).	S23
Figure S25. HMBC spectrum of 14b in DMSO- d_6	S23
Figure S26. ^1H NMR spectrum of 14c in acetone- d_6 (500 MHz).	S24
Figure S27. ^1H NMR spectrum of 17b in DMSO- d_6 (500 MHz).	S24
Figure S28. $^{13}\text{C}\{^1\text{H}\}$ NMR spectrum of 17b in DMSO- d_6 (125 MHz).	S25
Figure S29. HMBC spectrum of 17b in DMSO- d_6	S25
Figure S30. ^1H NMR spectrum of 17b in acetone- d_6 (500 MHz).	S26
Figure S31. ^1H NMR spectrum of 17c in acetone- d_6 (500 MHz).	S26
Figure S32. ^1H NMR spectrum of 18b in DMSO- d_6 (500 MHz).	S27
Figure S33. $^{13}\text{C}\{^1\text{H}\}$ NMR spectrum of 18b in DMSO- d_6 (125 MHz).	S27
Figure S34. HMBC spectrum of 18b in DMSO- d_6	S28
Figure S35. ^1H NMR spectrum of 29b in CDCl_3 (500 MHz).	S28

SUPPORTING INFORMATION

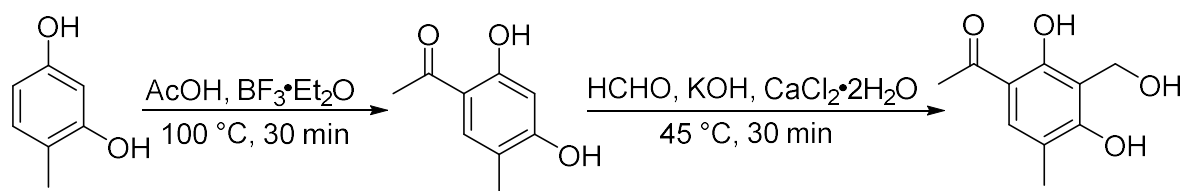
Figure S36. $^{13}\text{C}\{^1\text{H}\}$ NMR spectrum of 29b in CDCl_3 (125 MHz).....	S29
Figure S37. HMBC spectrum of 29b in CDCl_3	S29
Figure S38. ^1H NMR spectrum of 35b in $\text{DMSO}-d_6$ (500 MHz).....	S30
Figure S39. $^{13}\text{C}\{^1\text{H}\}$ NMR spectrum of 35b in $\text{DMSO}-d_6$ (125 MHz).....	S30
Figure S40. HMBC spectrum of 35b in $\text{DMSO}-d_6$	S31
Figure S41. ^1H NMR spectrum of 41b in $\text{DMSO}-d_6$ (500 MHz).....	S31
Figure S42. $^{13}\text{C}\{^1\text{H}\}$ NMR spectrum of 41b in $\text{DMSO}-d_6$ (125 MHz).....	S32
Figure S43. HMBC spectrum of 41b in $\text{DMSO}-d_6$	S32
Figure S44. ^1H NMR spectrum of 44b in $\text{DMSO}-d_6$ (500 MHz).....	S33
Figure S45. $^{13}\text{C}\{^1\text{H}\}$ NMR spectrum of 44b in $\text{DMSO}-d_6$ (125 MHz).....	S33
Figure S46. HMBC spectrum of 44b in $\text{DMSO}-d_6$	S34
Figure S47. ^1H NMR spectrum of 45b in acetone- d_6 (500 MHz).....	S34
Figure S48. ^1H NMR spectrum of 47b in $\text{DMSO}-d_6$ (500 MHz).....	S35
Figure S49. $^{13}\text{C}\{^1\text{H}\}$ NMR spectrum of 47b in $\text{DMSO}-d_6$ (125 MHz).....	S35
Figure S50. HMBC spectrum of 47b in $\text{DMSO}-d_6$	S36
Figure S51. ^1H NMR spectrum of 50b in acetone- d_6 (500 MHz).....	S36
Figure S52. ^1H NMR spectrum of 61b in $\text{DMSO}-d_6$ (500 MHz).....	S37
Figure S53. $^{13}\text{C}\{^1\text{H}\}$ NMR spectrum of 61b in $\text{DMSO}-d_6$ (125 MHz).....	S37
Figure S54. ^1H NMR spectrum of (\pm)-65b in acetone- d_6 (500 MHz).....	S38
Figure S55. ^1H NMR spectrum of (\pm)-65c in $\text{DMSO}-d_6$ (500 MHz).....	S38
Figure S56. $^{13}\text{C}\{^1\text{H}\}$ NMR spectrum of (\pm)-65c in $\text{DMSO}-d_6$ (125 MHz).....	S39
Figure S57. HMBC spectrum of (\pm)-65c in $\text{DMSO}-d_6$	S39
Figure S58. HSQC spectrum of (\pm)-65c in $\text{DMSO}-d_6$	S40
Figure S59. ^1H NMR spectrum of (\pm)-65c in acetone- d_6 (500 MHz).....	S40
Figure S60. ^1H NMR spectrum of 72b in CDCl_3 (500 MHz).....	S41
Figure S61. ^1H NMR spectrum of 76b in CDCl_3 (500 MHz).....	S41
Figure S62. ^1H NMR spectrum of 77b in $\text{DMSO}-d_6$ (500 MHz).....	S42
Figure S63. ^1H NMR spectrum of 79b in CDCl_3 (500 MHz).....	S42
Figure S64. ^1H NMR spectrum of 79b in $\text{DMSO}-d_6$ (500 MHz).....	S43
Figure S65. $^{13}\text{C}\{^1\text{H}\}$ NMR spectrum of 79b in $\text{DMSO}-d_6$ (125 MHz).....	S43
Figure S66. HMBC spectrum of 79b in $\text{DMSO}-d_6$	S44
Figure S67. ^1H NMR spectrum of 79c in CDCl_3 (500 MHz).....	S44
Figure S68. ^1H NMR spectrum of 79d in CDCl_3 (500 MHz).....	S45
Figure S69. ^1H NMR spectrum of 80b in acetone- d_6 (500 MHz).....	S45
Figure S70. $^{13}\text{C}\{^1\text{H}\}$ NMR spectrum of 80b in acetone- d_6 (125 MHz).....	S46
Figure S71. HMBC spectrum of 80b in acetone- d_6	S46
Figure S72. ^1H NMR spectrum of 80c in acetone- d_6 (500 MHz).....	S47
Figure S73. ^1H NMR spectrum of 95b in $\text{DMSO}-d_6$ (500 MHz).....	S47
Figure S74. $^{13}\text{C}\{^1\text{H}\}$ NMR spectrum of 95b in $\text{DMSO}-d_6$ (125 MHz).....	S48
Figure S75. HMBC spectrum of 95b in $\text{DMSO}-d_6$	S48
Figure S76. ^1H NMR spectrum of 98b in $\text{DMSO}-d_6$ (500 MHz).....	S49
Figure S77. $^{13}\text{C}\{^1\text{H}\}$ NMR spectrum of 98b in $\text{DMSO}-d_6$ (125 MHz).....	S49
Figure S78. HMBC spectrum of 98b in $\text{DMSO}-d_6$	S50

SUPPORTING INFORMATION

Figure S79. ^1H NMR spectrum of 101b in acetone- d_6 (500 MHz).....	S50
Figure S80. $^{13}\text{C}\{^1\text{H}\}$ NMR spectrum of 101b in acetone- d_6 (125 MHz).....	S51
Figure S81. HMBC spectrum of 101b in acetone- d_6	S51
Figure S82. ^1H NMR spectrum of 101c in acetone- d_6 (500 MHz).....	S52
Figure S83. ^1H NMR spectrum of 101d in acetone- d_6 (500 MHz).....	S52
Figure S84. ^1H NMR spectrum of 102b in CD_3OD (500 MHz).....	S53
Figure S85. $^{13}\text{C}\{^1\text{H}\}$ NMR spectrum of 102b in CD_3OD (125 MHz).....	S53
Figure S86. HMBC spectrum of 102b in CD_3OD	S54
References	S55

SUPPORTING INFORMATION

Scheme S1. Chemical synthesis of hydroxyclovatol.



4-Methyl-6-acetylresorcinol was firstly synthesized by a Friedel-Craft acylation of 4-methylbenzene-1,3-diol (BLDpharm, Shanghai, China) as reported.¹ Introducing the hydroxymethylene group onto 4-methyl-6-acetylresorcinol was achieved by using a modified method reported for the synthesis of luminacin D.²

SUPPORTING INFORMATION

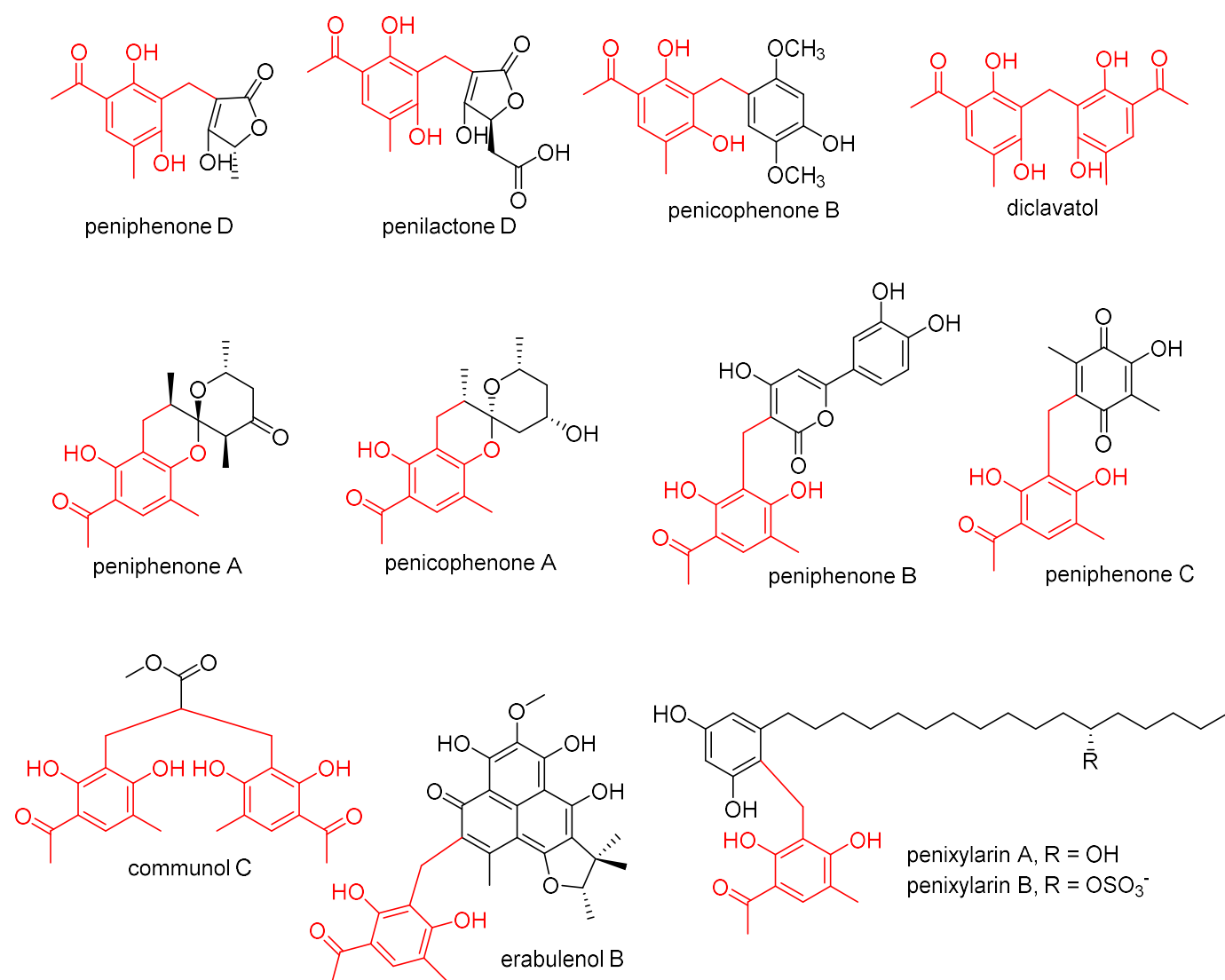


Figure S1. Examples of fungal clavatul-containing natural products.³⁻⁹

SUPPORTING INFORMATION

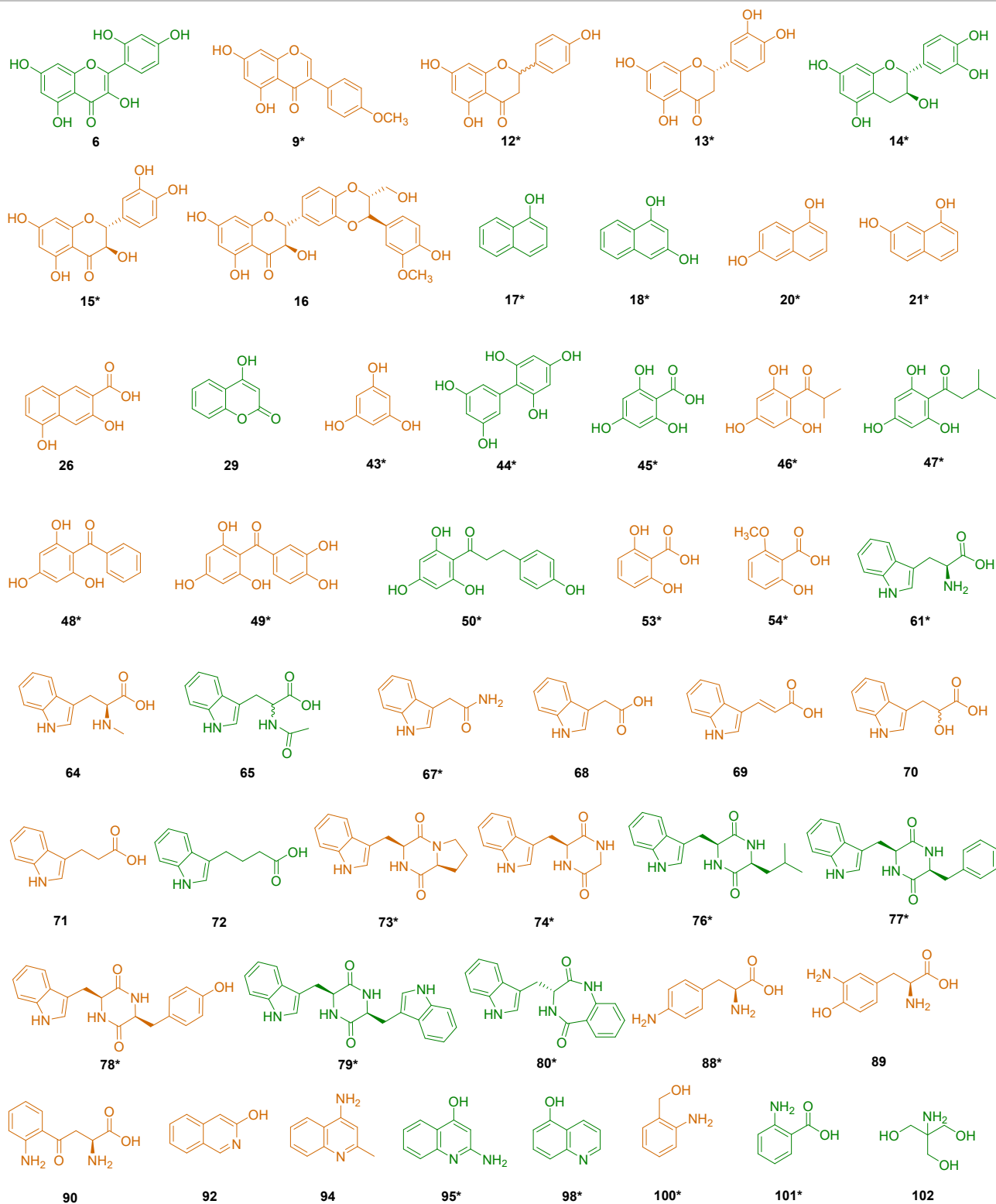


Figure S2. Structures of tested reactants with conversions between 10% – 55%.

Products of reactants in green were further identified by NMR after isolation. Products of reactants in orange were only identified by LC-MS analysis. Products with two clavotol moieties were detected from reactants labeled with *. Reaction mixtures (50 μ L) containing 0.4 mM hydroxyclovatol and 0.4 mM reactants were incubated at 25 $^{\circ}$ C for 16 h before sent to LC-MS analysis. The conversion (%) was calculated by peak areas with UV detection.

SUPPORTING INFORMATION

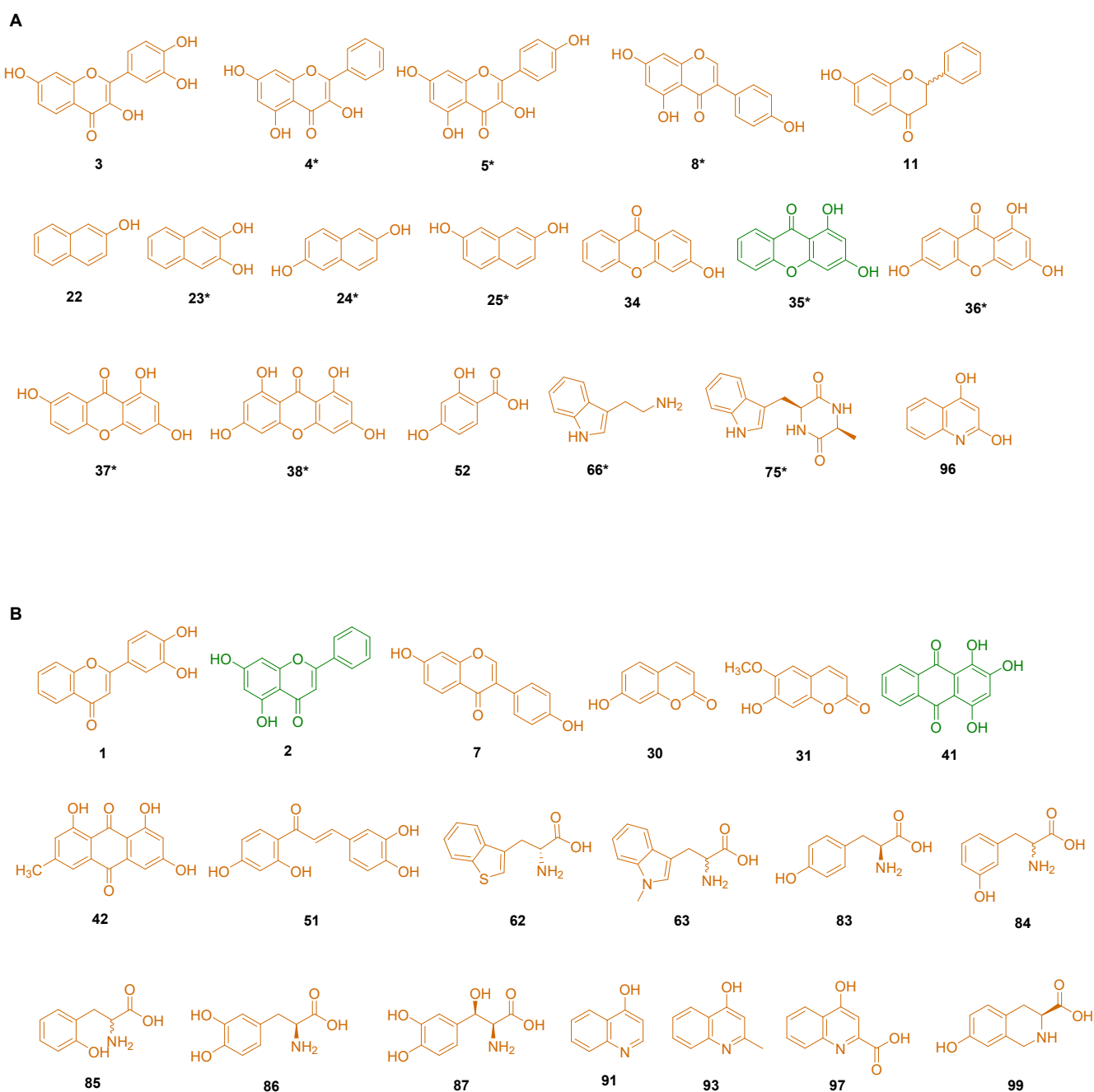


Figure S3. Structures of tested reactants with conversions between 1% – 10% (A), and only detected by EIC of $[M+H]^+/[M-H]^-$ ions (B).

Reaction mixtures (50 μ L) containing 0.4 mM hydroxyclovatol and 0.4 mM reactants were incubated at 25 $^{\circ}$ C for 16 h before sent to LC-MS analysis. Products of reactants in green were isolated from incubations at 95 $^{\circ}$ C for 30 min. Products of reactants in orange were only identified by LC-MS analysis. Products with two clavatol moieties were detected from reactants labeled with *. The conversion (%) was calculated by peak areas with UV detection.

SUPPORTING INFORMATION

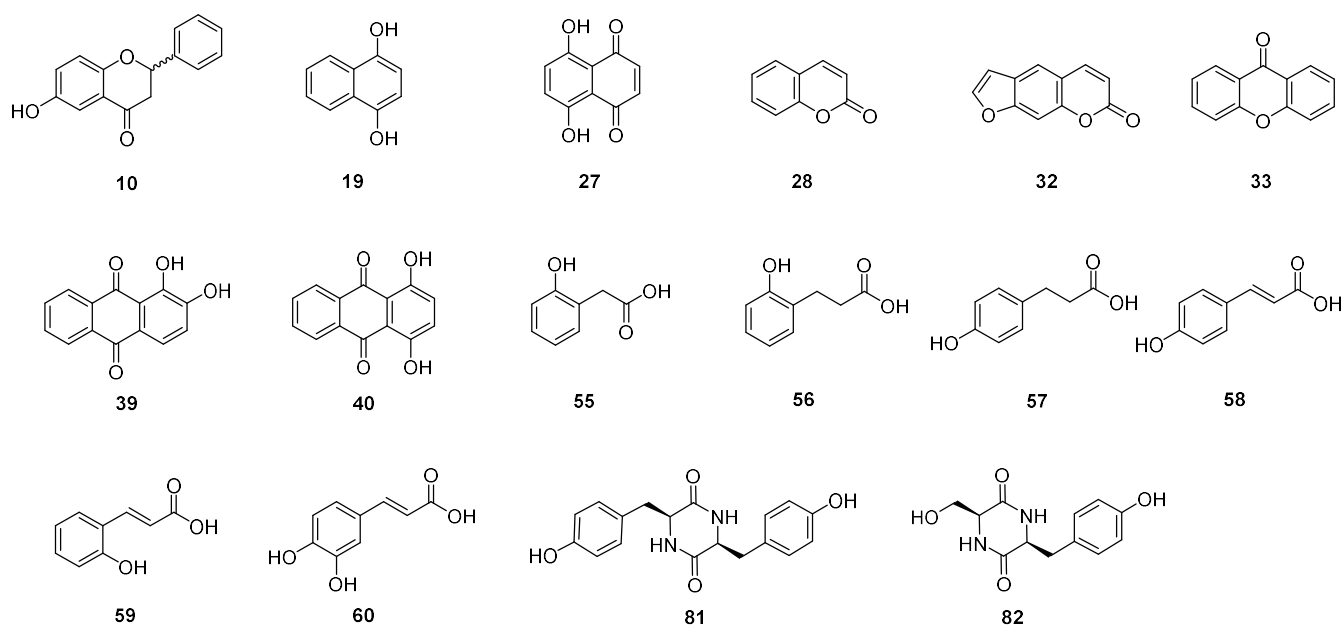


Figure S4. Structures of tested reactants with no detectable product by EIC of $[M+H]^+/[M-H]^-$ ions.

Reaction mixtures (50 μ L) containing 0.4 mM hydroxyclovatol and 0.4 mM reactants were incubated at 25 $^{\circ}$ C for 16 h before sent to LC-MS analysis.

SUPPORTING INFORMATION

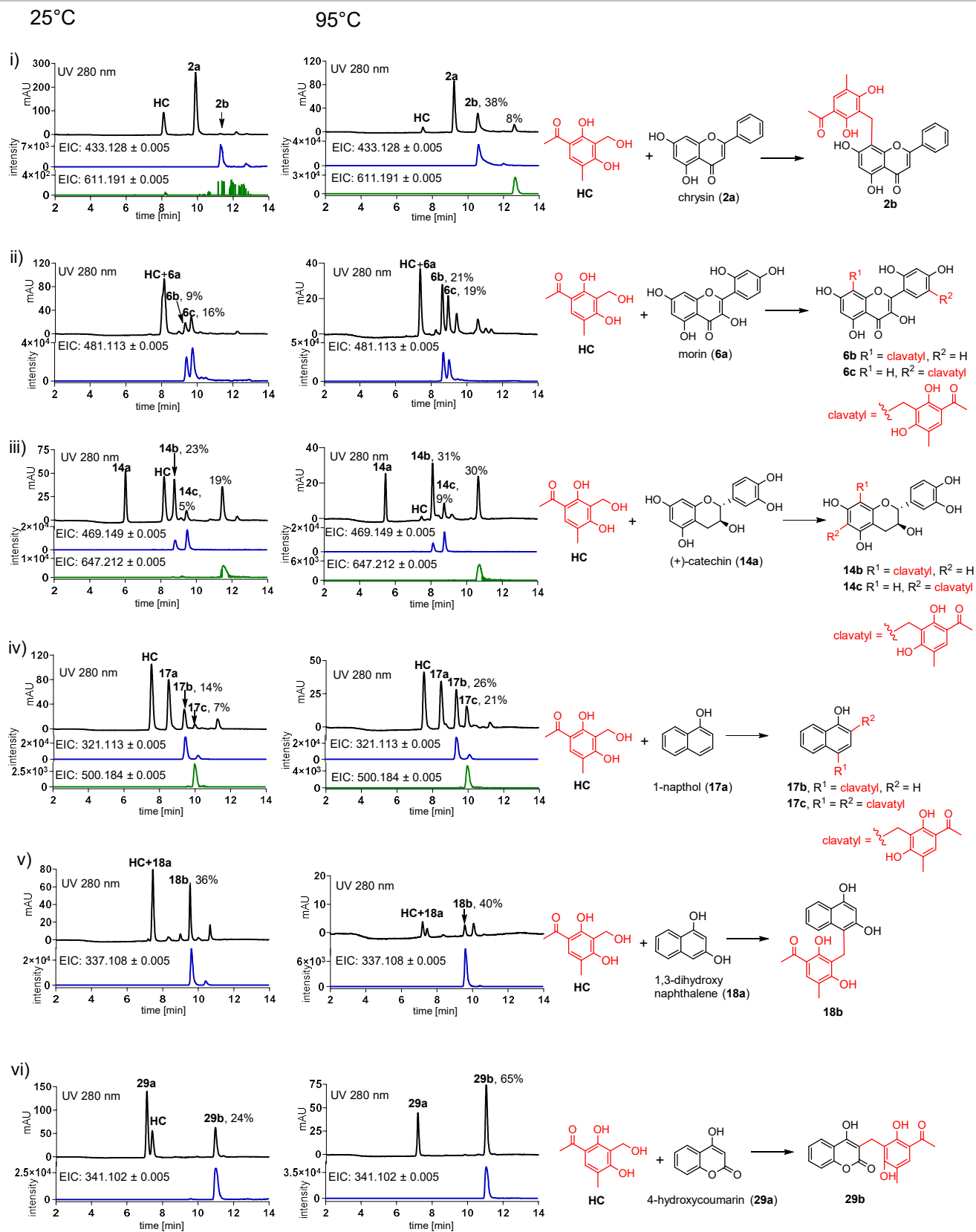


Figure S5. LC-MS analysis of reaction mixtures of hydroxyclovatol with different reactants.

HC: hydroxyclovatol, UV absorptions at 280 nm (black) are illustrated. EICs in blue or green refer $[M+H]^+$ of products with one or two clavatol moieties with a tolerance range of ± 0.005 . EICs refer $[M-H]^-$ of **17b**, **17c**, and **18b**.

SUPPORTING INFORMATION

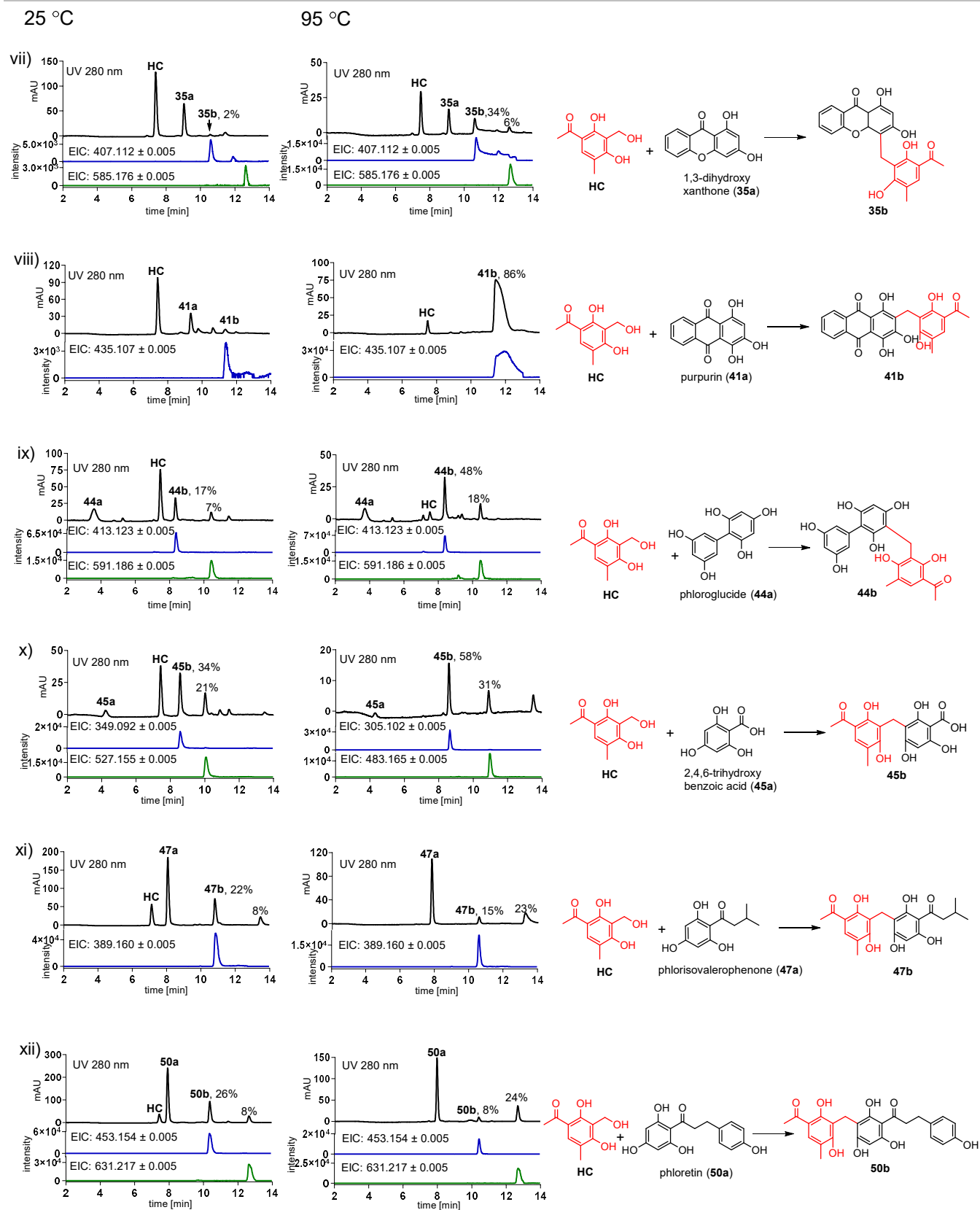


Figure S6. LC-MS analysis of reaction mixtures of hydroxyclovatol with different reactants.

HC: Hydroxyclovatol, UV absorptions at 280 nm (black) are illustrated. EICs in blue or green refer $[M+H]^+$ of products with one or two clavatol moieties with a tolerance range of ± 0.005 .

SUPPORTING INFORMATION

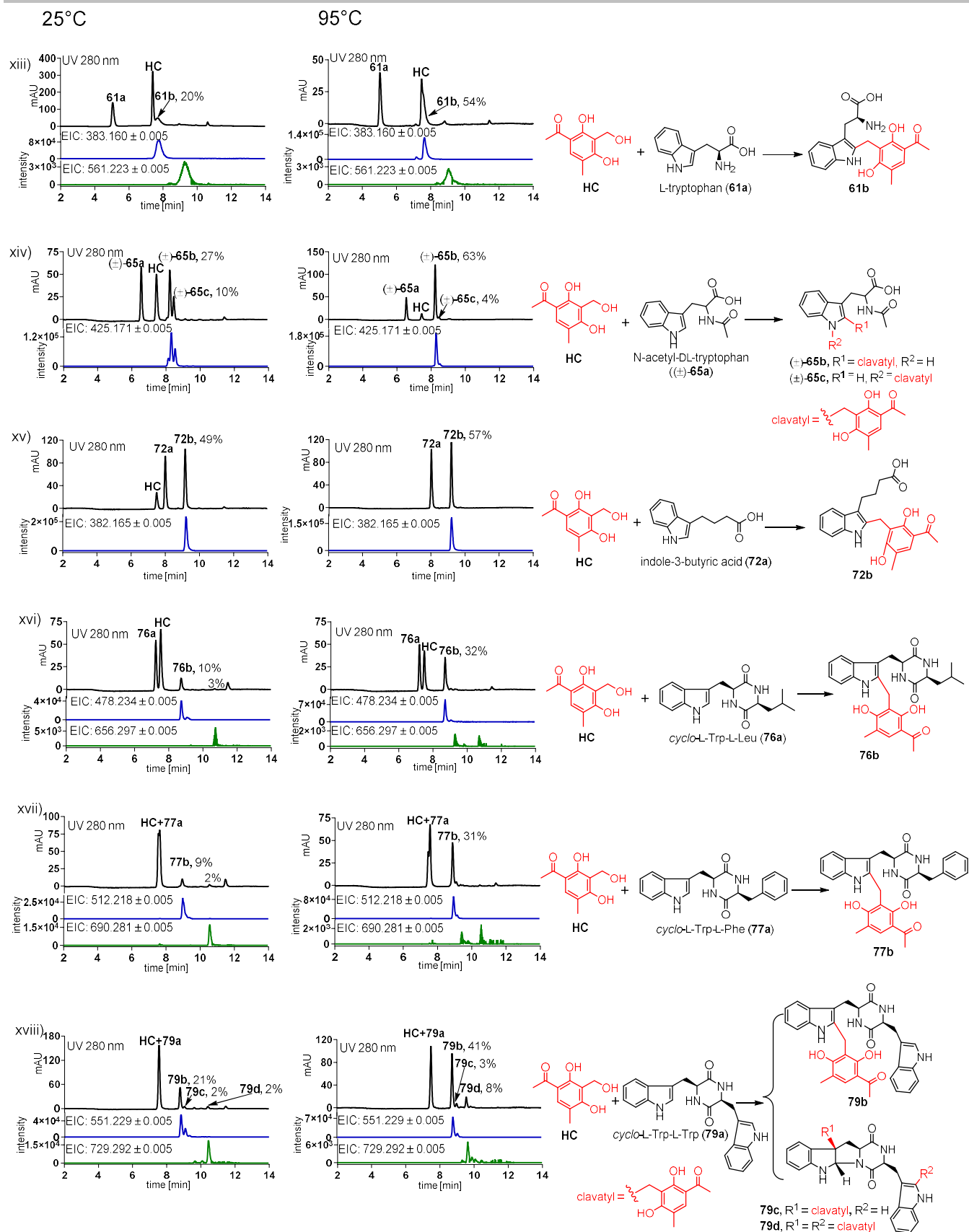


Figure S7. LC-MS analysis of reaction mixtures of hydroxyclavatul with different reactants.

HC: hydroxyclavatul, UV absorptions at 280 nm (black) are illustrated. EICs in blue or green refer [M+H]⁺ of products with one or two clavatul moieties with a tolerance range of ± 0.005.

SUPPORTING INFORMATION

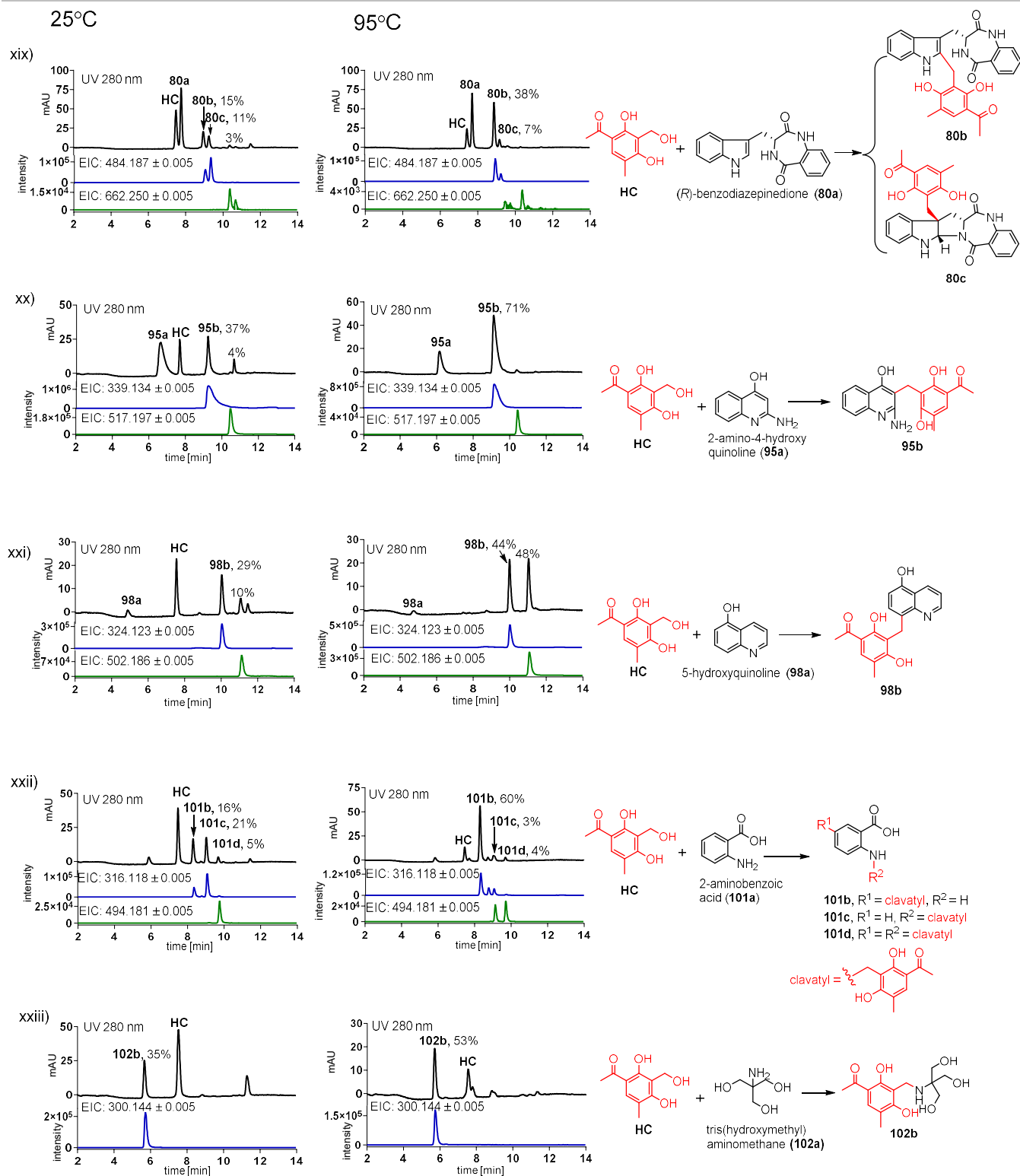


Figure S8. LC-MS analysis of reaction mixtures of hydroxyclovatol with different reactants.

HC: hydroxyclovatol, UV absorptions at 280 nm (black) are illustrated. EICs in blue or green refer $[M+H]^+$ products with one or two clavatol moieties with a tolerance range of ± 0.005 .

SUPPORTING INFORMATION

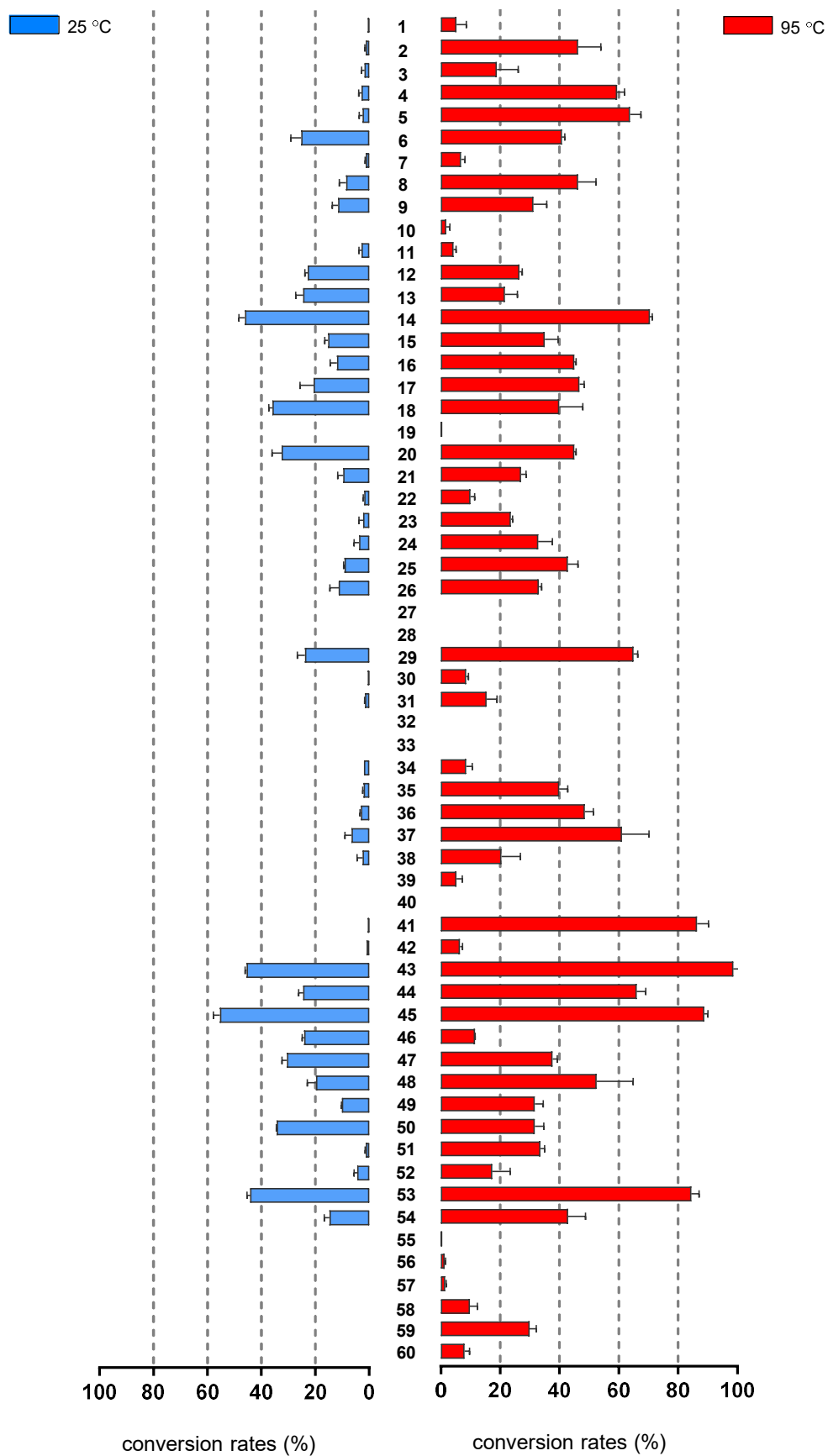


Figure S9. Conversions of hydroxylclavatol reactions with nitrogen-free reactants at 25 °C (left) or 95 °C (right).

SUPPORTING INFORMATION

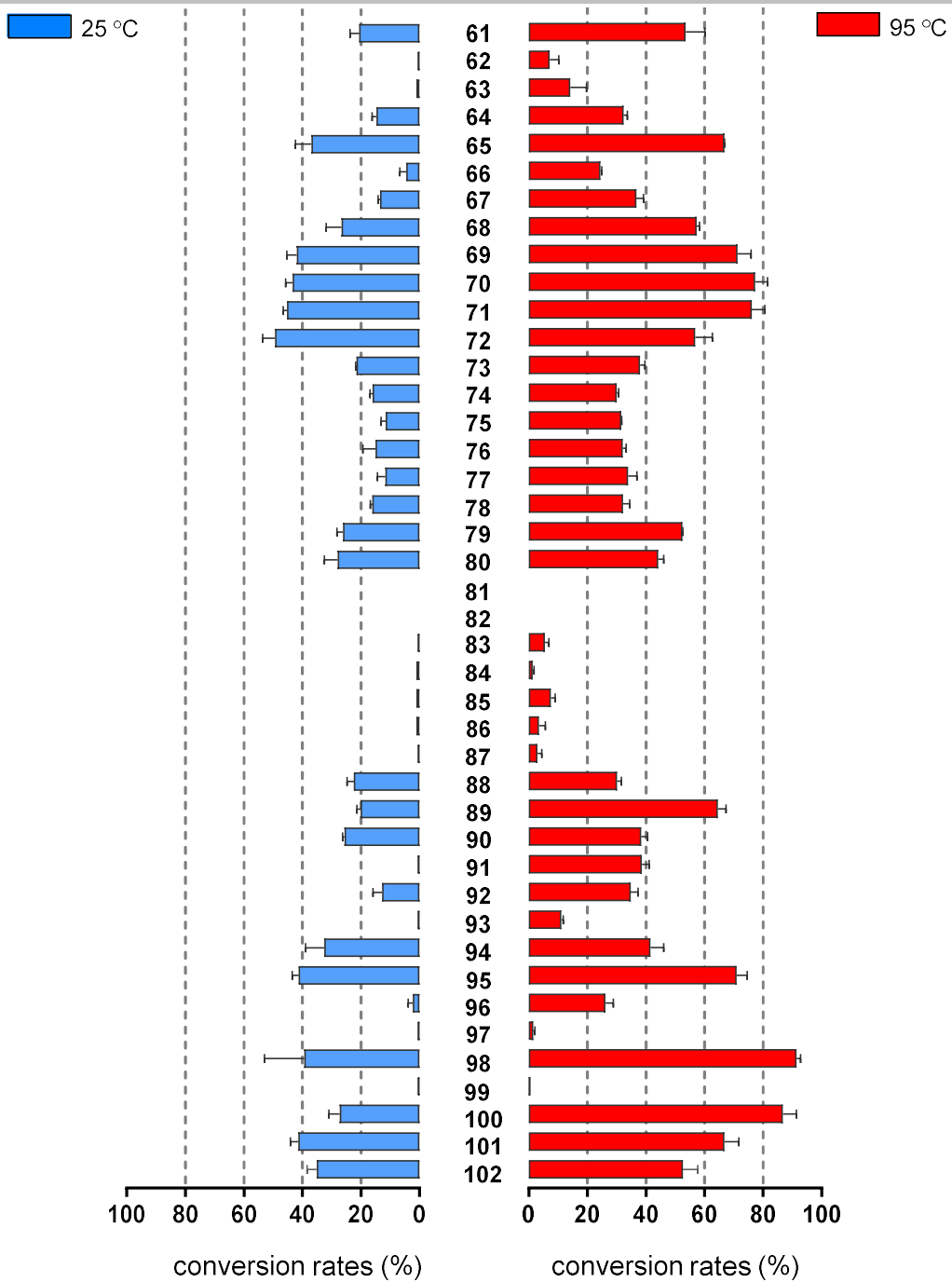


Figure S10. Conversions of hydroxycavato reactions with nitrogen-containing reactants at 25 °C (left) or 95 °C (right).

SUPPORTING INFORMATION

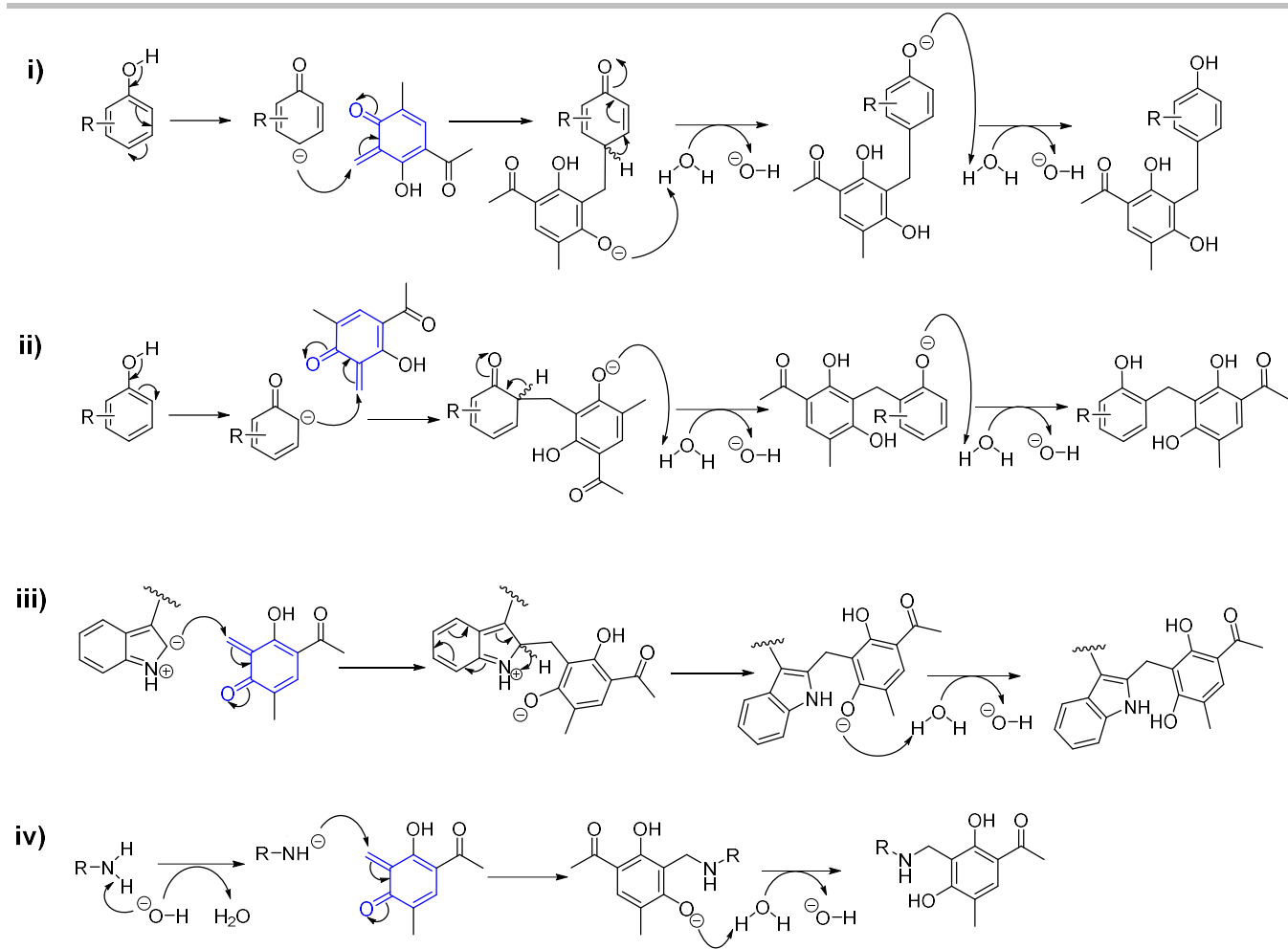
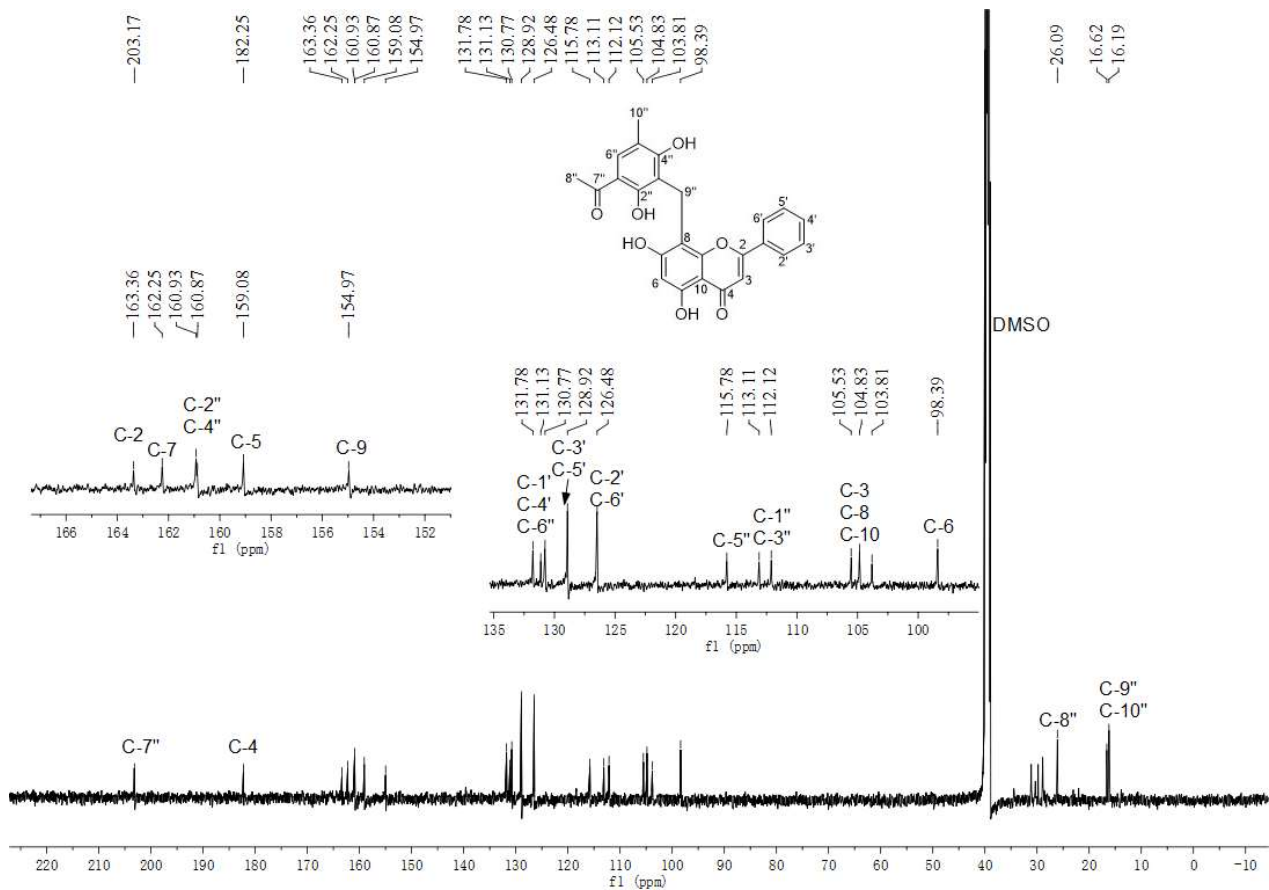
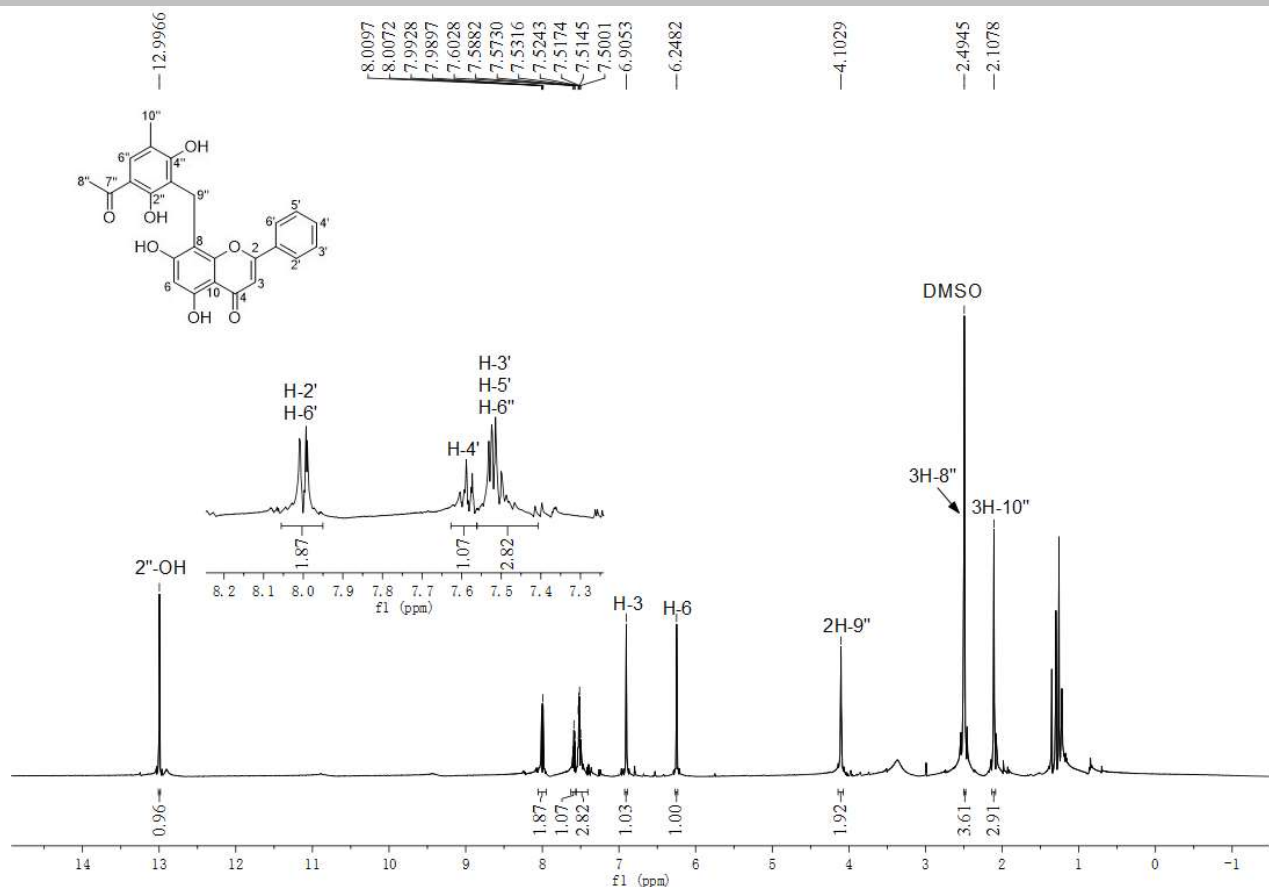


Figure S11. Reaction mechanisms of different nucleophile additions to the *ortho*-quinone methide intermediate.

SUPPORTING INFORMATION



SUPPORTING INFORMATION

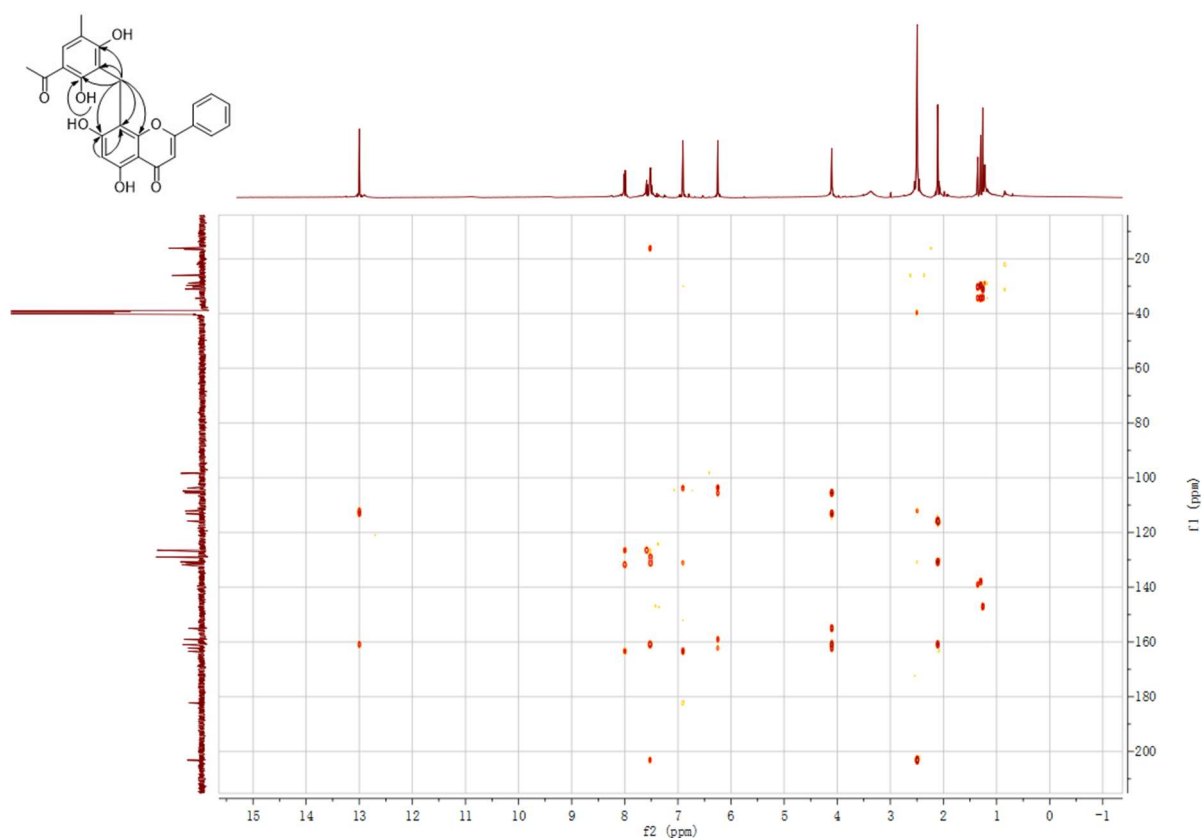


Figure S14. HMBC spectrum of **2b** in DMSO-*d*₆.

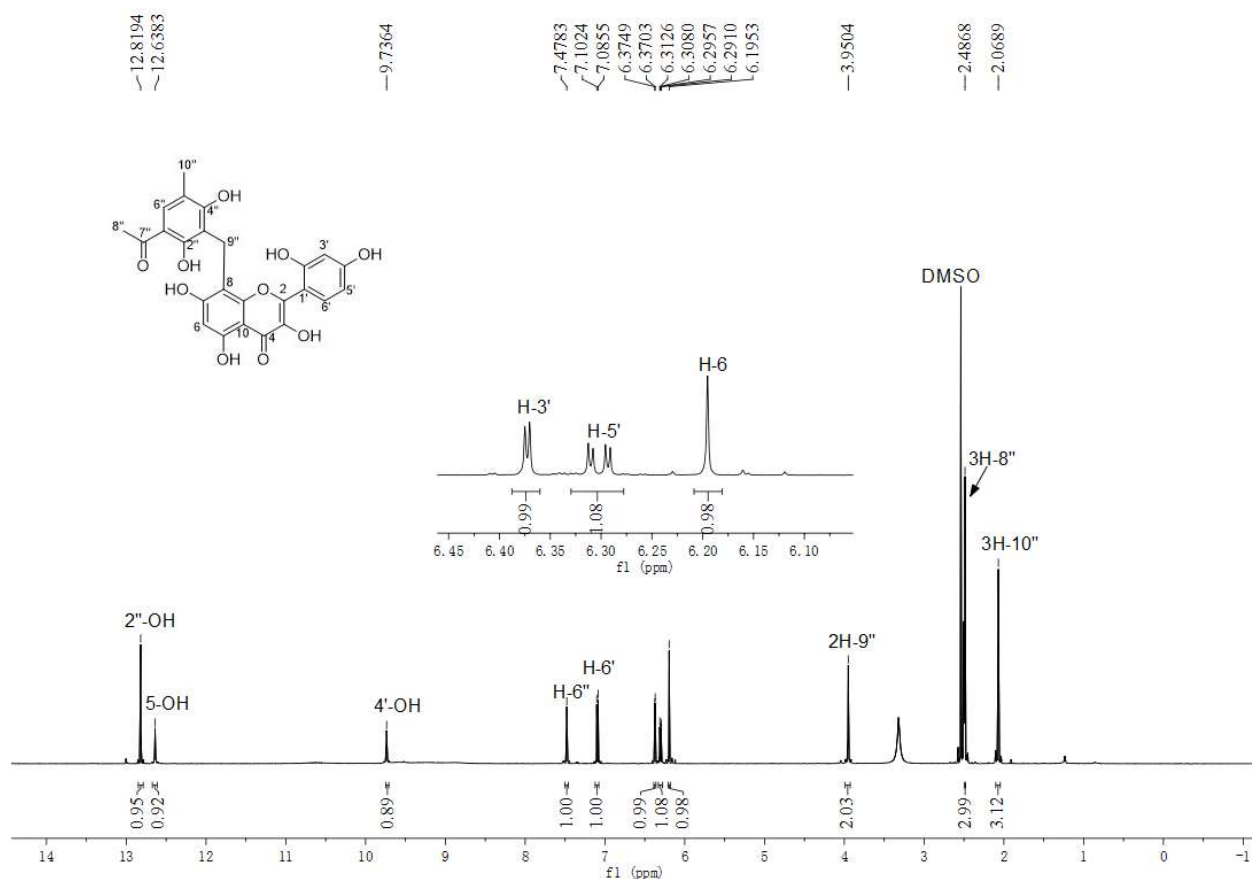
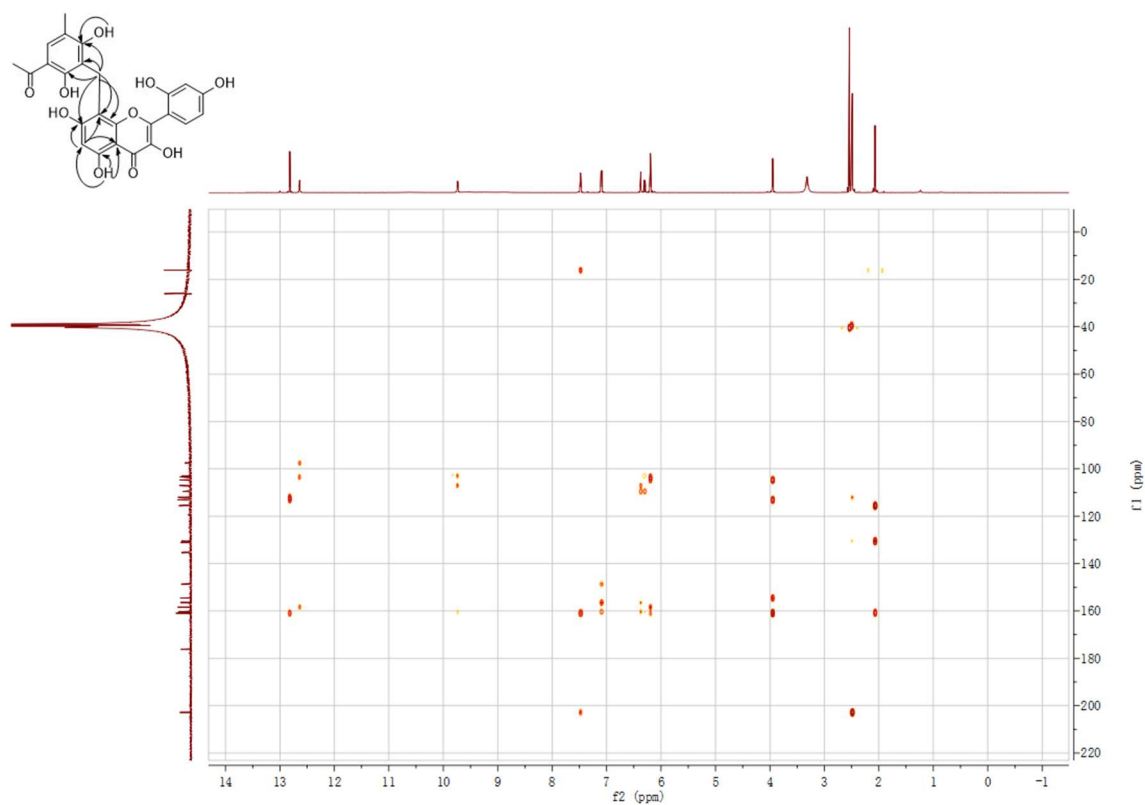
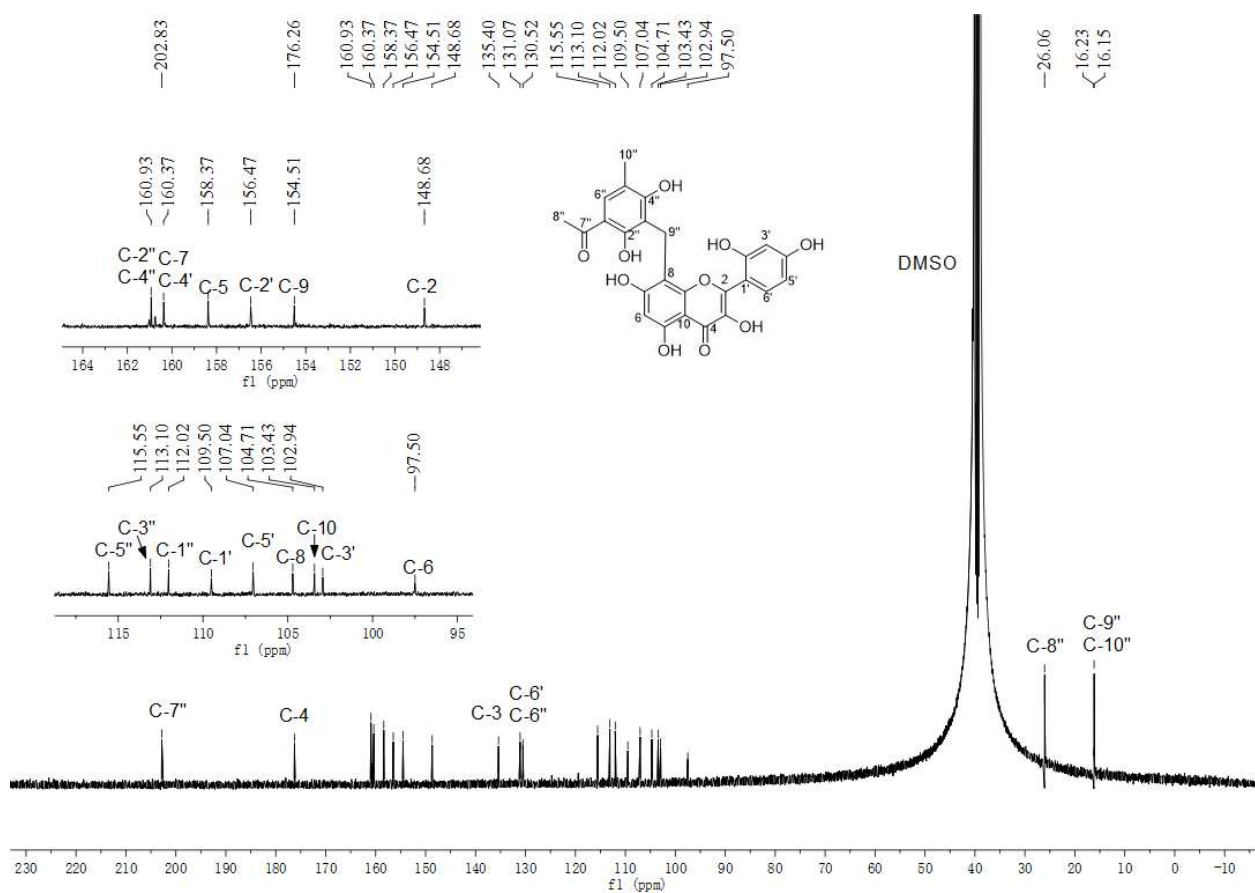
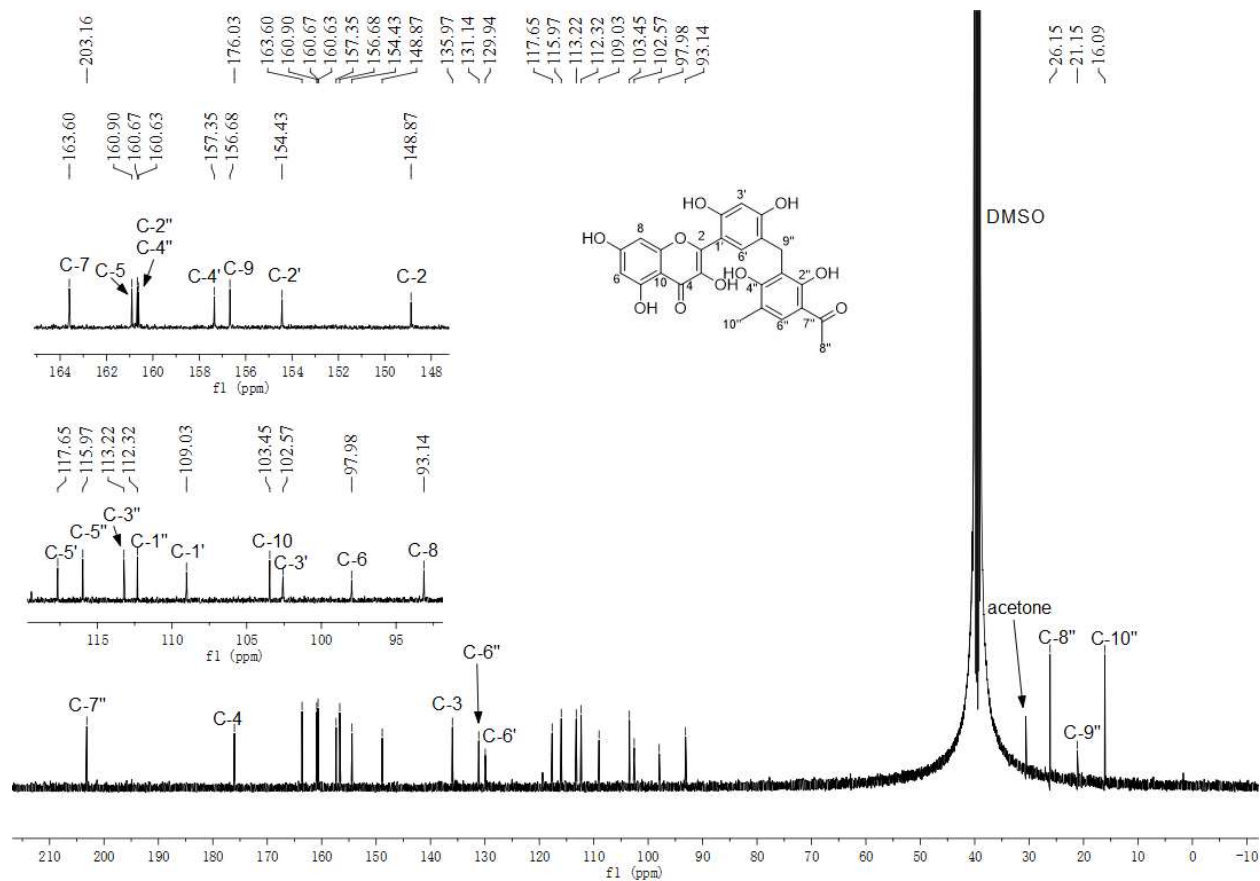
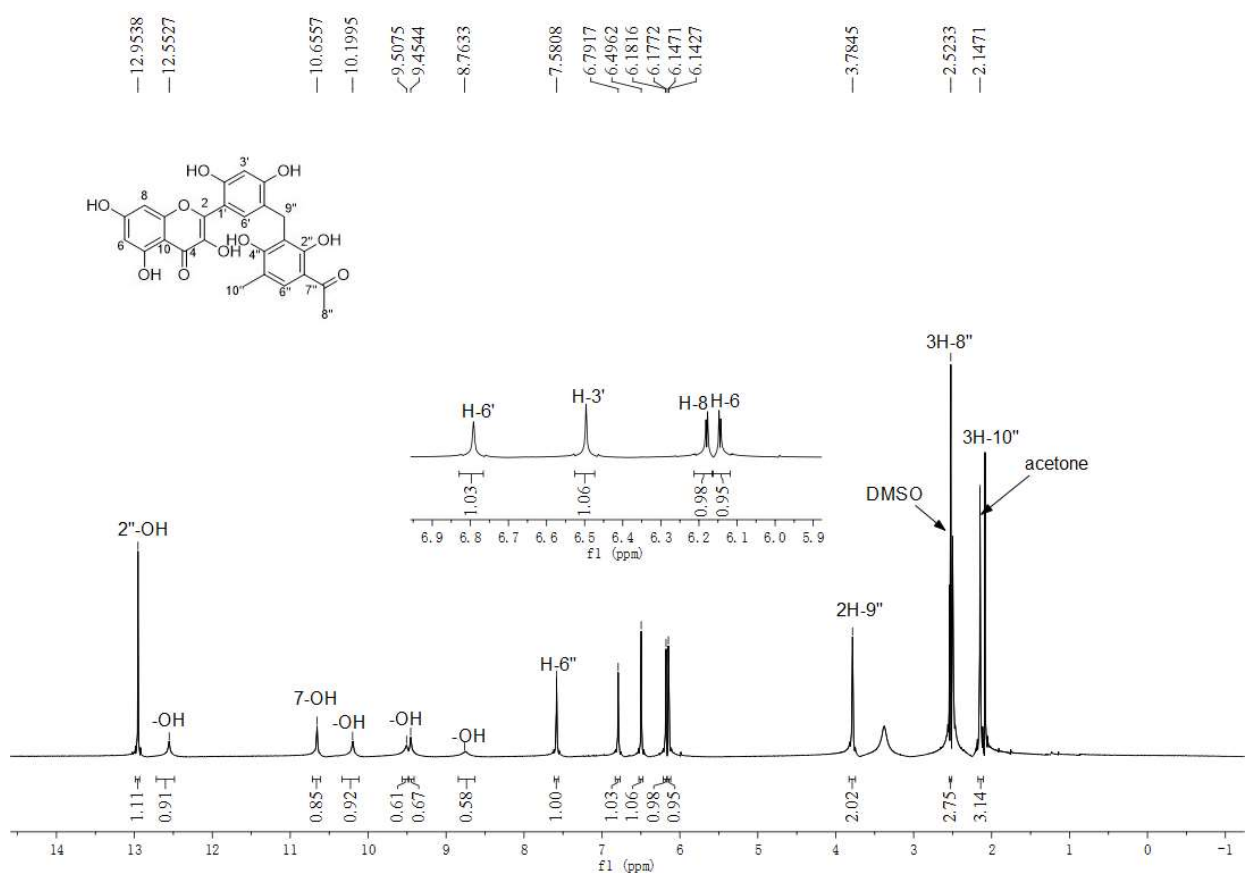


Figure S15. ¹H NMR spectrum of **6b** in DMSO-*d*₆ (500 MHz).

SUPPORTING INFORMATION



SUPPORTING INFORMATION



SUPPORTING INFORMATION

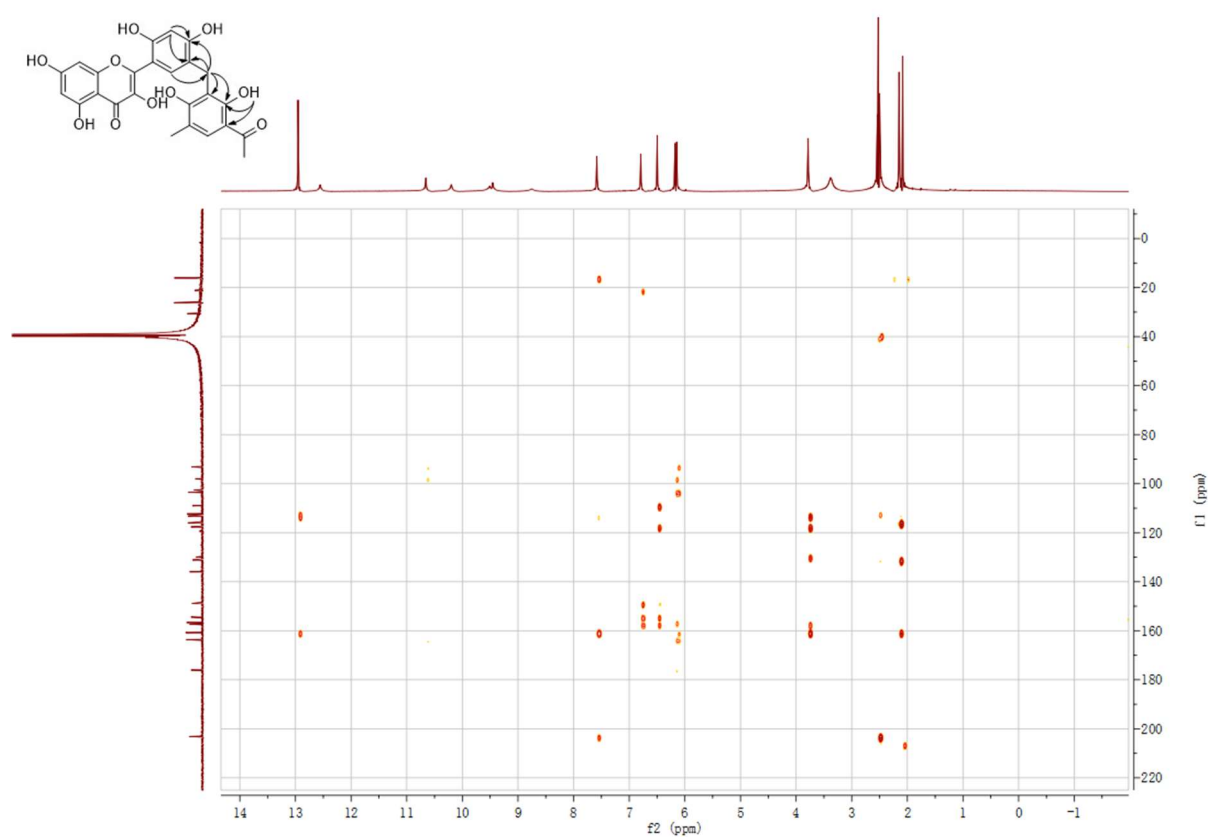


Figure S20. HMBC spectrum of **6c** in DMSO-*d*₆.

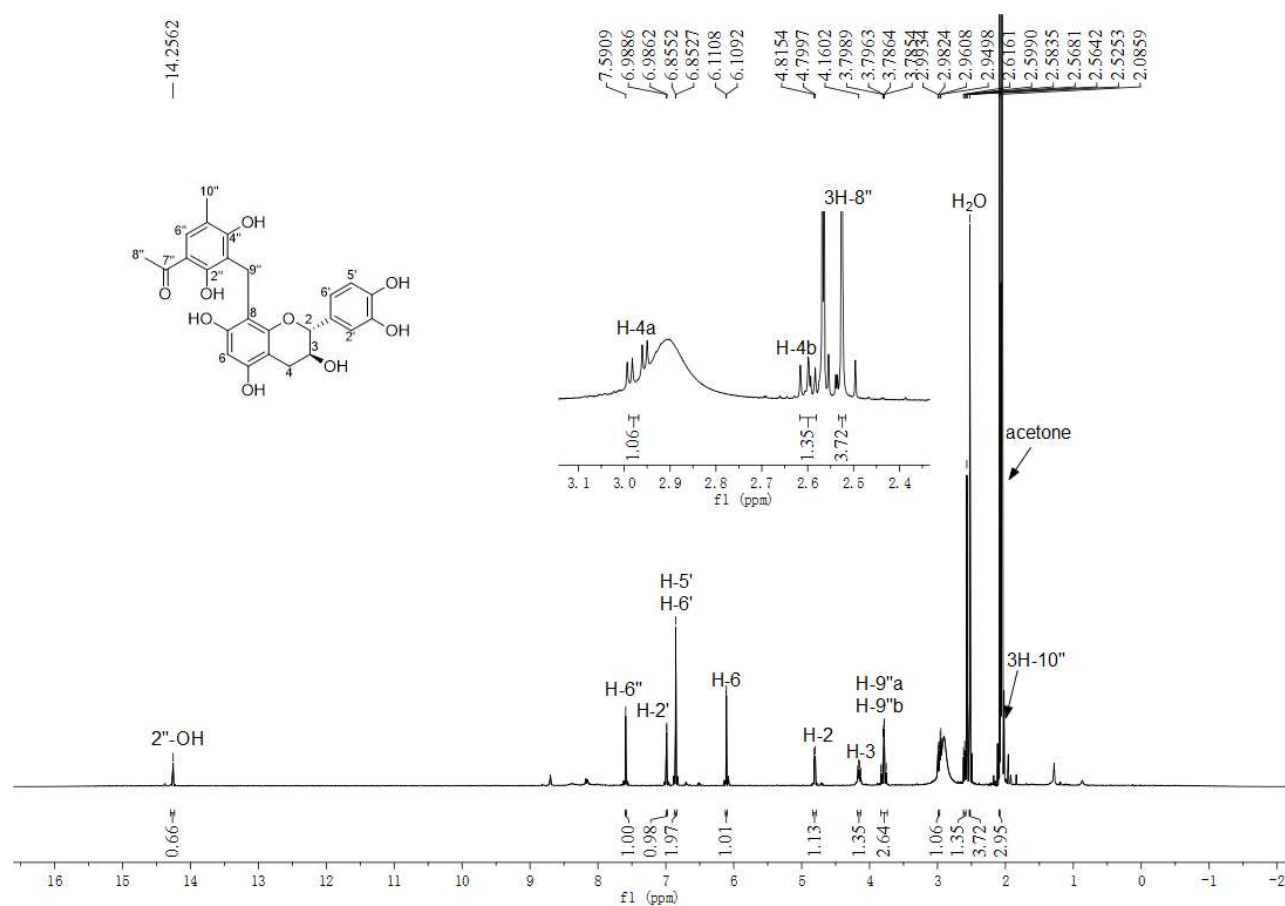


Figure S21. ¹H NMR spectrum of **14b** in acetone-*d*₆ (500 MHz).

SUPPORTING INFORMATION

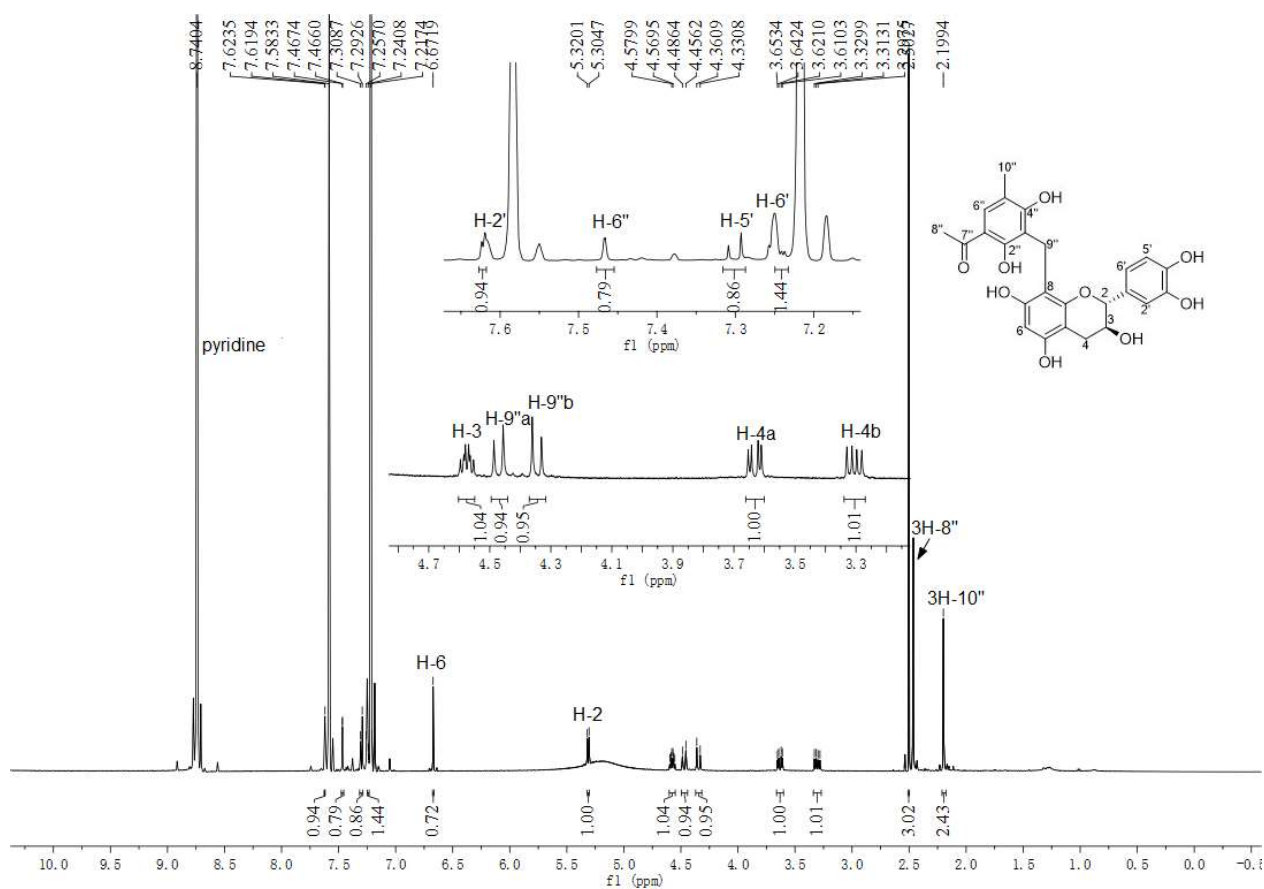


Figure S22. ^1H NMR spectrum of **14b** in pyridine- d_5 (500 MHz).

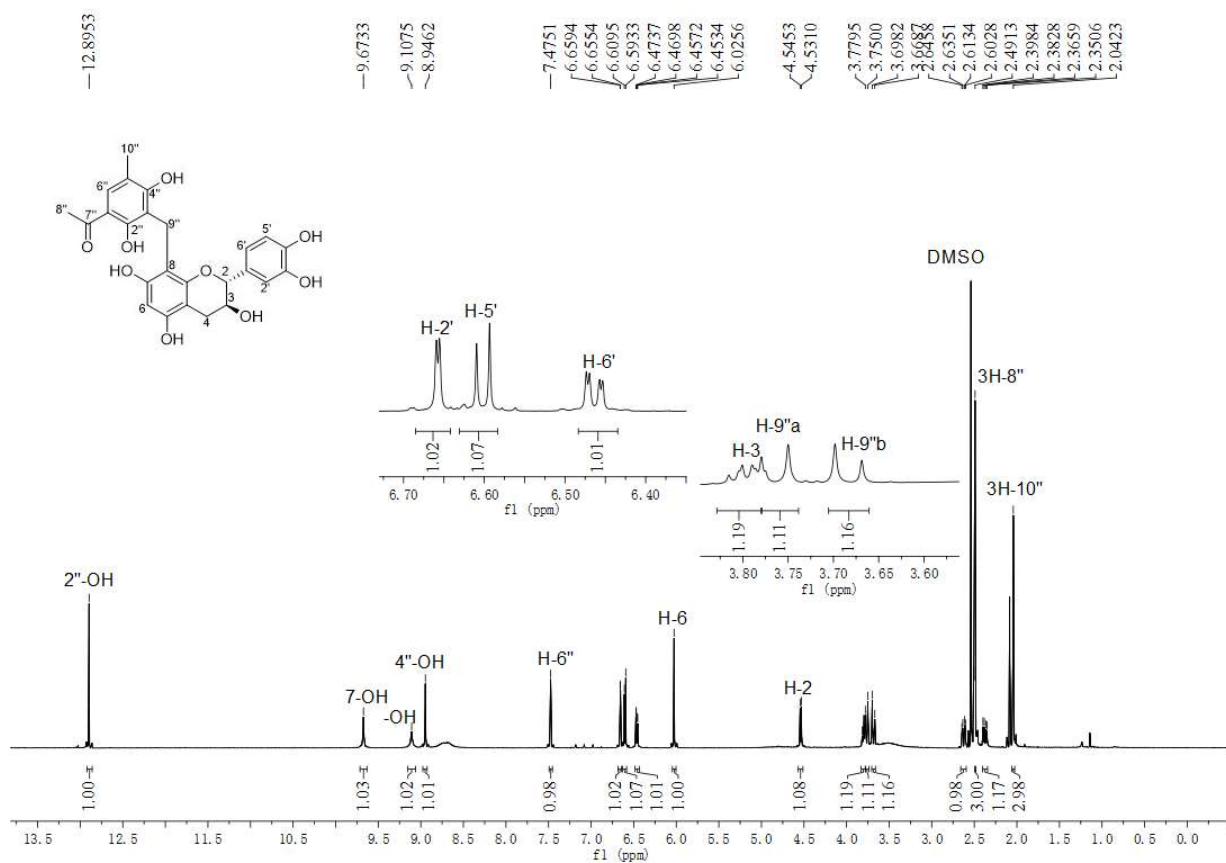


Figure S23. ^1H NMR spectrum of **14b** in DMSO- d_6 (500 MHz).

SUPPORTING INFORMATION

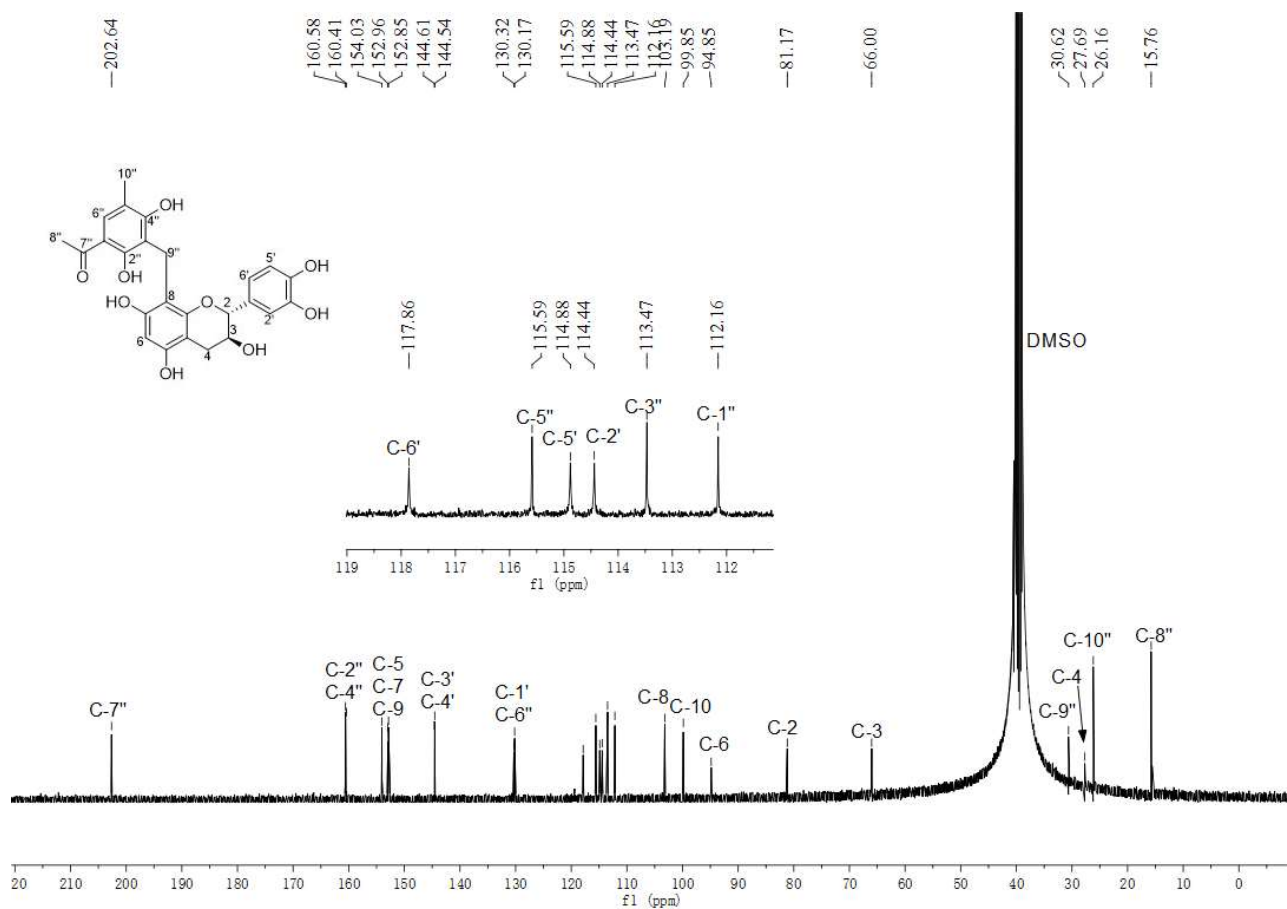


Figure S24. $^{13}\text{C}\{^1\text{H}\}$ NMR spectrum of **14b** in $\text{DMSO-}d_6$ (125 MHz).

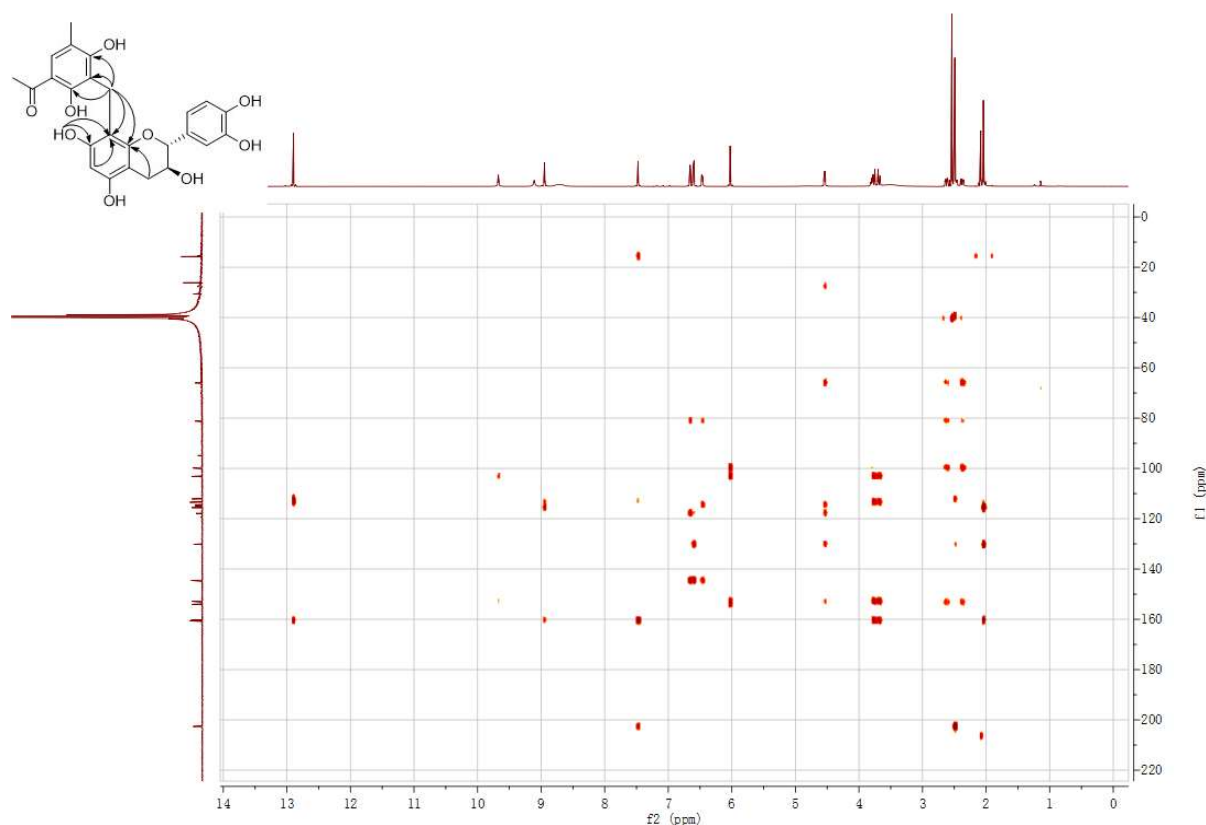
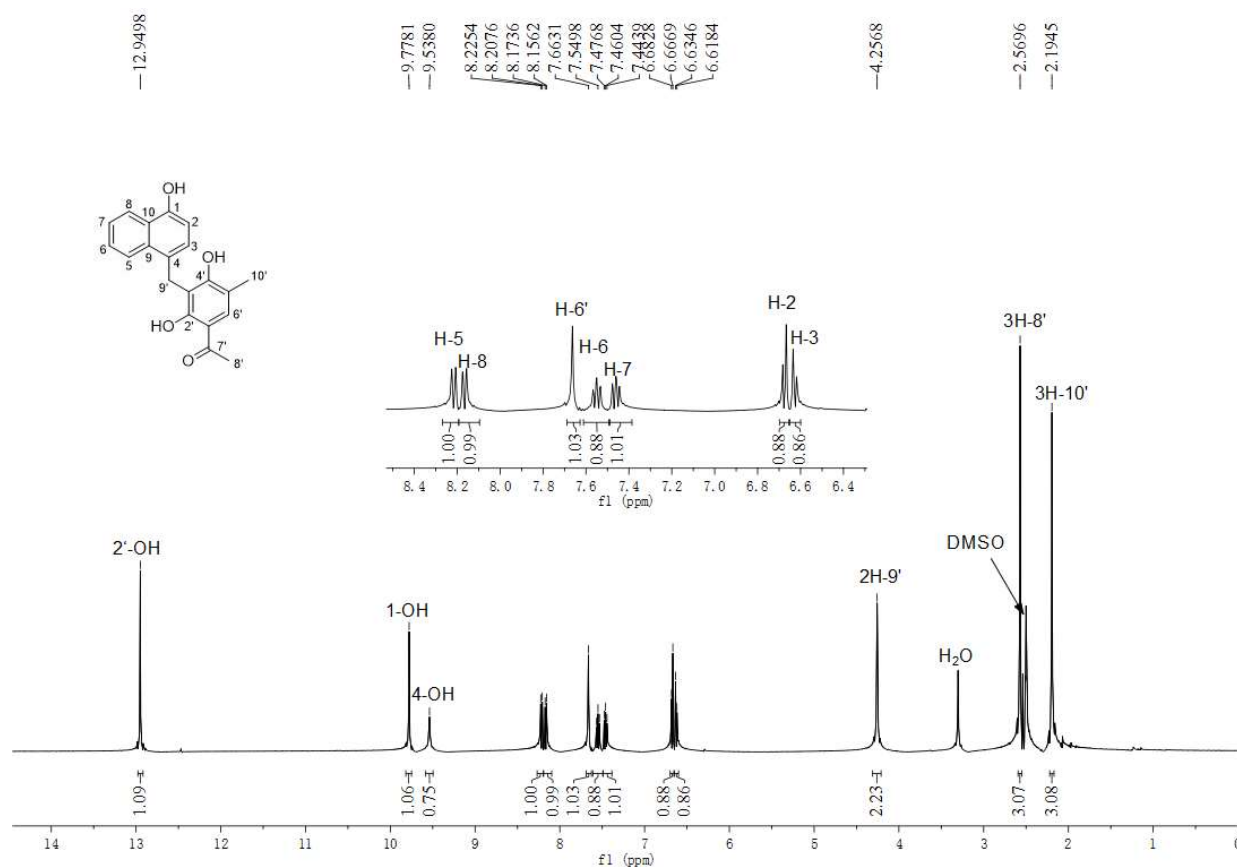
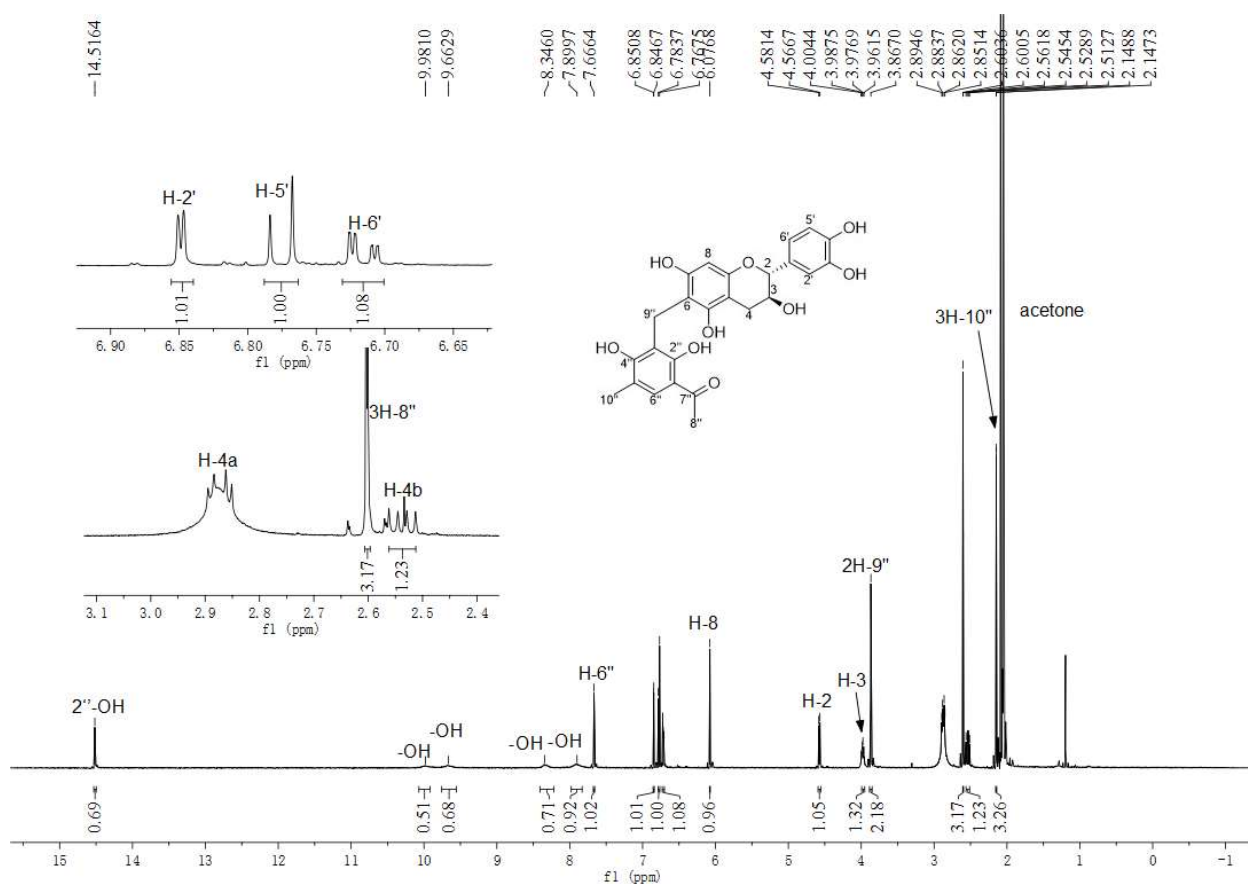


Figure S25. HMBC spectrum of **14b** in $\text{DMSO-}d_6$.

SUPPORTING INFORMATION



SUPPORTING INFORMATION

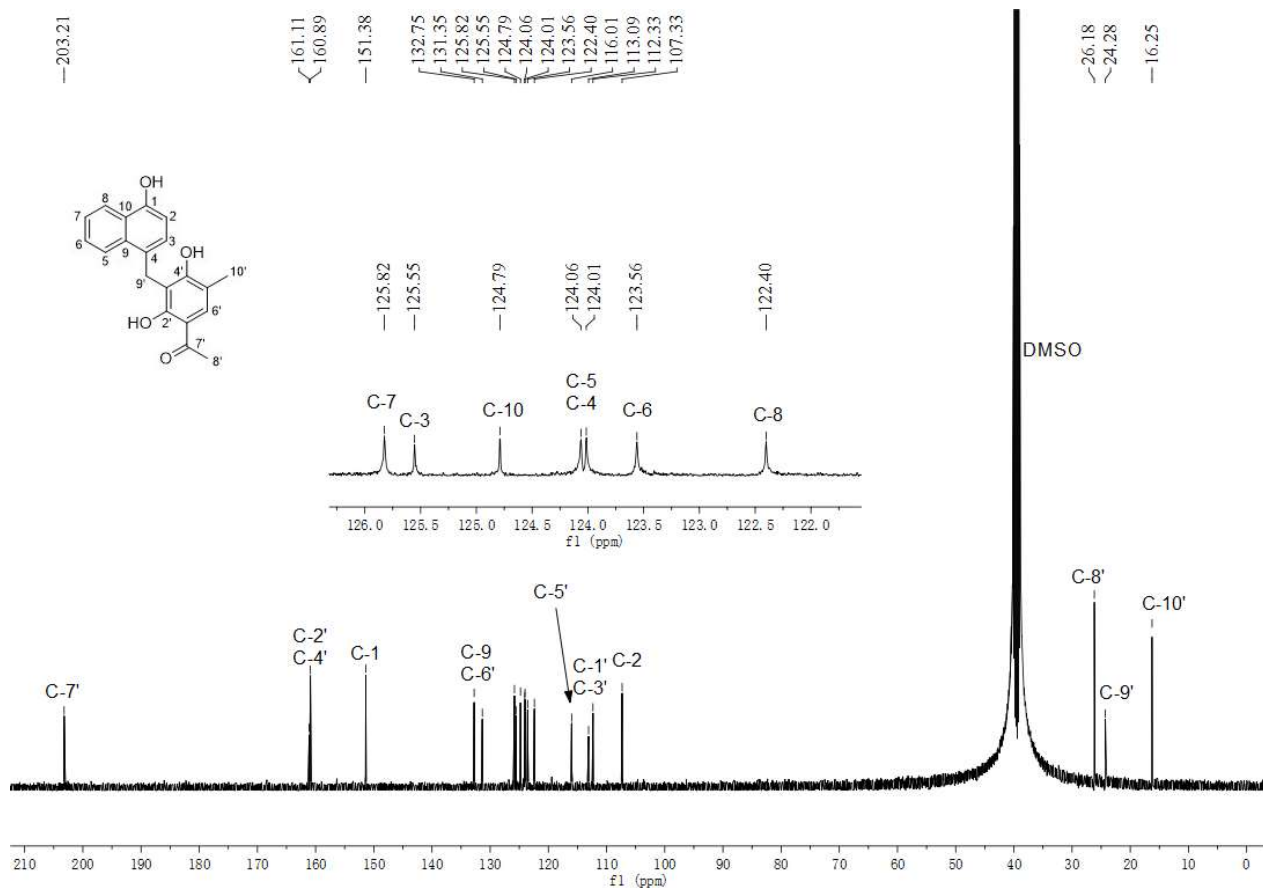


Figure S28. $^{13}\text{C}\{^1\text{H}\}$ NMR spectrum of **17b** in $\text{DMSO-}d_6$ (125 MHz).

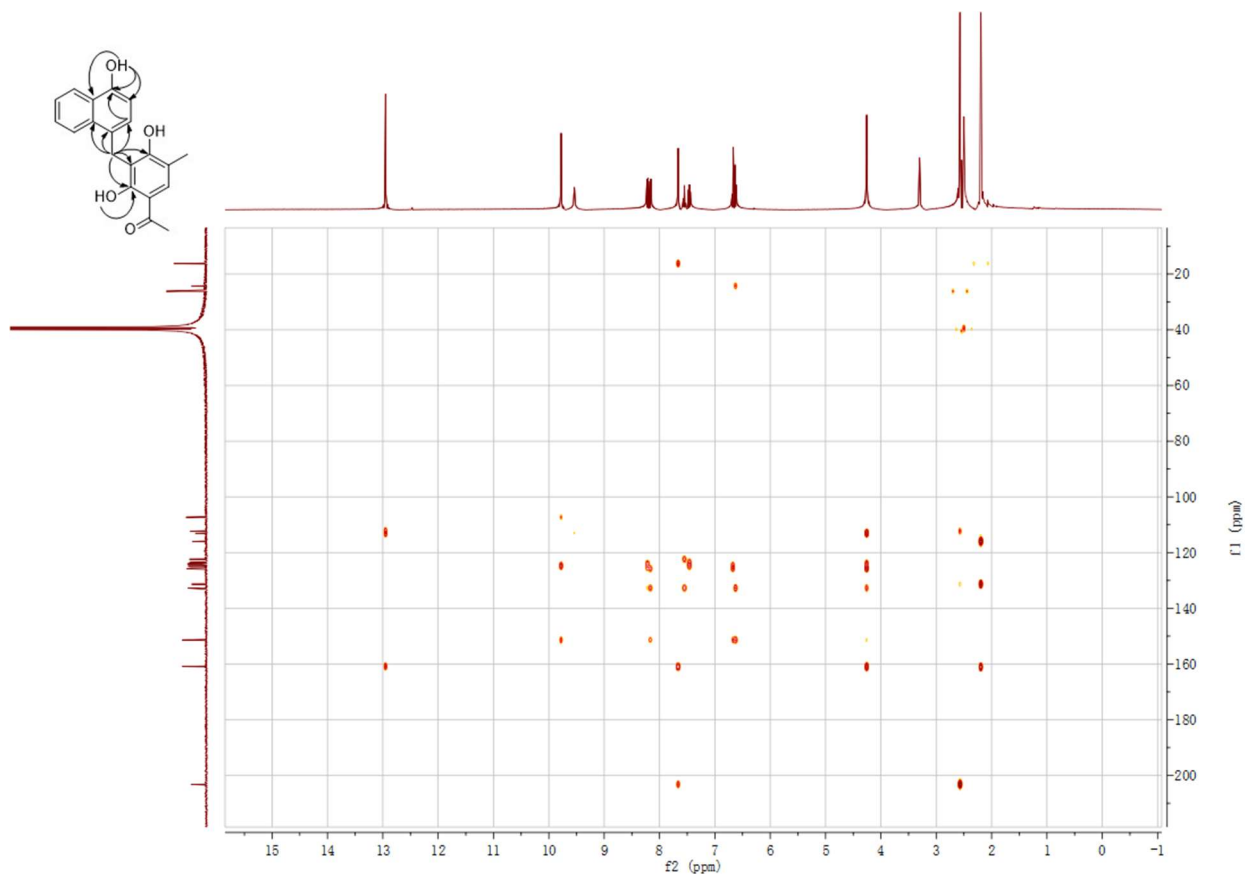


Figure S29. HMBC spectrum of **17b** in $\text{DMSO-}d_6$.

SUPPORTING INFORMATION

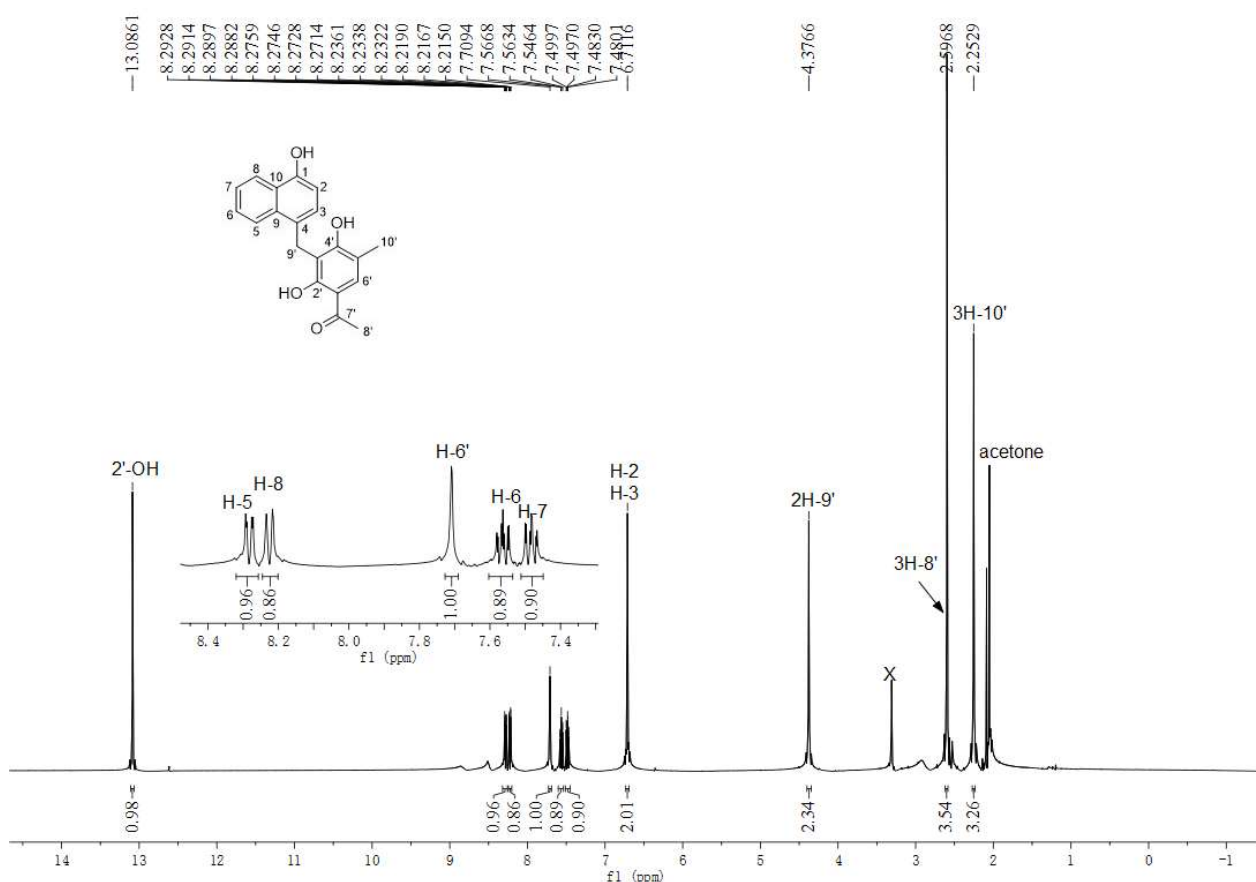


Figure S30. ^1H NMR spectrum of **17b** in acetone- d_6 (500 MHz).

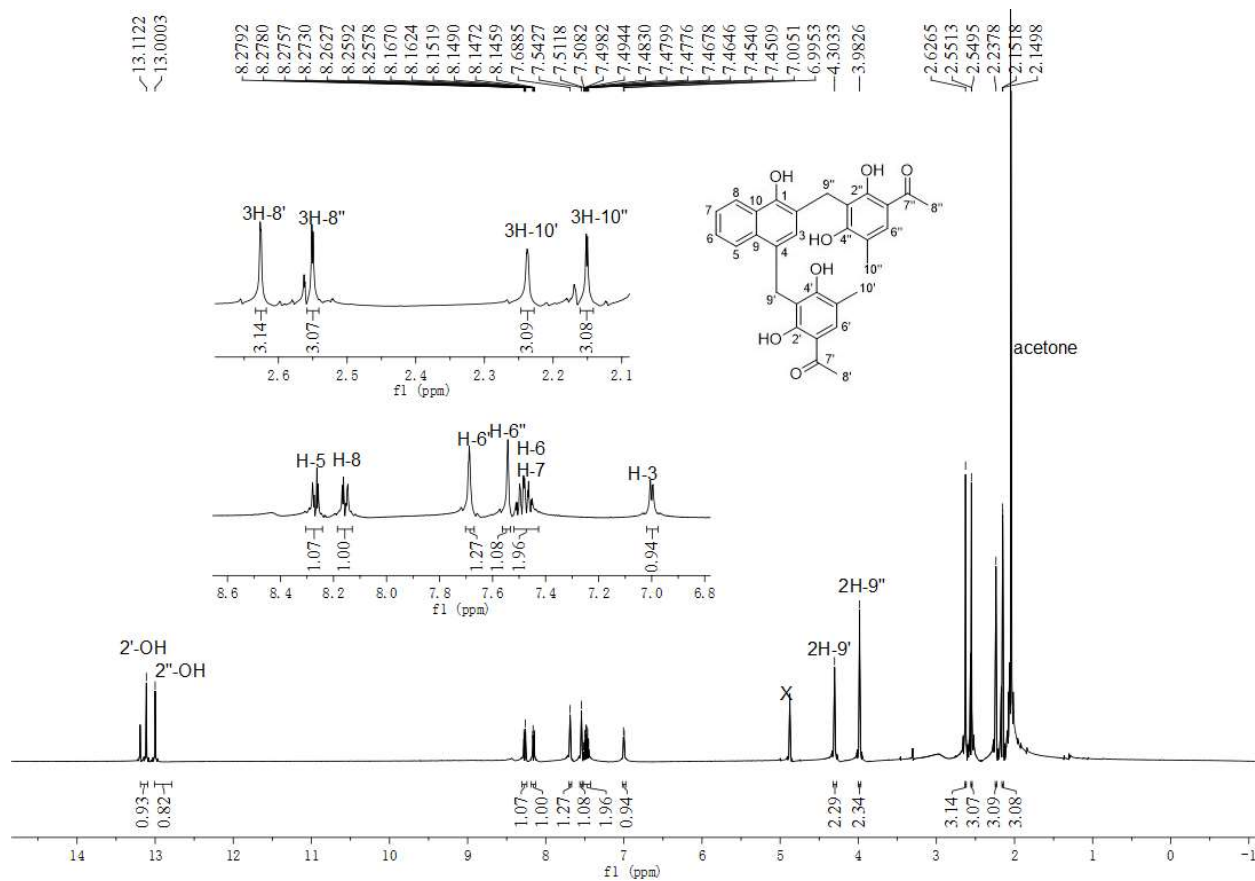


Figure S31. ^1H NMR spectrum of **17c** in acetone- d_6 (500 MHz).

SUPPORTING INFORMATION

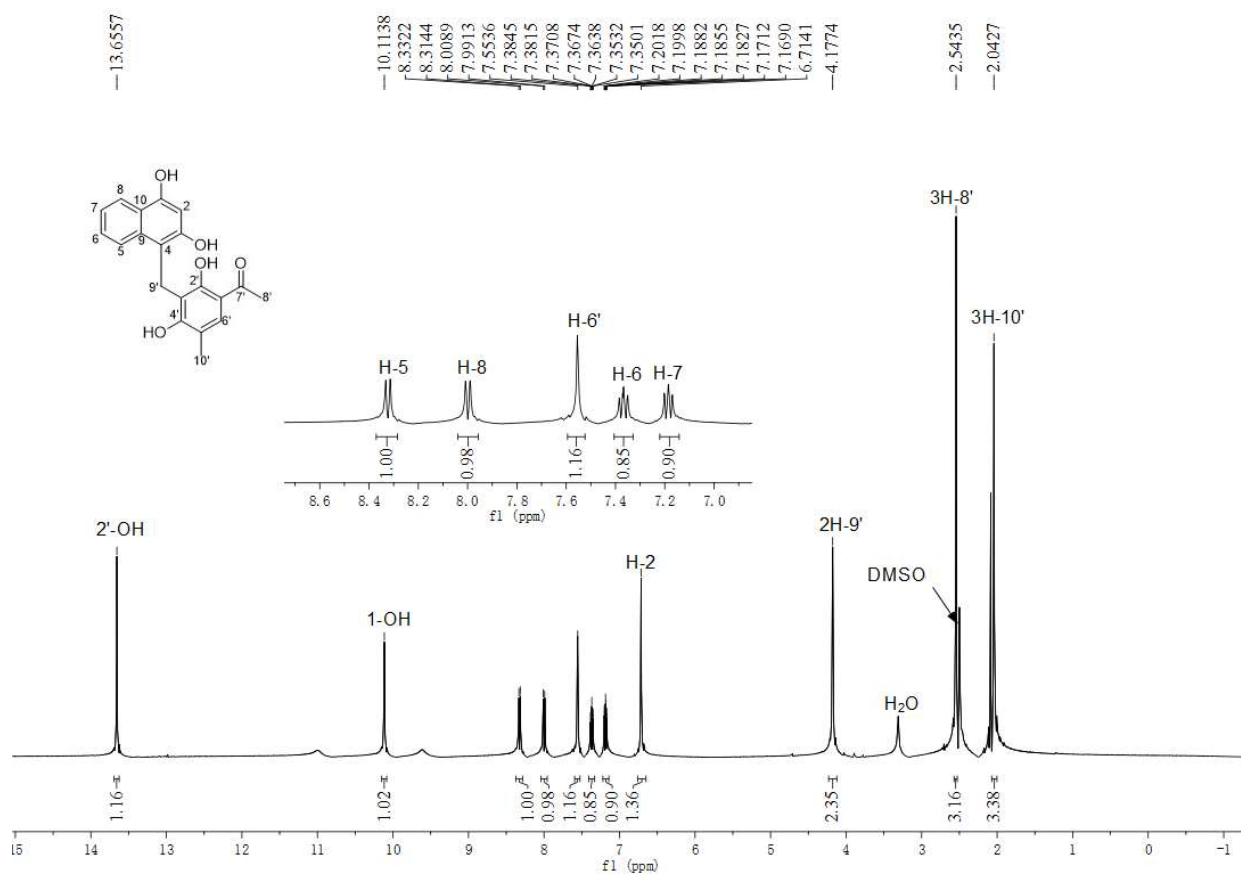


Figure S32. ^1H NMR spectrum of **18b** in $\text{DMSO-}d_6$ (500 MHz).

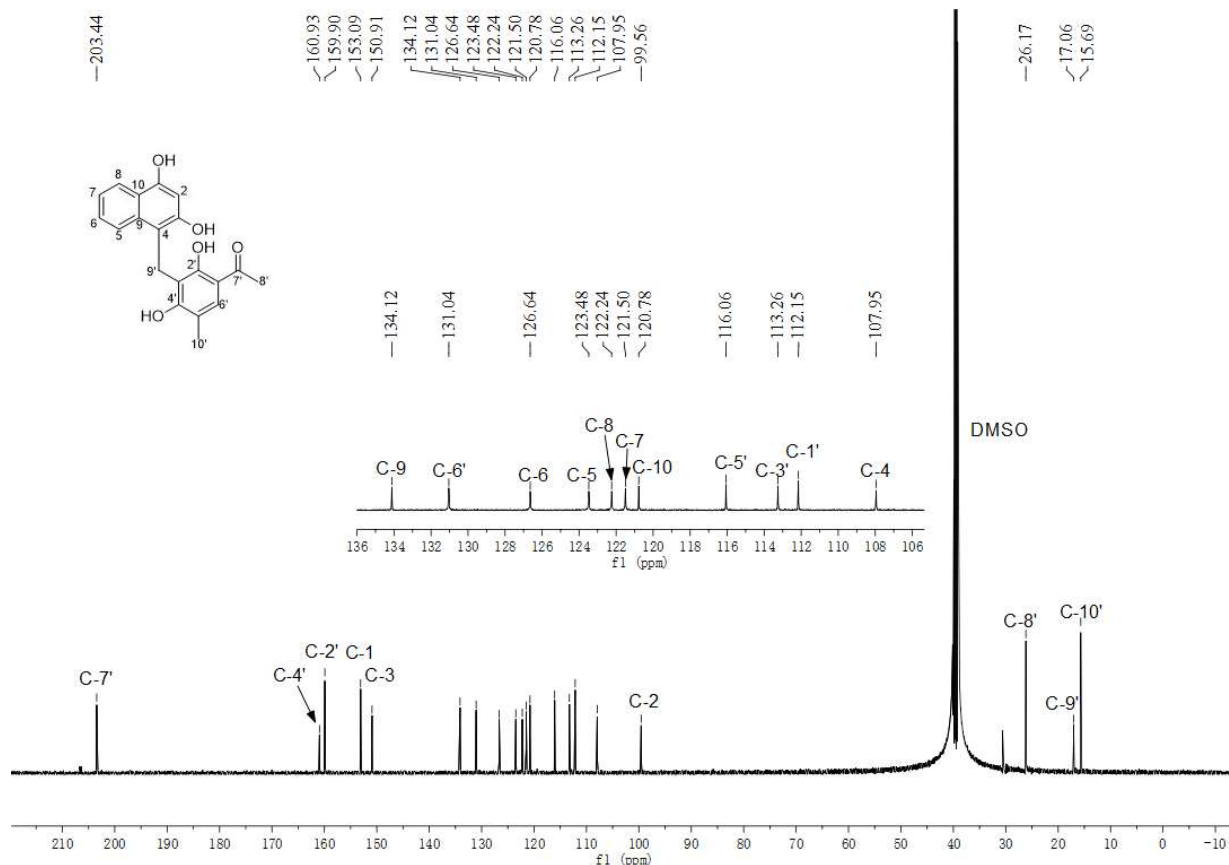


Figure S33. $^{13}\text{C}\{^1\text{H}\}$ NMR spectrum of **18b** in $\text{DMSO-}d_6$ (125 MHz).

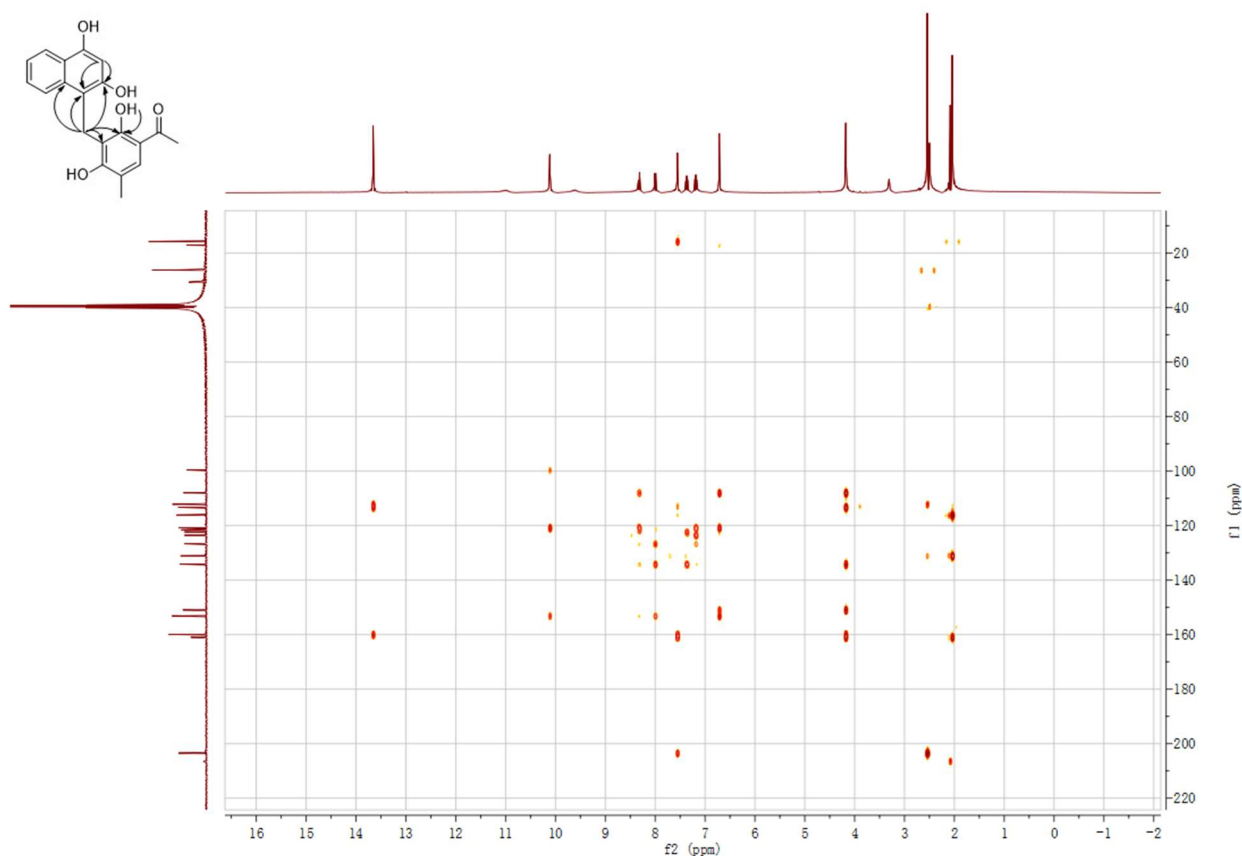


Figure S34. HMBC spectrum of **18b** in DMSO-*d*₆.

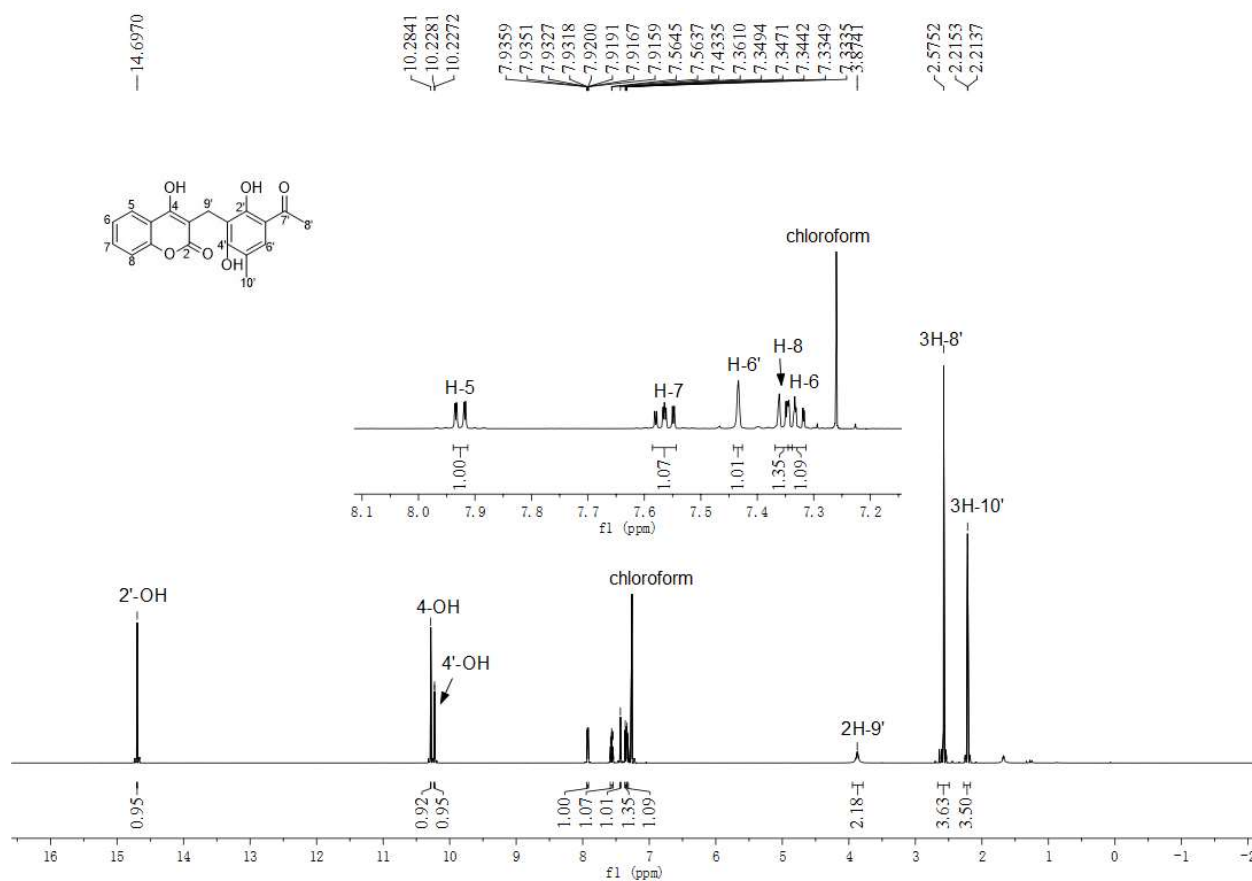


Figure S35. ¹H NMR spectrum of **29b** in CDCl₃ (500 MHz).

SUPPORTING INFORMATION

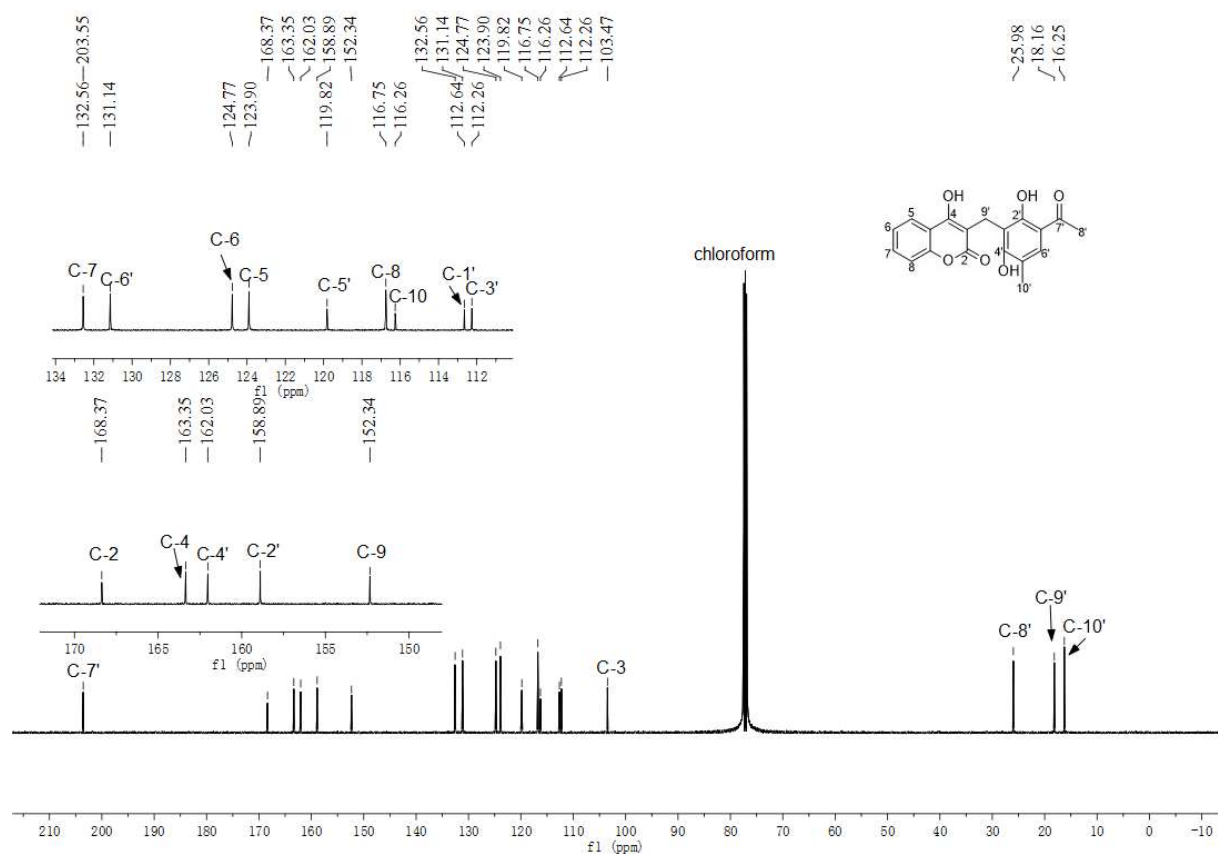


Figure S36. $^{13}\text{C}\{^1\text{H}\}$ NMR spectrum of **29b** in CDCl_3 (125 MHz).

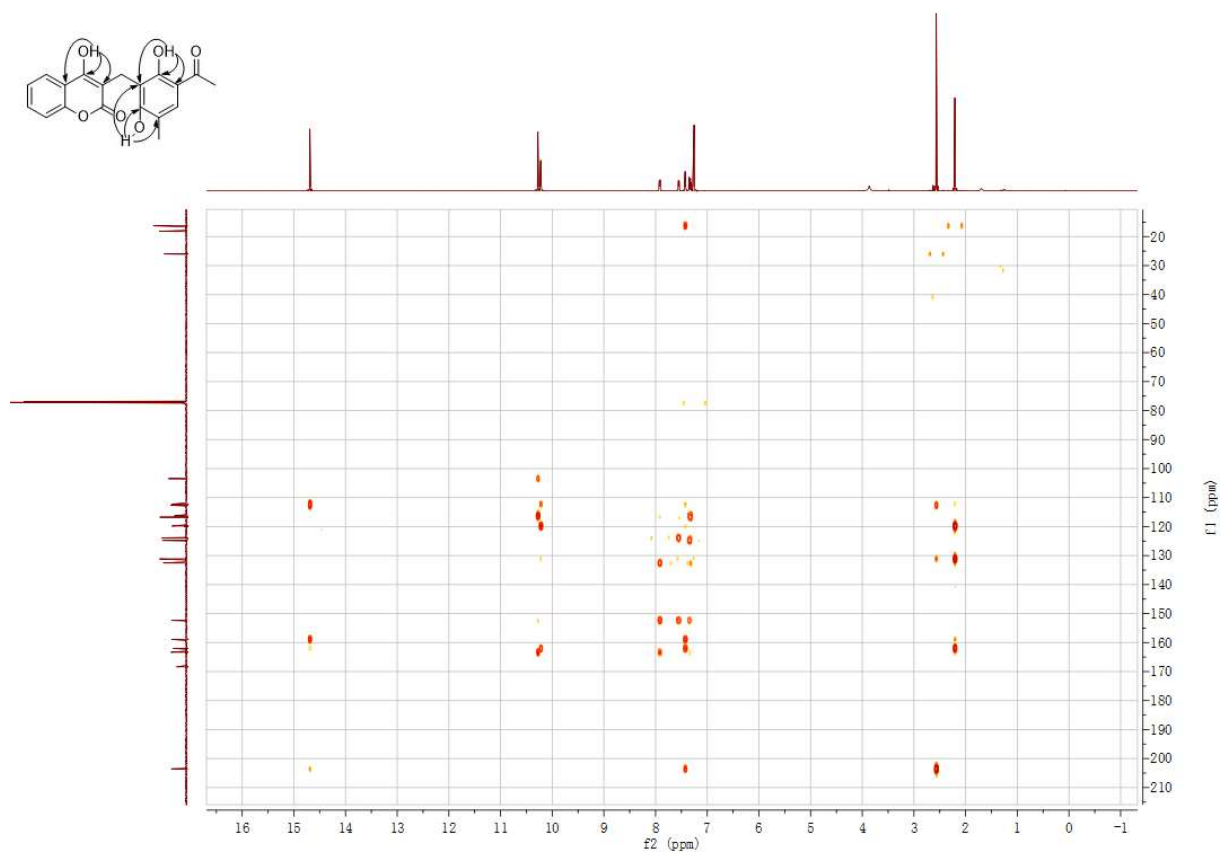


Figure S37. HMBC spectrum of **29b** in CDCl_3 .

SUPPORTING INFORMATION

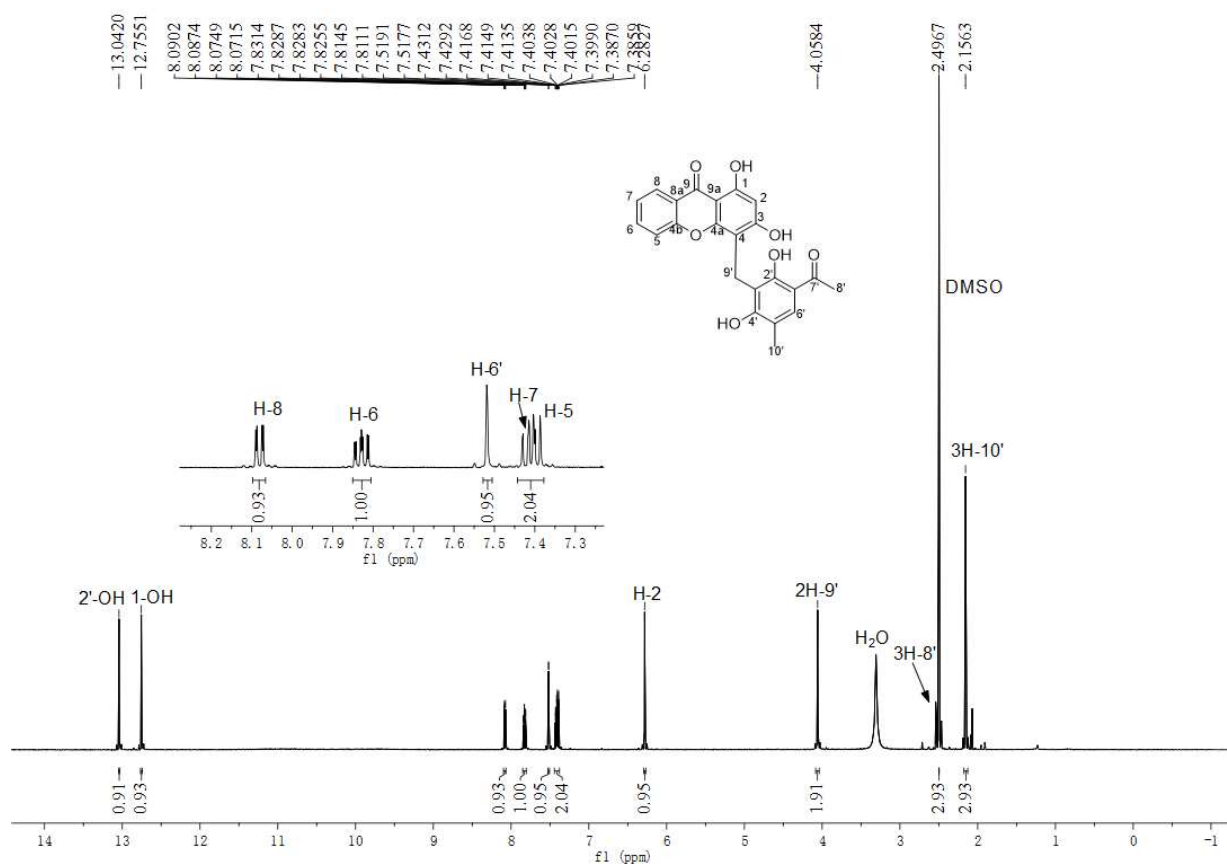


Figure S38. ^1H NMR spectrum of **35b** in $\text{DMSO}-d_6$ (500 MHz).

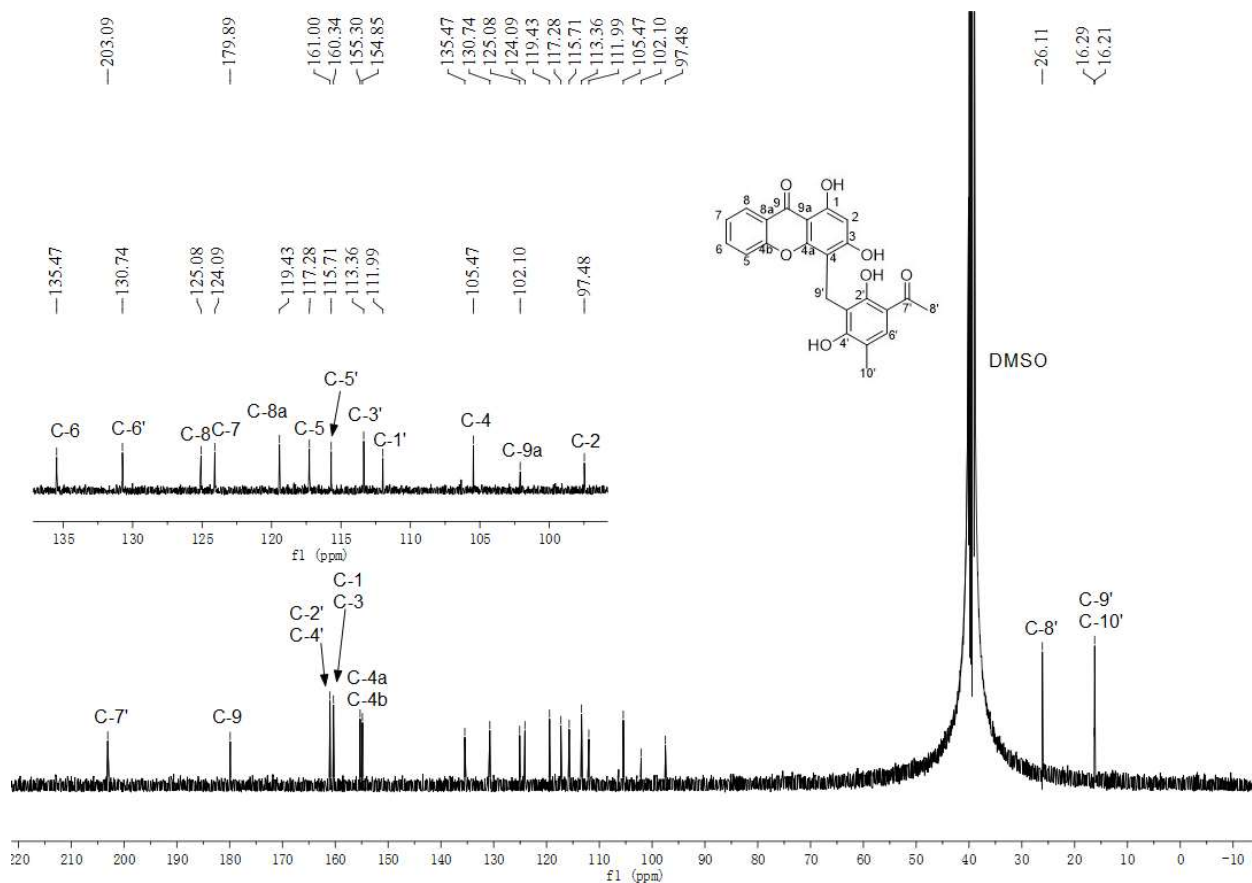


Figure S39. $^{13}\text{C}\{^1\text{H}\}$ NMR spectrum of **35b** in $\text{DMSO}-d_6$ (125 MHz).

SUPPORTING INFORMATION

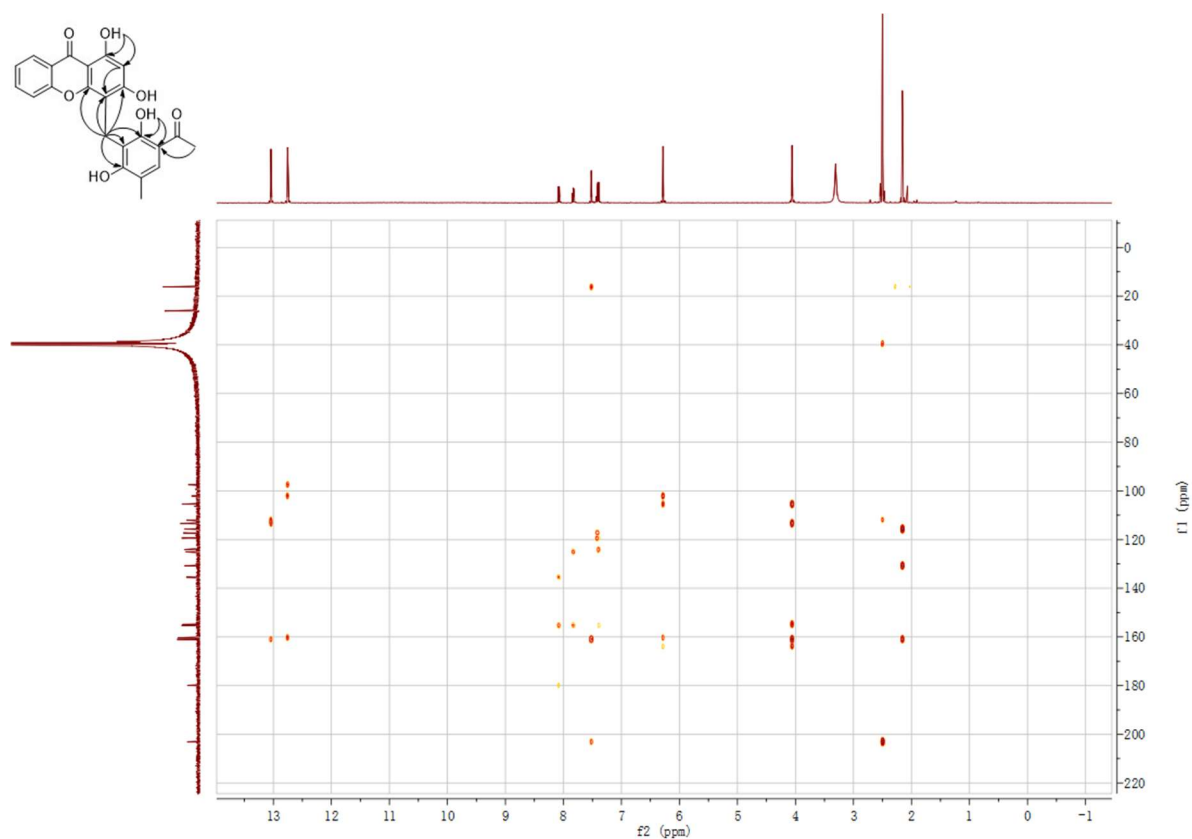


Figure S40. HMBC spectrum of **35b** in DMSO-*d*₆.

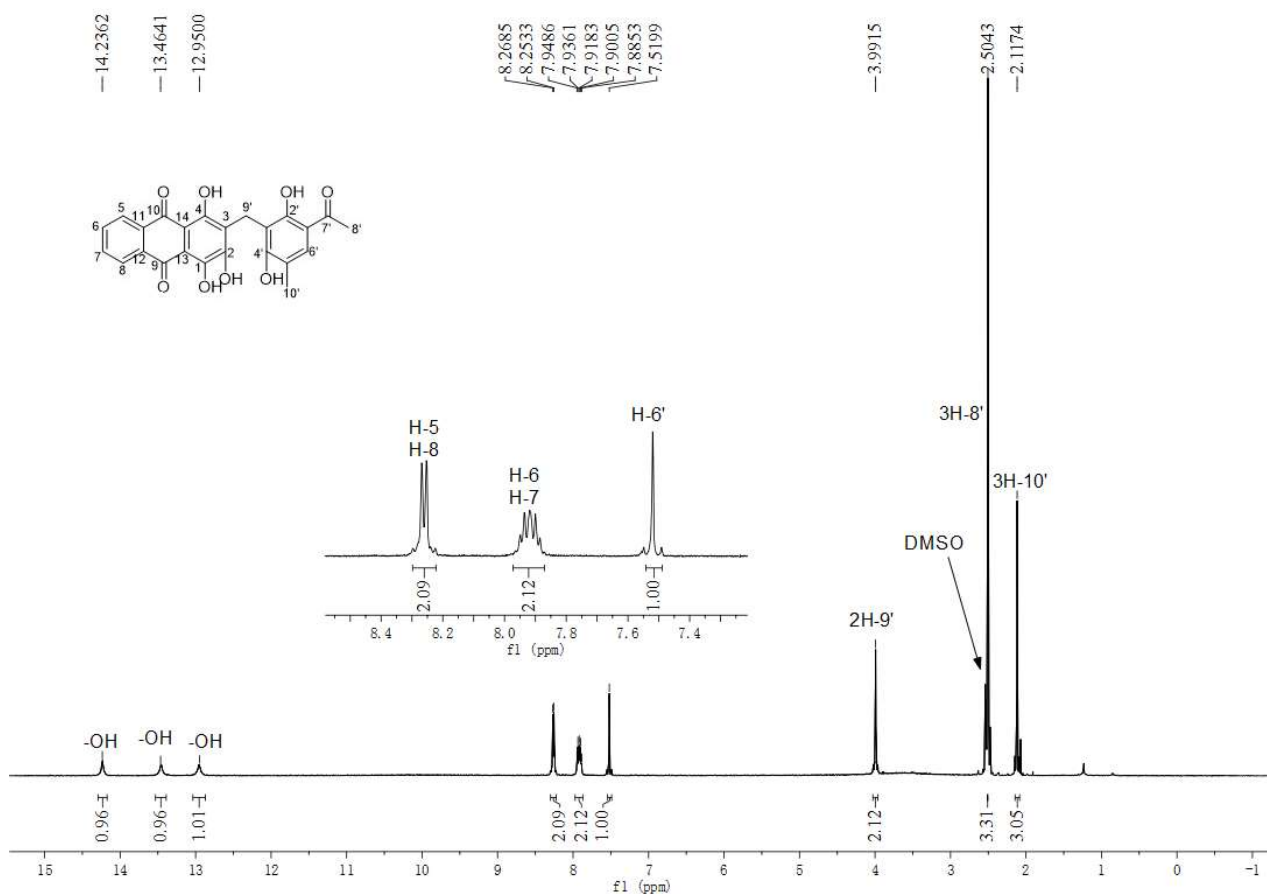
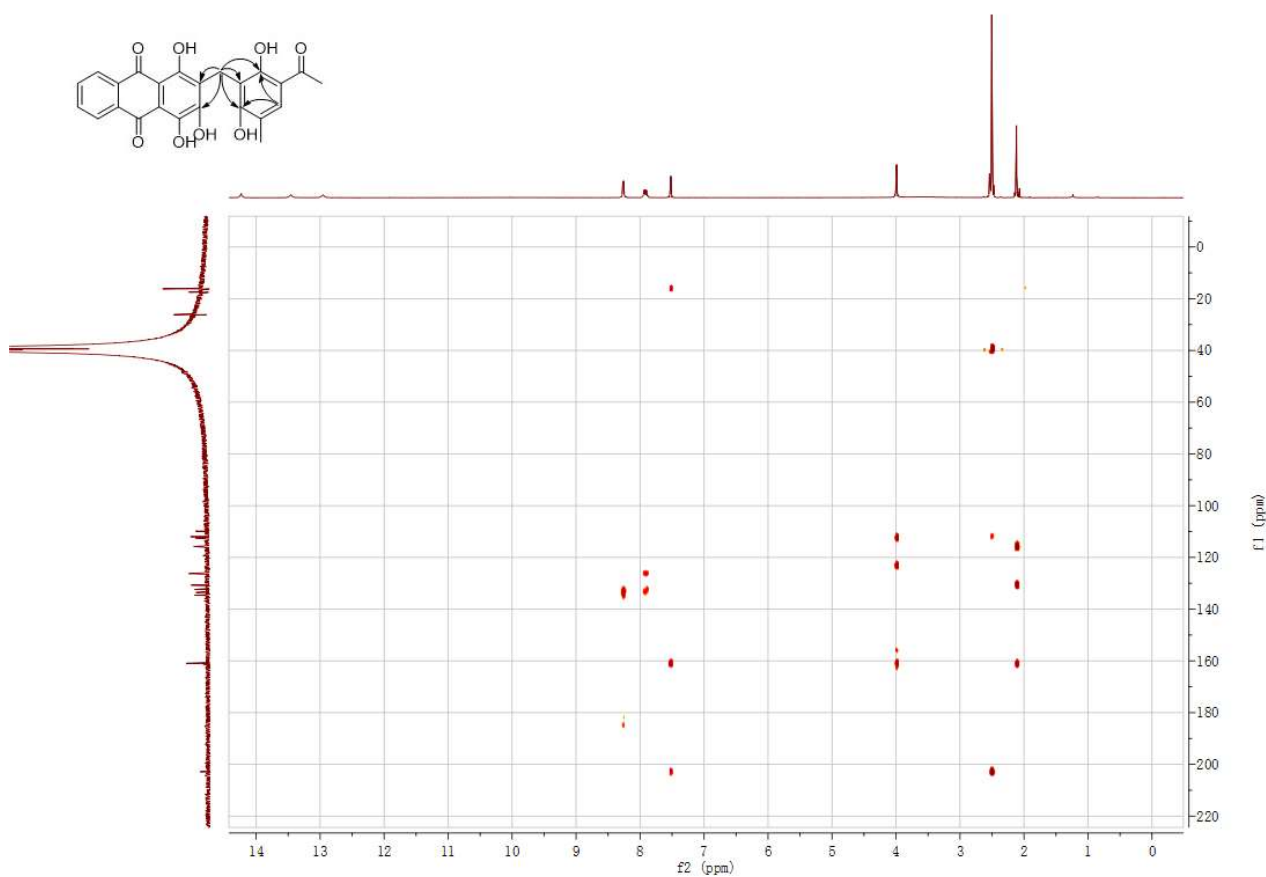
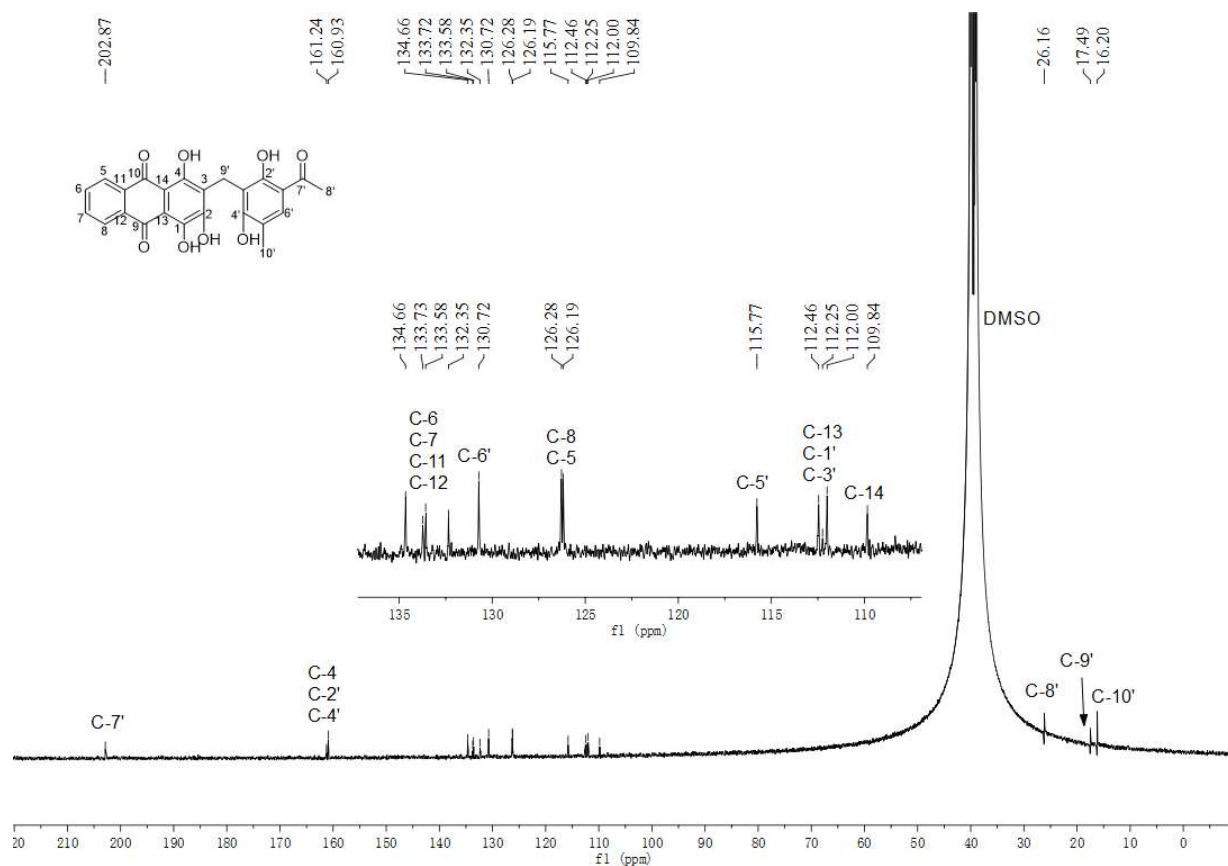
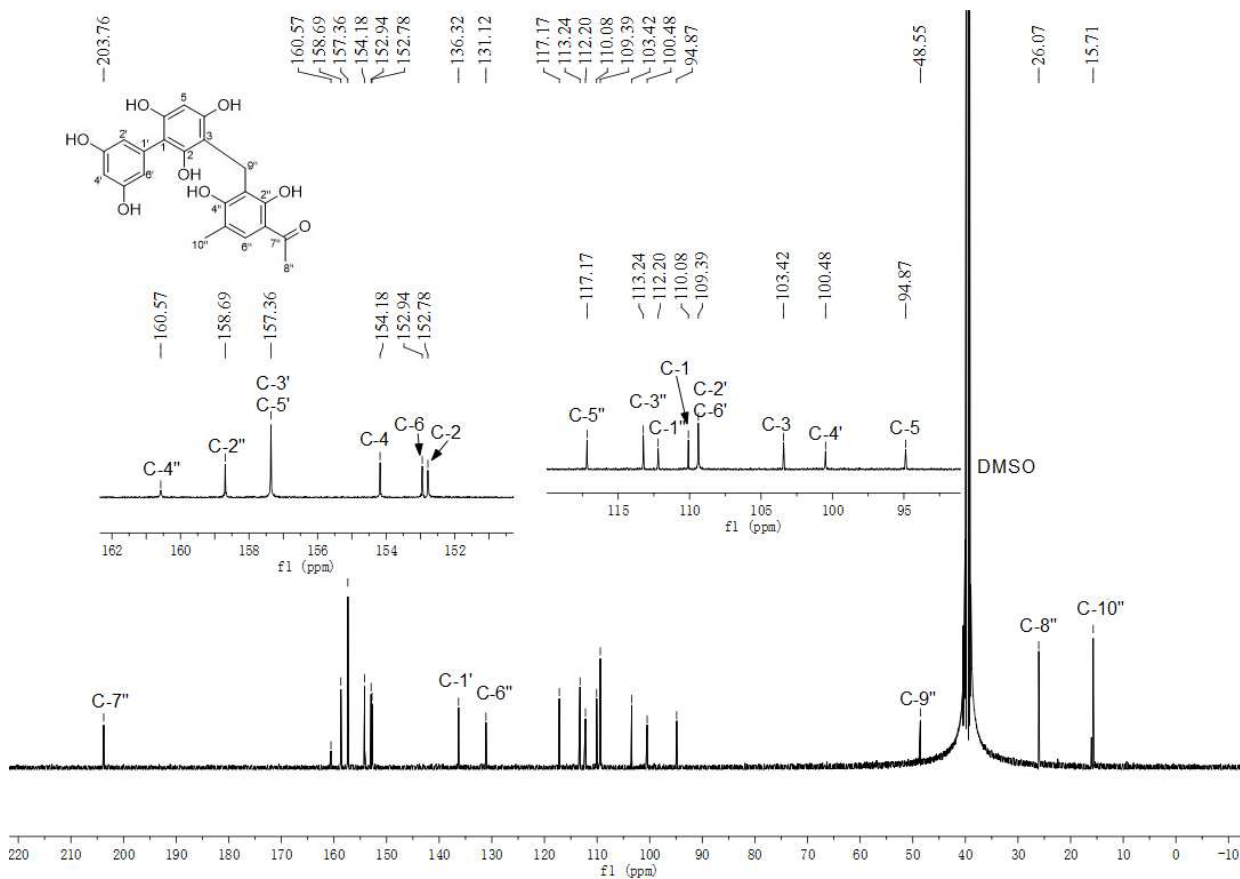
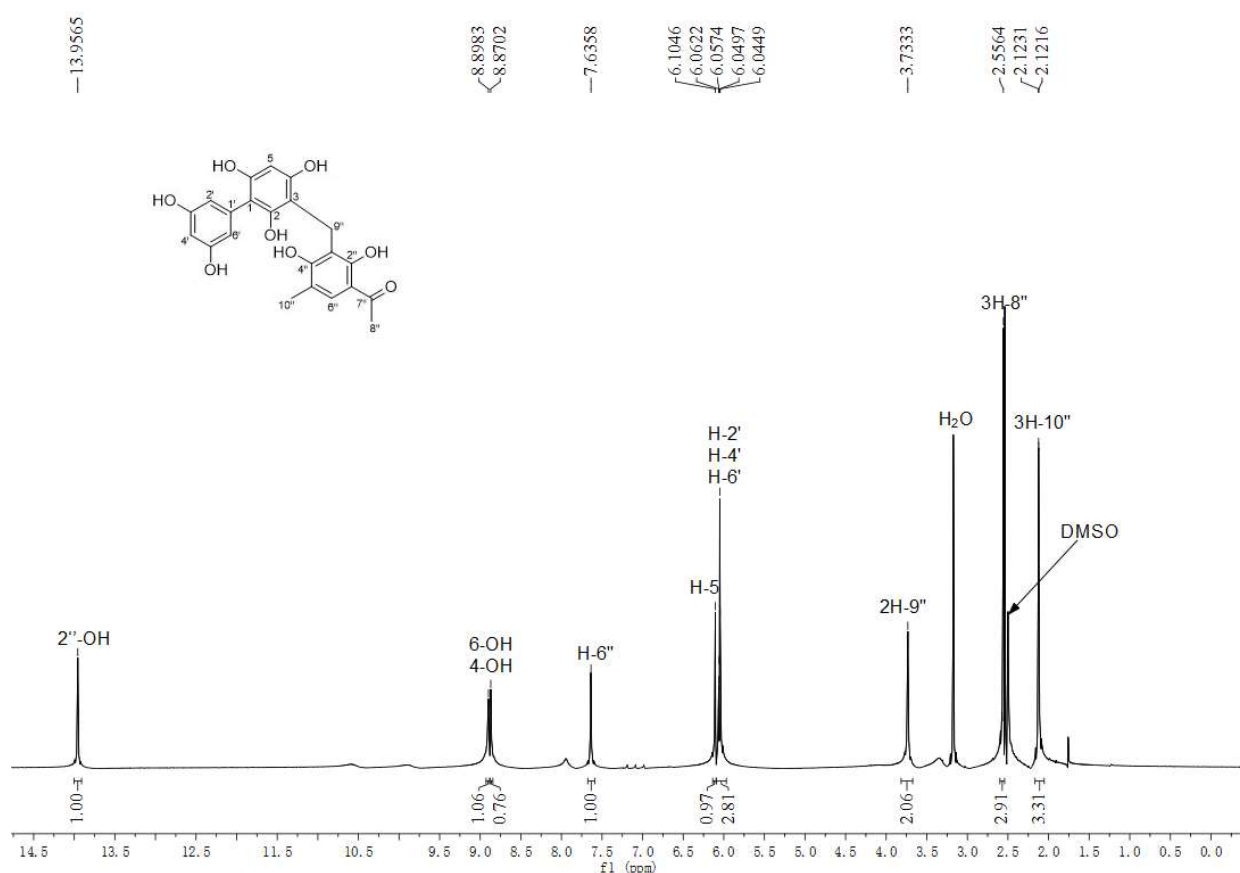


Figure S41. ¹H NMR spectrum of **41b** in DMSO-*d*₆ (500 MHz).

SUPPORTING INFORMATION



SUPPORTING INFORMATION



SUPPORTING INFORMATION

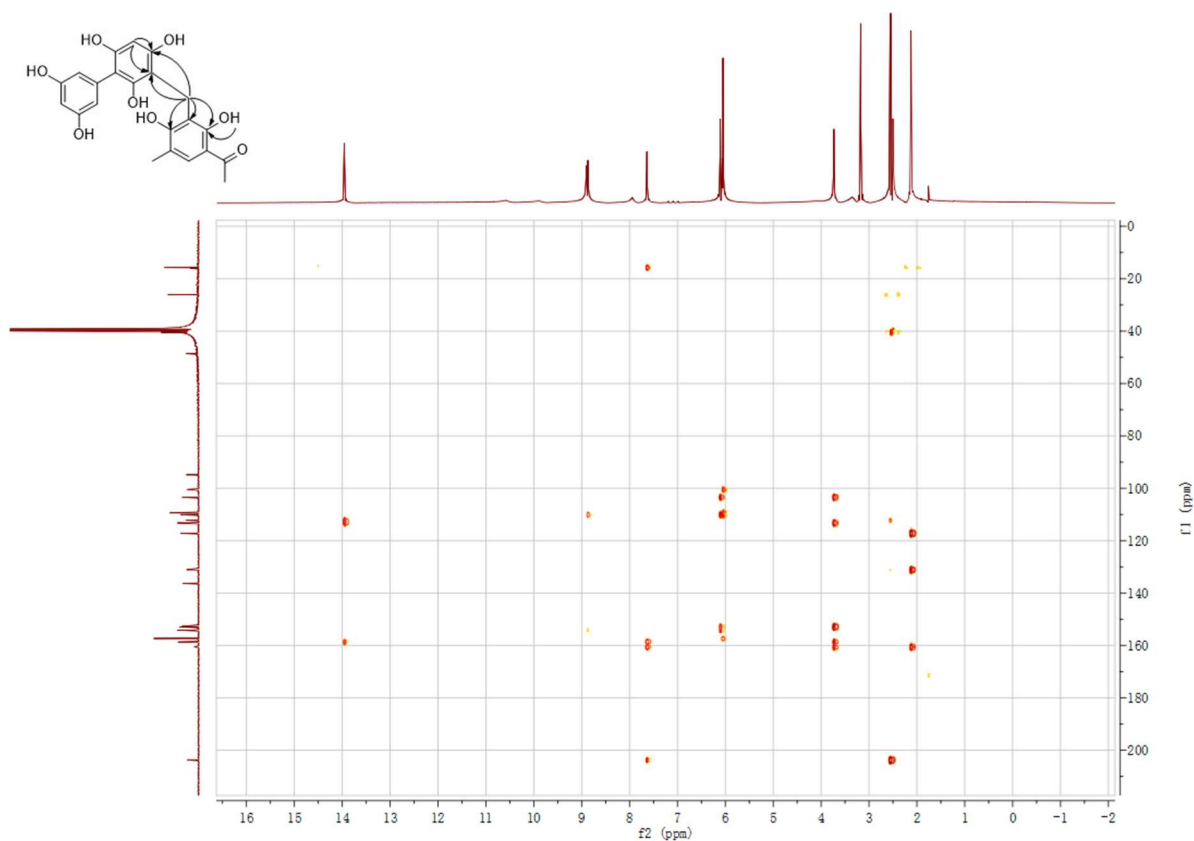


Figure S46. HMBC spectrum of **44b** in DMSO- d_6 .

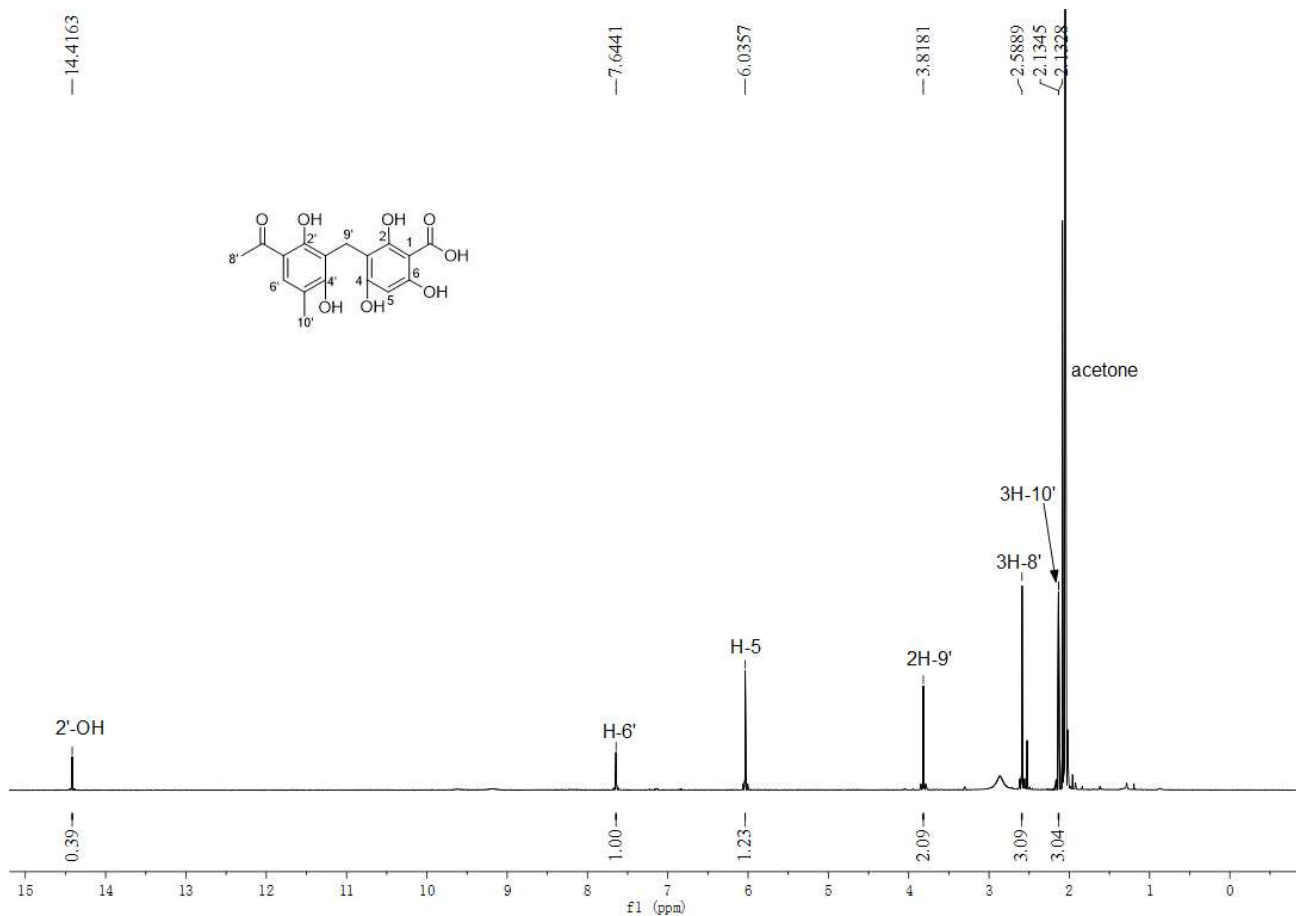


Figure S47. ^1H NMR spectrum of **45b** in acetone- d_6 (500 MHz).

SUPPORTING INFORMATION

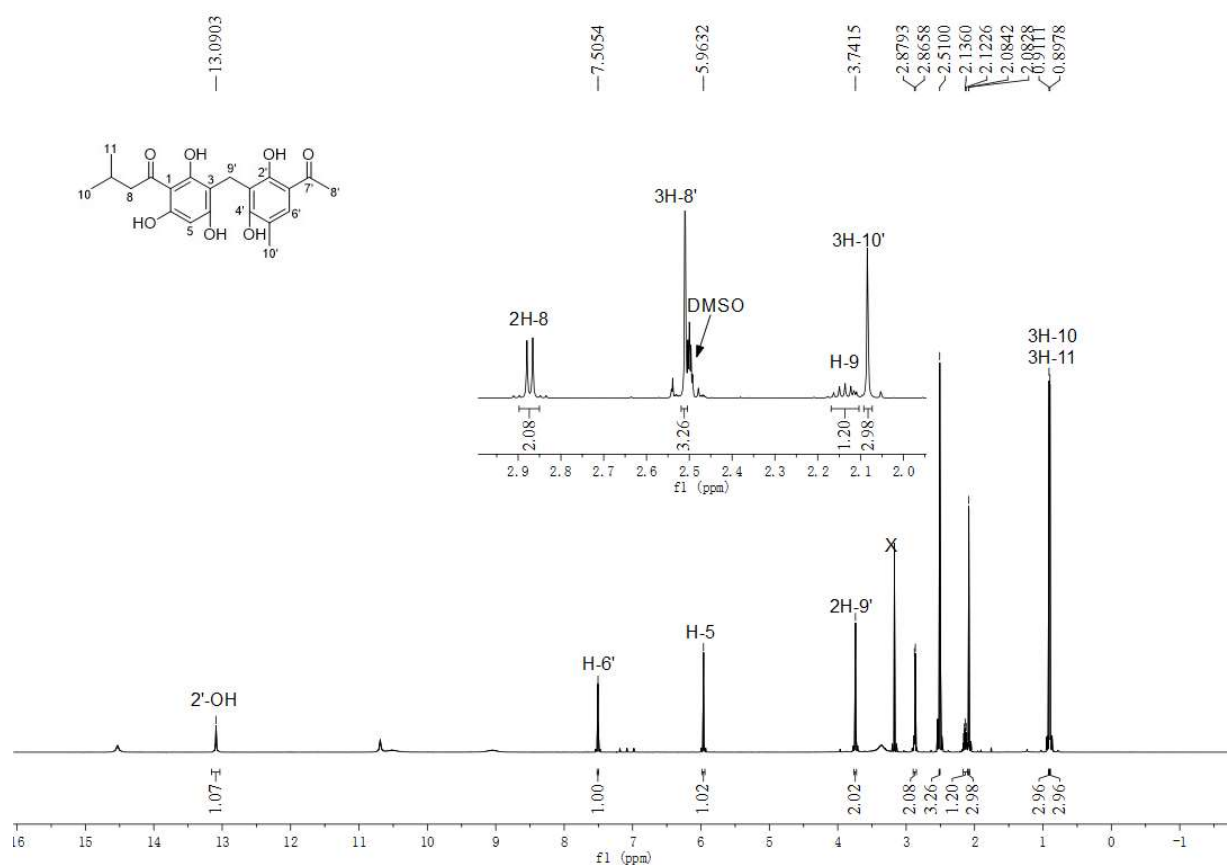


Figure S48. ^1H NMR spectrum of **47b** in $\text{DMSO-}d_6$ (500 MHz).

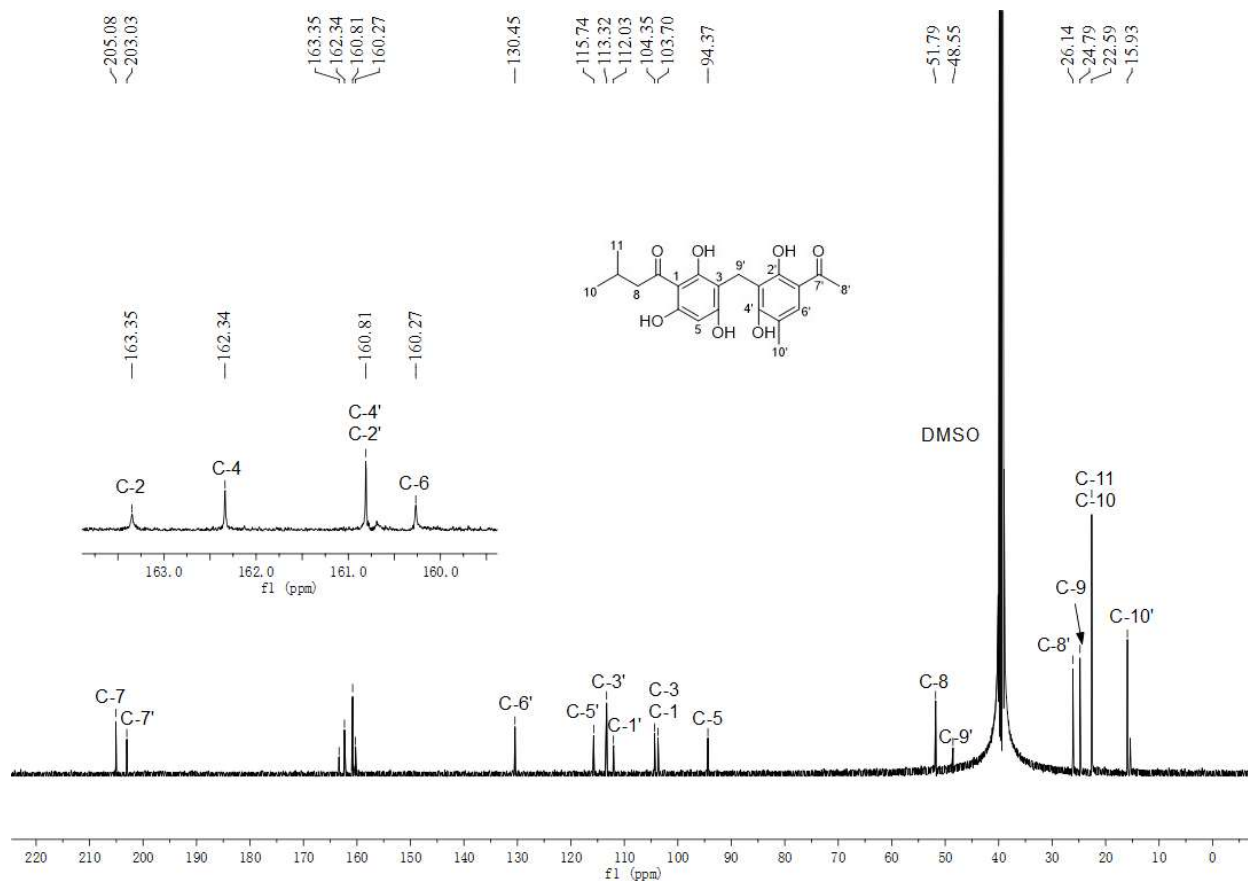


Figure S49. $^{13}\text{C}\{^1\text{H}\}$ NMR spectrum of **47b** in $\text{DMSO-}d_6$ (125 MHz).

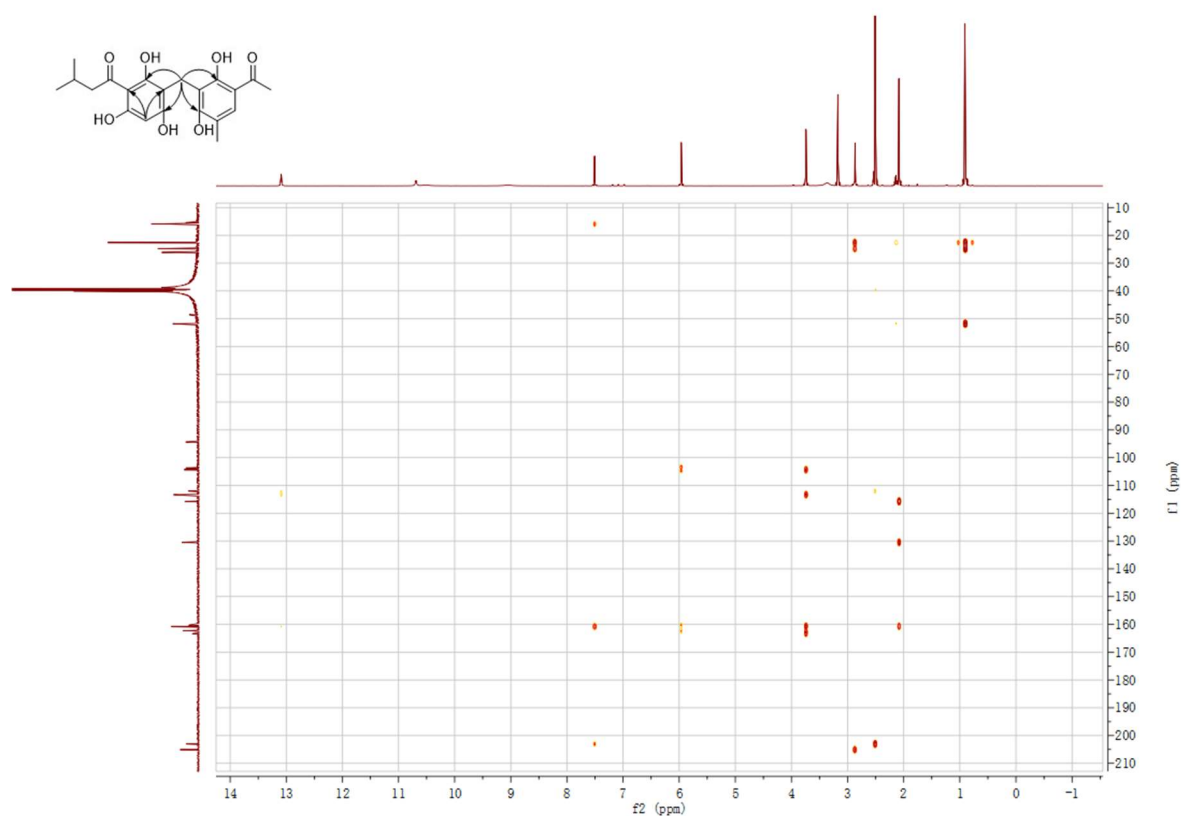


Figure S50. HMBC spectrum of **47b** in DMSO-*d*₆.

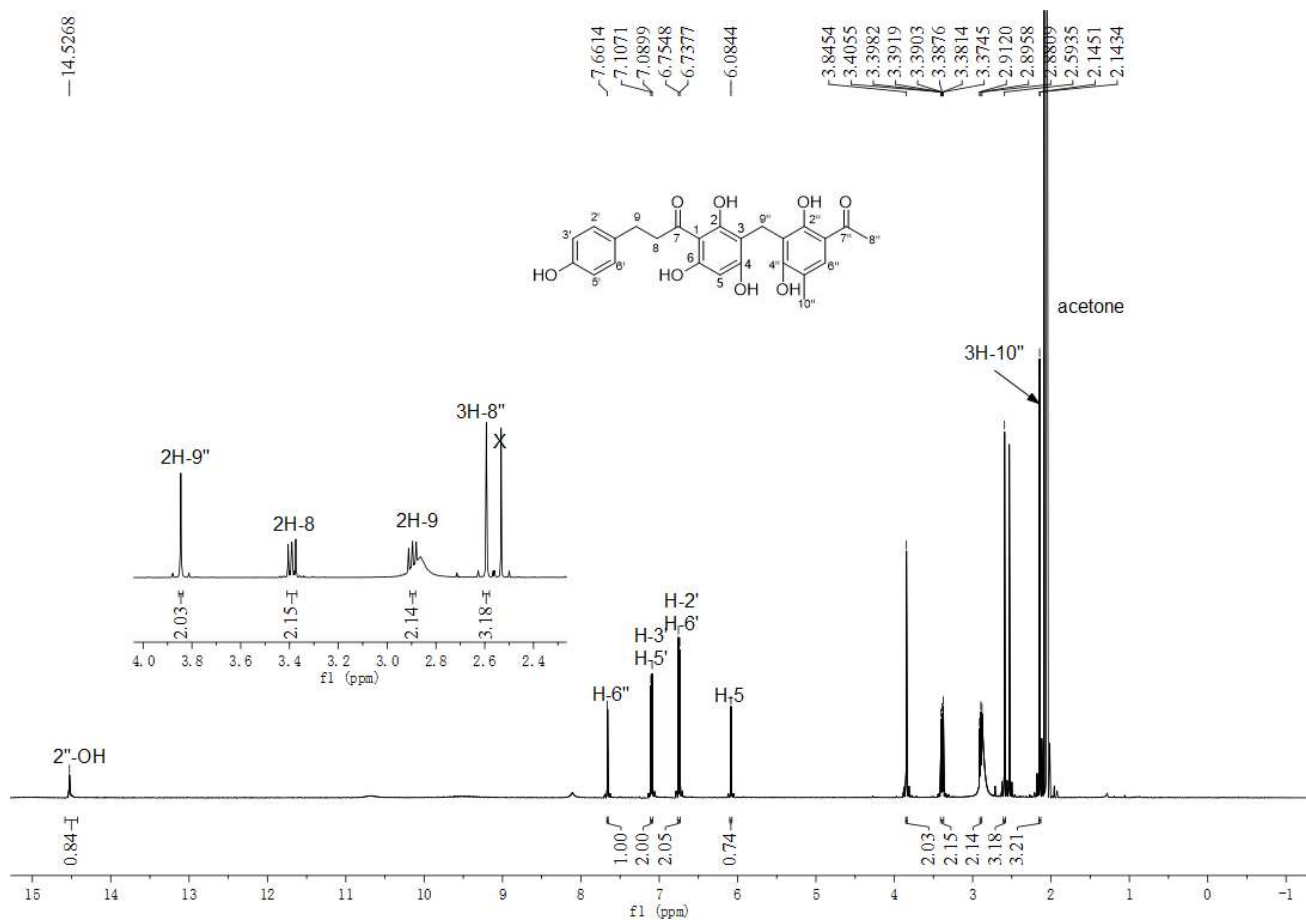
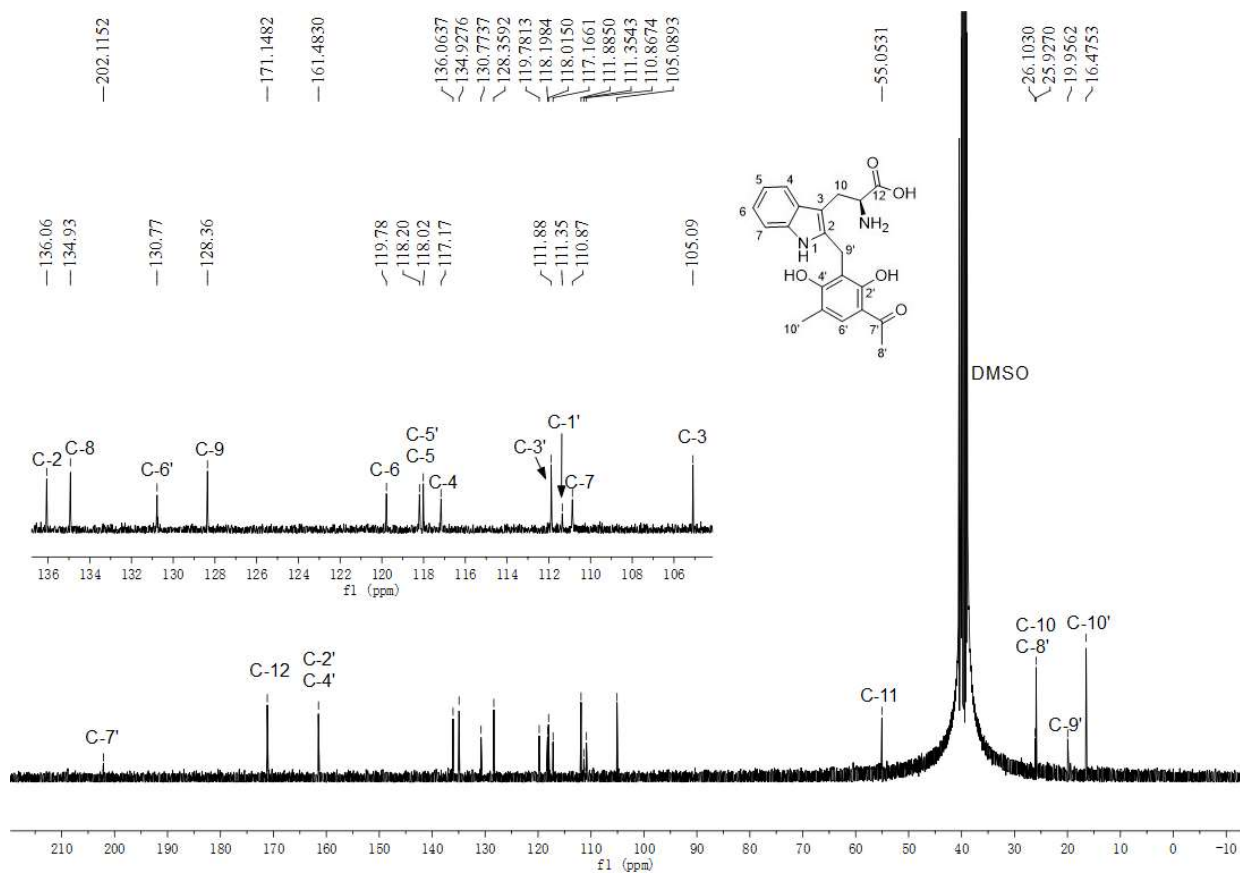
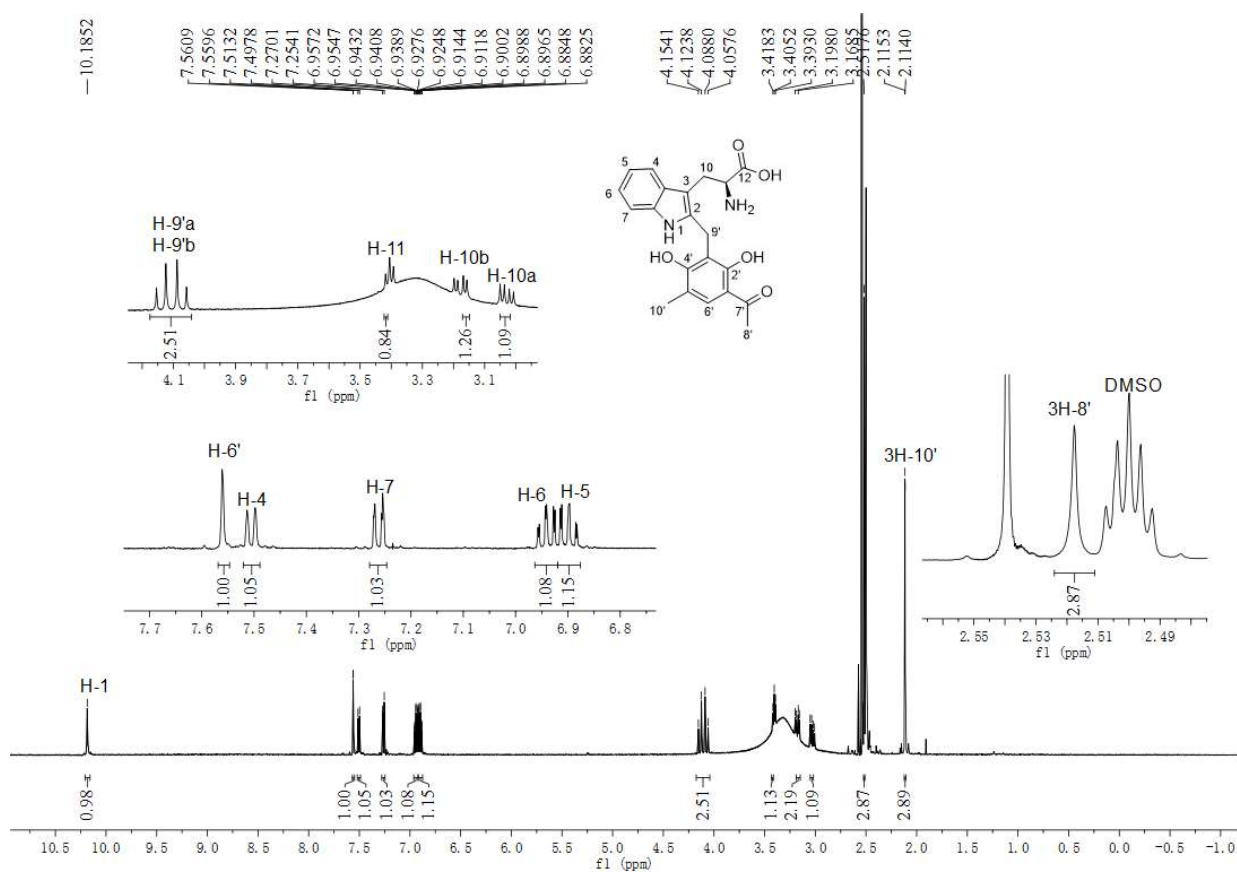


Figure S51. ¹H NMR spectrum of **50b** in acetone-*d*₆ (500 MHz).

SUPPORTING INFORMATION



SUPPORTING INFORMATION

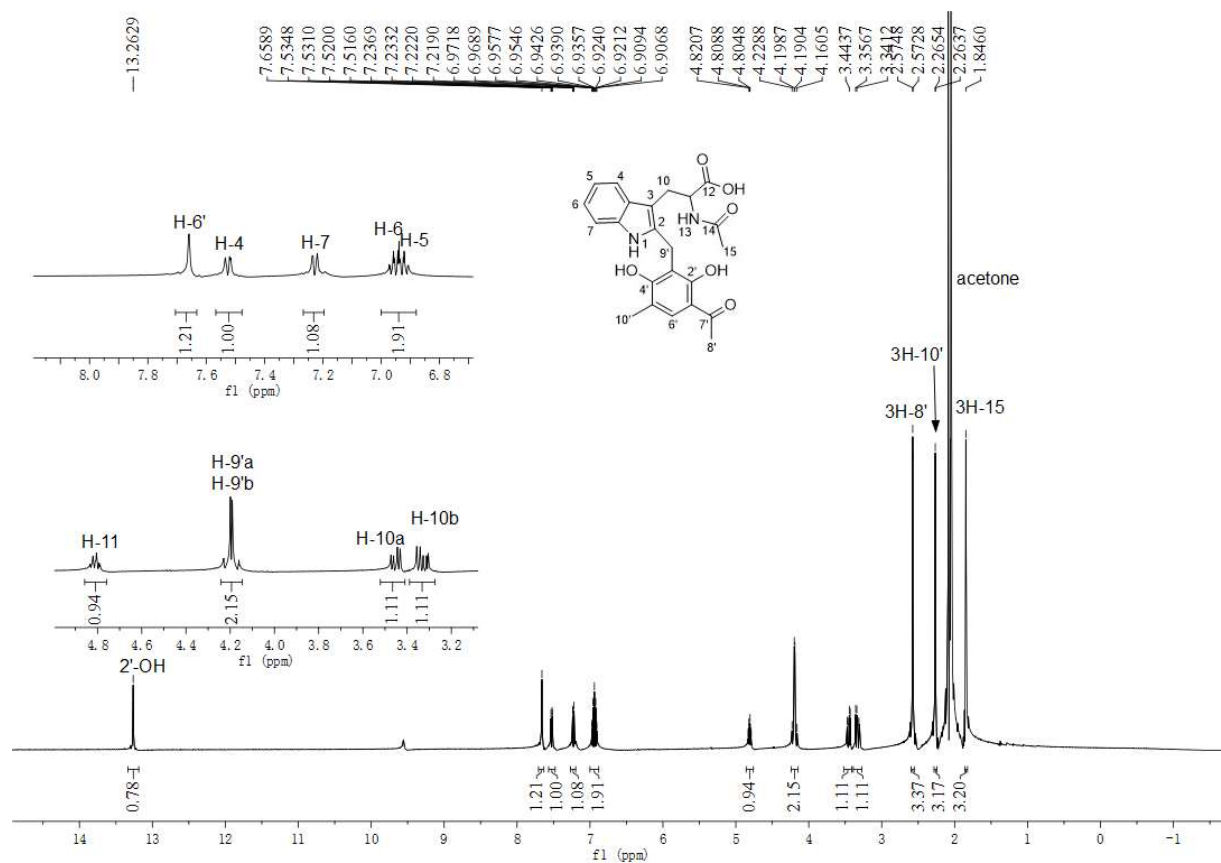


Figure S54. ¹H NMR spectrum of (±)-65b in acetone-d₆ (500 MHz).

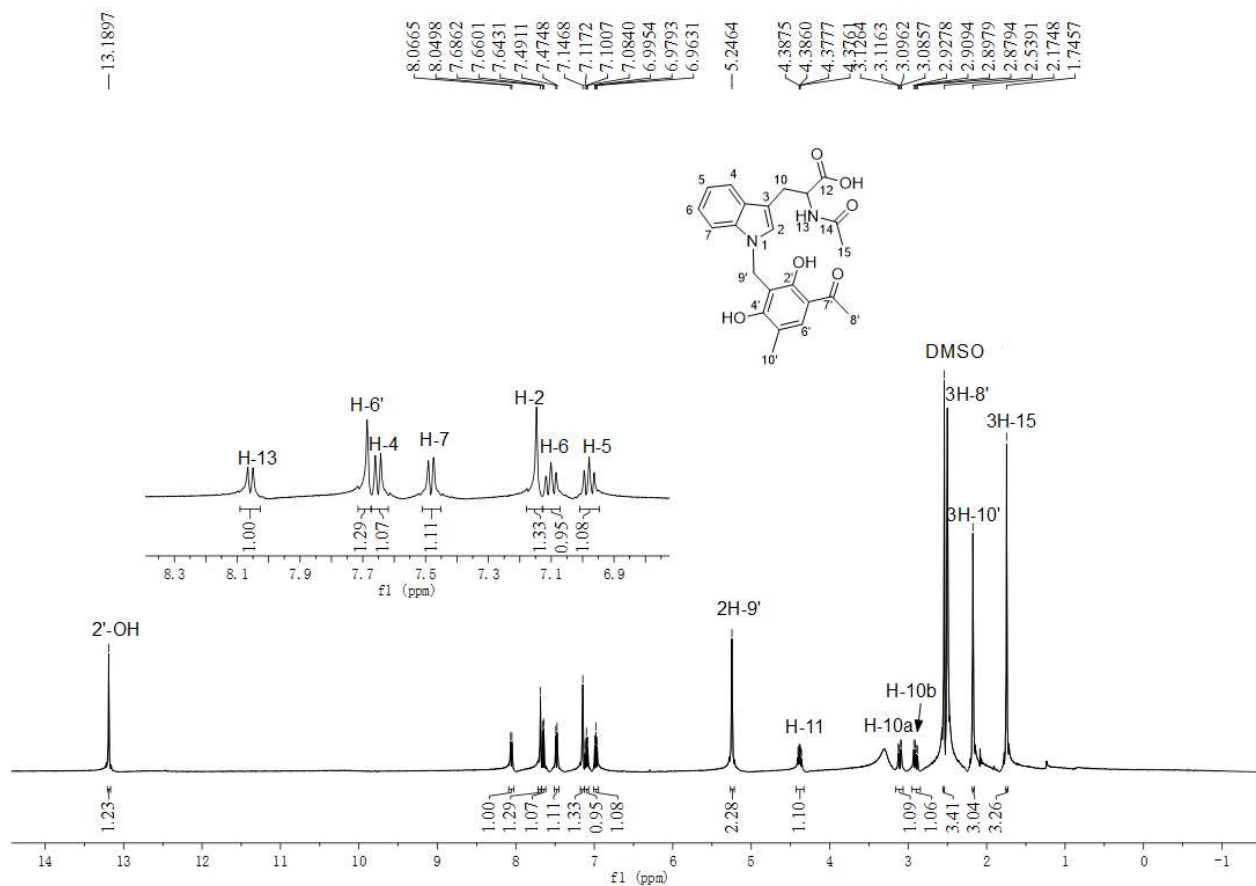


Figure S55. ¹H NMR spectrum of (±)-65c in DMSO-d₆ (500 MHz).

SUPPORTING INFORMATION

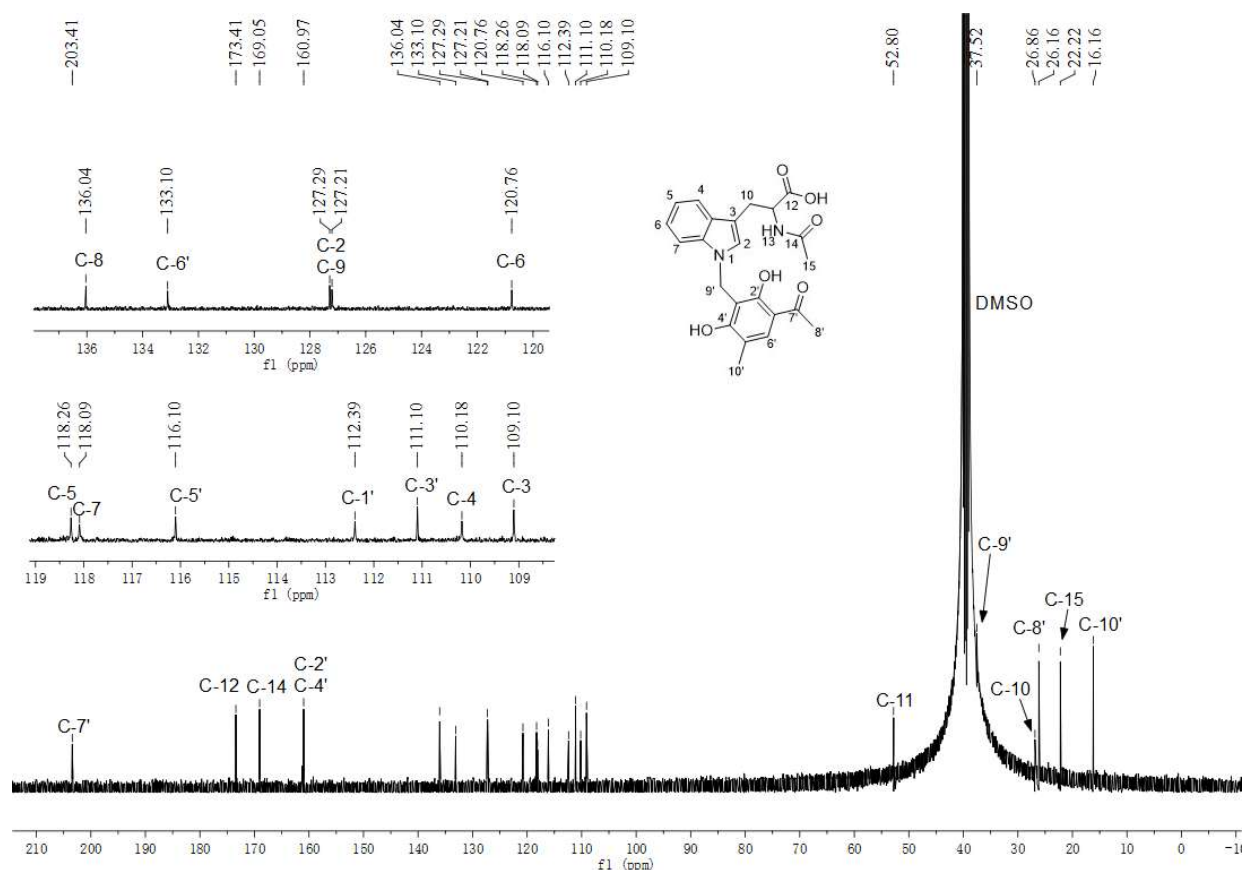


Figure S56. $^{13}\text{C}\{^1\text{H}\}$ NMR spectrum of (±)-65c in DMSO- d_6 (125 MHz).

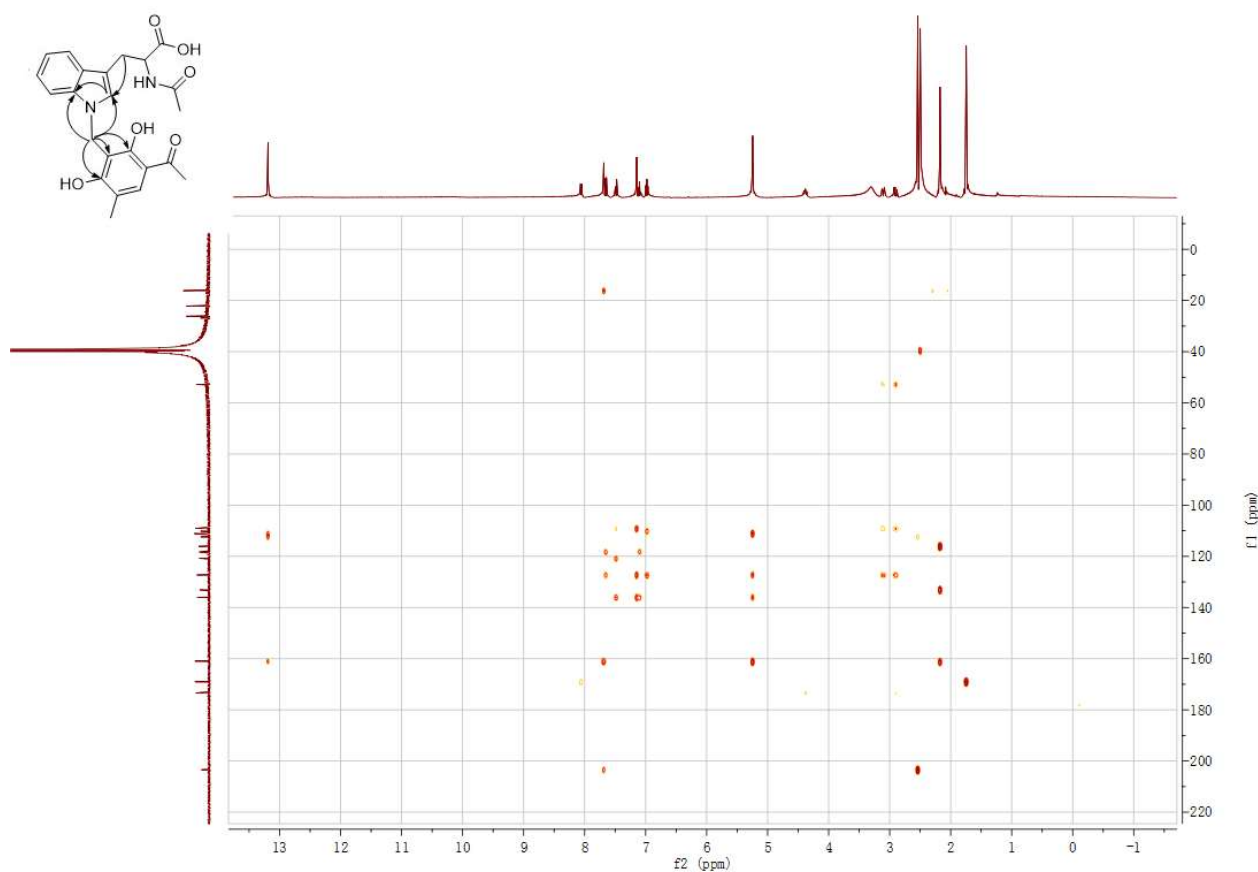


Figure S57. HMBC spectrum of (±)-65c in DMSO- d_6 .

SUPPORTING INFORMATION

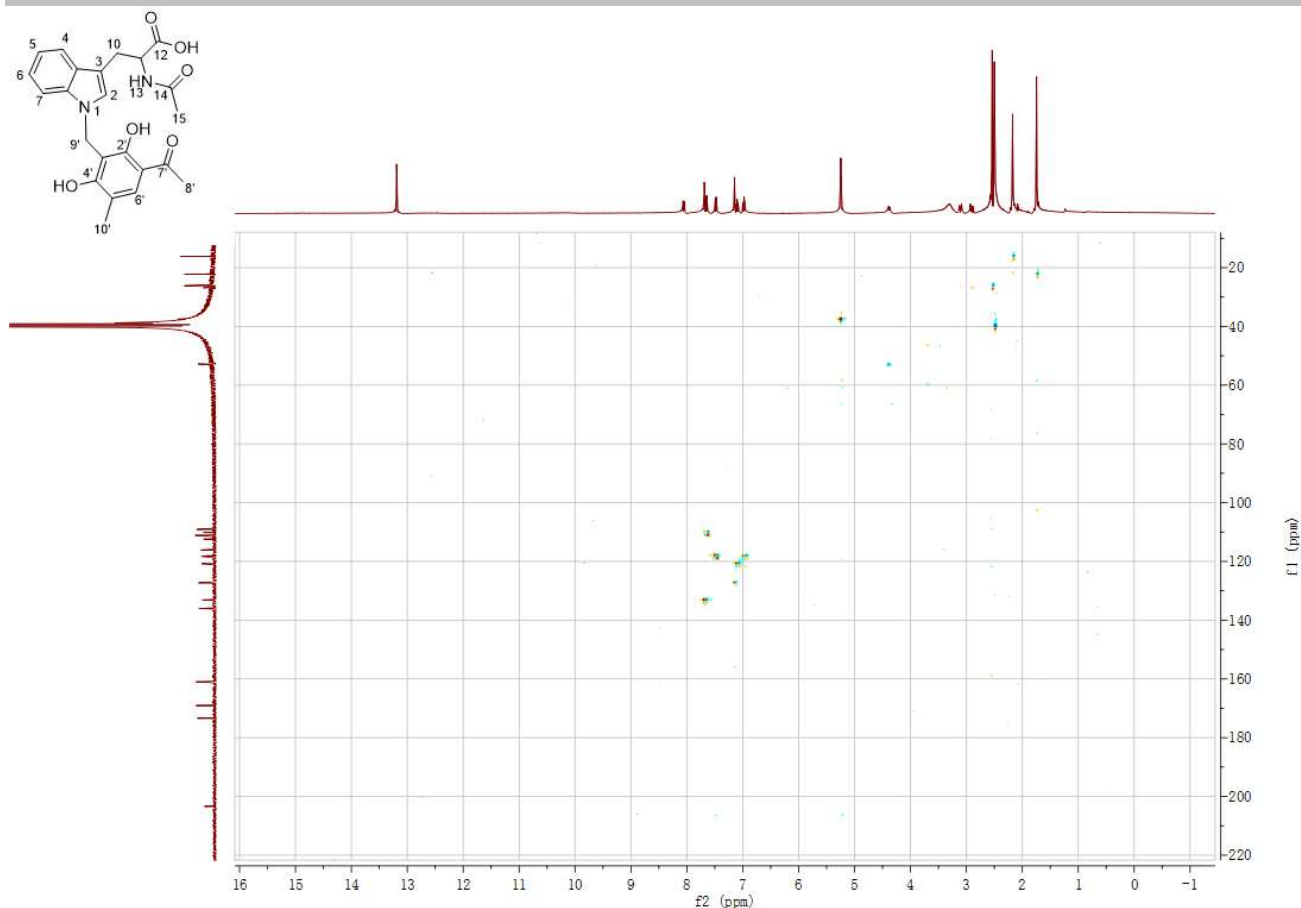


Figure S58. HSQC spectrum of (±)-65c in DMSO-*d*₆.

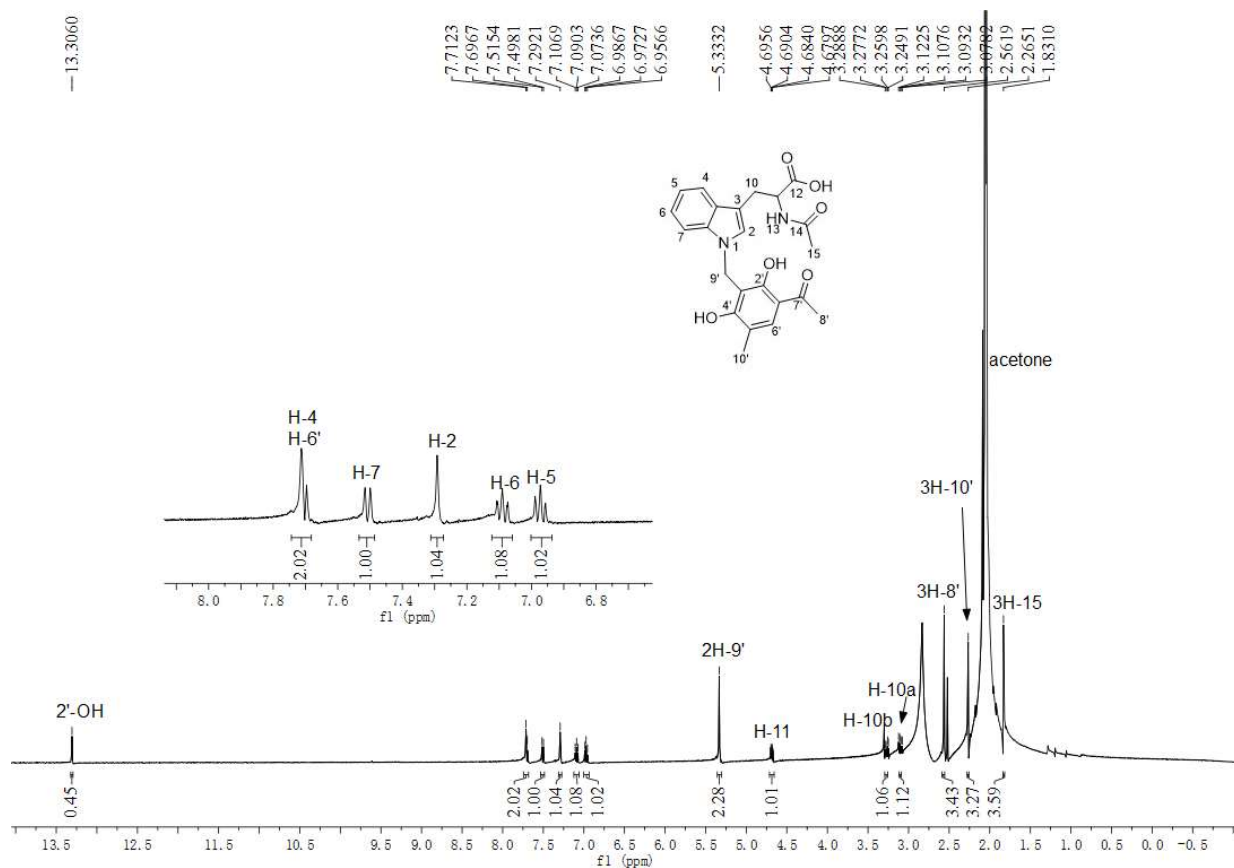
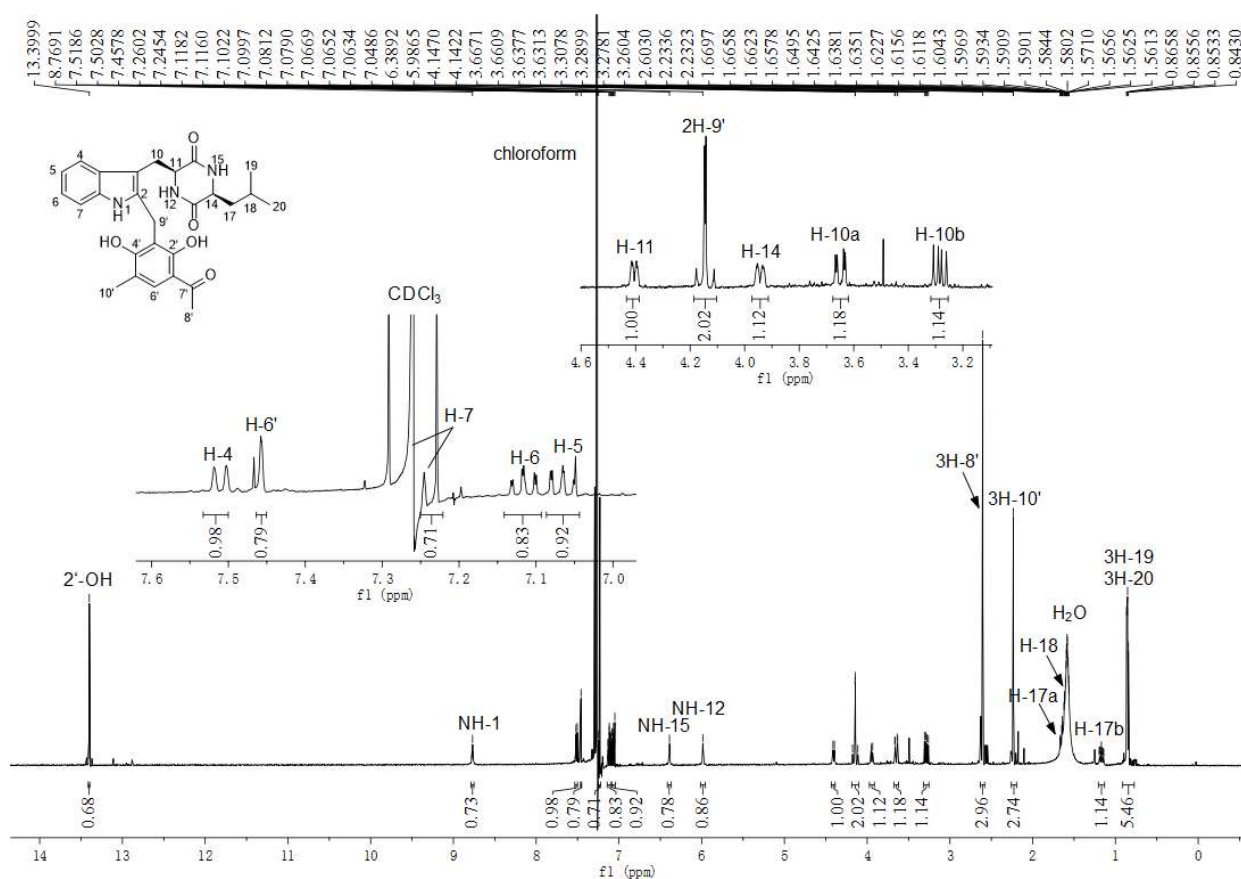
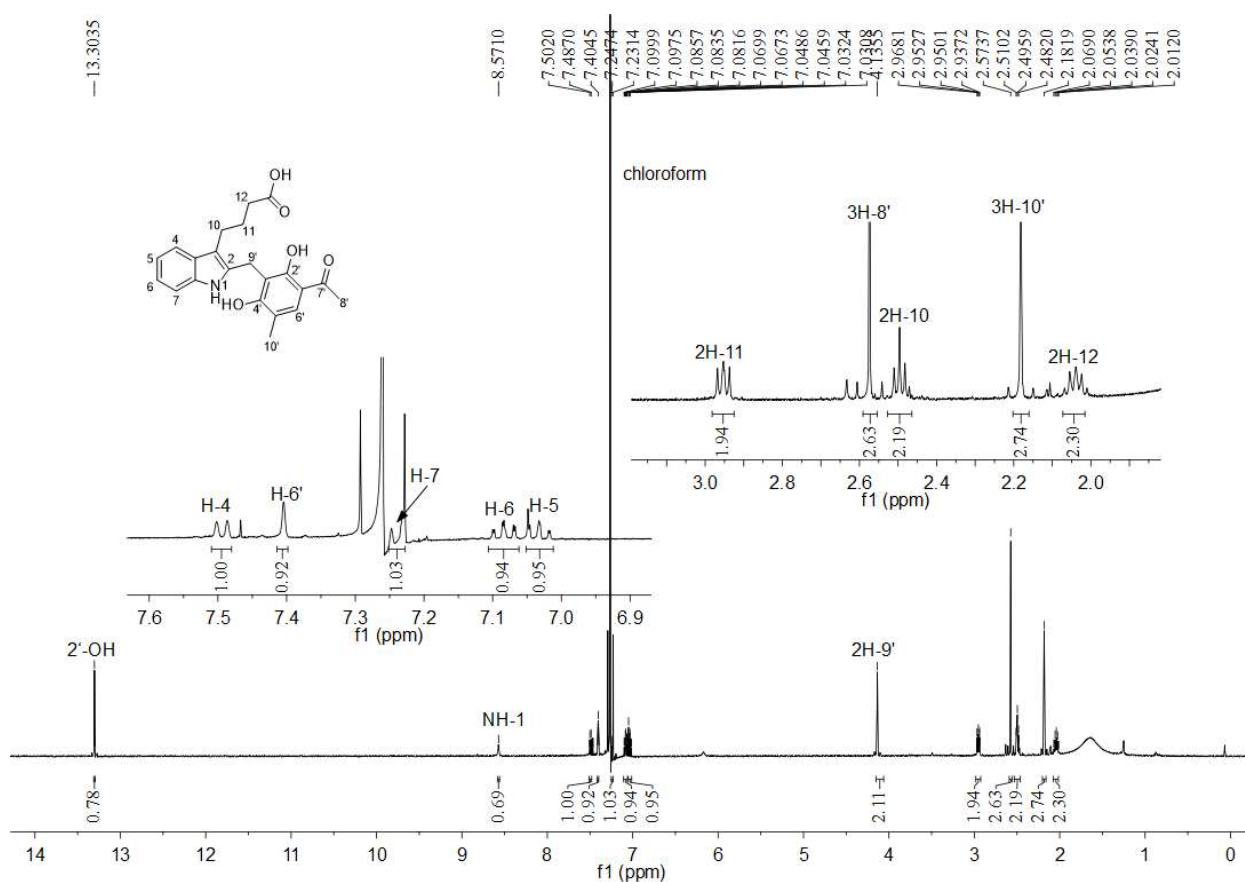
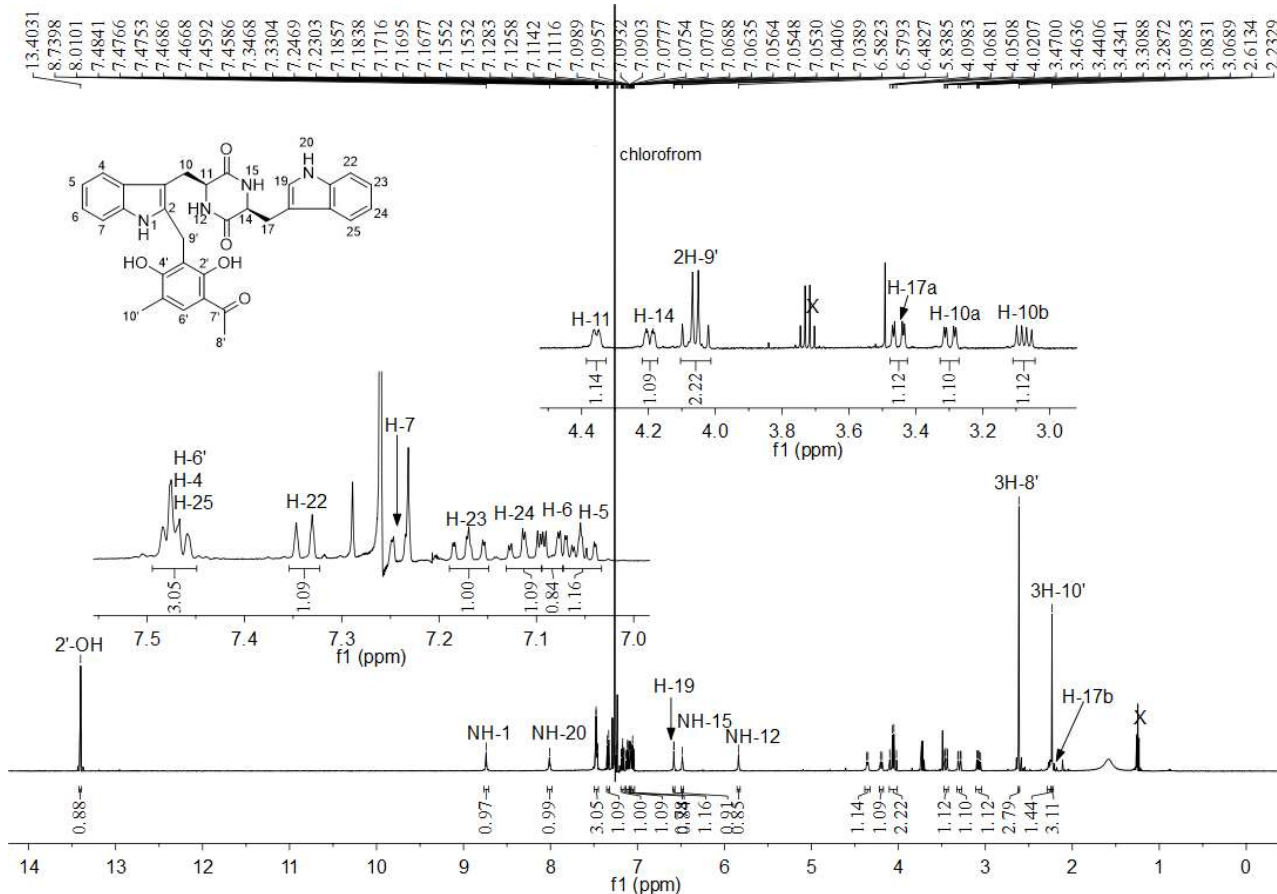
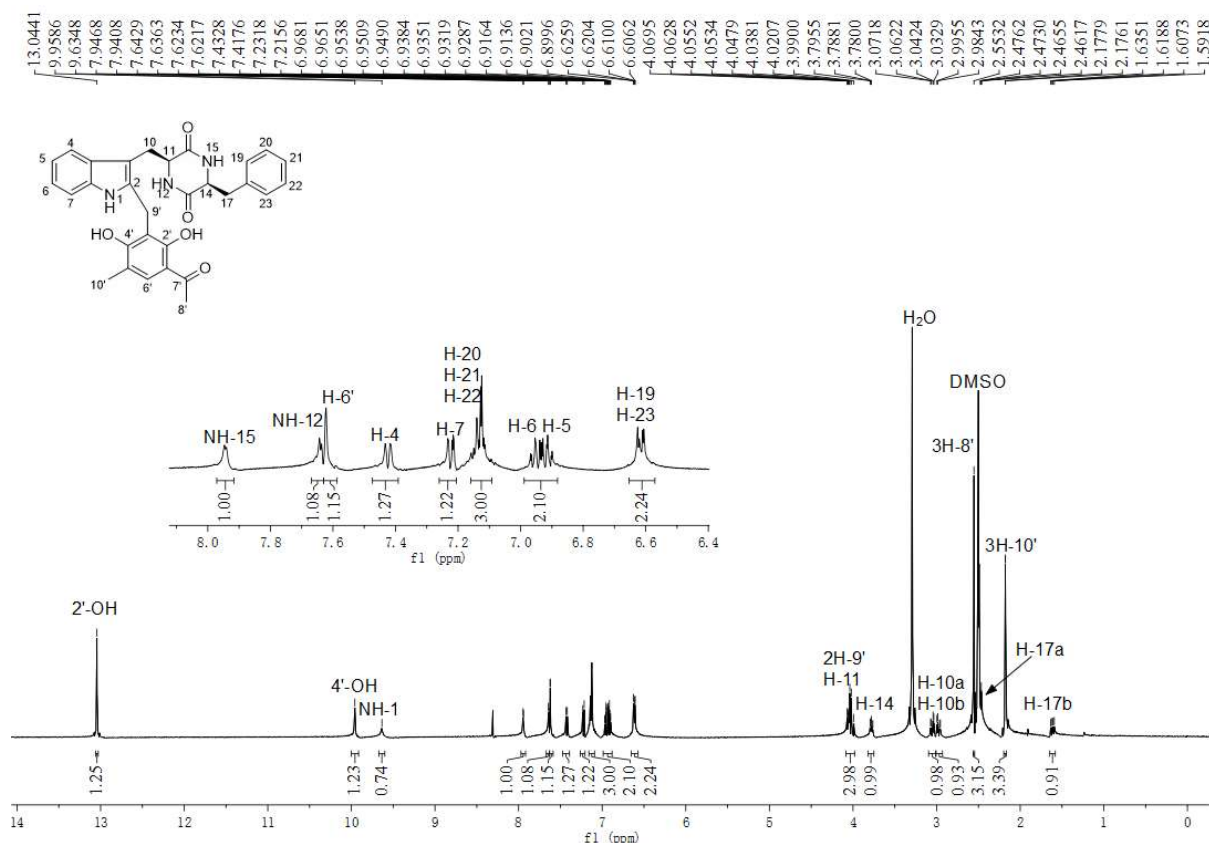


Figure S59. ¹H NMR spectrum of (±)-65c in acetone-*d*₆ (500 MHz).

SUPPORTING INFORMATION



SUPPORTING INFORMATION



SUPPORTING INFORMATION

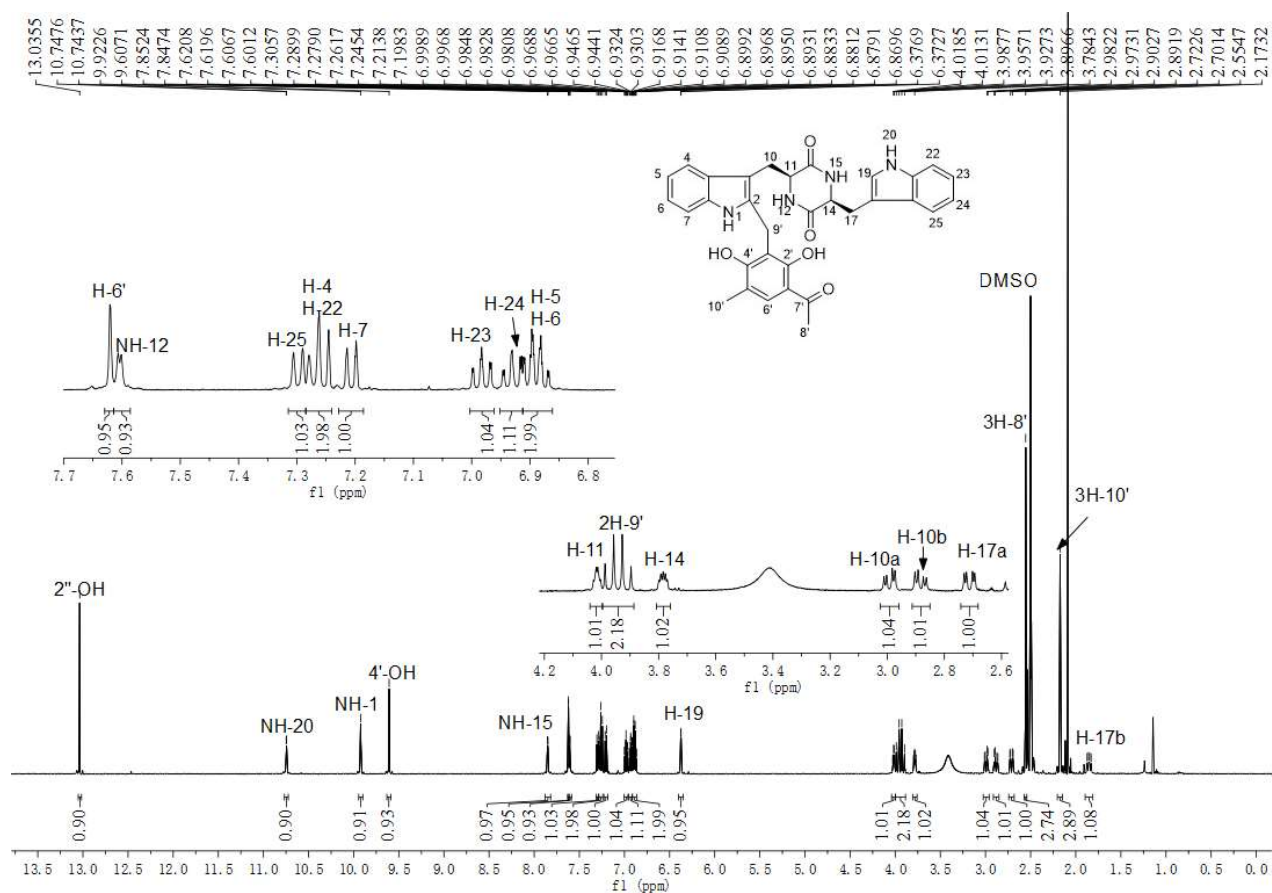


Figure S64. ^1H NMR spectrum of **79b** in $\text{DMSO-}d_6$ (500 MHz).

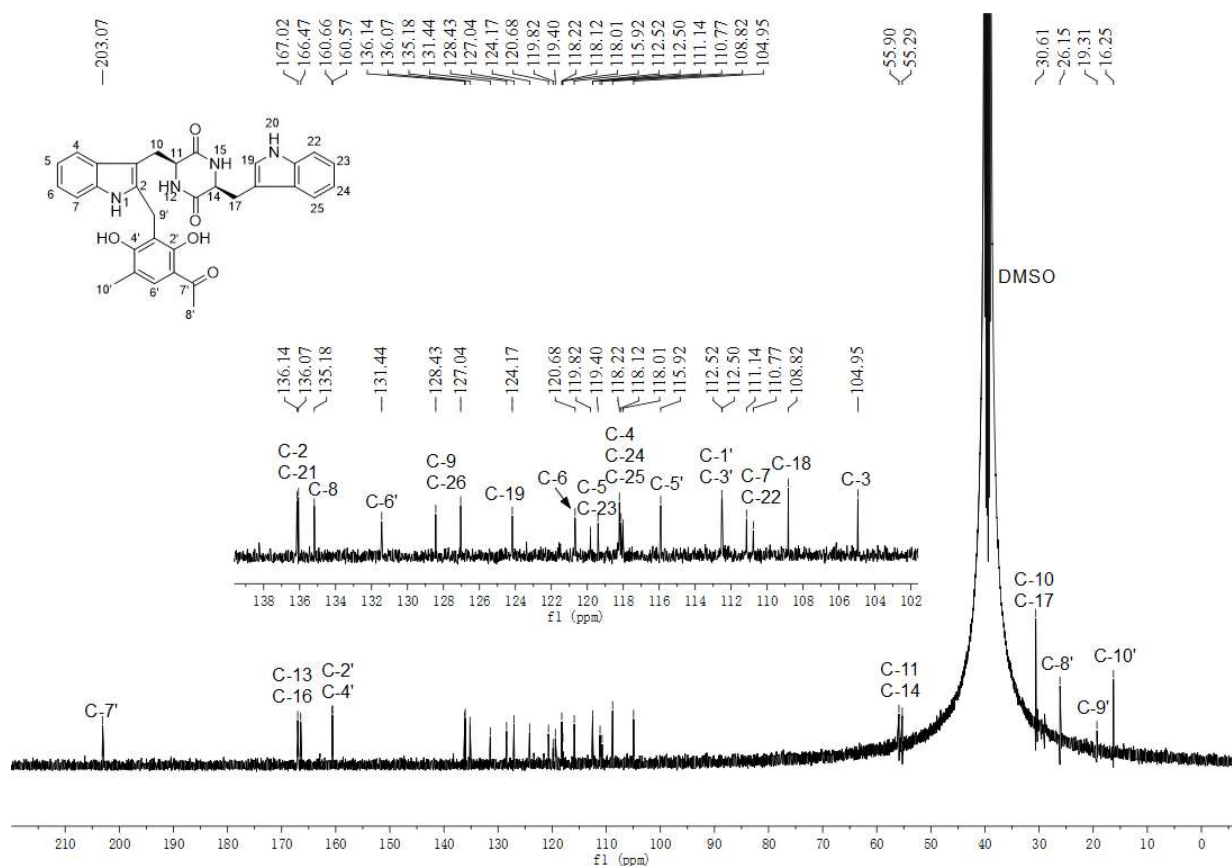


Figure S65. $^{13}\text{C}\{^1\text{H}\}$ NMR spectrum of **79b** in $\text{DMSO-}d_6$ (125 MHz).

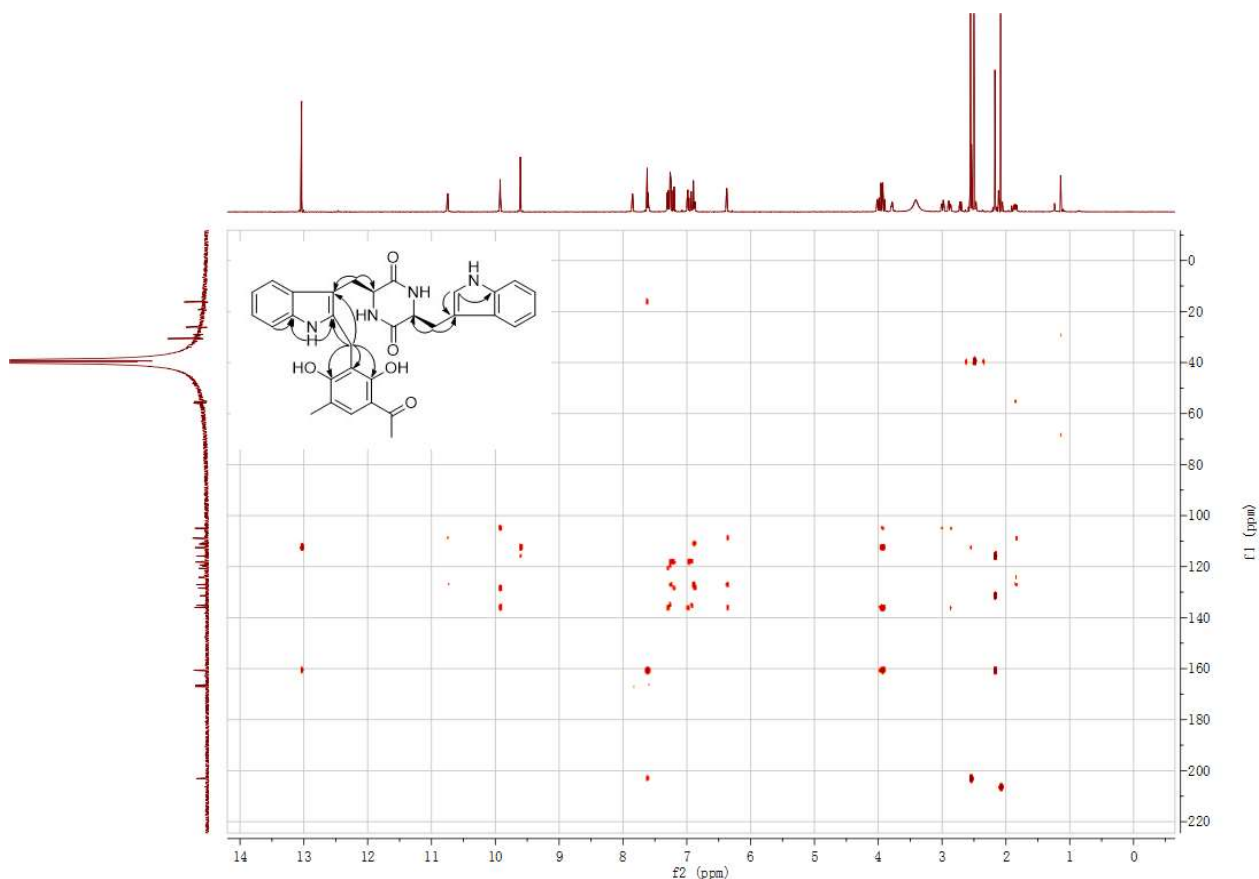


Figure S66. HMBC spectrum of **79b** in DMSO-*d*₆.

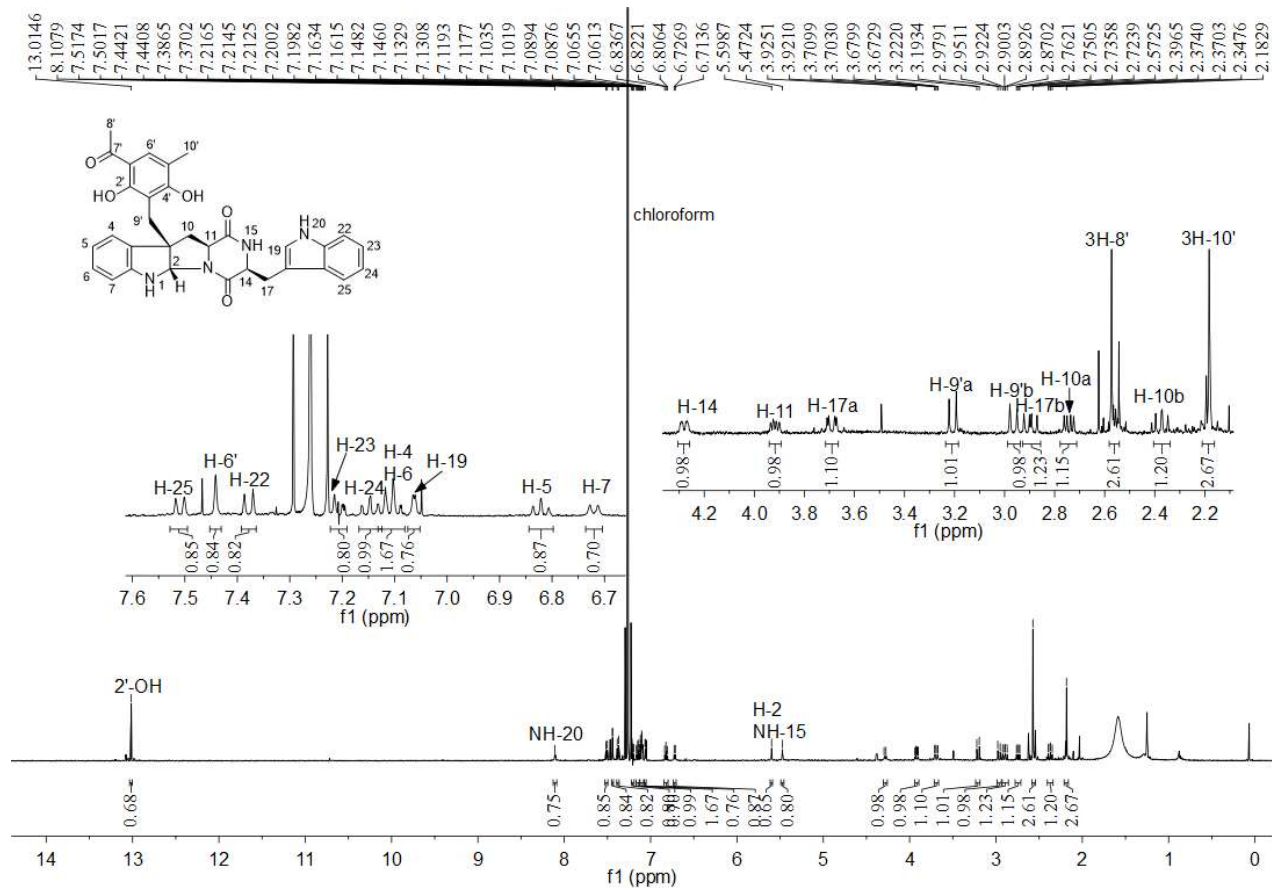
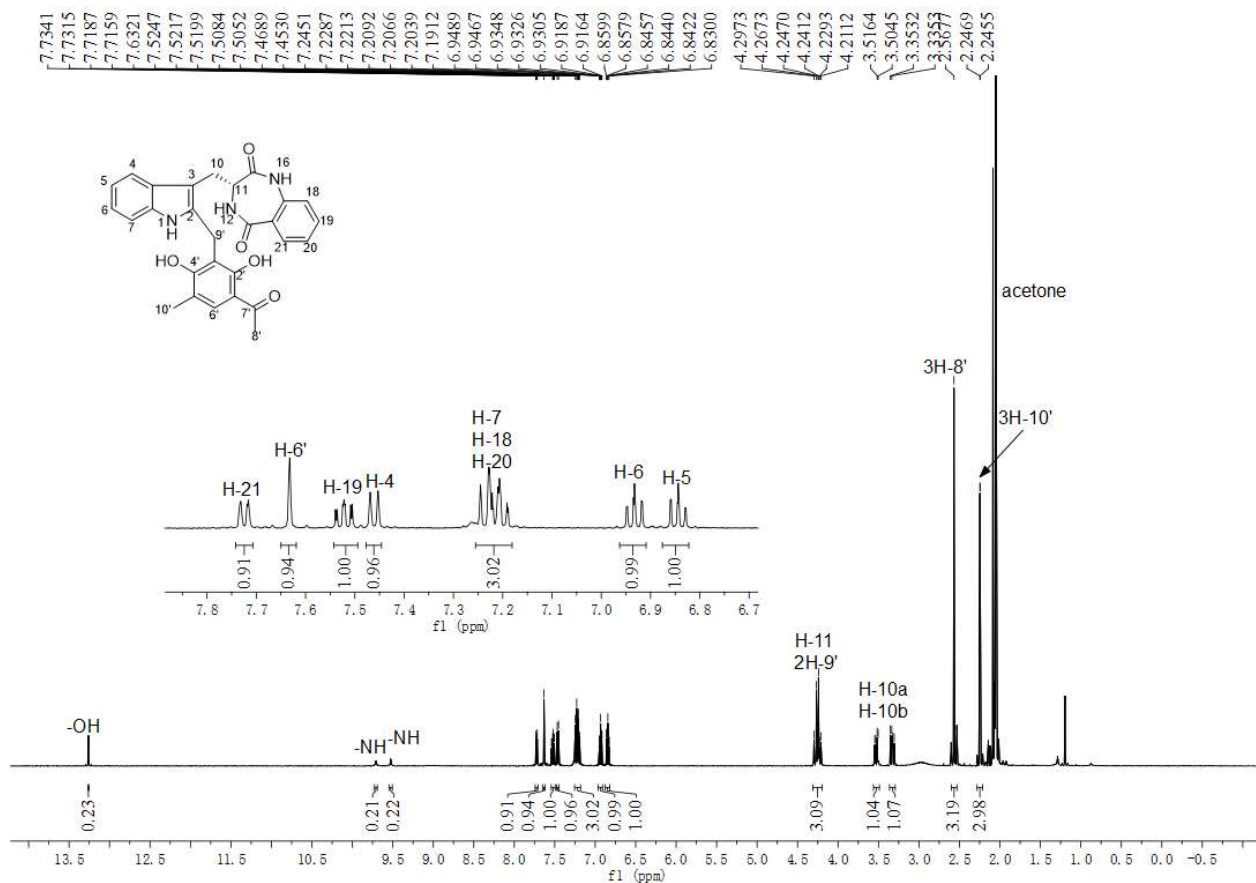
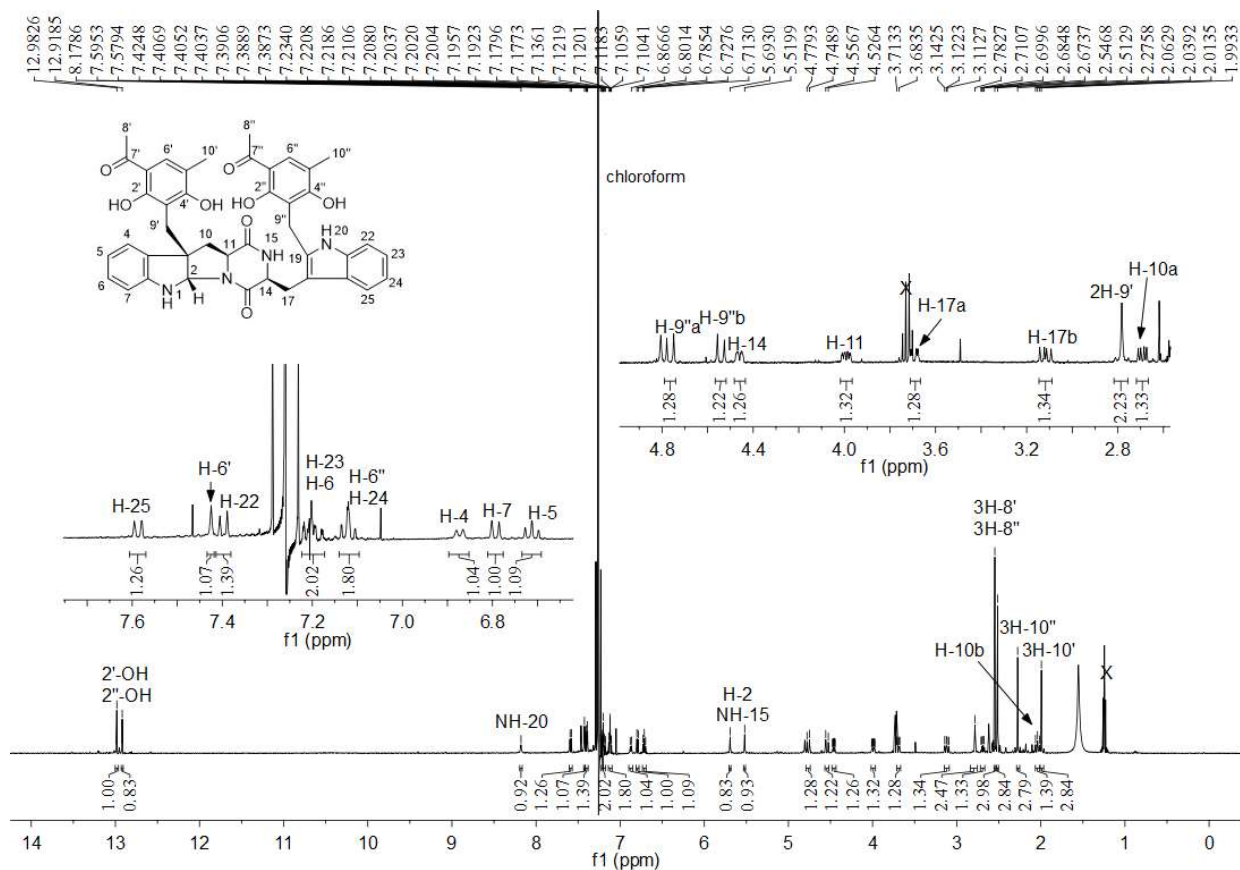
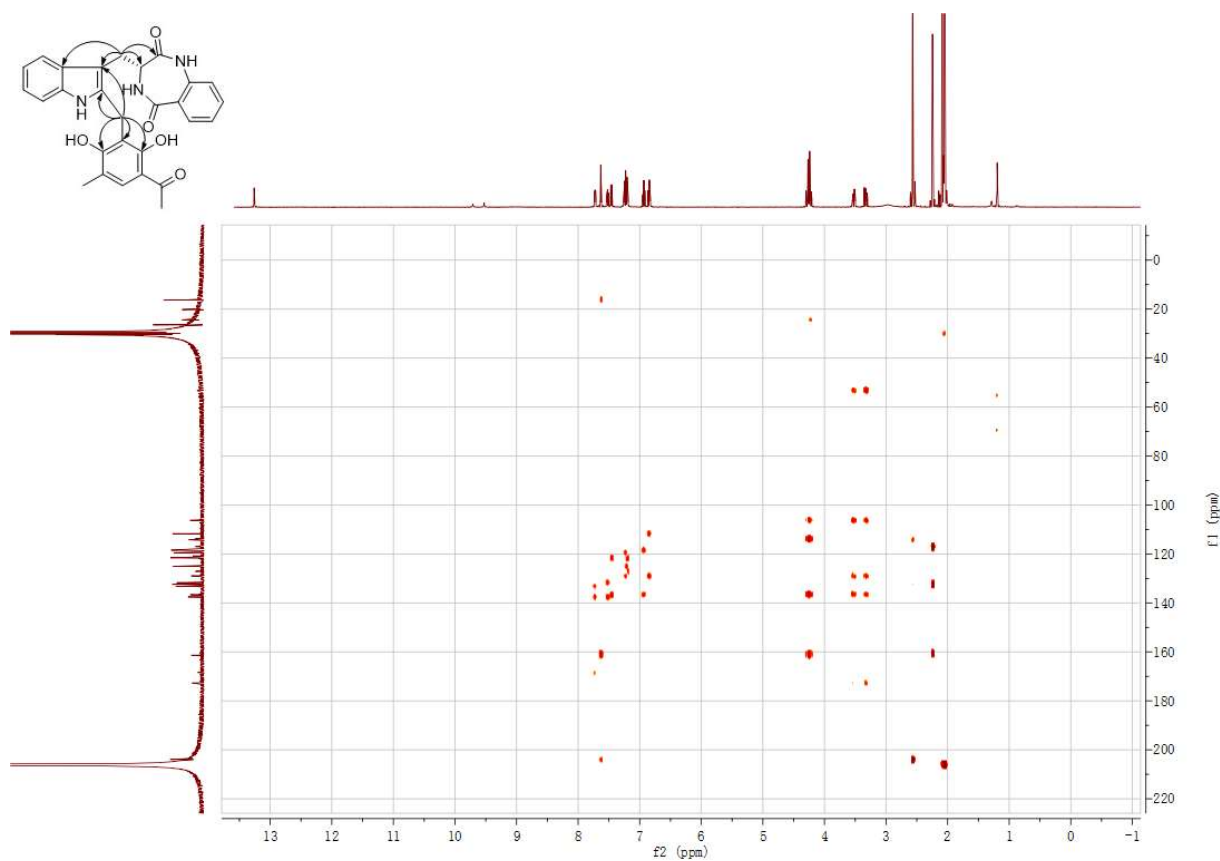
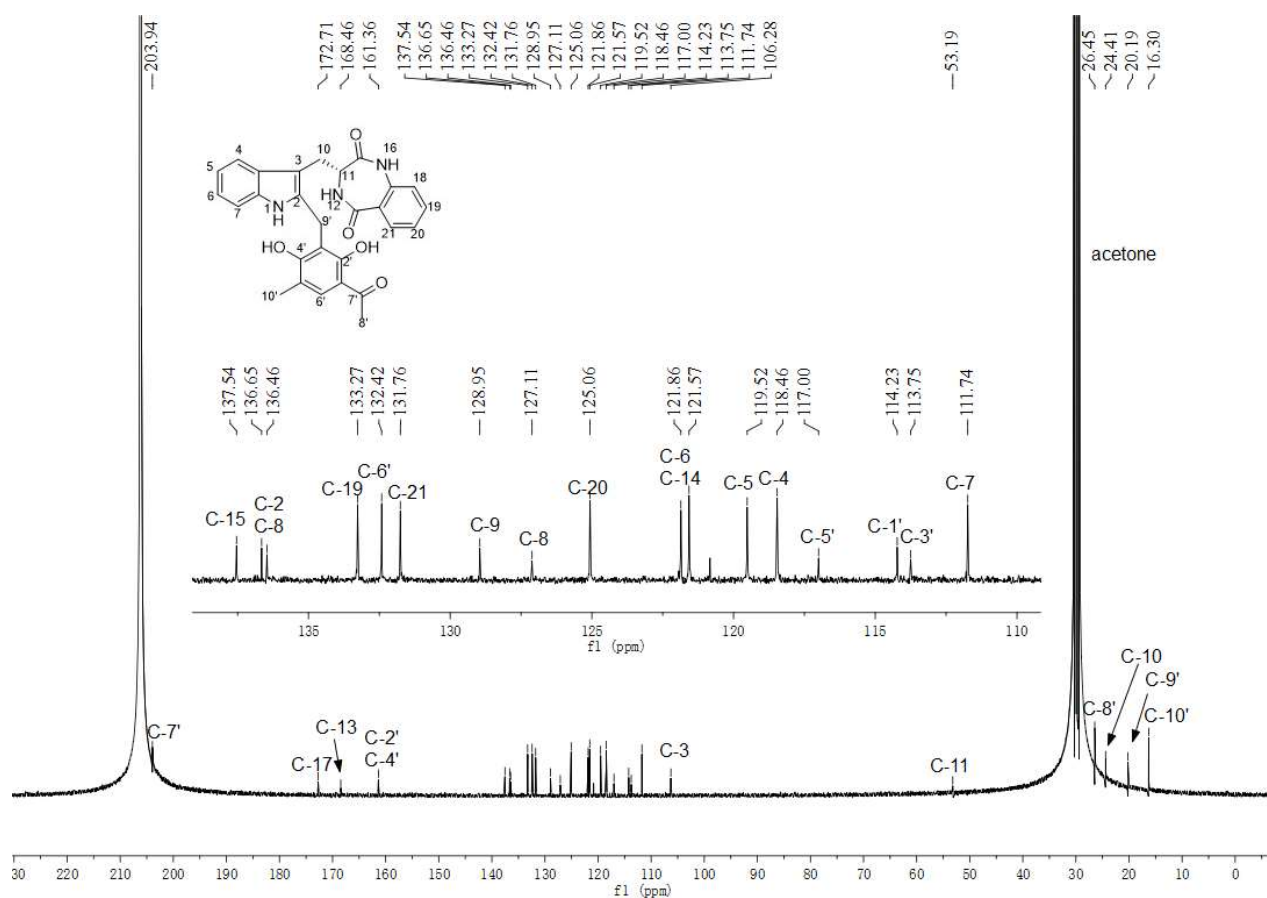


Figure S67. ¹H NMR spectrum of **79c** in CDCl₃ (500 MHz).

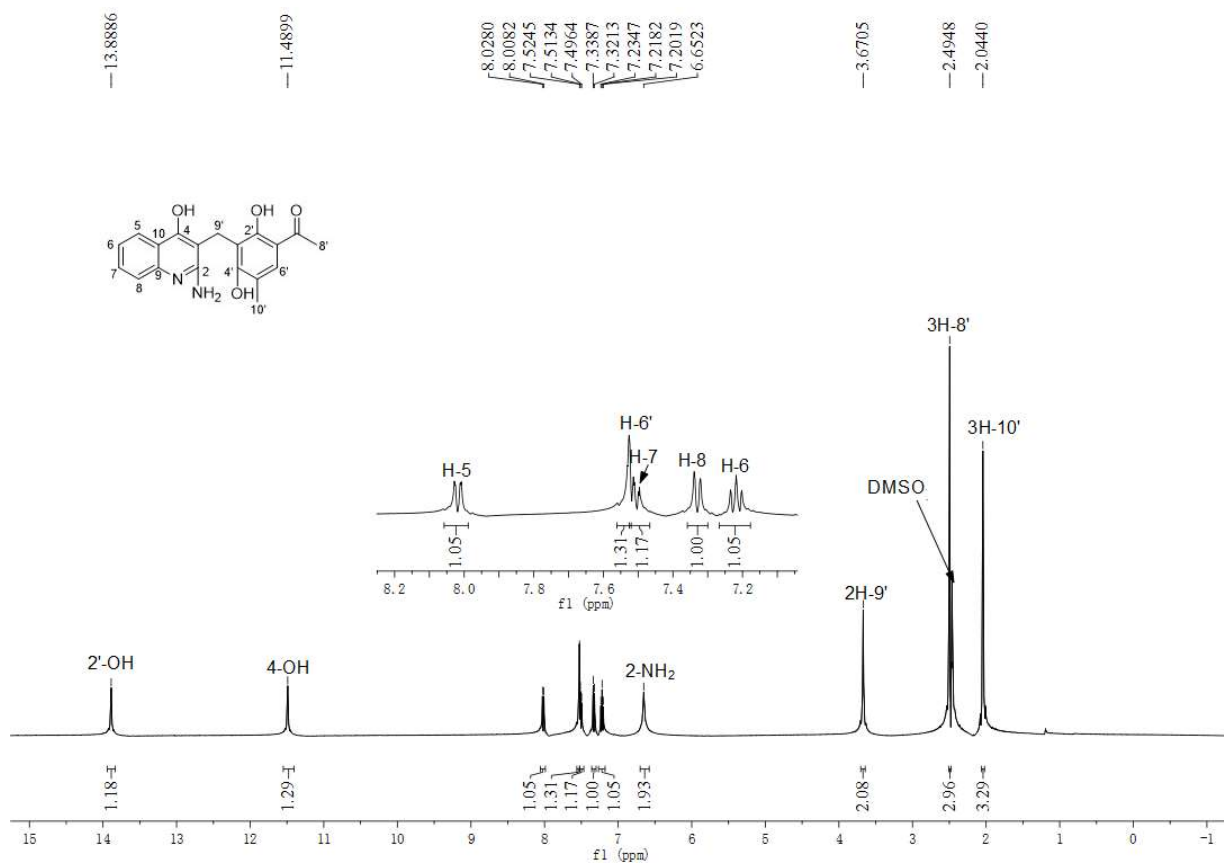
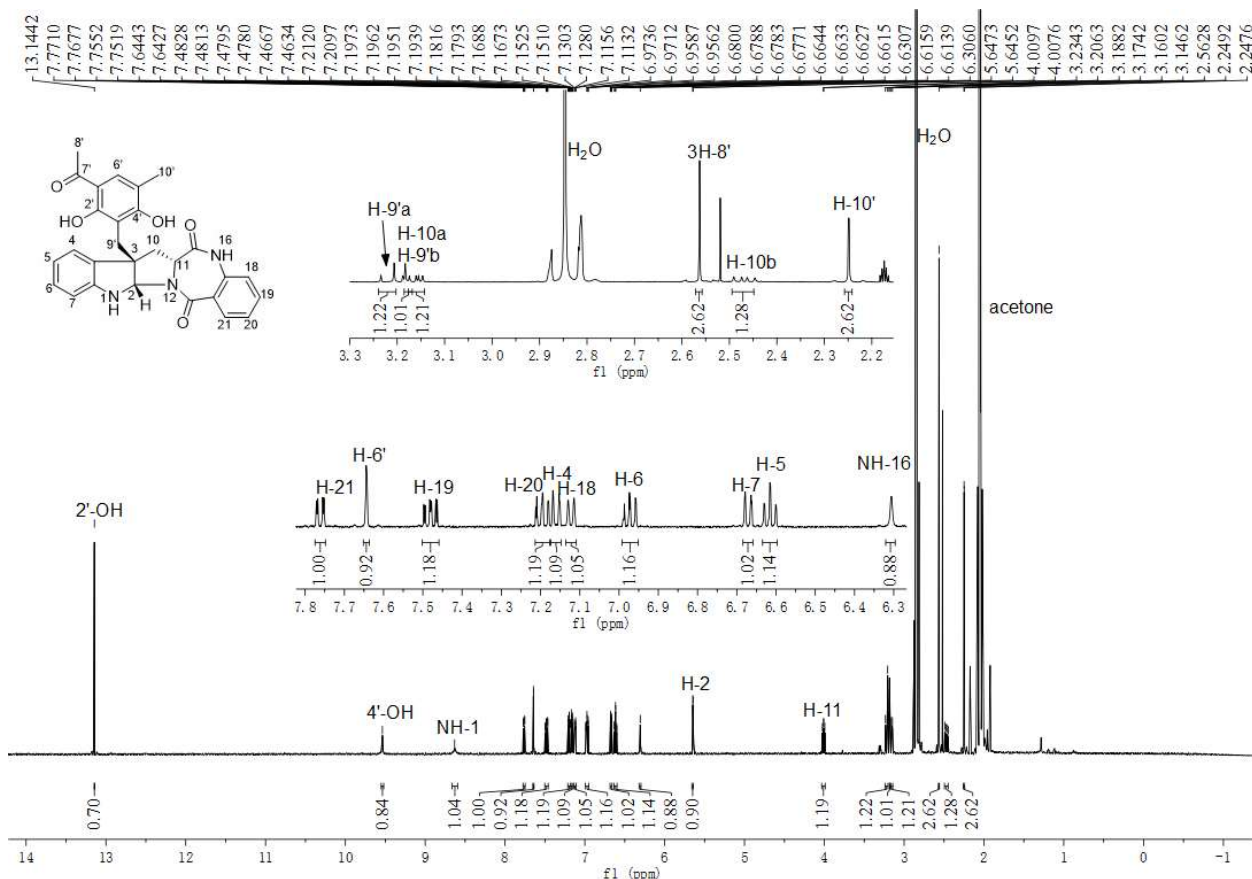
SUPPORTING INFORMATION



SUPPORTING INFORMATION



SUPPORTING INFORMATION



SUPPORTING INFORMATION

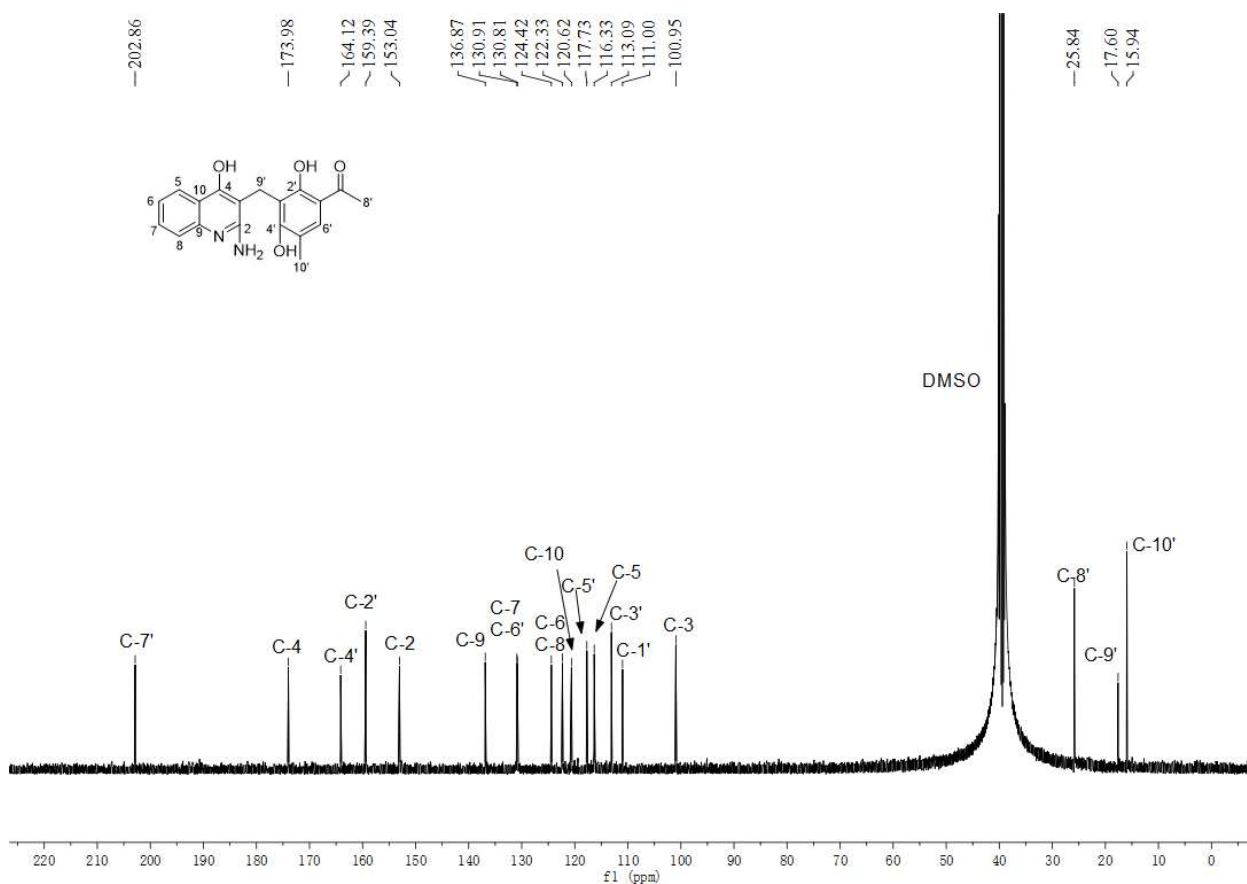


Figure S74. $^{13}\text{C}\{^1\text{H}\}$ NMR spectrum of **95b** in $\text{DMSO-}d_6$ (125 MHz).

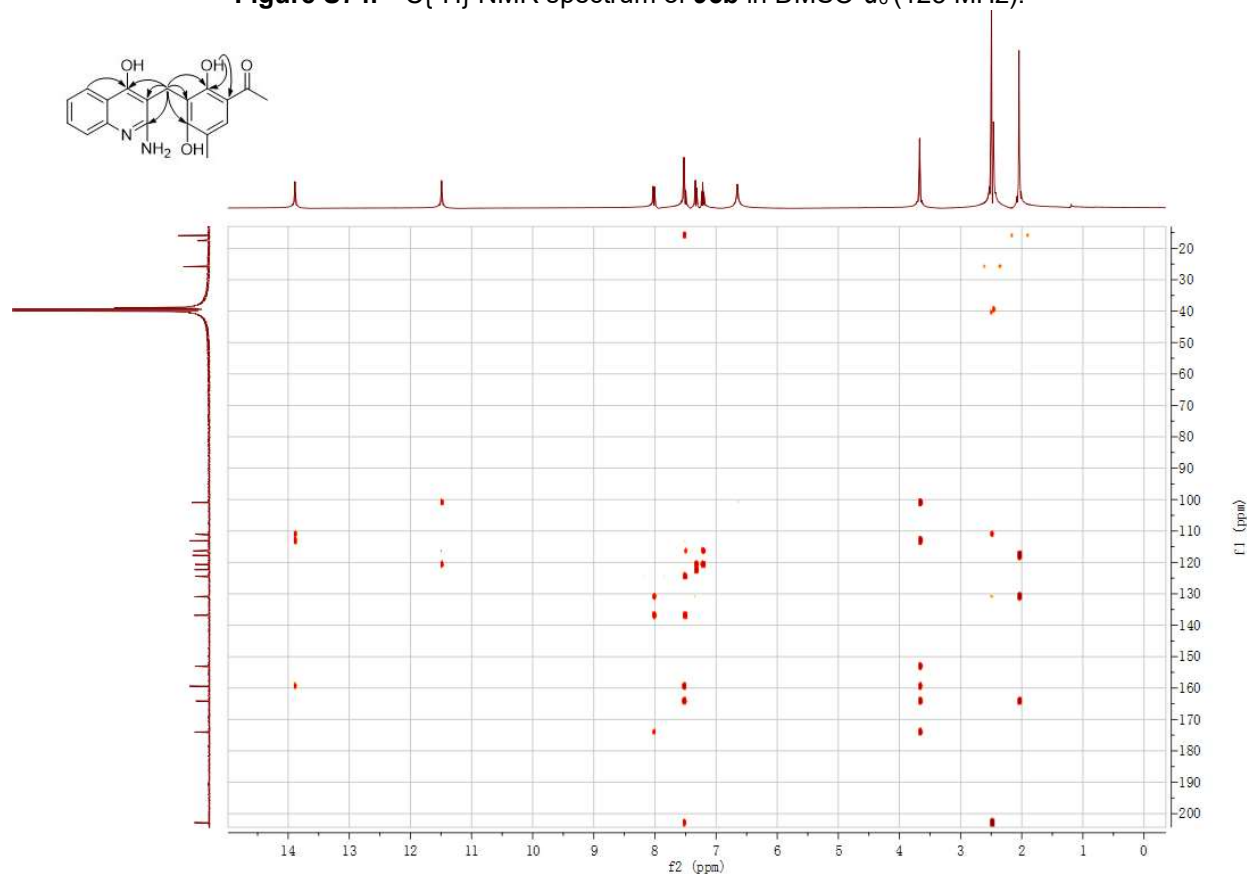
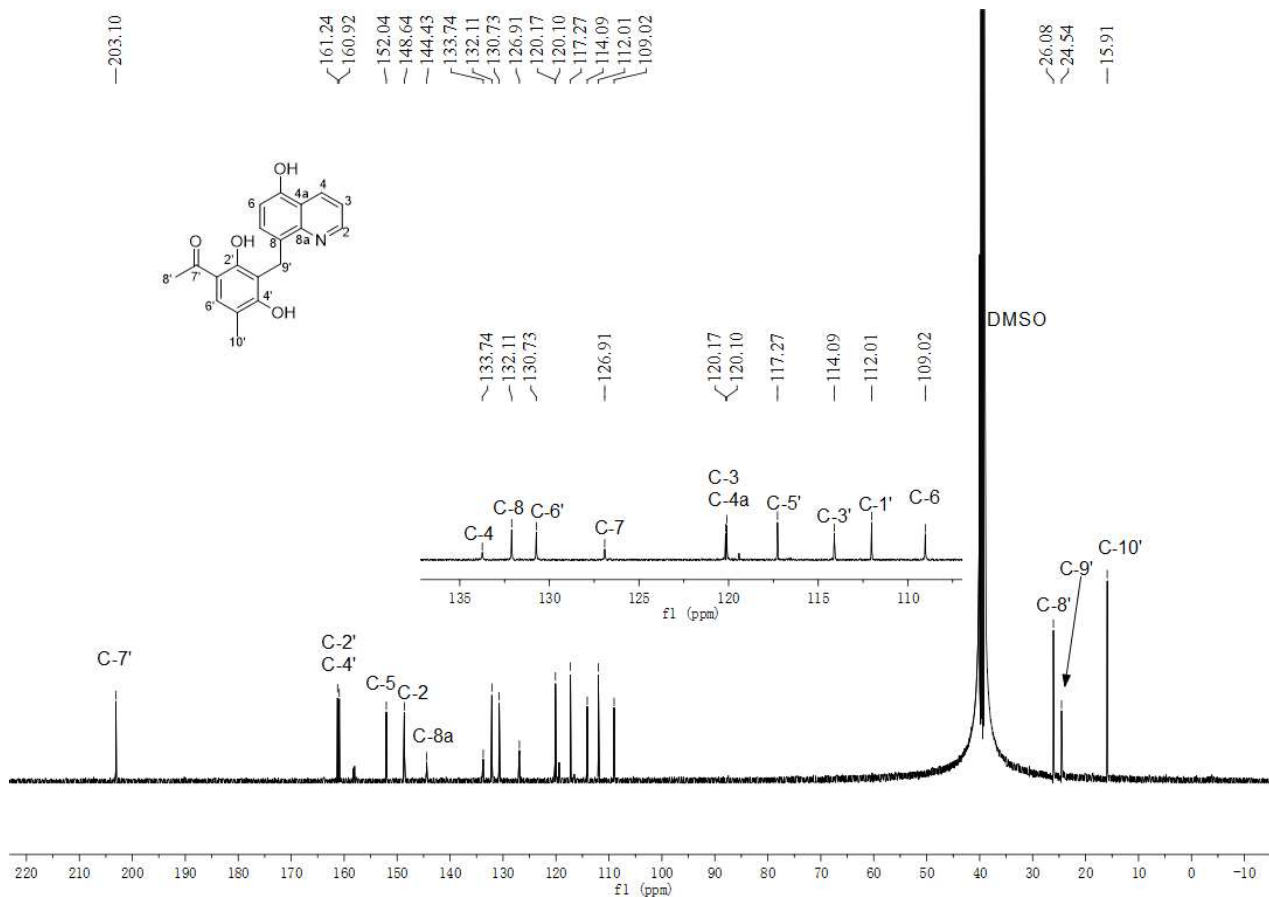
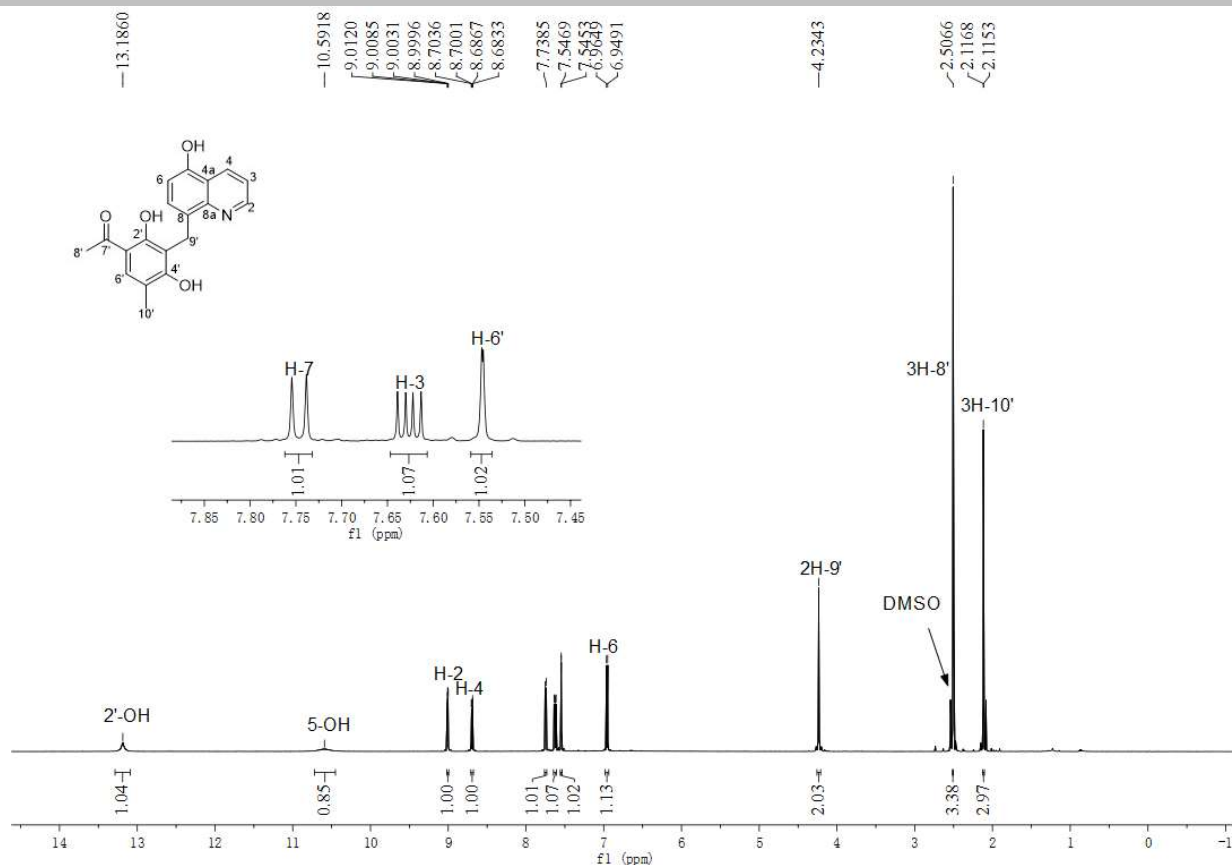


Figure S75. HMBC spectrum of **95b** in $\text{DMSO-}d_6$.

SUPPORTING INFORMATION



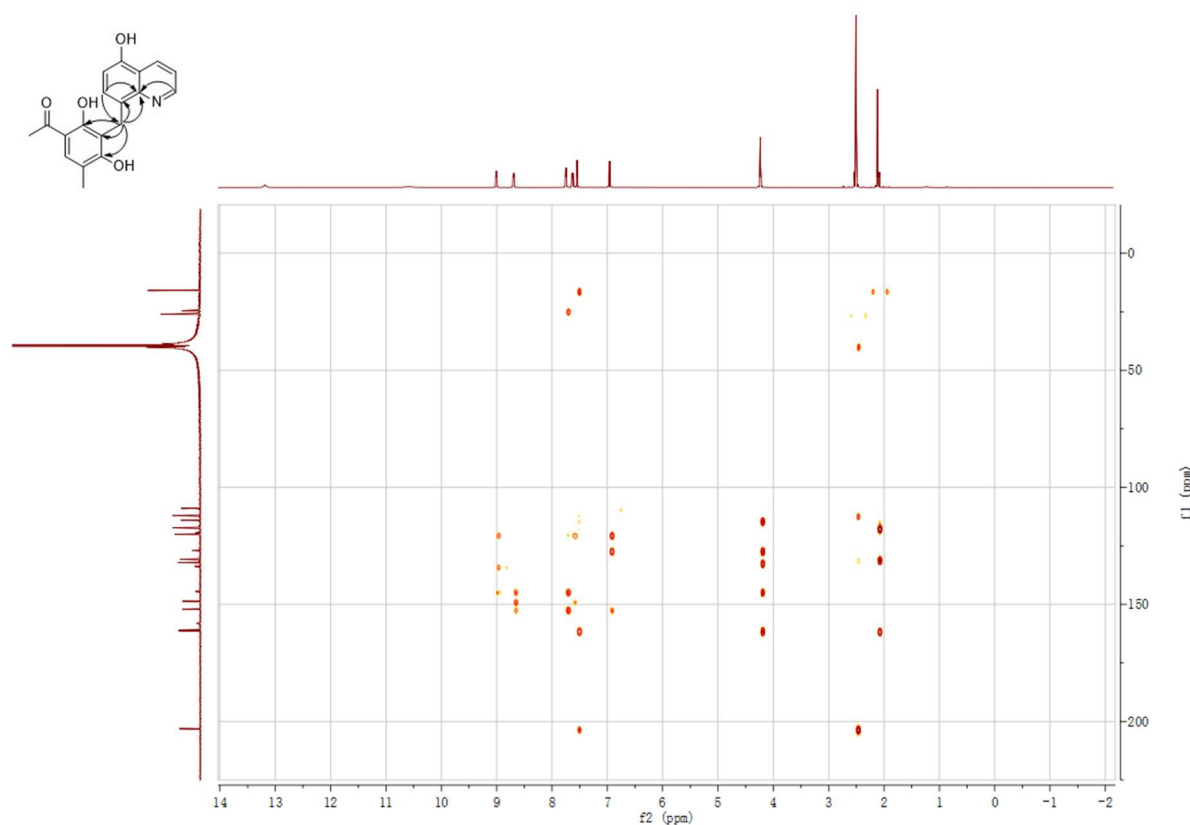


Figure S78. HMBC spectrum of **98b** in DMSO- d_6 .

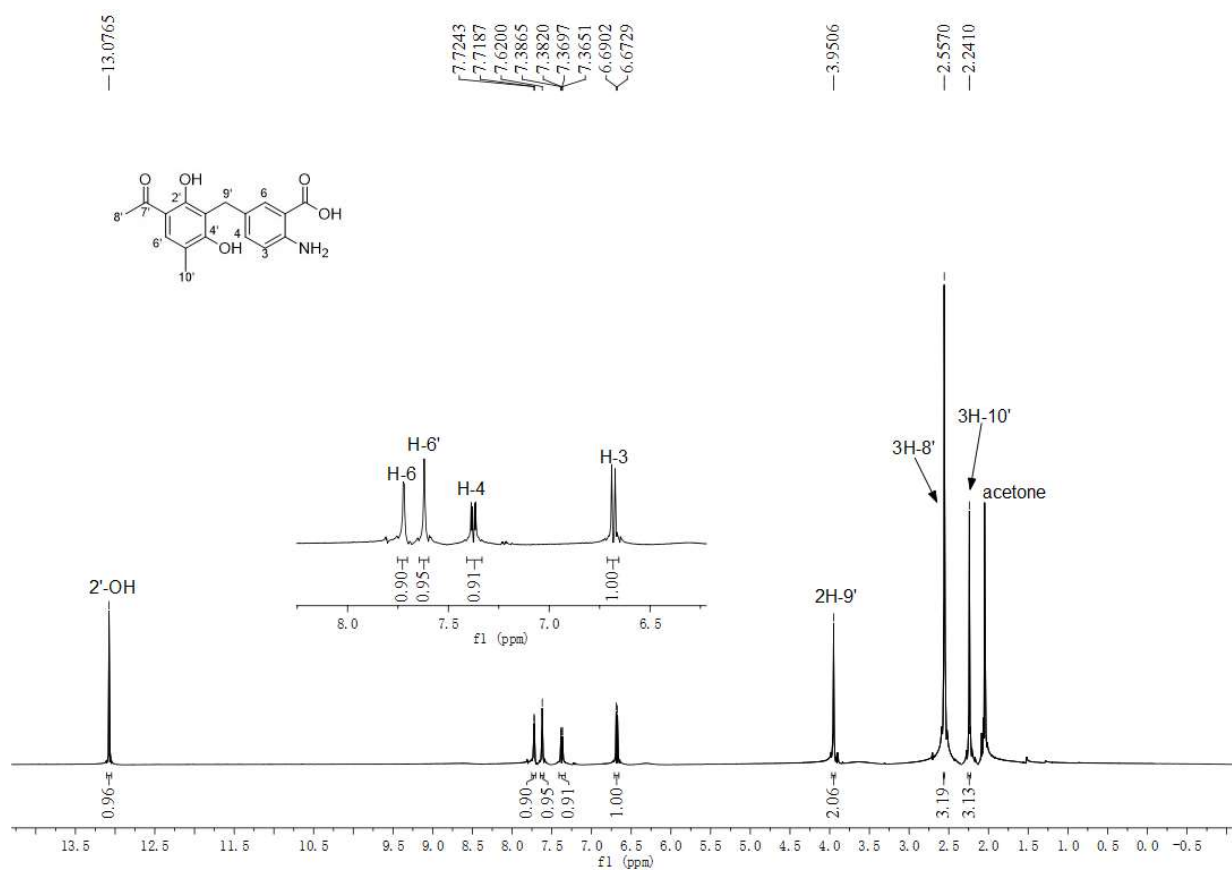
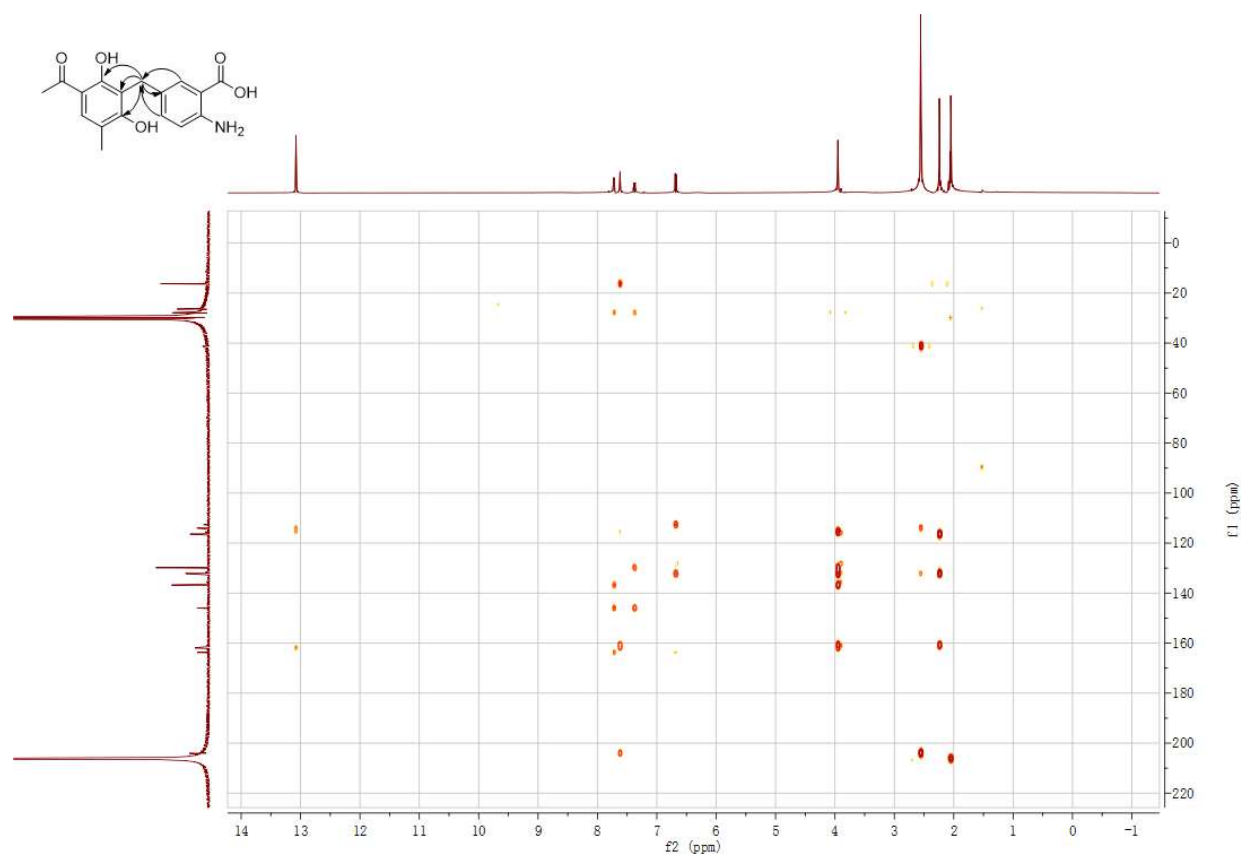
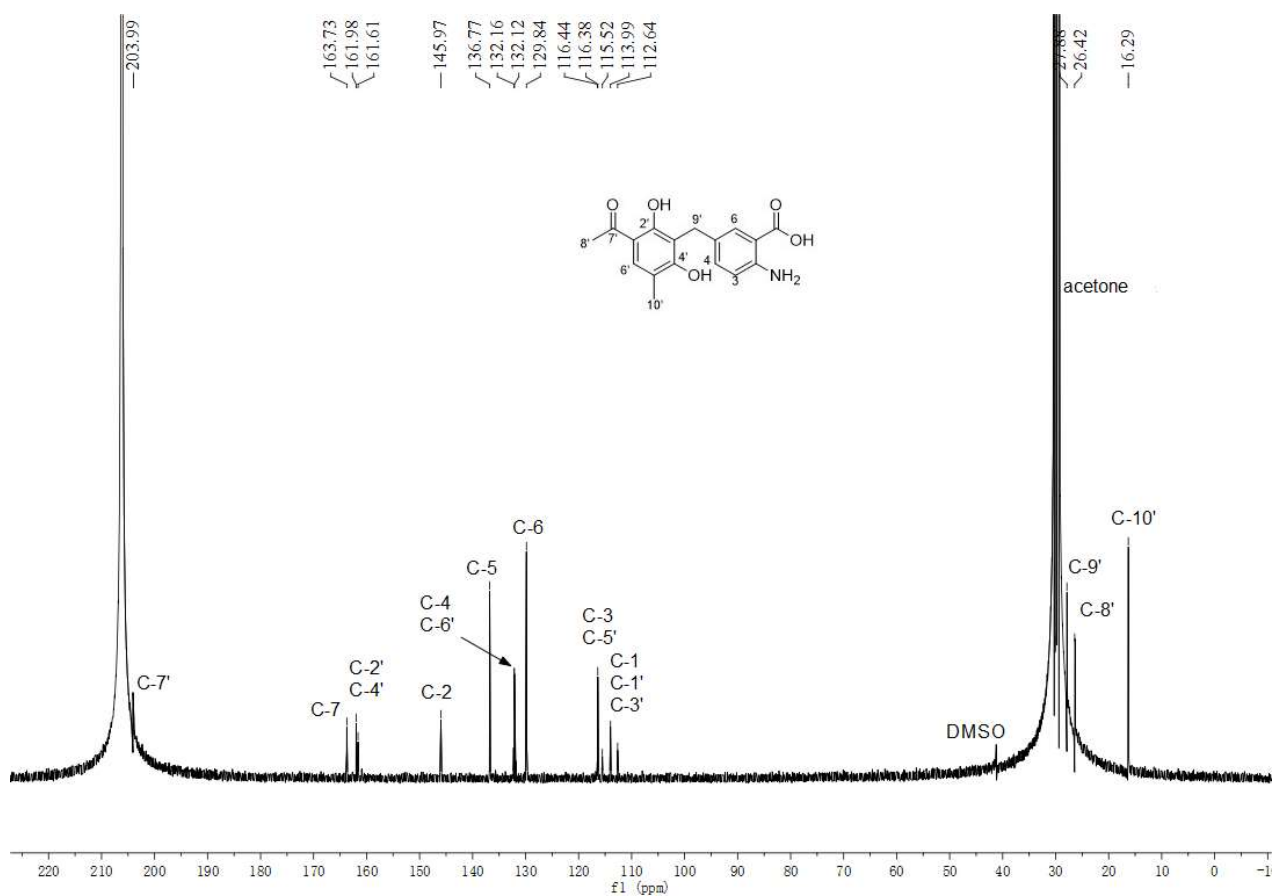


Figure S79. ^1H NMR spectrum of **101b** in acetone- d_6 (500 MHz).

SUPPORTING INFORMATION



SUPPORTING INFORMATION

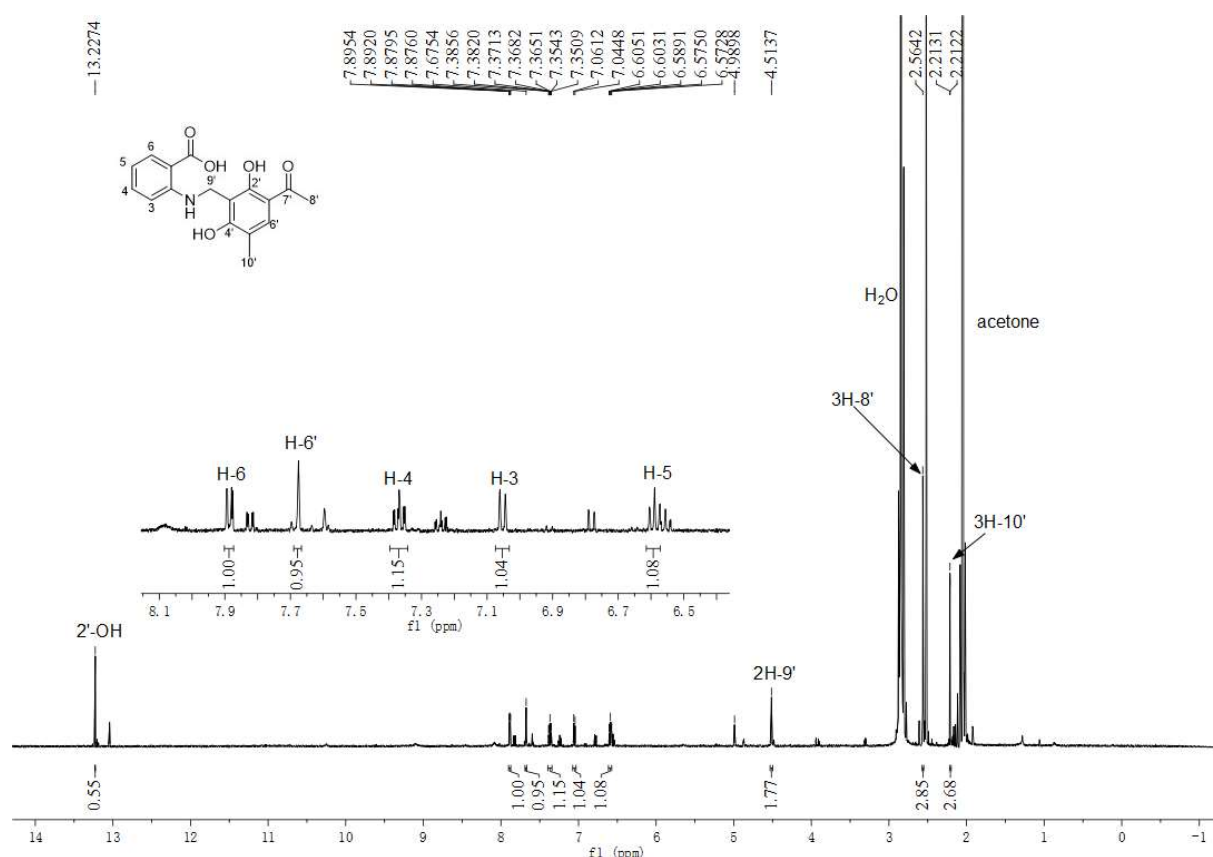


Figure S82. ^1H NMR spectrum of **101c** in acetone- d_6 (500 MHz).

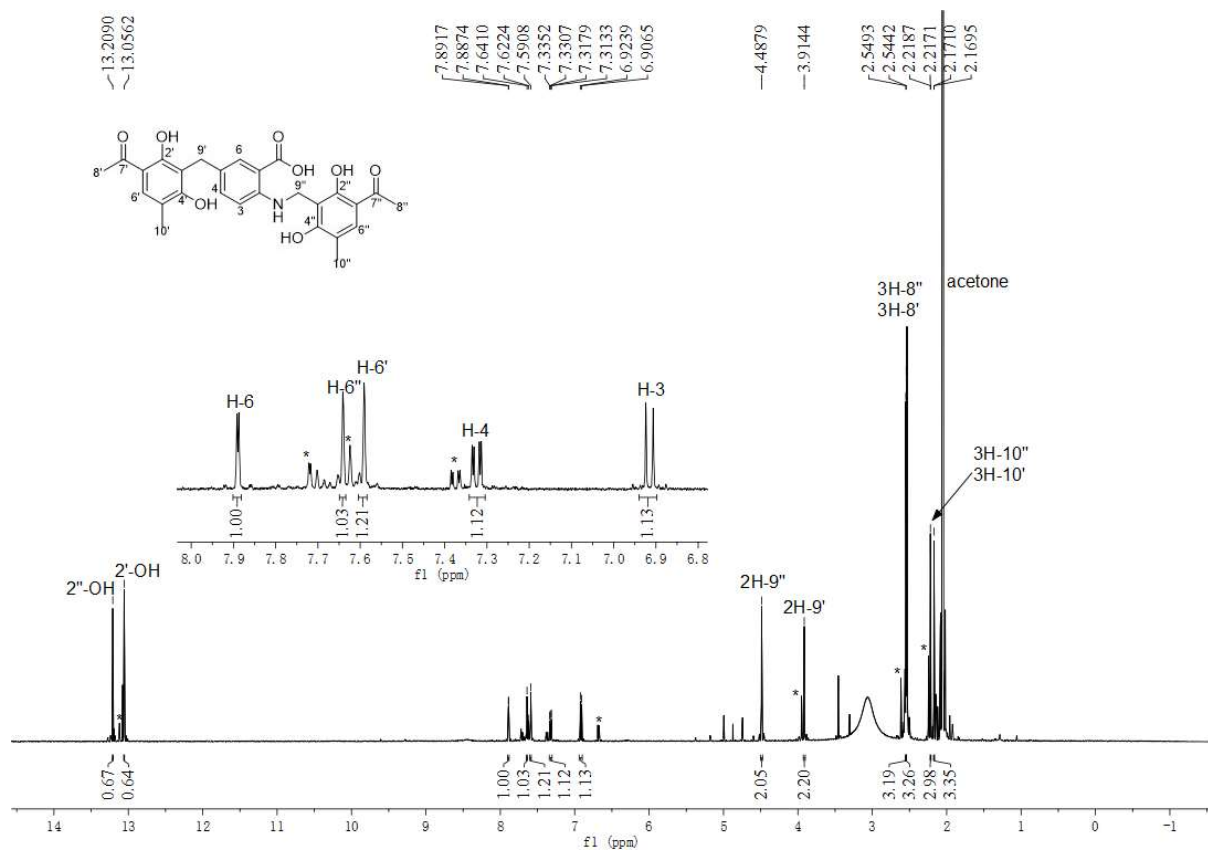


Figure S83. ^1H NMR spectrum of **101d** in acetone- d_6 (500 MHz).

Peaks labelled with * are signals belong to **101b**.

SUPPORTING INFORMATION

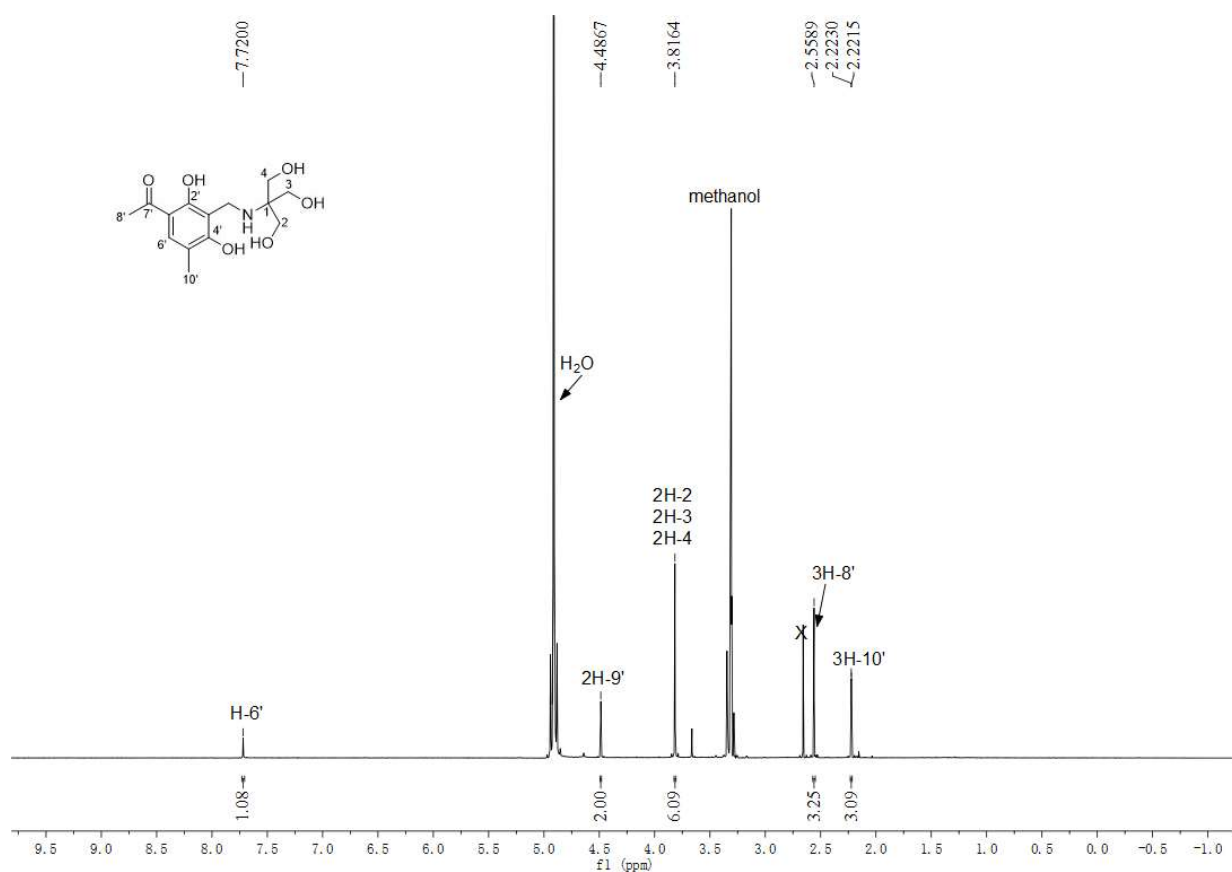


Figure S84. ^1H NMR spectrum of **102b** in CD_3OD (500 MHz).

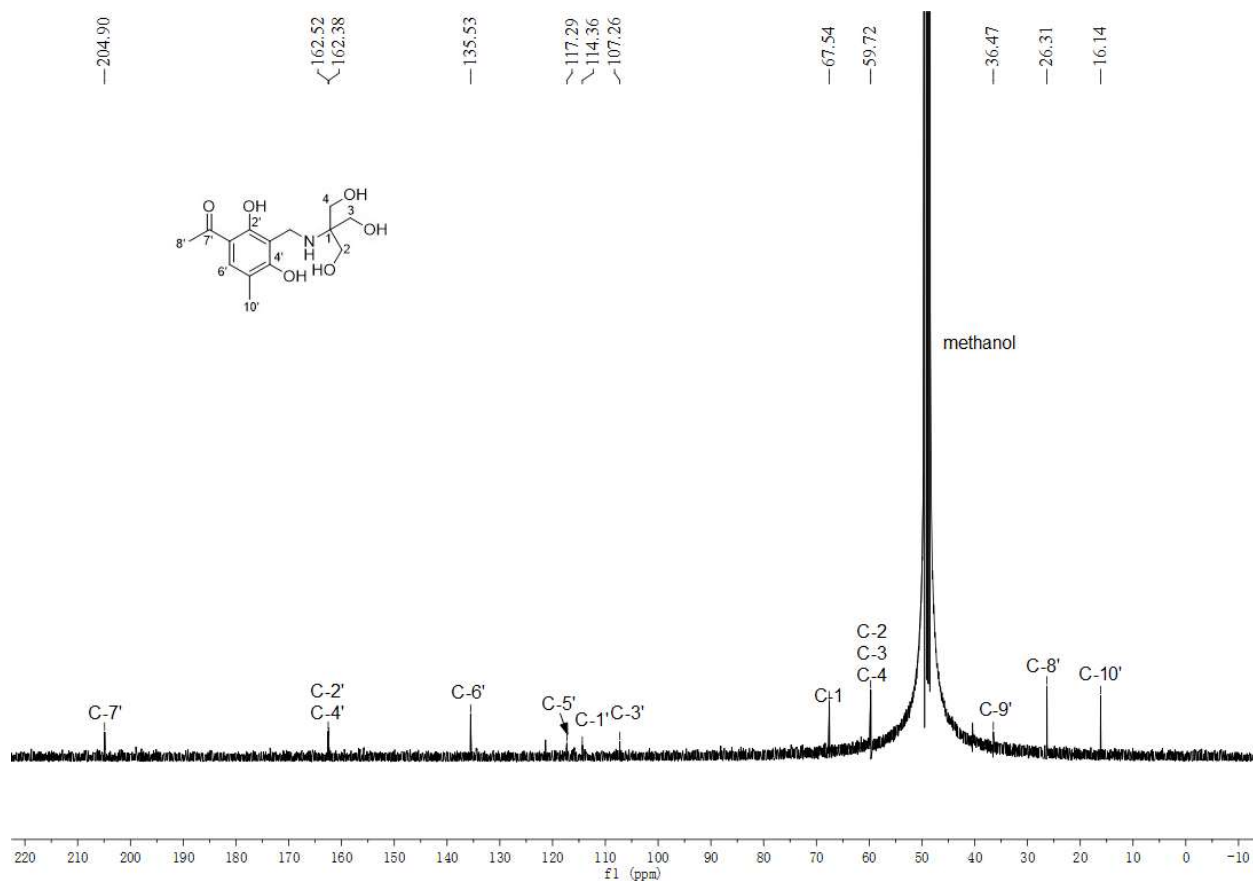
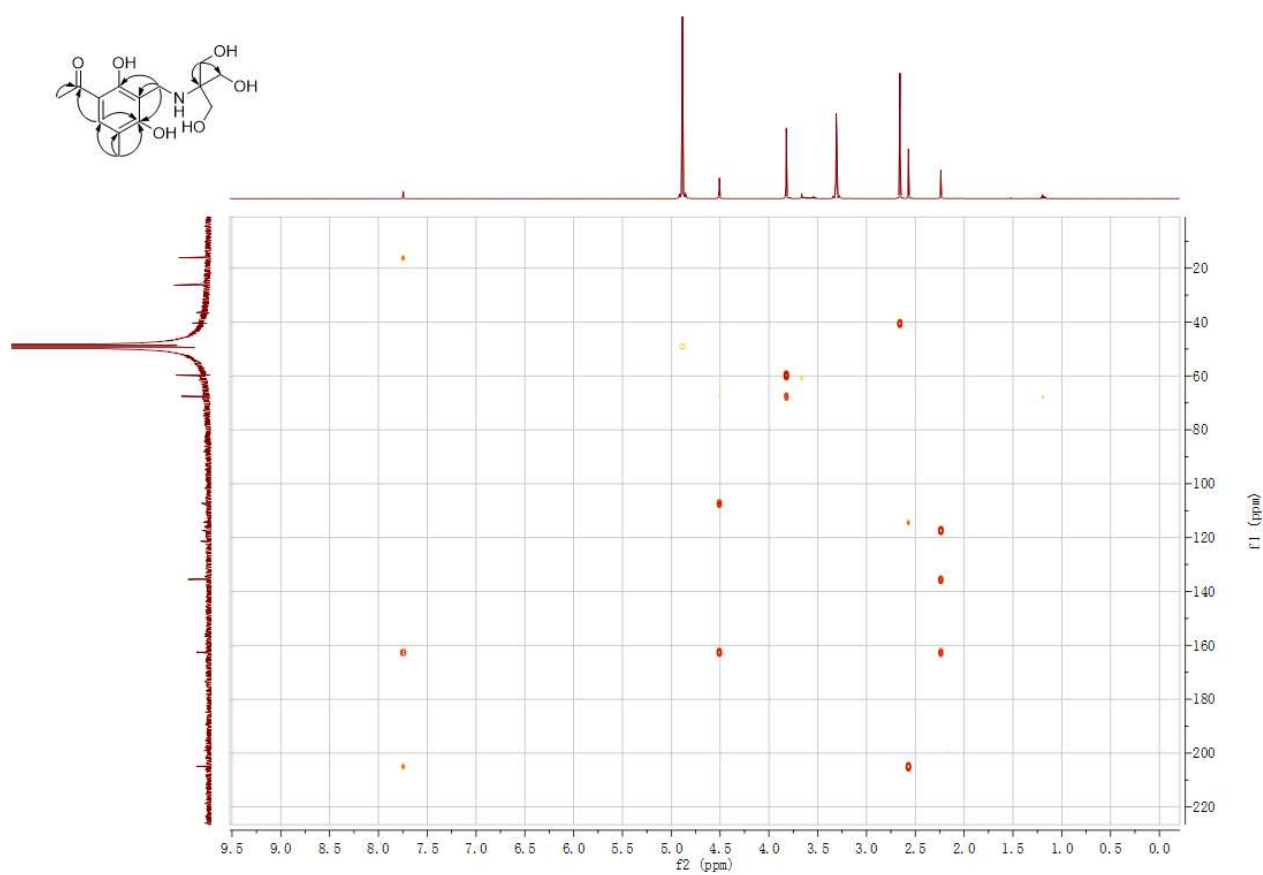


Figure S85. $^{13}\text{C}\{^1\text{H}\}$ NMR spectrum of **102b** in CD_3OD (125 MHz).

SUPPORTING INFORMATION



References

1. Spence, J. T.; George, J. H. Biomimetic total synthesis of *ent*-penilactone A and penilactone B. *Org. Lett.* **2013**, *15* (15), 3891-3893.
2. Davies, M. W.; Maskell, L.; Shipman, M.; Slawin, A. M.; Vidot, S. M.; Whatmore, J. L. Studies toward the synthesis of luminacin D: assembly of simplified analogues devoid of the epoxide displaying antiangiogenic activity. *Org. Lett.* **2004**, *6* (22), 3909-3912.
3. Wu, G.; Ma, H.; Zhu, T.; Li, J.; Gu, Q.; Li, D. Penilactones A and B, two novel polyketides from Antarctic deep-sea derived fungus *Penicillium crustosum* PRB-2. *Tetrahedron* **2012**, *68*, 9745-9749.
4. Wang, J.; Liu, P.; Wang, Y.; Wang, H.; Li, J.; Zhuang, Y.; Zhu, W. Antimicrobial aromatic polyketides from Gorgonian-associated fungus, *Penicillium commune* 518. *Chin. J. Chem.* **2012**, *30*, 1236-1242.
5. Li, H.; Jiang, J.; Liu, Z.; Lin, S.; Xia, G.; Xia, X.; Ding, B.; He, L.; Lu, Y.; She, Z. Peniphenones A-D from the mangrove fungus *Penicillium dipodomycicola* HN4-3A as inhibitors of *Mycobacterium tuberculosis* phosphatase MptpB. *J. Nat. Prod.* **2014**, *77* (4), 800-806.
6. Sun, W.; Chen, X.; Tong, Q.; Zhu, H.; He, Y.; Lei, L.; Xue, Y.; Yao, G.; Luo, Z.; Wang, J.; Li, H.; Zhang, Y. Novel small molecule 11beta-HSD1 inhibitor from the endophytic fungus *Penicillium commune*. *Sci. Rep.* **2016**, *6*, 26418.
7. Yu, G.; Sun, Z.; Peng, J.; Zhu, M.; Che, Q.; Zhang, G.; Zhu, T.; Gu, Q.; Li, D. Secondary metabolites produced by combined culture of *Penicillium crustosum* and a *Xylaria* sp. *J. Nat. Prod.* **2019**, *82* (7), 2013-2017.
8. Tomoda, H.; Tabata, N.; Masuma, R.; Si, S. Y.; Omura, S. Erabulenols, inhibitors of cholesteryl ester transfer protein produced by *Penicillium* sp. FO-5637. I. Production, isolation and biological properties. *J. Antibiot. (Tokyo)* **1998**, *51* (7), 618-623.
9. da Silva, B. F.; Rodrigues-Fo, E. Production of a benzylated flavonoid from 5,7,3',4',5'-pentamethoxyflavanone by *Penicillium griseoroseum*. *J. Mol. Catal. B - Enzyme* **2010**, *67* (3-4), 184-188.

5 Conclusions and future prospects

This thesis presented multiple approaches to study the biosynthetic pathways of fungal secondary metabolites. Historically, characterization of the inventory of natural products from fungi by isolation and structural elucidation has spurred many of the conceptual and practical advances in natural product discovery. Developed bioinformatic tools and genetic manipulation strategies supplied the availability to explain the enzymatic assembly lines of different product scaffolds.

In the course of biosynthetic machinery in *Penicillium crustosum*, two separate gene clusters containing NR-PKS ClaF and hybrid PKS-NRPS TraA were identified by gene deletion, heterologous expression, and precursor feeding experiments for the biosynthesis of key building blocks, *i.e.* clavatul and γ -butyrolactone (tetronic acid) moieties, of the rare natural products penilactones and peniphenones. The biochemical characterization of enzymes with respect to their specific reaction conditions, substrates and cofactors proved the oxidation of clavatul by a nonheme Fe^{II}/2-OG-dependent oxygenase ClaD to yield hydroxycavatul, the oxidative decarboxylation of crustosic acid by another nonheme Fe^{II}/2-OG-dependent oxygenase TraH to yield dehydroterrestric acid, and its stereospecific C-C double bond reduction by a flavin-containing oxidoreductase TraD to produce the predominant metabolite terrestric acid. Subsequently, hydroxycavatul spontaneously undergoes the dehydration to an active intermediate *ortho*-quinone methide. The cross-cluster coupling to form penilactones A and B was further demonstrated by nucleophilic attack of γ -butyrolactones derived from terrestric acid and crustosic acid to *ortho*-quinone methide via non-enzymatic 1,4-Michael additions. The formation of penilactones and peniphenones provided new example for complex natural product biosynthesis by separate clusters through both enzymatic and non-enzymatic strategies. The conversion of crustosic acid to terrestric acid represents the stereochemistry relationships in biosynthetic pathway of fungal acyltetronates.

Inspired by the post-biosynthetic non-enzymatic reactivity of the *ortho*-quinone methide derived from hydroxycavatul, more natural or natural like-products from 11 subgroups were screened and incubated with hydroxycavatul to produce more clavatul-containing products. As a result, 32 new coupling products were identified by isolation and structural elucidation, proving that the *ortho*-quinone methide can be used as a Michael acceptor to increase structural diversity via spontaneous 1,4-Michael additions under mild conditions. The conjugation between clavatul moiety with diverse nucleophiles occurs preferentially with C-C bond formation via *para*- or *ortho*-positions of phenolic hydroxyl/amino groups and C2-position of the indole skeleton. Non-enzymatic C-N formation was also identified in a few cases. Encouraged by the increasing structures, more clavatul-containing products might be synthesized in a similar way in nature. Although chemical synthesis and chemoenzymatic synthesis are developed these days, the reactivity of *ortho*-quinone methide supplied a faster and easier route to synthesize products with complex structures.

CONCLUSION AND FUTURE PROSPECTS

For future prospects, the following works can be performed:

- Ongoing the biosynthetic machinery of other clavatul-containing metabolites from other *Penicillium* strains
- Targeted mechanism of other tailoring enzyme(s) responsible for the hydroxylation at the acyl chain of viridicatic acid to form crustosic acid
- Investigation of other enzymes in clavatul and terrestrial gene clusters by heterologous expression, overexpression, activation or biochemical characterization
- Analysis of other fungal acyltetronates with different stereochemistry and substituent groups
- Further characterization of more nonheme Fe^{II}/2-OG-dependent oxygenases to expand the structural diversity by chemoenzymatic strategy
- Improving the applicability of *ortho*-quinone methide to produce more clavatul-containing products

6 References

- (1) Watkinson, S. C.; Boddy, L.; Money, N. P. *The fungi*; Academic Press: 2015.
- (2) Kirk, P. M.; Cannon, P. F.; Minter, D. W.; Stalpers, J. A. *Dictionary of the Fungi*, 10th edition CABI. Wallingford, UK . 2008.
- (3) Webster, J. and Weber, R. *Introduction to fungi*; Cambridge University Press: 2007.
- (4) Bennett, R. J. and Turgeon, B. G. Fungal sex: The Ascomycota. *Microbiol.Spectr.* 4[5]. 2016.
- (5) Mérillon, J. M. and Ramawat, K. *Fungal metabolites*. Springer, Cham . 2016. Springer.
- (6) Schueffler, A. and Anke, T., Fungal natural products in research and development, *Nat.Prod.Rep.* **2014**, 31, 1425.
- (7) Staunton, J. and Weissman, K. J., Polyketide biosynthesis: a millennium review, *Nat.Prod.Rep.* **2001**, 18, 380.
- (8) Finking, R. and Marahiel, M. A., Biosynthesis of nonribosomal peptides, *Annu.Rev.Microbiol.* **2004**, 58, 453.
- (9) Ajikumar, P. K.; Tyo, K.; Carlsen, S.; Mucha, O.; Phon, T. H.; Stephanopoulos, G., Terpenoids: opportunities for biosynthesis of natural product drugs using engineered microorganisms, *Mol.Pharm.* **2008**, 5, 167.
- (10) Cushnie, T. P. T.; Cushnie, B.; Lamb, A. J., Alkaloids: an overview of their antibacterial, antibiotic-enhancing and antivirulence activities, *Int.J.Antimicrob.Agents* **2014**, 44, 377.
- (11) Fisch, K. M., Biosynthesis of natural products by microbial iterative hybrid PKS–NRPS, *RSC Adv.* **2013**, 3, 18228.
- (12) Keller, N. P., Fungal secondary metabolism: regulation, function and drug discovery, *Nat.Rev.Microbiol.* **2019**, 17, 167.
- (13) Ray, L. and Moore, B. S., Recent advances in the biosynthesis of unusual polyketide synthase substrates, *Nat.Prod.Rep.* **2016**, 33, 150.
- (14) Chan, Y. A.; Podevels, A. M.; Kevany, B. M.; Thomas, M. G., Biosynthesis of polyketide synthase extender units, *Nat.Prod.Rep.* **2009**, 26, 90.
- (15) Beck, J.; Ripka, S.; Siegner, A.; Schiltz, E.; Schweizer, E., The multifunctional 6-methylsalicylic acid synthase gene of *Penicillium patulum*. Its gene structure relative to that of other polyketide synthases, *Eur.J.Biochem.* **1990**, 192, 487.
- (16) Davis, N. D.; Dalby, D. K.; Diener, U. L.; Sansing, G. A., Medium-scale production of citrinin by *Penicillium citrinum* in a semisynthetic medium, *Appl.Microbiol.* **1975**, 29, 118.
- (17) He, Y. and Cox, R. J., The molecular steps of citrinin biosynthesis in fungi, *Chem.Sci.* **2016**, 7, 2119.
- (18) Li, F. Q.; Yoshizawa, T.; Kawamura, O.; Luo, X. Y.; Li, Y. W., Aflatoxins and fumonisins in corn from the high-incidence area for human hepatocellular carcinoma in Guangxi, China, *J.Agric.Food Chem.* **2001**, 49, 4122.
- (19) Minto, R. E. and Townsend, C. A., Enzymology and molecular biology of aflatoxin biosynthesis, *Chem.Rev.* **1997**, 97, 2537.
- (20) Hesseltine, C. W.; Shotwell, O. L.; Ellis, J. J.; Stubblefield, R. D., Aflatoxin formation by *Aspergillus flavus*, *Bacteriol.Rev.* **1966**, 30, 795.

REFERENCES

- (21) Alberts, A. W.; Chen, J.; Kuron, G.; Hunt, V.; Huff, J.; Hoffman, C.; Rothrock, J.; Lopez, M.; Joshua, H.; Harris, E.; Patchett, A.; Monaghan, R.; Currie, S.; Stapley, E.; Albers-Schonberg, G.; Hensens, O.; Hirshfield, J.; Hoogsteen, K.; Liesch, J.; Springer, J., Mevinolin: a highly potent competitive inhibitor of hydroxymethylglutaryl-coenzyme A reductase and a cholesterol-lowering agent, *Proc.Natl.Acad.Sci.U.S.A* **1980**, *77*, 3957.
- (22) Bomke, C. and Tudzynski, B., Diversity, regulation, and evolution of the gibberellin biosynthetic pathway in fungi compared to plants and bacteria, *Phytochemistry* **2009**, *70*, 1876.
- (23) Lee, S. Y.; Kim, M.; Kim, S. H.; Hong, C. Y.; Ryu, S. H.; Choi, I. G., Transcriptomic analysis of the white rot fungus *Polyporus brumalis* provides insight into sesquiterpene biosynthesis, *Microbiol.Res.* **2016**, *182*, 141.
- (24) Talapatra, S. K. and Talapatra, B. Chemistry of plant natural products; Springer: 2015.
- (25) Proctor, R. H. and Hohn, T. M., Aristolochene synthase. Isolation, characterization, and bacterial expression of a sesquiterpenoid biosynthetic gene (Ari1) from *Penicillium roqueforti*, *J.Biol.Chem.* **1993**, *268*, 4543.
- (26) Starks, C. M.; Back, K.; Chappell, J.; Noel, J. P., Structural basis for cyclic terpene biosynthesis by tobacco 5-epi-aristolochene synthase, *Science* **1997**, *277*, 1815.
- (27) Firn, R. Nature's chemicals: the natural products that shaped our world; Oxford University Press, USA: 2010.
- (28) Rohmer, M.; Seemann, M.; Horbach, S.; Bringer-Meyer, S.; Sahm, H., Glyceraldehyde 3-phosphate and pyruvate as precursors of isoprenic units in an alternative non-mevalonate pathway for terpenoid biosynthesis, *J.Am.Chem.Soc.* **1996**, *118*, 2564.
- (29) Du, L. and Lou, L., PKS and NRPS release mechanisms, *Nat.Prod.Rep.* **2010**, *27*, 255.
- (30) Houbraken, J.; Frisvad, J. C.; Samson, R. A., Fleming's penicillin producing strain is not *Penicillium chrysogenum* but *P. rubens*, *IMA Fungus.* **2011**, *2*, 87.
- (31) Diez, B.; Gutierrez, S.; Barredo, J. L.; van, S. P.; van der Voort, L. H.; Martin, J. F., The cluster of penicillin biosynthetic genes. Identification and characterization of the *pcbAB* gene encoding the alpha-aminoadipyl-cysteinyl-valine synthetase and linkage to the *pcbC* and *penDE* genes, *J.Biol.Chem.* **1990**, *265*, 16358.
- (32) MacCabe, A. P.; Riach, M. B.; Unkles, S. E.; Kinghorn, J. R., The *Aspergillus nidulans npeA* locus consists of three contiguous genes required for penicillin biosynthesis, *EMBO.J.* **1990**, *9*, 279.
- (33) Smith, D. J.; Burnham, M. K. R.; Edwards, J.; Earl, A. J.; Turner, G., Cloning and heterologous expression of the penicillin biosynthetic gene cluster from *Penicillium chrysogenum*, *Biotechnology (N.Y.)* **1990**, *8*, 39.
- (34) Brakhage, A. A.; Thon, M.; Sprote, P.; Scharf, D. H.; Al-Abdallah, Q.; Wolke, S. M.; Hortschansky, P., Aspects on evolution of fungal beta-lactam biosynthesis gene clusters and recruitment of *trans*-acting factors, *Phytochemistry* **2009**, *70*, 1801.
- (35) Schroeckh, V.; Scherlach, K.; Nutzmann, H. W.; Shelest, E.; Schmidt-Heck, W.; Schuemann, J.; Martin, K.; Hertweck, C.; Brakhage, A. A., Intimate bacterial-fungal interaction triggers biosynthesis of archetypal polyketides in *Aspergillus nidulans*, *Proc.Natl.Acad.Sci.U.S.A* **2009**, *106*, 14558.

REFERENCES

- (36) Gardiner, D. M. and Howlett, B. J., Bioinformatic and expression analysis of the putative gliotoxin biosynthetic gene cluster of *Aspergillus fumigatus*, *FEMS Microbiol.Lett.* **2005**, *248*, 241.
- (37) Dittmann, J.; Wenger, R. M.; Kleinkauf, H.; Lawen, A., Mechanism of cyclosporin A biosynthesis. Evidence for synthesis via a single linear undecapeptide precursor, *J.Biol.Chem* **1994**, *269*, 2841.
- (38) Gerhards, N.; Neubauer, L.; Tudzynski, P.; Li, S.-M., Biosynthetic pathways of ergot alkaloids, *Toxins.(Basel)* **2014**, *6*, 3281.
- (39) Funayama, S. and Cordell, G. A. Alkaloids: a treasury of poisons and medicines; Elsevier: 2014.
- (40) Yang, B.; Dong, J.; Lin, X.; Zhou, X.; Zhang, Y.; Liu, Y., New prenylated indole alkaloids from fungus *Penicillium* sp. derived of mangrove soil sample, *Tetrahedron* **2014**, *70*, 3859.
- (41) Hoffmeister, D. and Keller, N. P., Natural products of filamentous fungi: enzymes, genes, and their regulation, *Nat.Prod.Rep.* **2007**, *24*, 393.
- (42) Keller, N. P. and Hohn, T. M., Metabolic pathway gene clusters in filamentous fungi, *Fungal Genet.Biol.* **1997**, *21*, 17.
- (43) Wakefield, J.; Hassan, H. M.; Jaspars, M.; Ebel, R.; Rateb, M. E., Dual induction of new microbial secondary metabolites by fungal bacterial co-cultivation, *Front.Microbiol.* **2017**, *8*, 1284.
- (44) Wang, J. P.; Lin, W. H.; Wray, V.; Lai, D. W.; Proksch, P., Induced production of depsipeptides by co-culturing *Fusarium tricinctum* and *Fusarium begoniae*, *Tetrahedron Lett.* **2013**, *54*, 2492.
- (45) Andersen, M. R.; Nielsen, J. B.; Klitgaard, A.; Petersen, L. M.; Zachariassen, M.; Hansen, T. J.; Blicher, L. H.; Gotfredsen, C. H.; Larsen, T. O.; Nielsen, K. F.; Mortensen, U. H., Accurate prediction of secondary metabolite gene clusters in filamentous fungi, *Proc.Natl.Acad.Sci.U.S.A* **2012**, *110*, E99.
- (46) Manzoni, M. and Rollini, M., Biosynthesis and biotechnological production of statins by filamentous fungi and application of these cholesterol-lowering drugs, *Appl.Microbiol.Biotechnol.* **2002**, *58*, 555.
- (47) Wiemann, P.; Willmann, A.; Straeten, M.; Kleigrew, K.; Beyer, M.; Humpf, H. U.; Tudzynski, B., Biosynthesis of the red pigment bikaverin in *Fusarium fujikuroi*: genes, their function and regulation, *Mol.Microbiol.* **2009**, *72*, 931.
- (48) Hartley, A. J.; de Mattos-Shiple, K.; Collins, C. M.; Kilaru, S.; Foster, G. D.; Bailey, A. M., Investigating pleuromutilin-producing *Clitopilus* species and related basidiomycetes, *FEMS Microbiol.Lett.* **2009**, *297*, 24.
- (49) Yang, X. L.; Awakawa, T.; Wakimoto, T.; Abe, I., Three acyltetronic acid derivatives: noncanonical cryptic polyketides from *Aspergillus niger* identified by genome mining, *Chembiochem* **2014**, *15*, 1578.
- (50) Chiang, Y. M.; Szewczyk, E.; Davidson, A. D.; Entwistle, R.; Keller, N. P.; Wang, C. C.; Oakley, B. R., Characterization of the *Aspergillus nidulans* monodictyphenone gene cluster, *Appl.Enviro.Microbiol.* **2010**, *76*, 2067.
- (51) König, C. C.; Scherlach, K.; Schroeckh, V.; Horn, F.; Nietzsche, S.; Brakhage, A. A.; Hertweck, C., Bacterium induces cryptic meroterpenoid pathway in the pathogenic fungus *Aspergillus fumigatus*, *Chembiochem* **2013**, *14*, 938.
- (52) Sørensen, J. L.; Hansen, F. T.; Sondergaard, T. E.; Staerk, D.; Lee, T. V.; Wimmer, R.; Klitgaard, L. G.; Purup, S.; Giese, H.; Frandsen, R. J. N., Production of novel fusarielins by ectopic activation of the polyketide synthase 9 cluster in *Fusarium graminearum*, *Environ.Microbiol.* **2012**, *14*, 1159.

REFERENCES

- (53) Chooi, Y. H.; Fang, J.; Liu, H.; Filler, S. G.; Wang, P.; Tang, Y., Genome mining of a prenylated and immunosuppressive polyketide from pathogenic fungi, *Org.Lett.* **2013**, *15*, 780.
- (54) Yin, W.-B.; Baccile, J. A.; Bok, J. W.; Chen, Y.; Keller, N. P.; Schroeder, F. C., A nonribosomal peptide synthetase-derived iron(III) complex from the pathogenic fungus *Aspergillus fumigatus*, *J.Am.Chem.Soc.* **2013**, *135*, 2064.
- (55) Lim, F. Y.; Hou, Y.; Chen, Y.; Oh, J. H.; Lee, I.; Bugni, T. S.; Keller, N. P., Genome-based cluster deletion reveals an endocrocin biosynthetic pathway in *Aspergillus fumigatus*, *Appl.Environ.Microbiol.* **2012**, *78*, 4117.
- (56) Forseth, R. R.; Amaike, S.; Schwenk, D.; Affeldt, K. J.; Hoffmeister, D.; Schroeder, F. C.; Keller, N. P., Homologous NRPS-like gene clusters mediate redundant small-molecule biosynthesis in *Aspergillus flavus*, *Angew.Chem.Int.Ed Engl.* **2013**, *52*, 1590.
- (57) Bouhired, S.; Weber, M.; Kempf-Sontag, A.; Keller, N. P.; Hoffmeister, D., Accurate prediction of the *Aspergillus nidulans* terrequinone gene cluster boundaries using the transcriptional regulator LaeA, *Fungal.Genet.Biol* **2007**, *44*, 1134.
- (58) Baba, S.; Kinoshita, H.; Nihira, T., Identification and characterization of *Penicillium citrinum* VeA and LaeA as global regulators for ML-236B production, *Curr.Genet.* **2012**, *58*, 1.
- (59) Fan, A.; Mi, W.; Liu, Z.; Zeng, G.; Zhang, P.; Hu, Y.; Fang, W.; Yin, W. B., Deletion of a histone acetyltransferase leads to the pleiotropic activation of natural products in *Metarhizium robertsii*, *Org.Lett.* **2017**, *19*, 1686.
- (60) Szewczyk, E.; Chiang, Y. M.; Oakley, C. E.; Davidson, A. D.; Wang, C. C.; Oakley, B. R., Identification and characterization of the asperthecin gene cluster of *Aspergillus nidulans*, *Appl.Environ.Microbiol.* **2008**, *74*, 7607.
- (61) Williams, R. B.; Henrikson, J. C.; Hoover, A. R.; Lee, A. E.; Cichewicz, R. H., Epigenetic remodeling of the fungal secondary metabolome, *Org.Biomol.Chem* **2008**, *6*, 1895.
- (62) Zheng, Y.; Ma, K.; Lyu, H.; Huang, Y.; Liu, H.; Liu, L.; Che, Y.; Liu, X.; Zou, H.; Yin, W.-B., Genetic manipulation of the COP9 signalosome subunit PfCsnE leads to the discovery of pestaloficins in *Pestalotiopsis fici*, *Org.Lett.* **2017**, *19*, 4700.
- (63) Chiang, Y. M.; Oakley, C. E.; Ahuja, M.; Entwistle, R.; Schultz, A.; Chang, S. L.; Sung, C. T.; Wang, C. C.; Oakley, B. R., An efficient system for heterologous expression of secondary metabolite genes in *Aspergillus nidulans*, *J.Am.Chem.Soc.* **2013**, *135*, 7720.
- (64) Ohashi, M.; Liu, F.; Hai, Y.; Chen, M.; Tang, M. C.; Yang, Z.; Sato, M.; Watanabe, K.; Houk, K. N.; Tang, Y., SAM-dependent enzyme-catalysed pericyclic reactions in natural product biosynthesis, *Nature* **2017**, *549*, 502.
- (65) Sakai, K.; Kinoshita, H.; Shimizu, T.; Nihira, T., Construction of a citrinin gene cluster expression system in heterologous *Aspergillus oryzae*, *J.Biosci.Bioeng.* **2008**, *106*, 466.
- (66) Bai, T.; Quan, Z.; Zhai, R.; Awakawa, T.; Matsuda, Y.; Abe, I., Elucidation and heterologous reconstitution of chrodriamanin B biosynthesis, *Org.Lett.* **2018**, *20*, 7504.
- (67) Harvey, C. J. B.; Tang, M.; Schlecht, U.; Horecka, J.; Fischer, C. R.; Lin, H. C.; Li, J.; Naughton, B.; Cherry, J.; Miranda, M.; Li, Y. F.; Chu, A. M.; Hennessy, J. R.; Vandova, G. A.; Inglis, D.; Aiyar, R.S., HEx: a heterologous expression platform for the discovery of fungal natural products, *Sci.Adv.* **2018**, *4*,

REFERENCES

eaar5459.

(68) Lyu, H. N.; Liu, H. W.; Keller, N. P.; Yin, W. B., Harnessing diverse transcriptional regulators for natural product discovery in fungi, *Nat.Prod.Rep.* **2020**, *37*, 6.

(69) Keller, N. P.; Turner, G.; Bennett, J. W., Fungal secondary metabolism - from biochemistry to genomics, *Nat.Rev.Microbiol.* **2005**, *3*, 937.

(70) Fernandes, M.; Keller, N. P.; Adams, T. H., Sequence-specific binding by *Aspergillus nidulans* AfIR, a C6 zinc cluster protein regulating mycotoxin biosynthesis, *Mol.Microbiol.* **1998**, *28*, 1355.

(71) Jiang, C.; Zhang, C.; Wu, C.; Sun, P.; Hou, R.; Liu, H.; Wang, C.; Xu, J. R., TRI6 and TRI10 play different roles in the regulation of deoxynivalenol (DON) production by cAMP signalling in *Fusarium graminearum*, *Environ.Microbiol.* **2016**, *18*, 3689.

(72) Bayram, O.; Krappmann, S.; Ni, M.; Bok, J. W.; Helmstaedt, K.; Valerius, O.; Braus-Stromeyer, S.; Kwon, N. J.; Keller, N. P.; Yu, J. H.; Braus, G. H., VelB/VeA/LaeA complex coordinates light signal with fungal development and secondary metabolism, *Science* **2008**, *320*, 1504.

(73) Bok, J. W.; Noordermeer, D.; Kale, S. P.; Keller, N. P., Secondary metabolic gene cluster silencing in *Aspergillus nidulans*, *Mol.Microbiol.* **2006**, *61*, 1636.

(74) Pfannenstiel, B. T.; Zhao, X.; Wortman, J.; Wiemann, P.; Throckmorton, K.; Spraker, J. E.; Soukup, A. A.; Luo, X.; Lindner, D. L.; Lim, F. Y.; Knox, B. P.; Haas, B.; Fischer, G. J.; Choera, T.; Butchko, R. A. E., Revitalization of a forward genetic screen identifies three new regulators of fungal secondary metabolism in the genus *Aspergillus*, *mBio.* **2017**, *8*, e01246-17.

(75) Oakley, C. E.; Ahuja, M.; Sun, W. W.; Entwistle, R.; Akashi, T.; Yaegashi, J.; Guo, C. J.; Cerqueira, G. C.; Russo, W. J.; Wang, C. C.; Chiang, Y. M.; Oakley, B. R., Discovery of McrA, a master regulator of *Aspergillus* secondary metabolism, *Mol.Microbiol.* **2017**, *103*, 347.

(76) Kindinger, F.; Nies, J.; Becker, A.; Zhu, T.; Li, S.-M., Genomic locus of a *Penicillium crustosum* pigment as an integration site for secondary metabolite gene expression, *ACS Chem.Biol.* **2019**, *14*, 1227.

(77) Walsh, C. T.; Tang, Y. *Natural Product Biosynthesis*; Royal Society of Chemistry: 2017.

(78) Butler, M. J.; Friend, E. J.; Hunter, I. S.; Kaczmarek, F. S.; Sugden, D. A.; Warren, M., Molecular cloning of resistance genes and architecture of a linked gene cluster involved in biosynthesis of oxytetracycline by *Streptomyces rimosus*, *Mol.Gen.Genet.* **1989**, *215*, 231.

(79) Petkovic, H.; Thamchaipenet, A.; Zhou, L. H.; Hranueli, D.; Raspor, P.; Waterman, P. G.; Hunter, I. S., Disruption of an aromatase/cyclase from the oxytetracycline gene cluster of *Streptomyces rimosus* results in production of novel polyketides with shorter chain lengths, *J.Biol.Chem.* **1999**, *274*, 32829.

(80) Austin, M. B. and Noel, J. P., The chalcone synthase superfamily of type III polyketide synthases, *Nat.Prod.Rep.* **2003**, *20*, 79.

(81) Khosla, C.; Tang, Y.; Chen, A. Y.; Schnarr, N. A.; Cane, D. E., Structure and mechanism of the 6-deoxyerythronolide B synthase, *Annu.Rev.Biochem.* **2007**, *76*, 195.

(82) Lambalot, R. H.; Gehring, A. M.; Flugel, R. S.; Zuber, P.; LaCelle, M.; Marahiel, M. A.; Reid, R.; Khosla, C.; Walsh, C. T., A new enzyme superfamily-the phosphopantetheinyl transferases, *Chem.Biol.* **1996**, *3*, 923.

(83) Walsh, C. T.; Gehring, A. M.; Weinreb, P. H.; Quadri, L. E.; Flugel, R. S., Post-translational modification of polyketide and nonribosomal peptide synthases, *Curr.Opin.Chem Biol.* **1997**, *1*, 309.

REFERENCES

- (84) Cox, R. J., Polyketides, proteins and genes in fungi: programmed nano-machines begin to reveal their secrets, *Org.Biomol.Chem.* **2007**, *5*, 2010.
- (85) Herbst, D. A.; Townsend, C. A.; Maier, T., The architectures of iterative type I PKS and FAS, *Nat.Prod.Rep.* **2018**, *35*, 1046.
- (86) Campbell, C. D. and Vederas, J. C., Biosynthesis of lovastatin and related metabolites formed by fungal iterative PKS enzymes, *Biopolymers* **2010**, *93*, 755.
- (87) Xie, X.; Watanabe, K.; Wojcicki, W. A.; Wang, C. C.; Tang, Y., Biosynthesis of lovastatin analogs with a broadly specific acyltransferase, *Chem.Biol.* **2006**, *13*, 1161.
- (88) Holm, D. K.; Petersen, L. M.; Klitgaard, A.; Knudsen, P. B.; Jarczynska, Z. D.; Nielsen, K. F.; Gotfredsen, C. H.; Larsen, T. O.; Mortensen, U. H., Molecular and chemical characterization of the biosynthesis of the 6-MSA-derived meroterpenoid yanuthone D in *Aspergillus niger*, *Chem.Biol.* **2014**, *21*, 519.
- (89) Crawford, J. M.; Dancy, B. C.; Hill, E. A.; Udway, D. W.; Townsend, C. A., Identification of a starter unit acyl-carrier protein transacylase domain in an iterative type I polyketide synthase, *Proc.Natl.Acad.Sci.U.S.A* **2006**, *103*, 16728.
- (90) Crawford, J. M.; Thomas, P. M.; Scheerer, J. R.; Vagstad, A. L.; Kelleher, N. L.; Townsend, C. A., Deconstruction of iterative multidomain polyketide synthase function, *Science* **2008**, *320*, 243.
- (91) Zhou, H.; Li, Y.; Tang, Y., Cyclization of aromatic polyketides from bacteria and fungi, *Nat.Prod.Rep.* **2010**, *27*, 839.
- (92) Crawford, J. M.; Korman, T. P.; Labonte, J. W.; Vagstad, A. L.; Hill, E. A.; Kamari-Bidkorpeh, O.; Tsai, S. C.; Townsend, C. A., Structural basis for biosynthetic programming of fungal aromatic polyketide cyclization, *Nature* **2009**, *461*, 1139.
- (93) Crawford, J. M. and Townsend, C. A., New insights into the formation of fungal aromatic polyketides, *Nat.Rev.Microbiol.* **2010**, *8*, 879.
- (94) Watanabe, A.; Fujii, I.; Sankawa, U.; Mayorga, M. E.; Timberlake, W. E.; Ebizuka, Y., Re-identification of *Aspergillus nidulans* wA gene to code for a polyketide synthase of naphthopyrone, *Tetrahedron Lett.* **1999**, *40*, 91.
- (95) Fujii, I.; Watanabe, A.; Sankawa, U.; Ebizuka, Y., Identification of Claisen cyclase domain in fungal polyketide synthase WA, a naphthopyrone synthase of *Aspergillus nidulans*, *Chem.Biol.* **2001**, *8*, 189.
- (96) Awakawa, T.; Yokota, K.; Funa, N.; Doi, F.; Mori, N.; Watanabe, H.; Horinouchi, S., Physically discrete β -lactamase-type thioesterase catalyzes product release in atrochrysone synthesis by iterative type I polyketide synthase, *Chem.Biol.* **2009**, *16*, 613.
- (97) Couch, R. D. and Gaucher, G. M., Rational elimination of *Aspergillus terreus* sulochrin production, *J.Biotechnol.* **2004**, *108*, 171.
- (98) Regueira, T. B.; Kildegaard, K. R.; Hansen, B. G.; Mortensen, U. H.; Hertweck, C.; Nielsen, J., Molecular basis for mycophenolic acid biosynthesis in *Penicillium brevicompactum*, *Appl.Environ.Microbiol.* **2011**, *77*, 3035.
- (99) Richter, C. D.; Nietlispach, D.; Broadhurst, R. W.; Weissman, K. J., Multienzyme docking in hybrid megasynthetases, *Nat.Chem Biol.* **2008**, *4*, 75.

REFERENCES

- (100) Weissman, K. J., The structural biology of biosynthetic megaenzymes, *Nat.Chem Biol.* **2015**, *11*, 660.
- (101) Miyanaga, A.; Kudo, F.; Eguchi, T., Protein-protein interactions in polyketide synthase-nonribosomal peptide synthetase hybrid assembly lines, *Nat.Prod.Rep.* **2018**, *35*, 1185.
- (102) Müller, S.; Garcia-Gonzalez, E.; Mainz, A.; Hertlein, G.; Heid, N. C.; Mösker, E.; van den Elst, H.; Overkleef, H. S.; Genersch, E.; Süssmuth, R. D., Paenilamicin: structure and biosynthesis of a hybrid nonribosomal peptide/polyketide antibiotic from the bee pathogen *Paenibacillus larvae*, *Angew.Chem Int.Ed Engl.* **2014**, *53*, 10821.
- (103) Cortina, N. S.; Revermann; Krug, D.; Müller, R., Identification and characterization of the althiomycin biosynthetic gene cluster in *Myxococcus xanthus* DK897, *Chembiochem* **2011**, *12*, 1411.
- (104) Xu, Y.; Kersten, R. D.; Nam, S. J.; Lu, L.; Al-Suwailem, A. M.; Zheng, H.; Fenical, W.; Dorrestein, P. C.; Moore, B. S.; Qian, P. Y., Bacterial biosynthesis and maturation of the didemnin anti-cancer agents, *J.Am.Chem.Soc.* **2012**, *134*, 8625.
- (105) Blodgett, J. A.; Oh, D. C.; Cao, S.; Currie, C. R.; Kolter, R.; Clardy, J., Common biosynthetic origins for polycyclic tetramate macrolactams from phylogenetically diverse bacteria, *Proc.Natl.Acad.Sci.U.S.A* **2010**, *107*, 11692.
- (106) Chen, H. and Du, L., Iterative polyketide biosynthesis by modular polyketide synthases in bacteria, *Appl.Microbiol.Biotechnol.* **2016**, *100*, 541.
- (107) Eley, K. L.; Halo, L. M.; Song, Z.; Powles, H.; Cox, R. J.; Bailey, A. M.; Lazarus, C. M.; Simpson, T. J., Biosynthesis of the 2-pyridone tenellin in the insect pathogenic fungus *Beauveria bassiana*, *Chembiochem.* **2007**, *8*, 289.
- (108) Bergmann, S.; Schumann, J.; Scherlach, K.; Lange, C.; Brakhage, A. A.; Hertweck, C., Genomics-driven discovery of PKS-NRPS hybrid metabolites from *Aspergillus nidulans*, *Nat.Chem.Biol.* **2007**, *3*, 213.
- (109) Xu, W.; Cai, X.; Jung, M. E.; Tang, Y., Analysis of intact and dissected fungal polyketide synthase-nonribosomal peptide synthetase in vitro and in *Saccharomyces cerevisiae*, *J.Am.Chem.Soc.* **2010**, *132*, 13604.
- (110) Sims, J. W.; Fillmore, J. P.; Warner, D. D.; Schmidt, E. W., Equisetin biosynthesis in *Fusarium heterosporum*, *Chem.Commun.* **2005**, 186.
- (111) Phonghanpot, S.; Punya, J.; Tachaleat, A.; Laoteng, K.; Bhavakul, V.; Tanticharoen, M.; Cheevadhanarak, S., Biosynthesis of xyrrolin, a new cytotoxic hybrid polyketide/non-ribosomal peptide pyrroline with anticancer potential, in *Xylaria* sp. BCC 1067, *Chembiochem* **2012**, *13*, 895.
- (112) Gressler, M.; Zaehle, C.; Scherlach, K.; Hertweck, C.; Brock, M., Multifactorial induction of an orphan PKS-NRPS gene cluster in *Aspergillus terreus*, *Chem.Biol.* **2011**, *18*, 198.
- (113) Boettger, D. and Hertweck, C., Molecular diversity sculpted by fungal PKS-NRPS hybrids, *Chembiochem.* **2013**, *14*, 28.
- (114) Yakasai, A. A.; Davison, J.; Wasil, Z.; Halo, L. M.; Butts, C. P.; Lazarus, C. M.; Bailey, A. M.; Simpson, T. J.; Cox, R. J., Nongenetic reprogramming of a fungal highly reducing polyketide synthase, *J.Am.Chem Soc.* **2011**, *133*, 10990.
- (115) Yun, C. S.; Motoyama, T.; Osada, H., Biosynthesis of the mycotoxin tenuazonic acid by a fungal NRPS-PKS hybrid enzyme, *Nat.Commun.* **2015**, *6*, 8758.

REFERENCES

- (116) Sattely, E. S.; Fischbach, M. A.; Walsh, C. T., Total biosynthesis: in vitro reconstitution of polyketide and nonribosomal peptide pathways, *Nat.Prod.Rep.* **2008**, *25*, 757.
- (117) Walsh, C. T., The chemical versatility of natural-product assembly lines, *Acc.Chem Res.* **2008**, *41*, 4.
- (118) Li, S.-M., Applications of dimethylallyltryptophan synthases and other indole prenyltransferases for structural modification of natural products, *Appl.Microbiol.Biotechnol.* **2009**, *84*, 631.
- (119) Punekar, N. S. ENZYMES: catalysis, kinetics and mechanisms; Springer: 2018.
- (120) De Montellano, P. R. O. Cytochrome P450: structure, mechanism, and biochemistry; Springer Science & Business Media: 2005.
- (121) Tang, M. C.; Zou, Y.; Watanabe, K.; Walsh, C. T.; Tang, Y., Oxidative cyclization in natural product biosynthesis, *Chem.Rev.* **2017**, *117*, 5226.
- (122) Nakamura, H.; Matsuda, Y.; Abe, I., Unique chemistry of non-heme iron enzymes in fungal biosynthetic pathways, *Nat.Prod.Rep.* **2018**, *35*, 633.
- (123) Peters, C. and Buller, R. M., Industrial application of 2-oxoglutarate-dependent oxygenases, *Catalysts* **2019**, *9*, 221.
- (124) Gao, S.-S.; Naowarojna, N.; Cheng, R.; Liu, X.; Liu, P., Recent examples of α -ketoglutarate-dependent mononuclear non-haem iron enzymes in natural product biosyntheses, *Nat.Prod.Rep.* **2018**, *35*, 792.
- (125) Martinez, S. and Hausinger, R. P., Catalytic Mechanisms of Fe(II)- and 2-oxoglutarate-dependent oxygenases, *J.Biol.Chem* **2015**, *290*, 20702.
- (126) Eriksson, M.; Myllyharju, J.; Tu, H.; Hellman, M.; Kivirikko, K. I., Evidence for 4-hydroxyproline in viral proteins. Characterization of a viral prolyl 4-hydroxylase and its peptide substrates, *J.Biol.Chem* **1999**, *274*, 22131.
- (127) Vedler, E.; Kõiv, V.; Heinaru, A., Analysis of the 2, 4-dichlorophenoxyacetic acid-degradative plasmid pEST4011 of *Achromobacter xylosoxidans* subsp. *denitrificans* strain EST4002, *Gene* **2000**, *255*, 281.
- (128) Hibi, M.; Mori, R.; Miyake, R.; Kawabata, H.; Kozono, S.; Takahashi, S.; Ogawa, J., Novel enzyme family found in filamentous fungi catalyzing *trans*-4-hydroxylation of L-pipecolic acid, *Appl.Environ.Microbiol.* **2016**, *82*, 2070.
- (129) Farrow, S. C. and Facchini, P. J., Dioxygenases catalyze O-demethylation and O,O-demethylenation with widespread roles in benzylisoquinoline alkaloid metabolism in opium poppy, *J.Biol.Chem* **2013**, *288*, 28997.
- (130) Akahori, H.; Guindon, S.; Yoshizaki, S.; Muto, Y., Molecular evolution of the TET gene family in mammals, *Int.J.Mol.Sci.* **2015**, *16*, 28472.
- (131) Hillwig, M. L.; Zhu, Q.; Ittiamornkul, K.; Liu, X., Discovery of a promiscuous non-heme iron halogenase in ambiguine alkaloid biogenesis: implication for an evolvable enzyme family for late-stage halogenation of aliphatic carbons in small molecules, *Angew.Chem.Int.Ed Engl.* **2016**, *55*, 5780.
- (132) Wang, X. C.; Liu, J.; Zhao, J.; Ni, X. M.; Zheng, P.; Guo, X.; Sun, C. M.; Sun, J. B.; Ma, Y. H., Efficient production of *trans*-4-hydroxy-L-proline from glucose using a new *trans*-proline 4-hydroxylase in *Escherichia coli*, *J.Biosci.Bioeng.* **2018**, *126*, 470.

REFERENCES

- (133) Hagel, J. M. and Facchini, P. J., Dioxygenases catalyze the O-demethylation steps of morphine biosynthesis in opium poppy, *Nat.Chem.Biol.* **2010**, *6*, 273.
- (134) Zhao, Z.; Zhang, Y.; Liu, X.; Zhang, X.; Liu, S.; Yu, X.; Ren, Y.; Zheng, X.; Zhou, K.; Jiang, L.; Guo, X.; Gai, Y.; Wu, C.; Zhai, H.; Wang, H.; Wan, J., A role for a dioxygenase in auxin metabolism and reproductive development in rice, *Dev.Cell* **2013**, *27*, 113.
- (135) Zhang, J.; Lin, J. E.; Harris, C.; Campos Mastrotti, P. F.; Wu, F.; Blakeslee, J. J.; Peer, W. A., DAO1 catalyzes temporal and tissue-specific oxidative inactivation of auxin in *Arabidopsis thaliana*, *Proc.Natl.Acad.Sci.U.S.A* **2016**, *113*, 11010.
- (136) Clifton, I. J.; Doan, L. X.; Sleeman, M. C.; Topf, M.; Suzuki, H.; Wilmouth, R. C.; Schofield, C. J., Crystal structure of carbapenem synthase (CarC), *J.Biol.Chem.* **2003**, *278*, 20843.
- (137) Stapon, A.; Li, R.; Townsend, C. A., Carbapenem biosynthesis: confirmation of stereochemical assignments and the role of CarC in the ring stereoinversion process from L-proline, *J.Am.Chem.Soc.* **2003**, *125*, 8486.
- (138) Chang, W. C.; Guo, Y.; Wang, C.; Butch, S. E.; Rosenzweig, A. C.; Boal, A. K.; Krebs, C.; Bollinger, Jr. J. M., Mechanism of the C5 stereoinversion reaction in the biosynthesis of carbapenem antibiotics, *Science* **2014**, *343*, 1140.
- (139) Kishimoto, S.; Hara, K.; Hashimoto, H.; Hirayama, Y.; Champagne, P. A.; Houk, K. N.; Tang, Y.; Watanabe, K., Enzymatic one-step ring contraction for quinolone biosynthesis, *Nat.Comm.* **2018**, *9*, 2826.
- (140) Ishikawa, N.; Tanaka, H.; Koyama, F.; Noguchi, H.; Wang, C. C.; Hotta, K.; Watanabe, K., Non-heme dioxygenase catalyzes atypical oxidations of 6,7-bicyclic systems to form the 6,6-quinolone core of viridicatin-type fungal alkaloids, *Angew.Chem.Int.Ed.Engl.* **2014**, *53*, 12880.
- (141) Steffan, N.; Grundmann, A.; Afiyatullo, A.; Ruan, H.; Li, S.-M., FtmOx1, a non heme Fe(II) and alpha-ketoglutarate-dependent dioxygenase, catalyses the endoperoxide formation of verruculogen in *Aspergillus fumigatus*, *Org.Biomol.Chem.* **2009**, *7*, 4082.
- (142) Yan, W.; Song, H.; Song, F.; Guo, Y.; Wu, C. H.; Sae, H. A.; Pu, Y.; Wang, S.; Naowarajna, N.; Weitz, A.; Hendrich, M. P.; Costello, C. E.; Zhang, L.; Liu, P.; Zhang, Y. J., Endoperoxide formation by an alpha-ketoglutarate-dependent mononuclear non-haem iron enzyme, *Nature* **2015**, *527*, 539.
- (143) Dunham, N. P.; Del Rio Pantoja, J. M.; Zhang, B.; Rajakovich, L. J.; Allen, B. D.; Krebs, C.; Boal, A. K.; Bollinger, Jr. J. M., Hydrogen donation but not abstraction by a tyrosine (Y68) during endoperoxide installation by verruculogen synthase (FtmOx1), *J.Am.Chem.Soc.* **2019**, DOI:10.1021/jacs.9b03567.
- (144) Busby, R. W.; Chang, M. D.; Busby, R. C.; Wimp, J.; Townsend, C. A., Expression and purification of two isozymes of clavaminic acid synthase and initial characterization of the iron binding site. General error analysis in polymerase chain reaction amplification, *J.Biol.Chem.* **1995**, *270*, 4262.
- (145) Zhou, J.; Kelly, W. L.; Bachmann, B. O.; Gunsior, M.; Townsend, C. A.; Solomon, E. I., Spectroscopic studies of substrate interactions with clavaminic acid synthase 2, a multifunctional α -KG-dependent non-heme iron enzyme: correlation with mechanisms and reactivities, *J.Am.Chem.Soc.* **2001**, *123*, 7388.
- (146) Rabe, P.; Kamps, J. J. A. G.; Schofield, C. J.; Lohans, C. T., Roles of 2-oxoglutarate oxygenases and isopenicillin N synthase in β -lactam biosynthesis, *Nat.Prod.Rep.* **2018**, *35*, 735.

REFERENCES

- (147) Tarhonskaya, H.; Szollossi, A.; Leung, I. K.; Bush, J. T.; Henry, L.; Chowdhury, R.; Iqbal, A.; Claridge, T. D.; Schofield, C. J.; Flashman, E., Studies on deacetoxycephalosporin C synthase support a consensus mechanism for 2-oxoglutarate dependent oxygenases, *Biochemistry* **2014**, *53*, 2483.
- (148) Huang, J. L.; Tang, Y.; Yu, C. P.; Sanyal, D.; Jia, X.; Liu, X.; Guo, Y.; Chang, W. C., Mechanistic investigation of oxidative decarboxylation catalyzed by two iron(II)- and 2-oxoglutarate-dependent enzymes, *Biochemistry* **2018**, *57*, 1838.
- (149) Yu, C. P.; Tang, Y.; Cha, L.; Milikisiyants, S.; Smirnova, T. I.; Smirnov, A. I.; Guo, Y.; Chang, W. C., Elucidating the reaction pathway of decarboxylation-assisted olefination catalyzed by a mononuclear non-heme iron enzyme, *J Am.Chem.Soc.* **2018**, *140*, 15190.
- (150) Chang, W. C.; Sanyal, D.; Huang, J. L.; Ittiamornkul, K.; Zhu, Q.; Liu, X., *In vitro* stepwise reconstitution of amino acid derived vinyl isocyanide biosynthesis: Detection of an elusive intermediate, *Org.Lett.* **2017**, *19*, 1208.
- (151) Harris, N. C.; Born, D. A.; Cai, W.; Huang, Y.; Martin, J.; Khalaf, R.; Drennan, C. L.; Zhang, W., Isonitrile formation by a non-heme iron(II)-dependent oxidase/decarboxylase, *Angew.Chem.Int.Ed Engl.* **2018**, *57*, 9707.
- (152) Clifton, I. J.; McDonough, M. A.; Ehrismann, D.; Kershaw, N. J.; Granatino, N.; Schofield, C. J., Structural studies on 2-oxoglutarate oxygenases and related double-stranded β -helix fold proteins, *J.Inorg.Biochem.* **2006**, *100*, 644.
- (153) Walsh, C. T., Flavin coenzymes: at the crossroads of biological redox chemistry, *Acc.Chem.Res.* **1980**, *13*, 148.
- (154) Alexeev, I.; Sultana, A.; Mäntsälä, P.; Niemi, J.; Schneider, G., Aclacinomycin oxidoreductase (AknOx) from the biosynthetic pathway of the antibiotic aclacinomycin is an unusual flavoenzyme with a dual active site, *Proc.Natl.Acad.Sci.* **2007**, *104*, 6170.
- (155) Davis, C.; Carberry, S.; Schrettl, M.; Singh, I.; Stephens, J. C.; Barry, S. M.; Kavanagh, K.; Challis, G. L.; Brougham, D.; Doyle, S., The role of glutathione S-transferase GliG in gliotoxin biosynthesis in *Aspergillus fumigatus*, *Chem.Biol.* **2011**, *18*, 542.
- (156) Schrettl, M.; Carberry, S.; Kavanagh, K.; Haas, H.; Jones, G. W.; O'Brien, J.; Nolan, A.; Stephens, J.; Fenelon, O.; Doyle, S., Self-protection against gliotoxin--a component of the gliotoxin biosynthetic cluster, GliT, completely protects *Aspergillus fumigatus* against exogenous gliotoxin, *PLoS.Pathog.* **2010**, *6*, e1000952.
- (157) Kallio, P.; Liu, Z.; Mäntsälä, P.; Niemi, J.; Metsä-Ketelä, M., Sequential action of two flavoenzymes, PgaE and PgaM, in angucycline biosynthesis: chemoenzymatic synthesis of gaudimycin C, *Chem.Biol.* **2008**, *15*, 157.
- (158) Kallio, P.; Patrikainen, P.; Suomela, J. P.; Mäntsälä, P.; Metsä-Ketelä, M.; Niemi, J., Flavoprotein hydroxylase PgaE catalyzes two consecutive oxygen-dependent tailoring reactions in angucycline biosynthesis, *Biochemistry* **2011**, *50*, 5535.
- (159) Huijbers, M. M.; Montersino, S.; Westphal, A. H.; Tischler, D.; van Berkel, W. J., Flavin dependent monooxygenases, *Arch.Biochem.Biophys.* **2014**, *544*, 2.
- (160) van Berkel, W. J.; Kamerbeek, N. M.; Fraaije, M. W., Flavoprotein monooxygenases, a diverse class of oxidative biocatalysts, *J.Biotechnol.* **2006**, *124*, 670.

REFERENCES

- (161) Walsh, C. T. and Wencewicz, T. A., Flavoenzymes: Versatile catalysts in biosynthetic pathways, *Nat.Prod.Rep.* **2013**, *30*, 175.
- (162) Benson, T. E.; Walsh, C. T.; Hogle, J. M., The structure of the substrate-free form of MurB, an essential enzyme for the synthesis of bacterial cell walls, *Structure.* **1996**, *4*, 47.
- (163) Benson, T. E.; Walsh, C. T.; Hogle, J. M., X-ray crystal structures of the S229A mutant and wild-type MurB in the presence of the substrate enolpyruvyl-UDP-N-acetylglucosamine at 1.8-Å resolution, *Biochemistry* **1997**, *36*, 806.
- (164) Lees, W. J.; Benson, T. E.; Hogle, J. M.; Walsh, C. T., (*E*)-enolbutyryl-UDP-N-acetylglucosamine as a mechanistic probe of UDP-N-acetylenolpyruvylglucosamine reductase (MurB), *Biochemistry* **1996**, *35*, 1342.
- (165) Walsh, C. T.; Benson, T. E.; Kim, D. H.; Lees, W. J., The versatility of phosphoenolpyruvate and its vinyl ether products in biosynthesis, *Chem.Biol.* **1996**, *3*, 83.
- (166) Muschiol, J.; Peters, C.; Oberleitner, N.; Mihovilovic, M. D.; Bornscheuer, U. T.; Rudroff, F., Cascade catalysis-strategies and challenges en route to preparative synthetic biology, *Chem.Commun.* **2015**, *51*, 5798.
- (167) Rudroff, F.; Mihovilovic, M. D.; Gröger, H.; Snajdrova, R.; Iding, H.; Bornscheuer, U. T., Opportunities and challenges for combining chemo- and biocatalysis, *Nat.Catal.* **2018**, *1*, 12.
- (168) Capon, R. J., Extracting value: mechanistic insights into the formation of natural product artifacts - case studies in marine natural products, *Nat.Prod.Rep.* **2019**, DOI: 10.1039/c9np00013e.
- (169) Van De Water, R. W. and Pettus, T. R. R., *o*-Quinone methides: intermediates underdeveloped and underutilized in organic synthesis, *Tetrahedron* **2002**, *58*, 5367.
- (170) Bai, W. J.; David, J. G.; Feng, Z. G.; Weaver, M. G.; Wu, K. L.; Pettus, T. R. R., The domestication of *ortho*-quinone methides, *Acc.Chem.Res.* **2014**, *47*, 3655.
- (171) Nielsen, C. D. T.; Abas, H.; Spivey, A. C., Stereoselective reactions of *ortho*-quinone methide and *ortho*-quinone methide imines and their utility in natural product synthesis, *Synthesis* **2018**, *50*, 4008.
- (172) Pathak, T. P. and Sigman, M. S., Applications of *ortho*-quinone methide intermediates in catalysis and asymmetric synthesis, *J.Org.Chem.* **2011**, *76*, 9210.
- (173) Willis, N. J. and Bray, C. D., *ortho*-Quinone methides in natural product synthesis, *Chemistry* **2012**, *18*, 9160.
- (174) Spence, J. T. and George, J. H., Biomimetic total synthesis of *ent*-penilactone A and penilactone B, *Org.Lett.* **2013**, *15*, 3891.
- (175) Spence, J. T. and George, J. H., Total synthesis of peniphenones A-D *via* biomimetic reactions of a common *o*-quinone methide intermediate, *Org.Lett.* **2015**, *17*, 5970.
- (176) Forest, K.; Wan, P.; Preston, C. M., Catechin and hydroxybenzhydrols as models for the environmental photochemistry of tannins and lignins, *Photochem.Photobiol.Sci.* **2004**, *3*, 463.
- (177) Chen, Y. and Steinmetz, M. G., Photoactivation of amino-substituted 1,4-benzoquinones for release of carboxylate and phenolate leaving groups using visible light, *J.Org.Chem.* **2006**, *71*, 6053.
- (178) Bishop, L. M.; Winkler, M.; Houk, K. N.; Bergman, R. G.; Trauner, D., Mechanistic investigations of the acid-catalyzed cyclization of a vinyl *ortho*-quinone methide, *Chemistry* **2008**, *14*, 5405.

REFERENCES

- (179) Patel, A.; Netscher, T.; Rosenau, T., Stabilization of *ortho*-quinone methides by a bis (sulfonium ylide) derived from 2, 5-dihydroxy-[1, 4] benzoquinone, *Tetrahedron Lett.* **2008**, *49*, 2442.
- (180) Fan, J.; Liao, G.; Kindinger, F.; Ludwig-Radtke, L.; Yin, W.-B.; Li, S.-M., Peniphenone and penilactone formation in *Penicillium crustosum* via 1,4-Michael additions of *ortho*-quinone methide from hydroxyclovatol to γ -butyrolactones from crustosic acid, *J.Am.Chem.Soc.* **2019**, *141*, 4225.
- (181) Huang, C.; Yang, C.; Zhang, W.; Zhang, L.; De, B. C.; Zhu, Y.; Jiang, X.; Fang, C.; Zhang, Q.; Yuan, C. S.; Liu, H.W.; Zhang, C., Molecular basis of dimer formation during the biosynthesis of benzofluorene-containing atypical angucyclines, *Nat.Commun.* **2018**, *9*, 2088.
- (182) Bourguet-Kondracki, M. L.; Lacombe, F.; Guyot, M., Methanol adduct of puupehenone, a biologically active derivative from the marine sponge *Hyrtios* species, *J.Nat.Prod.* **1999**, *62*, 1304.
- (183) Urban, S. and Capon, R. J., Absolute stereochemistry of puupehenone and related metabolites, *J.Nat.Prod.* **1996**, *59*, 900.
- (184) Hemphill, C. F. P.; Daletos, G.; Liu, Z.; Lin, W.; Proksch, P., Polyketides from the mangrove-derived fungal endophyte *Pestalotiopsis clavispora*, *Tetrahedron Lett.* **2016**, *57*, 2078.
- (185) Jansen, R.; Gerth, K.; Steinmetz, H.; Reinecke, S.; Kessler, W.; Kirschning, A.; Müller, R., Elansolid A3, a unique *p*-quinone methide antibiotic from *Chitinophaga sancti*, *Chemistry* **2011**, *17*, 7739.
- (186) Dehn, R.; Katsuyama, Y.; Weber, A.; Gerth, K.; Jansen, R.; Steinmetz, H.; Höfle, G.; Müller, R.; Kirschning, A., Molecular basis of elansolid biosynthesis: evidence for an unprecedented quinone methide initiated intramolecular Diels-Alder cycloaddition/macrolactonization, *Angew.Chem.Int.Ed.Engl.* **2011**, *50*, 3882.
- (187) Asai, T.; Tsukada, K.; Ise, S.; Shirata, N.; Hashimoto, M.; Fujii, I.; Gomi, K.; Nakagawara, K.; Kodama, E. N.; Oshima, Y., Use of a biosynthetic intermediate to explore the chemical diversity of pseudo-natural fungal polyketides, *Nat.Chem.* **2015**, *7*, 737.
- (188) Wu, G.; Ma, H.; Zhu, T.; Li, J.; Gu, Q.; Li, D., Penilactones A and B, two novel polyketides from Antarctic deep-sea derived fungus *Penicillium crustosum* PRB-2, *Tetrahedron* **2012**, *68*, 9745.
- (189) Li, H.; Jiang, J.; Liu, Z.; Lin, S.; Xia, G.; Xia, X.; Ding, B.; He, L.; Lu, Y.; She, Z., Peniphenones A-D from the mangrove fungus *Penicillium dipodomycicola* HN4-3A as inhibitors of *Mycobacterium tuberculosis* phosphatase MptpB, *J.Nat.Prod.* **2014**, *77*, 800.
- (190) Sun, W.; Chen, X.; Tong, Q.; Zhu, H.; He, Y.; Lei, L.; Xue, Y.; Yao, G.; Luo, Z.; Wang, J.; Li, H.; Zhang, Y., Novel small molecule 11beta-HSD1 inhibitor from the endophytic fungus *Penicillium commune*, *Sci.Rep.* **2016**, *6*, 26418.
- (191) Wu, G., Studies on secondary metabolites of three different marine environment-derived fungi: structures and bioactivities, *Dissertation, Ocean University of China* **2014**
- (192) Astudillo, L.; Schmeda-Hirschmann, G.; Soto, R.; Sandoval, C.; Afonso, C.; Gonzalez, M. J.; Kijjoo, A., Acetophenone derivatives from Chilean isolate of *Trichoderma pseudokoningii* Rifai, *World J.Microbiol.Biotechnol.* **2000**, 585.
- (193) Nukina, M., Terrestrial acid as a phytotoxic metabolite from *Pyricularia oryzae* Cavara, *Agric.Biol.Chem.* **1988**, *52*, 2357.
- (194) Adrian, J. and Stark, C. B., Total synthesis of muricadienin, the putative key precursor in the solamin biosynthesis, *Org.Lett.* **2014**, *16*, 5886.

REFERENCES

- (195) Stebbins, N. D.; Yu, W.; Uhrich, K. E., Enzymatic polymerization of an ibuprofen-containing monomer and subsequent drug release, *Macromol.Biosci.* **2015**, *15*, 1115.
- (196) Clutterbuck, P. W.; Haworth, W. N.; Raistrick, H.; Smith, G.; Stacey, M., Studies in the biochemistry of micro-organisms: The metabolic products of *Penicillium charlesii* G. Smith., *Biochem.J.* **1934**, *28*, 94.
- (197) Weber, T.; Blin, K.; Duddela, S.; Krug, D.; Kim, H. U.; Brucocoleri, R.; Lee, S. Y.; Fischbach, M. A.; Müller, R.; Wohlleben, W.; Breitling, R.; Takano, E.; Medema, M. H., antiSMASH 3.0 - a comprehensive resource for the genome mining of biosynthetic gene clusters, *Nucleic Acids Res.* **2015**, *43*, W237.
- (198) Tomoda, H.; Tabata, N.; Masuma, R.; Si, S. Y.; Omura, S., Erabulenols, inhibitors of cholesteryl ester transfer protein produced by *Penicillium* sp. FO-5637. I. Production, isolation and biological properties, *J.Antibiot.(Tokyo)* **1998**, *51*, 618.
- (199) da Silva, B. F. and Rodrigues-Fo, E., Production of a benzylated flavonoid from 5,7,3',4',5'-pentamethoxyflavanone by *Penicillium griseoroseum*, *J.Mol.Catal.B - Enzyme* **2010**, *67*, 184.
- (200) Wang, J.; Liu, P.; Wang, Y.; Wang, H.; Li, J.; Zhuang, Y.; Zhu, W., Antimicrobial aromatic polyketides from Gorgonian-associated fungus, *Penicillium commune* 518, *Chin.J.Chem.* **2012**, *30*, 1236.
- (201) Vieweg, L.; Reichau, S.; Schobert, R.; Leadlay, P. F.; Sussmuth, R. D., Recent advances in the field of bioactive tetronates, *Nat.Prod.Rep.* **2014**, *31*, 1554.
- (202) Schobert, R. and Schlenk, A., Tetramic and tetronic acids: an update on new derivatives and biological aspects, *Bioorg.Med.Chem.* **2008**, *16*, 4203.
- (203) Bentley, R.; Bhate, D. S.; Keil, J. G., Tetronic acid biosynthesis in molds I. Formation of carlosic and carolic acids in *Penicillium charlesii*, *J.Biol.Chem.* **1962**, *237*, 859.
- (204) Bracken, A. and Raistrick, H., Studies in the biochemistry of micro-organisms: 75. Dehydrocarolic acid, a metabolic product of *Penicillium cinerascens* Biourge, *Biochem.J.* **1947**, *41*, 569.
- (205) Pitt, J. I.; Lange, L.; Lacey, A. E.; Vuong, D.; Midgley, D. J.; Greenfield, P.; Bradbury, M. I.; Lacey, E.; Busk, P. K.; Pilgaard, B.; Chooi, Y.H.; Piggott, A.M., *Aspergillus hancockii* sp. nov., a biosynthetically talented fungus endemic to southeastern Australian soils, *PLoS.One.* **2017**, *12*, e0170254.
- (206) Grant, J. L.; Hsieh, C. H.; Makris, T. M., Decarboxylation of fatty acids to terminal alkenes by cytochrome P450 compound I, *J.Am.Chem.Soc.* **2015**, *137*, 4940.
- (207) Rachid, S.; Revermann, O.; Dauth, C.; Kazmaier, U.; Müller, R., Characterization of a novel type of oxidative decarboxylase involved in the biosynthesis of the styryl moiety of chondrochloren from an acylated tyrosine, *J.Biol.Chem.* **2010**, *285*, 12482.
- (208) Ji, X.; Mo, T.; Liu, W. Q.; Ding, W.; Deng, Z.; Zhang, Q., Revisiting the mechanism of the anaerobic coproporphyrinogen III oxidase HemN, *Angew.Chem Int.Ed Engl.* **2019**, *58*, 6235.
- (209) Rui, Z.; Li, X.; Zhu, X.; Liu, J.; Domigan, B.; Barr, I.; Cate, J. H. D.; Zhang, W., Microbial biosynthesis of medium-chain 1-alkenes by a nonheme iron oxidase, *Proc.Natl.Acad.Sci.U.S.A* **2014**, *111*, 18237.
- (210) Manley, O. M.; Fan, R.; Guo, Y.; Makris, T. M., Oxidative decarboxylase UndA utilizes a dinuclear iron cofactor, *J.Am.Chem.Soc.* **2019**, *141*, 8684.

REFERENCES

- (211) Steinmetz, H.; Zander, W.; Shushni, M. A. M.; Jansen, R.; Gerth, K.; Dehn, R.; Dräger, G.; Kirschning, A.; Müller, R., Precursor-directed syntheses and biological evaluation of new elansolid derivatives, *Chembiochem* **2012**, *13*, 1813.
- (212) Yu, G.; Sun, Z.; Peng, J.; Zhu, M.; Che, Q.; Zhang, G.; Zhu, T.; Gu, Q.; Li, D., Secondary metabolites produced by combined culture of *Penicillium crustosum* and a *Xylaria* sp, *J.Nat.Prod.* **2019**, *82*, 2013.
- (213) Davies, M. W.; Maskell, L.; Shipman, M.; Slawin, A. M.; Vidot, S. M.; Whatmore, J. L., Studies toward the synthesis of luminacin D: assembly of simplified analogues devoid of the epoxide displaying antiangiogenic activity, *Org.Lett.* **2004**, *6*, 3909.
- (214) Kasai, S.; Watanabe, S.; Kawabata, J.; Tahara, S.; Mizutani, J., Antimicrobial catechin derivatives of *Agrimonia pilosa*, *Phytochemistry* **1992**, *31*, 787.
- (215) Kim, H. W.; Park, J.; Kang, K. B.; Kim, T. B.; Oh, W. K.; Kim, J.; Sung, S. H., Acylphloroglucinolated catechin and phenylethyl isocoumarin derivatives from *Agrimonia pilosa*, *J.Nat.Prod.* **2016**, *79*, 2376.

Statutory Declaration

Ich, Jie Fan, versichere, dass ich meine Dissertation

„Biosynthesis of penilactones and peniphenones in *Penicillium crustosum*“

selbständig ohne unerlaubte Hilfe angefertigt und mich dabei keiner anderen als der von mir ausdrücklich bezeichneten Quellen bedient habe. Alle vollständig oder sinngemäß übernommenen Zitate sind als solche gekennzeichnet.

Die Dissertation wurde in der jetzigen oder einer ähnlichen Form noch bei keiner anderen Hochschule eingereicht und hat noch keinen sonstigen Prüfungszwecken gedient.

Marburg, den.....

.....
Jie Fan

Acknowledgements

I would like to express my special thanks to the people who accompanied and supported me during my PhD study.

Firstly, I would like to express my sincere gratitude to my supervisor Prof. Dr. Shu-Ming Li for his excellent mentoring and supervision during my PhD study. With a great knowledge on our biological and chemical research, he is always interested in the newest process and willing to learn more. Many great thanks go to him for his patience to me, for his scientific motivation, for his encouragement on my hard working, for his advices on my researches, and even for his help with my life in Germany.

I am grateful to Prof. Dr. Michael Keusgen for kindly agreeing to act as second referee and examiner. I would also like to take this opportunity to thank Ge Liao as my best partner on our projects. Also thanks very much to Lena Ludwig-Radtke for her chemical synthesis, Rixa Kraut for taking mass spectra, and Dr. Regina Ortmann and Stefan Newel for taking NMR spectra, as well as Prof. Dr. Andreas Heine for X-ray crystal analysis. I also express the deep appreciation to Prof. Dr. Wen-Bing Yin from Institute of Microbiology, Chinese Academy of Sciences for his help for the genome sequencing, genetic guidance and academic discussion. My special gratitude goes to Sina Stierle for translating and Lauritz Harken for proof reading this dissertation.

A heartfelt thank you goes to Huomiao with whom we can talk about everything at work and in my free time. I am thankful to Shuang Zhou, Huan Liu, Lindsay Coby, Florian Kindinger, and Johanna Schäfer for their friendly support on my life and research. Also special thanks go to Huili Yu, Jinglin Wang, and Zhengxi Zhang for their company to Mensa and life sharing. Great thanks to Haowen Wang and Liujuan Zheng for their help on my movement and their open ears for my private life.

More thanks to my current and former colleagues, Jing Liu, Pan Xiang, Bastian Kemmerich, Jonas Nies, Lena Mikulski, Wei Li, Alexander Frehse, Viola Wohlgemuth, Kirsten Brockmeyer, Peter Mai, Linus Naumann, Kristin Öqvist, Elisabeth Hühner, Wen Li, Jenny Zhou, Yiling Yang, Yu Dai, Marlies Peter, Danniell Jonathan Janzen, Andreas Martin, Dr. Katija Backhaus, Dr. Nina Gerhards, Dr. Kang Zhou, and Dr. Dieter Kreuzsch for the great and wonderful time. I also thank the short-term communication professors and students in our institute for the great experience together.

I further express my thanks to my friends outside of the laboratory for their wonderful friendship.

I thank the China Scholarship Council (CSC) for financial supports.

At last but not the least, I deeply thank my family for their encouragement and support over the past years.

Curriculum Vitae

Personal Information

Name: Jie Fan

Gender: Female

Birthday: 16.02.1991

Place of Birth: Guxian, Linfen, Shanxi Province, P. R. China

Address: Robert-Koch-Str. 4, 35032, Marburg

Email: fanjie@staff.uni-marburg.de

Education & Research

PhD candidate: 10.2015–now

Philipps-University Marburg, Germany

Institute for Pharmaceutical Biology and Biotechnology

Thesis title: “Biosynthesis of penilactones and peniphenones in *Penicillium crustosum*”

Supervisor: Prof. Dr. Shu-Ming Li

Master of Science: 09.2012–06.2015

Hainan University, China

Institute of Tropical Bioscience and Biotechnology (ITBB)

Plant Molecular Genetics

Thesis title: “Functional characterization involved in drought stress of galactinol synthase gene *MeGolS5* from *Manihot esculenta* Crantz”

Supervisor: Prof. Dr. Jianchun Guo

Bachelor of Science: 09.2008–06.2012

Hainan University, China

College of Life Sciences and Agriculture

Agricultural Resources and Environment

Project: Development of a method for the efficient release of N-glycans from glycoproteins generating native deglycosylated proteins

Supervisor: Prof. Dr. Lei Meng

Thesis title: “The correlation between rubber tree leaf Nutrition and latex production as well as protein”

Education:

09.2004-06.2008 Linfen No.3 Middle School